

★
Gaseous Nebulae
★

L. H. ALLER

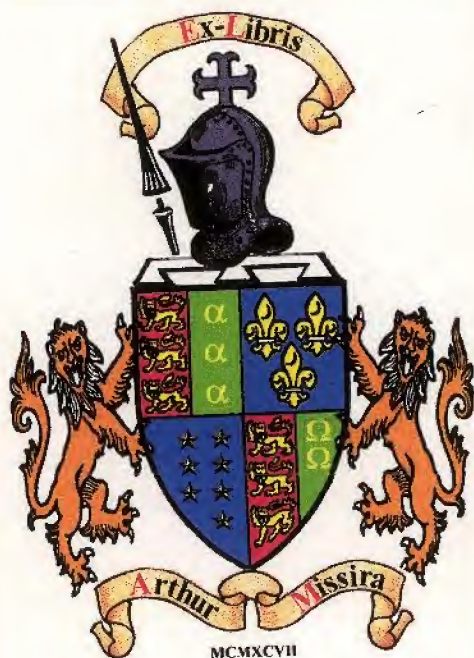
Gaseous Nebulae

L. H. ALLER

THE INTERNATIONAL ASTROPHYSICS SERIES

VOLUME THREE

C & H



GASEOUS NEBULAE

THE INTERNATIONAL ASTROPHYSICS SERIES
VOLUME THREE

THE INTERNATIONAL ASTROPHYSICS SERIES

Already published

The Aurorae	<i>L. Harang</i>
Comets and Meteor Streams	<i>J. G. Porter</i>
Gaseous Nebulae	<i>L. H. Aller</i>
General Relativity and Cosmology	<i>G. C. McVittie</i>

In preparation

Astronomical Photometry	<i>D. S. Evans</i>
The Earth and the Planets	<i>W. H. Ramsey</i>
Stellar Constitution	<i>D. H. Menzel and H. K. Sen</i>
Close Binary Systems	<i>Zdenek Kopal</i>
The Origin of Cosmic Rays	<i>L. Bierman</i>
Galactic and Extra-Galactic Emissions	<i>R. Hanbury Brown</i>

THE INTERNATIONAL ASTROPHYSICS SERIES

General Editors

M. A. Ellison, Sc.D., F.R.S.E., F.R.A.S.

The Royal Observatory, Edinburgh

A. C. B. Lovell, O.B.E., Ph.D., F.Inst.P., F.R.S., F.R.A.S.

Professor of Radio Astronomy

University of Manchester

VOLUME THREE

Gaseous Nebulae

L. H. ALLER

Professor of Astronomy

University of Michigan



LONDON

CHAPMAN & HALL LTD.

37 Essex Street, W.C.2

1956

First published 1956

CATALOGUE NO. 525/4

*Printed and bound in Great Britain by
Jarrold and Sons Limited, Norwich*

TO
DONALD H. MENZEL

Editors' Note

THE AIM of the International Astrophysics Series is to provide a collection of authoritative volumes dealing with the main branches of Astrophysics and Radio Astronomy. The need for such a series of books has arisen because of the great developments which have taken place in these fields of work during recent years.

The books will be suitable for both specialists and students. Some of the titles may have a wider and more popular appeal, but this will be secondary to their main purpose, which is to assist in the teaching of Astrophysics and Radio Astronomy and in the advancement of these subjects themselves.

Author's Preface

RECENT YEARS have seen a great increase in interest in gaseous nebulae and the interstellar medium. The relation of these subjects to galactic radio emission, stellar evolution, and even cosmic rays have attracted ever-increasing attention.

The first version of the present work was prepared by the writer while he was at Harvard University and at the University of California between 1940 and 1945. The profound changes which have occurred in the subject since then have required a complete revision of the older manuscript. Developments have been particularly striking in the observational side. Olin Wilson's measurements of the internal motions in the planetaries and Minkowski's beautiful direct photographs of these objects have drastically changed our concepts of these nebulae.

The study of diffuse gaseous nebulae has been accelerated by the development of techniques capable of studying objects of extremely low surface brightness. Radio-frequency observations may assist us greatly in the study of these extended nebulae.

On the theoretical side much basic work remains to be done. Although the fundamental physical processes appear to be well understood, the theory of certain necessary parameters such as target areas for collisional excitation of lines is not yet in a satisfactory state. The hydrodynamical theory of gaseous nebulae is only in the earliest stages of its development.

No attempt has been made to treat all topics in the same detail. For example, the diffuse nebulae form a component of the interstellar medium, a subject which will be treated in another volume of this series. Hence they have not been discussed as comprehensively as have the planetary nebulae.

L. H. A.

Ann Arbor, Michigan
March 23, 1954

Acknowledgments

THIS VOLUME could not have been written without the co-operation and helpful suggestions of many astronomers. Thanks are due to G. K. Batchelor, Roy Garstang, Mrs. C. H. P. Gaposchkin, D. H. Menzel, A. C. B. Lovell, D. McLaughlin, W. W. Morgan, D. Osterbrock, and H. Zanstra who read the manuscript and offered helpful suggestions. William Liller, M. J. Seaton, Henry J. Smith, and W. Baade contributed data in advance of publication, while original diagrams and photographs have been supplied by H. Arp, Albert Boggess III, Joseph Chamberlain, E. Dennison, K. G. Henize, James Milligan, N. U. Mayall, Bart J. Bok, and E. B. Weston. The isophotometer tracings of planetary nebulae were all made by Mrs. Nancy Boggess.

I am especially indebted to R. Minkowski and Olin C. Wilson, who not only contributed so much of the observational material reproduced, analysed, or discussed in these pages, but who also read the entire manuscript critically. To Director I. S. Bowen and the staff of the Mount Wilson and Palomar Observatories, I am deeply grateful for the opportunities for research extended to me as a guest investigator.

L.H.A.

Contents

CHAPTER	PAGE
I TYPES OF GASEOUS NEBULAE	1
II METHODS OF OBSERVATION	11
III THE DISTANCES, DIMENSIONS, AND SPECTRA OF THE GASEOUS NEBULAE	46
IV PHYSICAL PROCESSES IN GASEOUS NEBULAE	111
V THE FORBIDDEN LINES	164
VI THE STARS THAT ILLUMINATE THE GASEOUS NEBULAE	201
VII STRUCTURE AND INTERNAL MOTIONS OF THE PLANETARY NEBULAE	234
VIII THE DIFFUSE GASEOUS NEBULAE	279
NAME INDEX	315
SUBJECT INDEX	319

List of Plates

FIGURE NUMBER

I : 1.	<i>The Planetary Nebula</i>	<i>between 8 and 9</i>
I : 2.	<i>The Nebular Shell of DQ Herculis in 1942</i>	<i>8 and 9</i>
I : 3.	<i>NGC 6960, a portion of the Network Nebula</i>	<i>8 and 9</i>
I : 4.	<i>The Star Cluster (NGC 6530) and Nebula Messier 8 (NGC 6523)</i>	<i>8 and 9</i>
I : 5.	<i>Messier 8 as observed with an Objective Prism</i>	<i>8 and 9</i>
I : 6.	<i>The Large Magellanic Cloud and its Emission Nebulosities</i>	<i>8 and 9</i>
I : 7.	<i>Objective Prism Spectrogram of Messier 33</i>	<i>8 and 9</i>
II : 1.	<i>Bond's Drawing of the Orion Nebula</i>	<i>facing 12</i>
II : 2.	<i>The Orion Nebula</i>	<i>13</i>
II : 5.	<i>Slitless Spectrograms of the Ring Nebula and Comparison Star</i>	<i>21</i>
II : 14.	<i>A Monochromatic Planetary Nebular Image observed with O. C. Wilson's Multi-Slit</i>	<i>43</i>
III : 4.	<i>The Ring Nebula in Lyra</i>	<i>between 56 and 57</i>
III : 5.	<i>The Ring Nebula in Lyra (Minkowski)</i>	<i>56 and 57</i>
III : 6.	<i>NGC 7026</i>	<i>56 and 57</i>
III : 7.	<i>Slitless Spectra of Planetary Nebulae</i>	<i>56 and 57</i>
III : 8.	<i>The Behaviour of $\lambda 3727$ [OII] in certain Planetary Nebulae facing 74</i>	
III : 9.	<i>Slit Spectrograms of Planetary Nebulae</i>	<i>75</i>
III : 13.	<i>The η Carinae Nebula</i>	<i>between 96 and 97</i>
III : 14.	<i>The Diffuse Nebula Messier 17 (NGC 6618)</i>	<i>96 and 97</i>
III : 15.	<i>The Spectra of Four Diffuse Nebulae</i>	<i>96 and 97</i>

FIGURE NUMBER

III : 16.	<i>An Objective Prism Spectrogram of Emission Nebulosities in the Large Magellanic Cloud</i>	between 96 and 97
VI : 3.	<i>The Spectra of the Planetaries NGC 6751 and NGC 6905</i>	facing 210
VII : 11(a).	<i>Slitless Spectra and Isophotic Contours of NGC 7662</i>	255
VII : 12.	<i>Slitless Spectrograms and Isophotic Contours of NGC 2392</i>	256
VII : 13.	<i>Slitless and Slit Spectra of various Images in IC 418</i>	257
VII : 17.	<i>Internal Motion in the Planetary Nebulae NGC 7027 and NGC 7662</i>	276
VIII : 1.	<i>NGC 7023 photographed in Red and Blue Light</i>	280
VIII : 2.	<i>The Trifid Nebula</i>	281

(All other figures are in the text)

CHAPTER I

Types of Gaseous Nebulae

1. Introductory Remarks

The term nebula has been employed by astronomers to denote diffuse telescopic objects that cannot be resolved into stars. It is in some respects an unfortunate word since it includes both clouds of particles and gas and whole stellar systems. In our present survey we shall be concerned with objects of the first type and particularly those that are predominantly gaseous. It is customary to speak of these bodies as diffuse or galactic nebulae; stellar systems that are catalogued or described as nebulae are ordinarily referred to by such terms as extra-galactic nebulae, spiral nebulae, elliptical nebulae, external galaxies, or simply galaxies. The last-mentioned term will be employed throughout this book to denote all stellar systems of galactic dimensions outside our own Milky Way system. Unless otherwise qualified the term "nebula" will be used to denote *galactic nebulae*.

The best known of all galactic nebulae is the Orion nebula which, as far as naked-eye observations are concerned, contributes a misty appearance to the central star of the sword. Other nebulae were found shortly after the invention of the telescope. A number are included in Messier's catalogue, that list of nuisances to the searcher for comets. The first great contribution to the study of the nebulae was made by Sir William Herschel, who recognized the planetary nebulae as a distinct class of object and who catalogued great numbers of diffuse nebulae and galaxies. These studies were extended to the southern hemisphere by his son, Sir John Herschel. Later investigators added further objects; the nineteenth-century work culminates in Dreyer's compilation of the *New General Catalogue of Clusters and Nebulae*. The NGC, as it is abbreviated, gives the right ascensions, north polar distances ($90^\circ - \delta$), where δ is the declination, and brief descriptions of the object. There are two supplements or index catalogues. Thus IC 4997 or NGC II 4997 means object No. 4997 in the index catalogue, in this instance in the second index catalogue.

The number of known galactic nebulae has been greatly increased by the photographic surveys which have utilized narrow band-pass filters and objective prisms. Cederblad listed the diffuse galactic nebulae known up to about 1945. Further objects have been added since then by Strömgren, Sharpless and Osterbrock, and Morgan at the Yerkes Observatory, by

Shajn and Hase at Simeis, and by other observers. Minkowski at Mt. Wilson and, to a lesser extent, Henize in South Africa have added many new planetaries to our list.

The nineteenth-century observers recognized a distinction between two types of nebulae—objects that showed a faint greenish appearance when observed under optimum conditions and which tended to congregate towards the Milky Way, and “white” nebulae that avoided the Milky Way. The former were subsequently identified as galactic nebulae, the latter as galaxies.

In the early part of the nineteenth century a belief persisted in some quarters that all nebulae were really stellar systems seen at great distances. Herschel did not subscribe to this view; he believed that the planetaries, at least, consisted of a shining fluid and not of an aggregate of stars. Lord Rosse, at the other extreme, thought he resolved the Orion nebula into stars. The spectroscope solved the problem conclusively. Huggins found that the planetaries and the Orion nebula showed a bright-line spectrum, and therefore consisted of incandescent gases.* The dark-line spectra of the white nebulae are usually much more difficult to observe because of their low surface brightnesses, but subsequent work showed them to give spectra of the type to be expected from a clustering of stars at a great distance.

Let us now turn to a detailed consideration of the different types of galactic nebulae.

2. The Planetary Nebulae

The planetary nebulae owe their picturesque designation to their frequent resemblance to the pale green disks of the giant planets Uranus and Neptune. Their spectra are characterized by strong forbidden lines of oxygen, nitrogen, neon, etc., and the re-combination lines of hydrogen and helium. The radiation of each nebula is derived by the degradation of ultra-violet energy of a small, extremely hot central star. A typical planetary has a radius of about ten thousand astronomical units, a density between 10^3 and 10^4 ions/cm.³, and an electron temperature of the order of $10,000^\circ\text{K}$. or more.

Some planetaries such as the celebrated Ring nebula appear as disk or ring shapes, or even as double rings (e.g. NGC 3242). All these rings display irregularities or a filamentary structure when examined with a sufficient scale. Others show complicated forms which defy interpretation in terms of any simple geometrical model or physical theory of an outburst of the central star.

The planetaries belong to Baade's population Type II and have a spatial

* Objects such as the Orion nebula have been shown also to contain solid particles as well as gases.

distribution similar to that of the RR Lyrae stars. They show little galactic concentration, being dispersed to great distances from the galactic plane. They do show a very strong concentration towards the centre of the galaxy, i.e. towards the Sagittarius Star cloud, where most of them are found. The central stars appear to have absolute photo-visual magnitudes near 0, while the planetaries themselves may have magnitudes ranging up to -3 or -4 .

3. Shells Associated with Novae and Nova-like Stars

Among the gaseous nebulae we may place also the shells ejected by novae that are sometimes observed as small nebulae surrounding the old star some years after the outburst. Although these nebular shells are short-lived phenomena, the character of their spectra and the physical processes that occur in the attenuated envelopes bear a close relationship to what goes on in a planetary or other gaseous nebula.* For example, a month after the outburst of Nova Aquilae, 1918, the expanding shell had a radius about that of Neptune's orbit and its density and spectrum was of the nebular type. Some months later Barnard observed a small nebula around the star whose diameter grew at the rate of about two seconds a year, gradually growing dimmer until it had faded away. Nova Persei, 1901, had a somewhat irregular-looking nebular shell, which showed the characteristic radiations of a typical gaseous nebula, hydrogen, helium and forbidden lines of oxygen and neon.

Even more interesting features were exhibited by the shell that developed around Nova (DQ) Herculis, 1934.† In 1940, when photographed by W. Baade in the light of the $N_1 + N_2$ radiation, the nebula appeared as a small elliptical disk of uniform brightness. The nebula was so bright that the central star was hidden both in photographic and photo-visual light. By mid-1942 the surface brightness had fallen off 1.2 magnitudes and in the radiation of the green nebular lines the object appeared as an elliptical ring nebula of dimensions $4'' \times 3''$. The thickness of the shell was about half the outer radius of the nebula. The surface brightness in the blue regions and in the [OIII] lines seemed rather constant over the disk (see Fig. 2). In the light of the $\lambda 6548, \lambda 6584$ [NII] lines, however, the strongest emission was situated in two condensations along the minor axis, whereas two weaker condensations appeared at the end of the major axis. In addition to these concentrations a weaker general emission extended over the image. The [NII] images showed conspicuous changes in shape and intensity the following month. Marked changes in excitation conditions must have occurred in a short time.

* We must emphasize, however (see also Chapter VI), that nova shells are *not* related to the planetaries.

† BAADÉ, W., *Publ. A.S.P.*, **52**, 386 (1940); **54**, 244 (1942).

The similarity in spectra and appearance between old novae and planetary nebulae have led some writers to suggest that the planetaries originate from old novae. It is certain that they cannot have been produced by ordinary novae which eject their shells with speeds of hundreds or even thousands of km./sec. They may be produced by slow nova-like variables such as η Carinae or FU Orionis, but no observational evidence is available to settle this point. We do not know whether these objects belong to Baade's population Type II as do the planetary nebulae.

Certain nova-like, or *combination*, variables as they are sometimes called, also appear to have nebulous envelopes. In this class of objects we may mention BF Cygni, CI Cygni, Z Andromedae, AX Persei, and RW Hydrae. All are characterized by late-type spectra on which are superposed emission lines of hydrogen and helium and permitted high excitation lines of other elements, permitted and forbidden lines of iron in various stages of ionization, and forbidden lines characteristic of the planetaries. In BF Cygni, for example, the principal star, whose spectrum is usually smothered by a high-temperature continuum, is a late-type star for which Merrill has suggested a spectral class gM4. Associated with this is a strongly variable high-temperature source which provides the excitation for the bright lines. Surrounding these objects appears to be an extended envelope in which appear the lines of FeII, [FeII], and [FeIII] and perhaps also the recombination lines of H and He. Finally, there is an outer nebula where the well-known forbidden lines of [OIII] and [NeIII] are produced. Merrill's radial velocity measurements show that these different groups of lines have different mean displacements, indicating that these radiations originate in different strata. Unlike a planetary nebula in which the distribution of the various radiations can be identified quickly by a slitless spectrograph, the spatial distribution of the radiating gases in a system such as BF Cygni has to be inferred indirectly from the data of velocities and excitations. Of particular interest are the changes exhibited by the lines of [OIII] and [NeIII], which are more rapid than in any other star. The speed of the changes shows that the density in the nebular envelope where the [OIII] lines are produced must be as great as 10^6 ions/cm.³. Thus the densities are comparable with those existing in the envelopes of novae in their nebular stage rather than with those characteristic of planetary and diffuse gaseous nebulae. We shall not pursue the subject of nebular shells of novae further in this book other than to point out that much of the theory developed for the planetary nebulae is applicable to these shells also.

Mention must be made of the Crab nebula which has been identified as the remnants of a supernova that appeared in the year A.D. 1054. The bright emission lines originate in delicate filaments; the amorphous background mass radiates a continuous spectrum and appears to be at a

temperature of about $500,000^{\circ}\text{K}$. or even more. Significantly, the Crab nebula is a strong source of radio-frequency radiation as is also Tycho's supernova of 1572. All radio sources have not been identified with ex-supernovae, but some which have been associated with optically recognizable objects have been identified with unusual nebulosities not necessarily relics of supernovae. Some radio sources are normal external galaxies such as M31. Another is interpreted as galaxies in collision (Cygnus A source), while the elliptical nebula M81 in Virgo is an unusually strong radio source.

R Aquarii is an example of a system in which a hot source is associated with a long period M-type variable and a variable nebula. The usual nebular lines are strong in the composite spectrum and the bright lines of iron are also observed.

In the spectra of many stars such as Z Andromedae, CI Cygni, or AG Pegasi, strong forbidden and permitted emission lines of iron in various stages of ionization are present. Presumably these emission-line spectra are characteristic of much higher densities than exist in typical gaseous nebulae. Forbidden lines of iron, nickel, and various other metals in different stages of ionization are observed in many gaseous nebulae, but they are always weak in comparison with the forbidden lines of the lighter non-metals. We shall see (page 194) that these differences arise as a consequence of different densities rather than as a consequence of differences in chemical composition between the nebulae and the stars.

4. Gaseous Galactic Nebulae

The galactic nebulae associated with the Type I population are confined to the spiral arms of our galaxy. They include objects that appear to be purely gaseous as well as objects that contain great quantities of solid particles. When illuminated by nearby stars or by the general galactic radiation field they appear as bright nebulae; when not so illuminated the clouds that contain particles appear as dark lines or filaments hiding the stars behind them. Let us first consider the gaseous nebulae with the aid of a few illustrative examples of various types.

Among the objects with the highest aesthetic rating must be placed the Network or Veil nebula in Cygnus (see Fig. 3). It consists of two well-defined arcs, with some fainter nebulosity between them. Each of these larger patches is resolved into an intricate pattern of fine, thread-like filaments whose delicate structure was well exhibited on Ritchey's beautiful photographs secured forty years ago with the 60-in. reflector at Mt. Wilson. The pattern of the nebulosity suggests that it may be the remnants of an ancient nova (or supernova) explosion. Radial velocity measures do not lend any definite support to this hypothesis, however, as they do not indicate any clear-cut expansion. Spectroscopic observations and filter

photographs indicate that the radiation is almost if not entirely bright-line emission; there appears to be no contribution arising from reflection by particles. Similarly, the so-called California nebula, NGC 1499, appears to be entirely gaseous. Photographs taken in the red or green, where strong nebular lines appear, show the distinctive filaments of the nebula. On the other hand, if one uses a filter-plate combination that isolates a region in the yellow where there are no nebular lines of any consequence, no trace of the nebula appears!

The red radiation of $H\alpha + [NII]$ is usually among the stronger nebular emissions. Hence photographs taken with a red Plexiglas filter and Eastman 103a-E ($H\alpha$ —special) emulsion are particularly useful for picking up moderately faint emission nebulosities. The Palomar 48-in. Schmidt sky survey, which uses this combination of plate and filter, has recorded extended areas of nebulosity where little had been suspected before. In Cygnus, for example, vast areas interlaced with seemingly chaotic, faintly luminous clouds of hydrogen are revealed. These wisps have a distribution of sizes with a maximum frequency in the neighbourhood of 5 to 10 parsecs.* They give the impression of a complete lack of order and symmetry. Probably they derive their excitation from scattered groups of stars rather than from a single star or cluster of stars.

More orderly appearing, possibly only because the exciting radiation emanates from a single group of stars, is the Monoceros nebula described by R. Minkowski.† The open galactic cluster NGC 2244, whose brightest star is S Monocerotis, is surrounded by a diffuse nebula whose brightest parts had been catalogued previously as NGC 2237, 2238, and 2246. The spectrum shows lines of $[OIII]$, $[NeIII]$, and H . The distance of the nebula is 760 parsecs, so its diameter of 80' amounts to 17 parsecs. It appears that the interstellar medium forms a dense cloud in this region and the observed nebula is only the portion thereof which is ionized and caused to shine by the hot stars in the cluster NGC 2244. The surface brightness in $H\alpha$, as measured by G. E. Kron, is 1.3×10^{-3} erg/cm.²/sec. from which a density of 23 ions/cm.³ is derived on the assumption the electron temperature is 10,000°K. This result is in good agreement with the density estimated from the radius of the luminous shell and the magnitudes and temperatures of the illuminating stars in accordance with the Strömgren theory (see Chapter VII). The mass of the bright nebulosity amounts to about ten thousand times that of the sun.

With a specially designed nebular spectrograph, Struve and his co-workers photographed the lines of faint emission nebulosities along the Milky Way.‡ With this technique they were able to locate radiation from

* *Ap. J.*, **113**, 120 (1951).

† *Publ. A.S.P.*, **61**, 151 (1949).

‡ See, for example, *Journ. Wash. Acad. Science*, **31**, 217 (1931).

nebulae with densities of the order of 2 or 3 ions/cm.³, i.e. nebulosities of much lower density than could be photographed by ordinary procedures. Faint nebulae have also been studied with other fast spectrographs and by interference filter techniques (see Chapter II).

5. Diffuse Galactic Nebulae containing both Gas and Solid Particles

The best known of the nebulae that contain sizeable proportions of solid particles as well as gas are the Orion, Trifid, and Messier 8 nebulosities. The whole constellation of Orion is shown to be permeated with bright nebulosity, and there are dark clouds containing particles. The celebrated Horse-head nebula is the most striking example of these obscuring clouds. The Orion nebula is but a small illuminated volume in a vast cloud of stars, gas, and dust. The entire Orion group of stars has been shown to form a single aggregate at a distance from us of about 500 parsecs.*

Fig. 4 shows the Messier 8 nebulosity as photographed with the Curtis Schmidt telescope upon Eastman 103a-E emulsion through a red Plexiglas filter. Notice the dark lines of obscuring matter and small dark *globules* of obscuring matter projected against the bright nebula. Observe also the delicate filaments of luminous matter in the outer portions of the nebula. It is of interest to see if these filaments are emission-spectrum or continuous spectrum features. The question can be settled easily with the aid of an objective prism spectrogram taken with the same plate and filter combination (see Fig. 5). The stars are drawn out into short spectra but the delicate features of the nebula are still there, demonstrating that a good share of the radiation is of emission-line origin. The contrast between the sharp features and the background is less than on the direct exposure, indicating that at least some of the radiation is simply scattered light from the illuminating stars. Similar observations have been made for the Trifid and other nebulae.

From colour excesses of stars embedded in the nebulosity and from star counts, it is evident that there is much obscuring matter in this region. Both of these objects lie in the same spiral arm as the sun, apparently along a great broken filament of interstellar matter that includes also the southern Coal Sack and the great rift in the Milky Way.

Solid grains appear to play an important role in such objects as the Messier 8 nebulosity; the bright lines of *H*, [OII], [OIII], and [NeIII] which characterize the spectra of M8, M16, and M20 are produced by incandescent gas, much of which may have been liberated by the evaporation of grains. The continuous background is partly scattered starlight and partly surface fluorescence caused by the high-frequency radiation of the exciting star.

* SHARPLESS, S., *Ap. J.*, 116, 251 (1952).

6. Diffuse Nebulae in External Galaxies

Diffuse, emission-line nebulosities are characteristic of Type I populations and may be expected wherever these populations are found. Thus, emission nebulosities are found in the outer spiral arms of the Andromeda spiral, where a fringe of Type I objects seems to be appended to a galaxy which is predominantly of Type II. The Large Magellanic Cloud, which seems to be mostly a Type I system, reveals a great number of emission nebulosities of which the largest, brightest, and most intricate is the Loop nebula 30 Doradus, which is many times the size of the Orion nebula (see Fig. 6). In addition to large, irregular, filamentary nebulae, the Large Magellanic Cloud contains numerous, small, round condensations of high surface brightness. The Small Magellanic Cloud also contains gas and a population I, although its stellar population is predominantly Type II. The Australian radio measures show that this gas exists mostly in the neutral state and therefore cannot be observed by optical means.

One of the richest galaxies in terms of emission nebulosities is the Spiral M33. Fig. 7 shows an objective prism spectrogram secured with the Curtis Schmidt telescope and 6° objective prism. The red Plexiglas filter used in conjunction with a 103a-E plate isolates a small spectral region in the neighbourhood of $H\alpha$. The stars are drawn out into short spectra; the nebulae appear as small points or condensations. Some of these nebulae were known many years ago on the basis of direct photographs; many were found by Director G. Haro with the Schmidt telescope at Tonanzintla. The sizes of the nebulosities vary over a large range; from perhaps a couple of parsecs to 50 or 100 parsecs. The surface brightness of those large enough to appear as areas on our plates have been measured by comparison with widened spectra of stars of known magnitude in Selected Area 45 which can be photographed on the same plate (see Chapter II). On the assumption that the nebulae are roughly spherical in form, that the nebular radiation comes primarily from $H\alpha$ (see p. 147), and that the electron temperature is 10,000°K., the average densities given in Table I:1 are found. Similar studies have been made by Shajn and Hase.

Photographs taken with larger telescopes (e.g. the 60-in. reflector at Mt. Wilson and the 200-in. Hale telescope) show that these nebulosities are often quite complex aggregates of filamentary material. Hence the average densities in the filaments are larger than the values given in Table I:1. Further revisions are to be expected when more recent observations have been reduced.

These electron densities, while much smaller than those characteristic of the brighter diffuse nebulae (such as Orion or Messier 8) in our own galaxy, are higher than those found in the extended regions of emission observed by Struve and his co-workers. Regions of ionic densities lower than

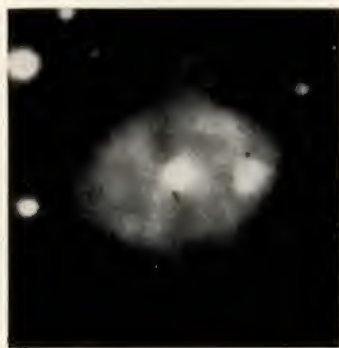


FIG. 1: 1. *The Planetary Nebula.*

$\alpha = 11^{\text{h}}26^{\text{m}}.2$, $\delta = -52^{\circ}39'$.

(Photographed at the Boyden station of the Harvard College Observatory, Bloemfontein, O.F.S., South Africa, March 15, 1948.)



FIG. 1: 2. *The Nebular Shell of DQ Herculis in 1942.*

Left. The star and nebula in blue light.

Centre. The nebula as photographed in the green radiation of [OIII]. The star is relatively faint in these wavelengths.

Right. The nebular shell as photographed with a plate and filter combination that isolates [NII] $\lambda 6548$, $\lambda 6584$; $H\alpha$ is weak.

(Photographs by Walter Baade, Mt. Wilson Observatory, 1942. Reproduced from an article by D. B. McLaughlin, *Sky and Telescope*, 5, No. 7, May (1946).)

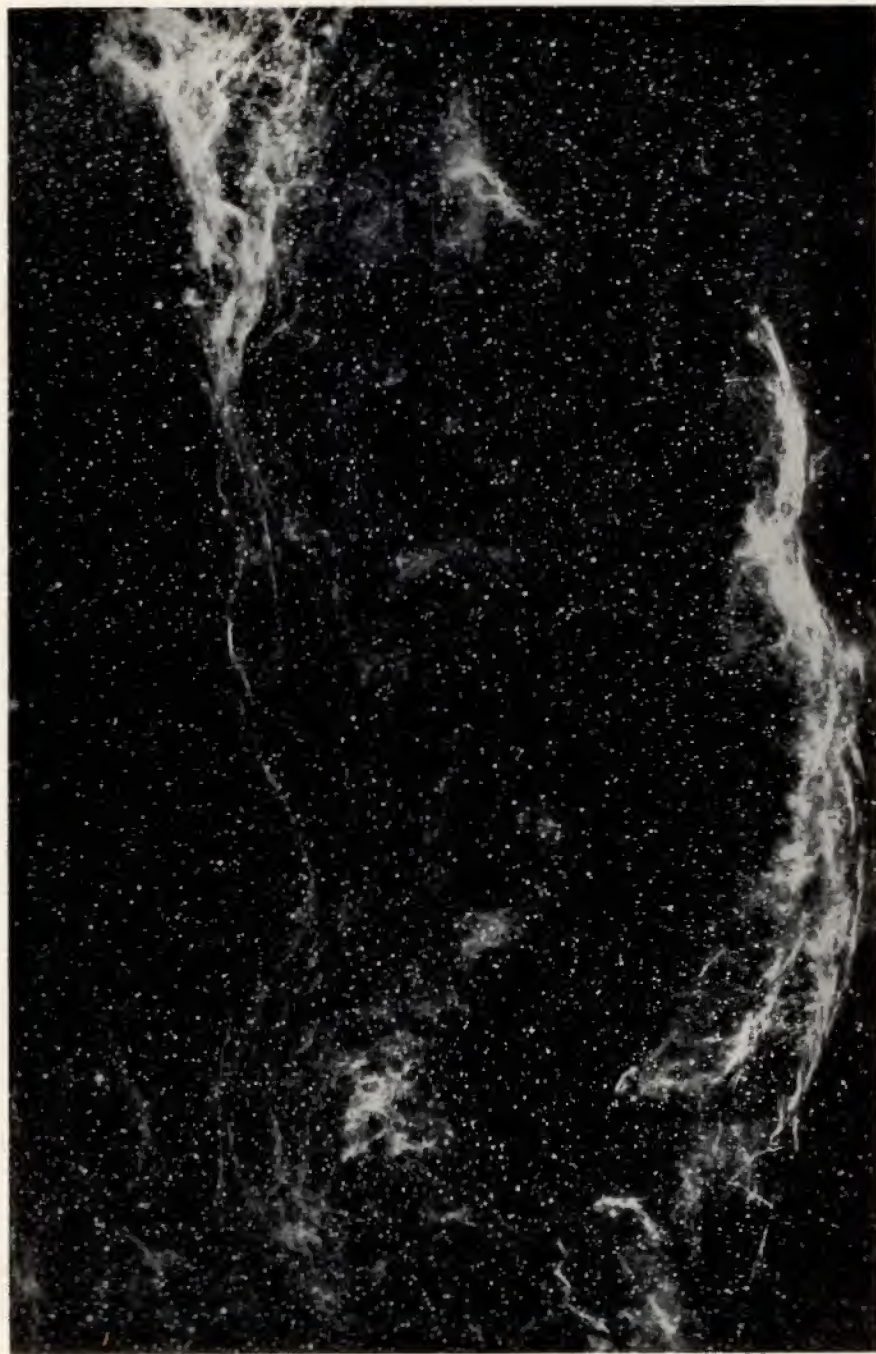


FIG. 1:3. *NGC 6960, a Portion of the Network Nebula.*

This exposure was taken on an Eastman 103a-O emulsion with a Wratten 18A filter. The radiation is primarily due to [OIII].
(Photographed with the Curtis Schmidt telescope at the University of Michigan by J. W. Chamberlain.)



FIG. 1:4. *The Star Cluster (NGC 6530) and Nebula Messier 8 (NGC 6523).*

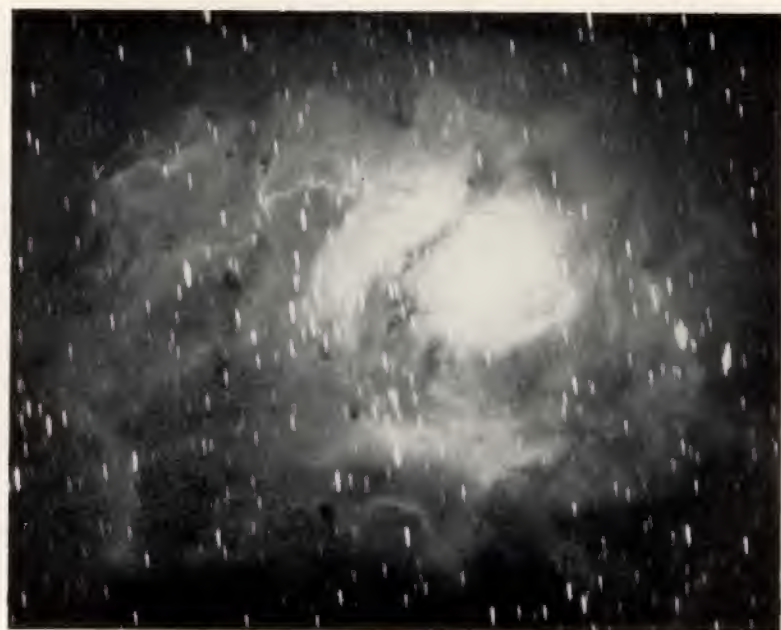


FIG. 1:5. *Messier 8 as observed with an Objective Prism.*

(Figs. 1:4, 1:5 photographed with the Curtis Schmidt telescope by Albert Boggess III.)

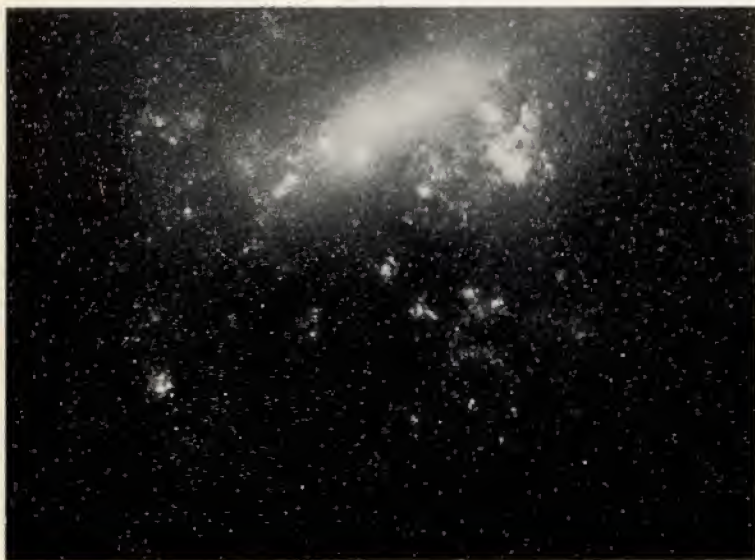


FIG. 1 : 6 (above). *The Large Magellanic Cloud and its Emission Nebulosity.*

(Photographed by Karl G. Henize with a 10-in. camera and objective prism loaned by the Mt. Wilson Observatory at Bloemfontein, O.F.S. The use of a red filter and 103a-E emulsion isolates the $H\alpha$ emission.)

FIG. 1 : 7 (right). *Objective Prism Spectrogram of Messier 33.*

Notice how the stellar spectra are drawn out into short lines while the emission nebulosities are recorded as short patches.

(Photographed with the Curtis Schmidt telescope.)



10/cm.³ probably contribute much to the background radiation in this spiral. Spectrographic observations show that the $\lambda 3727$ [OII] radiation permeates large regions of this spiral.

TABLE I:1
Typical Emission Nebulosities in Messier 33

Nebula	Assumed extent of radiating matter along line of sight (parsecs)	Surface brightness in <i>H</i> α ergs/cm. ² / sec./unit solid angle	Ionic density ions/cm. ³
NGC 604	24	19×10^{-4}	40
NGC 588			
dense portion	16	2.5×10^{-4}	25
faint portion	33	1.0×10^{-4}	10
NGC 595 (A)	33	1.6×10^{-4}	14
(B)	13	2.8×10^{-4}	27
Mayall No. 3	11	2.6×10^{-4}	28
IC 142	16	2.2×10^{-4}	21
IC 131	13	3.6×10^{-4}	30

A catalogue giving the positions and descriptions of the emission nebulae in the Magellanic Clouds has been prepared by Karl Henize. Measures of their surface brightnesses (or a quantity proportional to the integrated luminosity) and estimates of their densities have been made by Karl Henize, Lowell Doherty, and the writer. A similar catalogue of the emission nebulosities in Messier 33 is being prepared by the writer. Guillermo Haro has made a special search for emission nebulosities in external galaxies with the Tonanzintla Schmidt.

7. Gaseous Nebulae and the Interstellar Medium

The planetary nebulae and the shells associated with novae appear to be examples of pure gaseous nebulae, and although complications are introduced by the geometry of the distribution of the radiating gases, many problems posed by these objects are amenable to theoretical attack.

The gaseous nebulae associated with the Type I population pose problems of a much more complex sort. The range in density is enormous: from 1 or 2 ions/cm.³ for certain of the faint emission regions observed by Struve and by Strömgren and Hiltner to 10^3 – 10^4 ions/cm.³ in the Orion nebula. Furthermore, the diffuse galactic nebulae often contain solid particles as well as gas. These grains have a profound effect on the physical processes occurring in such nebulae and theoretical procedures

worked out for purely gaseous nebulae are not always available. The interstellar medium, grains and gas, is far from homogeneous in density and temperature. The fluctuations in density are so great that the use of an average density or coefficient of absorption is quite meaningless. Finally, the grains and gas tend to collect together in aggregates, so that when the space density of the grains is high, that of the gas will be high also.

In this book we are primarily concerned with gaseous nebulae, and therefore we shall emphasize objects such as planetary nebulae rather than diffuse objects that contain great quantities of solid material, although the latter will come in for some discussion.

REFERENCES

1 Catalogues and Lists of Gaseous Nebulae

(a) General

DREYER, J. L. E., "New General Catalogue of Nebulae and Clusters", and "Index Catalogues." *Memoirs R.A.S.*, **49** (1888); **51** (1895); **59** (1908). The epoch is 1860.

(b) Diffuse galactic nebulae

CEDERBLAD, SVEN, *Lund Medd.*, **2**, 119 (1946).

STROHMEIER, W., *Zeits. F. Ap.*, **27**, 49 (1950).

SHARPLESS, S., and OSTERBROCK, D., *Ap. J.*, **115**, 89 (1952).

(c) Planetary Nebulae

Publ. Lick Obs., **13** (1918).

VORONTSOV-VELYAMINOV, B., "General Catalogue of Planetary Nebulae", *Astronomical Journal of the Soviet Union*, **11**, 40 (1934).

MINKOWSKI, R., *Publ. A.S.P.*, **58**, 305 (1946); **59**, 257 (1947).

EVANS, DAVID S., and THACKERAY, A. D., *M.N.R.A.S.*, **110**, 429 (1950) (southern planetary nebulae).

2 Texts and General References

SPITZER, L., *The Interstellar Medium* (Chapman and Hall, London (*in press*)).

WURM, K., *Die Planetarische Nebeln* (Akademischer Verlag, Berlin 1951).

HYNEK, J. A., *Astrophysics—A Topical Symposium*, Chapter 13, by J. L. Greenstein (McGraw-Hill, New York 1951).

ALLER, L. H., *Astrophysics* (Nuclear Transformations, Stellar Interiors, and Nebulae) (Ronald Press Co., New York 1953), Chapters 4, 5, and 6.

GOLDBERG, LEO, and ALLER, L. H., *Atoms, Stars, and Nebulae* (Harvard University Press, Cambridge 1955).

VORONTSOV-VELYAMINOV, B., *Gasnebel u. Neue Sterne Verlag Kultur u. Fortschritt* (Berlin, 1953).

MINKOWSKI, R., and WILSON, O. C., *Planetary Nebulae* (North Holland Publishing Co., Amsterdam (*in press*)).

DUFAY, J., *Nebuleuses Galactiques et Matiere Interstellaire* (Albin Michel, Paris, 1954).

CHAPTER II

Methods of Observation

THE EARLIEST direct and spectroscopic observations of diffuse and gaseous nebulae had to be made visually. These observers must be given considerable credit for the detection of numerous faint and difficult objects. Many of these nebulae are elusive and not easy to see, even when one knows exactly where to look.

The drawings and descriptions were necessarily inadequate. Most of the details are at the limit of visibility and are extremely elusive. Many of the characteristic features of the planetary and diffuse nebulae were recognized by the visual observers. The filamentary character of the ring of NGC 6720 was recognized by visual observations made at the Lick Observatory in 1888.⁽¹⁾ The delicate *striae* or bands that cross the interior of the ring were noticed by Lord Rosse in 1844⁽²⁾ and confirmed by photographs secured by Keeler with the Crossley reflector fifty-five years later.

The celebrated Orion nebula has been studied in greater detail than any other galactic nebula. Huyghens made the first drawing in 1656. Since then many observers have published drawings and descriptions of this object.

One of the best drawings was that due to G. P. Bond of the Harvard College Observatory.⁽³⁾ We reproduce it to compare a sample of the best visual work with the best photographic work (see Fig. 2). E. S. Holden⁽⁴⁾ examined and critically compared the numerous early visual observations and drawings of this object. At the end of his monograph he published a single photograph obtained by Henry Draper with an 11-in. telescope. Even this early photograph gives a much more accurate idea of the nebula than does the best drawings.

Before the end of the nineteenth century, the photographic method had superseded the visual method for the study of the forms and shapes of the nebulae, although visual spectroscopic work was still carried on. The beginning of the modern era in nebular photography came with the work of James E. Keeler with the Crossley reflector at the Lick Observatory.⁽⁵⁾ His photographs included the Orion nebula, M8, M17, and M20 among the diffuse gaseous nebulae and NGC 3242, the Owl nebula M97, NGC 6543, the Ring nebula NGC 6720, NGC 7009, and NGC 7662.

1. Direct Photography—filters

The available type of telescope or camera determines the kind of object we can study. With a large reflector which is characterized by sizeable light-gathering power but with a small coma-free field, one may work to advantage on such things as planetary nebulae which have small angular diameters. On the other hand, a Schmidt camera permits us to work on much more extended nebulosities of lower surface brightness while a fast, wide-angle camera such as the Henyey-Greenstein camera or the Baker super-Schmidt permits the observer to study extended, very faint nebulae.

TABLE II : 1

Wavelength Region	Filter	Eastman Emulsion	Remarks
3727	Schott UG2 1 mm. thick	Ila-O, 103a-O	(1)
$N_1 + N_2$	glass GG7, Schott GG11	Ila-O	(2)
$\lambda 5200 - \lambda 5500$	W Fluorzine, T filter (gelatine)	103-G	(3)
$H\alpha$	RG2 or RG5	103a-E	(4)
$\lambda 6150$	Wratten 29F	C	(5)

- (1) This combination cuts out all wavelengths longward of $\lambda 3850$ A. and permits very long exposures.
- (2) Avoid process plates which are insensitive to the green nebular lines.
- (3) Corresponds to photo-visual region.
- (4) RG5 is better for a narrow wavelength range.
- (5) This combination is used to compare $H\alpha$ to the continuum from $\lambda 6150$ to the end of sensitivity of the "C" plate.

If the nebula has strong monochromatic radiations, considerable progress can also be made by the choice of appropriate filters and photographic emulsions. For example, one may choose one plate and filter combination such as the Eastman 103a-F emulsion plus a Corning 2403 filter to isolate a spectral region 300 A. wide centred on $H\alpha$ and another combination of a yellow filter with an orthochromatic plate to cover a region in the visual where no strong emission lines appear; one thus obtains photographs of the nebula in both its continuous and its line radiation. For purposes of illustration Table II : 1 lists some plate-filter combinations employed by Baade in order to isolate gaseous nebulae from other objects in external galaxies and to study particular features of selected gaseous nebulae. Minkowski used somewhat similar filter-plate combinations to great advantage in the photography of planetary nebulae. These objects can also be studied with the slitless spectrograph (see Section 3) with the aid of which it is possible to compare different monochromatic images. By filter photography alone, however, it is possible to photograph the nebula in the radiation of the visual or ultra-violet continuum and compare these results with those found for the Balmer and forbidden lines.



FIG. II:1. *Bond's Drawing of the Orion Nebula.*
(Reproduced from Vol. 5 of the *Annals of the Harvard College Observatory*, 1867.)



FIG. II : 2. *The Orion Nebula.*

(Photographed by N. U. Mayall with the Crossley reflector at the Lick Observatory.)

Filter techniques are advantageous for the photography of extended faint nebulae because the emissions of the nebula can be transmitted by the filter, whereas much of the background or night-sky illumination is cut out.

Among the most important types of filters are the recently developed *interference filters*⁽⁶⁾ which isolate a narrow wavelength region of the spectrum. Their action is based on the principle of the Fabry-Perot interferometer (Section 2) and they are best used in parallel light. A glass plate is coated with a thin film of silver and on top of this is evaporated a layer of magnesium fluoride. Then a second layer of silver is added and a glass

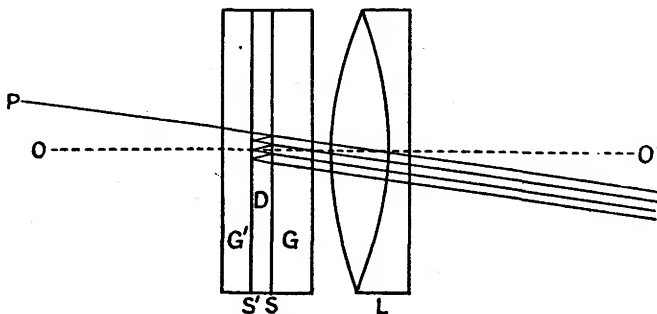


FIG. II:3. *The Interference Filter.*

A single ray from a point P in a nebula is depicted as passing through an interference filter which consists of a glass plate G upon which are deposited a silver coat, S , a dielectric layer D , and a second silver coat, S' . A cover glass G' is cemented on to protect the filter. We represent the filter as being used over the objective lens of a small patrol camera. Three orders of reflection are shown.

plate is put on to protect the optical surfaces. By making the dielectric layer between the silver surfaces very thin the interference fringes will be separated by many Ångströms. The exact position of a transmission peak will depend on the precise thickness of this dielectric layer. Since the evaporation process cannot be controlled with requisite accuracy, filters cannot be made with a maximum accurately centred at a given wavelength. If the peak of the filter transmission occurs a little on the long wavelength side of the desired point in the spectrum, the filter may be tilted slightly to shift the peak to a shorter wavelength. Care must be exercised, however, for if the filter is tilted by more than about 5° , undesirable polarization effects will enter.

Although when properly protected these filters are stable and permanent, they suffer from a number of disadvantages. Since they should be used in parallel light and cannot be made in sizes larger than about 8×8 in., they must be employed over the objectives of small telescopes (as

has been done by Fehrenbach and Strömgren at the Observatory at St. Michel in Haute Provence and is being done by Morgan and Strömgren at McDonald Observatory), or else between the elements of a coma corrector in a reflector, or in a specially designed optical device to make the rays parallel before they are focused on the photographic plate. The silver coat cannot be too thick or the peaks will be too narrow.

The great advantage of the interference filters is that they isolate such a narrow wavelength range of the spectrum. Two or more maxima may fall in the range of sensitivity of a given emulsion, but they are so far apart in wavelength that the undesirable one may be cut out easily with an ordinary filter. With an $f/1$ Schmidt camera and an 8×8 in. interference filter Morgan and Strömgren are able to reach nebulosities ten or fifteen times fainter than those that are photographed with the Palomar Schmidt. They employ a comparison filter centred at 6450 Å., to separate the nebulosity from the background.

2. Applications of the Fabry-Perot Etalon to Studies of the Nebulae

Interference filters represent a very special application of the *Fabry-Perot interferometer*.⁽⁷⁾ In its conventional form, this device has been used to yield much information of interest about the gaseous nebulae.

As most frequently employed, the Fabry-Perot etalon consists of two partially silvered quartz plates, mounted with their surfaces accurately parallel to one another, the partially silvered surfaces being face to face. Invar or quartz separators hold the plates apart. If parallel rays from an extended surface which emits monochromatic radiation are passed through this device and the emergent beam focused with a lens, an image of the original surface crossed by circular interference fringes will be produced.

Let φ denote the angle between the direction of a given ray and a normal drawn to the surfaces of the etalons. If d is the plate separation the condition for a maximum (completely constructive interference) is

$$2d \cos \varphi = n\lambda. \quad . \quad . \quad . \quad (1)$$

$$\text{If} \quad \delta = \frac{4\pi}{\lambda} d \cos \varphi, \quad . \quad . \quad . \quad (2)$$

the intensity in the fringes as observed with transmitted light will be given

$$\text{by} \quad I_T = \frac{I_0}{1 + \frac{4R \sin^2 \delta/2}{(1-R)^2}}, \quad . \quad . \quad . \quad (3)$$

where I_0 is the maximum intensity in the fringes and R is the reflectivity of the silvered surfaces. We assume that the two surfaces are equally

silvered. These fringes are often called *Haidinger fringes* and are sharper the heavier the coating of silver on the plates, i.e. the greater the value of R . This is evident from inspection of equation (3).

Charles Fabry and H. Buisson made the first application of the Fabry-Perot etalon to the study of the nebulae. They used the Marseilles reflector.⁽⁸⁾ The first work was visual; later investigations in collaboration with Bourget employed photographic techniques.⁽⁹⁾

The light of the nebula is focused in the usual way by the primary mirror. Then the beam is rendered parallel by an eyepiece, passes through the etalon, and through a short-focus lens to form an image of the nebula upon which are superposed rings corresponding to the monochromatic radiations of the nebula. They placed a cross-wire at the first focus to serve as a reference mark and photographed the fringes produced by a mercury vapour lamp before and after each nebular exposure in order to have suitable reference standards. In an attempt to isolate the various monochromatic radiations from one another they used the then available filters, a technique which was not entirely satisfactory.

Thus each observation consisted of three photographs—a calibration exposure on the mercury arc, the nebular exposure, and a final calibration exposure. Since the wavelengths of the mercury lines employed in the calibration are known, the wavelengths of the nebular radiations as modified by the Doppler shift can be found by well-known techniques in physical optics.

In practice, the rings are deformed as a consequence of the internal motions in the nebula. From measures of the radius of the warped ring at different points, together with measurements of the calibration rings, Fabry, Buisson and Bourget deduced the radial velocities at different points in the nebula.

They employed etalons with different spacers. For example, one etalon was constructed in such a way that the two components of the $\lambda 3727$ [OII] pair coincided to give sharp fringes so that this radiation could be used to measure the internal motion in the nebula. With another pair of etalons they made accurate measurements of the wavelengths of the two components, $\lambda 3726.10$ and $\lambda 3728.84$.

As a consequence of thermal motions and turbulence (large-scale disorganized motions) in the nebula, each spectral line has a finite width. Thus, if a sufficiently high order of interference is used, the rings will finally merge and cease to be visible. If n is the order of interference where the rings cease to be visible, and if the entire broadening can be attributed to thermal effects alone, the kinetic temperature, T , is given by

$$n = 1.22 \times 10^6 \sqrt{\frac{A}{T}}, \quad . \quad . \quad . \quad (4)$$

where A is the atomic weight of the atom responsible for the line. From measurements of the $H\gamma$ line it was found that $n=10,000$, which leads to a temperature of about $15,000^\circ\text{K}$. This is an upper limit to the kinetic temperature, as the influence of turbulence is neglected.

One of the principal difficulties encountered in the work of Fabry, Buisson, and Bourget was that filters could not adequately separate emission lines that fell close together. In a later investigation Baade, Goos, Koch, and Minkowski⁽¹⁰⁾ overcame these troubles by using a spectrograph to isolate neighbouring lines such as $H\beta$, N_2 , and N_1 . They placed a quartz Fabry-Perot etalon between the collimator lens and the prism of the spectrograph. With a wide slit each spectrum line is registered as a broad band crossed by fringes running parallel to the dispersion. The plates were photometrically calibrated so that tracings made across each line (\perp to the fringes) could be reduced to a true intensity scale. They measured the instrumental profiles, i.e. the shapes the fringes would have if a truly monochromatic source could be examined. The observed profiles were very much wider than the theoretical profiles.

The profile of a line that is broadened only by the thermal Doppler effect is given by

$$I = I_c e^{-(\Delta\nu/\Delta\nu_0)^2}, \quad . \quad . \quad . \quad . \quad (5)$$

where I_c is the central intensity and

$$\Delta\nu_0 = \frac{v}{c} v_p = \frac{\sqrt{\pi} v \bar{v}}{2c}, \quad . \quad . \quad . \quad . \quad (6)$$

where

$$v_p = \sqrt{\frac{2kT}{M}} \quad . \quad . \quad . \quad . \quad (7)$$

is the most probable velocity and \bar{v} is the average velocity. T is the kinetic temperature. Baade and his co-workers measured the widths of the lines at intensities 0.5 and 0.7 of the maximum intensity. If the lines are broadened by the Doppler effect, the width at intensity $i = I/I_c$ will be

$$(\Delta\nu)_i = 2 \Delta\nu_0 \sqrt{\ln \frac{I_c}{I}}. \quad . \quad . \quad . \quad . \quad (8)$$

The observations gave $\Delta_{0.5}/\Delta_{0.7} = 1.45$, which was in good agreement with the predicted value of 1.39. Thus the profiles represented a Maxwellian distribution of velocities reasonably well. A comparison of the widths of $H\beta$ and the green nebular lines showed that the latter were much too broad to be accounted for by thermal Doppler motion. In addition there must exist some large-scale motion or *turbulence*. On the assumption that these macroscopic motions are disorganized and follow a Maxwellian distribution with a mean velocity, v_m , which is constant along any given line of sight

(but dependent on the place in the nebula), and that the kinetic temperature is constant along the line of sight, one may replace \bar{v} in equation (6) by

$$V = \sqrt{\bar{v}_m^2 + \bar{v}^2}. \quad (9)$$

Then, for the hydrogen and oxygen atoms, one can write

$$V_H = \sqrt{\bar{v}_m^2 + \bar{v}_H^2} \quad V_0 = \sqrt{\bar{v}_m^2 + \bar{v}_0^2}, \quad (10)$$

where V_H and V_0 are the observed mean velocities obtained from the line profile $(\Delta\nu)_l$ with the aid of equation (6). The values of the turbulent velocities V_m obtained in this way were of the order of 10–12 km./sec. This is larger than the value of about 2 km./sec. obtained from the separation of the fringes, but if the velocities were truly Maxwellian there would be a net average fringe displacement of zero! The kinetic temperature turned out to be in the neighbourhood of 15,000° K. or 20,000° K.

We return to this topic in Chapter VIII, where we shall discuss the large-scale motions in the Orion nebula from the point of view of the turbulence theory. The Fabry-Perot etalon has been applied to other diffuse nebulae but not to the planetaries. On the one hand, the size of the smaller nebulae renders the etalon impracticable, as an insufficient number of fringes can be observed. On the other, the loss of light entailed in the use of etalons of high resolution (and therefore heavy silvering) is considerable.

Recently, Georges Courtes of the Marseilles Observatory has devised an improved Fabry-Perot interferometer that employs multiple layers of zinc sulphide and cryolite for the inner reflecting surfaces. With interferometer plates with five coatings, the light loss produced by absorption in the films is small. The interference fringes are narrow and sharp and he has been able to measure the velocity at different points in the Orion nebula with an accuracy of about 1 km./sec. Courtes has also studied the nebulosity near Gamma Cygni and the “elephant trunk” structure of M16. He finds that internal motions in areas as small as 10×10 in. may vary by 30 or 40 km./sec.

3. Spectrographic Techniques for the Study of small Gaseous Nebulae

The earliest spectroscopic work on the gaseous nebulae was done visually. Huggins⁽¹¹⁾ detected the green nebular lines of [OIII] and $H\beta$ in NGC 6543 in 1864. The concentration of the nebular radiations into a few emission lines made it possible to observe their spectra visually, whereas those of the so-called “white” nebulae (external galaxies) that emitted continuous spectra were too faint to be seen.

The enumeration of the stronger emission lines proceeded during the following years. Lockyer⁽¹²⁾ and Campbell⁽¹³⁾ measured a large number of lines with low dispersion. The visual method permits the measurement

of only the stronger lines over a limited wavelength range in the brighter nebulae. It is of interest, however, that Campbell was able to see faint emission lines in the green region of the spectrum of NGC 7027 that were not photographed until many years later.

Spectroscopic observations are now carried out photographically, although a few attempts have been made to make direct photo-electric tracings at the telescope. The advantages of photography—greater spectral range and detection of much weaker lines with the aid of fast cameras and long exposures—have led to a considerable increase in our knowledge of the nebulae.

Exclusive of the “stellar” planetaries whose angular dimensions are smaller than the seeing disk, the nebulae present finite areas, often of low surface brightness. The objects may have diameters of only a few seconds of arc or lengths of even degrees along the Milky Way. If we wish to study extended diffuse nebulae our spectrographic equipment will obviously differ from that required for a study of planetaries.

All nebular spectrographs (excluding a few stellar spectrographs occasionally used for work on bright nebulae) have one feature in common—a high photographic speed. Nearly all nebulae have low surface brightnesses, and a high camera speed is essential to secure exposures of usable densities in practical exposure times. Let us first consider nebular spectrographs designed for objects of small angular diameter, e.g. external galaxies, globular clusters, or planetaries.

The size of the image of a nebula on the slit of a spectrograph depends only on the focal length of the telescope, while its brightness depends also on the aperture of the objective. Thus the brightness on the slit will be controlled by the speed of the objective. The speed of the spectrograph, however, depends on the focal ratio of the camera and is independent of the speed of the telescope. In principle, a spectrograph with identical prisms and camera but, of course, different collimators would have the same speed on a 36-in. refractor of 57-ft. focal length as on a 36-in. reflector with a 15-ft. focal length. The efficiency of a spectrograph depends on the fraction of light that passes through the slit. With short cameras it is possible to gain speed by widening the slit, but this procedure should not be pushed far beyond the point where the impurity in the spectrum equals the resolution of the plate. The use of highly transparent optical materials and of non-reflection coatings of optical surfaces are all necessary to attain the highest speeds in any instrument, but these cannot compensate or offset the disadvantages of poor design. Various techniques have been employed to improve the efficiencies of nebular spectrographs. Bowen's *image slicer* is perhaps the most ingenious accessory that has been employed in conjunction with existing spectrographs.⁽¹⁴⁾ With the largest telescopes,

coudé spectrographs, in spite of the large number of reflections in the optical system, have proven useful. Bowen has demonstrated that by using a long collimator, large optical parts, and fast Schmidt cameras in the coudé spectrograph, speeds and dispersions satisfactory for most work on small gaseous nebulae can be attained.⁽¹⁵⁾ In the coudé spectrograph of the 200-in. Hale telescope a composite grating made of four separate gratings each of which has a ruled surface of $5\frac{1}{2} \times 7$ in. serves as the dispersing element. By this method a beam diameter of 12 in. can be attained. Schmidt cameras of speeds $f12$, $f6$, $f3$, $f1.5$, and $f0.7$ are provided, the fastest of these having a dispersion of 39 Å./mm. in the third order violet, or 59 Å./mm. in the second order red. An ingenious feature of the design

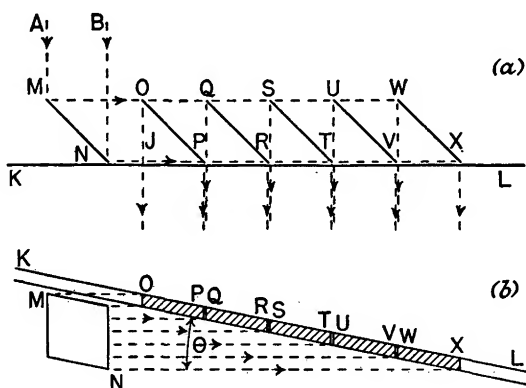


FIG. II : 4. *The Image Slicer.*

(After I. S. Bowen, courtesy *Astrophysical Journal*, 88, 115, 1938.)

of this particular spectrograph is the placing of the corrector plate almost in contact with the grating. Thus the beam traverses the plate twice, once before and once after dispersion by the grating. By this unconventional use of the Schmidt corrector plate, light loss by vignetting could be greatly reduced. With the shortest camera it is possible to use a very wide slit. Most of the light of a small nebula would go through such a slit.

In observations on small gaseous nebulae with telescopes of moderate aperture much of the light is lost on the slit jaws, and if the spectrum is widened by drifting, the exposure times become too great. Bowen and Wyse showed that much could be gained by the use of the former's image slicer. This device simply changes the shape of the image without modifying its area. An elliptical or circular image is divided up into long narrow strips and added end to end along the slit. The principle of this instrument may be understood with the aid of Fig. 4, in which two views of the system of plane mirrors necessary to accomplish this division of the image are shown. The beam of light from the objective limited by the rays AM

and *BN* strikes the mirror *MN*, which is tilted at an angle of 45° . This mirror (see Fig. 4*b*) is mounted near the end of the slit jaw. The beam is thus reflected along a path parallel to the plane of the slit jaws (see Fig. 4*a*). It then strikes a series of small mirrors *OP*, *QR*, *ST*, *UV*, and *WX* which are parallel to the mirror *MN*. Each tiny mirror intercepts a narrow strip of the beam equal in width to that of the slit, and reflects it through an angle of 45° . It continues on through the slit parallel to the original beam. Thus the original image is sliced into a number of strips which are placed end to end.

Since the mirrors placed over the slit have the same width as the slit (0.02–0.5 mm.) and a length of not more than 2 mm., individual tiny mirrors would be impractical. Instead, a stack of glass plates, whose individual thicknesses are equal to the perpendicular distances between the mirrors, is employed. The appropriate surfaces are aluminized to provide reflecting surfaces.

In the form employed by Bowen and Wyse in their work on planetary nebulae, the slicer was designed to take an image 1.2×1.8 mm. and included six aluminium-on-glass mirrors which divided the image into slices 1.2×0.3 mm. (or 14×4 in. at the focus of the 36-in. Lick refractor). Thus several spectral strips are photographed side by side and weak lines which might be missed on a single narrow strip may be detected if they appear on two or more strips.

For the study of very weak lines in bright gaseous nebulae it is necessary to use a fast camera with as high a dispersion as possible. Otherwise the weak lines may be lost in the strong nebular continuum. The usual nebular spectrographs that are intended primarily for work on external galaxies are designed to give high speed and low dispersion so as to record weak continuous spectra. Such instruments are valuable for studies of the strongest lines in very faint emission nebulae or the nebular continua, but are unable to reveal weak lines in nebulae of high surface brightness. With the Palomar coudé, Bowen was able to photograph lines of the higher series of *HeII* in NGC 7027 which had not previously been observed because of the strong nebular continuum.

Let us describe briefly some of the low dispersion high-speed nebular spectrographs. Much work can be done with fast cameras in conventional prism spectrographs ordinarily employed in stellar spectroscopy. Work on faint nebulae, however, usually requires modifications in the guiding system, since the object under scrutiny is often too faint to be easily seen on the slit. Offset guiding may be necessary and a guide star must be employed. One of the most successful of nebular spectrographs was that designed by N. U. Mayall for the Crossley reflector at the Lick Observatory.⁽¹⁶⁾ This prime-focus two-prism spectrograph contains ultra-violet

$\lambda 3727$ [OII]
 $\lambda 3868$ [NeIII]
 $\lambda 3969$ [NeIII] + H ϵ
 H δ
 H γ
 $\lambda 4686$ HeII
 $\lambda 4861$ H β
 $\lambda 4959, 5007$ [OIII]



BALMER CONTINUUM

BALMER
LIMIT

H β

H γ

H δ

H ϵ

H ζ

FIG. 11:5. Slitless Spectrograms of the Ring Nebula and Comparison Star.

The Ring Nebula NGC 6720 exhibits very strikingly the differing sizes of the various monochromatic images; compare especially $\lambda 4686$ HeII and $\lambda 3727$ [OII]. A few extremely faint images of permitted OIII lines are superposed on the weak continuum extending shortward of $\lambda 3727$. The images of a number of field stars are superposed on the nebula. The spectrum of the central star is faintly visible.

The comparison star, γ Lyrae (spectral class AO), shows the strong Balmer lines and continuum setting in near $\lambda 3650$.

(Photographed with the quartz slitless spectrograph attached to the Crossley reflector at the Lick Observatory.)

glass optics. The beam width is 1.8 in., while the camera has a speed of $f/1.3$. More recent nebular spectrographs employ gratings as dispersive elements rather than prisms. The "B spectrograph" of the McDonald Observatory employs an $f/4$ parabolic collimator mirror of 2 in. aperture and 7.65 in. focal length together with a plane aluminium-on-glass grating of 15,000 lines/in. ruled by H. D. Babcock.⁽¹⁷⁾ The camera consists of a solid $f/0.65$ UV glass Schmidt camera made by D. O. Hendrix. The film has to be pressed in contact with the oiled concave focal surface during the exposure. The dispersion is 350 Å./mm. For faint (chiefly extragalactic) objects the Palomar observers use a grating spectrograph with a 3-in. beam and cameras of focal ratios $f/0.47$ and $f/0.95$. Dispersions ranging from 105 Å./mm. to 430 Å./mm. are obtained with the different combinations of cameras and gratings.

Exposures with a nebular spectrograph can be continued until the spectrum of the night sky becomes strong. In so far as the night sky lines of atomic origin are concerned, little interference with the nebular spectrum is encountered, but the band systems in the auroral spectrum may constitute a real nuisance. In the nebulae of low surface brightness it is possible to observe only the very strongest lines. All others are lost in the faint background of night-sky radiation, zodiacal light, or the light of faint stars.

An extremely useful instrument for the study of small gaseous nebulae, particularly planetaries, is the slitless spectrograph. In the form used at the Lick Observatory a concave quartz lens is placed just inside the focus of the primary mirror so as to render the light rays parallel. The beam then passes through two quartz prisms and is focused by a convex quartz lens of the same focal length as the concave one. If a planetary nebula is photographed with such an instrument and the exposure carefully guided, the spectrum of the central star will be recorded as a long narrow streak whereas the nebular spectrum will consist of a series of monochromatic images of the nebula (see Fig. 5).

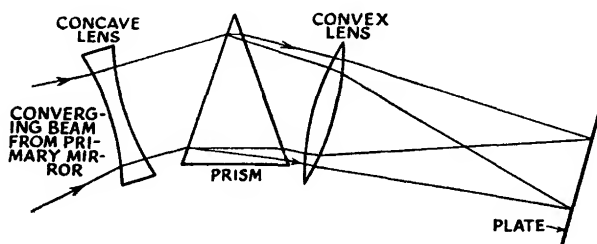


FIG. II : 6. *Principle of the Slitless Spectrograph.*

A concave quartz lens renders parallel the rays of light from the primary mirror. The beam then passes through the dispersing element (here depicted as a single quartz prism) and then through the convex quartz lens that focuses the rays on a photographic plate.

(Courtesy *Sky and Telescope*, 1, No. 10, p. 11, 1942.)

O. C. Wilson used the coudé spectrograph of the 100-in. reflector. He replaced the slit by a hinged mirror. In order to guide, he centres the nebular image with respect to the reticle in the guiding eyepiece, then raises the mirror to permit the light to enter the spectrograph. After a time the mirror is lowered, the image recentred, and the mirror is raised again. Guiding is thus intermittent and rather difficult with faint objects, but Wilson has obtained some excellent results by this method. Since the image at the coudé focus slowly rotates, it is necessary to compensate by means of an optical device referred to as an *image rotator*. The equivalent focal length of the 100-in. coudé is 250 ft., so that the scale at the focus is 2.7"/mm. With a collimator of 290-cm. focus and a camera of 81-cm. focus, the scale of the image on the plate is 9.64"/mm.

4. Spectrographs for the Study of Extended Nebulae

With small nebulae the scale of the final image is extremely important, and the use of the largest available instrumental equipment is indicated. For the study of very extended gaseous nebulae of low surface brightness the use of a large telescope, or even any kind of a telescope, is often unnecessary. A small scale is no longer a disadvantage, and everything depends on the speed of the camera and the transparency of the optics.

Struve and his associates⁽¹⁸⁾ studied the faint emission regions of the Milky Way with specially designed nebular spectrographs which employed telescopes for guiding purposes only. The original spectrograph consisted of two defining slits, two prisms, and a fast Schmidt camera fastened to the tube of the Yerkes refractor. No collimator lens is needed because the first slit is placed so far from the prisms (17.70 m.) that the beam is almost parallel upon reaching the latter. The distortion produced by the lack of collimator was smaller than the resolution of the photographic emulsion. Since the angle subtended by the slit on the sky is 16', the instrument has an advantage on any nebula whose angular size is more than half that of the moon. By the same token a star which happened to fall in the slit would have a width of 16'.

Observations with the original instrument inspired the construction of a yet larger spectrograph which was installed at the McDonald Observatory.⁽¹⁹⁾ The schematic arrangement of the optical parts is depicted in Fig. 7. The guide telescope, primary mirror, prisms, and camera are carried on an assembly mounted at the end of a polar axis. The light from the region to be observed is picked up by the rectangular mirror M_2 , which serves as the defining slit. Its width can be controlled by appropriate diaphragms. The light is then reflected a distance of 75 ft. to the fixed plane mirror M_1 of 2 ft. diameter, which points to the south celestial pole. M_1 reflects the light into two quartz prisms and an $f1$ Schmidt camera of

94-mm. aperture. Each star image is now only $6'$ long so that a considerable improvement in resolution results. Any part of the sky may be observed by rotating the polar axis and tilting the mirror M_2 north or south. Extensive studies of faint emission regions throughout the Milky Way were carried out with this spectrograph. The spectra of narrow strips of the sky are obtained. By the interference filter techniques, photographs of larger areas in one of the characteristic radiations, e.g. $H\alpha + [\text{NII}]$, may be obtained, but no information on the rest of the spectrum is found in this way.

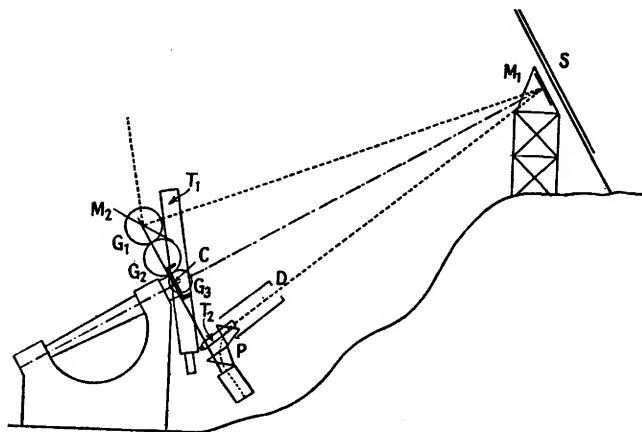


FIG. II : 7. *The McDonald Nebular Spectrograph.*
(Courtesy *Astrophysical Journal*, 87, 559, 1937.)

5. Quantitative Measures of Surface Brightnesses of Nebulae

The complete description of the radiation of a gaseous nebula would entail the determination of the total amount of energy in each of its characteristic emissions and the distribution of the emission over the surface of the nebula. Such detailed information is not available for any nebula, although for some objects, such as NGC 7662, fairly extensive measurements have been made.

Photometric measurements of gaseous nebulae cannot be made as easily as measurements on stars. In the first place, the nebulae are surfaces—the stars are effectively small “seeing disks”. It is true that one can compare stars and nebulae by photographing the latter in focus and the former out of focus, provided the telescope gives good out-of-focus images. Reflectors give more satisfactory results than do refractors or Schmidt cameras. Holmberg applied this procedure in his determination of the magnitudes of extra-galactic nebulae.⁽²⁰⁾ The comparison of stars and small nebulae can be carried out more easily by photo-electric photometry than by photographic methods (see Section 7). A more fundamental difficulty is imposed by the different character of nebular and stellar radiation.

A star radiates a continuous spectrum from which only a small amount of energy is subtracted by absorption lines. A nebula emits a bright-line spectrum with a relatively weak background continuum. Thus, if we were to measure the magnitudes of small planetary nebulae upon patrol camera plates so the images would be stellar in appearance and could be compared directly with stars, we would come out with a set of numbers whose exact values would depend not only on the brightness of the nebula but also on the plate sensitivity and instrument transparency.

In many planetary nebulae, most of the light is contributed by the green nebular lines which fall in a spectral region where the sensitivity of the emulsions ordinarily employed is low. Consequently, the photographic magnitude will depend very markedly on the sensitivity of the plate in this region, far more than is true for a star. On the other hand, in so far as faint light sources are concerned, the eye is most sensitive to the green. A visual observer, therefore, comparing a nebula with an out-of-focus stellar image might estimate the nebula systematically too bright. Unless something is known concerning the relative intensities of the emission lines in the spectrum and the plate-plus-instrument or eye sensitivity, it is difficult to interpret nebular magnitudes, expressed in the ordinary stellar scale, either visual or photographic. The measurements of the magnitudes of planetary nebulae is further complicated by their central stars.

Attempts to measure the surface brightnesses or so-called integrated magnitudes of planetary nebulae have been fragmentary and to a large degree unsatisfactory. Holetschek⁽²¹⁾ estimated the visual brightnesses of a number of nebulae on the B.D. scale by comparing them with out-of-focus images of stars. Later, Wirtz,⁽²²⁾ at Strasbourg, measured the visual surface brightnesses of a number of gaseous nebulae by comparing them with the diffused light of an artificial star. Extra-focal images of stars of known magnitude provided the calibration of the comparison source. Wirtz simply multiplied the surface brightness of the brightest part of the disk by the apparent surface of the nebula to get the total visual magnitude. The studies of Holetschek and Wirtz appear to be subject to large accidental and systematic errors.

Curtis⁽²³⁾ compared the exposure times necessary to record the brightest details in planetary nebulae with that needed to obtain a similar density on an exposure of a selected point in the Orion nebula. These *relative exposures* amount to estimates of the surface brightnesses of the planetaries. Hubble's investigations indicate that they are fairly good for large faint nebulae, but that Curtis estimated the small, bright nebulae as systematically too faint. He concluded that Curtis's relative exposures of less than two should be divided by 1.7, i.e. the surface brightnesses are too faint by this factor.⁽²⁴⁾

Vorontsov-Velyaminov and Parenago⁽²⁵⁾ estimated the combined magnitudes of nebulae plus central stars for a number of planetaries. They used short-focus cameras so that the nebular images would appear stellar. Comparisons with the north polar sequence, Harvard Standard regions, and selected areas provided magnitude standards. They tried to attain an accuracy of about 0.2^m. For the southern planetaries they estimated the magnitude from the Franklin-Adams charts with an error estimated to amount to 0.5^m. Their nebular magnitudes, not corrected for the contribution of the central star, are systematically fainter than those of Wirtz and Holetschek. Their catalogue also gives the nebular surface brightnesses expressed in stellar magnitudes per circle one minute of arc in diameter.

The apparent photographic magnitudes of the planetary nebulae tabulated in Berman's catalogue⁽²⁶⁾ represent the determinations by Vorontsov-Velyaminov and Parenago, or their values as revised by Berman according to Hubble's data.

For theoretical discussions, what we want is not the nebular magnitude, but rather the surface brightness in some particular radiation, e.g. $H\beta$, expressed in units such as ergs/cm.²/sec. Some years ago Menzel and the writer attempted⁽²⁷⁾ to derive monochromatic surface brightnesses from the nebular magnitudes as tabulated by Berman. The first step is to convert surface brightnesses expressed in magnitudes per square minute of arc to surface brightnesses expressed in ergs/cm.²/sec. To accomplish this step we may employ the sun as a fundamental reference standard. According to Kuiper⁽²⁸⁾ the apparent bolometric magnitude of the sun is -26.95. The apparent surface area amounts to 806 square minutes of arc. Hence the average surface brightness of the sun in magnitudes per square minute of arc will be

$$H_{\odot} = -19.68. \quad . \quad . \quad . \quad (11)$$

The rate of radiation by the solar surface (surface brightness) amounts to $S_{\odot} = 6.25 \times 10^{10}$ ergs/cm.²/sec. Let H_n denote the bolometric surface brightness of the nebula in magnitudes per square minute of arc. Then

$$\log S_n = -0.4(H_n - H_{\odot}) + \log S_{\odot} \quad . \quad . \quad (12)$$

or
$$S_n = 840(2.512)^{-H_n} \text{ ergs/cm.}^2/\text{sec.} \quad . \quad . \quad (13)$$

Ideally, this formula applies to a nebula which has a continuous spectrum and for which a meaningful bolometric correction can be given. In the present context we deal with an emission-line nebula, the observed quantities are the dimensions of the nebula and its photographic magnitude. We could develop the same type of formula for photographic magnitudes, but the procedure actually employed was to attempt to estimate the monochromatic magnitude in $H\beta$. It was assumed that the magnitude scale

taken from Berman's paper corresponded to a plate-plus-instrument sensitivity combination similar to that found by Yü for a Seed 23 plate and a silver-coated mirror.⁽²⁹⁾ The relative intensities of all the strong nebular lines (on the scale $H\beta=10$) were then multiplied by this plate-plus-instrument sensitivity factor and added together. The intensity (10) of $H\beta$ was then compared with this sum to give the amount by which the nebular magnitude had to be corrected to give an hypothetical $H\beta$ magnitude.

This procedure is unfortunately a crude one, and gave surface brightnesses that were systematically too high. A much better plan is to compare the surface brightness in a particular nebular line, λ , with the intensity in a range λ to $\lambda + \Delta\lambda$ in a star of known magnitude and of the same intrinsic colour (spectral class G2V) as the sun. This is the method of V. A. Ambarzumian for the photometry of a bright-line nebula.⁽³⁰⁾ W. Liller has developed a modification for photo-electric photometry which we shall discuss in Section 7.⁽³¹⁾

Barring absorption of light in space, the surface brightness of an extended object will be independent of its distance. Consider the emission in a particular bright line. The surface brightness will depend only on one quantity, I_λ , the amount of energy radiated by the nebular surface in the line, i.e. in the particular frequency of the bright line being considered per second per unit solid angle per cm.².

Ambarzumian photographed a number of nebulae with a spectrograph with a wide slit so as to obtain broad lines suitable for photometry. He also observed appropriate G0 comparison stars with the same instrument.* From tracings of the monochromatic images he obtained the brightness $i_{n,\lambda}$ of a square second of arc of the nebula in arbitrary units. Similar microphotometric tracings across the spectrum of the comparison star, combined with the known dispersion of the spectrograph, give the intensity $i_{s,\lambda}$ of 1 A. of its spectrum in the same arbitrary units. The ratio

$$P_\lambda = \frac{i_{n,\lambda}}{i_{s,\lambda}} \quad . \quad . \quad . \quad . \quad (14)$$

is independent of units.

The G0 star has essentially the same energy distribution as the sun. If $i_{\odot,\lambda}$ is the intensity of 1 A. of the continuous spectrum of the sun at the wavelength in question,

$$\log \frac{i_{\odot,\lambda}}{i_{s,\lambda}} = 0.4(m_s - m_\odot), \quad . \quad . \quad . \quad . \quad (15)$$

where m_s and m_\odot are respectively the apparent magnitudes of the star and sun. Let A denote the surface area of the sun in square seconds of arc, and

* He used G0 rather than G2V stars in his original application of the method.

h_λ the brightness of the emission in one square second of arc in 1 Å. of the solar surface. Then

$$\log \frac{h_\lambda}{i_{s,\lambda}} = 0.4(m_s - m_\odot) - \log A, \quad (16)$$

or
$$\log \frac{i_{n,\lambda}}{h_\lambda} = \log P_\lambda - 0.4(m_s - m_\odot) + \log A. \quad (17)$$

That is, the ratio of the surface brightnesses of the monochromatic nebular image and of the sun may be determined from the measured quantity P_λ and from the apparent magnitude of the sun and comparison star.

As an example, consider the measurement of the surface brightnesses of filamentary nebulae in the large Magellanic Cloud. The observational data give $i_{n,\lambda}$ the energy received on the plate per square second of arc from a certain point in the nebula, and I_α the energy received per Ångström unit at $H\alpha$ from a G2V ($m_{pv}=10.0$) star in the same arbitrary units. To get the surface brightness of the nebula in ergs/cm.²/sec./unit solid angle, S_n , we substitute in the expression

$$\begin{aligned} \log S_n &= 0.4(m_\odot - 10) + \log h_\lambda A + \log \frac{i_{n,\lambda}}{I_\alpha} \\ &= \log i_{n,\lambda}/I_\alpha - 1.82, \end{aligned}$$

with $h_\lambda = 2.88 \times 10^6$ ergs/cm.²/sec./Å/unit solid angle at $H\alpha$, $A = 2.893 \times 10^6$ seconds of arc, and $m_\odot = -26.84$. For a particular filament in nebula 163 in Henize's forthcoming catalogue we find $\log i_{n,\lambda}/I_\alpha = -1.86$. Hence $S_n = 2.1 \times 10^{-4}$ ergs/cm.²/sec./unit solid angle. Multiplication by 4π gives the energy radiated in the spectral line in one second by all the atoms in a cylinder of unit cross-section passing through the nebula and along the line of sight.

6. Determination of Isophotic Contours

The description of the radiation of a given monochromatic emission in a gaseous nebula requires a knowledge not only of the total amount of energy in the line but also of the distribution of energy in the image. This distribution can be described most conveniently with the aid of isophotic contours, drawn at equal steps in intensity.

Suitable monochromatic images of the stronger radiations can be obtained by appropriate filters and photographic emulsions as described in Section 2, or with the slitless spectrograph (see Section 3). When proper photometric calibrations are impressed on the plates, isophotic contours may be obtained by any one of several methods.

With an ordinary microphotometer one may make successive tracings across each image, measure the abscissa of every point corresponding to

a given intensity with respect to a fixed fiducial mark, and construct contours by laborious point-by-point plotting. Such a procedure was followed by Louis Berman in his pioneer spectrophotometric work on the planetary nebulae and has been employed by other workers since.

The determination of such contours is so extremely time-consuming that other methods must be developed. One answer is the cathode-ray tube isophotometer proposed by T. L. Page,⁽³²⁾ another is the balanced beam photometer which was developed by Hiltner and Williams at the University of Michigan.⁽³³⁾

The cathode-ray tube isophotometer is based on an instrument developed for the study of X-ray plates by the medical school of the University of Illinois. The principle of operation is as follows: the photograph to be studied is first scanned in transmitted light by a television tube. Then the tube output is amplified and "clipped" with the aid of appropriate circuits to eliminate high or low plate densities in a pre-assigned way. The clipping can be made sharp enough to give an accuracy of a few per cent in intensity in the resultant contours. The "clipped" output of the television tube is next supplied to a cathode-ray tube (a standard television-screen tube), and finally the pattern is photographed. The relation between film density and intensity is found from the photometric calibration of the plate. Page has published some preliminary results obtained for the diffuse nebula Messier 8 by this method, but further studies have not been published.

The balanced-beam photometer was originally developed as a direct-intensity microphotometer for the reduction of spectrophotometric observations. It was also designed for use as an isophotometer. Recently the machine has been greatly improved under the guidance of O. C. Mohler. This isophotometer has been employed by S. P. Wyatt (Jr.) in the measurement of contours in elliptical galaxies, by Edwin Dennison in the study of the brightness distribution in elliptical galaxies, by Albert Boggess (III) in the study of galactic nebulae, and by Mrs. Boggess in the analysis of slitless spectrograms of planetaries obtained by O. C. Wilson (Fig. 8).

The machine has two carriages; the photograph to be analysed is placed on one and the interpolation wedge plate on the other. The bright image of an illuminated slit is focused on each plate by a microscope objective. After passage through the emulsion, the light continues through collimating lenses and through two pieces of Polaroid so adjusted that the planes of polarization are at right angles. The two light beams are then reflected through a rotating Polaroid to the photo-cell. If the two beams of light are of equal intensity after passing through the photographic plates, the light incident upon the photo-cell will be of constant intensity; and the resulting constant voltage will not be amplified by the alternating current amplifier. If, for example, the beam from the photographic plate under

examination (F) is brighter than that from the interpolation wedge (F'), there will be a periodic variation of the light intensity, an alternating voltage will be produced and amplified. If the beam from the interpolation wedge is brighter, there will result a similar alternating voltage but of

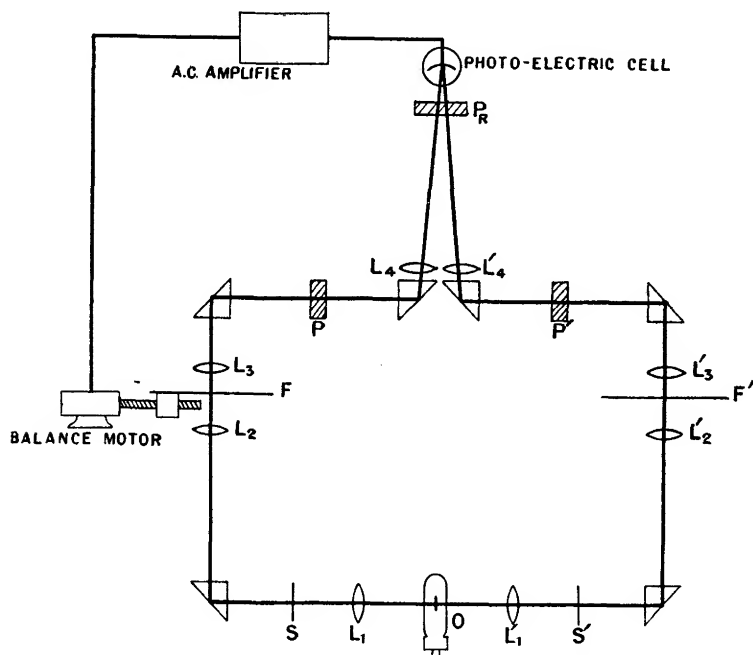


FIG. II : 8. *Schematic Diagram of the University of Michigan Balanced-beam Isophotometer.*

- O Ribbon filament lamp.
- S, S' Slits (circular or rectangular).
- F Photographic plate to be analysed.
- F' Interpolation wedge.
- P, P' Polaroid filters (planes of polarization mutually perpendicular).
- P_R Rotating filter (30 revolutions per second).
- L_1, L_1' Condensing lenses (images filament on L_2, L_2').
- L_2, L_2' Objective lenses (images slit on plates).
- L_3, L_3' Collimating lenses (images plates at infinity).
- L_4, L_4' Field lenses (images L_3, L_3' on photo-electric cell).

The photo-electric cell, A.C. amplifier, and balance motor automatically maintain the position of the plate F so that the density in the illuminated image remains constant. Plate F is driven at constant speed perpendicular to the plane of the diagram. The position of F is registered by a pen-and-paper recorder.

opposite phase. The output of the A.C. amplifier is fed to a two-phase balance motor whose direction of drive depends on the phase of the alternating voltage. When a density in the interpolation wedge is chosen, the plate under examination will be automatically driven in one coordinate until the density is matched.

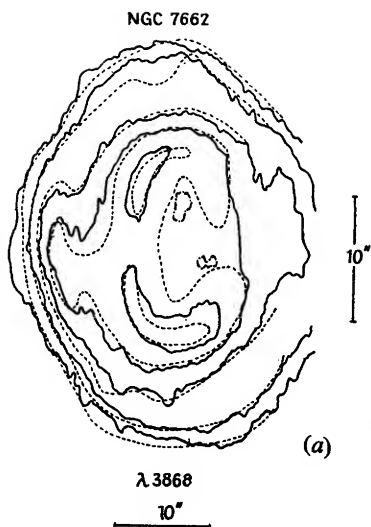


FIG. II : 9(a) NGC 7662, $\lambda 3868$ [NeIII]. The solid lines were traced with the isophotometer; the dotted lines by the method of successive tracings across the nebula. The latter process results in a great deal of smoothing. The contours refer to values of $\log I = 1.2, 0.9, 0.7, 0.3, 9.7$. The magnification by the spectrograph is greater perpendicular to the dispersion than parallel thereto.

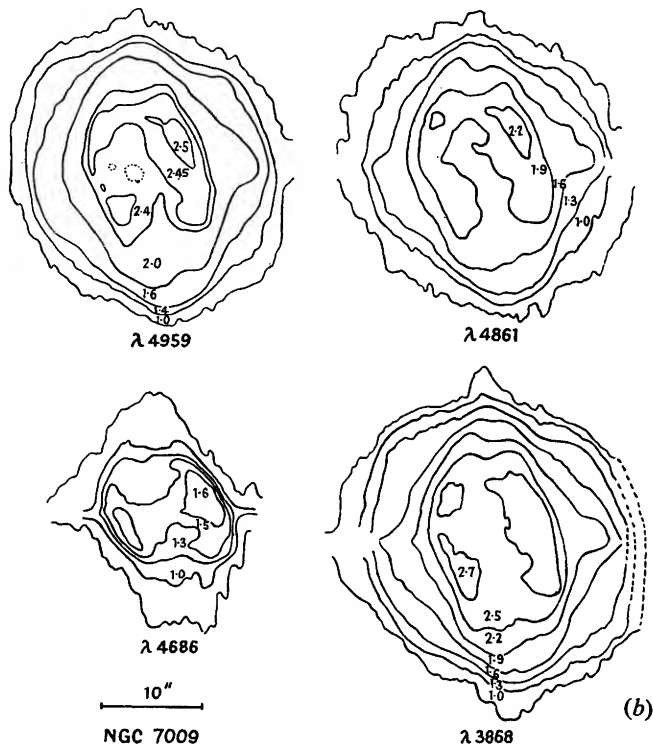


FIG. II : 9(b). NGC 7009, images of $\lambda 4959$ (N_2 [OIII], $\lambda 4861$, $H\beta$, $\lambda 4686$ HeII, and $\lambda 3868$ [NeIII]. The unequal magnifications perpendicular to and parallel to the dispersion have been corrected for in making the tracings.

FIG. II : 9. *Some Typical Isophotic Contours traced with the Balanced-beam Isophotometer.*

The slitless spectrograms were secured by O. C. Wilson at the coude spectrograph of the 100-in. reflector. Mrs. Nancy Boggess made the isophotometer tracings.

If the operator wishes to trace a series of isophotes of a nebula, he selects a series of densities D_1, D_2, D_3 , etc., on an interpolation wedge that corresponds to the desired intensity steps, I_1, I_2, I_3 , etc. If the density D_1 in the calibration wedge is chosen, the machine will trace the contour for I_1 . The plate F is driven at a constant rate in the other coordinate, and the position in both coordinates is simultaneously recorded by a servo-mechanism that connects F with a pen-and-ink recorder.

Each side of a given closed contour must be traced separately; a special selector device is provided for accomplishing this.

Symmetrical nebulae such as NGC 6210 can be easily traced with this instrument. Special care is required for more complicated forms which show numerous wisps and filaments. Nevertheless, nebulae as complicated as NGC 2392 or 30 Doradus have been successfully traced.

Some of the results obtained with the balanced-beam isophotometer for gaseous nebulae will be discussed in Chapters VII and VIII.

7. Photo-electric Photometry of Gaseous Nebulae

An inherent difficulty in the photometric measurement of small gaseous nebulae by photographic methods is that the nebulae have small but finite angular dimensions and cannot be compared with stellar images unless telescopes of very short focus are employed. Furthermore they are often associated with illuminating stars in such a way that the disentangling of stellar and nebular contributions is impossible. Some of these difficulties can be overcome by the use of slitless spectrograms, but the comparison of monochromatic nebular images with stars remains troublesome.

Many of the difficulties in the photometry of planetary nebulae and their central stars can be handled by photo-electric photometry. Essentially, two methods have been employed. One technique is to form a slitless spectrum with an objective prism, and scan it with a slit placed in front of the photo-cell. In this way MacRae and Stock and also Liller and the writer have made spectrophotometric measures of a number of planetaries.⁽³⁴⁾ In a variation on this method, due to John Hall and Arthur Hoag, a small slitless spectrum of the nebula is formed by a low dispersion spectrograph. A diaphragm with carefully spaced apertures only slightly larger than, and coincident with, the monochromatic nebular images is placed in front of the photo-cell so that the sky background is eliminated and the nebular radiations come through. In this fashion nebulae can be measured even against fairly bright sky backgrounds. Whitford and Code working at Mt. Wilson have also measured planetary nebulae with a spectrograph and photo-electric cell.

The second method is that of Liller.⁽³¹⁾ It aims to separate the contributions of the star and the nebula by taking advantage of the fact that the nebular radiation tends to be concentrated in bright lines, whereas the star has a more nearly continuous spectrum. Thus, if one uses filters to isolate spectral regions (e.g. one near $\lambda 5500$ and one near $\lambda 4200$) where there are no strong nebular emissions, it should be possible to measure the magnitude and colour of the central star. Then by the employment of a filter that transmits the green nebular lines $\lambda 5007$ and $\lambda 4959$ of [OIII] which are strong in most planetary nebulae, it is possible to measure the monochromatic brightness of the nebula since the contribution of the central star can be subtracted off. Unfortunately many planetaries, e.g. NGC 7662, have strong continuous spectra which overwhelm the contribution from the central star so that while it is possible to get good nebular brightness measurements, no data on the central star can be obtained with telescopes of modest size. If the nebula is large enough, and the seeing steady, the observer could measure the star and a known area of the surrounding nebulosity separately. If the isophotic contours of the nebula are known, the nebular light added to the central star could be determined and subtracted off. Such observations can be made for a few objects, e.g. NGC 6720, the Ring nebula in Lyra, with a telescope of moderate size (e.g. the 24-in. Cassegrain reflector of the McMath-Hulbert Observatory or the 40-in. reflector of the U.S. Naval Observatory). Most planetaries, however, are so small that the entire object, star plus nebula, must be observed at once. In this problem, as in others pertaining to planetary nebulae, much is to be gained by going to large telescopes which are available under conditions of good seeing.

Measurements of diffuse nebulae present difficulties of other sorts. Usually the surface brightnesses are very low. By using equipment of high sensitivity, an interference filter to cut out unwanted sky brightness, and a telescope with a high f -ratio it is possible to measure nebulae of very low surface brightness. Such studies have been carried out by Strömgren and Hiltner.⁽³⁵⁾

Since we shall make frequent use of his observational results, let us first describe in some detail the procedures followed by W. Liller in his studies of the planetaries.

The photometer, which was of rather conventional design, employed a 1P21 photomultiplier tube. To isolate the green nebular lines, Liller employed an all-dielectric, multilayer interference filter with a maximum transmission of 81 % at $\lambda 4985$ and a half-width of only 35 Å. When used with a conventional green filter, all other maxima were eliminated, and essentially only the radiations of the green nebular lines plus some emission from $H\beta$ were transmitted. In order to get the monochromatic magnitudes

in the green nebular lines from the measurements it is necessary to know the relative contributions of $H\beta$, the nebular continuum and the green lines. In most nebulae these corrections, which can be determined from photographic spectrophotometric studies, are small. Furthermore, in nebulae with bright central stars, the contribution of the latter in this region must be known. Liller tried to evaluate the stellar contribution by the previously mentioned method of observing the star plus nebula with filter combinations that transmitted regions of the spectrum with no strong nebular emission lines. For the visual region ($\lambda 5100$ – 6000) he employed a Wratten 40 plus Wratten 15 filter; for the violet ($\lambda 4100$ – $\lambda 4340$) region he used a conventional interference filter (150 Å. half-width) centred at $\lambda 4220$ plus a Schott BG12 2-mm. filter. For the green nebular lines he used the previously mentioned all-dielectric Bausch and Lomb interference filter plus a Wratten 40 and 2-mm. Schott GG7 filter. He measured the transmission curves of this 3-filter combination with the aid of the solar spectrograph in the 70-ft. McGregor Tower of the McMath-Hulbert Observatory. Such a high dispersion was necessary because of the steep slope of the transmission curve of the green interference filter. To determine the response curve of the 1P21 photomultiplier tube plus the optical system, Liller traced the spectrum of Vega produced by a 4-in., 12° prism placed over the aperture of the 24-in. reflector with which the nebular observations were made. A correction for the transmission of the prism (which was not used in the nebular work) had to be applied.

To measure the monochromatic surface brightnesses in the green nebular lines one may use essentially the method of Ambarzumian. Since the relative contributions of the nebular lines and of the central star are known, the deflection that would be produced by the selected nebular lines alone may be computed and compared with the green deflection of a nearby dwarf G-star of known magnitude. Since the sensitivity curve of the green system is known, the contribution from a one Ångstrom interval at the wavelength of the selected nebular line to the deflection can be calculated. Liller used 13 G0V to G4V comparison stars in the magnitude range 3 to 7.5. He measured their magnitudes and colours, using the same types of filters as employed by Stebbins, Whitford, and Johnson in their work on three selected areas.⁽³⁶⁾ He calibrated the filter plus photo-cell combination with the aid of the brighter stars in Selected Area 61 and certain stars observed by Johnson and Morgan so the observed colours could be transferred to the International System.

Ambarzumian's method utilizes stars of the same energy distribution as the sun so that it makes no difference whether visual or photographic magnitudes are used. In practice it is never possible to get stars of exactly

the same colour as the sun. Hence, in an effort to minimize these effects, Liller introduced a green magnitude defined by

$$P_{gr} = P_v + C_p/2, \quad . \quad . \quad . \quad (18)$$

where P_v and C_p are the international photo-visual magnitude and colour.

Since the energy curves of very hot nuclei do not differ greatly in the visual region, even over extreme temperature ranges, the relative I_λ can be estimated for the planetary nuclei with continuous spectra. See Chapter VI.

The reduction of the observations can be carried out in the following way. With any given filter-combination the potentiometer deflection will be given by

$$D_\lambda = a \Sigma I_\lambda(n) S_\lambda + a \int I_\lambda^c(n) S_\lambda d\lambda + b \int I_\lambda(s) S_\lambda d\lambda, \quad . \quad . \quad . \quad (19)$$

where $I_\lambda(n)$ denotes the intensity of the nebular line radiation, $I_\lambda^c(n)$ that of the nebular continuous radiation defined per unit wavelength interval, and $I_\lambda(s)$ the energy distribution in the spectrum of the central star. S_λ is the sensitivity of the photometer plus optical system at wavelength λ . Here a and b are constants that must be found for each nebula. The first term represents the contribution of the line emission, the second that of the continuum, and the third that of the central star. With each nebula, D_λ is observed with each of the three filter combinations. Now S_λ is known from the calibrations, the relative values of the line and continuous nebular radiation are known from the studies by photographic photometry, while the relative values of $I_\lambda(s)$ can be reliably estimated at the effective wavelengths of the yellow and green colour systems. For most planetary nuclei one may write

$$\int I_\lambda(s) S_\lambda d\lambda = A_\lambda \bar{I}_\lambda(s), \quad . \quad . \quad . \quad (20)$$

where A_λ is the total area under the S_λ curve and $\bar{I}_\lambda(s)$ is the value of $I_\lambda(s)$ at the effective wavelength of the particular colour system [$\lambda_y = 5435$ Å. (yellow), $\lambda_g = 4985$ Å. (green), and $\lambda_v = 4225$ Å. (violet)]. Since the relative values of $\bar{I}_y(s)$, $\bar{I}_g(s)$, and $\bar{I}_v(s)$ are known, the three equations for the three deflections D_y , D_g , and D_v involve the three unknowns, a , b , and $\bar{I}_v(s)$, which may be solved formally. The solution is made more determinate by the fact that D_y and D_v involve mostly the nebular continua and the star, whereas D_g usually involves mainly the contribution of the green nebular lines. That is, the contribution to the deflection from each of the three sources can be evaluated. Finally, from the observations of the comparison stars the contributions of the nebular emission lines, the nebular continuum, and the central star can all be put on the same scale.

With S_λ known, the deflection that would be produced by the radiation from one Ångström of the spectrum of any G2V star at the wavelengths

of the nebular lines can be calculated since the energy distribution in the solar spectrum is determined. Liller introduces a "reduced deflection" so defined that a G2V star 30 magnitudes fainter than the sun gives a green deflection of 10,000. Then the reduced deflection from a wavelength interval $\Delta\lambda$ at λ in the standard stars spectrum is

$$d_{\lambda}(G_s) = 10^4 \frac{I_{\lambda}(G) S_{\lambda} \Delta\lambda}{\int I_{\lambda}(G) S_{\lambda} d\lambda}, \quad (21)$$

where $\Delta\lambda$ is 1 Å. In Ambarzumian's equation

$$\log i_{n,\lambda} = \log P_{\lambda} - 0.4(m_s - m_{\odot}) + \log A + \log h_{\lambda,\odot} \quad (22)$$

P_{λ} is the quantity taken from the observations, $m_s - m_{\odot}$ is exactly 30, $\log A = 6.461$, and the values of h_{λ} were obtained from Pettit's measurements of the energy distribution in the solar spectrum. The dimensions of the nebulae are taken from the work of Curtis.

By way of orientation let us discuss the measures for a typical object NGC 6826. The "reduced deflections" d_1^n and d_2^n for the two green nebular lines are 269 and 72.2, the deflections of the central star at these same wavelengths are $d_1^s = 0.091$ and $d_2^s = 0.071$, whereas the values for the comparison star are $d_1^G = 68.8$ and $d_2^G = 53.8$. The ratio of the brightnesses of the central star at the effective wavelengths of the violet and yellow filter systems is $C_1 = 2.52$. Adopting an angular radius $A = 13''$ for this nebula, the surface brightness, S_{λ} , expressed in ergs/cm.²/sec. at the outer boundary is 0.23 and 0.080 for $\lambda 5007$ and $\lambda 4959$ respectively. Making use of the ratio of $N_1 + N_2$ to $H\beta$ found by photographic photometry, $S(H\beta) = 0.0294$ ergs/cm.²/sec. In the calculation of S it is assumed that the nebula is a disk of uniform surface brightness and of radius A . When the distribution of energy over the disk is known, the precise value of the emission at each point may be given.

The surface brightnesses found by Liller are considerably lower than those estimated by Menzel and the writer from the crude data that were available earlier. His results have been substantiated by the spectrophotometric measures described in Section 9.

To date, more than a hundred planetary and other gaseous nebulae have been measured by Liller's technique. Many were observed by him and the writer at the Mt. Wilson Observatory in 1954. When these measures are combined with the line and continuum intensity data which are available for most of them, fairly satisfactory photometric material will be available for the majority of planetary nebulae observable in the northern hemisphere.

The photometry of diffuse nebulae presents problems of other sorts. The brighter emission nebulae are not difficult to observe, but they occupy

perhaps only about 0.001 of the volume of the space in the spiral arms where they occur. The emission regions in Sagittarius, Cygnus, Cepheus, Auriga, Orion, and Monoceros observed by Struve and Elvey are much larger but are usually so much fainter than the sky background of the Milky Way that they can be detected only by techniques that isolate the emission lines. The regions of maximum surface brightness of Struve and Elvey's extended nebulosities can be photographed, however, with Schmidt cameras and appropriate plate-filter combinations (see Section 2).

Strömgren and Hiltner⁽³⁵⁾ used interference filters in conjunction with a photo-electric photometer attached to the 82-in. McDonald reflector to observe hydrogen emission regions as dim as the faintest ones found by Struve and Elvey. One filter was centred near $H\beta$, the other was used to monitor a comparison region near $\lambda 4600$ Å. Each filter had a width of about 150 Å. They avoided setting on stars brighter than the 17th magnitude and determined the deflections corresponding to the galactic+sky background and very faint stars. Since the filter characteristics were known, measures of comparison stars of known magnitude and colour permitted the reduction of the measures to absolute units.

The observed intensity, expressed in absolute units, can be expressed in terms of the number of atoms in the fourth level of hydrogen multiplied by the length of the column, and the transition probability. Since the hydrogen spectrum is produced by recombination, the emission will depend on $N_i N_e$ and the electron temperature (see Chapter IV). Furthermore, since the ionization of hydrogen in these nebulosities is essentially total, and since all other elements are much less abundant, we can equate N_i to N_e to the total number of hydrogen atoms per cm.³, N_H .

Strömgren defines hN_H^2 as the "emission measure", where h is the length of the radiating column in parsecs.⁽³⁷⁾ On this system, an average one of Struve's and Elvey's ionized hydrogen regions has an emission measure of about 800. If the length of the column is taken as 200 parsecs, $N_H = N_i = N_e = 2$. If the distribution is spotty, N_H will be larger in the regions of condensation. In IC 405, for which Strömgren finds an emission measure of 7000, an assumed diameter of 10 parsecs leads to $N_i \sim 30$.

With the aid of narrower filters it is possible to measure even fainter emission regions and further studies with this technique appear to be promising.

Photo-electric measures of diffuse nebulae have been made occasionally by other observers. What is urgently needed is a set of fundamental photometric standards in selected galactic nebulae. Preferably, these should be set up as monochromatic standards for emission nebulae. Selected regions in nebulae such as Orion, Messier 8, Messier 16, and a few other objects might well serve this purpose.

8. Spectrophotometric Studies of Gaseous Nebulae

The interpretation of photo-electric and photographic measures of nebular magnitudes and surface brightnesses requires a knowledge of the energy distribution in their spectra, i.e. the relative intensities in the various emission lines and in the continuum. Here we shall confine our attention to some of the techniques used and in the next chapter we shall discuss the results obtained.

The earliest spectrophotometric work on the gaseous nebulae was that by Wilsing and Scheiner,⁽³⁸⁾ who measured the intensity ratio of the green nebular lines, N_2/N_1 , to be 0.40 using visual methods.

Most spectrophotometric work on gaseous nebulae has been done photographically, although it has been demonstrated that it is practical to measure the stronger lines by photo-electric methods (see Section 9). A complete discussion of photographic photometry lies outside the scope of this book, but we shall summarize some of the important points here. The basic method involves photographing upon the same plate:

- (a) The spectrum of the nebula.
- (b) The spectrum of a source of known energy distribution (usually a comparison star).
- (c) Calibration spectra which enable the observer to relate the blackening of the photographic emulsion to the relative intensity of the light.

It is necessary to determine the atmospheric extinction coefficient, k_λ , as a function of wavelength. This step may be accomplished by photographing the comparison star at different zenith distances $z_1, z_2 \dots z_n$ and measuring the observed relative intensities $i_\lambda(z_1), i_\lambda(z_2)$, etc., at these zenith distances for a series of wavelengths, $\lambda_1, \lambda_2 \dots \lambda_n$. The law of extinction is

$$I_\lambda = I_\lambda^0 e^{-k_\lambda \sec z}, \quad . \quad . \quad . \quad (23)$$

where I_λ^0 is the true intensity outside the earth's atmosphere, and I_λ is the absolute intensity measured at the earth's surface. The relative intensities i_λ need not be converted to absolute intensities. Generally i_λ will differ from I_λ by a factor A_λ that will depend on the sensitivity of the plate and the transparency of the optics. Thus

$$\log i_\lambda(z) = -k_\lambda \sec z + C_\lambda. \quad . \quad . \quad . \quad (24)$$

If the data, $\log i_\lambda(z_1), \log i_\lambda(z_2)$, etc., are plotted against $\sec z$, the coefficient k_λ can be found from the slope of the straight line passing through the points. It turns out that

$$k_\lambda = k_0 + k_1 \lambda^{-4} \quad . \quad . \quad . \quad (25)$$

for spectral regions where there are no strong telluric lines. Here k_0 is a constant that is determined by the extinction produced by large-size

particles, whereas the $k_1\lambda^{-4}$ term corresponds to Rayleigh scattering. In relative spectrophotometry k_0 is not important.

The comparison of the spectrum of the nebula with that of the comparison star should be done at as nearly the same zenith distance as is possible. The exposure times on the star, nebula, and photometric calibration should be comparable. If it is necessary to cut the plate, putting the stellar and

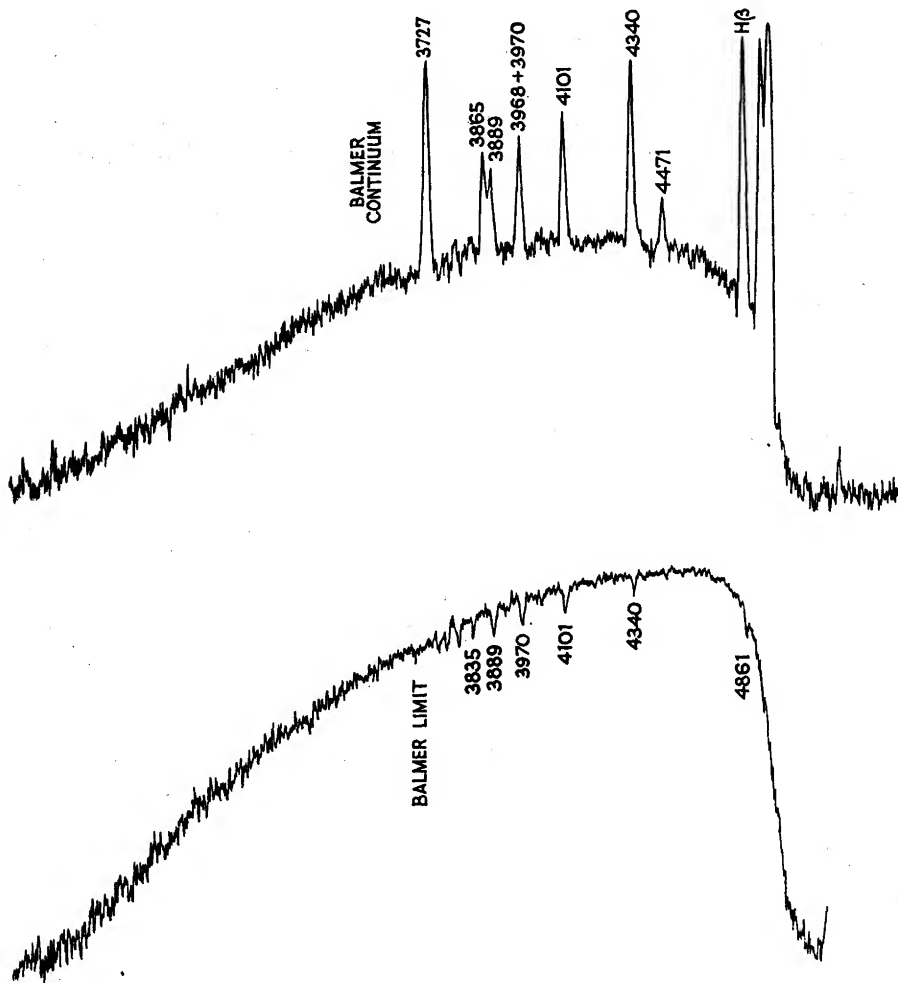


FIG. II : 10. *Tracings of the Spectra of a Planetary Nebula and a Comparison Star.*

The nebula IC 2149 has a bright central star; hence the strong continuous background on the tracing. A spectrogram of this nebula is reproduced in Fig. III : 7. The comparison star is 68 Cygni, spectral class Oe5. From observations secured with the Crossley quartz slitless spectrograph at the Lick Observatory, October 1944.

nebular exposures on one part and the calibration exposure on another, the two pieces should be developed together.

Stellar energy distributions have been measured by a number of observers. The Greenwich workers compared the energy distributions of stars.⁽³⁹⁾ Comparisons of stars with terrestrial sources (i.e. the measurement of the true energy distribution) have been made by R. C. Williams,⁽⁴⁰⁾ by Kienle and his co-workers,⁽⁴¹⁾ and by Barbier and Chalonge.⁽⁴²⁾ The French workers extended the energy measurements to the limit of transmission of the earth's atmosphere in the ultra-violet.

Spectrophotometric studies of gaseous nebulae have been made both with slitless and slit spectrographs. In either event the comparison of a star, which appears as a small seeing disk, with the nebula which is usually an extended surface, presents difficulties. With the slitless spectrograph the comparison star spectrum is often widened by letting the star drift in right ascension, the dispersion being in declination. With a slit spectrograph the star cannot be simply focused on the slit and the spectrum recorded in the usual way because of the effects of atmospheric dispersion. Different proportions of violet, green, and red light enter the slit so that the energy distribution in the resultant spectrum may be very different from what would be found with a slitless spectrograph. Nor can the star be run out of focus, for then the light path of the starlight through the spectrograph could be radically different from the path of the nebular light. Barbier⁽⁴³⁾ and also Minkowski and the writer placed a small quartz diffuser in front of the slit. T. L. Page employed a piece of Lucite.⁽⁴⁴⁾ If the star is now run out of focus a small patch of the surface of the quartz will be diffusely illuminated. Since this diffuse surface is at the focus of the collimator it will be optically similar to the nebula in many respects.

The spectra of the star and nebula being photographed side by side upon the plate, a direct measurement of the relative intensities of the nebular lines and continuum can now be made, provided the relation between photographic blackening and intensity is known. This information is provided by the *photometric calibration*. Numerous methods of photometric calibration have been proposed, and we shall mention only a few of them. The simplest is the *spot sensitometer* in which a lamp illuminates an opal glass diffuser behind which is placed a row of tubes. Each tube has a cap at the end with a hole of different aperture; the amount of light getting through the tube is proportional to the area of the hole. Different filters are used to isolate different regions of the spectrum. The plate sets behind the row of tubes. A better method is to employ a calibrating spectrograph with some device to vary the light reaching the plate as a known function of the distance along the slit. The calibrating spectrograph may or may not be identical with the nebular spectrograph.

In one version of the instrument a step or wedge slit is employed. This arrangement has the disadvantage with instruments of small dispersion that since the purity of the spectrum depends on the distance along the slit, the calibration is seriously affected in wavelength regions where the plate sensitivity changes rapidly.

A superior technique employs a rapidly rotating sector placed in front of a slit of constant width. The amount of light admitted into the spectrograph as a function of distance along the slit can be varied in an arbitrary fashion. If the sector is rotated rapidly, intermittency effects are eliminated.

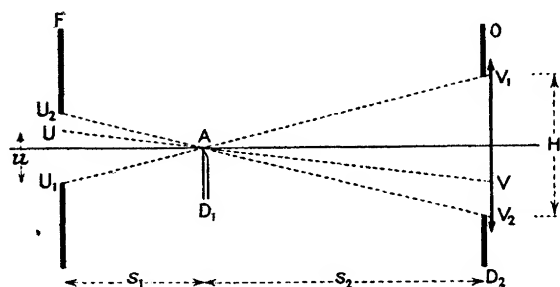


FIG. II : 11. Schematic Adaptation of the Collimator of a Calibration Spectrograph for the Method of von Hirsch and Schon.

O is the objective of the calibration spectrograph and F is its slit. A knife-edge D is oriented perpendicular to the slit with its edge on the optic axis at A . If the objective is a circle of diameter V_1V_2 , the rays from U_2 illuminate the objective completely, whereas those from U_1 are stopped by the knife-edge D .

(Courtesy D. Barbier, *Annales d'Ap.*, 7, 86 (1944).)

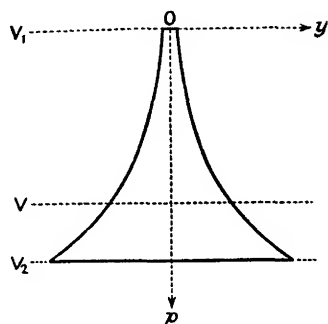


FIG. II : 12. Collimator Diaphragm for the Calibration Spectrograph.

Instead of using a circular aperture on the collimator, or a rectangle (as did von Hirsch and Schon), Barbier used a diaphragm limited by two exponential curves. In this way the light intensity upon the plate varies as the logarithm of the abscissa measured perpendicular to the dispersion of the spectrum.

(Courtesy D. Barbier, *Annales d'Ap.*, 7, 87 (1944).)

In his spectrophotometric work on the planetaries, T. L. Page⁽⁴⁴⁾ standardized his plates with an aluminium on quartz optical wedge placed over the slit. He calibrated the wedge on the spectrograph with rotating sectors having apertures from 10° to 340° and with slit widths from 0.10 to 1.00 mm. In this particular wedge the logarithm of the transmission was found to vary linearly with distance from the thin edge.

In his spectrophotometric study of the Orion nebula, Barbier⁽⁴³⁾ employed the method of R. von Hirsch and M. Schön in which no sector or wedge or other device is placed in front of the slit of the spectrograph. Rather a knife-edge perpendicular to the plane of the slit is introduced in the collimator in such a way that the top of the collimator receives light from the entire length of the slit, whereas the bottom of the collimator

receives no light from the slit at all. Instead of using a circular collimator, Barbier employed a special shaped diaphragm over the collimator so that the illumination falling on the plate varied logarithmically with the distance across the calibration spectrum. See Figs. 11 and 12.

If the calibration spectrum is so made that I or $\log I$ is proportional to the distance from some fixed fiducial work on the plate, the spectrogram may be analysed by a direct intensity microphotometer. H. W. Babcock has constructed a successful instrument for the analysis of stellar spectra at the Mt. Wilson and Palomar observatories. Such instruments have not been applied to nebular lines, although there is no reason why this cannot be done. Once the relative intensities of the emission lines in a nebular spectrum at a particular point in the image have been measured by the aforementioned techniques, the isophotic contours (which usually refer to fixed steps in $\log I$) may all be referred to the same zero point. The zero point itself is established by the Ambarzumian method or some equivalent thereof.

The photometric difficulties encountered in the measurement of nebular line intensities are legion. Unlike the photometry of stellar absorption lines where the line profile is simply referred to the stellar continuum, the nebular line intensities are usually referred to some particular line, e.g. $H\beta$ as standard. Hence all photometric errors that depend on wavelength enter with full effect upon the final results. Finally, there exists a 10^3 – 10^4 -fold intensity ratio between the weakest and strongest lines that have been measured. A series of graduated exposures ranging from seconds to many hours is necessary.

Particularly difficult is the measurement of the very strongest lines with respect to the others. For example, the ratio $I(N_1 + N_2)/I(H\beta)$ is troublesome to establish by photographic photometry because the sensitivity of the emulsions ordinarily employed falls off very rapidly towards the longer wavelengths in this region. Fortunately, the ratio can be measured very accurately by photo-electric methods. The system of nebular line intensities, like the system of stellar magnitudes, profits by a photo-electric check for at least the brighter nebulae.

9. Photo-electric Spectrophotometry of Planetary Nebulae

At the Warner and Swasey Observatory of the Case Institute of Technology, Donald MacRae and Jurgens Stock measured the intensity ratio $I(N_1 + N_2)/I(H\beta)$ by taking tracings across the nebular spectrum formed by a 6° objective prism attached to their 24-in. Schmidt camera. Subsequently, W. Liller and the writer measured the relative intensities of these radiations in a number of planetaries with the 24-in. Curtis Schmidt telescope equipped with a 10° objective prism. Measures were made both

by using a diaphragm and measuring the monochromatic images and the nearby continuum, and also by tracing the spectrum with a narrow slit. The latter method which is similar to that of MacRae and Stock, involves driving the telescope at a rate slightly different from the sidereal rate by means of a frequency control.

Tracings of Vega and Deneb at different zenith distances enable corrections for instrumental sensitivity and atmospheric extinction to be made. The results of the two kinds of measures are in good agreement with one another and with the observations of MacRae and Stock.

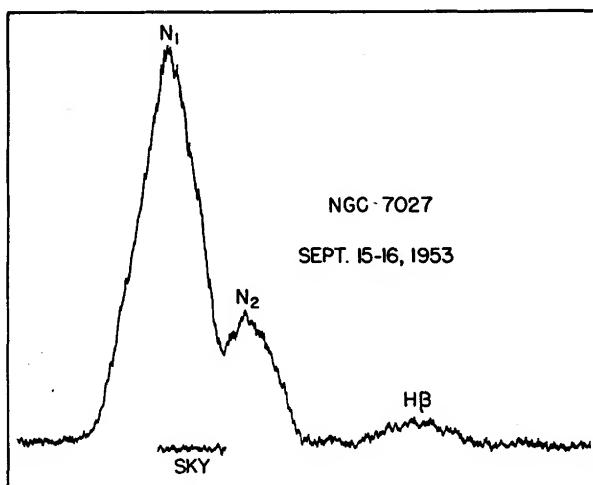


FIG. II : 13. *Tracing of the Green Nebular Lines and $H\beta$ in NGC 7027.*

This tracing was made with a photo-electric photometer and the 24-in. Curtis Schmidt telescope equipped with a 10° objective prism. The sensitivity of the photometer and the transmission of the optics change slowly with wavelength; hence the large intensity ratio of $N_1 + N_2$ to $H\beta$ is clearly shown.

Fig. 13 shows a sample tracing. The higher dispersion employed by the Michigan observers permitted a separation of the images of the two green nebular lines in most of the planetaries observed.

The method of reduction for surface brightnesses in which Vega and Deneb served as comparison stars involves a slight modification of the Ambarzumian method. The photo-visual magnitudes of the sun and Vega are, respectively, -26.87 and $+0.03$,⁽⁴⁵⁾ a difference of 26.90^m . Since the mean effective wavelength of the photo-visual system is $\lambda 5433$ a correction (depending on the energy distributions in the sun and Vega) must be made. This correction reduces the magnitude difference to 26.55 at $\lambda 4861$. After



FIG. 11 : 14. *A Monochromatic Planetary Nebular Image observed with O. C. Wilson's Multi-slit.*

The image of $\lambda 3868$ [NeIII] in NGC 7662.

Top. Slitless image photographed at the coudé focus of the 100-in. reflector. The $\lambda 3835$ image is faintly visible to the left.

Bottom. The same image photographed with Olin Wilson's multi-slit. Notice the splitting of the lines near the centre of the nebula. The small white square serves as a fiducial mark.

(Spectrograms obtained at the Mt. Wilson Observatory, October 1952.)

corrections have been made for the effects of differential atmospheric extinction, the slit width, and the size of the nebula, there results

$$\log P_{\lambda'} = \log i_{n\lambda} - \log i_{s\lambda},$$

where $i_{n\lambda}$ is the deflection that would be produced by a square second of arc of the nebula in the light of $H\beta$ and $i_{s\lambda}$ is the deflection that would be produced by 1 A. of the solar spectrum at $\lambda 4861$. We discuss some of the detailed results in Chapters III and IV. Liller and the writer have given average fluxes for each nebula in ergs/cm.²/sec. on the assumption that each nebula can be regarded as a uniform disk of radius a . When isophotic contours are available, these mean surface fluxes can be used to calibrate the zero point of the contour scale in terms of surface brightness in ergs/cm.²/sec./unit solid angle.

The relative intensities of N_1 , N_2 , and $H\beta$ follow at once from the reductions of the tracings. The chief uncertainty lies in the estimation of the star plus nebular continuum. Nevertheless, the results of different photo-electric observers are in good agreement.

At the Mt. Wilson Observatory, Arthur Code of Wisconsin has photo-electrically measured the intensities of the stronger lines $I > 0.1I(H\beta)$ in NGC 7027. His measures are in excellent accord with those made photographically by Bowen, Minkowski, and the writer.

10. Measurement of Internal Motions in the Gaseous Nebulae

In addition to data on the quantity and spatial distribution of the emitted quanta, a knowledge of the internal motions is necessary for an understanding of the gaseous nebulae. Mention has already been made of the application of the Fabry-Perot interferometer to the measurement of the internal motions in the Orion nebula.

Campbell and Moore⁽⁴⁶⁾ observed this object with slit spectrographs, using a slit length amounting to 80". Their velocity measurements were confined to N_1 , N_2 , and $H\beta$. They also measured the internal motions and radial velocities of a large number of planetary nebulae.

Whereas Campbell and Moore, working with a refractor, were able to make radial velocity measurements in only a limited region of the spectrum at a time, O. C. Wilson,⁽⁴⁷⁾ who observes at the coudé focus of the 100-in. reflector is able to photograph large regions of the spectrum at once. Hence simultaneous measurements of the internal motions in the radiations of several ions can be made. One disadvantage of the coudé focus is that the image rotates on the slit in the course of an exposure, but this trouble can be overcome with the aid of an image rotator. The field is small, but this is no disadvantage on small nebulae.

With a conventional slit spectrograph, the radial velocity distribution in

only one strip across the nebula can be observed at a time. Since the required exposures are very long, the accumulation of detailed information on any one nebula is slow. To overcome these difficulties Wilson employed a multi-slit instead of a single slit. The slit of the spectrograph is replaced by an aluminized quartz disk upon which are ruled a number of parallel lines which admit light into the spectrograph when the image of the nebula falls on the disk. The observer guides the exposure with the aid of a reticle placed in the eyepiece. Thus, instead of a single bowed, distorted, or split spectral line corresponding to a narrow strip across the nebula, each nebular emission gives a series of lines. Each one of these lines gives data on the radial velocities in a strip across the nebula. A single exposure tells the velocity story of a nebula.

Measurements of the internal motions in faint extended nebulae of the galaxy have been made by Georges Courtes who used interferometer techniques. Grating spectrographs with high dispersion and short cameras could be used also. Such studies will be rewarding for investigations of turbulence and large-scale motions in the emission nebulae.

More data on the motions of cool clouds of neutral hydrogen will be forthcoming from the 21-cm. radio observations. These measurements in turn are difficult to interpret because of the low resolution of the radio telescopes and the fact that emission along long paths in the galaxy are contributing to each observation.

Radio astronomy techniques must therefore be added to the list of tools for the investigation of gaseous nebulae. The 21-cm. radiations comes from large clouds of neutral hydrogen and when the methods are perfected valuable data on the density fluctuations, temperatures, and velocities of the gas will be obtained (see Chapter VIII).

REFERENCES

- (1) *M.N.R.A.S.*, **48**, 387 (1888).
- (2) *Phil. Trans. Roy. Soc.*, **134**, 19 (1844).
- (3) *Harvard Obs. Ann.*, **5** (frontispiece) (1867).
- (4) Washington Astron. and Meteorological Observations for 1878.
- (5) *Lick Obs. Publ.*, **8** (1908).
- (6) See the discussion by BAKER, J. G., *Harvard Obs. Mono.*, **7**, Centennial Symposia, 37, (1948).
- (7) For the theory of this instrument consult texts of physical optics, e.g. JENKINS, F. A., and WHITE, H. E., *Fundamentals of Physical Optics* (McGraw-Hill Book Co., New York, 1937), p. 93. J. Valasek, *Introduction to Theoretical and Experimental Optics* (John Wiley & Sons, New York, 1949), p. 147.
- (8) *Ap. J.*, **33**, 406 (1911).
- (9) *Ap. J.*, **40**, 241 (1914).
- (10) *Zeits. f. Ap.*, **6**, 355 (1933). In the formulae (9) and (10) of this paper, the "2" appearing in the denominator should be deleted. See also MINKOWSKI, R., *Zeits. f. Ap.*, **9**, 202 (1934).

- (11) *Phil. Trans. Roy. Soc.*, **154**, 437 (1964).
- (12) *Phil. Trans. Roy. Soc.*, **186A**, 73 (1894).
- (13) *Astronomy and Astrophysics*, **13**, 384, 494 (1894).
- (14) *Ap. J.*, **88**, 113 (1938).
- (15) *Ap. J.*, **116**, 1 (1952).
- (16) *Publ. A.S.P.*, **48**, 14 (1936).
- (17) See PAGE, T. L., *Ap. J.*, **108**, 157 (1948).
- (18) STRUVE, O., *Ap. J.*, **86**, 613 (1937), and STRUVE, O., VAN BIESBROECK G., and ELVEY, C. T., *Ap. J.*, **87**, 559 (1937).
- (19) *Ap. J.*, **111**, 279 (1950).
- (20) *Lund Medd.*, II, No. 128 (1950).
- (21) See for example the discussions by HOPMANN, A.N., **214**, 242 (1921), and by BERNHEIMER, *Lund Obs. Circ.*, **6**, 107 (1932). Zanstra (*Zeits. f. Ap.*, **2**, 26 (1931)) also employed a correction which was a compromise between Hopmann's correction of the BD-scale and the systematic Hopmann-Holetschek differences for nebulae. For objects brighter than 9.3 on Holetschek's scale no correction was applied; later Zanstra applied the correction of the BD-scale: 9.3+0.5; 9.4+0.7; 9.5+0.9; 9.6 or fainter +1.1 magnitudes.
- (22) *Lund Medd.*, II, 29 (1923).
- (23) *Lick Obs. Publ.*, **13**, 57 (1918).
- (24) *Mt. Wilson Contr.*, 250 (1922), or *Ap. J.*, **56**, 400 (1922).
- (25) *Russian Ast. Journ.*, **8**, 206 (1931); **11**, 40 (1934).
- (26) *Lick Obs. Bull.*, **18**, 57 (1937), (No. 486).
- (27) *Ap. J.*, **93**, 145 (1941).
- (28) *Ap. J.*, **88**, 429 (1938).
- (29) *Lick Obs. Bull.*, **12**, 104 (1926).
- (30) *Zeits. f. Ap.*, **6**, 107 (1933).
- (31) *Ap. J.*, **122**, 240 (1955).
- (32) *A.J.*, **55**, 76 (1950).
- (33) WILLIAMS, R., and HILTNER, W. A., *Publ. Obs. Univ. Mich.*, **8**, 45 (1940).
- (34) MACRAE, D., and STOCK, J., *Nature*, **173**, 589 (1954); LILLER, W., and ALLER, L. H., *Ap. J.*, **120**, 48 (1954).
- (35) See STRÖMGREN's article in *Problems of Cosmical Aerodynamics* (Central Air Documents Office, Dayton 2, Ohio), p. 20 (1951).
- (36) *Ap. J.*, **112**, 469 (1950).
- (37) Strictly speaking the use of the term "emission measure" is unfortunate in that the relation between N_H and the surface brightness involves the electron temperature which is often unknown. Confusion will be avoided, however, if agreement is obtained to use a fixed T_e , e.g. 10,000°K.
- (38) *Ap. J.*, **16**, 234 (1902).
- (39) GREAVES, DAVIDSON, and MARTIN, *M.N.R.A.S.*, **94**, 488 (1934).
- (40) *Publ. Obs. Univ. Mich.*, **7**, 93 (1938); **7**, 147, 159 (1939).
- (41) KIENTLE, STRASSL, and WEMPE, *Zeits. f. Ap.*, **16**, 201 (1938); KIENTLE, STRASSL, and BEILEKE, *Zeits. f. Ap.*, **20**, 91 (1940).
- (42) BARBIER and CHALONGE, *Ann. d'Astro.*, **3**, No. 2 (1940); **4**, 30 (1941).
- (43) *Ann. d'Astro.*, **7**, 80 (1944).
- (44) *Ap. J.*, **96**, 78 (1942).
- (45) The magnitude of Vega is that given by JOHNSON, H., and MORGAN, W. W., *Ap. J.*, **117**, 313 (1953). The magnitude of the sun is taken from the work of KUIPER, *Ap. J.*, **88**, 429 (1938), and of DE VAUCOLEURS, *Ann. d'Ap.*, **12**, 287 (1949).
- (46) *Lick Obs., Publ.*, **13**, 96 (1918).
- (47) *Ap. J.*, **111**, 279 (1950).

CHAPTER III

The Distances, Dimensions, and Spectra of the Gaseous Nebulae

THE PLANETARIES and diffuse objects form two distinct classes of gaseous nebulae. The determination of the distances of the two classes of objects is carried out by different methods, while their forms, dimensions, and stellar associations appear to be unrelated. We shall discuss first the planetaries, which are purely gaseous objects, then the gaseous diffuse nebulae, and finally touch on the galactic nebulae which contain solid particles as well as gas.

1. The Space Distribution of the Planetary Nebulae

The distribution of the planetary nebulae known at the beginning of the present century showed them to have no very strong concentration to the galactic plane as do the galactic nebulae and B-stars. Nebulae of large apparent diameter are widely scattered over the sky, whereas the small objects are concentrated mainly towards the galactic centre.

The observed distribution of the planetaries is strongly affected by space absorption and observational selection. In regions of high galactic latitude or elsewhere where space is clear, our statistics are probably complete. In other areas, such as the direction of the great rift in the Milky Way, many must be hidden by the absorbing material. The interstellar particles absorb selectively so that *H α* emission may still be observed in objects that are so heavily obscured that the [OIII] and other radiations are effectively extinguished.

The number of known planetary nebulae was greatly increased by the survey carried out by R. Minkowski,⁽¹⁾ who used objective prism plates secured with a small refractor through red and orange filters on a 103a-E emulsion. This 10-in. camera had been employed by P. W. Merrill for a survey of Be stars.

On such plates a small gaseous nebula is recorded as an *H α* emission image. A peculiar or faint Be star with an intrinsically weak continuum may have very nearly the same appearance. Hence it is necessary to supplement the objective prism spectrograms with direct photographs taken on a larger scale, e.g. with a large reflector. Minkowski also secured slit spectrograms in order to distinguish Be stars and planetary nebulae.

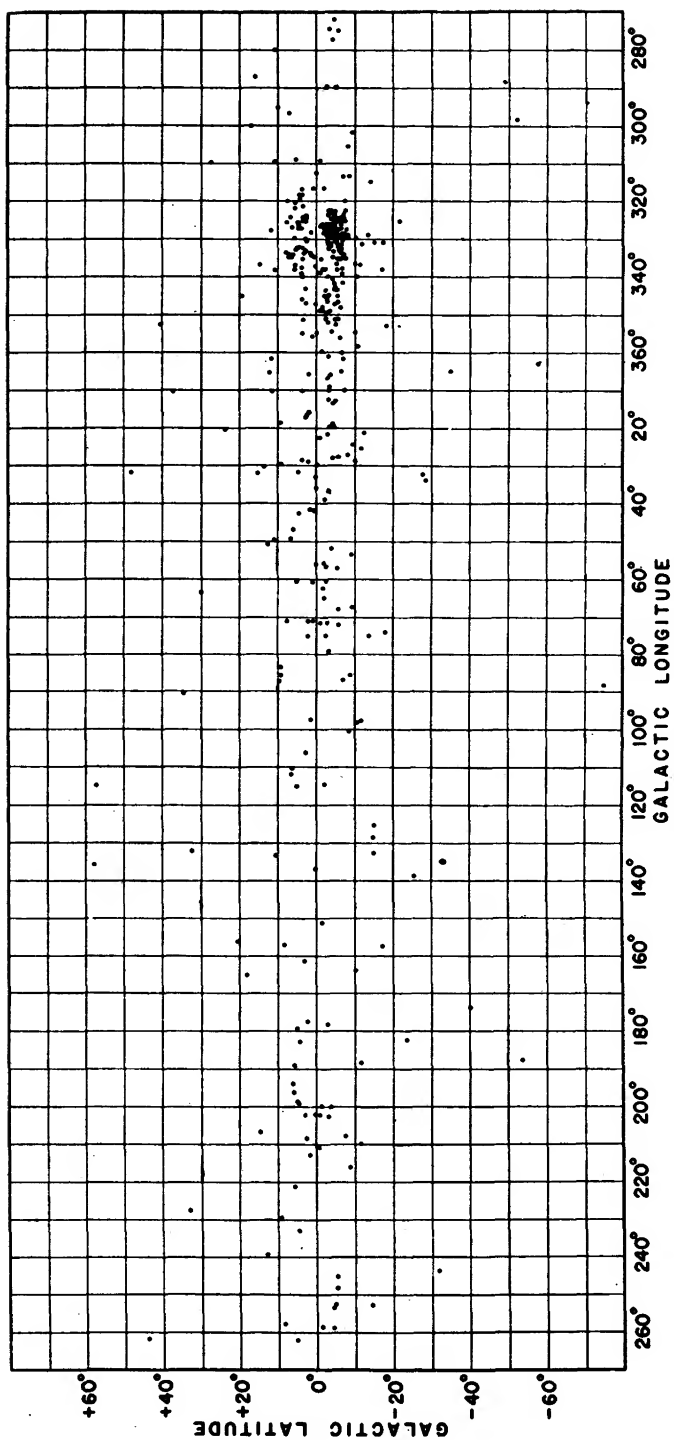


FIG. III : 1. Galactic Distribution of 371 Planetary Nebulae.

Notice the strong concentration of nebulae to the galactic centre (longitude $l=328^\circ$, latitude $b=0$).
 (Courtesy R. Minkowski, *Publ. Obs. Univ. Mich.*, 10, 26 (1951).)

In addition to the 10-in. camera plates, Minkowski also used objective prism plates obtained by J. C. Duncan and A. Wilson with the 18-in. Schmidt camera at Palomar. This survey added 216 new planetaries, bringing the total up to 371. Karl G. Henize used the 10-in. telescope at the Lamont-Hussey Observatory of the University of Michigan to extend the survey to the southern hemisphere; he has added about 137 objects, provisionally identified as planetary nebulae.

As might have been expected, Minkowski's and Henize's survey added relatively more new objects in areas of heavy obscuration where comparatively few planetaries had been known heretofore. For example, between

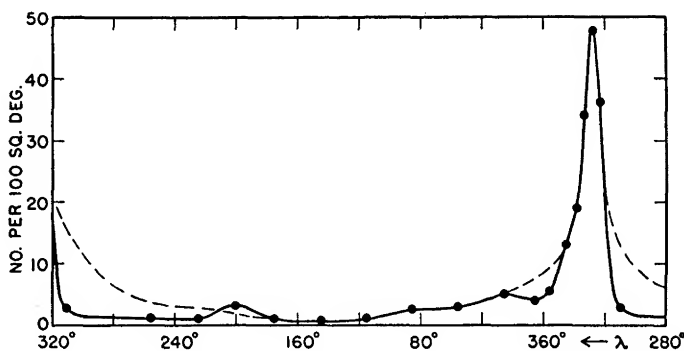


FIG. III:2. *Concentration of Planetary Nebulae between -10° and $+10^\circ$ Galactic Latitude as a Function of Galactic Longitude.*

The maximum near galactic longitude 328° arises because of the high concentration of the nebulae near the centre of the galaxy. Minimum near $l=10^\circ$ is produced by heavy obscuration in this direction. The broken line denotes the densities one might expect to observe in the absence of obscuration.

(Courtesy R. Minkowski, *Publ. Obs. Univ. Mich.*, 10, 29 (1951).)

galactic longitudes 0° and 30° and latitudes -5° to $+5^\circ$, they got fifteen planetaries in an area where none had been found before. South of -5° in a region of presumably low obscuration, no new nebulae were found. Henize finds the density of planetary nebulae in the southern branch of the Milky Way to be about twice that in the northern branch. It would appear that most of the previously known nebulae all fall in areas where the interstellar absorption is small.

The planetary nebulae appear to form a flattened system with a dispersion perpendicular to the galactic plane much greater than that of the B stars. Clearly the high concentration of the planetaries in the direction of Sagittarius means that large numbers of them must be found in the central bulge of our galaxy. The distribution appears to be very similar to that of the RR Lyrae stars, and there can be no doubt that the planetaries belong to the Type II population.

The space density of the planetaries is high in a central bulge of 1500 parsecs radius and then falls off slowly in the outer parts of the galaxy. A number are found at greater distances from the galactic centre than the sun.

A few appear to be located as far as 2000 or 3000 parsecs from the galactic plane. Berman's analysis⁽²⁾ gives a thickness of the nebular system as great as 3000 parsecs and assigns a number of objects to regions beyond the galactic centre. Actual evaluation of the space density would require detailed knowledge of the distances of these objects, and this information is not available at present.

2. The Distances of the Planetary Nebulae

A knowledge of the distances of the planetary nebulae is a prerequisite to any determination of their true dimensions and luminosities. Among the methods tried for the determination of the distances and absolute magnitudes of the planetary nebulae are the following:⁽³⁾

- (a) Trigonometric parallaxes.
- (b) Statistical parallaxes based on the tau and upsilon components of proper motion.
- (c) Galactic rotation.
- (d) Statistical methods based on apparent sizes and magnitudes.
- (e) Central bulge of galaxy.
- (f) Associations with clusters or stars of known distance.
- (g) Presence in external galaxies.

A number of astronomers of the nineteenth century measured positions of some of the brighter planetaries in connexion with extensive programmes of astrometric work. K. Lundmark⁽⁴⁾ has compiled a list of the early observations of Lalande, John Herschel, W. Struve, Auwers, Bruhns, and others. Parallax measurements were attempted by Wilsing, Newkirk, Bredichin, and particularly by van Maanen.⁽⁵⁾ The measured parallaxes are invariably of the order of, or smaller than, the errors of observation. For example, van de Kamp and Vyssotsky found a parallax for NGC 6826 of $-0.006'' \pm 0.007''$.⁽⁶⁾ Other lines of evidence demonstrate the remoteness of the planetary nebulae so that it is little wonder that the method of direct trigonometric parallaxes failed.

Although Wirtz⁽⁷⁾ and also Lundmark⁽⁴⁾ attempted to derive proper motions from the astrometric visual observations of the nineteenth century, H. D. Curtis was the first to measure proper motions by the photographic method.⁽⁸⁾ Other photographic measurements have been made,⁽⁹⁾ but the most extensive studies were those by A. van Maanen⁽¹⁰⁾ at Mt. Wilson and by Claude Anderson at Lick.⁽¹¹⁾

The proper motions (probable error $\sim 0.001''$) derived by van Maanen are based on plates taken at the Cassegrain focus of the 60-in. reflector with an average interval of 12.22 years. The derived motions are relative to comparison stars in each field, and van Maanen reduced them to absolute motions with the aid of Howard Willis's tables which give the parallactic motion for stars of photographic magnitude 12.6 to 15.0 for different galactic latitudes. He calculated mean parallaxes by Airy's method and from the τ and υ components of proper motion with an assumed average radial velocity of a planetary, V , of 26.1 km./sec. The mean parallaxes of twenty-three planetaries derived by the three methods were 0.00050, 0.00096, and 0.00046'', respectively. Weights of 2, 2, and 1 were adopted by van Maanen to obtain the mean value of 0.00068''. Actually, the value given by the τ component is to be preferred. The mean parallax does not lead directly to an estimate of the mean distance unless all the objects selected are roughly at the same distance.

Anderson used eighty-eight plates of thirty-three planetary nebulae photographed with the Crossley reflector at the Lick Observatory. The early plates were obtained by Keeler (1899-1901), Perrine (1904-8), and by Curtis (1910-17). Anderson's investigation (1928, 1931, and 1932) included the larger and supposedly nearer objects, although he did include two stellar planetaries. He also was able to derive only relative proper motions.⁽¹²⁾ An examination of his results show that the nebulae in high galactic latitudes are relatively nearer than those in low galactic latitudes. He found a tendency for the objects with brighter central stars to have smaller statistical parallaxes. This effect was probably a consequence of observational selection, since among the objects he chose, the larger nebulae tended to have fainter nuclei. It is of interest that the larger mean parallax is associated with the objects of larger mean diameter, suggesting that the angular diameter is the quantity most closely related to the distance, i.e. in general the larger the nebula appears to be, the closer it really is. On the other hand, the stellar planetaries are not necessarily all remote objects; many of them may be intrinsically small nebulae of relatively high density; in many instances their small apparent sizes must be a consequence of their dimensions rather than their distances. The mean parallax computed from the τ and υ components is 0.00070'', a value in good agreement with the one obtained by van Maanen, even though the individual proper motions are not in good agreement.

First epoch plates for proper motion studies of the southern planetaries have been obtained by Thackeray and Evans.⁽¹³⁾ Furthermore, it is now possible to more than double the base-line of many of Anderson's plates by means of a new series taken with the Crossley. The precision of the proper motions could be greatly increased, and it is to be hoped that the

number of objects reobserved will be extended to include all planetaries for which good early plates are available.

The study of the motions of the planetary nebulae is complicated because of their remoteness and their membership in the Type II population. Campbell and Moore, at Lick Observatory,⁽¹⁴⁾ made a complete study of the velocities of the emission nebulae north of -34°S , while R. E. Wilson at the Santiago station of the Lick Observatory observed the southern objects, including the ones in the Magellanic Clouds. If one adopts the apex of the sun's way as $\alpha=270^\circ$, $\delta=+30^\circ$, and the velocity of the sun with respect to the nearby stars as -19.5 km./sec. , the nebular velocities may be corrected for the solar motion. It turns out that six planetaries, all located in one small area of the sky $15.1^h < \alpha < 19.2^h$, $-9^\circ > \delta > -38^\circ$, have corrected velocities greater than 115 km./sec. ! Of the ninety-six remaining planetaries, thirty-one are of the so-called "stellar type" with diameters less than $5''$. These objects fall in the direction of the galactic centre and have an average radial velocity of 28 km./sec. , while the sixty-five nebulae with diameters greater than $5''$ give an average velocity of 31 km./sec. These nebulae probably all belong to the central bulge.

On the assumption that the planetary nebulae share the motion of galactic rotation defined by the B stars, Zanstra and also Vorontsov-Velyaminov⁽¹⁶⁾ attempted to derive statistical parallaxes for the planetaries. In view of the erroneous nature of the fundamental premise it is unlikely that the numerical results are of much significance.

Perhaps the most ambitious of these early studies was that by Louis Berman, who attempted to use all the then available information relevant to the determination of the distances of the planetaries. The data are: (1) mean parallaxes based on proper motions; (2) angular diameters (d); (3) radial velocities which he treated in conjunction with the theory of galactic rotation; and (4) the apparent magnitudes of the nebulae, m_n , and of their central stars, m_s .

As a zeroth approximation, Berman used the angular diameters of the planetaries as a measure of their distances. Unlike nebular magnitudes, they are comparatively unaffected by space absorption. He divided the planetaries into two groups: (I) the large objects with bright nuclei that are scattered well over the sky, and (II) the small objects which are concentrated in the Sagittarius region. The proper motion data then serve to fix the constant of proportionality, c , between parallax and angular diameter, $d=c\bar{p}$. Once c is known (Berman calculated it from the τ components of proper motion), one can obtain the mean parallax of any distance group from d . Before the mean distance of the group, r_d , can be found, however, it is necessary to correct $1/\bar{p}$ for the dispersion in the diameters. Berman computed mean absolute magnitudes of the nebulae, M_n , and used them to

establish the relative distances of the planetaries by means of the relation: $\log r = 0.2(m_n + 5 - M_n)$. Then, for the first approximation, he divided the nebulae into three distance groups and analysed the radial velocities of the nebulae in each group on the basis of the theory of galactic rotation. The latter discussion yielded three values of Ar_A , so that if A is known, it is possible to find the mean "rotational distance" of each group. Berman adjusted the value of A to make the r_A and r_D scales agree. One of the objectives of his study was to use the motions of the planetaries to study galactic rotation at great distances from the sun.

Next, Berman used the nebular magnitudes m_n to sort out the nebulae for yet another grouping to provide the material for the next approximation. One must know, however, not only the mean absolute magnitudes of the planetaries, M_n , but also the corrections to be applied for the absorption of light in space. Furthermore, one should allow for the temperature differences in the central stars and that the absolute magnitude of the nebula probably depends on the temperature T_1 of the central star. Berman introduced the quantity, $\delta(T_1) = m_s - m_n$, because the luminosity of the nebula depends ultimately upon the available ultra-violet energy which is a function of T_1 . The nebulae with cooler central stars will have bright nuclei, but those nebulae whose central stars have temperatures of the order of $100,000^\circ\text{K}$. will have relatively very faint nuclei. Berman calculated $\delta(T)$ theoretically and compared it with the observed $m_s - m_n$ to estimate T_1 . He also derived empirical corrections to $\delta(T_1)$, and computed the "reduced" nebular magnitude, m_n' , from the relation $m_n' + a\delta = m_n$. Now δ is known from the temperature estimates for the central stars, and for each of the distance groups a least-squares solution yields an estimate of a and \bar{m}_n' . By a combination of mean group distances and reduced magnitudes, m_n' , the absolute magnitude M_n' and k , the coefficient of interstellar absorption follows. Once M_n' and k are known, one can compute for each planetary

$$\log r = 0.2(m_n - a\delta - kr_1 - M_n' + 5),$$

where r_1 refers to the distance group. The improved estimates of r enable the rearrangement of the planetaries into new distance groups, and the determination of the new scale of distances from d and p . The new distances and the magnitude data yield better values of the space absorption and M_n' and the process was continued. Several approximations were utilized to obtain the finally adopted relations between \bar{p} , \bar{r} , and $\log r$. The determination of the distance of the galactic centre, 9360 parsecs, was in good agreement with that found by other studies at that time.

Many of the planetaries lie at a considerable distance above the galactic plane. In his discussion of the effects of absorption, Berman assumed an

exponential law for the density of the absorbing material perpendicular to the galactic plane. He sorted some of his objects into subgroups according to galactic latitude and made least-squares solutions for M_n' and k (the absorption per kiloparsec in the galactic plane). He found $M_n' = -0.88 \pm 0.12$ and $k = 0.55 \pm 0.06$ magnitude per kiloparsec. At the end of his paper he tabulated for each nebula, its photographic magnitude, m_n , the magnitude of its central star, m_s , the temperature of the central star, and the distance in parsecs.

While Berman's distance scale appears to be more nearly correct than those which preceded it, a number of objections may be raised against it. Oort⁽¹⁷⁾ criticized the assumed equality in absolute magnitude and size of the faint and bright planetaries together with the assumption that the diameters are not influenced by galactic absorption. Different planetaries probably are at different stages in their evolutionary development (Chapter VII), so we would not expect all of them to be of the same intrinsic size. For example, few would assert that the dense "stellar" planetary IC 4997 has the same dimensions as the giant Aquarius nebula NGC 7293. Nearby, faint, large planetaries can be detected easily if they are unobscured, whereas if the same objects were located behind even a small amount of obscuring matter they would be dimmed out by space absorption. The smaller planetaries of high surface brightness may be able to stand much more absorbing material in the line of sight before they are hidden from view. Berman's treatment of space absorption is too idealized to lead to satisfactory results. The planetaries used in his investigation are generally those seen through "windows" in the absorbing material. The interstellar material is so irregularly distributed that the use of an average absorption coefficient is meaningless.

Statistical methods to obtain the distances of the planetaries have also been employed by Camm⁽¹⁸⁾ and by P. Parenago.⁽¹⁹⁾ Camm postulated a linear relation between absolute magnitude, M_n , and linear diameter, D , viz. $D = aM_n + b$, where the constants a and b were determined by imposing the condition that the dispersion in linear diameter and absolute magnitude be as small as possible, consistent with the condition $\bar{M}_n = +0.2$. This postulated relation does not appear to be connected to any physical theory of these objects. Camm made no allowance for interstellar absorption nor for observational selection as he deemed his method "too crude to warrant such corrections". Except for the nebulae of large angular diameter for which Camm gets smaller distances than Berman, the distances appear to be of the same order of magnitude. Individual objects show considerable differences. Parenago's distances, on the other hand, are systematically smaller than those of Berman.

We have mentioned the strong concentration of the planetaries to

the central bulge of the galaxy. On the assumption that the sizes of the planetaries are, on the average, everywhere the same throughout the galactic system, Minkowski has used the apparent sizes of the planetary nebulae to test various distance estimates. If the average size of the planetary nebulae between $+10^\circ$ and -10° of galactic latitude is plotted against galactic longitude, it is found that the resultant curve has a maximum at $l=+10^\circ$ in the zone of greatest obscuration (where all distant objects are hidden) and a minimum ($5.9''$ is the mean diameter) in the direction of the galactic bulge between 320° and 340° . If the distance of

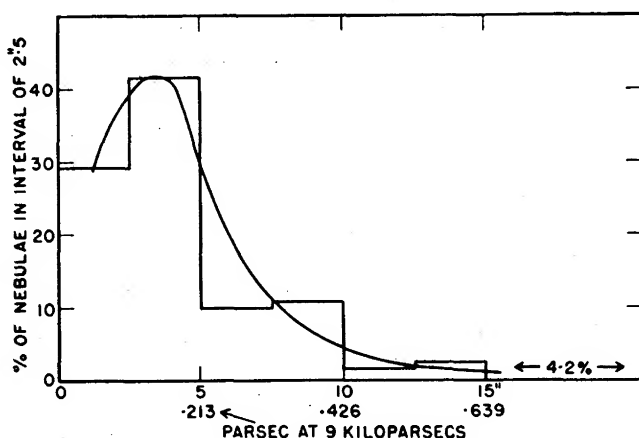


FIG. III : 3. *Size Distribution of Planetary Nebulae in the Central Bulge.*

(Courtesy, R. Minkowski, *Publ. Obs. Univ. Mich.*, 10, 31 (1951).)

the galactic centre is taken as 8500 parsecs (corresponding to a parallax of $0.00012''$), the ratio of angular diameter to parallax amounts to 5.0×10^4 . Now van Maanen obtained a parallax of $0.00096''$ from the τ components of proper motion for his nebulae which had a mean angular diameter of $53''$. The corresponding ratio is 5.5×10^4 , while Anderson, who selected a number of very large nebulae, obtained results which lead to a ratio of 10.2×10^4 . Berman's distance scale, which is ultimately based on the proper motions by van Maanen and Anderson, leads to one that is in harmony with the scale based on the nebular concentration at the galactic centre.

Minkowski finds that Berman has applied corrections for interstellar absorption that are too large for low galactic latitudes. That the planetaries studied by Berman are mostly in relatively "clear" regions in the Milky Way is confirmed also by studies of the Balmer decrement. Thus the objects in low galactic latitudes are larger and are at greater distances than Berman supposed. His distances for relatively faint nebulae are probably

too large. For objects far from the galactic plane, Berman's distances are statistically trustworthy. Parenago's distances appear to be systematically too small, and it would seem that he has over-corrected for space absorption.

Ultimately it should be possible to give mean absolute visual magnitudes for the planetaries in the central bulge. Several precautions are to be noted. First, the correction for space absorption must be determined from the Balmer decrement. Second, account must be taken of the level of excitation of the nebula. Our description is inadequate if we give the monochromatic magnitude of the nebula in the radiation of the $[OIII]$ emission, but do not give the relative intensities of the other lines and the correction for space absorption.

The association of planetary nebulae with Baade's Type II population is further illustrated by the object discovered in the globular cluster NGC 7078 by F. G. Pease.⁽²⁰⁾ Spectrograms secured by Minkowski show the characteristic emissions of a planetary nebula. The velocity of this object is the same as that of the cluster.⁽²¹⁾ The magnitude of this nebula may be measured by a judicious combination of photo-electric photometry (using the technique developed by Liller) and photographic photometry. Finally, it may be mentioned that the nucleus of the planetary NGC 246 has a companion whose spectrum indicates it to be a dwarf star of around F or G spectral class. Thus the spectroscopic parallax of at least one planetary nebula would appear to be determined, since the magnitude difference of the two stars has been measured photo-electrically by Liller and the writer.

3. The Dimensions and Forms of the Planetary Nebulae

When the distances of the planetaries have been established, their dimensions follow at once from their angular diameters. Anderson found the mean linear diameters of the ten largest planetaries studied by him to be 0.61 parsec. Minkowski has used the apparent sizes of the planetaries found in the central bulge to estimate the intrinsic size distribution in the planetary nebulae (see Fig. 3). The distribution has a maximum at about 0.14 parsec and falls off gradually for increasing sizes. Minkowski suggests that a distribution in sizes of this form results if, during the earlier stages of development, the observed size represents only the ionized portion of the expanding shell of gas and not the entire shell (see Chapter VII).

The assignment of dimensions to some planetary nebulae is no easy task when account is taken of their complexity. Detailed discussion of the forms of planetary nebulae with emphasis on quantitative results is given in Chapter VII, but we may mention here some of the earlier studies that form the background for the later theoretical investigations.

The variety and complexity of the forms exhibited by the planetary nebulae have attracted the attention of astronomers for many years. Although the best-known examples are large ring-shaped objects like NGC 6720, the Ring nebula in Lyra, the class includes small disk-structures like IC 418 (cf. Chapter VII, Section 2), stellar planetaries like IC 4634, and binuclear objects such as NGC 7026, which Keeler described as resembling "two sheaves of corn placed side by side"⁽²²⁾ (see Figs. 4, 5, and 6).

Careful drawings by Herschel, Lord Rosse, Lassell, Holden, and Schaeberle reveal the striking features of many of the planetaries. These early pictures exhibit a considerable subjective element, a factor that could be removed only by the application of the photographic plate to the problem.

Keeler's pioneer photographic work with the Crossley reflector was extended by H. D. Curtis's careful study of the forms of these subjects. He made careful drawings from his photographs of all the then-known planetaries north of 34° S.⁽²³⁾ Such a process was necessary to show the fine details, but scarcely could be expected to represent the great differences in brightness between the brighter and fainter parts of many planetaries. Although he found no central star in thirteen of seventy-eight planetaries, Curtis concluded that all planetaries had central stars; if they were not seen, it was because the nebular material was so bright as to obscure them.

Curtis classified the planetaries according to their ring and shell structures. He distinguished seven (not mutually exclusive) groups, including helical, annular, various kinds of disks, irregular or amorphous, and stellar objects. In agreement with the conclusions of earlier workers, Curtis concluded that the ring planetaries must be actually shell structures rather than rings. Such a shell, if homogeneous and transparent, should appear in projection as a disk with a brighter peripheral ring, and if d is the thickness of the shell expressed as a fraction of the outer radius, the brightest part of the ring will be $\sqrt{\frac{2}{d}-1}$ times as bright as the centre of the disk. Thus if the brightness of the centre of the disk is one-tenth that of the ring the thickness of the shell should be one-fifth that of the nebula. Definite discrepancies are found for the Ring nebula NGC 6720. Curtis found that the homogeneous ellipsoidal shell model would explain about twenty-five of the planetaries he observed, but failed for thirteen objects including such well-known nebulae as NGC 7662.

Curtis investigated the theoretical appearance of planetaries with various types of shells; he found the intensity curves graphically with the aid of small semi-transparent models suspended in a liquid of nearly the same

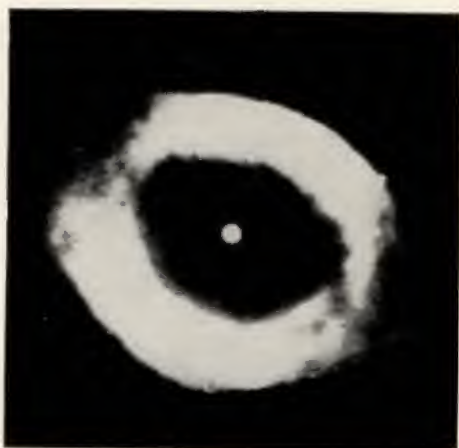
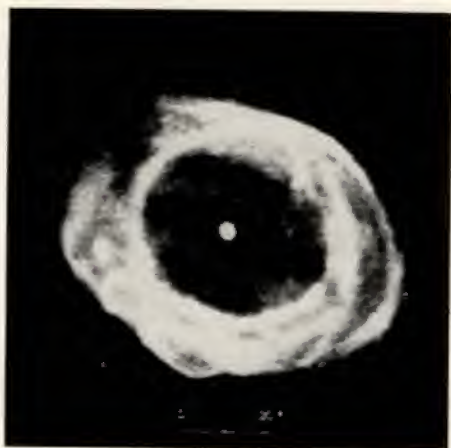


FIG. III : 4. *The Ring Nebula in Lyra.*

Right. Direct photograph secured with the Crossley reflector.

Left. Drawing based on exposures from 1^m to 2^h; the complex structural details are accentuated in the drawing. The outside dimensions of the nebula are about $83'' \times 59''$ in position angle 66° .

(Courtesy H. D. Curtis, *Publ. Lick Obs.*, 13, Fig. 46, Plate XVII (1919).)

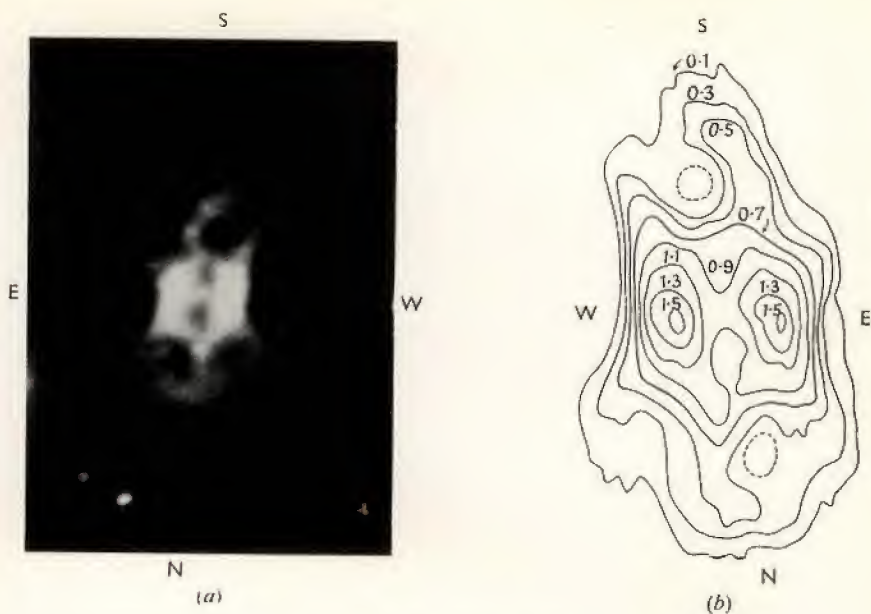


FIG. III : 6. *NGC 7026.*

(a) R. Minkowski obtained this photograph in the radiation of $H\alpha + [NII]$ with the 200-in. Hale telescope.

(b) The isophotic contours were derived from a graded series of exposures in steps of 0.1 in $\log I$. Notice the two centres of highest intensity and the symmetrically placed "arms" of this nebula. The scale of the isophotic contours is about twice that of the direct photograph. The orientation is indicated for each picture by the symbols, N, S, E, W.

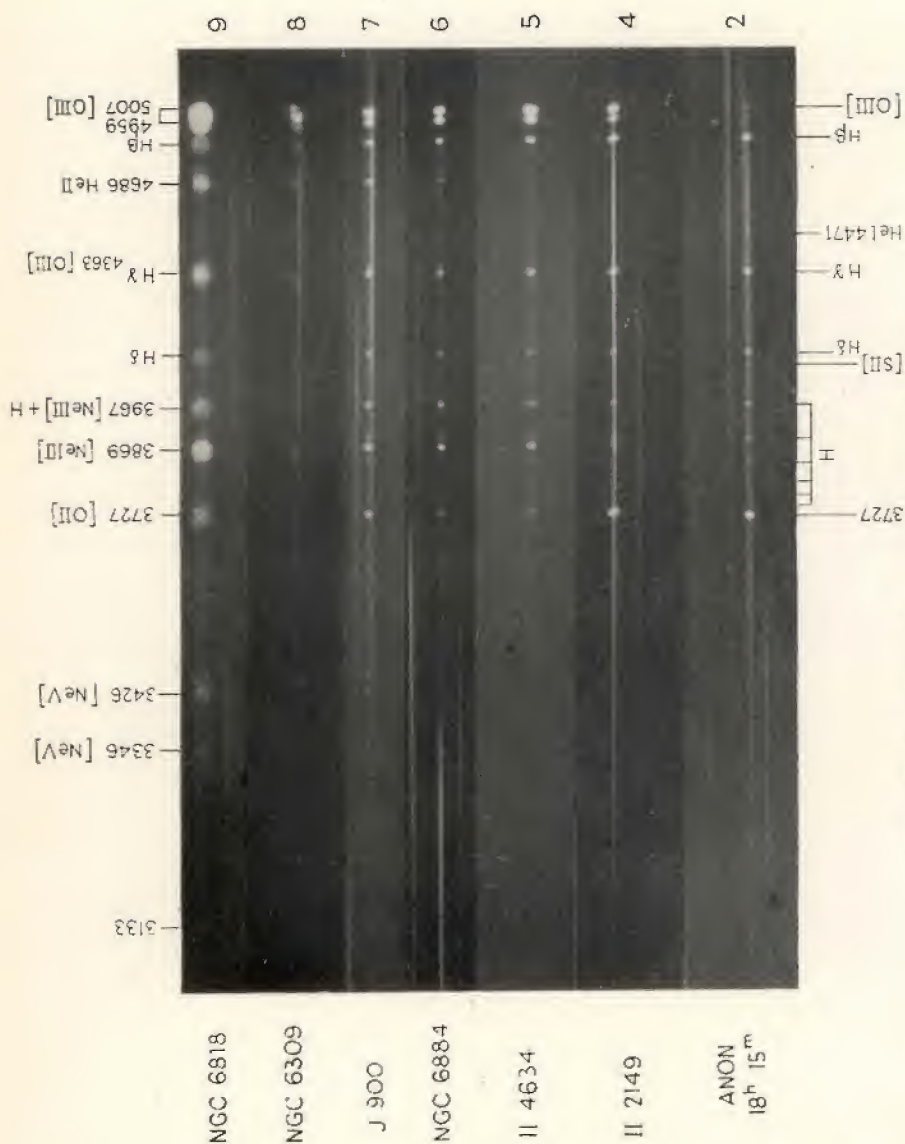


FIG. III : 7. *Slitless Spectra of Planetary Nebulae.*

The nebulae are grouped according to excitation class (*right*) following the scheme given in Table III : 2. Notice the progressive change in the intensity ratios (4959 + 5007)/H β , 3727/4949, 4686/H β , and 3426/H β from the low to the high excitation objects.

(Photographed with the 2-prism slitless spectrograph at the Crossley reflector of the Lick Observatory, 1944-5.)

refractive index and viewed by transmitted light. He found that a homogeneous oblate spheroidal shell much thinner in the equatorial zones than at the poles gave good agreement with many of the observed nebular forms. Small angles of inclination (0° – 30°) between the major axis and the line of sight appeared to represent nebulae that are fainter along the major axis, e.g. NGC 6818. Projections at angles 45° – 60° corresponded roughly to objects such as NGC 6853 or NGC 40. The truncated shell model explained other “regular” forms observed. The assumption of homogeneous shells, rings, and other structures is at best only a rough approximation and even if we ignore the “fine-structure” of the nebulae, it is not always possible to find a unique model that fits the observations.

In addition to the classification scheme proposed by Curtis, many others have been suggested. Some have been based on spectroscopic considerations. Others such as those of Stoy,⁽²⁴⁾ Vorontsov-Velyaminov,⁽²⁵⁾ or Thackeray and Evans⁽¹³⁾ are based on the geometrical forms. The photographs secured by Minkowski at Palomar show the complexities of most planetaries to be much greater than had been appreciated. We discuss his observations in Chapter VII and conclude this section with the theoretician’s planetary nebula. This mythological object (which is perhaps most closely approximated by IC 3568) consists of a hot central star surrounded by a spherical shell of radius large compared with that of the star. The shell is usually assumed to be thin compared with its radius, and often has a constant density. The complexities exhibited by most of the real nebulae are not amenable to theoretical discussion.

4. Spectroscopic and Spectrophotometric Studies of the Planetary Nebulae

Since 1864, when Huggins demonstrated the bright-line character of the spectra of the planetaries, investigations have been carried out by many observers, including Lockyer,⁽²⁶⁾ E. von Gothard,⁽²⁷⁾ Wolf,⁽²⁸⁾ and Campbell.⁽²⁹⁾ Extensive observations, with both slit and slitless spectrographs were carried out by W. H. Wright⁽³⁰⁾ at the Lick Observatory. He gave wavelength measures and intensity estimates of the nebular emission lines, discovered the Balmer recombination continuum, classified the nebulae according to their spectra, and described the distribution of the various radiations in the different parts of the planetaries. He found that $\lambda 4686$, *HeII*, tended to concentrate in the inner regions of the nebulae, whereas $\lambda 3727$, now known to be due to *[OII]*, was often concentrated in the outer regions and *ansae*. In fact, whenever size differences existed in the images, the $\lambda 3727$ image was always as large (and usually larger) than any other image while $\lambda 3426$ [*NeV*] was smaller than any other image. The green nebular *[OIII]* lines usually gave slightly larger images than did hydrogen, although in the low excitation nebula IC 418 they are smaller.

Certain emissions always seem to have about the same spatial distributions and relative intensities. Thus we may mention $\lambda 4959$ and $\lambda 5007$ [OIII], $\lambda 6548$ and $\lambda 6584$ [NII], $\lambda 3869$ and $\lambda 3967$ [NeIII], $\lambda 3726$ and $\lambda 3729$ (the 3727 pair of [OII]), $\lambda 3426$ and $\lambda 3346$ [NeV], and $\lambda 3313$, $\lambda 3342$, and $\lambda 3445$ of OIII. The identifications of the forbidden lines were made many years later, particularly by Bowen and by Swings and Edlén.

Later, Stoy⁽³¹⁾ observed a few of the fainter lines in the visual region ($\lambda 5400$ – $\lambda 7300$) in NGC 6572 and NGC 7027, but the most extensive study was that carried out by Bowen and Wyse at the Lick Observatory.⁽³²⁾ They employed Bowen's image slicer and carefully examined the spectra of NGC 6572, NGC 7027, and NGC 7662. As mentioned in Chapter II, with this device it is possible to secure widened spectra without drifting the telescope and thereby requiring a longer exposure. Also, since successive strips of the nebula are placed side by side, faint lines may be more easily distinguished from spurious ones than would be true for a narrow spectrum. They made exhaustive tests to find the photographic emulsions best suited for the long exposures on the nebula. The exposure times ranged from 15 minutes to 19 hours and 20 minutes in order to record both strong and weak lines with measurable intensity. They obtained both the wavelengths and rough estimates of the intensities of the nebular lines.

The levels of excitation of the three nebulae differ in an interesting fashion. In NGC 6572 Bowen and Wyse found no ions with ionization potentials greater than 65 e.v. In NGC 7027, lines of ions from neutral O to Ne^{++++} appear with high intensity. In NGC 7662 the high excitation lines are strong; those of low excitation are relatively weaker. Hence a great range of excitation appears to exist in NGC 7027.

Bowen and Wyse detected lines of a number of metals previously unobserved in gaseous nebulae, thus removing one of the conspicuous qualitative differences between the elements represented in nebulae and stars. Furthermore, when they took into account the mode of excitation of the various emissions in the gaseous nebulae, they found that quantitatively the composition of the planetary nebulae seemed to be about the same as that of the sun.

These investigations were continued by Wyse, who in his last paper,⁽³³⁾ published detailed results obtained for ten gaseous nebulae. This careful investigation, the most exhaustive study ever made of the spectra of representative planetary nebulae, provides a wealth of material for theoretical studies. Wyse was particularly interested in the chemical compositions of the nebulae and wanted to find whether NGC 7027 was typical in composition, whether there were important differences in the chemical compositions of the diffuse and planetary nebulae, and whether the planetaries exhibited

a nitrogen and a carbon sequence as do the classical Wolf-Rayet stars. He employed appropriate spectrographs on the 36-in. refractor of the Lick Observatory with an image slicer replacing the slit except for exposures on the Orion nebula. Exposures ranging from a few minutes to several nights' duration were required in order to compare the weak and the strong lines. Wyse estimated the intensities of the lines on his spectrograms with the aid of scale plates, obtained by photographing the spectrum of a helium discharge tube, the intensity of the source being varied from one exposure to the next. He compared his estimated intensities for NGC 7027 with Plaskett's value for the visual region and those obtained by the writer for the photographic region, in order to establish systematic corrections for the variation of plate sensitivity, instrumental absorption, and atmospheric extinction, and applied these systematic corrections to all the nebulae observed. Unfortunately, no attempt was made to allow for the variation of atmospheric extinction from one exposure of one object to another. This omission of extinction corrections may be important for some of the far southern objects.

Although the accidental errors in the eye estimates of the line intensities may be large in individual instances, the scale of the intensity system as checked by subsequent spectrophotometric work appears to be remarkably good. Wyse's exposures were limited by the intensity of the background nebular continuum. More recently, Bowen, by using higher dispersions at the Palomar coudé, has been able to suppress this continuum to the extent that he has been able to observe substantially fainter lines.

The list published by Wyse includes about 270 nebular (and sometimes perhaps nuclear) lines, only about a third of which were known before the beginnings of the investigation by Bowen and Wyse. The unidentified lines numbered about 40% of the total, although they contributed less than 5% of the energy. Wyse estimated the chemical composition of the planetaries and the Orion nebula to be about the same, and concluded their chemical compositions did not differ conspicuously from that of the sun.

Since the investigations of Wyse, spectroscopic studies of the planetaries in the infra-red have been made by Minkowski and the writer⁽³⁴⁾ and by Swings and Jose.⁽³⁵⁾ A very detailed study of the rich, bright-line spectrum of NGC 7027 has been carried out at Palomar and Mt. Wilson by Bowen, Minkowski, and the writer. Lines of the following ions appear: *H*, *HeI*, *HeII*, *CII*, *CIII*, *CIV*, *NI*, *NII*, *NIII*, *OI*, *OII*, *OIII*, *OIV*, *OV*, *FIV*, *NeIII*, *NeIV*, *NeV*, *MgI*, *SiII*, *SiIII*, *SI*, *SII*, *SIII*, *ClIII*, *ClIV*, *AlII*, *AIV*, *AV*, *KIV*, *KV*, *KVI*, *CaV*, *CaVII*, *MnV*, *MnVI*, *FeIII*, *FeV*, *FeVI*, and *FeVII*. We list the identifications and intensities (when measured or estimated) in Table III : 1.

TABLE III : 1

Spectrum of NGC 7027

(Based on observations of Bowen, Minkowski, and Aller; Mt. Wilson and Palomar, 1954)

λ	Element	Origin	<i>I</i>
3132.82	OIII	$3p^3S-3d^3P_2$	20:
3203.16	HeII	3^2D-5^2F	7:
3299.58	OIII	$3s^3P_0-3p^3S$	3.5
3312.35	OIII	$3s^3P_1-3p^3S$	11.3
3340.78	OIII	$3s^3P_2-3p^3S$	16.0
3345.82	[NeV]	$3^3P_1-1^1D$	24:
3386.03	—	—	0.5
3411.84	OIV	$3^2P_{3/2}-3^2D_{5/2}$	1.1
3414.76	—	—	0.8
3425.84	[NeV]	$3^3P_2-1^1D$	60:
3428.70	OIII	$3p^3P_1-3d^3P_2$	
3444.05	OIII	$3p^3P_2-3d^3P_2$	30:
3554.4	HeI	2^3P-10^3D	0.3
3587.05	HeI	2^3P-9^3D	0.8
3634.20	HeI	2^3P-8^3D	0.8
3666.00	H I	2^2P-27^2D	—
3667.68	H I	2^2P-26^2D	—
3669.47	H I	2^2P-25^2D	—
3671.48	H I	2^2P-24^2D	0.6
3673.70	H I	2^2P-23^2D	0.8
3676.31	H I	2^2P-22^2D	0.9
3679.39	H I	2^2P-21^2D	0.9
3682.81	H I	2^2P-20^2D	1.0
3686.88	H I	2^2P-19^2D	1.1
3691.53	H I	2^2P-18^2D	1.3
3697.21	H I	2^2P-17^2D	1.4
3703.81	H I	2^2P-16^2D	1.7:
3705.04	HeI	2^3P-7^3D	0.7:
3711.95	H I	2^2P-15^2D	1.8
3715.27	HeII	4^2F-29^2G	0.7
3721.81	H I	2^2P-14^2D	4.3
	[SIII]	$3^3P_1-1^1S$	
3725.99	[OII]	$4^4S-2^2D_{3/2}$	9.4
3728.76	[OII]	$4^4S-2^2D_{5/2}$	4.6
3732.97	HeII	4^2F-26^2G	0.7
3734.34	H I	2^2P-13^2D	2.3
3736.70	OIV	$3p^4D_{7/2}-3d^4F_{9/2}$	0.9
3740.16	HeII	4^2F-25^2G	0.6
3748.77	HeII	4^2F-24^2G	0.6
3750.19	H I	2^2P-12^2D	2.7
3754.69	OIII	$3s^3P_1-3p^3D_2$	1.4
3757.24	OIII	$3s^3P_0-3p^3D_1$	0.8
3759.87	OIII	$3s^3P_2-3p^3D_3$	3.8
3768.86	HeII	4^2F-22^2G	0.7
3770.66	H I	2^2P-11^2D	3.3
3773.95	OIII	$3s^3P_1-3p^3D_1$	0.7
3781.74	HeII	4^2F-21^2G	0.8
3791.29	OIII	$3s^3P_2-3p^3D_2$	0.7
3797.91	H I	2^2P-10^2D	3.5

2.4*

TABLE III : 1—*contd.*

λ	Element	Origin	I
3813.50	HeII	4^2F-19^2G	0.7
3819.66	HeI	2^3P-6^3D	1.1
3833.75	HeII	4^2F-18^2G	0.6:
3835.41	HI	2^2P-9^2D	4.6 } 7.6*
3856.17	SiII	$3p^2\ 2D_{5/2}-4^2P_{3/2}$	0.3
3857.99	HeII	4^2F-17^2G	0.8
3862.67	SiII	$3p^2\ 2D_{3/2}-4^2P_{1/2}$	0.3
3868.73	[NeIII]	$3P_2-1D$	51
3888.91	HI	2^2P-8^2D	8.5
	HeI	2^3S-3^3P	0.3 } 8.8*
3891.28	[FeV]	$^5D_4-^3F_4$	0.4
3895.61	[FeV]	$^5D_3-^3P_2$	0.4
3923.56	HeII	4^2F-15^2G	0.6
3926.50	HeI	2^1P-8^1D	0.4
3956.82	—	—	0.2
3964.88	HeI	2^1S-4^1P	—
3967.46	[NeIII]	$^3P_1-1D$	} 24.4
3970.06	HI	2^2P-7^2D	
3997.36	[FIV]	$^3P_1-1D$	0.2
4009.17	HeI	2^1P-7^1D	0.4
4026.12	HeI	2^3P-5^3D	2.0
4060.26	[FIV]	$^3P_2-1D$	0.3
4068.62	[SII]	$^4S-2P_{3/2}$	4.5 } 4.9*
4070.27	CIII	$4^3F_4-5^3G_5$	0.4
	[FeIII]	$^5D_4-^3G_5$	
4072.14	[FeV]	$^5D_2-^3P_1$	0.3
4076.33	[SII]	$^4S-2P_{1/2}$	2.2
4097.37	NIII	$3^2S-3^2P_{3/2}$	2.0
4100.08	HeII	4^2F-12^2G	—
4101.74	HI	2^2P-6^2D	} 16.3
4103.46	NIII	$3^2S-3^2P_{1/2}$	
4120.80	HeI	2^3P-5^3S	0.3
4122.60	[KV]	$^4S-2D_{5/2}$	0.2
4128.74	—	—	0.3
4143.76	HeI	2^1P-6^1D	0.5
4156.35	CIII	$3^3D_2-5^3F_3$	0.4
4163.33	[KV]	$^4S-2D_{3/2}$	0.3
4180.92	[FeV]	$^5D_1-^3P_0$	0.2
4186.98	CIII	4^1F-5^1G	0.5
4199.88	HeII	4^2F-11^2G	1.5
4227.39	—	—	0.5
4267.13	CII	3^2D-4^2F	0.9
4338.62	HeII	4^2F-10^2G	} 33
4340.44	HI	2^2P-5^2D	
4363.19	[OIII]	^1D-1S	21
4379.07	NIII	4^2F-5^2G	0.5
4387.97	HeI	2^1P-5^1D	1.7
4471.50	HeI	2^3P-4^3D	3.9
4510.79	[KIV]	^1D-1S	0.7:
4541.60	HeII	4^2F-9^2G	2.3
4552	SiIII	$4^3S-4^3P_2$	0.4
4571.24	MgI	$3^1S-3^3P_1$	0.9
4606.51	[FeIII]	$^5D_4-^3F_3$	0.5
4625.54	[AV]	^1D-1S	0.5†

TABLE III : 1—continued

λ	Element	Origin	I
4631.96	—	—	—
4634.15	NIII	$3^2P_{1/2}-3^2D_{3/2}$	2.8
4640.62	NIII	$3^2P_{3/2}-3^2D_{5/2}$	3.6:
4641.93	NIII	$3^2P_{3/2}-3^2D_{3/2}$	0.6:
4647.46	CIII	$3^3S-3^3P_2$	1.4:
4649.08	OII	$3s^4P_{5/2}-3p^4D_{7/2}$	0.4:
4650.27	CIII	$3^3S-3^3P_1$	0.6
4657.68	—	—	—
4658.42	CIV	5^2G-6^2H	—
	[FeIII]	$5D_4-3F_4$	1.6
4685.71	HeII	3^2D-4^2F	45
4701.45	[FeIII]	$5D_3-3F_3$	—
4711.34	[AlIV]	$4S-2D_{5/2}$	2.8
4713.17	HeI	2^3P-4^3S	0.7
4714.26	[NeIV]	$2D_{5/2}-2P_{3/2}$	0.8
4715.65	[NeIV]	$2D_{5/2}-2P_{1/2}$	0.5
4724.16	[NeIV]	$2D_{3/2}-2P_{3/2}$	1.3
4725.60	[NeIV]	$2D_{3/2}-2P_{1/2}$	1.3
4733.68	[FeIII]	$5D_2-3F_2$	—
4740.20	[AlIV]	$4S-2D_{3/2}$	11
4754.9	[FeIII]	$5D_3-3F_4$	0.4
4859.32	HeII	4^2F-8^2G	—
4861.30	HI	2^2P-4^2D	100
4893.42	[FeVII]	$3F_2-3P_1$	0.6
4921.96	HeI	2^1P-4^1D	3.1
4930.97	[OIII]	$3P_0-1D$	< 0.5:
4944.01	[FeVII]	$3F_3-3P_2$	—
4950.48	—	—	—
4958.95	[OIII]	$3P_1-1D$	420
4972.12	[FeVI]	$4F_{5/2}-2G_{7/2}$	—
5006.88	[OIII]	$3P_2-1D$	1170
5015.55	HeI	2^1S-3^1P	—
5041.31	SiII	$4^2P_{1/2}-4^2D_{3/2}$	1.6:
5047.92	HeI	2^1P-4^1S	1.4:
5056.45	SiII	$4^2P_{3/2}-4^2D_{5/2}$	1.5:*
5090	—	—	0.5
5112	OV	3^1S-3^1P	0.5
5131.18	—	—	0.6
5145.78	[FeVI]	$4F_{7/2}-2G_{7/2}$	0.9
5158.94	[FeVII]	$3F_3-3P_1$	—
5161.67	—	—	0.6
5176.42	[FeVI]	$4F_{9/2}-2G_{9/2}$	0.9
5191.81	[AlIII]	$1D-1S$	0.9:
5197.95	[NI]	$4S-2D_{3/2}$	1.2:
5200.41	[NI]	$4S-2D_{5/2}$	0.3:
5216	—	—	0.5
5232	—	—	0.4
5262.00	—	—	—
5270.28	[FeIII]	$5D_3-3P_2$	0.3:
5277.76	[FeVII]	$3F_4-3P_2$	0.3:
5309.17	[CoV]	$3P_2-1D$	1.7
5323.26	[ClIV]	$1D-1S$	1.0
5335.22	[FeVI]	$4F_{3/2}-4P_{1/2}$	1.2
5345.98	—	—	1.2

TABLE III: 1—continued

λ	Element	Origin	I
5411.54	HeII	4^2F-7^2G	9
5423.87	[FeVI]	$4^4F_{5/2}-4^4P_{3/2}$	0.4:
5426.57	[FeVI]	$4^4F_{7/2}-4^4P_{5/2}$	0.2:
5470.93	—	—	0.4:
5484.79	[FeVII]	$4^4F_{5/2}-4^4P_{1/2}$	0.5:
5517.72	[CIII]	$4^4S-2^4D_{5/2}$	1.0
5537.80	[CIII]	$4^4S-2^4D_{3/2}$	2.7
5577.36	[OI]	1^1D-1^1S	1.5
5592.17	OIII	$3s^1P-3p^1P$	1.1
5604	[KVI]	$3^3P_1-1^1D$	0.6
5614.65	[CaVII]	$3^3P_2-1^1D$	—
5630.88	[FeVI]	$4^4F_{7/2}-4^4P_{3/2}$	0.7
5677.01	[FeVI]	$4^4F_{9/2}-4^4P_{5/2}$	1.1
5696.06	CIII	3^1P-3^1D	—
5721.13	[FeVII]	$3^3F_2-1^1D$	1.2
5726.12	—	—	—
5754.59	[NII]	1^1D-1^1S	12
5776.37	[MnVI]	$3^3F_3-3^3P_1$	—
5786.59	HeII	5^2G-40^2H	—
5790.85	HeII	5^2G-39^2H	—
5794.64	HeII	5^2G-38^2H	—
5801.38	CIV	$3^2S-3^2P_{3/2}$	2.2
5806.29	HeII	5^2G-36^2H	—
5812.12	CIV	$3^2S-3^2P_{1/2}$	1.1
5820.14	HeII	5^2G-34^2H	—
5828.64	HeII	5^2G-33^2H	—
5836.50	HeII	5^2G-32^2H	0.3:
5847.14	HeII	5^2G-31^2H	—
5858.33	HeII	5^2G-30^2H	—
5862.34	[MnV]	$4^4F_{7/2}-2^4G_{7/2}$	—
5864.81			
5867.82	HeII	5^2G-29^2H	—
5875.63	HeI	2^3P-3^3D	24
5882.35	HeII	5^2G-28^2H	—
5885.90	—	—	—
5890.98	[MnV]	$4^4F_{9/2}-2^4G_{9/2}$	—
5894.01	[MnVI]	$3^3F_4-3^3P_2$	—
5896.87	HeII	5^2G-27^2H	—
5913.52	HeII	5^2G-26^2H	—
5932.22	HeII	5^2G-25^2H	0.8
5953.00	HeII	5^2G-24^2H	0.9
5977.05	HeII	5^2G-23^2H	0.7
6004.81	HeII	5^2G-22^2H	1.2
6037.16	HeII	5^2G-21^2H	1.1
6074.30	HeII	5^2G-20^2H	1.1†
6086.88	[CaV]	$3^3P_1-1^1D$	2.5
	[FeVII]	$3^3F_3-1^1D$	
6101.76	[KIV]	$3^3P_2-1^1D$	2.5
6118.31	HeII	5^2G-19^2H	1.1†
6151.43	—	—	—
6166.22	[MnV]	$4^4F_{7/2}-4^4P_{5/2}$	0.3
6170.73	HeII	5^2G-18^2H	1.1
6218.64	[MnV]	$4^4F_{5/2}-4^4P_{1/2}$	—
6221.04			

TABLE III : 1—continued

λ	Element	Origin	I
6228.41	[KVI]	$3P_2-1D$	—
6233.80	HeII	5^2G-17^2H	0.9*
6300.31	[OI]	$3P_2-1D$	20
6312.10	[SIII]	$1D-1S$	16
6347.54	SiII	$4^2S-4^2P_{3/2}$	—
6363.82	[OI]	$3P_1-1D$	10
6371.34	SiII	$4^2S-4^2P_{1/2}$	0.3*
6393.62	[MnV]	$4^4F_{9/2}-4^4P_{5/2}$	—
6406.53	HeII	5^2G-15^2H	0.8
6435.11	[AV]	$3P_1-1D$	5.2
6518.34	[MnVI]	$3F_2-1D$	—
6527.31	HeII	5^2G-14^2H	0.8:†
6548.09	[NII]	$3P_1-1D$	80
6560.24	HeII	4^2F-6^2G	—
6562.90	HI	2^2P-3^2D	650
6583.36	[NII]	$3P_2-1D$	240
6598.76	[FeVII]	$3F_4-1D$	—
6678.16	HeI	2^1P-3^1D	10
6716.52	[SII]	$4^4S-2^4D_{5/2}$	5.4
6730.74	[SII]	$4^4S-2^4D_{3/2}$	7.5
6890.80	HeII	5^2G-12^2H	2.1
7005.67	[AV]	$3P_2-1D$	14
7065.31	HeI	2^3P-3^3S	20
7135.78	[AIII]	$3P_2-1D$	56
7170.62	[AIV]	$2^4D_{3/2}-2^4P_{3/2}$	3:
7177.77	HeII	5^2G-11^2H	2:
7237.26	[AIV]	$2^4D_{5/2}-2^4P_{3/2}$	2.6
7262.77	[AIV]	$2^4D_{3/2}-2^4P_{1/2}$	3.1
7281.32	HeI	2^1P-3^1S	2.8†
7319.92	[OII]	$2^4D_{3/2}-2^4P$	} 77
7330.19	[OII]	$2^4D_{3/2}-2^4P$	
7530.54	[CIV]	$3P_1-1D$	1.4
7592.79	HeII	5^2G-10^2H	>1.2§
7726.51	[SI]	$1D-1S$	—
7751.04	[AIII]	$3P_1-1D$	20
8045.58	[CIV]	$3P_2-1D$	5.3
8196.61	—	—	2.0
8236.64	HeII	5^2G-9^2H	5.2
8502.5	HI	3^2D-16^2F	0.6
8545.53	HI	3^2D-15^2F	0.8
8598.35	HI	3^2D-14^2F	2.6
8665.0	HI	3^2D-13^2F	2.7
8750.5	HI	3^2D-12^2F	3.1
8862.8	HI	3^2D-11^2F	3.5
9014.9	HI	3^2D-10^2F	5.5
9069	[SIII]	$3P^1-1D_2$	40:

NOTES TO TABLE III : 1

* When the lines are not resolved on the tracings of high dispersion plates, the allocation of relative intensities is very rough.

† Intensity interpolated from tracing of high dispersion plate.

‡ Intensity of 6548.09 estimated by comparison with 6583.26 on the basis of theoretical A-values.

§ In atmospheric absorption band.

These intensities are uncorrected for space absorption. In order to allow for the effects of interstellar extinction the following corrections have been deduced from a comparison of observed and predicted Balmer decrements (cf. Chapter 4).

Correction $\Delta \log I$ to be added to the logarithms of the line intensities to allow for space absorption.

$\lambda 3200$	+0.53	$\lambda 4000$	+0.27	$\lambda 4800$	+0.02	$\lambda 5400$	-0.13	$\lambda 6500$	-0.37
3400	+0.45	4200	+0.20	4861	0.00	5600	-0.17	7000	-0.47
3600	+0.39	4400	+0.14	5000	-0.04	5800	-0.21	7500	-0.57
3800	+0.33	4600	+0.08	5200	-0.08	6000	-0.26	8000	-0.66

These corrections should be applied to the observed line intensities when they are used, for example, for theoretical discussions.

Attempts to classify the gaseous nebulae, particularly the planetaries, on the basis of their spectra have been attempted by a number of workers. The earliest classification was that proposed by Miss Cannon in the Henry Draper catalogue.⁽³⁶⁾ She used the 4686 line as her principal criterion and since this line is conspicuous in class O stars, she placed spectra in which this line was strong in the later divisions near class O. She employed low dispersion, small-scale spectra. The Lick work showed this classification to be inadequate.⁽³⁰⁾ Later, Miss Payne regarded the O stars and nebulae as constituting parallel sequences and arranged the nebulae in a sequence from P1, characterized by a strong 4686, e.g. NGC 2440, to P10, characterized by a continuous spectrum of reflected starlight.⁽³⁷⁾ Her classification runs in the same order as that suggested by Bowen.⁽³⁸⁾

Page⁽³⁹⁾ has classified the spectra of the planetary nebulae according to their excitation on a scale from 1 to 8. For low excitations he used the ratio $\lambda 3727$ [OII] 4959 [OIII], and for high excitations the ratio 4686 (HeII)/ $H\beta$. Extended objects of low surface brightness present a special problem. They often show strong $\lambda 4686$ simultaneously with strong [OII]. Whenever this is the case, the [OII] usually is concentrated in the outer regions of the nebula and 4686 in the inner regions. For such objects Page selected the $\lambda 4686/H\beta$ criterion and added the designation "pec" to the excitation class.

Since photometric measures of the line intensities are now available for many planetary nebulae, a somewhat more refined classification scheme is practicable. In the lowest excitation nebulae, the $(N_1 + N_2)/H\beta$ ratio may be used to supplement the $(3727)/(N_1 + N_2)$ ratio. To differentiate between nebulae of the highest excitation the [NeV]/ $H\beta$ ratio or the [NeV]/[NeIII] ratio is useful. The application of these various criteria to a group of nebulae of different excitation is illustrated in Table III:2. Our proposed system of classification differs from that of Page in that ten classes are employed and different quantitative criteria are used. Excitation class 1 is reserved for these nebulae that do not show the [OIII] lines. If $\lambda 4686$ is

not present the nebula is to be placed in classes 1–5, depending on the $3727/4959$ or $(5007+4959)/4861$ ratio. Class 6 refers to objects that show $\lambda 4686$ but not $[\text{NeV}]$. If $[\text{NeV}]$ is present, we use the ratios $[\text{NeV}]/H\beta$ and $[\text{NeV}]/3869$, which are more sensitive than the $4686/H\beta$ criterion.

TABLE III : 2

Classification of Planetary Nebulae on Basis of Excitation Level of Spectrum

CRITERION	Anon 18 ^h 15 ^m	IC 418	IC 2149	IC 4634	NGC 7026	J 900	NGC 6309	IC 2165	Anon 21 ^h 31 ^m
$(N_1+N_2)/H\beta$	0.21	1.9	5.5	10.6	12.4	16.7	14.1	18.1	10.4
$3727/4959$	32	3.1	0.20	0.03	0.04	0.03	0.03	0.02	0.04
$4686/H\beta$	—	—	—	—	00.13	0.47	0.77	0.6	0.9
$[\text{NeV}]/H\beta$	—	—	—	—	—	0.28	0.5	0.8	2.4
$[\text{NeV}]/3869$	—	—	—	—	—	0.38	0.5	0.95	3.8
Excitation class	2	3	4	5	6	7	8	9	10

The spectral characteristics of planetary nebulae of low surface brightness have been studied particularly by R. Minkowski,⁽⁴⁰⁾ who used a slit spectrograph with a dispersion of 500 Å./mm. at $H\gamma$ and estimated the line intensities by comparing the spectra of these objects with nebulae in which the relative line intensities had been measured. In a number of nebulae the Balmer decrement (relative intensities of the Balmer lines) was very steep because of space reddening; the most strongly affected objects being planetaries of moderate intrinsic surface brightness. The objects with the lowest surface brightnesses seem to be large, relatively near by, intrinsically faint planetaries. Minkowski found a number of striking differences between the spectra of planetaries of low and of high surface brightness. The faint nebulae often show spectra in which $\lambda 3727$ is stronger than $H\beta$ and $\lambda 4686$ of HeII is prominent, a phenomena which is rather rare among nebulae of high surface brightness. If the seventy-one nebulae for which good spectroscopic data are available are grouped according to surface brightness as follows: (I) Curtis relative exposure $e \leq 1$; (II) $1 < e \leq 15$; and (III) $e < 15$; only 6 and 12% of the nebulae in group I show strong $\lambda 3727$ and $\lambda 4686$, respectively, while 11 and 26% of those in group II and 42 and 26% of those in group III show these lines with prominence. The temperatures of the nuclear stars, as computed by the Zanstra theory (cf. Chapter VI), are higher for the nebulae of low surface brightness showing strong $\lambda 3727$ than they are for those objects which show strong $\lambda 4686$. Minkowski explains this anomalous result by suggesting that in these objects the nebular shells are probably thin and the absorption of the nuclear radiation is incomplete so that the conditions of Zanstra's theory are not

fulfilled. Furthermore, in the planetaries in which $\lambda 4686$ is strong, this line extends through the nebula just as the hydrogen lines do. Probably the temperatures of the nuclei showing $\lambda 4686$ are really very high. In Chapter VII we consider the problem of stratification in nebulae and discuss some of these matters in more detail.

Studies of additional nebulae of low surface brightness have been made by the writer on slit spectrograms made available to him by N. U. Mayall of the Lick Observatory.⁽⁴¹⁾ The spectra of planetaries of similar appearance often closely resemble one another. Thus the irregular disk objects NGC 6772, 7139, and 7048 show similar spectra with a $\lambda 4686$ line of moderate intensity confined to the central regions and an intense $\lambda 3727$ [OII] in the outer strata. The spectra of the two diffuse appearing, low excitation, irregular nebulae NGC 7635 and IC 1470 resemble that of the small bright planetary IC 418, i.e. strong $\lambda 3727$, prominent Balmer series, and moderately strong green nebular lines. They closely approach the level of excitation of certain of the diffuse galactic nebulae in our own and other galaxies. In structure, surface brightness, and spectra, NGC 7635 and IC 1470 simulate the diffuse galactic nebulae.

In addition to the descriptive studies of the nebular spectra which catalogue the observed emission lines it is necessary to have quantitative measures of the intensities of the observed emission lines. As mentioned in Chapter II, the description of the intensity of an emission line in a gaseous nebula is not necessarily simple. One should specify the surface brightness in $\text{ergs/cm}^2/\text{sec.}$ at a fixed point in the monochromatic nebular image, and give the isophotic contour of the image. Such detailed information is rarely available. Usually our data consist of measurements of the relative intensities of the nebular lines (referred to $H\beta$ as 10, for example). Sometimes the relative intensities are measured on slitless spectrograms or objective prism plates, and refer to intensities integrated over the entire nebular image. Other studies may involve slit spectrograms and give the relative intensities at some fixed point in the nebular image.

The general spectrophotometric procedures have been described in Chapter II, and we shall give here a description of some of the studies that have been made for the planetary nebulae. The earliest spectrophotometric work was done visually. Photographic spectrophotometry was undertaken by L. Berman⁽⁴²⁾ at the Lick Observatory and by H. H. Plaskett at Victoria.⁽⁴³⁾ Plaskett employed a wedge method of photometry with a calibrated carbon arc as a "standard lamp" to measure the intensities of a few of the brighter lines between $H\alpha$ and $\lambda 4000$ in six planetaries. Berman measured the isophotal contours and relative integrated brightnesses of monochromatic nebular images registered on slitless spectrograms obtained with the quartz spectrograph at the Crossley reflector. He

standardized his plates with a spot sensitometer. To correct for the wavelength variation of plate sensitivity, spectrographic transmission, etc., Berman compared the energy distribution in the sun with that of 16 Pegasi and used the standard star merely as an intermediary in reducing the nebular intensities. His paper gives the relative intensities of the strongest lines for the five nebulae NGC 6543, 6826, 6572, 7009, and 7027. These data were supplemented later by observations of other nebulae.

One of the most extensive spectrophotometric programmes on the planetary nebulae was that carried out at the McDonald Observatory by Thornton Page,⁽³⁹⁾ who secured some two hundred calibrated spectra of fifty-eight planetaries with the Cassegrain spectrograph at the 82-in. reflector. He employed an *f*1 Schmidt camera and quartz spectrograph, giving a dispersion of 360 Å./mm. at *H*δ and also an *f*2 camera of twice this dispersion; his spectra extended, in good definition to λ3100 Å. Page observed with a wide slit, equivalent to about 50 Å. on the plate, thereby combining to some extent the advantages of the slit and slitless spectrograph. The overlapping of lines was somewhat reduced. Photometric calibration was provided by a wedge and rotating sectors, while for comparison stars he used the objects observed in the spectrophotometric programme of Barbier and Chalonge.⁽⁴⁴⁾ Page photographed these standard stars at the same altitudes as the nebulae so as to reduce errors arising from atmospheric reddening to a second-order effect. Since the stars were very much brighter than the nebulae, he employed a Lucite plate over the slit as a diffusing screen and ran the star out of focus on the slit.

Page was primarily concerned with the continuous spectra of the planetaries (see p. 71). His plates, however, should also be useful for the measurement of the intensities of the stronger lines.

Some years ago the present writer, then at the University of California, made a spectrophotometric study of forty-four planetary nebulae with the Crossley reflector.⁽⁴⁵⁾ These data supplemented an earlier study (1938-9) of eleven planetaries which included objects of low excitation such as NGC 40 or IC 418, objects of intermediate excitation such as NGC 6826 or NGC 6543, objects of high excitation such as NGC 7662, and also stellar planetaries such as IC 4997. The earlier programme involved the determination of the relative total intensities of the nebular lines. In the second series, relative total intensities were given only for the stellar planetaries. For the other objects, the intensities measured at a particular point (or sometimes two or more points in the nebula) are usually tabulated. A spot sensitometer and filters plus widened exposures on a suitable comparison star with the mirror diaphragmed provided the photometric calibration.

In the 1943-5 programme emphasis was first placed on the nebulae studied by Wyse: NGC 2165, 2440, 6741, and IC 5217 (which had not been observed in the earlier study) in order to provide data on the line intensities in the ultra-violet. Secondly, there were added a number of objects of moderate surface brightness that show interesting structural details. Finally, the programme included a number of stellar nebulae of interest because of their high surface brightnesses, central stars, and the problem of the Balmer decrement. Of the fifty-five planetaries included in the entire study, thirty-seven have also been observed by Page, five by Minkowski, and a few have also been observed by Stoy.

These Lick programmes give the most extensive available spectrophotometric data on the brighter lines in the planetaries. The weaker lines are measured with much greater difficulty, and often appear to have been estimated too weak on slitless spectrograms because of the difficulty in estimating the continuous background. In particular, the intensities of the weak lines are all too small in the 1938-9 series. At the other extreme, the measurement of the relative intensities of the green nebular lines is often difficult because they are so very bright. Measurements of the fainter planetaries with a slitless spectrograph is troublesome because of the effects of the background sky fog which does not have the same colour as the spectral line under consideration.

Andrillat⁽⁴⁶⁾ has measured the relative intensities of $N_1 + N_2$ and $\lambda 4363$ in a number of planetaries in order to estimate electron temperatures. He does not give the details of his observations, so it is not possible to make a critical comparison with the results of other observers. The published electron temperatures indicate a somewhat lower $(N_1 + N_2)/4363$ ratio than that found by other observers for many planetaries.

Photo-electric measures of the relative intensities of some of the stronger lines in the brighter planetary nebulae have been undertaken by several observers (see Section 9 of Chapter II). These observations of the $(N_1 + N_2)/H\beta$ intensity ratio are in excellent agreement with one another and substantiate the photographic measures published by the writer. Except for NGC 6818 and 1535, for which the photographic results were based on a single plate apiece, the average error of the published $(N_1 + N_2)/H\beta$ intensity ratios is about 12%.

For theoretical studies of radiative and collisional processes in gaseous nebulae it is necessary to have photometric data on the weaker as well as on the stronger lines. The intensities of the weaker lines can be measured only with the aid of slit spectrographs equipped with fast cameras. It is desirable to set the slit on a pre-assigned position in the nebula and keep it there with the aid of a guide-star arrangement.

With the aid of Cassegrain spectrographs at the 60-in. and 100-in.

telescopes of the Mt. Wilson Observatory, Minkowski and the writer observed a number of the brighter planetaries. The programme included the double-ring nebula NGC 7662, the complex-ring planetary NGC 2392, and the ring structures NGC 2022 and 1535. All of these objects are high excitation nebulae. To the list was added NGC 40, one of the lowest excitation planetaries. Miscellaneous observations of a number of other planetaries were also made. The calibration system of the 100-in. coudé spectrograph provided the relation between blackening of the emulsion and light intensity as a function of wavelength. Vega, ϵ Persei, and η Ursae Majoris, chosen from the spectrophotometric programmes of R. C. Williams,⁽⁴⁷⁾ Kienle and his associates,⁽⁴⁸⁾ and Barbier and Chalonge⁽⁴⁴⁾ served as comparison stars.

The spectral range covered was from the Balmer limit to about 48800 (the limit of sensitivity of the Eastman spectroscopic *I-N* emulsion). The spectrum of NGC 7027 was investigated in the same way by Bowen, Minkowski, and the writer, but the Mt. Wilson observations were supplemented by higher dispersion plates secured at Palomar.

Exposures ranging from a few seconds to 8 hours were required in order to compare lines of different intensity. A glance at Table III : 1, which gives the preliminary results for NGC 7027, will show the very great intensity range involved.

Relative intensities have been measured at two points in NGC 7027 and small differences are found. In NGC 1535, 2022, 2392, and 7662 it is necessary to place the nebular image in the slit so as to avoid light from the central star. Measurements in these objects are therefore confined to selected points in the bright inner and fainter outer rings. The difference in excitation between the inner and outer rings are clearly exhibited by the measured intensities.

A comparison of the photometrically determined intensities and Wyse's scale plate estimates shows that the scale of the Wyse system of intensities agrees with that found by Bowen, Minkowski, and the writer, although there appears to be a zero-point error in the visual region where Wyse's zero-point was set by comparison with the Plaskett intensities. The Palomar plates add many lines that were not seen on the earlier spectrograms. Recent photo-electric spectrophotometric measures by Code and Whitford at Mt. Wilson show an excellent agreement with the line intensities measured by Bowen, Minkowski, and the writer.

The number of lines photographed in any nebula depends very critically upon its surface brightness. Weaker lines are observable only in the brighter objects. In the fainter ones the lines become lost against the background of the night sky. Thus, relatively few lines could be measured in NGC 40 in spite of the long exposures employed.

Measurements of the continuous spectra of the planetary nebulae as well as of the emission-line spectra are of great interest. Unlike the line emission whose origin appears to be well established, the background continuum of the planetaries is not completely understood. The continuum at the head of the Balmer series, produced by the recapture of free electrons in the second level (cf. Section 5), is prominent in many nebulae. Measures of the intensity of a 20 Å. interval of this Balmer continuum (with the contribution of the underlying continuum subtracted off) have been made by the writer for thirty planetaries.

The most extensive study of the continuous spectra of the planetary nebulae is due to Page, who has published measurements of the intensity of this continuum in terms of that of $H\delta$. He finds that on the average the nebulae of lower excitation have a stronger Balmer continuum (with respect to $H\delta$) than do the nebulae of high excitation. The general underlying continuous emission also appears to be weaker in nebulae of high excitation than in those of low excitation. If the electron temperature is taken in the neighbourhood of $10,000^\circ\text{K.}$, he found indications that the continuous Balmer emission was weaker than indicated by the theoretical calculations made by Cillie,⁽⁴⁹⁾ based upon the hypothesis of a pure recombination spectrum with complete self-reversal of the Lyman lines. More recent work suggests that the intensity of the Balmer continuum is greater than Page or the writer found it to be. Page also measured the energy distribution in the Balmer continuum. If it is assumed that the underlying continuum has a constant intensity distribution with wavelength, the electron temperature may then be estimated. He found values in fair agreement with those suggested by Menzel, Hebb, and the writer,⁽⁵⁰⁾ but in view of the theoretical uncertainties involved no emphasis can be placed on the agreement.

The general continuous spectrum of the planetary nebulae, which Page refers to as the visual continuum, has an integrated strength in the region $\lambda 4400$ to $\lambda 5000$ comparable with that of $H\delta$. Page estimated that throughout the whole spectrum its intensity might be comparable with that of all the hydrogen lines. Some of it is certainly due to the smeared contributions from many faint lines, but it does not seem probable that all of it can be accounted for in this way. Page estimated that the intensity was roughly constant with wavelength.

The difficulty with photometric observations of the nebular continuum secured with a wide slit is that the effects of the weaker lines cannot be taken into account properly. If a narrow slit is used, as did Minkowski and the writer, a spectrum of greater purity is obtained, but only the very brightest nebulae may be studied and the required exposures are much longer. The Mt. Wilson results for the continuous energy distribution

are not in agreement with those of Page, but further work will be necessary before fully trustworthy results will be forthcoming. From his photo-electric measures of selected planetaries Liller finds evidence that in at least some objects the intensity in the visual continuum as measured by Page is too high, by something of the order of 20%.

We may summarize the present status of the spectroscopic data on the planetary nebulae somewhat as follows: the wavelengths, relative intensities for selected objects, and identifications of nearly all of the stronger lines have been established. Many weaker lines, not yet identified, undoubtedly will be assigned to their correct atomic origins when term analyses of various atoms in higher stages of ionization are completed. The internal motions in the nebulae have been observed by Campbell and Moore and particularly by Olin Wilson. We discuss this work in Chapter VII.

For a few nebulae, particularly NGC 7662 and NGC 2392, measures of isophotic contours in the stronger lines, the relative intensities of all the moderately strong lines at certain points in the nebular image, and measures of the surface brightness in the $[OIII]$ lines are all available. If the distances of these objects were known, estimates of the emission per unit volume and the densities could be made. Discussions of the isophotic contours, structural features, and internal motions will be given in Chapter VII. We now turn our attention to the qualitative interpretation of the spectra of the nebulae.

5. Interpretation of the Spectra of the Gaseous Nebulae

Table III : 3 gives the wavelengths, identifications, and intensities of the stronger lines observed in the spectra of nine representative planetary nebulae. The objects are listed roughly in order of the increasing intensity of the highest excitation lines (cf. Table III : 2). Notice that there is a great range in the relative intensities of the "forbidden" lines with respect to those of the Balmer series of hydrogen. Furthermore, the forbidden line intensities show a great range among themselves. Consider first the small stellar planetary Anon 18^h15^m. In this nebula $\lambda 3727 [OII]$ is stronger than $H\beta$, but the 5007 and 4959 lines of $[OIII]$ are much weaker. The Balmer series is strong, $[NeIII]$ is missing, and $[SII]$ is weak. Helium is represented by $\lambda 4471$. In IC 418 the $[OIII]$ lines are stronger, while in IC 2149 $[NeIII]$ puts in its appearance. In IC 4634, $\lambda 3727$ is much weaker than the green nebular lines of $[OIII]$ which dominate the spectrum. In NGC 7026 the high excitation lines of $HeII$ and $[AIV]$ appear, while in J900, NGC 6309, IC 2165, and Anon 21^h31^m the very high excitation $[NeV]$ lines appear. In these same nebulae there are also selected strong permitted lines of $OIII$.

Thus the planetaries exhibit a range of excitation from objects whose spectra are characterized by a strong Balmer series plus $\lambda 3727$ of [OII] to others in which the hydrogen lines are relatively inconspicuous in

TABLE III : 3

Emission-line Intensities in Planetary Nebulae

λ	IDEN	Anon 18 ^h 15 ^m	IC 418	IC 2149	IC 4634	NGC 7026	J 900	NGC 6309	IC 2165	Anon 21 ^h 31 ^m
3132.86	OII	—	—	—	—	—	3.1	—	8.8	3.5
3187.74	HeI	—	—	—	—	—	—	—	0.8	—
3203.10	HeII	—	—	—	—	—	1.4	—	1.9	3.0
3299.36	OIII	—	—	—	—	—	—	—	0.7	—
3312.30	OIII	—	—	—	—	—	0.57	—	1.0	—
3345.82	[NeV]	—	—	—	—	—	1.0	—	2.2	5.6
3425.86	[NeV]	—	—	—	—	—	1.8	4.7	6.0	18.0
3444.10	OIII	—	—	—	—	—	1.7	—	2.2	1.0
3726.06	{[OII]}	16	15.7	11	3.1	4.7	5.2	4.7	3.1	4.5
3728.82										
3750.15	H12	0.47	—	0.73	—	—	0.5	—	0.56	0.3
3770.63	H11	0.47	—	0.9	—	—	0.4	—	0.4	0.4
3797.90	H10	0.50	0.34	0.92	—	—	0.5	—	0.5	0.5
3835.39	H9	0.81	0.64	1.2	—	—	0.74	—	0.5	0.7
3868.77	[NeIII]	—	—	2.4	6.0	7.4	7.4	9.5	8.7	6.2
3889.05	H8	1.1	1.3	1.5	2.0	2.1	1.6	—	1.8	1.7
3889.65	HeI									
3967.48	[NeIII]									
3970.07	He	1.6	1.5	2.3	4.0	3.6	3.4	4.5	4.3	3.4
4026.20	HeI	0.2	0.1	—	—	—	0.3	—	0.2	0.3
4068.62	{[SII]}	0.5	0.21	—	—	0.41	0.3	—	0.2	0.3
4076.36										
4101.74	H δ	2.6	2.4	3.0	2.3	2.2	2.1	2.6	2.6	2.3
4199.83	HeII	—	—	—	—	—	—	—	0.1	—
4340.47	H γ	5.1	4.5	5.2	3.9	4.4	4.2	4.2	4.6	4.6
4363.22	[OIII]	—	—	0.60	0.52	—	1.3	—	2.1	2.0
4471.50	HeI	0.3	0.4	0.76	0.46	0.6	0.4	—	0.3	0.5
4541.59	HeII	—	—	—	—	—	0.3	—	0.2	0.8
4634	{NIII}	—	—	—	—	0.5	0.3	—	0.5	0.2
4640										
4685.68	HeII	—	—	—	—	1.3	4.7	7.7	6.0	9.0
4711.36	[AlV]	—	—	—	—	0.4	—	—	0.72	1.0
4740.22	[AlV]	—	—	—	—	—	0.4	—	0.65	0.5
4861.33	H β	10	10	10	10	10	10	10	10	10
4958.91	[OIII]	0.5	5	14	28	40	39	40	53	29
5006.85	[OIII]	1.6	13.9	41	78	84	126	101	128	75

comparison with the intense forbidden lines of [OIII], [NeIII], [NII], and [NeV]. Our first question is: Why do the gaseous nebulae exhibit spectra of this type, and, second, why do they show conspicuous variations in excitation from one to another? Why are the forbidden lines so outstandingly strong and why do selected permitted lines of OIII appear, while other lines equally strong in the laboratory do not appear?

The planetary nebulae have no sources of energy of their own. The radiation they emit is borrowed from the stars embedded within them, and the fact that the nebulae are often visually brighter than the stars from which they derive their energy is a datum of considerable interest. The explanation of this observation is that the central stars are so very hot they radiate most of their energy in the far ultra-violet. This energy is absorbed in the surrounding gaseous envelope and degraded into radiations that fall in observable regions of the spectrum.

The lines of hydrogen and helium and certain weak lines of ionized carbon and oxygen are produced by what is called the *primary mechanism*. High-frequency quanta from the central star are absorbed by atoms or ions in their ground-level and photo-ionization results. As these free electrons are recaptured by various ions a recombination emission spectrum is produced.

Hydrogen, the most abundant of the elements composing the nebulae, will serve as a good illustration. Essentially all neutral hydrogen atoms are in the lowest level, so photo-ionization from the higher levels can be neglected entirely. The atom absorbs a quantum from beyond the Lyman limit and ejects the electron, which continues to wander about until it is recaptured. Although, in the nebulae, photo-ionizations take place only from the ground-level, recaptures may take place on any level. An important consequence of this circumstance is that if the electron is recaptured in the third or higher level, the atom may emit a line of the Balmer series as it returns to its ground-level. If it is recaptured on the second level directly, it will emit a quantum of the Balmer continuum which falls beyond the limit of the Balmer series at $\lambda 3646$.

There is an important theorem, established independently by Zanstra⁽⁵¹⁾ and by Menzel,⁽⁵²⁾ to the effect that if the nebula is sufficiently thick each quantum emitted by the central star beyond the limit of the Lyman series will be degraded ultimately into a quantum of the Balmer series or continuum and a Lyman α quantum. The argument goes as follows: Let us first define as *ultra-violet quanta* those corresponding to frequencies beyond the Lyman limit. Consider one of these stellar ultra-violet quanta absorbed by a hydrogen atom. The atom becomes ionized, and when the electron is recaptured by another hydrogen atom a new quantum or quanta are produced. If the electron is recaptured on the ground-level, a new ultra-violet quantum similar to the original is reborn. If it is recaptured on the third, fourth, or higher level, an infra-red quantum is created, and then, as the atom cascades to the ground-level, certain line quanta are emitted. If, for example, an atom cascades directly from the third level to the ground-level, a Lyman β quantum will be emitted. If it goes from the third level to the second level and thence to the ground-level, an $H\alpha$ and then a Lyman

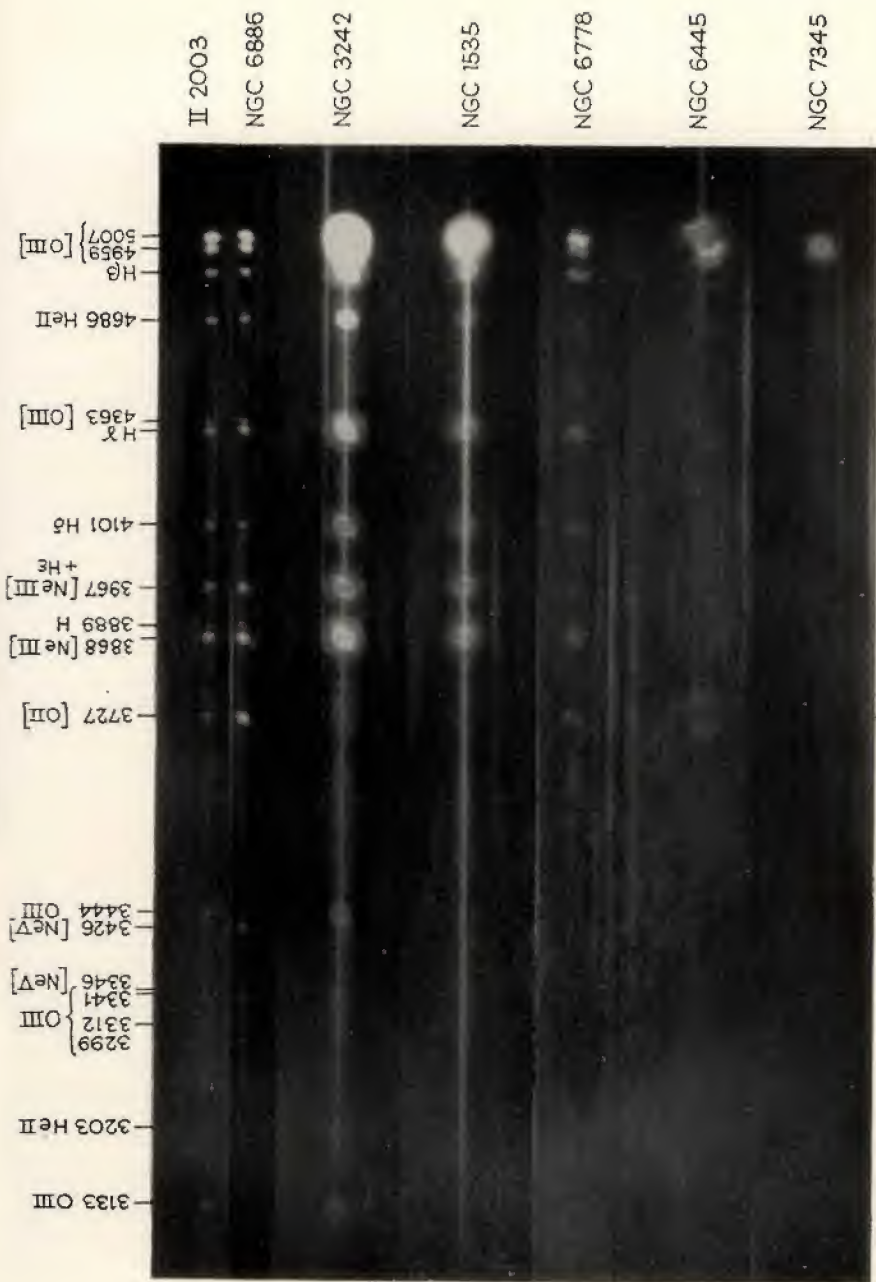


FIG. III : 8. *The Behaviour of $\lambda 3727$ [O II] in certain Planetary Nebulae.*

In the high excitation nebulae NGC 3242, 1535, 7345, and II 2003 the [O II] lines are weak, as one might anticipate for such objects. NGC 6445 and NGC 6886 show strong [O II] and $\lambda 4686$ He II lines simultaneously. Page classifies both of them as "peculiar". In the binuclear nebula NGC 6778, $\lambda 4686$ appears relatively weak and confined to the central regions. The highest excitation object, NGC 6886, shows the strongest 3727 line.

(Photographed with the Crossley reflector at the Lick Observatory, 1944-5.)

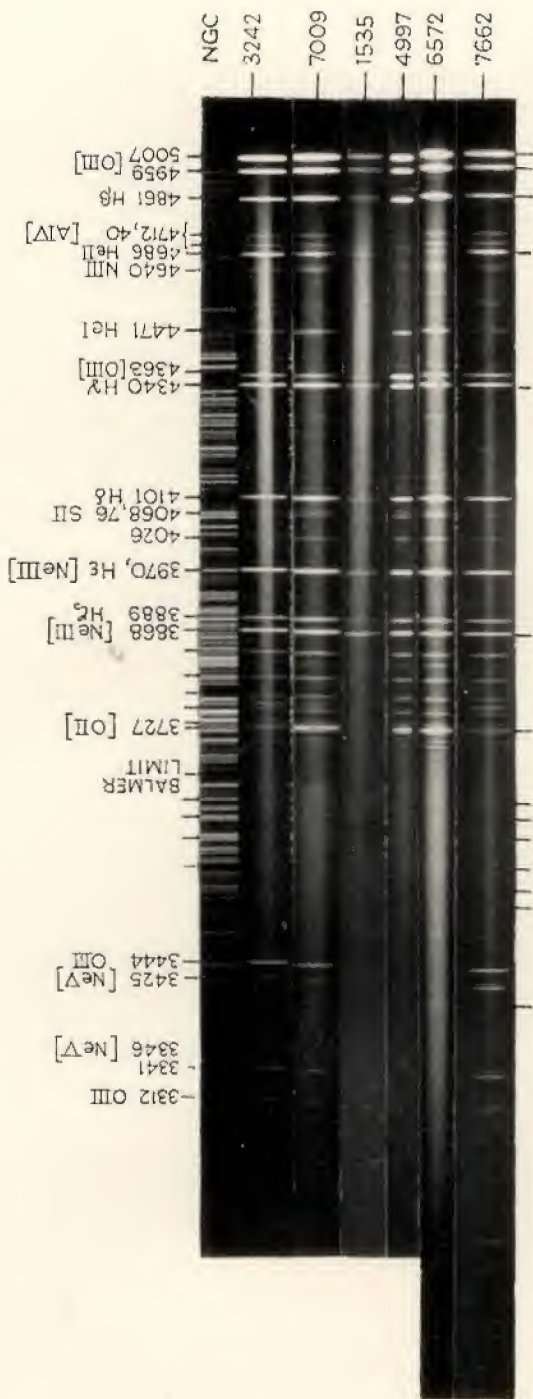


FIG. III : 9. Slit Spectrograms of Planetary Nebulae.

Compare these slit spectra of NGC 3242 and NGC 1535 with the slitless spectra in Fig. 8. A. B. Wyse found many weak recombination lines of [O III] in NGC 7009. The spectra of the nuclei of NGC 7662 and NGC 7009 appear to be continuous with no bright or dark lines. Notice the great strength of the 4363 [O III] line in the high-density planetary IC 4997. The spectrum and appearance of NGC 7662 closely resemble that of NGC 3242. Notice the ultra-violet lines of helium and other elements in the spectrum of NGC 5572 that do not appear in these spectrograms of the other planetary nebulae.

(Photographed with the 82-in. reflector of the McDonald Observatory, 1945-6.)

α are emitted. The $H\alpha$ and infra-red quanta escape immediately from the nebula, the $L\gamma\alpha$ quantum is repeatedly absorbed and re-emitted, i.e. scattered, until it finally escapes from the nebula. The $Ly\beta$ quantum ultimately becomes broken down into an $H\alpha$ and a $L\gamma\alpha$ quantum. Every time a Balmer or infra-red (Paschen, Brackett, Pfund, etc.) quantum is created, it escapes from the nebula, whereas every ultra-violet quantum ultimately becomes degraded into a $L\gamma\alpha$ quantum and Balmer quantum. Hence from a measurement of the intensities of all the Balmer emissions we obtain the number of Balmer quanta which will equal the number of quanta emitted by the central star beyond the limit of the Lyman series. In practice the number of ultra-violet quanta is compared with the number emitted at selected wavelengths in the spectrum of the central star. If the star radiates as a black body, an estimate of its temperature may be made. By this method (see Chapter VI) Zanstra found temperatures of the order of $25,000^\circ\text{K.}$ – $100,000^\circ\text{K.}$ for the central stars of the planetaries.

The formal theory of ionized helium is similar to that of hydrogen, and there is independent evidence that the $L\gamma\alpha$ of $HeII$, $\lambda 303$, attains great strength in those nebulae where the $HeII$ lines are prominent.

The recombination lines of neutral helium are often strong in the planetary nebulae; quantitative analyses show that helium is the most abundant element after hydrogen. The high metastable 2^1S and 2^3S levels of helium produce some interesting effects as were first noted by Ambarzumian.⁽⁵³⁾ As with hydrogen, nearly all neutral atoms find themselves in the ground-level and photo-ionizations take place from this level. Recaptures may occur in either singlet or triplet terms. Since helium is in almost pure LS coupling, intercombination lines are forbidden.

Atoms which find themselves in the high n^1P terms may cascade directly to the ground 1^1S term with the emission of quanta of the principal series. If they reach the 2^1S_0 level, they find themselves in a metastable state which has a lifetime of about $1/7$ sec. in the absence of collisional de-excitation. Atoms may escape from the 2^1S level with the emission of two photons which escape from the nebula as part of the continuous radiation field (see p. 151, Chapter IV). A similar phenomenon occurs in hydrogen where the two-photon emission may contribute to the nebular continuum. In helium the first line of the principal series does not build up to a high intensity as does Lyman α . Consider, as an example, the 1^1S – 3^1P transition. From 3^1P the atom may return to 1^1S , restoring the original quantum, or it may go to 3^1S and thence to 2^1P and on to 2^1S or 1^1S , or it may go to 2^1S directly. A 1^1S – 2^1P quantum may be reabsorbed by an atom, which then goes to the 2^1S metastable level. Quanta of the types 3^1S – 3^1P , 2^1S – 3^1P , and 2^1P – 3^1S escape from the nebula without further reabsorptions unless the metastable level becomes very heavily populated. Thus quanta of the

1^1S - n^1P series become broken down into low-frequency quanta plus continuous radiation from the 2^1S - 1^1S transition.

The atoms which recapture electrons in triplet levels ultimately cascade to the 2^3S level. Breit and Teller⁽⁵⁴⁾ found that for atoms in this level, the

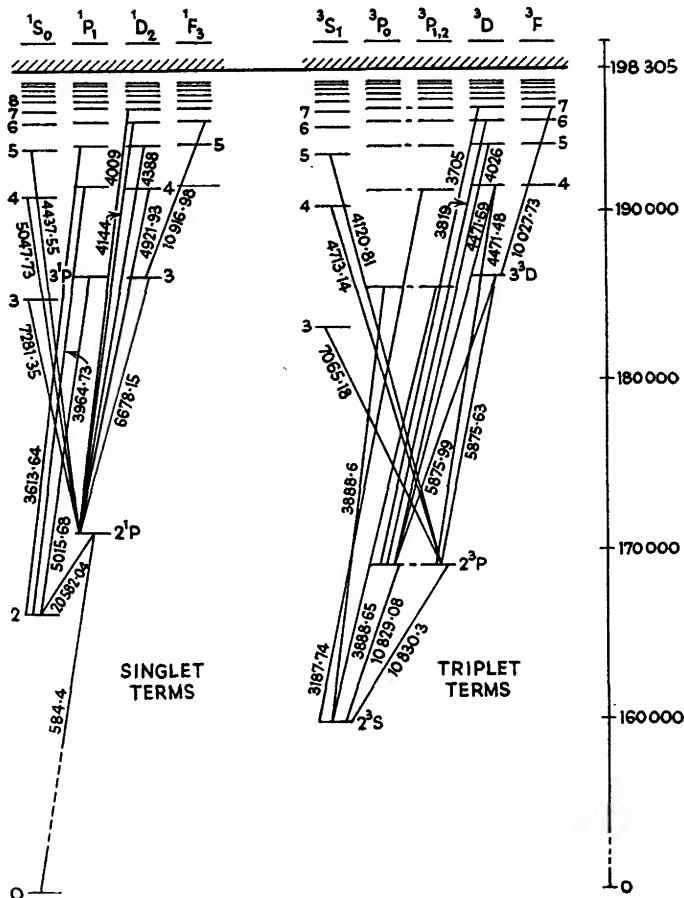


FIG. III : 10. *Energy Level Diagram of Helium.*
The energy is given in wave number units. The singlet and triplet levels are plotted separately.

probability of a spontaneous emission of two photons is about a million times smaller than for atoms in the 2^1S level, so that the 2^3S level must be de-excited only by collisional processes.

Ambarzumian regarded the 2^3S level as strictly metastable so that the 2^3S - 2^3P $\lambda 10,830$ transition plays the role of Lyman α , and the 2^3S - 3^3P $\lambda 3889$ line the role of Lyman β . Nebulae photographed in the light of $\lambda 10,830$ with a slitless spectrograph should appear as bright disks.

Unhappily $\text{HeI } \lambda 3889$ is blended with $H\epsilon$ of hydrogen from which it cannot be separated.

Quantitative predictions of the relative intensities of the helium lines for a nebula in pure radiative equilibrium were made by Goldberg.⁽⁵⁵⁾ He treated the 2^1S and 2^3S levels as strictly metastable, i.e. the two-photon transitions of the type 2^1S-1^1S are ignored. Collisional effects were likewise neglected. This theory predicts a very great weakening of the singlet lines with respect to the triplets. The observed weakening of the singlets is much less. For example, at an electron temperature of $10,000^\circ\text{K.}$ and a central star temperature of $50,000^\circ\text{K.}$, $I(4143)/I(4471)$ is predicted to be 0.013, whereas the observed intensity ratio is 0.077 for NGC 7662. The discrepancy is probably to be explained in terms of collisional and radiative processes that Goldberg could not take into account.

Encounters between electrons and atoms in metastable levels produce several effects. Super-elastic collisions may de-excite the 1^1S and 3^1S levels. Furthermore, inelastic collisions may excite atoms from the metastable levels to the higher permitted ones. Excitations from the 3^1S to higher singlet levels are more frequent than from the 3^1S to higher triplet levels because at low electron velocities, *exchange collisional transitions* (i.e. singlets-triplets) are more likely than singlet to singlet or triplet to triplet excitations. If collisions are important in redistributing atoms among the highly excited levels of helium, the singlet levels will become more highly populated than would be predicted from the theory of pure recapture processes. Until the relevant collisional cross-sections and nebular densities are known, precise predictions of the relative intensities of the singlet and triplet lines is not possible. A careful study of the role of collisional processes would be very much worth while. Also, a more detailed study of radiative processes would be fruitful; in particular the transfer of resonance helium radiation in the nebula ought to be investigated. The central star might also be of influence. If the radiation of this object is rich in resonance helium emission, the singlet levels could be excited by direct transitions from the 1^1S term.

Finally, it might be expected that changes in density throughout the nebula can produce marked changes in the populations of the helium levels and in the relative intensities of the spectral lines. That is, in the spectrum of helium, the effects of density fluctuations ought to be apparent in one stage of ionization, whereas for other elements density effects become evident usually only when more than one stage of ionization is studied.

Carbon, like hydrogen and helium, is observed only by means of its recombination lines. Singly ionized carbon is represented only by $\lambda 4267$, which corresponds to the $3d^2D-4f^2F$ transition, while $\lambda 4187$ of CIII is also observed. Wyse found lines of CIV in a number of planetaries, indicating

that four-times ionized carbon atoms must exist in such objects as NGC 7662 and NGC 7027. Quantitative interpretations of the line intensities in terms of recombination theories is extremely difficult.

The recombination spectrum of OII, which Wyse observed to be especially strong in NGC 7009, is of particular interest for the following reason. The intensities of these OII lines will depend directly on the recombination rate, and therefore on the concentration of OIII ions and electrons and on the electron temperature. Likewise, the intensity of the [OIII] lines will depend on these same quantities, although through different functional relationships. Hence, a comparison of the intensities of the OII and [OIII] lines in NGC 7009 by means of the appropriate theoretical relationships should yield the same concentration of OIII ions. Some years ago Menzel and the writer,⁽⁵⁶⁾ using the then available data on the collisional cross-sections and the estimated electron temperatures, found the OIII ion concentrations determined by these two methods to be in harmony with one another. This calculation should be repeated with improved observational data and with better values of the electron density and temperature and of the basic physical parameters.

Reference to Table III:3 shows that in most planetary nebulae the strongest lines are not those of hydrogen and helium, but are the green lines now known to be due to [OIII], the ultra-violet [OII] $\lambda 3727$ lines, and other radiations that have never been observed in any terrestrial laboratory. For nearly three-quarters of a century after their discovery, these radiations defied all attempts at identification. It was suggested that they might be due to a hypothetical element, *nebulium*, which had not yet been isolated on the earth. It was also believed that this element had a small atomic weight. The advances of chemistry and physics, particularly the brilliant investigations of X-ray spectra by Moseley, showed that all the light elements were known and there was no place for this elusive element to which the mysterious radiations might be assigned.

Spectral term analyses of the lighter atoms by I. S. Bowen⁽⁵⁷⁾ and by Boyce, Menzel, and Payne⁽⁵⁸⁾ showed that the unidentified nebular radiations arose from transitions between terms of the same configuration, i.e. to transitions that were *forbidden* according to the ordinary selection rules for dipole radiation. Hence they were called *forbidden lines*. Perhaps the most common type of forbidden radiation, *magnetic dipole radiation*, is analogous to the radiation from a loop type of antenna, whereas ordinary radiation is analogous to the radiation from a vertical "dipole" antenna.⁽⁵⁹⁾ In Chapter V the identification of the [NeV] lines by Edlén and Swings⁽⁶⁰⁾ is given as an illustration of one of the procedures used for ions of high ionization.

The forbidden lines of NII, OII, OIII, NeIII, NeV, SII, SIII, AIV, etc.,

which are prominent in the gaseous nebulae arise from transitions between the various terms of the p^2 , p^3 , and p^4 configuration. In the ground $2p^2$ configuration of NII, for example, the 3P_0 , 3P_1 , and 3P_2 levels, respectively, are the lowest. The 1D_2 term lies 1.89 e.v. above the ground 3P_0 level and the 1S_0 term is highest of all with an excitation potential of 4.04 e.v. above the ground-level. Transitions from the 1D_2 level to the 3P_2 and 3P_1 levels,

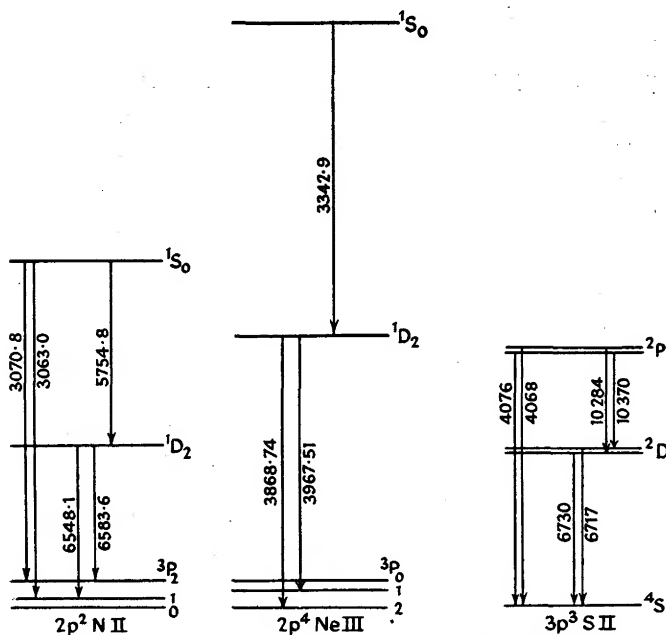


FIG. III: 11. *Transition Schemes for Typical Forbidden Lines in Gaseous Nebulae.*

The 6548, 6584 [NII], 3868, 3967 [NeIII], and 6730, 6717 [SII] transitions are of the so-called nebular type. Transitions like 5755 [NII], 3343 [NeIII], and 10284, 10317, 10336, 10370 [SII] are of the auroral type, while 3071, 3063 [NII] and 4068, 4076 [SII] are of the transauroral type.

respectively, give the $\lambda 6584$ and $\lambda 6548$ lines which flank $H\alpha$. The 1S_0 – 1D_2 transition gives a line at $\lambda 5755$. The p^4 configuration has the same terms as the p^2 configuration, but the 3P term is inverted. The strongest of the [NeIII] lines, $\lambda 3868.74$, corresponds to a transition from the 1D_2 term to the ground 3P_2 level. A p^3 configuration gives a ground $^4S_{3/2}$ level with 2D and 2P terms above it. Transitions between the two highest terms of the configuration are called *auroral transitions*, those between the middle term and the lowest term are referred to as *nebular transitions*, while jumps from the highest to the lowest term produce the so-called *transauroral lines*.⁽⁵⁸⁾ Examples are illustrated in Fig. 11.

The mechanism for the production of the forbidden lines must be vastly

different from that responsible for the permitted recombination lines of *H* and *He*. The observed emissions are produced by downward transitions from the higher metastable levels of the ground configuration. Were these levels populated by recombination, i.e. by the ions capturing electrons directly in these metastable levels, there would also be many recaptures in higher normal levels and the characteristic recombination lines of *OIII*, *NII*, etc., should be strong. Actually, the recombination lines, when observed at all, are extremely weak. With these considerations in mind, Bowen⁽⁶¹⁾ pointed out that electrons which had been photo-electrically ejected from hydrogen and helium atoms could collide with ions of nitrogen, oxygen, neon, sulphur, etc., in their ground terms and excite them to metastable terms, lying but a few volts above the ground term. As the ions returned from these metastable levels to lower levels with the emission of energy, they radiated the so-called forbidden lines. All subsequent work on forbidden lines in gaseous nebulae has substantiated Bowen's explanation.

The forbidden lines dominate the spectra of the planetary nebulae because the normal or "permitted" lines of these same ions are so hard to produce under conditions existing there. In the spark or glow discharge the intensity of the permitted lines and continuous spectra vastly overwhelms the weak radiations of the forbidden lines. In the gaseous nebulae, on the other hand, there are no fast electrons capable of exciting the higher configurations which lie approximately 15–30 e.v. above the ground configuration. Hence the normal permitted lines cannot be collisionally excited in the nebulae. On the other hand, at electron temperatures from 10,000° K. to 25,000° K. there are sufficient electrons with energy sufficient to excite the metastable levels. Although the total emission of energy per unit volume is very small, the vast extent of the nebula permits its surface brightness in the forbidden radiation to build up to an amount which can be easily detected.

Nevertheless, the nebula is almost completely transparent to the forbidden radiation as may be shown by calculating its optical thickness in the line. The average absorption coefficient of an ion over the Doppler profile of the line will be

$$\bar{\alpha}_\nu = \frac{\pi e^2}{mc} f \frac{1}{\Delta\nu}, \quad . \quad . \quad . \quad (1)$$

where e and m are the charge and mass of the electron, c is the velocity of light and $\Delta\nu$ is the effective half-width of the line in frequency units as determined by the random kinetic motions of the atoms. We assume there is no large-scale turbulent or mass motion in the nebula. Thus the minimum value of $\Delta\nu$ will be⁽⁶²⁾

$$\Delta\nu = \frac{2.15 \times 10^4}{\lambda} \sqrt{\frac{T}{\mu}}, \quad . \quad . \quad . \quad (2)$$

where μ is the molecular weight of the ion in question. The gas kinetic temperature is equated to the electron temperature, as the momentum exchange between ions and electrons will quickly lead to an equipartition of energy. If we consider an O^{++} ion and an electron temperature of $10,000^\circ\text{K.}$, $\Delta\nu \sim 1.08 \times 10^{10}$. The Ladenburg f or *oscillator strength* is related to the Einstein coefficient of spontaneous emission for the transition involved by the well-known expression⁽⁶²⁾

$$f = \frac{\varpi_n}{\varpi_{n'}} \frac{mc^3}{8\pi^2\varepsilon^2\nu^2} A_{nn'}, \quad (3)$$

where ϖ_n and $\varpi_{n'}$ are the statistical weights of the upper and lower levels, respectively, and ν is the frequency of the line. Putting in numerical values for the strong $\lambda 5007$ [OIII] line which corresponds to the transition $p^2\ ^1D_2 - p^2\ ^3P_2$, i.e. $\varpi_{n'} = (2J+1) = \varpi_n = 5$, $A(^3P_2 - ^1D_2) = 0.021$, together with the numerical values of the other factors of the equation, we find $f = 7.9 \times 10^{-11}$. Then $\bar{a} = 1.93 \times 10^{-22}$.

If the total thickness of the nebular shell D is 10^{17} cm. and the number of atoms in the 3P_2 level of O^{++} is $1/\text{cm.}^3$, we find for the total optical thickness τ_0 in the strongest of the green nebular lines,

$$\tau_0 = N\bar{a}D \sim 2 \times 10^{-5}, \quad (4)$$

so that the chance of reabsorption of a given quantum of $\lambda 5007$ is utterly negligible.

This conclusion may be easily verified by taking the observed surface brightness in the green nebular lines S ([OIII]), as measured, for example, by Liller, and a minimum value of $\Delta\lambda$ as estimated from T_e and comparing it with $B_\lambda(T_e)\Delta\lambda$, where $B_\lambda(T_e)$ is the Planckian function for a temperature T_e .

Quantitative considerations concerning the production of forbidden lines in gaseous nebulae are given in Chapter V.

The far ultra-violet spectra of high excitation planetaries (cf. Table III:3) contain not only the prominent [NeV] and HeII 3203 lines, but also certain permitted lines of doubly ionized oxygen. The most remarkable characteristic of these OIII lines is that they represent a highly selected group of transitions. Other lines of the OIII spectrum that are even stronger in laboratory spectra or in the high excitation Wolf-Rayet stars are completely missing.

The OIII lines observed in the planetaries are confined to transitions that would be produced by an initial excitation of the $2p3d\ ^3P_2$ level with subsequent cascade to the $^3P_{2,1}$ and 3S_1 levels of the $2p3p$ configuration and to the 3P level of the $2p3s$ configuration.

The explanation for the selective excitation of this particular atomic level was given by Bowen.⁽⁶³⁾ He noticed the existence of a very close coincidence

between the frequencies of the Lyman α line of $HeII$ ($1s^2S-2p^2P^0$) and the resonance $2p^2\ ^3P_2-2p3d\ ^3P_2^0$ transition of $OIII$. The "fractional multiplets" of $OIII$ occur only in nebulae with strong $HeII$ recombination lines. In the same way as the quanta beyond the limit of the Lyman series of hydrogen are degraded ultimately into quanta of $L\gamma$ and Balmer quanta, so are the quanta beyond the limit of the Lyman series of ionized helium ultimately degraded into the $\lambda 303.780$ line of ionized helium. In a nebula surrounding a high-temperature star a considerable energy density in this radiation may be built up with the result that doubly ionized oxygen atoms in the $2p^2\ ^3P_2$ level are readily excited to the $2p3d\ ^3P_2^0$ level. The wavelength of this transition, $\lambda 303.799$, does not quite coincide with that of the helium line, but Doppler shifts produced by mass motion within the nebula will bring the two frequencies into coincidence for many $OIII$ atoms in the nebula. Other levels of the $2p3d\ ^3P$ term are not excited because the wavelengths do not coincide.⁽⁶⁴⁾

Once in the $2p3d\ ^3P_2$ level the atom will most likely return to the ground-levels, but there is a finite probability that it will cascade successively to the $2p3p$ and $2p3s$ configurations with the emission of the fractional multiplets. The observed transitions are depicted in Fig. 12. Jumps to levels in the $2p3p$ configuration give the $\lambda 3133$, 3429 , and 3444 lines. Transitions from the 3S and from $2p3p\ ^3P_2$ levels to the $2p3s\ ^3P$ term account for most of the observed lines. The 3760 line, which arises from the $2p3p\ ^3D_3$ level, is connected with the $2p3d\ ^3P_2$ term by the unobservable $\lambda 2836.35$ line.

A further astonishing coincidence is provided by the $\lambda 374.436$ ($2p3s\ ^3P_1^0-2p^2\ ^3P_2$) transition, one of the end-products of the fluorescent cycle in $OIII$. This line coincides closely in wavelength with the resonance $2p^3P_{3/2}-3d^2D_{3/2}$ $\lambda 374.442$ line of $NIII$. Thus a somewhat similar fluorescent cycle involving the excitation of certain fractional multiplets in $NIII$ is initiated.

Bowen's suggestion gives an excellent qualitative explanation of the observations. Menzel and the writer have subjected it to a quantitative test.⁽⁶⁵⁾ A few obvious consistency checks are to be noted. The number of quanta in $\lambda 3133$ should equal the total number of quanta in the three lines $\lambda 3299$, $\lambda 3312$, and $\lambda 3341$. In a more sophisticated vein it is possible to write down the equations of *statistical equilibrium* for each level involved in the process, e.g. we equate the number of atoms entering, say, $2p3p\ ^3P_2$ by cascade from $2p3d\ ^3P_2$ to the number leaving by cascade. A series of equations for a steady state may be obtained from which it is possible to predict the relative intensities of all the lines in the fluorescent $OIII$ mechanism. The predicted relative intensities of the $OIII$ lines then may be compared with the observed relative intensities to provide a check on the theory. To within the rather large limits of error of the measured

intensities, theory and observation appear to be in agreement. The concentration of atoms in the $2p3d^3P_2$ level in a typical planetary amounts to something of the order of 10^{-14} to 10^{-15} atoms/cm.³. This is a very small concentration compared with that in the ground-levels (1/cm.³), or the numbers in the metastable 1D_2 level (10^{-3} /cm.³). The strongest ultra-violet OIII lines have intensities of the order of a tenth that of the green

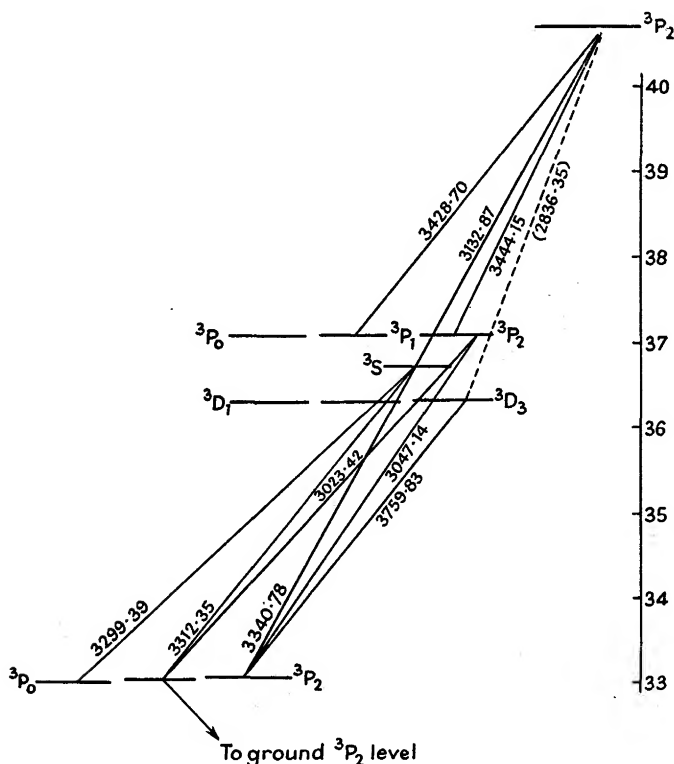


FIG. III:12. *Fractional Multiplets of OIII in the Bowen Fluorescent Mechanism.*

This partial energy level diagram shows only the levels of the $3s$, $3p$, and $3d$ configurations that are involved in the cascade of an ion from the $2p3d^3P_2$ level. The ground configuration and transitions thereto are not depicted.

nebular lines. The ratio of transition probabilities for the lines arising from the two kinds of levels is of the order of 10^{10} . Hence the speed of “cycling” of an atom through the fluorescent mechanism is vastly greater than for a forbidden line.

Detailed calculation shows that in an optically thick nebula in which helium is doubly ionized in the inner layers, the intensity of the radiation in OIII $\lambda 303.80$ is built up a hundred- or a thousand-fold over that radiated by the central star. Thus it is easy to understand why permitted lines of

OIII, other than those originating by cascade from $2p3d^3P_2$ are not observed.

The Lyman α radiation of ionized helium escaping from the He^{++} shell tends to be used up in the excitation of OIII since the O^{++} shell is much larger than the He^{++} shell. Thus the slitless images of OIII should be slightly larger than those of HeII; detailed computation indicates they should be of the order of 3–5% larger—a prediction which also appears to be in agreement with the observations.

The quantitative theory of the excitation of the NIII lines by the Bowen mechanism has been given by T. Hatanaka.⁽⁶⁶⁾

Shortley and Menzel pointed out that since the levels $p^2\ ^3P_2$ of OIII and $p^2P_{3/2}$ of NIII from which the initial fluorescent excitation takes place are not the ground-levels of their respective terms, collisions must maintain an appreciable number of OIII and NIII ions in the appropriate levels.⁽⁶⁷⁾ The densities in the planetaries therefore must be much greater than in interstellar space, where T. L. Dunham found that the only observed interstellar absorption lines of ionized titanium are those arising from the lowest level of the lowest term. Density estimates based on the surface brightness in the hydrogen lines and continua and the dimensions of the planetaries indicate electron densities of the order of 10^3 to $10^4/\text{cm}^3$, as contrasted with densities of the order of 0.1 to $10/\text{cm}^3$ for typical regions of interstellar space.

6. The Discovery of and Catalogues of Diffuse Galactic Nebulae

Unlike the planetary nebulae which are all telescopic objects, two diffuse nebulae are visible to the unaided eye. Only one of these, the Orion nebula, is visible in northern latitudes. The η Carina nebula discovered by Lacaille appears to have been variable in brightness as Herschel could not see it without a telescope in 1834–8, although it was bright in 1865–70, and later faded again although it is still faintly visible to the naked eye.

Both the η Carina and Orion nebulae were discovered telescopically. Until the time of Herschel the rate of discovery of galactic nebulae was relatively slow. Messier's catalogue contained several, viz. M1, 8, 16, 17, 20, 42, 43, 45, 78. Systematic work by the Herschels contributed many more objects in both the northern and southern hemispheres. Other visual observers added many additional objects.⁽⁶⁸⁾ The application of photography opened a new era in the study of nebulae. With a wide-angle lens, Barnard found sixty bright diffuse galactic nebulae and verified that some of the *dark* nebulae were faintly luminous. Max Wolf discovered sixteen objects by photographic methods.

More recent investigations have emphasized the detection of nebulae of low surface brightness and the study of faint extensions of well-known

nebulae. In Chapter II we mentioned the use of narrow band-pass filters and the nebular spectrographs employed by Struve and his colleagues.⁽⁶⁹⁾

A catalogue of bright diffuse galactic nebulae known up to 1945 has been prepared by S. Cederblad.⁽⁷⁰⁾ His list gives the positions, description, approximate dimensions, and estimated distances of both reflection and emission nebulae. The use of red-sensitive plates, filters to isolate $H\alpha$, and fast cameras have added greatly to the list of known nebulae.⁽⁷¹⁾ Many of these were photographed with the 18-in. Schmidt telescope at Palomar through a red Plexiglas filter on a 103a-E emulsion.⁽⁷²⁾ Very recently S. Sharpless has prepared a catalogue of emission nebulosities photographed near the galactic plane with the 48-in. Schmidt.⁽⁷³⁾ His survey covers galactic longitudes 315° to 105° and galactic latitudes between 1° and 5° on either side of the galactic equator. His catalogue gives the coordinates, angular diameters, forms (circular, elliptical, or irregular), structure (amorphous, filamentary, or intermediate), surface brightness on a scale of 3 and associated early type stars. Mention must also be made of the beautiful photographs obtained by G. A. Shajn and B. F. Hase,⁽⁷⁴⁾ who have given a catalogue with descriptions of many galactic nebulae. They have also discussed the orientations of many of the nebulous filaments.⁽⁷⁵⁾

The investigation of the ionized hydrogen, HII , regions of extremely low surface brightness requires the use of either the nebular spectrograph or narrow band-pass filters. The Strömgren-Morgan programme for the study of these objects was briefly mentioned in Chapter II. S. Sharpless and D. Osterbrock used the Greenstein-Henyey wide-angle camera plus a Corning 2403 filter and Eastman 103a-F plates to isolate a spectral band 300 Å. wide centred on $H\alpha$ to identify the nearest HII regions of moderately low surface brightness.⁽⁷⁶⁾ Exposures taken with no filter enabled them to find the emission regions by a direct comparison. They identified the O and B0 stars responsible for the excitation of the nebulosity, estimated the absorption from the colour measures of Stebbins and Whitford and the spectral classes by Morgan. Their catalogue gives for each nebulae the galactic coordinates, distance modulus, diameter and linear dimensions, together with the electron densities from the Strömgren theory (see Chapter VII, Section 1). They found two new nebulae, near ζ Ophiuchi, and near λ Orionis.

Emission nebulosities in external galaxies have been studied by a number of observers. We shall discuss them in Section 11.

Studies of faint emission nebulae in the southern hemisphere have been made by B. J. Bok, M. V. Bester, and Campbell M. Wade,⁽⁷⁷⁾ and by Arthur Code. Bok, Bester, and Wade used a 3-in. Zeiss $f1.5$ lens with a Corning 2403 red filter and a Baird interference filter to isolate $H\alpha$. Code

used an interference filter and the Greenstein-Henyey camera. Dorrit Hoffleit has described the $H\alpha$ emission regions between 250° and 265° , while Bok, Bester, and Wade give the galactic coordinates and descriptive remarks pertaining to sixteen $H\alpha$ emission regions between galactic longitudes 265° and 355° .

7. Dimensions and Descriptions of the Diffuse Galactic Nebulae

Examination of photographs of typical diffuse galactic nebulae will convince anyone that the variety in form, dimensions, fine structure, and surface brightness in these objects would preclude any classification scheme. Many resemble nothing as closely as terrestrial clouds, but a meteorological classification scheme would not seem practical as due allowance could not easily be made for the illuminating stars. On the other hand, disk or ring-like structures such as the Rosette nebula described by Minkowski are occasionally found. Amorphous structures are fairly common, while the intermixture of light and dark material in such objects as the Trifid, ρ Ophiuchi, and Messier 8 nebulae contribute to the complex appearance of these nebulae.

Curtis simply spoke of the Great Diffuse nebulae and the planetaries. Hubble differentiated between dark and luminous diffuse nebulae and distinguished between emission and reflection objects among the second group. Cederblad decided that surface brightness, concentration and size were not useful criteria for classification, and based his classification scheme primarily on the relation of the nebula to stars and secondly on the general appearance of the object.⁽⁷⁰⁾ He divides the nebulae into three main groups: (a) nebulous clusters; (b) nebulae associated mainly with one (possibly multiple) star; and (c) nebulae having no definite relationship with stars. The appearance of the nebula then determines into what sub-class it is to be fitted.

The classification of purely emission nebulae is somewhat less difficult. The simple system used by Sharpless has been mentioned. Bok and Wade proposed a classification based on shape, structural features, and surface brightness. The apparent or linear size of the nebula and the spectral class and luminosity of the exciting star do not enter in their classification scheme. Their Type I is of high surface brightness with a Strömgren emission measure of 10,000 or more, a diameter of 10–50 parsecs, and associated dark material (e.g. M8, M20, or the η Carinae nebula). Type II is moderately faint, irregular and often filamentary in structure, while spherical emission structure and bright ring structures belong respectively to their Classes III and IV.

The actual dimensions of diffuse gaseous nebulae show an enormous range. The thread-like filaments are often but a few hundred astronomical

units in diameter, and some of the smaller emission nebulae are of the order of 0.05 parsec. At the other extreme stand objects such as NGC 604 in the Triangulum galaxy with a diameter of about 140 parsecs!

8. The Distances and Galactic Distribution of Diffuse Nebulae

Before many conclusions concerning their nature and origin may be drawn, it is necessary to know the distances of the diffuse gaseous nebulae. The problem is simplified by the fact that the diffuse nebulae all belong to the Type I population which is closely confined in the galactic plane to the spiral arms. The bright-line gaseous nebulae are associated with luminous O and B stars. The connexion is not as intimate as in the planetaries, where each nebula surrounds a particular central star. Rather, the material of the interstellar medium appears to be distributed in each spiral arm in a lumpy fashion. If a concentration of particles and gas finds itself in the neighbourhood of a hot star, it is likely to fluoresce and yield a bright-line spectrum. If no luminous, hot star is near by, the masses of small solid particles appear as dark lanes or clouds projected against the fields of yet more distant stars, e.g. the dark lanes in Taurus.

A luminous O star can ionize a considerable volume of hydrogen gas in its neighbourhood, while a cluster of O and B stars as in Orion can produce a nebula of considerable surface brightness. Thus the determination of the distance of a given nebula usually involves the measurement of the distance of the associated high-temperature star.

Reliable trigonometric parallaxes cannot be obtained for the O and B stars because most of them lie at distances such that the probable error of the parallax is much larger than the parallax itself. Parallaxes of foreground stars projected on the nebulae have sometimes been used to get a lower limit to the distance.

The intensities of the interstellar lines have also been used to get distances for the associated O and B stars. The method may give a rough idea of the distances but will yield large errors for individual stars.

Since the B stars partake of galactic rotation, their distances may also be estimated from their radial velocities, V (referred to the average of the nearby stars), in accordance with the Oort relation,

$$V = rA \sin 2(l - l_0) \cos^2 b + K, \quad (5)$$

where r is the distance of the B star, l and b are its galactic longitude and latitude, l_0 is the longitude of the galactic centre, the K -term is supposed known, and A is the Oort constant which is usually poorly determined.

The best method is that employed by W. W. Morgan⁽⁷⁸⁾ to establish the scale of distances of the B stars. First, accurate spectral classes are established for each of the stars of interest and for the B stars in galactic

clusters. Then, from a comparison of all available galactic clusters containing O and B stars, the relative absolute magnitude of each spectral subdivision is established. The determination of the zero-point, e.g. the absolute magnitude of B3V-B5V stars may be accomplished from a statistical analysis of the v -components of proper motion of stars over a narrow range of actual distance, from proper-motion studies of aggregates such as the Scorpio-Centaurus cluster of B stars, or by the accurate determination of the parallax of some cluster which contains B stars.

Once the intrinsic luminosities of the B stars are known, it is necessary only to classify the spectrum of the star on the Morgan-Keenan system to determine its intrinsic luminosity or absolute magnitude, M_{vis} . The measurement of the apparent visual magnitude, m_{vis} , then gives the distance modulus, $y = m - M$, from which the actual distance can be found if the correction for space absorption is known. The space absorption, A , in magnitudes is usually estimated from the colour excess, the difference between the intrinsic colour of the star which depends only on its spectral type and the observed colour which depends also on the space absorption. If the colour is measured photo-electrically on the Stebbins-Huffer-Whitford E_1 system with effective wavelengths $\lambda 4260$ and $\lambda 4770$, the ratio A_{vis}/E_1 is 6.1, according to the recent work of W. W. Morgan, D. Harris, and H. Johnson.

From such studies Morgan and his associates were able to establish the distances of all the brighter B stars, and in particular those associated with emission nebulae and regions of ionized hydrogen. The climax of this investigation came with the identification by W. W. Morgan, S. Sharpless, and D. Osterbrock of the spiral arms of the galaxy in the neighbourhood of the sun.⁽⁷⁹⁾ The hydrogen emission regions and their associated B stars define parts of three spiral arms. The nearest arm extends from galactic longitude 40° to 190° , and at its closest point its centre lies about 300 parsecs from the sun in the opposite direction from the galactic centre. The observed length of the arm is about 3000 parsecs and its overall width is probably in the neighbourhood of 600 parsecs. Included in this arm are the bright nebulosities near P Cygni, NGC 6871, the North America nebula, the ξ Persei nebulosity, the Orion nebulosity, the Rosette nebula in Monoceros surrounding NGC 2244, and the ionized hydrogen regions near λ Orionis and S Monocerotis. Also included are the dark nebulosities in Taurus, Perseus and the great rift in the Milky Way. The southern Coal Sack and the Scorpio-Centaurus cluster lie on the inner side of the spiral arm.

Morgan, Sharpless, and Osterbrock traced a second outer spiral arm from 70° to 140° . This arm includes NGC 7380, NGC 7635, and the double cluster in Perseus. It is parallel to the arm that includes the

sun, and is located about 2000 parsecs away from it in the anti-centre region.

The blue supergiants with absolute visual magnitudes brighter than -4.0 also define the same structure.

More recent work by Morgan, Whitford, and Code⁽⁸⁰⁾ on the distances of high-luminosity O-A stars identifies a total of twenty-seven large-scale groupings or aggregates. Seven of these aggregates, including Messier 8 and M16, lie between galactic longitudes 311° and $346'$. They define a spiral arm located between the sun and the galactic centre at a distance of about 1400 parsecs. Furthermore, the arm in which the sun is located appears to have a spur running off in the direction of the outer spiral arm: the branch point lies a few hundred parsecs from the sun.

The dimensions and frequency of occurrence of the ionized hydrogen regions are comparable with those found by Baade in the Andromeda galaxy.⁽⁸¹⁾ Furthermore, the great aggregates of luminous O and B stars such as the Orion, Scorpio-Centaurus, and Perseus double cluster groups are concentrations in the arms similar to those observed in the Andromeda spiral.

The distribution of the galactic nebulae reflect on the one hand the influence of interstellar absorption, and on the other the influence of the spiral structure. Many years ago Hubble found a zone of avoidance for galactic diffuse nebulae above $b=2^\circ$, and in the great rift of the Milky Way.⁽⁸²⁾ Sharpless⁽⁷³⁾ found similar results from his studies of the 48-in. Schmidt plates. On the other hand, he points out that the scarcity of nebulae between longitudes 60° and 70° is real, since the number of apparently faint but intrinsically bright O and B stars in this region is appreciable. The inference is that along the more remote spiral arm of the galaxy, the interstellar hydrogen has a spotty distribution. Sharpless calls attention to the gradual decrease of the angular size of the nebulae from $l=315^\circ$ to $l=360^\circ$, which is in harmony with the suggestion of an inner spiral arm along which we are looking in the direction of Scutum. The diminishing sizes of the nebulae are merely an effect of perspective.

The general features of the spiral arm structure are confirmed by observations of the 21-cm. radio-frequency radiation. There appear to be some discrepancies, but some of these must arise from difficulties with the interpretation of the radio-frequency line profile data on the one hand and the corrections for space absorption in the distance determination of the B stars on the other. Detailed information on the dimensions, distances, and descriptions of individual diffuse nebulae may be found in the previously cited references.

As an example of an association of a star cluster containing many early-type stars, bright nebulosity, and solid particles, we may mention Messier 8,

the so-called "Lagoon nebula", $\alpha=17^{\text{h}}58^{\text{m}}$; $\delta=-24^{\circ} 53'$ (1900). It consists of a bright diffuse nebula (NGC 6523) and an open cluster. Early descriptions of it were given by Messier and by the Herschels.⁽⁸³⁾ Photographs of it have been published by Keeler,⁽⁸⁴⁾ Barnard,⁽⁸⁵⁾ H. D. Curtis,⁽⁸⁶⁾ Paraskevopoulos,⁽⁸⁷⁾ and by J. C. Duncan,⁽⁸⁸⁾ who described it as one of the most extraordinary objects in the sky. The spectrum has been described by Campbell and Moore⁽⁸⁹⁾ and by Hubble.⁽⁸²⁾ The latter attributed the source of the nebular emission to HD 164794, $m=6.9$, spec. Oe5, and CPD-24° 6146, a B0 star of 7.6 magnitude. Morgan, Whitford, and Code also list the hot stars HD 164906, B1 IV, and HD 165052, O7. Trumpler⁽⁹⁰⁾ determined the spectral classes for twenty-five stars brighter than 13.0 and estimated the distance of the cluster. Wallenquist⁽⁹¹⁾ studied the relationship of the nebula and cluster and from the associated O stars as well as the B stars of the cluster he derived a distance modulus of 11.0, which would correspond to a distance of 1600 parsecs if there were no space absorption. Actually, the involved stars show a considerable range in colour-excess; some are heavily reddened, others are much less so. Morgan, Whitford, and Code give a distance of 1300 parsecs for the cluster and associated nebula. Wallenquist finds the cluster to consist mostly of B stars brighter than $m_{pg}=11.5$. Below this limit he finds an even distribution of stars with no trace of any cluster. Above this limit there is a pronounced clustering corresponding to NGC 6530. Some of the cluster stars are hidden by the dark rift in the nebula.

The longer diameter of the nebula (Cederblad, Sharpless) is about 90', which corresponds to a linear diameter of about 34 parsecs. It is much larger than the associated star cluster NGC 6530 for which Trumpler obtained an apparent diameter of 14'.

The surface brightness, which has been measured by Boggess, places the Messier 8 nebula among the brightest galactic nebulae. Unfortunately, it is not conveniently placed for observers in the northern hemisphere. Boggess has also measured the isophotic contours. His $H\alpha$ photographs show that, as observed in this wavelength region, the bulk of the radiation from the main body of the nebula as well as from the delicate outlying filaments must come from $H\alpha+[NII]$. The Messier 8 nebula is relatively dense as galactic nebulae go; it is similar in many respects to the nearby somewhat smaller Trifid nebula which shows even more conspicuous lanes. Radio-frequency radiation, presumably of thermal origin, has been detected from Messier 8 and several similar objects.

9. The Spectra of the Diffuse Gaseous Nebulae

The earliest spectroscopic observations of the diffuse gaseous nebulae were those by Sir William Huggins,⁽⁹²⁾ who observed the bright lines of

hydrogen and [OIII] in the central region of the Orion nebula. Shortly thereafter Lord Oxmantown⁽⁹³⁾ observed an extremely faint continuous spectrum in Orion, which many people were inclined to attribute to faint stars. Later, Huggins⁽⁹⁴⁾ succeeded in photographing the spectrum of this object, and discovered the prominent $\lambda 3726-29$ radiations of [OII]. In 1886 Copeland⁽⁹⁵⁾ observed the 5876 line of HeI in this nebula. Near the end of the century W. W. Campbell⁽⁹⁶⁾ found variations in the $(N_1 + N_2)/H\beta$ ratio from one point to another in the Orion nebula, a phenomenon which had been noted earlier by Huggins. He observed a similar effect in the Trifid nebula.

The spectrum of the Orion nebula has been studied in great detail by a number of observers. We have already mentioned the work of Wyse, who included this object in his survey of the spectra of gaseous nebulae and observed the largest number of spectral lines. The line spectrum was also studied by Tcheng Mao-Lin and J. Dufay,⁽⁹⁷⁾ who give the wavelengths, intensities, and origins of spectral lines in the interval $\lambda 3700-45000$. Osterbrock has studied the variation of the $\lambda 3726/\lambda 3729$ radiation ratio in this nebula.⁽⁹⁸⁾

The continuous spectrum of the Orion nebula is partly produced by light scattered by particles and partly by recombination and other processes within the nebula itself. Greenstein⁽⁹⁹⁾ and Henyey used the nebular spectrograph of the McDonald Observatory to observe the Orion and the Pleiades nebulosities, and verified that both nebulae were bluer than the exciting stars. Later, Barbier⁽¹⁰⁰⁾ observed the continuous spectrum of the Orion nebula with a quartz spectrograph, and compared the nebular energy distribution with that of nearby stars of known energy distribution. He found an energy distribution corresponding to a colour temperature of $10,300^\circ\text{K.}$ in the ultra-violet beyond the Balmer limit. Later observations yielded a colour temperature of $23,500^\circ\text{K.}$ for the energy distribution in the interval ($\lambda 4550-6250$). Subsequently, Greenstein⁽¹⁰¹⁾ used the two-prism quartz *f*1 camera in the Cassegrain spectrograph at the McDonald Observatory to make a spectrophotometric comparison of the energy distribution in the Orion nebula with that of θ_1 Orionis C, whose colour temperature was based on photo-electric measures and photographic gradients. He found the nebular continuum to have a colour temperature of $12,000^\circ\text{K.}$ on both sides of the Balmer limit and suggested that the nebula is optically thick (see Chapter VIII).

It is of interest that O. C. Wilson⁽¹⁰²⁾ observed a sharp $\lambda 3889$ HeI line of nebular origin superposed on the spectra of stars seen through the Orion nebula. Thus the population in the metastable 2^3S level must be appreciable.

The spectra of other diffuse nebulae have been observed in less detail than that of Orion.⁽⁸²⁾ In general, the diffuse gaseous nebulae show spectra

similar to low excitation planetaries such as IC 418. The Balmer lines are usually prominent and $\lambda 3727$ [OII] is often quite strong. In some objects the green nebular lines of [OIII] are present, but often they are weak or missing) see Fig. 15, p. 96).

The spectra of very faint emission nebulosities have been observed by Struve and Elvey.⁽¹⁰³⁾ These extended regions of low surface brightness show the Balmer lines, [OII] $\lambda 3727$, [OIII] $\lambda 4959$, 5007 and [NII] $\lambda 6548$, 6584. Their linear dimensions are often of the order of 40 parsecs (λ Orionis patch) to 130 parsecs (Cygnus patch). The boundaries are often roughly circular in appearance with sharp outer boundaries. When [OIII] is observed, it is found in the centres of these regions and fades out gradually. A significant feature of these ionized hydrogen (HII) regions is that they tend to be associated with O stars, although they show but little concentration to individual early-type stars and clusters of such stars as do the bright galactic nebulae. Furthermore, the physical conditions of excitation vary from one part of the sky to another. For example, the [OII]/($H\alpha$ + [NII]) ratio is large in the Canis-Major region and small in the summer Milky Way between Cepheus and Sagittarius. From the observed surface brightnesses of these nebulosities, Struve estimated the density to be of the order of 1–3 hydrogen ions/cm.³.

The observations of Struve and Elvey were made with a very low dispersion. The [NII] lines were blended with $H\alpha$, [SII] $\lambda 6731$, 6717 were not found, while the D_3 line of helium $\lambda 5876$ was blended with the sodium lines in the airglow. T. L. Page⁽¹⁰⁴⁾ used the McDonald B spectrograph to separate the [NII] and $H\alpha$ radiation; he verified that in typical emission regions the $H\alpha/\lambda 6584$ ratio ranges from about 2 to 10.

Recently, Hugh M. Johnson,⁽¹⁰⁵⁾ at the Yerkes Observatory, has carried out a detailed survey of the spectra of emission nebulosities with the B spectrograph so adjusted as to isolate a band 7 Å. wide and 12° of arc long in the sky. Spectra of a standard lamp and of a diffusing screen illuminated by a neon lamp with known intensity steps provided the photometric calibration. He corrected for atmospheric extinction, but did not correct for the interstellar absorption. In order to calibrate his intensities in terms of surface brightness expressed as Strömgren's "emission measure", he observed the central region of IC 405 for which Strömgren has published an emission measure of 7200. His data then could be reduced to yield numbers of hydrogen atoms per cm.³. The Johnson catalogue lists for each nebula the relative intensities of the observed lines, the emission measure, the dimensions of the nebula, and the illuminating stars. Johnson concludes that the extended HII regions are ionized by radiation from O stars. The distances of the O stars are not well known: hence the distances of the corresponding HII regions are uncertain.

Struve and Elvey had noticed that the emission regions were confined closely to the galactic plane; none were observed at high galactic latitudes. Johnson found that every O star within 270 parsecs of the galactic plane was associated with an *HII* emission, whereas the seven O stars more remote than this from the galactic plane had no associated emission at all. That is, the interstellar gas must be confined to a band 500 parsecs thick centred on the galactic plane. The O stars that acquire sufficient velocity to take them out of the plane to distances of the order of 300–700 parsecs drift into regions where there is no interstellar gas.

Hugh Johnson also found the angular extents of the emission regions to be usually greater than those found by *H α* photography by Shajn and Hase⁽⁷⁴⁾ and by Sharpless and Osterbrock.⁽⁷⁶⁾ For example, Johnson finds an angular extent of 5.4° for NGC 1499, whereas Hase and Shajn find $200' \times 60'$ and Sharpless and Osterbrock get $2.4^\circ \times 0.8$. There is a faint extension of the emission in which NGC 1499 appears as a dense cloud. In Monoceros, Minkowski found a disk of $80'$ diameter around the cluster NGC 2244, whereas Johnson finds the entire region of $5^\circ \times 6^\circ$ between NGC 2237 and NGC 2264 to be filled with emission. He suggests that the brighter photographic disk is a dense core in a rarer stratum rather than a sphere of ionized hydrogen in a much more extended medium of uniform density.

The average value of the *H α* /6584 ratio is 3.2, and there appears to be a tendency for the ratio to increase as the surface brightness in *H α* increases. Johnson's spectroscopic data pertain primarily to the visual region, although he gives intensity estimates for $\lambda 3727$. His $I(H\alpha)/I(H\beta)$ ratio is very much larger than that found in the planetaries or that found by other observers for the Orion nebula. Further work on the spectra of emission nebulae is needed.

10. The Illumination of Diffuse Galactic Nebulae

The nature of the diffuse galactic nebulae was resolved only by spectroscopic observations and the establishment of a distance scale. Maupertius believed the nebulae to be rotating masses, which are either self-luminous or shining with borrowed light. J. D. Cassini and Lacaille believed all nebulae to be vast systems of stars. As early as 1797, Von Hahn discussed the question of possible dark matter in the Orion nebula versus the effect of contrast between the nebula and an empty sky background, and concluded in favour of the existence of a cloud of absorbing matter intermingled with the luminous material of the nebula.

Application of the spectroscope showed that some diffuse nebulae, e.g. Orion, M8, and the Trifid, had an emission-line spectrum superposed on a continuum. Other nebulae, such as the reflection nebula in the Pleiades

or NGC 7023, showed a spectrum that was simply a reflection of the spectrum of the central star.⁽¹⁰⁶⁾ A crucial fact for the interpretation of the diffuse galactic nebulae was established by Hubble, who found that if the spectrum of the illuminating star was later than B1 the nebula would simply reflect the spectrum of the star.

The diffuse galactic nebulae contain both solid particles (presumably grains of frozen H_2O , CH_4 , CO_2 , and other familiar compounds of abundant elements) and gas (mostly hydrogen, but with some helium and other permanent gases). If the temperature of the illuminating star is high, there will be a rich source of ultra-violet radiation and the gas will fluoresce, the hydrogen lines being produced by the primary mechanism. If the star is cooler than about $20,000^\circ\text{K}$., there will be an insufficient amount of ultra-violet radiation to ionize the hydrogen, the gas will not be excited, and the particles will tend to reflect the starlight. Some fluorescence by solid particles may also occur. The continuous spectrum in emission nebulae frequently seems to be weaker than in reflection nebulae. In some instances the grains are probably evaporated, leaving only the gas behind, and in others the concentration of light in the lines may be so very much stronger that by contrast the impression is left that the continuous background is weaker.

An exception to Hubble's rule must be noted for certain nebulae associated with the T Tauri variable stars (see Section 12) whose spectra show them to be dwarf G and K stars.

Hubble pointed out an important relationship between the apparent size of a diffuse nebula and the magnitude of the illuminating star, provided the following conditions are fulfilled:

- (1) The light falling upon an elementary area dS of a nebula is proportional to the inverse square of its distance from the star. That is, there is no absorption of light between the star and the elementary volume that scatters the light in the direction of the observer.
- (2) All starlight that is intercepted in each elementary volume is scattered evenly in all directions without change in colour, i.e. the nebular material is essentially white.
- (3) The light escapes from the point in the nebula at which it was scattered without further absorption.
- (4) There is no absorption of light in space between the star or nebula and the observer.

The well-known relation established by Hubble is⁽¹⁰⁷⁾

$$m+5 \log a_1=B, \quad . \quad . \quad . \quad (6)$$

where m is the apparent magnitude of the star (or equivalent magnitude of a cluster of stars) and a_1 is the maximum angular distance from the star

(or geometrical centre of the cluster) to the boundary of the nebular image as photographed on a Seed 30 plate exposed 60^m with an *f*5 reflector. If other exposure times are used, the observed angular diameters of the nebula must be corrected. If the various spatial orientations of the nebula are neglected, the theoretical value of the constant, *B*, as given by Hubble; is 11.61. Hubble suggested -0.98 as the correction to be applied to *B* to allow for the random distribution of directions of the scattering surfaces, but Zanstra⁽¹⁰⁸⁾ concluded that the correction should be -0.52.

The remarkable result Hubble obtained was that the observed $m - \log a_1$ plot fitted the theoretical line, the empirical constant on the right-hand side of equation (6) being 11.02. The agreement is startling for, *a priori*, we would suppose that the $m + \log a_1 = B$ relation would be a limiting line to the area in the diagram filled by scattered observed points. That is, almost everything we can think of would make the brightness of the nebular surface lower than predicted by equation (6). First, extinction of the incident starlight before it is scattered and second, extinction of the scattered starlight should make the nebular surface dimmer. Third, a high reflectivity of the scattering particles is demanded; they must be about as white as snow. We must assume that the nebular material is spread out smoothly. There must be no lumps or density concentrations. Difficulties are therefore presented by objects such as the wonderfully intricate nebula, NGC 6888, where the surface brightness is a maximum at the outer boundary and the observed angular size does *not* depend on the exposure time!

Some nebulae are actually brighter than the theoretical relation predicts. In other words, they scatter more visible light than they appear to receive from the star. In some instances this discrepancy may be due to an absorbing cloud in front of the star. In others it appears to arise from actual fluorescence in the solid grains. That is, ultra-violet radiation impinging upon the tiny crystals is degraded into radiation in the visible wavelengths. Without a knowledge of the specific qualities of the material involved, an actual calculation of the amount and the energy distribution of the emitted radiation is not possible.

Hubble concluded that both reflection and emission nebulae obeyed the same $m - \log a_1$ relationship, but a more recent discussion of somewhat more extended material by Cederblad indicates that there is a slight difference in the two relationships.⁽⁷⁰⁾ For the reflection nebulae he finds

$$m + (4.82 \pm 0.22) \log a_1 = 10.41, \quad . \quad . \quad (7)$$

while the emission nebulae obey a law of the form

$$m + (4.66 \pm 0.61) \log a_1 = 11.08. \quad . \quad . \quad (8)$$

The displacement of the line representing the emission nebulae is in such a direction as would be expected if all diffuse galactic nebulae were similar in composition. Cederblad attributes the smallness of the displacement to a smaller optical thickness of the emission nebulae as had been suggested by the investigations by Struve and Miss Story.⁽¹⁰⁹⁾

Statistical discussions of the above type probably cannot be pursued further with great profit. At the moment it appears that much more is to be gained by detailed photometric, polarization, and spectroscopic studies of individual nebulae. The diffuse nebulae exhibit such complex structures that progress in detailed interpretation is necessarily slow.

Photometric studies of the distribution in brightness as a function of the distance from the existing star have been carried out by L. Rosino⁽¹¹⁰⁾ and by others for the Orion nebula. The reflection nebula, NGC 7023, has been studied by P. C. Keenan⁽¹¹¹⁾ and more recently in greater detail by E. B. Weston. Messier 8, the Trifid nebula, M16, M17, NGC 6888, and others have been studied by Albert Boggess III.

Polarization investigations have been carried out for a number of diffuse nebulae.⁽¹¹²⁾ These studies are of particular value for estimating the sizes of the particles responsible for the scattering of light.

11. Emission Nebulosities in External Galaxies

The Large Magellanic Cloud contains large numbers of luminous early-type stars, Wolf-Rayet stars, supergiants, and quantities of absorbing material. It appears to be largely a Type I population. Although a Type II component seems to be present, no bona-fide planetaries have been identified. The spectra of the brighter stars have all been observed, and photo-electric colours and magnitudes have been measured.

The Large Magellanic Cloud contains a great number of diffuse nebulous objects. Many were observed by Sir John Herschel,⁽⁸³⁾ who noticed that they were irresolvable but apparently situated at about the same distance as stars of the seventh or eighth magnitude and open star clusters exhibiting every degree of resolvability. R. E. Wilson mentions 278 of them, but the actual count is probably more if extended wisps are counted as separate objects and the faint areas of low surface brightness are included. Early observations showed them to differ greatly in size, shape, and surface brightness.

An idea of the character of these objects can best be gained by inspection of Fig. 16. From the extremely large intricate structure of NGC 2070 down to the smallest stellar nebulosities that are distinguishable from stars only on objective prism plates, every conceivable form and shape seems to be represented from nearly symmetrical ring or shell objects to extremely wispy forms. Miss Cannon⁽¹¹³⁾ has described the spectra of the brighter



FIG. III : 13. *The η Carinae Nebula*

This photograph was obtained on a red sensitive 103a-E emulsion with a red filter (Wratten 25A), May 7, 1951, with the Armagh-Dunsink-Harvard Baker-Schmidt telescope at Bloemfontein, O.F.S., South Africa. The plate is centred at $\alpha=10^{\text{h}}43^{\text{m}}$, $\delta=-59^{\circ}4$.

(Courtesy Bart J. Bok, Harvard College Observatory.)



FIG. 11 : 14. *The Diffuse Nebula Messier 17 (NGC 6618), (Left) [OIII]; (centre) visual continuum; (right) H α + [NII].*

Notice the extreme dimness of the nebula in the radiation of the visual continuum. Some weak line radiation may contribute in this region.
(Photographed by Albert Boggess III with the Curtis Schmidt telescope at the University of Michigan.)

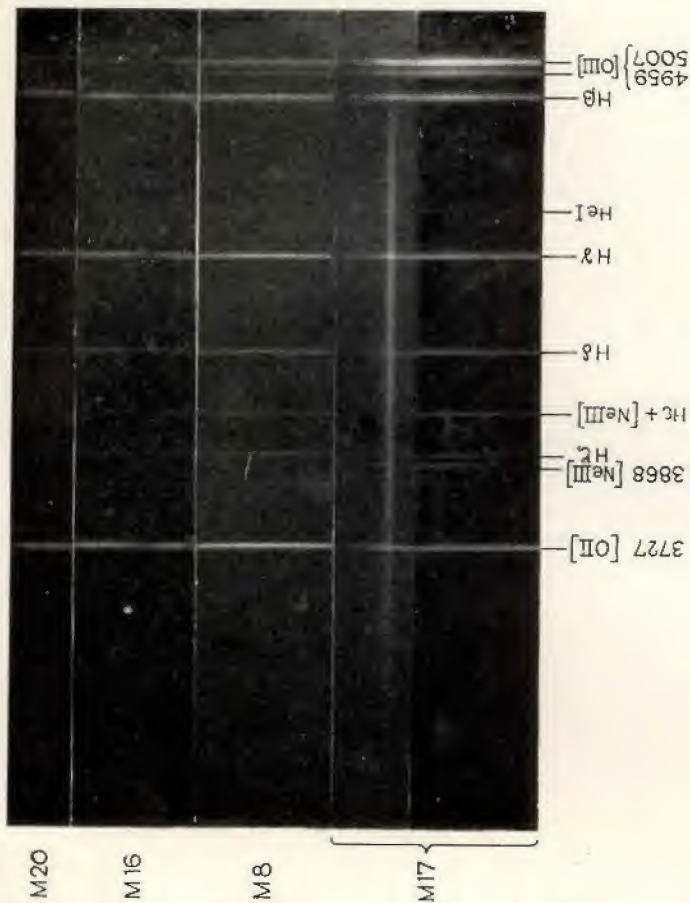


FIG. III : 15. *The Spectra of Four Diffuse Nebulae.*

Notice the relative weakness of the $[OIII]$ lines in Messier 20, Messier 16, and their relative strength in the two spectrograms of Messier 17. The $[NeIII]$ lines appear in the higher excitation M17 nebula. The $[OII] \ 3727$ line is strong in all these diffuse nebulae.

(Photographed at the McDonald Observatory, August 1946.)

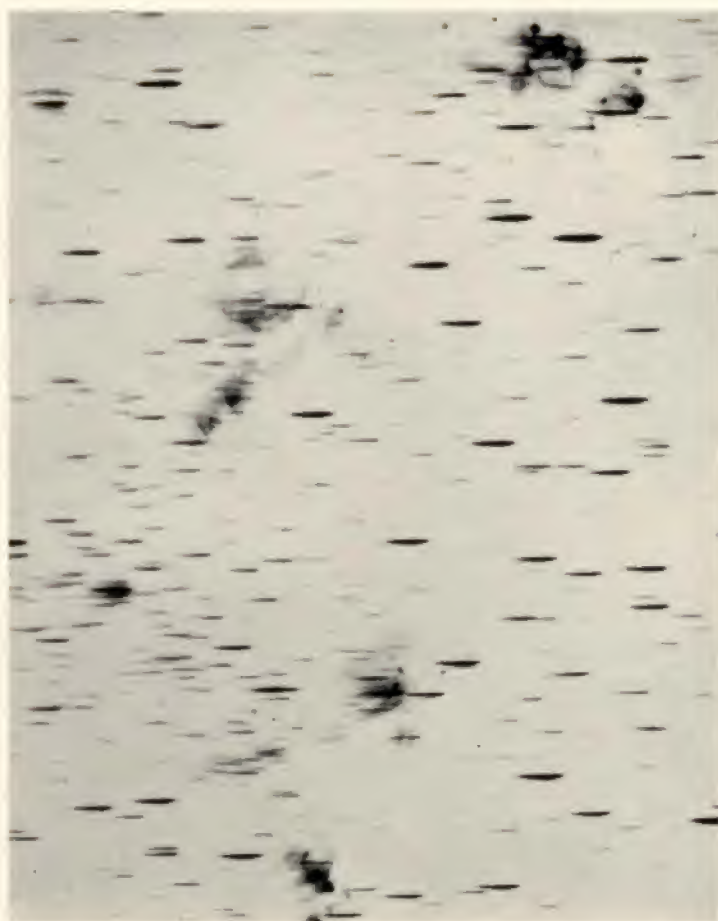


FIG. III ; 16. *An Objective Prism Spectrogram of Emission Nebulosities in the Large Magellanic Cloud.*

On this negative print the stellar images are recorded as short, stubby spectra. The emission nebulosities which radiate a strong $H\alpha$ are recorded as they would be upon a direct photograph. Notice the intricate structure of some of these nebulosities and the number of small, round nebulosities.

(Photographed by Karl G. Henize with the Mt. Wilson 10-in. camera and objective prism upon a 103a-E emulsion at the Lamont-Hussey Observatory of the University of Michigan, Bloemfontein, O.F.S., South Africa.)

objects, giving the relative intensities of N_1 , N_2 , and $H\beta$. R. E. Wilson⁽¹¹⁴⁾ measured the radial velocity of seventeen of these nebulae, verifying that all of them belonged to the Large Magellanic Cloud. He also called attention to the fact that the $(N_1 + N_2)/H\beta$ intensity ratio was much closer to the values found for the diffuse gaseous nebulae in our own system than it was to the planetary nebulae. He was able to measure the velocity of only one gaseous nebula in the Small Magellanic Cloud.

Shapley and Miss Harvia H. Wilson⁽¹¹⁵⁾ described the twenty-two brightest nebulae in the Large Cloud and made estimates of their integrated absolute magnitudes. They concluded that most of these nebulae were brighter than the Orion nebula to which they assign an absolute magnitude of -3 . One of them in particular, NGC 2070 or 30 Doradus, turned out to be the largest and brightest gaseous nebula known, so luminous that were it to replace the Orion nebula it would more than fill the whole constellation with a bright, shining surface!

Recently, Karl G. Henize has photographed the Magellanic Clouds with the 10-in. visually corrected photographic telescope used by Merrill at Mt. Wilson in his search for Be stars. Both direct and prismatic exposures are necessary to separate $H\alpha$ emission areas from star clusters, etc. Widened exposures permit an approximate reduction of the surface brightnesses of the nebulosities to an absolute scale by the method of Ambarzumian, provided the colours, magnitudes, and spectra of appropriate comparison stars are known. A catalogue of these emission nebulosities has been prepared by Henize. For each object listed, the position, dimensions, description, and data concerning the illuminating stars are given. The surface (and sometimes total) brightnesses of most of these nebulosities have been measured by Henize, Lowell Doherty, and the writer. For the more complicated nebulosities the surface brightnesses at representative points and, in some instances, the isophotic contours are given. The densities of the nebulae are comparable with the brighter objects in our own galaxy, but exact figures cannot be given as the electron temperature and density fluctuations of the material are not known. Probably the total mass of the gas is comparable with that found in a similar volume in a spiral arm in our own galaxy. The Small Magellanic Cloud also contains gas and a stellar population of Baade's Type I, although the Type II stellar population may actually predominate (see Chapters VII and VIII).

Patches of emission nebulosity are well known in many other galaxies. The outer spiral arms of M31, the Andromeda galaxy, contain many emission nebulae and hydrogen ionization regions.⁽¹¹⁶⁾ Seyfert identified emission nebulosities in M101,⁽¹¹⁷⁾ while G. Haro⁽¹¹⁸⁾ has identified many such objects in a number of external galaxies. Haro used the Tonanzintla Schmidt and 26-in. prism together with $H\alpha$ sensitive plates and a red filter.

He found strong $H\alpha$ in emission in fifty-eight objects in the spiral arms of M31 and noticed that many of them were exactly in or near the edges of conspicuous dark lanes.

The predominantly Type I population galaxy Messier 33 has an unusually large number of emission nebulosities. The bright-line spectra of certain of the nebulous condensations in this galaxy, NGC 588, 595, and 604, were observed many years ago by V. M. Slipher,⁽¹¹⁹⁾ by F. G. Pease,⁽¹²⁰⁾ and by E. P. Hubble.⁽¹²¹⁾ N. U. Mayall and the writer observed additional objects with the nebular spectrograph on the Crossley reflector at the Lick Observatory in a study of the rotation of this spiral galaxy.⁽¹²²⁾ Haro found ninety-seven objects with $H\alpha$ emission, thirty-one of which were previously known as emission nebulosities. He finds that these patches are systematically brighter than the ones observed in the Andromeda spiral by between a half and one magnitude. Objective prism spectrograms obtained at Michigan have added yet a few additional objects (see Fig. 7, Chapter I), while photometric measures on these plates have shown that the nebulosities are comparable in density with the brighter objects in the Milky Way.⁽¹²³⁾ These results have been substantiated recently by Shajn and Hase.⁽¹²⁴⁾

A preliminary catalogue of M33 emission nebulosities giving their relative brightnesses as measured on Curtis Schmidt plates and sizes as obtained from a direct photograph obtained by Mayall was prepared by the writer with the assistance of G. Newkirk and made available to those interested in such problems. Since then it has not only been possible to obtain much better Schmidt plates, but this material has been supplemented with observations secured at Mt. Wilson and Palomar. Large-scale direct photographs taken by Sandage at Palomar will make it possible not only to give improved descriptions and more precise dimensions of the nebulosities, but also magnitudes of the illuminating stars.

In his classical investigation of Messier 33,⁽¹²¹⁾ Hubble called attention to the large number of emission nebulosities involved with bright blue stars. The brightest of these patches, NGC 604, has an extremely intricate structure which is visible even upon plates taken with the 24-in. Schmidt camera. If the distance of the Messier 33 galaxy is taken as 220,000 parsecs the diameter of this object is about 70 parsecs. Actually the distance of M33 is probably closer to 400,000 parsecs so that the NGC 604 nebulosity is nearer 130 parsecs in diameter! Compare this with the dimensions of the inner luminous portion of the Orion nebula whose radius is less than 1 parsec! The nebula is illuminated by a cluster of blue, exceedingly luminous stars, which range in brightness up to $M = -7.5$! Sandage's and Baade's plates obtained with the 200-in. telescope show that many of the illuminating stars associated with emission nebulosities

are actually resolved into multiple stars (reminiscent of θ Orionis) or small clusters.

A detailed study⁽¹²⁵⁾ of the emission spectra of the nebulosities observed to determine the rotation of Messier 33 shows that most of them are low excitation objects—falling in our excitation classes 1 to 4. A typical diffuse nebulosity has a spectrum similar to that of Orion or IC 418 with strong $\lambda 3727$ [OII], Balmer lines of hydrogen, and the green nebular [OIII] lines. In some objects the [NeIII] lines are visible. The nebulosities of highest excitation are NGC 588, IC 132, and IC 133. The absence of [OIII] does not mean that O^{++} is necessarily absent; the N_1 and N_2 lines may be weak as in NGC 40 or BD+30° 3639. Certain nebulosities show only $\lambda 3727$ [OII], and this line appears in the inconspicuous nucleus of the spiral.

When the green nebular lines are weak as in the diffuse nebulae, the $\lambda 5007/\lambda 3727$ ratio is a very sensitive indicator of excitation. At the same time, the $H\beta/\lambda 3727$ intensity ratio is insensitive to changes in excitation. The reason for this effect is that in typical diffuse gaseous nebulae which show spectra of the IC 418 or Orion type, most of the oxygen is neutral or singly ionized and very little is doubly ionized. If the energy density in the far ultra-violet radiation field is even slightly increased, O^+ will tend to become ionized to O^{++} with a consequent strengthening of the green nebular lines. The percentage decrease in the number of O^+ ions may be small, so that the absolute intensity of $\lambda 3727$ may be changed by an undetectable amount. Stellar spectra exhibit a somewhat analogous phenomenon; with rising temperature along the spectral sequence the lines of the ionized atom may strengthen appreciably before any effect is noticed on the lines of the neutral atom. Since the ionization potentials of neutral oxygen and hydrogen are very nearly equal, the intensity of the radiation field just beyond the Lyman limit at $\lambda 912$ determines the rate at which both oxygen and hydrogen will be ionized. Collisions between electrons and O^+ ions excite the atoms to the 2D term from which they can cascade with the emission of the $\lambda 3727$ pair. The intensity of $\lambda 3727$ will therefore depend on the product $N_e N(O^+)$, while that of the Balmer lines will depend on the recombination rate and therefore on N_e^2 . If the electron temperature is kept constant and if the exciting stars are not so hot that O^+ is appreciably ionized, the hydrogen lines and $\lambda 3727$ will tend to increase or decrease in absolute intensity together. Such quantitative discussions as are possible (cf. Chapter V) show that for equal intensities of $N_1 + N_2$ and $\lambda 3727$ more of the oxygen atoms are concentrated as O^+ than as O^{++} . The difference is smaller the higher the electron temperature! Curiously, the higher excitation nebulae tend to be found at greater distances from the centre of the spiral than do the low excitation nebulosities!

The irregular dwarf galaxy NGC 6822 also shows a number of prominent emission patches, five of which have been described by Hubble.⁽¹²⁶⁾

In more remote galaxies, emission patches are less easy to identify. Incandescent gases frequently reveal their presence by their characteristic emission lines. The most persistent of the nebular radiations appears to be $\lambda 3727$ [OII], which Mayall⁽¹²⁷⁾ and also Humason⁽¹²⁸⁾ have found in the spectra of a very large number of galaxies. Out of seventy-seven nebulae observed with the UV-glass spectrograph Mayall found $\lambda 3727$ in thirty of them. The appearance or non-appearance was strongly dependent on nebular type in that nearly 50% of all spirals showed $\lambda 3727$, whereas only one of the fourteen elliptical nebulae observed showed this emission.

This result is, of course, readily understandable in terms of the population types. The elliptical nebulae are examples of the Type II population which is characterized by an absence of O and B stars and an interstellar medium. The Type I population is represented by the spiral arms of galaxies like our own or Messier 31; it is characterized by bright blue stars, supergiants, and an interstellar medium of gas and solid particles. The fact that even some elliptical nebulae show $\lambda 3727$ is of considerable interest. The irregular nebulae often contain a large Type I population component (e.g. the Magellanic Clouds and NGC 6822). Mayall found $\lambda 3727$ in the integrated spectra of two of the six objects he observed. As one might anticipate, Mayall found a relation between the intensity of $\lambda 3727$ and the presence of other bright lines in the sense that when $\lambda 3727$ was very faint, other emissions are absent, when it is moderately strong [OII], [NeIII], and the Balmer lines might or might not appear, whereas when $\lambda 3727$ was very strong, the characteristic lines of diffuse nebulae did appear. He found no correlation of the intensity of $\lambda 3727$ with the width of the absorption lines nor with the spectral type of the underlying continuum, although he did find that nebulae with strong ultra-violet continua tended to have strong $\lambda 3727$. He found that in NGC 3310, 4736, and 7742, galaxies characterized by bright, prominent spiral arms, $\lambda 3727$ is strong in the spiral structure.

Whether the $\lambda 3727$ radiation originates in discrete diffuse nebulae, illuminated by early-type stars, as appears to be true in the spiral arms of M33, for example, or whether it is emitted over large regions of the interstellar medium cannot be settled easily. In the nuclear region of M33, for example, $\lambda 3727$ is observed as a long, relatively structureless bright line indicative of excitation from a large volume of gas excited by the contributions of many stars. Until more is known concerning the character of the illuminating radiation and the structure of the diffuse nebulae or medium in which the line is produced little further progress can be made in the interpretation of the observations.

Not all external galaxies have low excitation spectra. A small number have spectra with high excitation emission lines similar to those exhibited by NGC 7027. Of the twelve galaxies of this class,⁽¹²⁹⁾ most are intermediate-type spirals with poorly defined amorphous arms, but all have exceedingly bright nuclei to which the high excitation emission spectrum is confined. The underlying absorption spectrum is of the solar type. Many years ago E. A. Fath,⁽¹³⁰⁾ V. M. Slipher,⁽¹³¹⁾ and Campbell and Moore⁽¹³²⁾ observed some of these objects. More recent observations were obtained by E. P. Hubble,⁽¹³³⁾ M. L. Humason,⁽¹³⁴⁾ N. U. Mayall⁽¹³⁵⁾ and particularly by Carl K. Seyfert,⁽¹³⁶⁾ who made an intensive spectrographic study of the six brightest of these "high excitation" galaxies, viz. NGC 1068, 1275, 3516, 4051, 4151, and 7469. High dispersion studies were made of the three having the brightest nuclei, NGC 1068, 3516, and 4151. Seyfert measured the intensities of all the brighter lines with respect to the background continua, whose colour temperature he established by comparison with stars of known energy distribution.

Except for the recombination lines of hydrogen and helium, all the radiations correspond to forbidden transitions. In NGC 1068, 4051, and 4151 the $HeII$ $\lambda 4686$ is strong; $[FeVII]$ is present in NGC 1068 and NGC 4151, indicating a very high excitation. Of considerable interest is the great strength of $[OII]$ in these objects as compared with planetaries of similar excitation. The $[NII]$ radiations are often also quite strong. The relative intensities of the lines show large differences from one nebula to another.

The most striking characteristic of the emission lines, however, is their enormous width. Campbell and Moore had called attention to the broad lines in NGC 1068 and NGC 4151. From a study of the line profiles, Seyfert found all emission lines to be widened, probably by Doppler motion, by amounts up to 8500 km./sec. for the total spread of the Balmer lines in NGC 3516 and NGC 7469. In NGC 4151 the Balmer lines exhibited narrow cores and broad wings corresponding to a total width of 7500 km./sec.! The other emission lines gave asymmetrical profiles that were similar in shape and corresponded to velocities less than 1800 km./sec.! The widths of these emission lines seem to be correlated with the brightness of the nucleus in the sense that the brighter the nucleus and the greater the concentration of light in it, the greater the breadth of the hydrogen lines.

These broad lines present a great puzzle. The emission lines in the brighter nebulosities in M101, M33, and in 30 Doradus or our own galaxy, show no evidence of such large broadening. Evidently these large velocities tend to be restricted to high excitation nebulosities. Since lines of such diverse ions as ionized helium and triply ionized argon show essentially

the same profiles, the broadening cannot be of thermal origin, but must represent large-scale mass motions of material. The velocities in question would appear to exceed the velocity of escape for the most massive galaxy-nucleus. Dissipation of mechanical energy might well account for the character of the spectrum, but the source of the high velocities is difficult to understand.

A high excitation colliding galaxy in Cygnus has been identified as a radio source.⁽¹³⁷⁾ We might expect the galaxies observed by Seyfert also to be strong radio sources, but such appears not to be true.

13. Variable Nebulae and the Associated Stars

We have already mentioned the variability of the η Carinae nebula which is associated with a slow nova. In addition to the nebulae associated with novae, there are variable nebulae associated with other types of variables, the so-called T Tauri stars and related objects.

A century ago J. R. Hind found a nebula, NGC 1555, about 45'' to the west of the irregular variable, T Tauri.⁽¹³⁸⁾ Subsequent observations by H. L. d'Arrest, O. Struve, Lassell, and others showed that this nebula was variable. O. Struve, in 1868, found another variable nebula, NGC 1554, about 4' to the west of T Tauri. In 1890, S. W. Burnham⁽¹³⁹⁾ at Lick found a small, condensed nebula with a maximum length of about 4.4'' immediately surrounding the star; this nebula also proved to be variable. In 1948-9, G. H. Herbig succeeded in observing this nebula spectroscopically with the McDonald reflector.⁽¹⁴⁰⁾ By placing the spectrograph slit in various position angles he was able to measure the extent of the nebula in the different directions. The strongest lines in the spectrum are $\lambda 3726$, $\lambda 3729$ of [OII], followed by $\lambda 4068$, 4076 [SII], and finally the Balmer lines. The [OIII] radiation is definitely missing, although [OI] has been observed. On the other hand, in 1952, Herbig found Hind's variable nebula to show a reflection spectrum which is a precise replica of the T Tauri itself.

T Tauri has a $dG5$ spectrum with broad absorption lines that are presumably widened by rotation.⁽¹⁴¹⁾ Overlying this absorption spectrum are the strong emission lines of H , $CaII$, $CrII$, $TiII$, FeI , $FeII$, and sometimes HeI and $HeII$. The strong [SII] and [OI] lines presumably originate in the small nebula surrounding the star. The emission spectrum resembles that of the solar chromosphere except that the lines are enormously stronger and broader. The H and K lines show self-reversal.

Other faint dwarf stars with late-type absorption spectra and bright emission lines have been observed by Joy in the Taurus region.⁽¹⁴²⁾ All appear to be associated with the dark nebulosity. In an area of 45 square degrees he found forty stars brighter than the fifteenth magnitude with bright $H\alpha$. On the basis of estimates of the size of the dark cloud and the

luminosity function for dwarf stars, Greenstein concluded that every late-type dwarf star within the boundary of the dark cloud showed emission lines.⁽¹⁴³⁾ On the other hand, variable stars associated with nebulosity do not necessarily have bright lines. Investigations by Struve and Greenstein,⁽¹⁴⁴⁾ Herbig,⁽¹⁴⁵⁾ Haro,⁽¹⁴⁶⁾ and others have shown that dwarf variable stars of earlier spectral classes in the Orion nebula are not variables of the T Tauri type. Among the fainter and cooler G and K stars, objects resembling T Tauri are found, although none show such rich emission-line spectra as that of XZ Tauri or RW Aurigae.

Another type of association is exhibited by Hubble's fan-shaped variable nebula, NGC 2261, which is illuminated by the remarkable variable R Monocerotis. The nebula shows an intricate structure in which knots and wisps disappear, only to reappear again after considerable time intervals as though they had been hidden by material passing between them and the star. The R Monocerotis nebula appears to be connected with the extended dark nebula that envelops the nebulous cluster NGC 2264, which is 450 parsecs away.⁽¹⁴⁷⁾ Greenstein finds weak, sharp Balmer lines that may be traced to H15 even on plates of low dispersion. The hydrogen absorption lines are stronger in the nebula than in the star, and appear to become stronger the greater the distance from the star. Apparently the absorption lines become stronger the longer the light path in the nebula. Greenstein concludes that the illuminating star is a main-sequence B or a giant A, F, or G star.⁽¹⁴⁸⁾

Another object resembling R Monocerotis in its connexion with a cometary variable and spectroscopic features is R Coronae Australis, which was studied by Greenstein and the writer with the McDonald reflector.⁽¹⁴⁹⁾ The star spectrum shows weak, sharp Balmer absorption lines plus emission $H\beta$ and $FeII$ lines characteristic of low excitation T Tauri stars. The associated nebula, NGC 6729, has a striking blue continuous spectrum with sharp, strong absorption lines, easily resolved up to $H11$ in spite of the low dispersion of 300 Å./mm. ! The $CaII$ K line appears in absorption and seems to strengthen with increasing distance from the central star. Weak, diffuse lines of HeI $\lambda\lambda 4471, 4026$ also appear. The continuous spectrum of the nebula and the weak emission $H\beta$ and $FeII$ lines appear to be due to the light of R CrA reflected and scattered by small solid grains.

Except for the helium lines, the spectrum of the nebula could be classified as that of a supergiant A5 star. Since the distance of the nebula is about 150 parsecs, were R CrA actually an A5 supergiant, an obscuration of fourteen magnitudes would be required in order to account for its apparent faintness. Since the star and nebula do not appear to be highly reddened, it seems likely that their observed absorption spectra, and

possibly the continuous background as well, may be abnormal and originate in dense clouds of gas and dust completely hiding the star! Spectrophotometric studies of the energy distribution in the continuum of the nebula and its illuminating star show that both NGC 6729 and R CrA are unexpectedly blue compared with other objects deeply immersed in dark nebulae.

The integrated brightness of NGC 1999 is greater than that of the illuminating star BD-6° 1253, which Herbig⁽¹⁵⁰⁾ and independently Morgan and Sharpless⁽¹⁵¹⁾ recognized as a nebular variable. This star shows strong emission lines of *H*, *FeII*, *TiII*, *CrII*, and *CaII* superposed on an underlying absorption spectrum between A0 and F0. Thus it is definitely earlier than typical T Tauri stars and appears to be more luminous than normal dwarf stars of the same spectral class.

Herbig⁽¹⁵²⁾ suggests that practically all emission-line stars found exclusively in association with nebulae can be assigned to one of four groups on the basis of their spectral characteristics, viz.:

- (a) *T Tauri Stars*. The absorption spectra range from F8 to M and are often overlaid by continua. Subdivision on the basis of emission lines is possible. Objects with strong emission lines, e.g. RW Aurigue, XZ Tauri, or RU Lupi, are relatively rare.
- (b) *Stars with Strong Balmer Absorption Lines*. This group includes BD-6° 1253, R CrA, and R Mon; each member illuminates a reflection nebula.
- (c) *Stars whose Spectra suggest Luminosities above the Main Sequence*. These objects may actually be only peculiar members of groups A and B. The prototype is BF Orionis.
- (d) *Peculiar Emission Objects with Strong Emission Spectra and Weak Continua*. They were first found in the dark nebula surrounding BD-6° 1253, and show both permitted and forbidden lines covering a wide excitation range.

Detailed studies of the absolute magnitudes of the K-M type emission-line variables connected with the obscuring clouds in Taurus and Auriga show them to be too bright for their spectral classes. That is, their luminosities would place all of them above the main sequence by amounts ranging up to about three magnitudes!

The next question we might ask concerns the relationship of more luminous stars to diffuse nebulosity in which they are immersed. More specifically, what traces of interaction between the interstellar matter and normal giant stars and main-sequence stars of types A0 and earlier can be found? To answer these questions Greenstein and the writer observed a dozen stars which illuminate bright diffuse nebulae, mostly of the

reflection type.⁽¹⁴⁹⁾ Most of the stars involved were less than 200 parsecs from the sun, and the reddening they showed must have originated from the nebula, a portion of which they illuminate. These stars were, on the average, four magnitudes brighter than Joy's T Tauri stars and almost eight magnitudes brighter than the faint emission objects he found in the Taurus dark nebula. In none of these stars were the usual peculiarities characteristic of the T Tauri stars or of the Orion nebular variables observed. The stars, ranging from B2 to gK2, seemed normal and unaffected by the surrounding nebulosity. In other words, only faint dwarf stars appear to be appreciably affected by the surrounding particles and gas of diffuse clouds.

One possible exception to the above rule might be noted. The diffuse nebula NGC 7023 shows a spectrum that appears to be a faithful reflection of the illuminating star HD 200775. This central star is a Be shell star with rotationally broadened hydrogen lines underlying emission lines with a sharp central reversal. E. B. Weston has made a detailed study of its spectrum.⁽¹⁵³⁾ He has identified the lines of [FeII], and traces of [OIII] and possibly [CrII]. These lines may originate in a portion of the nebula in the immediate neighbourhood of the star; they seem to show small variations in time.

Briefly, stars of intrinsically high luminosity seem to be little affected by surrounding nebulous material, whereas dim dwarf stars may be profoundly affected. The explanation may lie in the circumstance that radiation pressure depends very critically upon the luminosity of the star. A bright star will tend to drive gas molecules and particles away, but they may approach a faint star rather closely. Solid grains of ice, frozen methane, etc., may approach close enough for evaporation to occur and gas to be liberated. V. A. Ambazumian and P. Kholopov called the groups of dwarfish irregular variables in Taurus, Auriga, etc., "*T* associations" and suggested that they were main-sequence stars actually being formed from the interstellar medium on the spot. In their early life they are unstable and behave as irregular variables. Another possibility is that these irregular variables are normal stars that wander into dense regions of the interstellar medium and accrete material. The material falling into the star produces a high excitation "chromosphere". Still a third possibility, favoured by Greenstein,⁽¹⁵⁴⁾ is that the infall of material triggers flares on the stellar surface, and these flares produce the high excitation spectra that are observed.

The broadening of the underlying absorption lines observed by Herbig in the spectra of the T Tauri stars, if interpreted as rotation, suggests average velocities of 50 km./sec., which is much larger than is observed for normal dwarf stars of spectral classes G, K, and M.

If the stars are accreting large quantities of material from a non-quiescent cloud, they would inevitably pick up angular momentum, and we would expect them to have appreciable rotation. If the stars are built up *in toto* from the interstellar medium they would originate rotating even if most of the angular momentum is carried off in the process of their formation.⁽¹⁵⁵⁾

The matter of short-term variations in the spectra of the T Tauri stars is of interest in this connexion. Observations of T Tauri obtained at Ann Arbor show that the spectrum of this star is subject to short-term, i.e. night-to-night, variations in the intensity of the hydrogen lines. Other features of the spectrum also change with time. A similar, but less complete, series of observations on RY Tauri do not reveal any conspicuous changes. RY Tauri illuminates a faint fan-shaped nebula. Observations of R Monocerotis are much more difficult because of the faintness of the star and confusion with the associated cometary nebula. There is some evidence for short-term changes in the Balmer lines. For example, on December 2nd, 1948, $H\gamma$ appeared as a strong absorption line with weak emission on either side; two nights later the emission component of $H\gamma$ was of the P Cygni type.

The strong chromospheric-type emission of the T Tauri stars is certainly connected with the surrounding dense clouds of absorbing material. The exact mechanisms by which the infall of material produces the intense bright-line spectrum is not known. The short period fluctuations in the Balmer line intensities favour some kind of a flare-triggering mechanism as a possible cause of the luminosity. Minkowski⁽¹⁵⁶⁾ has proposed radiation pressure as the cause operating to produce the fan-shaped nebulae, but a satisfactory quantitative theory has not been worked out.

In this chapter we have reviewed some of the principal characteristics of gaseous nebulae and of nebulae that contain both gas and solid particles. Following some material on the theoretical aspects and the illuminating stars, a further account of the planetary and diffuse nebulae will be found in Chapters VII and VIII. Radio "stars" will be discussed in Chapter VIII.

W. Baade has recently* determined the absolute magnitude of the brightest planetaries in the Andromeda spiral to be -2.2 . For these particular objects he estimates the difference in magnitude between the nebula and the central star to be $\delta = m_s - m_n = 4$. Putting $\delta = 4$ in Berman's formula, cf. page 52, for the "reduced" magnitude,

$$M_n = \bar{M}_n' + a\delta = -(0.88 + 0.32\delta),$$

an excellent accord is found between Berman's and Baade's results. An improved value for the absolute magnitude of the galactic planetaries ought to come from the photo-electric measures of the objects in the central bulge of our galaxy.

* This last paragraph was added in proof (April 1955).

REFERENCES

- (1) *Publ. Obs. Univ. Mich.*, **10**, 25 (1951).
- (2) *Lick Obs. Bull.*, **18**, 57 (1938).
- (3) It is of interest that the first accurate estimates of the distances of the planetary nebulae were obtained by purely astrophysical methods; see MENZEL, D. H., *Publ. A.S.P.*, **43**, 334 (1931).
- (4) *Lund. Medd.*, Series II, No. 39 (1938).
- (5) WILSING, *Astron. Nach.*, **136**, 349 (1894); NEWKIRK, *Lick Obs. Bull.*, No. 299 (1917); VAN MAANEN, A., *Proc. Nat. Acad. Sci.*, **3**, 133 (1917). *Mt. Wilson Contr.*, **204** (1921); **290** (1925); and **356** (1928). Table 13 of MWC 356 shows a number of negative parallaxes and many objects with parallaxes smaller than the probable errors 0.0056–0.0104" quoted for this series of observations.
- (6) *Publ. A.S.P.*, **52**, 275 (1930).
- (7) *Astron. Nach.*, **219**, 165 (1923).
- (8) *Publ. A.S.P.*, **27**, 214 (1915), gives a mean proper motion of 0.028" for seventeen objects.
- (9) See, for example, MAKEMSON, *Publ. A.S.P.*, **40**, 136 (1928) (NGC 7662); and VAN DE KAMP and VYSSOTSKY (ref. 6) for NGC 6826.
- (10) *Mt. Wilson Contr.*, **406** (1930); and **463** (1933).
- (11) *Lick Obs. Bull.*, **17**, 21 (1933).
- (12) Anderson points out that the relative proper motion of an object is subject to a probable error which is a combination of three factors:
 - (1) The probable error of a measurement of the object.
 - (2) The probable error of a measurement of the comparison star.
 - (3) The average peculiar motion per year of the comparison stars in any area. The first two depend only on the uncertainty in setting the micrometer wire on the stellar images. The latter may be computed like a probable error, assuming a random distribution of velocities. Its effect on the proper motions of objects is not reduced by measuring additional plates. This mean proper motion of the comparison stars depends on the magnitude and galactic latitude. Anderson found the mean probable error of a proper motion of a planetary nebula to be 0.0033".
- (13) *M.N.R.A.S.*, **110**, 429 (1950).
- (14) *Lick Obs. Publ.*, **13**, 77 (1918).
- (15) *Zeits. f. Ap.*, **2**, 239 (1939).
- (16) *Zeits. f. Ap.*, **8**, 195 (1934). Discussions of galactic rotation have also been given by OGÓRODNIKOFF, *Pulk. Obs. Circ.*, **21**, 15 (1937).
- (17) *M.N.R.A.S.*, **99**, 376 (1939).
- (18) *M.N.R.A.S.*, **99**, 71 (1938).
- (19) *Astr. J. Soviet Union*, **23**, 69 (1946).
- (20) *Publ. A.S.P.*, **40**, 342 (1928).
- (21) See JOY, A. H., *Ap. J.*, **110**, 112 (1949).
- (22) *Lick Obs. Publ.*, **3**, 214 (1894).
- (23) *Lick Obs. Publ.*, **13**, 57 (1918).
- (24) *Observatory*, **56**, 269 (1933).
- (25) *Russ. Ast. Jour.*, **11**, 40 (1934).
- (26) *Phil. Trans. Roy. Soc.*, **186A**, 73 (1894).
- (27) *Astron. and Astrophys.*, **12**, 51 (1893).
- (28) WOLF, *Heidel. Akad. Wiss.*, **35**, Ab. (1911).
- (29) *Astron. and Astrophys.*, **13**, 384, 494 (1894).
- (30) *Lick Obs. Publ.*, **13**, 193 (1918).
- (31) *Lick Obs. Bull.*, **17**, 179 (1935).
- (32) *Lick Obs. Bull.*, **19**, 1 (1939).
- (33) *Ap. J.*, **95**, 356 (1942).
- (34) *Publ. A.S.P.*, **58**, 258 (1946).
- (35) *Publ. A.S.P.*, **61**, 181 (1949).
- (36) *Harvard Annals*, **76**, 20 (1916).
- (37) *Harv. Bull.*, 855 (1928).

- (38) *Ap. J.*, **67**, 1 (1928).
 (39) *Ap. J.*, **96**, 78 (1942).
 (40) *Ap. J.*, **95**, 243 (1942).
 (41) *Publ. Amer. Astron. Soc.*, **10**, 327 (1944).
 (42) *Lick Obs. Bull.*, **15**, 86 (1930).

The total intensities have to be corrected for an error in dispersion. This correction factor, expressed in magnitudes is as follows:

N_1	—0.09	$H\delta$	0.58	3869	0.83
$H\beta$	0.00	$H\epsilon$	0.70	$H\eta$	0.85
$H\gamma$	0.38	$H\zeta$	0.80	3727	1.00

- (43) *Publ. D.A.O.*, **4**, 187 (1931).
 (44) *Ann. d'Ap.*, **4**, 30 (1941).
 (45) *Ap. J.*, **113**, 125 (1951); **93**, 236 (1941).
 (46) *Comptes Rendu Paris Academy*, **231**, 1432 (1950); **234**, 62 (1952).
 (47) *Publ. Obs. Univ. Mich.*, **7**, 93 (1938); **8**, 147, 159 (1939).
 (48) *Zeits. f. Ap.*, **16**, 201 (1938); **20**, 91 (1940).
 (49) *M.N.R.A.S.*, **96**, 771 (1936). These numerical results have been supplanted by the more accurate values calculated by BAKER, J. G., and MENZEL, D. H., *Ap. J.*, **88**, 60 (1938).
 (50) *Ap. J.*, **96**, 230 (1941). The target areas for collisional excitation are probably much too large. M. J. Seaton has obtained greatly improved values for these parameters recently.
 (51) *Ap. J.*, **65**, 50 (1927).
 (52) *Publ. A.S.P.*, **38**, 295 (1926).
 (53) *Pulkova Obs. Bull.*, **13**, No. 3 (1933); *M.N.R.A.S.*, **93**, 50 (1932).
 (54) *Ap. J.*, **91**, 215 (1940).
 (55) *Ap. J.*, **93**, 244 (1941).
 (56) *Ap. J.*, **102**, 252 (1945).
 (57) *Ap. J.*, **67**, 1 (1928).
 (58) *Proc. Nat. Acad. Sci.*, **19**, 581 (1933).
 (59) See the author's *Astrophysics—the Atmospheres of the Sun and Stars*, p. 114, 151 (Ronald Press Co., New York, 1953), hereafter abbreviated as *Astrophysics I*.
 (60) *Comptes Rendu Paris Academy*, **198**, 1842 (1934).
 (61) *Ap. J.*, **81**, 1 (1935).
 (62) See, for example, *Astrophysics I*, p. 130.
 (63) *Publ. A.S.P.*, **46**, 146 (1934).
 (64) One exception to this rule must be noted. The $\lambda 3121.71$ line which is observed in a number of nebulae arises from the $2p3d^3P_1$ level. It may arise from resonance absorption of $\lambda 303$ by atoms moving with relative velocities of 90 km./sec., speeds which are rather higher than in most planetary nebulae.
 (65) *Ap. J.*, **94**, 436 (1941).
 (66) *Jap. Journ. Astr. and Geophys.*, **20**, 505 (1944).
 (67) *Ap. J.*, **91**, 307 (1940).
 (68) The earlier literature has been summarized by HOLDEN, E. S., *Index Catalogue of Books and Memoirs relating to Nebulae and Clusters*, Smithsonian Misc. Coll. 311 (Washington, 1877).
 (69) See STRUVE, O., and ELVEY, C. T., *Ap. J.*, **89**, 119 (1939); **90**, 301 (1939).
 (70) *Lund Medd.*, Series II, No. 119 (1946). This paper also contains an extensive bibliography of the literature on galactic nebulae.
 (71) See, for example, STROHMEIER, W., and GOLLNOW, H., *A.N.*, **275**, 167 (1947) (diffuse nebulae at $\alpha = 6^h 26.8^m$, $\delta = +2^\circ 34'$ (1855) and $\alpha = 6^h 28.2^m$, $\delta = +9^\circ 30'$ (1855), the latter being associated with a red star), STROHMEIER, W., *Himmelswelt*, **55**, 94 (1948); **56**, 84 (1949); *Sterne*, **25**, 150 (1948); and MINKOWSKI, R., *Publ. A.S.P.*, **61**, 151 (1949).
 (72) Red photographs of the region of Orion, Sagittarius, Serpens, Scutum, and Cygnus were published in *Sky and Telescope*, **8**, 255 (1949). See also DUNCAN, J. C., *Ap. J.*, **109**, 479 (1949), for descriptions of the nebulous regions in Cygnus.
 (73) *Ap. J.*, **118**, 362 (1953).
 (74) *Publ. Crimean Astrophys. Obs.*, **7**, 87 (1951); **9**, 52, 123 (1952).
 (75) *Publ. Crimean Astrophys. Obs.*, **8**, 3 (1952).
 (76) *Ap. J.*, **115**, 89 (1952).

- (77) *Astr. Journ.*, **58**, 36 (1953).
- (78) See Chapter I by MORGAN, W. W., KEENAN, P. C., in *Astrophysics, A Topical Symposium* (McGraw-Hill, New York, 1951).
- (79) *Astr. Journ.*, **57**, 3 (1952).
- (80) *Ap. J.*, **118**, 318 (1953).
- (81) *Publ. Obs. Univ. Mich.*, **10**, 7 (1951).
- (82) *Ap. J.*, **56**, 174 (1922).
- (83) HERSCHEL, SIR WILLIAM, *Collected scientific papers*, II, 651 (1912), London. HERSCHEL, SIR JOHN, *Cape Observations 1834-1838*, 14 (1847), London, gives a drawing of it.
- (84) *Lick Obs. Publ.*, **8**, plate 56 (1908).
- (85) *Lick Obs. Publ.*, **11**, plates 49, 51, 52 (1913). See also *Astron. Nach.*, **177**, 234 for a description of the nebula.
- (86) *Lick Obs. Publ.*, **13**, plate VII, fig. 81 (1918).
- (87) *Harvard Observatory Annals*, **105**, 241, plate I (1936).
- (88) *Ap. J.*, **51** (1919), plate II.
- (89) *Lick Obs. Publ.*, **13**, 134 (1918).
- (90) *Lick Obs. Bull.*, **14**, 154 (1930).
- (91) *Upsala Annals*, No. 3 (1940). Approximate isophotic contours of the nebular radiation are given in this paper.
- (92) *Phil. Trans. Roy. Soc.*, **154**, 437 (1864).
- (93) *Phil. Trans. Roy. Soc.*, **158**, 72 (1868).
- (94) *Proc. Roy. Soc. London*, **33**, 425 (1882).
- (95) *M.N.*, **48**, 360 (1888).
- (96) *Ap. J.*, **8**, 317 (1898); **2**, 161 (1895).
- (97) *Ann. d'Astrophys.*, **7**, 143 (1944).
- (98) *Ap. J.*, **122**, 235, 1955.
- (99) *Ap. J.*, **89**, 647 (1938).
- (100) *Ann. d'Ap.*, **7**, 80 (1944); **12**, 6 (1949).
- (101) *Ap. J.*, **104**, 414 (1946).
- (102) *Publ. Amer. Astron. Soc.*, **9**, 274 (1939).
- (103) STRUVE has summarized these observations in *Journ. Wash. Acad. of Sciences*, **31**, 217 (1941).
- (104) *Ap. J.*, **108**, 157 (1948).
- (105) *Ap. J.*, **118**, 370 (1953).
- (106) See SLIPHER, V. M.; *Lowell Obs. Bull.*, **55** (1913); (Pleiades), **75**, 1916, (ρ Ophiuchi nebula); **81** (1918); *Publ. A.S.P.*, **30**, 63 (1918); (NGC 7023), **31**, 212 (1919); *Publ. Amer. Astron. Soc.*, **9**, 168, 229 (1939).
- (107) *Ap. J.*, **56**, 400 (1922). Derivations of this equation may also be found in J. L. Greenstein's chapter in HYNEK, J. A., *Astrophysics* (McGraw-Hill Book Co., New York 1951), and in the author's *Stellar Interiors, Nuclear Transformations, and Nebulae* (Ronald Press Co., New York 1953).
- (108) *Ap. J.*, **65**, 60 (1927).
- (109) *Ap. J.*, **84**, 204 (1936).
- (110) *Bologna Obs. Publ.*, **5**, No. 4 (1947).
- (111) *Ap. J.*, **84**, 600 (1936).
- (112) See, for example, the study of the reflection nebula NGC 6729 by WHITNEY, W. T., and WESTON, E. B., *Ap. J.*, **107**, 371 (1948).
- (113) *Harvard Observatory Annals*, **76**, 3.
- (114) *Lick Obs. Publ.*, **13**, 187 (1918).
- (115) *Harvard Observatory Circular*, 271 (1925).
- (116) See, for example, BAADE, W., *Publ. Mich. Obs.*, **10**, 12 (1951), fig. 5.
- (117) *Ap. J.*, **91**, 261 (1940).
- (118) *Astr. Journ.*, **55**, 66 (1950).
- (119) *Pop. Astron.*, **23**, 23 (1915); *Proc. Amer. Phil. Soc.*, **56**, 406 (1917).
- (120) *Publ. A.S.P.*, **27**, 239 (1915).
- (121) *Ap. J.*, **63**, 236 (1926).
- (122) *Ap. J.*, **95**, 5 (1942).
- (123) ALLER, L. H., *Astr. Journ.*, **56**, 34 (1951).
- (124) *Publ. Crimean Astrophys. Obs.*, **9**, 13 (1952).
- (125) ALLER, L. H., *Ap. J.*, **95**, 52 (1942).
- (126) *Ap. J.*, **62**, 409 (1925).

- (127) *Lick Obs. Bull.*, **19**, 33 (1939).
- (128) *Ap. J.*, **83**, 10 (1936).
- (129) NGC 1068, 1275, 2782, 3077, 3227, 3516, 4051, 4151, 4258, 5548, 5814, and 7569.
- (130) *Lick Obs. Bull.*, **5**, 71 (1908).
- (131) *Pop. Astron.*, **25**, 36 (1917); *Proc. Amer. Phil. Soc.*, **56**, 403 (1917); *Lowell Obs. Bull.*, **3**, 59 (1917).
- (132) *Lick Obs. Publ.*, **13**, 88 (1918).
- (133) *Ap. J.*, **64**, 328 (1926).
- (134) *Publ. A.S.P.*, **44**, 267 (1932).
- (135) *Publ. A.S.P.*, **46**, 134 (1934).
- (136) *Ap. J.*, **97**, 28 (1943).
- (137) BAADÉ, W., and MINKOWSKI, R., *Ap. J.*, **119**, 206 (1954).
- (138) BARNARD, E. E., *M.N.R.A.S.*, **55**, 442 (1895); **59**, 372 (1899), summarized the early visual observations.
- (139) *Lick Obs. Publ.*, **2**, 175 (1894).
- (140) *Ap. J.*, **111**, 11 (1950).
- (141) See JOY, A. H., *Ap. J.*, **102**, 168 (1945), for an account of the spectra of these stars.
- (142) *Publ. A.S.P.*, **58**, 244 (1946); *Ap. J.*, **110**, 424 (1949).
- (143) *Harvard Obs. Monographs*, No. 7, Centennial Symposia, 19 (1948).
- (144) *Publ. A.S.P.*, **58**, 366 (1946).
- (145) *Ap. J.*, **111**, 15 (1950).
- (146) *Astr. Journ.*, **55**, 72 (1950).
- (147) See TRUMPLER, R. J., *Lick. Obs. Bull.*, No. 420 (1930).
- (148) *Ap. J.*, **107**, 375 (1948).
- (149) *Publ. A.S.P.*, **59**, 139 (1947).
- (150) *Publ. A.S.P.*, **58**, 163 (1946).
- (151) *Ap. J.*, **103**, 249 (1946).
- (152) *Journ. Roy. Astron. Soc. Canada*, **46**, 222 (1952).
- (153) *Publ. A.S.P.*, **61**, 265 (1949).
- (154) *Publ. A.S.P.*, **62**, 156 (1950).
- (155) See VON WEIZSÄCKER, C. F., *Ap. J.*, **114**, 165 (1951).
- (156) *Publ. A.S.P.*, **54**, 190 (1942).

CHAPTER IV

Physical Processes in Gaseous Nebulae

1. The Radiative Equilibrium of a Gaseous Nebula

We must now turn to the theoretical analysis (in so far as it is possible) of the gaseous nebulae. As a starting-point we shall consider as a first approximation to a planetary nebula a homogeneous, spherical shell of hydrogen gas surrounding a very hot star. We postulate that the state is a steady one. To idealize the problem yet further we shall suppose that the star radiates as a black body at a temperature T_1 , at least beyond the Lyman limit.

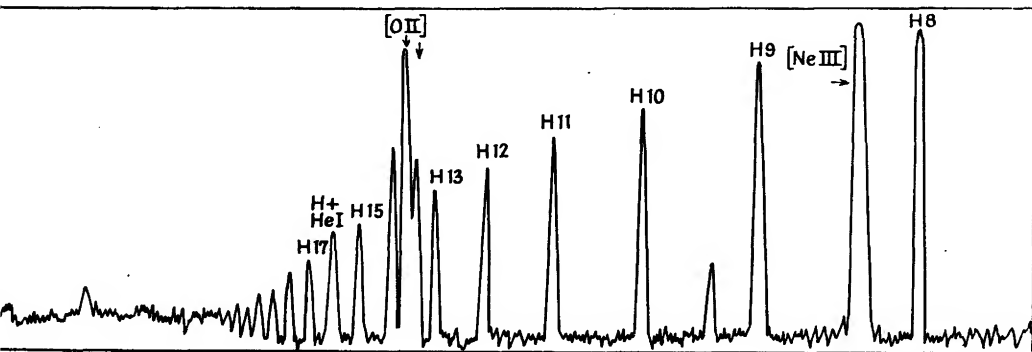


FIG. IV : 1. *Tracing of the Spectrum of IC 4997 ($\lambda 3600\text{--}\lambda 3900$).*

This spectrogram was secured with the Cassegrain spectrograph on the 82-in. McDonald Observatory reflector, September 1945. Notice the confluence of the hydrogen lines to the Balmer limit near $\lambda 3650$. A few lines of [OII], [NeIII], and HeI fall in this region. Compare with Fig. 9 of Chapter III.

In spite of the fact that the nebular gases must derive all their energy from the central star, the visual brightness of the planetary nebula is often many times greater than that of this star. As we have seen in Chapter III, the explanation lies in the circumstance that most of the stellar radiation is emitted in the ultra-violet and degraded by the nebular gases into visible light. Hydrogen, the most abundant of the chemical constituents in stars and nebulae, plays a major role in the softening of the ultra-violet star-light.

The mathematical analysis is greatly simplified by the fact that ionizations and excitations occur only from the ground-level. Recaptures occur

in all levels so that the observed Balmer spectrum is predominantly a recombination one, although in a thick nebula or one surrounding a star with bright lines some line excitation may occur.

The first problem will be to examine the distribution of the atoms among the various energy levels, i.e. the statistical equilibrium of the nebula. If we can calculate the populations of the various excited levels we can predict the relative intensities of the hydrogen lines, i.e. the intensity *decrement* in the Balmer series, a quantity that can be observed. Fig. 1

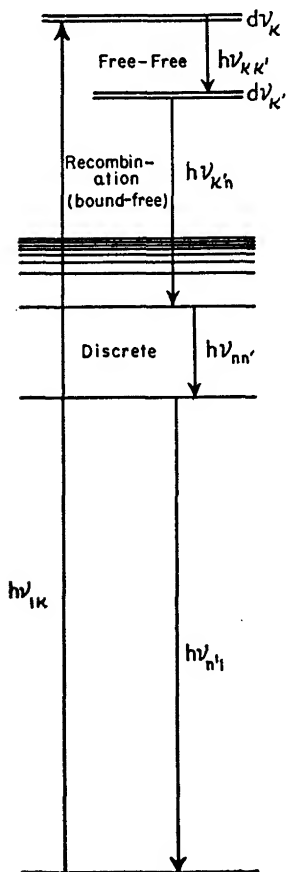


FIG. IV: 2.
Transitions in Hydrogen.

shows a tracing of the higher members of the Balmer series in the planetary nebula, IC 4997.

In our first reconnaissance of the problem we shall neglect all collisional excitations, although this limitation is not a fundamental one. Later we shall see how the theory can be modified in a straightforward way to take care of line excitation by electron collision.

Historically, two methods of approach to this problem were used. The first, due to H. H. Plaskett,⁽¹⁾ amounts to what might be called a "mechanistic" argument. He computed the number of captures in a particular energy level and then traced the ensuing history of these atoms as they cascaded to lower levels, following them through successive transitions all the way to the ground-level. Carroll⁽²⁾ and later Cillie⁽³⁾ followed an "equilibrium" approach in which they equated the number of atoms leaving a particular energy level by radiative transitions to the number so entering it. Carroll was able to give an exact solution for a hypothetical atom with seven bound levels and a continuum. Cillie made calculations for a fourteen-level atom. The method of Carroll and Cillie is unsatisfactory in that it does not allow for the continuity of energy levels through the higher terms and on into the continuum.*

In this connexion Plaskett's seven-level atom treatment was superior, in that by a mechanistic argument he was able to make some allowance for the levels and transitions Carroll had to neglect.

* The use of exact hydrogenic Einstein A 's for transitions involving the bound levels and exact recapture coefficients for the bound-free transitions leads to inconsistencies if only a small number (e.g. 7 or 14) levels are considered.

Actually, if we consider real hydrogen atoms with an infinite number of levels, the mechanistic and equilibrium points of view turn out to be the same. Menzel and Baker⁽⁴⁾ showed that an exact solution of the problem of statistical equilibrium for the hydrogen atom with an infinite number of levels is possible. They treated first the problem where the radiation impinging upon the nebula comes from beyond the limit of the Lyman series. Hence atoms enter the discrete levels only by recapture from the continuum or cascade from higher levels. Their method is not restricted to this special condition, however, but may be applied whenever the nature of the radiation field is specified. We shall see that the "equilibrium" point of view is often simpler, but for some problems such as the evaluation of the relation between the electron temperature and that of the exciting star, the "mechanistic" argument is useful.

The constancy of the number of atoms in a given level n , the condition of *statistical equilibrium*, is ensured by requiring that the number of atoms entering the level be equal to the number of atoms leaving. Let us first consider the ground-level. Atoms may enter this level by direct captures from the continuum and by cascades from higher levels. They may leave by line excitation to higher levels or by photo-ionization. If F_{n1} denotes the number of downward transitions from level n to 1, F_{1n} the number of upward transitions from 1 to n , while $F_{\kappa 1}d\nu$ denotes the captures from the continuum in the energy range $h d\nu$ of the free electron, then

$$\sum_2^{\infty} F_{n1} + \int_{\nu_1}^{\infty} F_{\kappa 1} d\nu = \sum_2^{\infty} F_{1n} + \int_{\nu_1}^{\infty} F_{1\kappa} d\nu. \quad (1)$$

cascades
from higher
levels

captures
from
continuum

excitation
to higher
levels

photo-
electric
ejections

The summations are taken over all discrete levels. The integrations over the continuum are taken from the Lyman limit ν_1 .*

The significance of the symbol κ employed in this and following equations may be clarified with the aid of the following discussion.

Consider a free electron moving with a velocity v . Its kinetic energy is $\frac{1}{2}mv^2$, and when it is recaptured by a hydrogen atom in a level n' , it radiates an amount of energy

$$\frac{1}{2}mv^2 + \frac{hRZ^2}{n'^2}.$$

* In the integral on the right-hand side of equation (1) we should have written $dF/d\nu$ instead of $F_{1\kappa}$. In the present notation, which is that of Menzel, the physical dimensions of $F_{1\kappa}$ are therefore not identical with those of F_{1n} . Furthermore, in the expressions for F , the variable κ should be retained, and we should write $F_{1\kappa}d\kappa = F_{1\nu}d\nu$. Menzel uses the less cumbersome notation, $F_{1\kappa}d\nu$.

Here Z is the charge on the ion and R is the Rydberg constant. Menzel and Pekeris⁽⁵⁾ suggested that if one writes $n = i\kappa$, where κ is a real number, the frequency of the emitted quantum could be expressed by the Rydberg formula

$$\nu = RZ^2 \left(\frac{1}{n'^2} + \frac{1}{\kappa^2} \right),$$

with the understanding that

$$\frac{RZ^2}{\kappa^2} = \frac{1}{2} \frac{mv^2}{h}.$$

By means of this substitution, formulae developed for transitions between discrete levels may be adopted to transitions involving continuous states.

Throughout all this work we postulate that the velocity distribution of the free electrons is Maxwellian, corresponding to some temperature T_e , the gas kinetic temperature of the electrons and ions. The justification for this assertion may be found in a detailed comparison of the processes tending to destroy a Maxwellian distribution with those tending to restore it. The electrons photo-electrically ejected into the continuum have a velocity distribution dependent upon the energy distribution of the incident radiation at the point in question. Similarly, the electrons are recaptured at a rate that depends on their velocity. The slow ones are much more readily recaptured. Free-free emissions and the collisional excitation of metastable levels also tend to destroy a Maxwellian distribution. The only process tending to maintain a Maxwellian distribution is the coulombic encounters between charged particles. Detailed calculations⁽⁶⁾ show that in a typical planetary nebula the lifetime of a free electron is of the order of ten years, it will lose energy in an inelastic collision once every two or three months, and will dissipate its energy in free-free transitions in a matter of many weeks. On the other hand, an electron will exchange an amount of energy equal to $3/2 kT$ in the matter of a second or two! Hence an electron entering the continuum will almost instantaneously share its energy with the other free electrons. Likewise, an electron that has lost excessive energy in an inelastic collision will quickly regain energy from its neighbours. The systematic loss of the slower electrons by recapture will not influence the velocity distribution, as new slow electrons will be supplied by the encounter processes. Deviations from a Maxwellian distribution will be negligible not only in a gaseous nebula but in the interstellar medium as well!

In the derivation of the equation of statistical equilibrium for an excited level, n , the extreme dilution of radiation throughout the gaseous envelope is of decisive importance. The chance that an atom in an excited level will

ascend to a yet higher one by the absorption of a subordinate-line quantum is negligibly small compared with the chance that it will descend to a lower level with the spontaneous emission of radiation. That is, we can neglect all transitions from level n to a higher level n'' .

The number of atoms entering an excited level n by cascade from higher levels n'' , by recombinations with electrons from the continuum, and by excitation by line radiation from the ground-level must equal the total number cascading downwards from level n to all lower levels n' . Thus,

$$\sum_{n+1}^{\infty} F_{n''n} + \int_{\nu_n}^{\infty} F_{\kappa n} d\nu + F_{1n} = \sum_1^{n-1} F_{nn'}. \quad (2)$$

The steady-state condition for the continuum requires that the number of photo-ionizations/sec. be equal to the number of recaptures. Although atoms can be ionized only from the ground-level, recaptures may occur from any level. Thus,

$$\begin{array}{l} \text{ionizations from} \\ \text{ground-level} \end{array} \int_{\nu_1}^{\infty} F_{1\kappa} d\nu = \sum_1^{\infty} \int_{\nu_n}^{\infty} F_{\kappa n} d\nu \quad \begin{array}{l} \text{recaptures on} \\ \text{all levels.} \end{array} \quad (3)$$

This equation can also be regarded as a mechanistic equation, since it traces the history of electrons photo-electrically ejected from the ground-level which are subsequently captured on all the levels of the atom. Now equations (1), (2), and (3) suffice to fix the relative populations of the levels if the character of the radiation field is specified. That is, the condition of statistical equilibrium or *stationarity*, as it is sometimes called, suffices to fix the Balmer decrement, if the incident radiation field and the electron temperature are known. Notice that F_{1n} , $F_{1\kappa}$, etc., involve I_ν as well as known atomic parameters, whereas $F_{\kappa n}$, $F_{nn'}$, etc., do not depend directly on I_ν . If we wish to determine, for example, the electron temperature of a gas exposed to a given radiation field, we need another relationship. This is the equation of *conservation of energy* which expresses the condition that the energy absorbed/cm.³/sec. be equal to that emitted. We neglect collision processes and assume the nebula to be purely hydrogenic. Later we shall see what effects the "impurities" such as O, Ne, and N may have.

With each radiative transition nn' , there is associated an energy $h\nu_{nn'}$. Consider the energy radiated by captures of electrons on discrete levels, by subsequent cascading, and by free-free transitions. The sum of these contributions is the total energy emitted/cm.³/sec. The amount of energy emitted by recapture from the continuum to a discrete level n will be

$$\int_{\nu_n}^{\infty} F_{\kappa n} h\nu_{\kappa n} d\nu.$$

We sum over all the energies $h\nu_{nn}$ emitted in recaptures in level n , and then over all levels n of the atom, thus,

$$\sum_1^{\infty} \int_{\nu_n}^{\infty} F_{nn} h\nu_{nn} d\nu.$$

This is the total energy radiated in the recaptures. Next there are the discrete emissions. An atom in level n may go to any lower level n' with the emission of energy $h\nu_{nn'}$. Hence the total amount of energy emitted by atoms cascading downwards from the particular level n will be

$$\sum_1^{n-1} F_{nn'} h\nu_{nn'}.$$

When we sum over all the levels n , we obtain

$$\sum_2^{\infty} \sum_1^{n-1} F_{nn'} h\nu_{nn'}.$$

Finally, there are the free-free emissions. When in the presence of an ion, an electron whose energy falls in the range $d\nu_{\kappa}$ at κ jumps to a state of lower energy at κ' , it emits energy $h\nu_{\kappa\kappa'}$. The sum of all downward jumps from the interval $d\nu_{\kappa}$ yields the emission

$$d\nu_{\kappa} \int_0^{\infty} F_{\kappa\kappa'} h\nu_{\kappa\kappa'} d\nu_{\kappa'}.$$

The summation over all downward transitions will be

$$\int_0^{\infty} \int_0^{\infty} F_{\kappa\kappa'} h\nu_{\kappa\kappa'} d\nu_{\kappa} d\nu_{\kappa'}.$$

The absorptions consist solely of photo-ionizations from the ground-level and discrete transitions to the upper level, viz.,

$$\int_{\nu_1}^{\infty} F_{1\kappa} h\nu_{1\kappa} d\nu \quad \text{and} \quad \sum_2^{\infty} F_{1n} h\nu_{1n}.$$

We now equate the total energy absorbed in each unit volume to the energy emitted. The equation for the conservation of energy in a gaseous nebula in pure radiative equilibrium is

$$\begin{aligned} \sum_1^{\infty} \int_{\nu_n}^{\infty} F_{nn} h\nu_{nn} d\nu + \sum_2^{\infty} \sum_1^{n-1} F_{nn'} h\nu_{nn'} + \int_0^{\infty} \int_0^{\infty} F_{\kappa\kappa'} h\nu_{\kappa\kappa'} d\nu_{\kappa} d\nu_{\kappa'} \\ = \int_{\nu_1}^{\infty} F_{1\kappa} h\nu_{1\kappa} d\nu + \sum_2^{\infty} F_{1n} h\nu_{1n}. \quad (4) \end{aligned}$$

This equation can be employed to derive the relation between the electron temperature T_e and the temperature of the central star T_1 for a thin nebular shell. The same relation may be derived more easily with the aid

of an additional equation for processes involving the free electrons. Energy supplied to the electrons by photo-detachment must equal that emitted in free-free transitions, captures on all levels of the atom, and subsequent cascade to the ground-level. The number of electrons captured in each level n per cm.³ per sec. must equal the number contributed by n to the ground-level, both by direct transition and by cascade through lower levels n' . In passing from level n to level 1, such atoms will emit a total energy $h\nu_{n1}$. Hence

$$\begin{aligned}
 \text{energy absorbed by} &= \text{energy emitted in} + \text{energy emitted in recapture and} \\
 \text{photo-ionization} &\quad \text{free-free transitions} \quad \text{subsequent cascade to ground-level} \\
 \int_{\nu_1}^{\infty} F_{1\nu} h\nu_{1\nu} d\nu &= \int_0^{\infty} \int_0^{\infty} F_{\kappa\kappa'} h\nu_{\kappa\kappa'} d\nu_{\kappa} d\nu_{\kappa'} + \sum_1^{\infty} \int_{\nu_n}^{\infty} F_{\kappa n} h(\nu_{\kappa n} + \nu_{n1}) d\nu \\
 &= \int_0^{\infty} \int_0^{\infty} F_{\kappa\kappa'} h\nu_{\kappa\kappa'} d\nu_{\kappa} d\nu_{\kappa'} + \sum_2^{\infty} h\nu_{n1} \int_{\nu_n}^{\infty} F_{\kappa n} d\nu + \sum_1^{\infty} \int_{\nu_n}^{\infty} F_{\kappa n} h\nu_{\kappa n} d\nu.
 \end{aligned} \tag{5}$$

This equation may be regarded as of a mechanistic nature.

We must now write down the explicit equations for the F 's and cast the equations (1) to (5) into a form that will permit actual calculations to be made. To accomplish this we will have to look into some of the physics involved a little more closely.

The total amount of radiation absorbed in a transition between two discrete levels n' and n will be

$$E_{n'n} = F_{n'n} h\nu_{n'n} = \left(N_{n'} - \frac{\varpi_{n'}}{\varpi_n} N_n \right) 4\pi I_{\nu} \frac{\pi e^2}{mc} f_{n'n}, \tag{6}$$

where $N_{n'}$ and N_n are, respectively, the numbers of atoms in the lower and upper levels of the transition, $\varpi_{n'}$ and ϖ_n are the *statistical weights* of the two levels, and I_{ν} represents the intensity of the radiation impinging upon the atoms in the volume element considered. That is,

$$I_{\nu} = W_{\nu} \frac{2h\nu^3}{c^2} \frac{1}{e^{h\nu/kT_1} - 1}, \tag{7}$$

where W_{ν} is the dilution factor which in general will depend both upon the position of the volume element in the nebula and on the density. T_1 appears as a parameter which we may associate with the ultra-violet colour temperature of the central star. We assume that I_{ν} is constant over the effective width of the absorption coefficient a_{ν} , so that we may make use of the relation

$$\int_0^{\infty} a_{\nu}(n'n) d\nu = \frac{\pi e^2}{mc} f_{n'n}. \tag{8}$$

For hydrogen, the *oscillator strength*, $f_{n'n}$, is given by⁽⁵⁾

$$f_{n'n} = \frac{2^6}{3\sqrt{3}\pi} \frac{1}{\varpi_{n'}} \frac{1}{\left(\frac{1}{n'^2} - \frac{1}{n^2}\right)^3} \left| \frac{1}{n^3} \frac{1}{n'^3} \right| g_{nn'}, \quad (9)$$

where $g_{nn'}$ is the so-called *Gaunt correction factor* to Kramers' formula. Mehzel and Pekeris have given expressions for the calculation of $g_{nn'}$, while Baker and Menzel have calculated adequate tables of this quantity.

The factor in parenthesis on the right-hand side of equation (6) takes into account the stimulated emissions which more properly should be called *negative absorptions*. Because of the extreme dilution of the radiation in a gaseous nebula we may neglect these negative absorptions. Thus, if I_ν is constant over the width of the line, the number of transitions from level n' to n per cm.³ per sec will be

$$F_{n'n} = 4\pi N_{n'} I_\nu \frac{\pi e^2}{mc} f_{n'n} \frac{1}{h\nu_{n'n}}. \quad (10)$$

Now the electrons in the gas will have a velocity distribution which is very closely Maxwellian, appropriate to some temperature T_e . Menzel pointed out that a considerable simplification in the treatment would result if we refer all processes to this kinetic temperature of the electrons, T_e ⁽⁷⁾. Except for stimulated captures, electrons will recombine with ions at the same rate as in thermal equilibrium at temperature T_e . Menzel expresses the number of atoms in level n in terms of the number of ions/cm.³, N_i , and the electron density, N_e , by means of the combined ionization and Boltzmann equation for hydrogen, viz.,

$$N_n = b_n N_i N_e \frac{h^3}{(2\pi m k T_e)^{3/2}} \frac{\varpi_n}{2} e^{hRZ^2/n^2 k T_e}, \quad (11)$$

where b_n is a factor that measures the degree of departure from thermodynamic equilibrium at the electron temperature T_e and for concentrations of electrons and ions N_e and N_i respectively. In strict thermodynamic equilibrium $b_n=1$. The calculation of the statistical equilibrium in a gaseous nebula and the Balmer decrement for a given set of initial conditions is essentially the problem of the determination of the b_n 's. The atomic number, Z , is one for hydrogen.

Anticipating the results of Section 2, we might remark that if the nebula is so thin that Lyman line radiation can freely escape, b_1 depends on the incident radiation field (i.e. T_1 and W_ν), while b_2 , b_3 , b_4 , etc., will depend only on T_e . If the optical depth in the Lyman lines is large, the factors b_3 , b_4 , etc., still are functions of T_e only, but will differ from the values for the thin nebula because of the breaking down of the Lyman line quanta.

If we now recall that the frequency, $\nu(n'n)$ of a hydrogen line is given by

$$\nu = RZ^2 \left(\frac{1}{n'^2} - \frac{1}{n^2} \right), \quad (12)$$

where R is the Rydberg constant, and if we let

$$X_n = \frac{hRZ^2}{n^2 k T_e} = \frac{1.570 \times 10^5}{n^2 T_e}, \quad (13)$$

and make use of equations (7), (9), and (11), we can write equation (10) in the form

$$F_{n'n} = N_i N_e W_\nu \frac{KZ^4}{T_e^{3/2}} \frac{b_{n'} g}{n'} \frac{e^{h\nu/kT_e}}{e^{h\nu/kT_e} - 1} \frac{2e^{X_n}}{n(n^2 - n'^2)}, \quad (14)$$

where $g_{nn'}$ is denoted by g and K is given by⁽⁷⁾

$$K = \frac{h^3}{(2\pi m k)^{3/2}} \frac{8\pi^2 \epsilon^2 R^2}{m c^3} \frac{2^4}{3\sqrt{3}\pi} = 3.260 \times 10^{-6}. \quad (15)$$

Similarly, the number of downward transitions/cm.³/sec. from level n to n' is

$$F_{nn'} = N_n A_{nn'}, \quad (16)$$

where $A_{nn'}$ is the Einstein coefficient of spontaneous emission. $A_{nn'}$ is related to the oscillator strength $f_{n'n}$ by⁽⁸⁾

$$A_{nn'} = \frac{\omega_{n'}}{\omega_n} \frac{8\pi^2 \epsilon^2 \nu^2}{m c^3} f_{n'n}. \quad (17)$$

Using this relationship in equation (16), together with equations (9), (11), and (15), we obtain

$$F_{nn'} = N_i N_e \frac{KZ^4}{T_e^{3/2}} b_n \frac{g}{n'} \frac{2}{n} \frac{e^{X_n}}{(n^2 - n'^2)}. \quad (18)$$

Notice that the radiation field $I_\nu(n'n)$ does not enter explicitly into this expression.

For the energies involved in the $n'-n$ transitions we shall have, similarly

$$E_{n'n} = N_i N_e \frac{KZ^4}{T_e^{3/2}} \frac{W b_{n'} e^{h\nu/kT_e}}{e^{h\nu/kT_e} - 1} \frac{g}{n^3} \frac{2hRZ^2}{n'^3} e^{X_n}, \quad (19)$$

and

$$E_{nn'} = N_i N_e \frac{KZ^4}{T_e^{3/2}} b_n \frac{g}{n'^3} \frac{2hRZ^2}{n^3} e^{X_n}. \quad (20)$$

The number of photo-ionizations from level n' to the interval ν to $\nu + d\nu$ is

$$F_{n'n} d\nu = 4\pi I_\nu \frac{a_{n'}(\nu)}{h\nu} N_{n'} d\nu, \quad (21)$$

where $\alpha_n(\nu)$ is the coefficient of continuous absorption. It is given by

$$\alpha_n(\nu) = \frac{32}{3\sqrt{3}} \frac{\pi^2 \epsilon^6}{ch^3} \frac{RZ^4}{n^5 \nu^3} g_{n\kappa}, \quad (22)$$

where $g_{n\kappa}$ is the Gaunt factor. If we now employ equations (7), (11), (21), and (22) we shall get

$$F_{n'\kappa} d\nu = N_i N_e \frac{KZ^4}{T_e^{3/2}} \frac{b_{n'} W_\nu}{e^{h\nu/kT_1} - 1} \frac{g}{n'^3} e^{x_{n'}} \frac{d\nu}{\nu}. \quad (23)$$

Similarly,

$$F_{n'\kappa} h\nu d\nu = E_{n'\kappa} d\nu = N_i N_e \frac{KZ^4}{T_e^{3/2}} \frac{b_{n'} W_\nu}{e^{h\nu/kT_1} - 1} \frac{g}{n'^3} e^{x_{n'}} h d\nu. \quad (24)$$

is the energy absorbed in transitions from level n' to the interval ν to $\nu + d\nu$ in the continuum.

The number of recaptures/cm.³/sec. from the interval ν to $\nu + d\nu$ in the continuum to the level n' is given by⁽⁹⁾

$$F_{n'\kappa} d\nu = N_i N_e \frac{KZ^4}{T_e^{3/2}} \frac{g e^{x_{n'}}}{n'^3} e^{-h\nu/kT_e} \frac{d\nu}{\nu}. \quad (25)$$

and the corresponding energy emitted will be

$$E_{n'\kappa} d\nu = N_i N_e \frac{KZ^4}{T_e^{3/2}} \frac{g e^{x_{n'}}}{n'^3} e^{-h\nu/kT_e} h d\nu. \quad (26)$$

To handle equations of the type (1), (2), (3), (4), and (5) we need the integrals over the entire continuum. The total number of transitions from the ground-level to the continuum is obtained by setting $n' = 1$ in equation (23) and integrating from the Lyman limit, $\nu_1 = RZ^2$, to infinity. Thus

$$\int_{\nu_1}^{\infty} F_{1\kappa} d\nu = N_i N_e \frac{KZ^4}{T_e^{3/2}} b_1 e^{x_1} \int_{\nu_1}^{\infty} \frac{W g dy}{y(e^y - 1)}, \quad (27)$$

where we put

$$y_1 = \frac{hRZ^2}{kT_1} = \frac{h\nu_1}{kT_1}. \quad (28)$$

The corresponding energy absorbed/cm.³/sec. in the bound-free transitions will be

$$\int_{\nu_1}^{\infty} E_{1\kappa} d\nu = N_i N_e \frac{KZ^4}{T_e^{3/2}} b_1 kT_1 e^{x_1} \int_{\nu_1}^{\infty} \frac{W g dy}{e^y - 1}. \quad (29)$$

The frequency dependence of g may be taken from the work of Menzel and Pekeris. The total number of recaptures/cm.³/sec. on n' may be computed with the aid of equation (25), viz.,

$$\int_{\nu_{n'}}^{\infty} E_{n'\kappa} d\nu = N_i N_e \frac{KZ^4}{T_e^{3/2}} \frac{\bar{g}}{n'^3} S_{n'}, \quad (30)$$

where

$$S_n = e^{X_n} E_1(X_n). \quad (31)$$

Here $E_1(x)$ is the exponential function defined by

$$E_1(x) = \int_1^\infty \frac{e^{-yx}}{y} dy. \quad (32)$$

The mean value of the Gaunt factor over the continuum is denoted by \bar{g} . Similarly, the total energy emitted in transitions from the continuum to the level n' is

$$\int_{\nu_{n'}}^\infty E_{\kappa n'} d\nu = N_i N_e \frac{k K Z^4 g}{T_e^{1/2}} \frac{1}{n'^3}. \quad (33)$$

We must now calculate the energy emitted in a free-free transition for an electron moving with a velocity between v and $v+dv$, which, after radiating a quantum, moves with a velocity between v' and $v'+dv'$. In other words, we want to calculate the energy $E_{\kappa \kappa'} d\nu_\kappa d\nu_{\kappa'}$ radiated in the transition from the frequency range $d\nu_\kappa$ at κ to the frequency range $d\nu_{\kappa'}$ at κ' . In equation (26) let us replace n' by $-i\kappa'$, so that

$$\nu_{n'} \rightarrow -\nu_\kappa = -\frac{RZ^2}{\kappa^2}$$

and

$$h d\nu = m v d v = -\frac{2 h R Z^2}{\kappa^3} d\kappa. \quad (34)$$

If we then integrate the resulting expression for $E_{\kappa \kappa'}$ over all values of κ' greater than κ we obtain for the free-free emission at ν

$$d\nu \int_0^{\nu_\kappa} E_{\kappa \kappa'} d\nu_{\kappa'} = N_i N_e \frac{k K Z^2}{2 R T_e^{1/2}} \bar{g} e^{-h\nu/kT_e} d\nu. \quad (35)$$

Finally, it is necessary to integrate over all $d\nu$ to get the total energy radiated in the free-free transitions

$$\int_0^\infty \int_{\nu_{\kappa'}=0}^{\nu} E_{\kappa \kappa'} d\nu d\nu_{\kappa'} = N_i N_e \frac{\bar{g} k^2 K Z^2 T_e^{1/2}}{2 R h}. \quad (36)$$

These formulae comprise the set of equations needed for the discussion of a hydrogen nebula. To calculate the relative intensities of the Balmer lines we may employ equation (2) in conjunction with equations (18), (27), and (30) and solve for the b_n 's as did Menzel and Baker. If there is no line radiation, $F_{ln}=0$, and the solution of the equations of statistical equilibrium for any level is relatively simple. If, however, there is line radiation in the Lyman lines, the populations of the excited levels and hence the Balmer decrement will be profoundly affected.

2. The Balmer Decrement

For a specified set of initial conditions, the Balmer decrement is one quantity that may be calculated exactly and compared with the observations and experimental results.⁽⁹⁾ Menzel and Baker⁽³⁾ considered first the example where the line radiation may be neglected. That is, the central star is supposed to have perfectly black Lyman lines. Electrons are photoionized by radiation beyond the Lyman limit and are recaptured in various levels. The atoms then cascade downward to the ground-level. For $n \geq 2$, each level has an equation of the form

$$\sum_{n''=n+1}^{\infty} F_{n''n} + \int_{\nu_n}^{\infty} F_{nn} d\nu = \sum_{n'=1}^{n-1} F_{nn'}. \quad (37)$$

If we write

$$U_{n''n} = \frac{2n^2}{n''(n''^2 - n^2)} \quad \text{and} \quad t_n = + \sum_1^{n-1} U_{nn'} g_{nn'} \quad (38)$$

and employ equations (18) and (30) together with the relevant definitions, we obtain for each level, n , an equation of the form

$$N_i N_e \frac{KZ^4}{T_e^{3/2}} \left\{ \sum_{n''=n+1}^{\infty} b_{n''} e^{x_{n''}} g_{n''n} U_{n''n} + \bar{g} S_n - b_n e^{x_n} t_n \right\} = 0. \quad (39)$$

Since $2 \leq n < \infty$, equation (39) amounts to an infinite set of simultaneous equations with the b_n 's as the unknowns. As a first approach we may set $g=1$ and solve the equations by the method of successive approximations. Dividing out the common factor $N_i N_e KZ^4 T_e^{-3/2}$, we may solve for b_n as follows

$$b_n = \frac{S_n + \sum_{n''=n+1}^{\infty} b_{n''} e^{x_{n''}} U_{n''n}}{e^{x_n} t_n}, \quad (40)$$

and by successive substitutions

$$\sum_{n''=n+1}^{\infty} b_{n''} e^{x_{n''}} U_{n''n} = \sum_{n''=n+1}^{\infty} \frac{S_{n''} U_{n''n}}{t_{n''}} + \sum_{n''=n+1}^{\infty} \frac{U_{n''n}}{t_{n''}} \sum_{j=n''+1}^{\infty} \frac{S_j U_{jn''}}{t_j} + \text{etc.} \quad (41)$$

so that we may write

$$b_n = \frac{S_n + V_n}{e^{x_n} t_n}, \quad (42)$$

where

$$\begin{aligned} V_n = & \sum_{n+1}^{\infty} \frac{S_i U_{in}}{t_i} + \sum_{j=n+1}^{\infty} \sum_{i=j+1}^{\infty} \frac{S_i U_{ij} U_{jn}}{t_i t_j} \\ & + \sum_{k=n+1}^{\infty} \sum_{j=k+1}^{\infty} \sum_{i=j+1}^{\infty} \frac{S_i U_{ij} U_{jk} U_{kn}}{t_i t_j t_k} + \dots \quad (43) \end{aligned}$$

Each of these summations can be shown to converge. Now b_n approaches 1 as n increases without bound. Similarly, $S_n \rightarrow 2 \ln n$ and $t_n \rightarrow 3 \ln n$. Hence $S_n/t_n \rightarrow 2/3$ as n increases without bound, and

$$\sum_{n+1}^{\infty} \frac{S_i}{t_i} U_{in} < \frac{2}{3} \sum_{n+1}^{\infty} U_{in} < \frac{2}{3} \ln n. \quad (44)$$

Menzel and Baker considered two models which they called *A* and *B*. Model *A* is the one we have already described. Equation (37) is valid. In sub-model A_1 the Gaunt factor g is set equal to unity throughout, and in the sub-model A_2 the exact values of the g factors as calculated by the formulae of Menzel and Pekeris⁽⁵⁾ are employed. A comparison of the b_n 's computed for the approximate (A_1) and exact (A_2) models will show to what extent calculations based on the simpler assumption may be applied. In their model *B*, Menzel and Baker take care of the Lyman line radiation that is produced in the nebula itself by the degradation of Lyman continuous quanta by assuming that the number of absorptions from level 1 to n is exactly equal to the number of emissions from level n to 1. That is, $F_{1n} = F_{n1}$, so that

$$\sum_{n''=n+1}^{\infty} F_{n''n} + \int_{\nu_n}^{\infty} F_{nn} d\nu = \sum_2^{n-1} F_{nn'}. \quad (45)$$

If we redefine t_n as

$$t_n = \sum_2^{n-1} U_{nn'} g_{nn'} \quad (\text{case B}) \quad (46)$$

the solution may be carried out as before.

Menzel and his colleagues⁽¹⁰⁾ also treated a model of a relatively transparent nebula, similar to *A*, in that all the Lyman line radiation produced in the nebula as a result of cyclical processes is allowed to escape. The nuclear star, however, is assumed to radiate like a black body in the region of the Lyman lines. The stellar line radiation profoundly steepens the decrement, making *H α* much stronger than *H β* . The equation of statistical equilibrium for this model *C* may be written down with the aid of equations (2), (14), (18), and (30).

$$\frac{N_i N_e K Z^4}{n^3 T_e^{3/2}} \left\{ \sum_{n''=n+1}^{\infty} b_{n''} e^{x_{n''}} g_{n''n} U_{n''n} + \bar{g} S_n + \left[W_{1n} \frac{b_1 e^{h\nu/kT_e}}{e^{h\nu/kT_1} - 1} \right] \frac{2n^2 e^{x_n}}{n^2 - 1} - e^{x_n} b_n t_n \right\} = 0. \quad (47)$$

Here b_1 measures the deviation of the population in the ground-level from thermodynamic equilibrium. It may be evaluated from the ionization formula for hydrogen (see equation (50)) for any electron temperature T_e and radiation field.

Equation (47) may be solved in the same way as equation (37) was solved. We have

$$b_n e^{x_n t_n} = S_{nr} + V_{nr}, \quad (48)$$

where

$$S_{nr} = S_n + W_{1n} \left[\frac{b_1 e^{h\nu/kT_e}}{e^{h\nu/kT_1} - 1} \right] \frac{2n^2 e^{x_n}}{n^2 - 1}, \quad (49)$$

where V_{nr} is defined in terms of S_{nr} in the same way as V_n was expressed in terms of S_n . The two terms in S_{nr} , although grouped together for convenience, do not represent physically similar quantities, since S_n refers to the recaptures of electrons on level n_1 , whereas the second term arises from line excitations from the first level to the n th level.

Before we can calculate S_{nr} we must obtain an expression for b_1 . Let us substitute equations (27) and (30) into equation (3), which states that the number of recaptures on all levels equals the number of photo-ionizations from the ground-level. We obtain

$$N_i N_e \frac{KZ^4}{T_e^{3/2}} b_1 e^{x_1} \int_{y_1}^{\infty} \frac{W_{1x} g dy}{y(e^y - 1)} = N_i N_e \frac{KZ^4}{T_e^{3/2}} \sum_{n=1}^{\infty} \frac{\bar{g} S_n}{n^3},$$

which reduces to

$$b_1 = \frac{G_{T_e}}{e^{x_1} \int_{y_1}^{\infty} W_{1x} \frac{dy}{y(e^y - 1)}}, \quad (50)$$

where

$$G_{T_e} = \sum_{n=1}^{\infty} \frac{\bar{g} S_n}{n^3}, \quad (51)$$

which depends only on the electron temperature. Equation (50) enables us to compute the ionization of hydrogen since, once b_1 is specified, $N_1/N_i N_e$ can be found at once from equation (11). The order of magnitude of b_1 is determined by the dilution factor; i.e. b_1 varies as $1/W$. The reason for this may be easily seen. In the gaseous nebula, recaptures must go on at essentially the same rate as in thermodynamic equilibrium at a temperature T_e . On the other hand, the rate of photo-ionization is cut down by a factor which depends on T_1 and W .* Hence a great concentration of atoms is built up in the ground-level. If equation (50) is now substituted in equation (49)

$$S_{nr} = S_n + \frac{W_{1n}}{W_{1x}} \int_{y_1}^{\infty} \frac{G_{T_e}}{dy} \frac{2n^2(n^2 - 1)^{-1}}{(e^{h\nu/kT_1} - 1)}. \quad (52)$$

* There is no exact proportionality because T_e is in general not equal to T_1 .

For an optically thin nebula surrounding a star radiating as a black body at temperature T_1 , W will be determined by the geometrical dilution and $W_{1n}=W_{1\kappa}$. If the nebula is optically thick, the radiation field will be appreciably modified by photo-ionizations and recaptures in the nebula. Then W_{1n} and $W_{1\kappa}$ may become no longer even approximately equal and the Balmer decrement can become appreciably modified. Model C corresponds to an optically thin nebula which will be one of very low surface brightness. Hence it will not be applicable to ordinary planetary nebulae, but may be of value in discussions of gaseous diffuse nebulae of very low surface brightness.

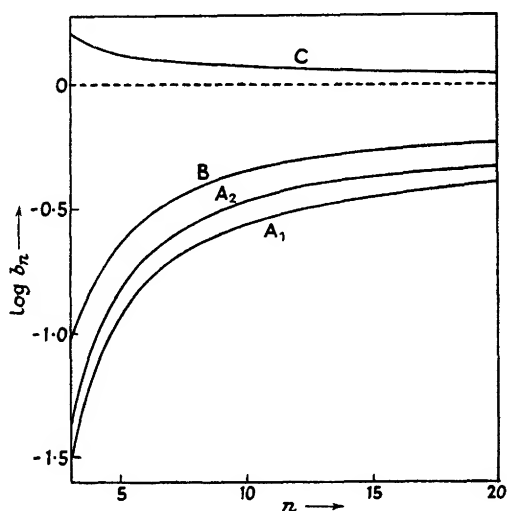


FIG. IV : 3. Relation between n and $\log b_n$ for $T_e=10,000^\circ \text{K}$. for models A_1 , A_2 , B , and C .

The computed values of b_n depend upon the temperature and particularly upon the mode of excitation.^(4, 10) In Fig. 3 we plot the variation of b_n with n for $10,000^\circ \text{K}$. for each of the three models A_1 , A_2 , B , and C . Notice that the difference between the curves for A_1 and A_2 is not small. That is, the neglect of the g factor in A_1 has a pronounced effect on the computed value of b_n . The effect on the Balmer decrement is much smaller. As n increases without bound, $b_n \rightarrow 1$ for all models.

The relative intensities of the Balmer lines may be expressed in terms of the intensity of $H\beta$ as unity. With the aid of equation (20) we find

$$\frac{I_{n2}}{I_{42}} = \frac{F_{n2} h \nu_{n2}}{F_{42} h \nu_{42}} = \frac{b_n g_{n2}}{b_4 g_{42}} \frac{4^3}{n^3} e^{x_n - x_{n4}} = \frac{b_n I_{n2}^0}{b_4 I_{42}^0}, \quad (53)$$

where I^0 is the intensity in thermodynamic equilibrium at temperature T_e .

Table IV : 1 gives the theoretical Balmer decrements for models A_1 , A_2 , B , and C . The decrement is sensitive to the mode of excitation, i.e. to the radiation field, but not to the electron temperature.

TABLE IV : 1

The Theoretical Balmer Decrements for Models A_1 , A_2 , B , and C .

(The Balmer line intensities are tabulated in terms of $H\beta$ as 1.0)

Model A_1 ($g \equiv 1.0$)

λ	n	$T_e = 5000^\circ$	10,000°	20,000°	40,000°
6563	3	1.953	2.035	2.118	2.205
4861	4	1.000	1.000	1.000	1.000
4340	5	0.592	0.576	0.561	0.546
4101	6	0.389	0.368	0.350	0.334
3969	7	0.271	0.252	0.235	0.220
3889	8	0.198	0.180	0.165	0.152
3835	9	0.149	0.135	0.121	0.111
3797	10	0.115	0.104	0.091	0.083
3770	11	0.092	0.081	0.071	0.063
3750	12	0.074	0.065	0.056	0.050
3734	13	0.060	0.052	0.045	0.040
3722	14	0.050	0.043	0.037	0.032
3712	15	0.042	0.036	0.030	0.026
3683	20	0.020	0.017	0.014	0.012
3669	25	0.011	0.009	0.007	0.006
3662	30	0.007	0.005	0.004	0.004

Model A_2 ($g=g$)

λ	n	$T_e = 5000^\circ$	10,000°	20,000°	40,000°
6563	3	1.859	1.915	1.984	2.073
4861	4	1.000	1.000	1.000	1.000
4340	5	0.598	0.576	0.560	0.548
4101	6	0.396	0.374	0.353	0.338
3969	7	0.274	0.255	0.236	0.221
3889	8	0.199	0.182	0.165	0.153
3835	9	0.149	0.136	0.120	0.111
3797	10	0.114	0.105	0.091	0.082
3770	11	0.090	0.081	0.070	0.062
3750	12	0.073	0.065	0.055	0.050
3734	13	0.059	0.052	0.043	0.039
3722	14	0.049	0.042	0.036	0.032
3712	15	0.041	0.035	0.030	0.025
3683	20	0.019	0.016	0.014	0.012
3669	25	0.011	0.009	0.007	0.006
3662	30	0.006	0.005	0.004	0.003

Model B

λ	n	$T_e=5000^\circ$	10,000°	20,000°	40,000°
6563	3	2.43	2.50	2.59	2.71
4861	4	1.00	1.00	1.00	1.00
4340	5	0.53	0.51	0.50	0.49
4101	6	0.33	0.31	0.30	0.29
3969	7	0.223	0.206	0.192	0.179
3889	8	0.157	0.143	0.130	0.120
3835	9	0.115	0.105	0.093	0.085
3797	10	0.087	0.079	0.069	0.062
3712	15	0.030	0.025	0.021	0.018
3683	20	0.014	0.012	0.010	0.009
3669	25	0.007	0.006	0.005	0.004
3662	30	0.004	0.003	0.003	0.002

Model C

λ	n	$T_e=5000^\circ$	10,000°	20,000°	40,000°
6563	3	11.8	5.3	3.6	3.0
4861	4	1.0	1.00	1.0	1.0
4340	5	0.25	0.35	0.42	0.46
4101	6	0.095	0.16	0.21	0.25
3969	7	0.048	0.090	0.125	0.15
3889	8	0.027	0.054	0.070	0.096
3835	9	0.017	0.036	0.054	0.066
3797	10	0.012	0.025	0.038	0.048
3770	11	0.0080	0.018	0.027	0.035
3750	12	0.0059	0.013	0.020	0.027
3734	13	0.0043	0.010	0.016	0.021
3722	14	0.0033	0.008	0.013	0.017
3712	15	0.0026	0.006	0.010	0.013

The numerical values for models A_1 , A_2 , and B are reproduced from BAKER, J. G., and MENZEL, D. H., *Ap. J.*, **88**, 52 (1938), Tables 7 and 8.

The data for Model C are based on the b_n factors calculated by BAKER, J. G., MENZEL, D. H., and ALLER, L. H., *Ap. J.*, **88**, 427 (1938). The corresponding intensity values for $T_e=10,000$, 20,000, and 40,000°K have been published by CHAMBERLAIN, J. W., *Ap. J.*, **117**, 387 (1953).

First, how do the calculations of the decrement by Menzel and Baker compare with the earlier ones by Cillie? Cillie's procedure amounts to taking only the first fourteen equations of the type (45), taking n'' only up to 14, putting in accurate $g_n n$ values and setting \bar{g} for the recaptures equal to unity and solving for the b_n 's. The effect of the neglect of all levels beyond $n=14$ is particularly serious for the higher transitions. Cillie's Balmer decrements are systematically too slow and the higher the electron temperature the greater the discrepancy.

Comparison between theory and observation is not easy, because the observed Balmer decrements are affected by space absorption. If we knew

the amount of absorbing material between us and the nebula we could calculate the corrections to be applied to the observed intensities. Many years ago G. A. Shajn⁽¹¹⁾ showed that the observed Balmer decrement depended on the galactic latitude of the planetary. The nebulae in low latitudes show a sensibly greater decrement than those in high latitudes, a result understandable in view of the concentration of absorbing particles near the Milky Way. Louis Berman⁽¹²⁾ made a much more detailed study of the problem. In order to eliminate the effects of any possible relationship between the Balmer decrement and the degree of excitation of the

TABLE IV : 2

The Balmer Decrement as Measured by Berman

λ	n	Group I 8 Nebulae	Group II 13 Nebulae	Group III 17 Nebulae
6563	3	39	—	27.7
4861	4	10	10	10
4340	5	4.5	4.8	5.0
4101	6	2.1	2.4	2.6
3969	7	1.3	1.4	1.8
3889	8	1.1:	1.0	1.2
3835	9	0.8:	0.5	0.9

Monthly Notices, Royal Astron. Soc., 96, 898 (1936).

nebula, he grouped these nebulae into three classes, I, II, and III, according to the brightness of the principal nebular lines N_1 and N_2 as compared with $H\beta$. Berman corrected for space absorption on the assumption that the interstellar absorbing material was evenly distributed in galactic longitude and fell off exponentially with height above the galactic plane. Then utilizing the distance of each nebula (which he had estimated from statistical investigations,⁽¹³⁾ the observed line intensities, and the galactic latitude, he made a solution for the coefficient of absorption per kiloparsec at $\lambda 4861$, the exponent n in an assumed law of selective absorption λ^{-n} , and the Balmer decrement for each group. He derived an absorption coefficient of 0.53 magnitude per kiloparsec at $H\beta$, and an absorption varying as $\lambda^{-2.27}$. We summarize Berman's results for the Balmer decrement in Table 2. The decrement is steeper than in either case *A* or *B* and varies for the different groups. The extreme patchiness of the distribution of the absorbing material throughout the galaxy vitiates Berman's method. Much more extensive photometric data on hydrogen line intensities are now available. For a comparison of theory with observations therefore we may utilize a series of measurements obtained at the Lick Observatory in 1943–5 with the Crossley reflector and quartz spectrograph.⁽¹⁴⁾ The nebulae were

divided into three groups, stellar objects, low excitation objects of diameter 5" or more, and high excitation objects. Within each group, space absorption produces considerable scatter, but its effect is always to steepen the gradient. Hence we may suppose that the nebulae showing the slowest gradient are least affected by space absorption. If one reduces the gradient for each nebula (by correcting for space absorption) to agree in the mean with the results for the nebulae of lowest gradient in each group, there is

TABLE IV : 3
The Balmer Decrement
Comparison Between Theory and Observation

λ	n	Observed			Theoretical		
		Low Excitation		High Excitation	$T_e = 14,000^\circ \text{K}$		
		Stellar Nebulae	Non-stellar Nebulae	Nebulae	<i>A</i>	<i>B</i>	<i>C</i>
4861	4	—	—	—	—	—	—
4340	5	5.25	5.66	5.65	5.68	5.05	3.85
4101	6	2.97	3.31	3.13	3.62	3.05	1.79
3969	7	1.93	2.20	1.99	2.46	1.99	1.08
3889	8	1.44	1.50	1.32	1.74	1.37	0.62
3835	9	1.00	1.03	0.93	1.28	0.99	0.45
3797	10	0.74	0.85	0.66	0.98	0.74	0.32
3770	11	0.57	0.56	0.49	0.75	0.57	0.22
3750	12	0.45	0.46	0.36	0.60	0.46	0.16
3734	13	0.42	—	—	0.48	0.35	0.13
3722	14	0.38	—	—	0.39	0.28	0.10
3712	15	0.30	—	—	0.33	0.23	0.08

The observational data are taken from *Astrophysical Journal*, **113**, 138 (Univ. of Chicago Press, 1951). The theoretical intensities are interpolated from Table 1.

obtained an upper limit to the steepness of the Balmer decrement. Table IV : 3 compares the observed Balmer decrement for the three groups with the theoretical calculations *A*, *B*, and *C* for $T_e = 14,000^\circ \text{K}$., the mean electron temperature of the fifteen planetaries for which the most accurate photometric data are available. The Balmer decrement is closely similar for the three groups of nebula, and there is no evidence that the high excitation nebulae show a steeper gradient than do the others. The decrements are not as steep as those obtained by Berman. They agree reasonably well with the predictions of model *B*, a conclusion that is not surprising in view of the fact that *B* applies to a thick shell, whereas models *A* and *C* apply to thin shells of necessarily low surface brightness.

Although a rigorous theoretical treatment of the Balmer decrement would require a solution of the transfer problem in the Lyman lines with

rather awkward boundary condition, model *B* should be a rather good approximation for an optically thick nebula. For such an object the influence of the energy distribution in the ultra-violet spectrum of the central star will not be important; the controlling factor will be the electron temperature.

The Balmer spectrum observed in a discharge tube arises as a consequence of collisional excitation by electrons which do not even follow a Maxwellian distribution. Hence the Balmer decrement is sensitive to the exact conditions of excitation and bears little resemblance to the decrement observed in the nebulae or stars.

To overcome these difficulties M. C. Johnson⁽⁹⁾ measured the Balmer decrement produced in the recombination spectrum of an after-glow. Mixtures of pure hydrogen, hydrogen-neon, or hydrogen-helium mixtures at 0.1 mm. pressure were excited in an electrode-less cylinder by a 350-watt, 3.5 megacycles/sec. r.f. oscillator. The after-glow was isolated by a revolving shutter synchronized with a cut-off circuit in the r.f. generator.

Comparison with the theoretical decrements may be made to infer the conditions in the after-glow and to study the possible influences of super-elastic collisions, non-compensated fluorescent cycles, etc.

Such experiments should prove useful for explaining the Balmer decrement phenomena in stellar atmospheres. The nebular conditions of extremely long relaxation times, because of the low densities involved, are impossible to duplicate experimentally.

One defect in the theoretical calculations of the Balmer decrement must be mentioned. In the work of Menzel and Baker and of Cillie, all the levels of a given n are treated together, and it is assumed that throughout the cascading process the atoms are distributed among the different levels of the same n , but different l according to their statistical weights. Actually each term characterized by a given (n, l) should have been treated separately. The equations of statistical equilibrium should be written for each (n, l) value in terms of appropriate expressions for $F_{nl, n'l'}$, etc. In place of equation (9), for example, we should then use the corresponding expression for $f(n'l'; nl)$.

3. The Theoretical Electron Temperature

The conditions of a steady state (statistical equilibrium) and conservation of energy in radiative processes impose a relation between the electron temperature T_e and the ultra-violet colour temperature of the central star, T_1 , provided collisional processes can be neglected.

We would expect the relation between T_1 and T_e to involve only processes concerning the continuum, i.e. the nature of the ultra-violet radiation field and the dissipation of energy by processes such as free-free emissions. The

line excitation in the nebula should have no influence on the relationship. Therefore we make use of equation (5) and substitute from equations (29), (30), (33), and (36). After cancellation of the factor $2N_iN_eKZ^6hRT_e^{-3/2}$ and neglecting g we have

$$b_1 e^{x_1} \frac{k}{(2hRZ^2)} T_1 \int_{y_1}^{\infty} W_{1\kappa} \frac{dy}{e^y - 1} = \left(\frac{k}{2hRZ^2} \right)^2 T_e^2 + \left(\frac{k}{2hRZ^2} \right) a T_e + \frac{1}{2} G_{T_e} - \frac{1}{2} \sum_1 \frac{S_n}{n^5}, \quad (54)$$

where

$$a = \sum \frac{1}{n^3}$$

and G_{T_e} was defined in equation (51). If b_1 is eliminated between equations (50) and (54) there results

$$\frac{\left(\frac{k}{2hRZ^2} \right) T_1 \int_{y_1}^{\infty} \frac{W dy}{e^y - 1}}{\int_{y_1}^{\infty} \frac{W dy}{y(e^y - 1)}} = \frac{\left(\frac{k}{2hRZ^2} \right)^2 T_e^2 + a \left(\frac{k}{2hRZ^2} \right) T_e + \frac{1}{2} G_{T_e} - \frac{1}{2} \sum \frac{S_n}{n^5}}{G_{T_e}}. \quad (55)$$

The right-hand side of the equation depends only on T_e , whereas the left-hand side depends only on the incident radiation field. If $W_{1\kappa}$ depends only on geometrical factors and not on the frequency it can be cancelled out of the equation, and this side of the equation will depend only on T_1 , the temperature of the central star. We would expect this to be true for a nebula that is optically thin in the Lyman continuum. A nebula of optical thickness 0.1 in the continuum may still have an optical thickness of 10^2 or 10^3 in Lyman α , however. Then we can write, symbolically

$$f_1(T_1) = f_2(T_e). \quad (56)$$

The solution may be found by numerical methods (see Table IV : 4). When T_1 is small, $T_e \sim T_1$, but as T_1 increases, T_e departs more and more from T_1 . The reason that T_e falls farther and farther behind T_1 is to be sought in the free-free emissions which are responsible for the T_e^2 term in equation (54). If collisional processes are taken into account T_e will become even smaller.

It is of interest to see what the relationship between T_1 and T_e will be for a nebula of finite optical thickness, i.e. one where the shell is sufficiently thick for the original intensity distribution of the radiation from the central star to be appreciably modified by absorption and re-emission by atoms within the nebula. The problem of the transfer of radiation in the Lyman continuum through a pure hydrogen nebula in which no collisional

processes occur can be solved by a method of successive approximations. A radial expansion of the nebula will introduce great complications in the treatment of the transfer of radiation in the lines, but will have no effect on the continuum. Milne⁽¹⁵⁾ showed that the boundary conditions for a thin spherical shell were very simple, while Ambarzumian⁽¹⁶⁾ set up the transfer equation with the continuum regarded as though it were a single state. He used the Schuster-Schwarzschild approximation while Chandrasekhar⁽¹⁷⁾ gave a treatment of the same problem with the Eddington

TABLE IV : 4

*The Theoretical Relation between the Electron Temperature and the Temperature of the Central Star for a Thin Nebula consisting of pure hydrogen.**

<i>Temperature of Central Star</i>	<i>Electron Temperature</i>
T_1	T_e
5,000° K	5,000° K
10,000	9,500
20,000	18,000
40,000	34,000
80,000	57,000
160,000	92,000
320,000	132,000

* *Astrophysical Journal*, 88, 426 (1938).

approximation. Actually, even in the first approximation, the continuum cannot be treated as though it were a single state. There are $F_{1\kappa}d\nu$ photo-ionizations per cm^3/sec . by absorption of radiation between the frequency ν and $\nu + d\nu$. The number of recaptures on the ground-level/ cm^3/sec . $F_{\kappa 1}d\nu$ will not be simply $F_{1\kappa}p\nu d\nu$, where $p\nu$ is the probability of recapture on the ground-level, because the velocities of the electrons have been reshuffled by collisions and energy has been lost by free-free emissions. The electrons are recaptured from a Maxwellian velocity distribution appropriate to a temperature T_e , whereas the velocity distribution of the electrons injected into the continuum by photo-ionization is very different from a Maxwellian distribution. Thus there is an interlocking between the various states, $d\nu$, of the continuum which must be taken into account in the treatment of the transfer of radiation. The effect of this interlocking is to subtract energy from the higher frequencies and transfer it to frequencies near the series limit.

Calculations have been carried out for geometrically thin shells of optical thicknesses $\tau_0 = 1, 3$, and 10 at the Lyman limit which are illuminated by a star shining as a black body at 80,000° K. The results for the shells of

optical thicknesses $\tau_0=1$ and 10 are shown in Fig. 4(a).⁽¹⁸⁾ At the inner boundary of the shell an excess of ultra-violet radiation is built up near the Lyman limit. At $\tau \sim 0.7$ in the thin nebula ($\tau_0=1$), at $\tau \sim 1.3$ in the thicker nebula ($\tau_0=3$), and at $\tau \sim 2$ in the thickest nebula ($\tau_0=10$), the dilution factor is very near the geometrical value and it diminishes towards the outer boundary. In the nebula of optical thickness 10, the dilution factor at the inner boundary shows about the same dependence on the frequency as it does in the nebula of optical thickness 3. Notice that as ν increases, $W_{1\kappa} \rightarrow 1.0$, as is to be expected since $\tau \rightarrow 0$. Equation (55) permits a calculation of the electron temperature, since W is known at each point in the shell. The results show that in all three shells the theoretical electron temperature at the inner boundary lies near the value derived for the thin shell. It rises gradually outwards, reading $76,000^\circ\text{K.}$ at the outer boundary of the shell of optical thickness 3 and $130,000^\circ$ at the boundary of the shell of optical thickness 10.

These results apply, of course, only to a hypothetical steady-state nebula in which only radiative processes occur. If inelastic collisions are permitted the temperature of the electron gas is lowered drastically, and even in a pure hydrogen nebula could never reach values such as $100,000^\circ\text{K.}$ Actually there are strong reasons for believing that the electron temperatures in the luminous rings of most planetary nebulae lie in the neighbourhood of $10,000^\circ\text{K.}$ to $20,000^\circ\text{K.}$ Hence the transfer of radiation in the Lyman continuum will be not only quantitatively but also qualitatively different from the results given in Fig. 4(a).

The physical picture of the extinction of the ultra-violet starlight in a thick nebular shell may be seen with the aid of the following considerations. Consider a frequency interval ν to $\nu + d\nu$ in the continuum. Energy will be absorbed at a rate proportional to $g\nu^{-3}$ (of equation (22)), where g depends slowly on the frequency. The re-emission of Lyman continuous radiation in the same frequency interval depends on the number of electrons with velocities between v and $v + dv$, where

$$h\nu = hR + 1/2mv^2,$$

that are recaptured/cm.³/sec. on the ground-level. That is, it will depend $ge^{X_1}e^{-h\nu/kT_e}$ (cf. equation (25)). Looking at the process in a slightly different way, we may remark that the absorption depends on the energy distribution in the incident radiation field, whereas the re-emission depends on the rate of recapture of electrons from a Maxwellian velocity distribution appropriate to some temperature T_e . Since T_e is of the order of $10,000^\circ$ or $20,000^\circ\text{K.}$, few electrons will have energies as high as 5 or 10 volts, the recaptures will be principally of electrons with energies up to 2 or 3 e.v. Hence re-emission will occur in frequencies near the Lyman limit where

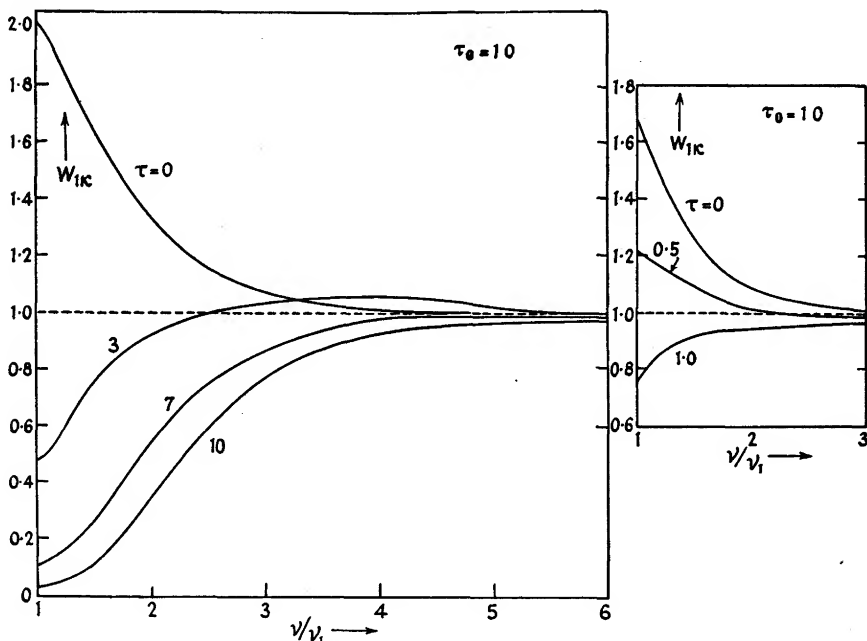


FIG. IV : 4 (a). The Variation of Dilution Factor with Frequency and Optical Depth for Nebulae of Total Optical Thicknesses $\tau_0=1$ and 10 at the Lyman limit.

The dilution factor W_{IX} is expressed in units of the geometrical dilution factor $W_g=R^2/4r^2$; the frequency, ν , is expressed in terms of that of the Lyman limit, ν_1 . Curves are given for $\tau=0, 0.5$, and 1.0 for the nebula of optical thickness $\tau_0=1$ and for $\tau=0, 3, 7$, and 10 for the nebula of optical thickness 10. Similar curves for $\tau_0=3$ were published in *Ap. J.*, 90, 607 (1939), by Menzel, Baker, and the writer. The electron temperature at each point is calculated from equation (55).

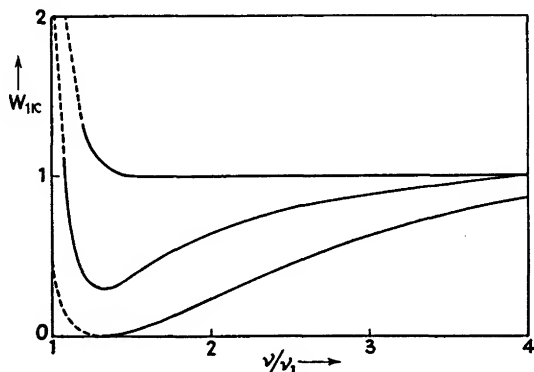


FIG. IV : 4 (b). The Qualitative Variation of Dilution Factor with Optical Depth in a Nebula of Total Optical Thickness $\tau_0=10$ at the Lyman limit.

The frequency is expressed in terms of the frequency at the Lyman limit and the dilution factor in terms of the geometrical dilution factor. The electron temperature is held constant at $10,000^\circ\text{K}$. Compare with Fig. IV : 4 (a).

radiation will be piled up at the expense of energy absorbed at higher frequencies. The latter radiation is simply extinguished in the nebula. Fig. 4(b) shows schematically the behaviour of the radiation in a nebula of optical thickness 10 at the Lyman limit. At the inner boundary there is some piling up of radiation at frequencies just above the Lyman limit, but this excess radiation falls right at frequencies where it is most voraciously absorbed. The net effect of the non-equality of T_1 and T_e is seen to be an enhancement of the rate at which ultra-violet energy is extinguished. These results are quite general. More than 3 or 4 e.v. beyond the ionization potential of any atom the radiation is simply absorbed and re-emitted at longer wavelengths. We shall discuss some aspects of this problem further in Chapter VII.

We must now look more carefully at the reason why T_e is depressed, even though the temperature of the central star is very high. In a pure hydrogen nebula the electron temperature would be regulated by the collisional excitation of the discrete levels and by collisional ionization. A real gaseous nebula contains "impurities" in the form of oxygen, nitrogen, neon, and other elements. The ions of these substances possess metastable levels a few volts above the ground-level, and the excitation of these levels by electron collision acts as a steady attrition on the kinetic energies of the free electrons. Once the atom is in the upper level there exists a probability, β , that it will be de-excited by a super-elastic encounter, and a probability $(1-\beta)$ that it will emit a quantum of energy $h\nu_F$ in the form of a forbidden transition. If \mathcal{F}_{AB} represents the number of collisional excitations to the excited level B from the lower level A /cm.³/sec., then the emission/cm.³/sec. in the forbidden radiation will be⁽¹⁹⁾

$$E_F = (1-\beta)\mathcal{F}_{AB}h\nu_F.$$

We saw in Chapter III that once a forbidden quantum is created it simply escapes from the nebula without any reabsorption. Therefore the electron gas is losing energy in the form of forbidden line radiation.

The equation of radiative equilibrium for the continuum is now to be replaced by the equation of conservation of energy. In place of equation (5) we now have

$$\int_{\nu_1}^{\infty} E_{ik} d\nu = \sum_1^{\infty} \int_{\nu_n}^{\infty} E_{kn} d\nu + \sum_2^{\infty} \int_{\nu_n}^{\infty} F_{kn} h\nu_{n1} d\nu + \int_0^{\infty} \int_0^{\infty} E_{kk'} d\nu_k d\nu_{k'} + \sum E_i, \quad (57)$$

where E_i represents the energy radiated in forbidden line radiation by the ions of type i . Measurements of the forbidden line intensities give us values of I in terms of the intensity of $H\beta$, $I(H\beta)$. If the forbidden line radiation

is emitted in the same regions in the nebula as are the Balmer lines, we may write

$$E_i = E(H\beta) \frac{I_i}{I(H\beta)}. \quad (58)$$

By equation (20) we have that

$$E(H\beta) = b_4 \frac{N_i N_e 2h R K Z^6 g_{42} e^{x_i}}{T_e^{3/2} 512}. \quad (59)$$

Now substitute from equations (29), (30), (33), (36), and (59) into equation (57) and cancel out the factor $2N_i N_e K Z^6 h R T_e^{-3/2}$ and we recover an expression equivalent to equation (54), but with an added term on the right-hand side. If we now eliminate b_1 with the aid of equation (50) we find that the equation for the determination of the electron temperature is

$$\frac{\frac{k}{2hRZ^2} T_1 \int_{y_1}^{\infty} \frac{W dy}{e^y - 1}}{\int_{y_1}^{\infty} \frac{W dy}{y(e^y - 1)}} = \frac{\left[\frac{k}{2hRZ^2} \right]^2 T_e^2 + a \left[\frac{k}{2hRZ^2} \right] T_e + \frac{1}{2} G_{T_e} - \frac{1}{2} \sum_1^{\infty} \frac{S_n}{n^5}}{G_{T_e}} + 1.61 \times 10^{-3} \frac{b_4(T_e) e^{x_i}}{G_{T_e}} \frac{\Sigma I_i}{I(H\beta)}, \quad (60)$$

which may be written in the symbolic form (similar to equation (56), viz.

$$f_1(T_1) = f_2(T_e) + C(T_e), \quad (61)$$

where $C(T_e)$, which is the last term on the right-hand side of equation (61), is the correction term to the $T_1 - T_e$ relation for a pure hydrogen nebula in strict radiative equilibrium and optically thin in the Lyman continuum. We may write it as

$$C(T_e) = A(T_e) \frac{\Sigma I_i}{I(H\beta)}, \quad (62)$$

where $A(T_e)$ varies slowly with the temperature.

As examples of the application of these formulae let us consider two nebulae, IC 418, in which the forbidden nebular lines are relatively weak, and NGC 6826 in which they are moderately strong.

For these two objects $\Sigma I_i / I(H\beta)$ is 3.5 and 11.5 respectively. We choose a series of values of T_e , take $f_2(T_e)$ from the calculations of the Harvard Nebular Series and compute

$$A(T_e) = 1.61 \times 10^{-3} \frac{b_4(T_e) e^{x_i}}{G_{T_e}}, \quad (63)$$

where $b_4(T_e)$ is adapted from Baker and Menzel's calculations for model B. Then $C(T_e)$ may be calculated for each model and the sum $f_2(T_e) + C(T_e)$

formed. Now $f_1(T_1)$ is given as a function of the temperature of the central star so that for a given value of $f_1=f_2+C$, T_1 may be found. The corresponding values of T_1 are given in the fifth and seventh columns of Table IV : 5. From their spectral classes the temperatures of the central stars of IC 418 and NGC 6826 have been estimated as 33,200°K. and 34,600°K. respectively. In IC 418 the electron temperature could be above 20,000°K.,

TABLE IV : 5
Theoretical Relation between T_1 and T_e for a nebula containing Ions of Oxygen, Neon, etc.

			IC 418		NGC 6826	
T_e	$f_2(T_e)$	$A(T_e)$	$C(T_e)$	T_1	$C(T_e)$	T_1
8,000	0.524	5.54 10 ⁻³	0.025	18,000	0.064	31,000
10,000	0.531	5.33	0.024	20,000	0.061	33,000
12,000	0.537	5.14	0.023	22,000	0.059	35,000
14,000	0.544	5.00	0.022	24,000	0.057	37,000
16,000	0.550	4.86	0.022	26,000	0.056	40,000
18,000	0.557	4.76	0.021	28,000	0.055	42,000
20,000	0.563	4.68	0.021	31,000	0.054	44,000
25,000	0.580	4.49	0.020	37,000	0.052	52,000
30,000	0.600	4.36	0.020	46,000	0.050	62,000

whereas in NGC 6826 we would expect an electron temperature near 11,000°K. These numbers are to be compared with $T_e=18,000$ and 11,300 found from the forbidden line intensities (Chapter V). Thus the electron temperature depends strongly on the intensities of the forbidden lines as compared with the recombination lines of hydrogen and helium.

The aforementioned argument is strictly of a qualitative character since we have tacitly assumed that W can be cancelled from the expression for $f_1(T_1)$. Such a cancellation is not permissible if W depends strongly on the frequency. The shells of IC 418 and NGC 6826 and similar nebulae are thick so that modifications in the energy distribution in the Lyman continuum will be produced by radiative processes in the shells. Throughout most of the luminous body of the nebula the optical depth τ , as measured from the inner boundary of the shell, will be small (see Section 1 of Chapter VII), and in this region detailed calculation leads us to expect that

$$f_1(T_1)=\frac{\left(\frac{k}{2hRZ^2}\right) T_1 \int_{y_1}^{\infty} \frac{W_\nu dy}{e^y-1}}{\int_{y_1}^{\infty} \frac{W_\nu dy}{y(e^y-1)}} \quad (64)$$

will be very nearly the same as in the thin shell.

Furthermore, the radiation from the central star is not necessarily that of a black body at the temperature corresponding to the excitation temperature of the central star (see Chapter VI, p. 229). Given the specific model atmosphere of the central star, and the optical thickness τ_0 of the nebula, we could make definite calculations.

In general, unless hydrogen is practically all ionized, the temperature of a typical planetary nebula cannot rise above about $25,000^\circ\text{K}$.

Estimates of T_e may be made by several methods, none of them completely satisfactory. The profiles of emission lines might be used if it is possible to disentangle the effects of mass motion and gas kinetic motion. In Chapter II we mentioned Baade, Goos, Koch, and Minkowski's study of the Orion nebula for which they found electron temperatures from $12,000^\circ\text{K}$. to $20,000^\circ\text{K}$. Methods based on the intensity in the nebular continuum and on the amount of the Balmer jump in the continuum will be discussed in Section 6. In Chapter V we shall discuss estimates of T_e based on intensity ratios of forbidden lines, particularly $I(N_1 + N_2)/I(4363)$ of [OIII].

4. The Ionization Equation for the Gaseous Nebulae

The ionization equilibrium in a gaseous nebula differs from that in a stellar atmosphere to a very marked degree. In the nebula all ionizations take place from the ground-level of whatever ion or atom is considered, whereas recaptures take place on all the levels. Let us consider first the ionization of hydrogen. From equations (11) and (50) we write down the ionization equation at once:

$$\frac{N_i N_e}{N_1} = \frac{(2\pi m k T_e)^{3/2}}{h^3} \frac{2\varpi_i}{\varpi_1} e^{-x_i} \frac{1}{b_1} = \frac{(2\pi m k T_e)^{3/2}}{h^3} \frac{\int_{y_1}^{\infty} W_{1*} \frac{dy}{y(e^y - 1)}}{G_{T_e}}. \quad (65)$$

This equation can be solved as soon as W_{1*} , T_e , and T_1 are known. Here $y = h\nu/kT_1$, and $y_1 = h\nu_1/kT_1$. To illustrate the order of magnitude of the factors involved let us consider the state of ionization in the shell of NGC 6826. We adopt a stellar radius of 0.8 that of the sun, i.e. 5.6×10^{10} cm. and a radius for the nebular shell of 2.04×10^{17} cm. The geometrical dilution factor

$$W = \frac{R^2}{4r^2} = 1.88 \times 10^{-14} \sim 2 \times 10^{-14}.$$

If the temperature of the central star is taken as $34,600^\circ\text{K}$., $y_1 = 4.57$. Then

$$\int_{y_1}^{\infty} \frac{dy}{y(e^y - 1)} \sim 0.00191.$$

For an electron temperature of $11,000^\circ\text{K}$., $G_{T_e}=0.144$. Putting these numbers into the ionization equation (65) we get

$$\frac{N_i N_e}{N_1} = 7.0 \times 10^5,$$

corresponding to $b_1=0.25 \times 10^{10}$. Photometric measures of the surface brightness indicate that $N_e=N_i \sim 2200$ so that $N_1 \sim 6.5$. Compare this number with that appropriate to thermal equilibrium at the same electron temperature and density, viz. $N_1=2.7 \times 10^{-9}$.

The ionization equation for any kind of atom exposed to a dilute radiation field may be derived in a straightforward way. The number of ionizations from the ground-level, viz.

$$\int_{\nu_1}^{\infty} N_1 \frac{4\pi I_\nu a_1(\nu)}{h\nu} d\nu = \frac{8\pi N_1}{c^2} \int_{\nu_1}^{\infty} \frac{W_\nu a_1(\nu) \nu^2}{(e^{h\nu/kT_1}-1)} d\nu, \quad (66)$$

must equal the number of recaptures on all levels, i.e.

$$\sum_j \int F_{j\lambda} d\lambda = \sum_j \int_0^{\infty} N_i N_e f(\nu) \nu \sigma_j d\nu, \quad (67)$$

here $a_1(\nu)$ denotes the absorption coefficient for photo-ionizations from the ground-levels by absorption of radiation of frequency ν . I_ν is given by equation (7). N_1 is the number of atoms or ions of the kind considered per cm^3 and N_i the corresponding number of such particles in the next higher stage of ionization, e.g. if N_1 refers to the number of OII ions/ cm^3 , N_i will refer to the number of OIII ions/ cm^3 . Recaptures occur on all levels (denoted by j) of the atom. Here $f(\nu)$ is the Maxwellian distribution of velocities, viz.

$$f(\nu) d\nu = 4\pi \left(\frac{m}{2\pi kT_e} \right)^{3/2} \nu^2 e^{-m\nu^2/2kT_e} d\nu, \quad (68)$$

which obeys the normalization condition

$$\int_0^{\infty} f(\nu) d\nu = 1. \quad (69)$$

Hence the number of electrons with velocities between ν and $\nu+d\nu/\text{cm}^3$ will be $N_e f(\nu) d\nu$. If $\sigma_j(\nu)$ is the cross-section for the recapture of electrons moving with a velocity ν into level j , the total number collected by N_i ions/ cm^3/sec . from the velocity range ν to $\nu+d\nu$ will be the number swept up in a cylinder of dimensions $\nu \sigma_j$, i.e. $N_e f(\nu) d\nu N_i \nu \sigma_j$. The total number of recaptures from all velocity ranges on all levels is then obtained by integrating over all velocities and summing over all energy states of the

atoms which gives us the right-hand side of equation (67). The cross-section for capture $\sigma_j(v)$ is related to the absorption coefficient $\alpha_j(v)$ for an atom in level j by

$$\frac{\alpha_j(v)}{\sigma_j(v)} = \frac{m^2 v^2 c^2}{v^2 h^2} \frac{\varpi_e \varpi_j}{2 \varpi_j}, \quad (70)$$

an equation due to Milne.⁽²⁰⁾ Here ν and v are related by

$$\frac{1}{2} m v^2 + \chi_j = h \nu,$$

where χ_j is the ionization energy for the j th level. We now equate equations (66) and (67) and substitute from equation (68) to obtain the general ionization equation, viz.

$$\frac{N_i N_e}{N_1} = \frac{(2\pi m k T_e)^{3/2}}{h^3} \frac{\varpi_e \varpi_i}{\varpi_1} \frac{\varpi_1 \int_{\nu_i}^{\infty} \frac{W_\nu \nu^2 \alpha_1(\nu)}{e^{h\nu/kT_1} - 1} d\nu}{\sum_{j=1}^{\infty} \varpi_j \int_0^{\infty} \frac{m}{h} e^{-m\nu^2/2kT_e} \alpha_j(\nu) \nu^2 v dv}. \quad (71)$$

We may reduce this equation to a more familiar form if we assume that I_ν may be represented by the *Wien approximation*, viz.

$$I_\nu \sim W_\nu \frac{2h\nu^3 e}{c^2} e^{-h\nu/kT_1}, \quad (72)$$

which is valid for $h\nu/kT_1 \gg 1$. Then

$$[e^{h\nu/kT_1} - 1] \sim e^{h\nu/kT_1} = e^{x_1/kT_1 + m\nu^2/2kT_1}. \quad (73)$$

Further, let us take

$$x = \frac{m\nu^2}{2kT} \quad z = \frac{m\nu^2}{2kT_1}. \quad (74)$$

Then equation (71) becomes

$$\frac{N_i N_e}{N_1} = \left[\frac{2\pi m k}{h^2} \right]^{3/2} \frac{2\varpi_i}{\varpi_1} T_1^{3/2} e^{-x_1/kT_1} \left[\frac{T_e}{T_1} \right]^{1/2} D, \quad (75)$$

since $\varpi_e = 2$, and where we put

$$D = \frac{\varpi_1 \int_0^{\infty} W_\nu \alpha_1(\nu) \nu^2 e^{-z} dz}{\sum_{j=1}^{\infty} \varpi_j \int_0^{\infty} \alpha_j(\nu) \nu^2 e^{-x} dx}. \quad (76)$$

Equation (75) is essentially the equation given by Strömberg. D depends primarily on the dilution factor W_ν . If we suppose that for the ion in

question $\alpha(\nu)$ varies as ν^{-2} , that W_r can be replaced by an average over ν , and that recaptures on levels higher than the first may be neglected, $D = \bar{W}$ and the ionization equation becomes

$$\frac{N_i N_e}{N_1} = \frac{(2\pi m k)^{3/2}}{h^3} \frac{2\varpi_1}{\varpi_1} T_1^{3/2} e^{-x_1/kT_1} \bar{W} \sqrt{\frac{T_e}{T_1}}, \quad (77)$$

which is the form of the equation employed by Strömberg in his discussion of the ionization of interstellar hydrogen around a hot star.⁽²¹⁾ Actually the neglect of the recaptures on the higher level is not justified, as detailed calculations for elements like calcium and sodium show. The number of neutral atoms tends to be greater than the number calculated by equation (77).

Detailed calculations of the factor D requires a knowledge of $\alpha_j(\nu)$ for the various energy levels of the atom in question. For hydrogen $\alpha(\nu)$ varies as ν^{-3} , but for other elements the dependence of $\alpha_j(\nu)$ on ν is often more complicated. Computations for atoms in the first row of the periodic tables have been made by D. R. Bates⁽²²⁾ and by Bates and Seaton,⁽²³⁾ while Goldberg and Aller calculated $\alpha_1(\nu)$ for oxygen in various stages of ionization, and made estimates for other atoms and ions of astrophysical interest.

It is not permissible to assume hydrogenic absorption coefficients for complex atoms because, as Bates pointed out, the free electron moves in a field of different effective charge Z_{eff} than does the bound electron. Consider, for example, a carbon atom in its ground-level. The photo-electric ejection of one of the outer $2p$ electrons occurs when the atom is ionized. When the electron is in the $2p$ shell, it is incompletely screened by the other five electrons and $Z_{eff} > 1$. When this $2p$ electron becomes photo-ionized to a d -state, the screening by the remaining electrons is complete and $Z_{eff} = (Z - \sigma) = 1$.

To develop the relevant formulae we may proceed as follows. The frequency of the radiation absorbed when an atom is excited from a ground $2p$ configuration to an excited nd configuration may be expressed as

$$\nu = RZ^2 \left(\frac{1}{n_0^{*2}} - \frac{1}{n^2} \right), \quad (78)$$

where R is the Rydberg constant in frequency units, Z is the net charge of the nucleus plus remaining electrons, and n_0^* is chosen in such a way as to reproduce the term value of the ground-level. We suppose that the d -levels are hydrogenic so that their term values may be expressed as $T = -RZ^2/n^2$. Likewise, following Menzel and Pekeris,⁽⁵⁾ we suppose that the term values of states in the continuum may be written as $T_c = RZ^2/\kappa^2$.

Hence the frequency of radiation emitted or absorbed in bound-free transitions will be given by

$$\nu = R \left[\frac{\chi_1}{\chi_H} + \frac{Z^2}{\kappa^2} \right], \quad (79)$$

where χ_1 is the ionization potential of the atom from the ground-level and χ_H is that of hydrogen.

The *continuous absorption coefficient* is related to the oscillator strength by

$$\alpha_\nu = \frac{\pi e^2}{mc} f \frac{d\kappa}{d\nu} = \frac{\pi e^2}{mc} f \frac{\kappa^3}{2RZ^2}, \quad (80)$$

since the oscillator strength is $f d\kappa$ for the interval κ to $\kappa + d\kappa$. The oscillator strength f for transitions to the continuum is given by

$$f(n, l'; \kappa l) = \frac{1}{2J'+1} \frac{8\pi^2 m \nu}{3h} \frac{a_0^2}{4l^2-1} S \varrho^2, \quad (81)$$

where a_0 is the radius of the first Bohr orbit, J is the total quantum number of the lower level, l is the larger of the two quantum numbers l and l' , S is the strength of the transition expressed in units of

$$\sigma^2 = \frac{1}{4l^2-1} \varrho^2, \quad (82)$$

ϱ is the radial quantum integral,

$$\varrho = \int_0^\infty r^3 R(nl') R(\kappa l) dr. \quad (83)$$

Here $R(nl')$ is the radial quantum wave function for the ground-level, while $R(\kappa l)$ is the radial quantum wave function for a free electron. Difficulties may sometimes arise in the application of equation (83) to the practical calculation of oscillator strengths, because the method employed to determine $R(nl)$ may fix the wave function in the neighbourhood of the origin, whereas the chief contribution to the absorption coefficient may arise at large values of r . If the wave functions are determined by the application of the Ritz principle, $R(nl)$ may be poorly determined at r -values that are important in the evaluation of ϱ . The calculation of the continuous absorption coefficient of the negative hydrogen ion illustrates these troubles particularly vividly. To overcome them Chandrasekhar proposed two additional alternative formulae.⁽²⁴⁾ These formulae are based on the fact that the rate of radiation of a classical dipole oscillator can be expressed in terms of its dipole moment, its momentum, or its acceleration.

That is, the matrix element

$$(n'l'|P|nl) = (n'l'|\varepsilon z_i|nl)$$

may be defined as

$$(n'l'|P|nl) = \int \psi^*(nl) \varepsilon z_i \psi(n'l') d\tau \quad (\text{dipole moment}),$$

as

$$\begin{aligned} (n'l'|P|nl) &= \frac{\varepsilon}{(E-E')} \int \frac{\partial \psi^*(nl)}{\partial z_i} \psi(n'l') d\tau \quad (\text{momentum operator}) \\ &= -\frac{\varepsilon}{(E-E')} \int \psi^*(nl) \frac{\partial \psi(n'l')}{\partial z_i} d\tau, \end{aligned} \quad (84)$$

or as

$$(n'l'|P|nl) = \frac{\varepsilon}{(E-E')^2} \int \psi^*(nl) \frac{\partial V}{\partial z_i} \psi(n'l') d\tau \quad (\text{acceleration}),$$

for the coordinate z_i of the i th electron. Here all quantities are measured in Hartree's atomic units, E and E' are the energies of the upper and lower states of the transition, and V is the potential energy due to electrostatic interactions between the particles. It is advantageous to calculate matrix elements by all three methods and compare the results. Su Shu Huang⁽²⁵⁾ has done this for helium. Here, however, we shall confine our attention to the calculation of the dipole moment.

As a specific example let us consider the transition from a bound p -state to a free d -state. The ps transitions contribute so very much less to the continuous absorption coefficient that they usually may be neglected. Let us suppose that the radial wave function for the ground-level can be represented by

$$R(2p) = \sqrt{\frac{4S_1^5}{3}} r e^{-S_1 r}, \quad (85)$$

where $S_1 = Z_2/2$, Z_2 being the effective charge on the nucleus. For the bound d -levels (which we assume to be hydrogenic) we adopt wave functions of the form

$$R(nd) = \sqrt{\frac{\mu^7(n+2)!}{2n^8(n-3)!(5!)^2}} r^2 e^{-\mu r/2n} F\left(-n+3, 6, \frac{\mu r}{n}\right), \quad (86)$$

where $\mu = 2Z_1$. Z_1 is the effective charge under whose influence the d electron moves. $Z_1 = 1$ for a neutral atom, 2 for a singly ionized atom, etc. $F(-)$ is the confluent hypergeometric equation. The radial quantum integral for a $2p$ - nd transition is⁽²⁶⁾

$$Q = \sqrt{\frac{4S_1^5 \mu^7(n+2)!}{6n^8(n-3)!(5!)^2}} \int_0^\infty r^6 e^{-[S_1 + \frac{\mu}{2n}]r} F\left(-n+3, 6, \frac{\mu r}{n}\right) dr,$$

which reduces to

$$\begin{aligned} \varrho^2 &= 3 \cdot 2^{17} \cdot n^6 \frac{S_1^5 \mu^7 (n+2)!}{(n-3)!} \frac{(2nS_1 - \mu)^{2n-6}}{(2nS_1 + \mu)^{2n+8}} \left[\frac{n \left(3 \frac{2S_1}{\mu} - 1 \right)}{3 \left(n \frac{2S_1}{\mu} - 1 \right)} \right]^2 \\ &= 3^{-12} 2^{12} S^5 (2Z_1)^{-2} n^9 (n^2 - 1)(n^2 - 4) \frac{(nS - 1)^{2n-8}}{(nS + 1)^{2n+8}} (3S - 1)^2, \quad (87) \end{aligned}$$

where

$$S = 2S_1/\mu = Z_2/2Z_1. \quad (88)$$

To obtain an expression for the radial quantum integral for the bound-free transitions we replace n by $i\kappa'$ (see p. 114), and take the absolute value of the resulting formula

$$\begin{aligned} \varrho &= 3^{-1/2} 2^6 \left(\frac{Z_2}{2Z_1} \right)^{5/2} (2Z_1)^{-1} \left(3 \frac{Z_2}{2Z_1} - 1 \right) \kappa^{9/2} (\kappa^2 + 1)^{1/2} (\kappa^2 + 4)^{1/2} \\ &\quad \left(1 + \frac{Z_2^2}{4Z_1^2} \kappa^2 \right)^{-4} e^{-2\kappa \tan^{-1} \frac{2Z_1}{Z_2 \kappa}}. \quad (89) \end{aligned}$$

In this calculation it is assumed that the wave function for the free d electron is hydrogen-like.

For many atoms or ions the representation of the radial wave function for the ground p configuration by equation (85) is inadequate. If Hartree wave functions are available for the ground-level, it is often possible to represent the tabulated values in analytic form, viz.,

$$R(2p) = r(ae^{-br} + ce^{-dr}) \quad (90)$$

as suggested by J. C. Slater.⁽²⁷⁾ By making the simple replacements

$$Z_2/2 \rightarrow b, \quad d \sqrt{\frac{Z_2^5}{24}} \rightarrow a, \quad c \quad (91)$$

equation (89) can be adapted for the calculation of ϱ . Since $l=2$ for d electrons, we find from equations (79), (80), and (81) that for pd bound-free transitions

$$a_\nu = \frac{\pi e^2}{c} \frac{4\pi^2 a^2}{45h} \frac{S}{2J+1} \left[\frac{\chi_1}{\chi_H} + \frac{Z^2}{\kappa^2} \right] \frac{|\kappa^{-3} \varrho^2}{Z^2}. \quad (92)$$

The strengths S may be calculated from available tables of multiplet strengths, due account being taken of the parentages of the various spectral terms.

For atoms for which ground-level wave functions are not available, effective values of Z_2 may be calculated by rules due to Slater.⁽²⁸⁾ A comparison of absorption coefficients based on wave functions obtained

from Slater's rules with those obtained from the Hartree wave functions for oxygen, shows that the Slater wave function gives rather serious errors in the neighbourhood of the series limit. On the other hand, the Slater approximation becomes less inaccurate for the oxygen atom in higher stages of ionization. The lighter the atom and higher the degree of ionization, the more nearly valid is the Slater approximation. This means that with a single exponential term it is not possible to get an adequate representation of the radial quantum integral. One qualitative result of the calculations must be mentioned. In neutral atoms and even to some extent in singly ionized atoms there is a tendency for the continuous

TABLE IV : 6
Absorption Coefficient for Bound-Free Transitions in Oxygen

OI		OII		OIII
$\tilde{\nu}$	α_{ν}	$\tilde{\nu}$	α_{ν}	α_{ν}
112,000	3.7×10^{-18}	300,000	10.0×10^{-18}	—
120,000	4.1	400,000	6.2	—
135,000	4.2	500,000	4.2	3.26×10^{-18}
	9.9	600,000	3.2	2.27
	10.8	700,000	2.5	1.66
150,000	14.4	800,000	2.0	1.25
	14.45	1×10^6	1.4	0.80
160,000	14.0	1.2×10^6	1.0	0.50
170,000	12.5	1.5	0.6	0.24
200,000	10.0	2.0	0.3	0.12
250,000	8.1			
300,000	7.1			
350,000	6.2			
400,000	4.9			
500,000	4.4			
600,000				

absorption coefficient to rise to a maximum above the series limit and then to diminish again. Among highly ionized atoms the absorption coefficient diminishes monotonically beyond the series limit.

The absorption coefficients of oxygen in various stages of ionization for bound-free transitions as computed by Leo Goldberg and the writer are given in Table IV : 6 as a function of wave-number, $\tilde{\nu}$.

Recaptures on the higher levels involve wave functions that are more nearly hydrogenic, and a good start may be made by using the corresponding hydrogenic functions for many of them.

D. R. Bates has carefully reviewed the use of quantum mechanics in the calculation of the continuous absorption coefficients of neutral atoms and positive ions with particular regard to the practical difficulties imposed by the nature of the wave functions. He has also derived approximate

formulae that may be used for other light ions, somewhat along the lines we have already discussed. The use of wave functions based on Slater's rules is of dubious value.

Continuous absorption coefficients for helium have been derived by Vinti,⁽²⁹⁾ by Goldberg,⁽²⁶⁾ and by Su Shu Huang.⁽²⁵⁾ We may calculate the continuous absorption coefficients for photo-ionizations from the 1^1S , 2^1S , and 2^3S levels from Huang's tables. For the continuum at the head of the 2^1P - n^1S series, Goldberg's results may be expressed by the formula

$$\log \alpha_\nu(2^1P-n^1S)=35.48-3.6 \log \nu, \quad (93)$$

and for the continuum at the head of the 2^3P - n^3S series, there occurs

$$\log \alpha_\nu(2^3P-n^3S)=31.06-3.3 \log \nu. \quad (94)$$

For the higher levels and for the free-free transitions the helium atom must be regarded as hydrogen-like.

5. The Continuous Spectra of the Gaseous Nebulae; Electron Densities

Galactic nebulae generally possess a continuous as well as a discrete line spectrum. Objects of low surface brightness such as NGC 1499 (the "California nebula") presumably emit a continuum of such low intensity that it is lost against the background of galactic light. In Chapter III we saw that diffuse galactic nebulae often show spectra similar to those of luminous stars near them. Such objects as the Pleiades nebulosity, for example, contain great numbers of small solid particles that reflect and scatter the starlight. Electron scattering, which seems to be responsible for the continuous spectrum of the corona, apparently plays no important roles in these nebular continua.

We are concerned here with the continuous spectra of the purely gaseous nebulae where physical processes are not complicated by the presence of small solid particles.

Photometric measures of the continuous spectra of the planetary nebulae have been made by T. L. Page⁽³⁰⁾ and by Minkowski and the writer, as well as more recently by Barbier and Andrillat.⁽³¹⁾ Page used a very wide slit so that the contribution of the weaker nebular lines was added to that of the true continuum. Minkowski and the writer used a narrow slit which enabled the weak lines to be observed, but the continuum was relatively much weaker so that long exposures with corresponding photometric difficulties were required. The Balmer continuum is easily recognized and measured; an underlying continuum is also observed, but its exact intensity dependence on frequency is not yet known. Page suggested that the intensity of this underlying or "visual" continuum changed slowly with wavelength, but his measures appear to be largely influenced by the effects of overlapping lines.

In the observable region of the spectra the following processes have long been known to contribute to the nebular continuous spectra:

- (1) Recombination of electrons with protons to give rise to the Balmer, Paschen, Brackett, and higher continua.
- (2) Free-free transitions involving hydrogen and helium ions and electrons.
- (3) Recombination of electrons with helium ions in excited levels. Menzel has observed the recombination continua of helium in NGC 6543.

Continuous recombination spectra involving atoms heavier than helium are unimportant because of the rarity of these elements as compared with hydrogen. Even helium contributes relatively little compared with the emission by hydrogen.

Let us consider first the recombination Balmer emission. The amount of energy emitted/unit frequency interval/cm.³/sec. will be (cf. equation 26)

$$E_{n2}d\nu = N_i N_e \frac{hKZ^4}{T_e^{3/2}} \frac{g}{8} e^{X_2} e^{-h\nu/kT_e} d\nu. \quad (95)$$

Near the series limit, Menzel and Pekeris give the following asymptotic expression for g^5

$$g \simeq 1 - 0.1728 \left(\frac{\nu}{RZ^2} \right)^{1/3} \left[\frac{Z}{n'^2} \left(\frac{RZ^2}{\nu} \right) - 1 \right]. \quad (96)$$

Then, noting that $hK = 21.6 \times 10^{-33}$, we get

$$E_{n2}d\nu = 2.70 \times 10^{-33} N_i N_e T_e^{-3/2} g e^{X_2 - h\nu/kT_e} d\nu. \quad (97)$$

At the Balmer limit $g = 0.876$, $h\nu_2/kT_e = X_2$, and the total amount of energy emitted by a nebula of constant electron temperature T_e and density will be

$$Ed\nu = 2.37 \times 10^{-33} N_i N_e T_e^{-3/2} V d\nu, \quad (98)$$

where V is the total volume occupied by the radiating atoms. Let S_{Bac} denote the average flux through the surface of the nebula in ergs/cm.²/sec. in a wavelength interval $\Delta\lambda$. If the nebula consists of a hollow shell of inner radius r_i and outer radius r_o , then

$$S_{Bac} = 1.78 \times 10^{-22} N_i N_e T_e^{-3/2} \left[\frac{r_o^3 - r_i^3}{r_o^2} \right] \Delta\lambda, \quad (99)$$

where $\Delta\lambda$ is given in Angstroms and r is expressed in cm.

Measures of the intensity of the Balmer continuum compared with $H\beta$ and other emission lines have been made by T. L. Page⁽³⁰⁾ and by the writer.⁽³²⁾ The results are in good agreement for most of the objects common to the two programmes; the chief uncertainty lies in estimating the position of the background continuum.

Menzel and the writer defined S_{Bac} for $\Delta\lambda$ selected as 20 Å. Equation (99) then becomes

$$S_{Bac} = 3.56 \times 10^{-21} N_i N_e T_e^{-3/2} r_0 \left[1 - \left(\frac{r_i}{r_0} \right)^3 \right]. \quad (100)$$

In some nebulae the Balmer continuum is so weak that it cannot be measured easily. Under these circumstances we may use the observed flux in $H\beta$, adopt b_4 from the assumed value of T_e for Menzel and Baker's model *B*, and calculate $N_i N_e$ from an equation derived from equation (20) in the same way as equation (100) was obtained from equation (26).

Table IV: 7 summarizes the results obtained for several planetaries. It is assumed that the nebulae can be approximated as spheres or hollow spherical shells. Column 2 gives the apparent radius of the nebula, column 3 the value for r_i/r_0 estimated by H. D. Curtis (*Lick Publ.* 13), column 4 the distance according to Berman (Chapter III, p. 51), and column 5 the corresponding value of r_0 in cm. Column 6 gives the surface flux in $H\beta$ in ergs/cm.²/sec., from the work of Liller and the writer; column 7 gives the ratio of the fluxes in the Balmer continuum and $H\beta$, $S_{Bac}/S_{H\beta}$ as measured by photographic photometry. The electron temperature entered in column 8 is derived from the [OIII] lines. The value of $\log b_4$ in column 9 is interpolated from the data of Baker and Menzel (see Table IV: 1). Columns 10 and 11 give the electron densities found from $H\beta$ and the Balmer continuum, respectively. The former are considered to be much more reliable and the adopted values in column 12 are primarily based on them.

The lack of a systematic difference between the data of columns 10 and 11 permits the conclusion that the $S_{Bac}/S_{H\beta}$ ratio is in satisfactory agreement with the theory of the Balmer decrement as given by Baker and Menzel. Discrepancies can be accounted for by the difficulty in measuring the Balmer continuum.

We shall use the $\log N_i$'s given in column 12 in later applications to specific nebulae. The numerical values involve (in addition to the simplifying geometric assumptions): (a) the assumed distance of the nebula; (b) its electron temperature. Both of these are likely to be uncertain.

Returning to the problem of the continuous spectrum, we notice that T_e can be estimated if the intensity in the pure Balmer continuum can be measured at two different frequencies. Thus, if I_{ν_2} is the intensity at the Balmer limit and I_ν that at some other frequency, we have

$$\frac{I_{\nu_2}}{I_\nu} = \frac{g(\nu_2)}{g(\nu)} e^{+h(\nu-\nu_2)/kT_e} \quad (101)$$

as the equation from which T_e can be derived.

TABLE IV : 7

The Electron Densities of Typical Planetary Nebulae

1	2	3	4	5	6	7	8	9	10	11	12
Nebula	r_0''	$\frac{r_i}{r_0}$	Distance (parsecs)	r_0 $\times 10^{-17}\text{cm.}$	$\log S_{H\beta}$	$\log \frac{S_{Bac}}{S_{H\beta}}$	T_e (Chap. 5)	$\log b_4$	$\log N_e$		
									$H\beta$	Bac	<i>Adopt</i>
NGC 1535	9"	0.7:	1720	2.32	-1.62	-0.72	14,300	-0.55	3.41	3.56	3.45
NGC 2149	6"	1.0	2250	2.02	-1.40	-1.04	14,150	-0.56	3.46	3.46	3.46
IC 418	6"	0.8	1800	1.62	-0.41	-1.14	18,300	-0.43	4.21	4.20	4.21
NGC 2392	23"	0.8	860	2.96	-2.44	-1.62:	19,600	-0.40	3.06	2.83	3.05
NGC 3242	10"	0.8	1640	2.45	-1.16	-1.10	17,700	-0.44	3.74	3.74	3.74
IC 4593	5"	1.0	2000	1.49	-1.29	-1.14	7,700	-1.02	3.47	3.34	3.47
NGC 6210	4"	1.0	1720	1.03	-0.60	-0.75	10,800	-0.72	3.94	4.06	3.95
NGC 6543	10"	0.8	1080	1.61	-0.94	-1.07	9,500	-0.82	3.81	3.75	3.81
NGC 6572	7"	1.0	1230	1.29	-0.83	-1.17	13,500	-0.58	4.02	3.76	4.02
NGC 6803	2.5"	1.0	2640	0.99	-1.30	-0.62:	12,800	-0.62	3.64	3.63	3.63
NGC 6818	9"	0.7	2380	3.20	-1.40	-1.00	15,700	-0.50	3.47	3.51	3.48
NGC 6826	13"	1.0	1050	2.04	-1.49	-1.12	11,200	-0.70	3.36	3.31	3.35
NGC 7009	9"	0.7	930	1.25	-1.04	-1.06	13,900	-0.57	3.82	3.81	3.81
NGC 7027	5"	1.0	2130	1.59	-0.88	-1.01	16,800	-0.46	3.70	3.75	3.70
NGC 7662	8"	0.8	1200	1.44	-1.18	-1.21	15,000	-0.52	3.84	3.78	3.83

The essential difficulty in the application of this equation to the determination of electron temperatures lies in allowing for the influence of the background continuum. The resultant temperature will depend strongly on the frequency dependence of this continuum. In the absence of any specific knowledge on this matter the usual practice has been to take the intensity as constant. On the basis of this assumption T. L. Page found that the energy distributions in the continua of several planetaries were consistent with the temperatures obtained from the ratio of the intensities of the auroral and nebular lines of [OIII] by Menzel, Hebb, and the writer, i.e. in the neighbourhood of 8000°K. to $10,000^{\circ}\text{K.}$ By a similar method, the writer found a somewhat higher electron temperature in NGC 7662. It should be emphasized that if the background continuum diminishes in intensity towards the ultra-violet, the electron temperature will be higher than $10,000^{\circ}\text{K.}$, whereas if it increases in intensity the temperature will be lower.

This background continuum is stronger than can be accounted for by recombinations and free-free transitions. It cannot be explained by electron scattering nor by the negative hydrogen ion. Reflection and scattering by solid particles seems also to be excluded. If particles were present in sufficient numbers they would dim the light from the side of the nebula opposite to the observer. Many nebula show spectral lines that are widened or doubled because of the expansion of the shell. If internal absorption occurred in the nebulae we would expect the red components to be systematically dimmer than the violet components. Yet the intensity ratios of the components vary from one object to another in a random fashion. The differences are caused by variations in the initial ejection process or in the subsequent motions of the gases, not by absorption by particles.

A possible mechanism for the production of a continuous emission in the gaseous nebulae is provided by the escape of atoms from the metastable $2s$ level in hydrogen with the radiation of two photons. A hydrogen atom that finds itself, say by direct capture or by cascade in the $2s$ level, may escape by one of several processes. Photo-ionization by the absorption of a quantum in the Balmer continuum is unlikely. A super-elastic collision may enable it to get rid of all its $10\cdot16$ e.v. of energy, or an electron collision may jostle it into the $2p$ level, whence it returns to the ground-level very quickly. If T_e is about $10,000^{\circ}\text{K.}$ the probability of this latter process is of the order of $5 \times 10^{-5} N_e \text{ sec.}^{-1}$. Macroscopic electric fields would also enable the atom to escape from the $2s$ to the $2p$ level, but such fields are not anticipated in gaseous nebulae. Even at very low electron densities, in the absence of electric fields, and in very weak radiation fields, the atom cannot remain in the $2s$ level longer than about $1/8$ th second.

Maria Goeppert Mayer⁽³³⁾ pointed out that an atom could escape from a metastable level such as the $2s$ level in hydrogen by a double-photon emission. It is as though the atom conjured a virtual p level lying between the ground-level and the metastable $2s$ level. Since this virtual level may lie anywhere between $1s$ and $2s$, the two photons can have any frequency subject to the condition

$$\nu' + \nu'' = \nu(2s-1s) = \frac{E(2s) - E(1s)}{h}, \quad (102)$$

where $E(2s)$ is the energy of the $2s$ level, $E(1s)$, that of the ground $1s$ level. Thus $\nu(2s-1s)$ is very nearly the frequency of Lyman α . Hence a continuous spectrum is emitted and we immediately ask two questions: (a) Does this continuum have the right dependence on frequency to explain the background continuum in the planetary? (b) Under the conditions of density and temperature thought to exist in the gaseous nebulae does it give the right amount of energy?

Some years ago Minkowski and the writer examined this mechanism to see if it would account for the strong background nebular continuum. The predicted intensity distribution did not agree with what appeared to be the observed energy distribution. The latter is uncertain, however, and more recent theoretical work by Spitzer and Greenstein⁽³⁴⁾ makes it appear that the two-photon emission may suffice to explain the elusive continuum.

Breit and Teller⁽³⁵⁾ made a detailed application of Mrs. Mayer's theory to the $2s-1s$ transition in hydrogen, and their work has been refined and extended by Spitzer and Greenstein. Let us denote the frequencies of the two quanta by

$$\nu' = y\nu(2s-1s); \quad \nu'' = (1-y)\nu(2s-1s). \quad (103)$$

If $A(y)dy$ is the probability that a photon is emitted with a frequency between $y\nu(2s-1s)$ and $\nu(2s-1s)(y+dy)$,

$$A(y) = \frac{9\alpha^6 R}{2^{10}} \varphi(y), \quad (104)$$

according to Breit and Teller. Here

$$\alpha = \frac{2\pi\epsilon^2}{hc}. \quad (105)$$

is the fine-structure constant, R is the Rydberg constant, and the function $\varphi(y)$ involves certain radial quantum integrals that have been defined by Breit and Teller. The emission per unit volume and time interval, $E_{2s}(\nu)$, is proportional to $h\nu A(y)$ and therefore to $y\varphi(y)$. The integration of $\varphi(y)$ gives

$$\int_0^1 \varphi(y) dy = 3.770. \quad (106)$$

The Einstein coefficient of spontaneous emission A_{2s-1s} for the two-photon transitions is

$$A_{2s-1s} = \frac{1}{2} \int_0^1 A(y) dy = \frac{9\alpha^6 R}{2^{11}} \times 3.77 = 8.227 \text{ sec.}^{-1}. \quad (107)$$

The factor of $1/2$ comes from the fact two photons are emitted per transition. The function $\varphi(y) = \varphi(1-y)$ is tabulated by Spitzer and Greenstein as follows:*

y	λ	$\varphi(y)$	y	λ	$\varphi(y)$
0.10	12,157	2.783	0.30	4052	4.546
0.15	8,105	3.481	0.35	3473	4.711
0.20	6,078	3.961	0.40	3039	4.824
0.25	4,862	4.306	0.50	2431	4.907

Atoms may enter the $2s$ level by direct recapture from the continuum, by recapture on higher levels and subsequent cascade, and sometimes by a collisional transition from $2p$ to $2s$. This latter process has an extremely low probability, but the Lyman α quanta are scattered such a huge number of times before their escape from the nebula that under certain favourable circumstances some two-quantum emission may be produced in this way. Ordinarily, however, atoms enter the $2s$ level by recapture and subsequent cascade. Spitzer and Greenstein estimate that the probability, X , that an atom will pass through the $2s$ level on its way to the ground-level will be about 0.32.

The total emission, E_{2q} , between ν and $\nu + d\nu$ in two quantum jumps will depend on the energy $h\nu$ of the jump, the probability function $\varphi(y)$, the total number of recaptures on the second and higher levels, the factor X , and finally a factor 2 because two quanta are liberated in each jump. Thus, using equations (30), (104), (106), we get

$$E_{2q} d\nu = N_i N_e \frac{Kh}{T_e^{3/2}} \sum_2 \frac{e^{x_n}}{n^3} \bar{g} E_1(X_n) 2X \frac{y\varphi(y)}{3.77} d\nu. \quad (108)$$

Similarly the energy liberated in the same frequency range in the bound-free recombinations and free-free transitions will be

$$E_{(bf+ff)} d\nu = N_i N_e \frac{Kh}{T_e^{3/2}} e^{-h\nu/kT_e} \left\{ \sum_{n_m} \frac{\bar{g}_{n'}}{n'^3} e^{x_n} + \frac{kT_e}{2hR} \right\} d\nu, \quad (109)$$

where we have used equations (26) and (35). There n_m is given by the condition that $\nu > \nu_{n_m} = \frac{hRZ^2}{n_m^2}$. The total emission is given by the sum of these two contributions, viz.

$$[E_{2q} + E_{(bf+ff)}] = E_{total}. \quad (110)$$

* *Ap. J.*, **114**, 409 (1951): Table 1.

Fig. 5 shows the results of the calculations. Our results differ from those of Spitzer and Greenstein, who did not take into account the contributions of the higher series limits nor the free-free transitions. The factor in brackets in equation (109) is evaluated by the approximate procedure employed by Unsöld⁽³⁶⁾ in the calculation of the stellar absorption coefficient except that the \bar{g}_n factors are chosen as in the writer's calculation of the stellar absorption coefficient.⁽³⁷⁾

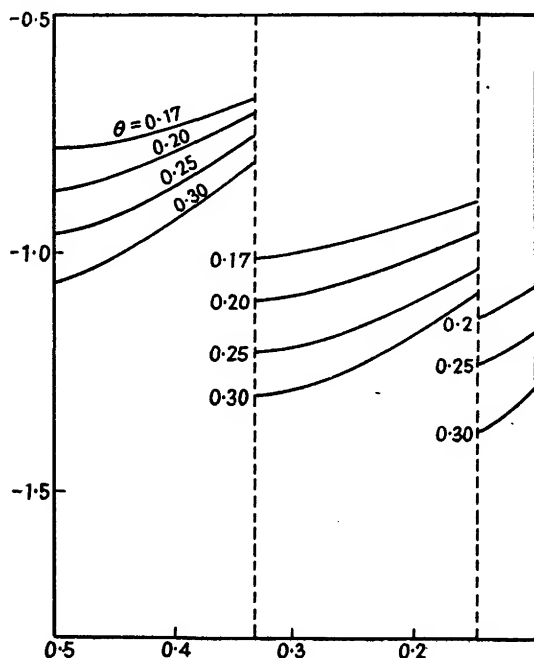


FIG. IV:5. Theoretical Continuous Energy Emission in Gaseous Nebulae.

The quantity $\log E / N_i N_e h K T_e^{-3/2}$ is plotted against $1216/\lambda$ (λ in Ångströms) as a function of $\theta = 5040/T_e$. The calculations are carried out according to the theory of Spitzer and Greenstein, *Ap. J.*, 114, 407 (1951).

The contribution of the two-quantum emissions greatly diminishes the Balmer discontinuity. The latter depends on the electron temperature, becoming smaller the greater the value of T_e . The discontinuity, $\log I_S/I_L$, where I_S denotes the intensity just to the short wavelength side of Balmer limit, and I_L the intensity just to the long wavelength side, amounts to 0.50 at $T_e = 15,000^\circ\text{K.}$, about 0.40 at $24,000^\circ\text{K.}$ and 0.30 at $34,000^\circ\text{K.}$ If the theory is correct, measure of the Balmer discontinuity should give some estimate of the electron temperature. In NGC 7027 the discontinuity is strikingly large, $\log I_S/I_L \sim 0.7$, which would imply an electron temperature less than $10,000^\circ\text{K.}$, whereas the [OIII] line intensities indicate an

electron temperature of $16,000^\circ\text{K}$. Seaton suggests that at the higher densities the $2s$ level tends to be depopulated by collisional excitation to the $2p$ level rather than by the two-photon emission. Hence the magnitude of the Balmer discontinuity will depend on both the electron temperature and the electron density. He has used Barbier and Andrillat's measures of the Balmer discontinuity and of the energy distribution in the continuum to estimate the required densities and temperatures. These tend to agree with those obtained from the forbidden lines.

Much further work on the nebular continua is necessary in order to test the theoretical considerations of Spitzer and Greenstein, of Seaton, and of others. A spectrograph for this programme is now under construction at Michigan where also Liller has designed a photo-electric monochromator for the study of the lines and continua in the brighter planetaries.

By use of appropriate plate filter combinations (cf. Chapter II) Minkowski has photographed nebulae in wavelength regions where there are no spectral lines, i.e. in the light of their continuous radiations. The image of IC 418 in the light of its visual continuum resembles the hydrogen images, a conclusion which is substantiated by photometric measures. Photographs of the Orion nebula in the Balmer continuum show different features than do photographs secured in the visual regions or in the light of $H\alpha + [NII]$. In this object there occur contributions to the continuum from small solid particles as well as from gases.

6. Collisional Excitation of the Hydrogen Lines

In most nebulae it appears to be rather well established that the lines of hydrogen and helium are excited by the so-called primary mechanism, photo-ionization followed by recapture in higher levels. In some objects direct collisional excitation may play an important role. J. H. Oort⁽³⁸⁾ suggested that the shells ejected by novae might collide with the material of interstellar space. The mingling gases become quickly heated, the temperature is raised and a bright-line spectrum is excited by inelastic collisions between electrons and atoms. He also supposed that the Network nebula in Cygnus, the faintly luminous edges of dark clouds, and even such objects as the extended "North America" nebula (NGC 7000) might be excited by collisions between interstellar clouds of gas and particles.

Although subsequent work indicates that the Network nebula probably owes its excitation to radiation rather than to gas-cloud collisions, examples of collisional excitation seem to occur in other objects. In particular collisional excitation would appear to dominate in certain radio sources (see Chapter VIII) and might occur to some extent in other gaseous nebulae, as for example NGC 7027 (p. 200).

The characteristic feature of the pure collisional excitation of the hydrogen lines is a steep Balmer decrement. Sixty years ago W. W. Campbell compared the Balmer lines in the Orion nebula with those of a laboratory discharge tube and called attention to the differences in the $H\alpha:H\beta:H\gamma$ ratios. The fact that unreddened planetary nebulae show a Balmer decrement that approaches the one predicted by pure radiative processes leads us to suppose that collisional excitations are usually not important in these objects. Nevertheless, it is important to examine the conditions under which collisional excitation can become significant.

The first attempt to calculate the effects of electron collisions on the Balmer decrement was that of S. Miyamoto.⁽³⁹⁾ The then available measurements of the Balmer decrement disagreed with the theoretical predictions in the sense that the observed decrement appeared to be too steep. Miyamoto treated an optically thick nebula illuminated by a central star and assumed that the higher levels were excited both by inelastic electron collisions and by the primary mechanism. Although his calculations were based on a hypothetical atom with five states plus a continuum and the target areas for collisional excitation were too large, especially at the lower electron velocities, the results are qualitatively correct in showing a sharp dependence of the $H\alpha/H\beta$ intensity ratio on the electron temperature.

The most detailed treatment of the collisional excitation of the hydrogen lines in gaseous nebulae was carried out by Jos. W. Chamberlain,^(40, 41) who generalized the methods of the Harvard Nebular Series to include collisions as well as radiation. We shall present his method in some detail.

Collisional and radiative excitations take place from the ground-level to excited levels n and to the continuum. The number of collisional excitations from the ground-level to the level n will be

$$\mathcal{F}_{1n} = N_1 N_e \int_{v_n}^{\infty} Q_n(v) v f(v) dv, \quad . \quad . \quad (111)$$

where $f(v)$ is the Maxwellian velocity distribution function for temperature T_e (see equation 68), and $Q_n(v)$ is the target area for collisional excitation from the ground to the n th level. The integration is performed over all velocities v greater than the velocity v_n corresponding to the collisional excitation energy of level n , i.e.

$$\frac{1}{2} m v_n^2 = \chi_n = h R \left(1 - \frac{1}{n^2} \right). \quad . \quad . \quad (112)$$

Let us define

$$\alpha_n(T_e) = \int_{v_n}^{\infty} Q_n(v) v f(v) dv. \quad . \quad . \quad (113)$$

Analogously, the number of collisional ionizations can be written as

$$\int_{v_1}^{\infty} \mathcal{F}_{1*} dv = N_1 N_e a_c(T_e), \quad (114)$$

where

$$a_c(T_e) = \int_{v_1}^{\infty} Q_*(v) f(v) v dv. \quad (115)$$

Here $Q_*(v)$ denotes the ionization cross-section for electrons moving with a velocity v .

Our next task is the estimation of the cross-sections $Q_n(v)$ and $Q_*(v)$ by quantum mechanical methods. The problem is somewhat different from the collisional excitation of the forbidden lines in that the energies involved are much larger. It appears that the Born approximation may give reasonable results, although it tends to overestimate the cross-section at low velocities.

Fortunately the absolute values of the cross-section are of less interest than is the ratio

$$\beta_n(T_e) \equiv \frac{a_n(T_e)}{a_c(T_e)} = \frac{\int_{v_n}^{\infty} Q_n(v) v f(v) dv}{\int_{v_1}^{\infty} Q_*(v) v f(v) dv}, \quad (116)$$

which can be estimated more reliably than can the cross-sections themselves.

Fundaminsky⁽⁴²⁾ has calculated target areas for the collisional excitation of the $2s$, $2p$, $3s$, $3p$, and $3d$ configurations from the ground-level as a function of velocity. To estimate the target areas to the $n=4$ and higher levels, Chamberlain employed an asymptotic formula due to Bethe,⁽⁴³⁾ and corrected the results following a suggestion made by Fundaminsky.

From detailed numerical computations Chamberlain found that for $n \geq 6$, the quantity $\beta_n(T_e)$ could be approximated by

$$\beta_n = \beta_6 \left(\frac{6}{n} \right)^{3.20}. \quad (117)$$

The rate of collisional excitation of the higher levels falls off rapidly, and it is found that for n greater than about 30 the levels tend to be populated by direct recaptures from the continuum, rather than by direct collisional excitation. Representative values of the α 's are given in Table IV:8.

Following Chamberlain, let us first consider the problem of pure collisional excitation of the hydrogen lines. Atoms in the ground-level suffer inelastic collisions with electrons, are excited to the various levels n , whence they cascade to lower levels with the emission of radiation. Others are

ionized from the ground-level by electron collision and subsequently recombine with electrons to emit the Lyman, Balmer, Paschen, and other continua. If the nebula is optically thick in the Lyman lines, the situation

TABLE IV : 8
*Values of Collisional Excitation Parameters**
 $\alpha_n(T_e)$ and $\alpha_{\kappa}(T_e)$

<i>n</i>	10,000° K.	20,000° K.	40,000° K.
2	231×10^{-15}	89×10^{-12}	23.2×10^{-10}
3	6.32	6.65	3.05
4	1.50	1.86	0.92
5	0.435	0.69	0.404
6	0.201	0.36	0.218
κ	25.7	5.31	6.25

To get the number of collisional excitations or ionizations per cm.³/sec. multiply tabular values by N_1N_e .
* Adapted from a table by CHAMBERLAIN, J. W., *Ap. J.*, 117, 392 (1953).

of greatest astrophysical interest, we take $F_{1n}=F_{n1}$. The equation of statistical equilibrium is obtained from equation (2) by adding on the left-hand side the quantity, \mathcal{F}_{1n} , the number of collisional excitations/cm.³/sec. Thus

$$\sum_{n''=n+1}^{\infty} F_{n''n} + \int_{\nu_n}^{\infty} F_{\kappa n} d\nu + F_{1n} + \mathcal{F}_{1n} = \sum_{n'=1}^{n-1} F_{nn'}. \quad (118)$$

We may also suppose that the number of collisional ionizations equals the number of recaptures, viz.

$$\int_{\nu_1}^{\infty} \mathcal{F}_{1\kappa} d\nu = \sum_{n=1}^{\infty} \int_{\nu_n}^{\infty} F_{\kappa n} d\nu, \quad (119)$$

since the number of photo-ionizations must be very small.

Now equations (118) and (119) may be transformed with the aid of equations (11), (13), (14), (15), (18), (30), (31), (32), (111), (113), and equations (30), (31), (51), (114), and (115), respectively. The solution for b_n may be found in a manner analogous to that employed by Menzel and Baker. Thus Chamberlain finds

$$b_n = b_n(B) + G_{T_e} \frac{e^{-x_n}}{t_n} \left\{ n^3 \beta_n + \sum_{i=n+1}^{\infty} \frac{i^3 \beta_i u_{in}}{t_i} + \dots \text{etc.} \right\}, \quad (120)$$

where

$$t_n = \sum_{n'=2}^{n-1} \frac{2n^2 g_{nn'}}{n'(n^2 - n'^2)}, \quad (121)$$

and U is defined by equation (38) and $b_n(B)$ is the value of b_n for Menzel and Baker's model B . For the thin nebula, $b_n(B)$ is replaced by $b_n(A_2)$, while the lower limit of the sum in equation (121) is $n'=1$ instead of $n'=2$.

Chamberlain carried out detailed calculations both for models that were optically thin in the Lyman lines (analogous to models A_2 and C) and for models that were optically thick (analogous to model B). Below $10,000^\circ\text{K}$., collisional excitation may be neglected completely. In the thin model at $10,000^\circ\text{K}$., b_n passes through a minimum at $n=5$ and then rises again as n increases. The lower levels are populated chiefly by direct collisional excitation from the ground-level. Since at low temperatures \mathcal{F}_{1n} falls off

TABLE IV : 9

The b_n -factors and Balmer Decrements for an Optically Thick Nebular Excited by Collisions

n	b_n			$I_n/I(H\beta)$		
	10,000	20,000	40,000	10,000	20,000	40,000
3	1.50	3.47	4.00	5.76	4.79	4.06
4	1.22	2.32	2.60	1.000	1.00	1.00
5	0.96	1.82	2.07	0.291	0.347	0.383
6	0.93	1.67	1.88	0.136	0.169	0.194
7	0.92	1.59	1.75	0.076	0.097	0.112
8	0.94	1.52	1.66	0.048	0.060	0.070
9	0.95	1.48	1.60	0.033	0.040	0.047
10	0.95	1.44	1.55	0.023	0.028	0.033
15	0.93	1.30	1.40	0.006	0.007	0.009

(Courtesy CHAMBERLAIN, J. W., *Ap. J.*, 117, 387 (1953).)

rapidly with n , b_n declines until recombination and subsequent cascade become the dominant factors populating the levels. Then b_n begins to rise once more. At a temperature of $40,000^\circ\text{K}$. the b_n 's for the thin collisional model resemble those for model C .

The b_n 's and Balmer decrements for the collisional excitation of a nebula that is optically thick are given in Table IV : 9. A comparison of the Balmer decrements with those of Table IV : 1 shows that the collisional decrement is always much steeper.

Finally, Chamberlain treated the situation in which the nebula is excited both by inelastic collision processes and by stellar radiation. Under these circumstances the Balmer decrement will depend on the electron temperature T_e , the electron density, N_e , and the character of the radiation from the central star. The expression for b_n may be written in the form

$$b_n = (1 - \mathcal{H})b_n^0 + \mathcal{H}b_n^c, \quad . \quad . \quad . \quad (122)$$

where b_n^c represents the value of b_n calculated for pure collisional excitation, and b_n^0 is the value for model B, A_2 or C, depending on whether the nebula is thick or thin in the Lyman lines. Here

$$\mathcal{H} = 1 - \frac{b_1 e^{x_1}}{G_{T_e}} \int_{y_1}^{\infty} \frac{W g dy}{y(e^y - 1)} = \frac{\alpha_c(T_e) T_e^{3/2} N_1}{G_{T_e} K N_e}. \quad (123)$$

When there is no external radiation $W=0$, $\mathcal{H}=1$, and the ionization equation is

$$\frac{N_1}{N_e} = \frac{3 \cdot 26 \times 10^{-6} G_{T_e}}{\alpha_c(T_e) T_e^{3/2}}. \quad (124)$$

Application of this formula shows that at 10,000° K. the nebula would be only about 1% ionized, at 20,000° K. about 95% ionized, and virtually completely ionized at 40,000° K.

When there is no collisional ionization, $\mathcal{H}=0$, and equation (50) holds. Since the radiative and collisional processes proceed independently, it is not difficult to understand how the resultant value of b_n may be found by a straightforward combination of the results for the two extremes. If N_1 and b_1 are eliminated from equation (123) with the aid of equation (11), we find

$$\begin{aligned} \frac{1 - \mathcal{H}}{\mathcal{H}} &= \frac{(2\pi m k)^{3/2} K}{N_e \alpha_c(T_e) h^3} \int_{y_1}^{\infty} \frac{W g dy}{y(e^y - 1)} \\ &\sim \frac{(2\pi m k)^{3/2} K}{h^3} \frac{W E_1(y)}{N_e \alpha_c(T_e)}. \end{aligned} \quad (125)$$

For a given set of values of T_1 , T_e , and N_e we may assume a series of values of \mathcal{H} and calculate the corresponding values of W from equation (125). If the assumption of an optically thin shell is retained, the geometrical dilution factor is simply $W=R^2/4r^2$. Thus for each value of \mathcal{H} , the corresponding value of r may be found. Since the b_n 's may be computed from equation (122) as soon as \mathcal{H} is known, the Balmer decrement may be calculated as a function of r .

In an extended nebulous region whose state of ionization and electron temperature was the result of the dissipation of mechanical energy or the relic of some previous excitation stage, the collisional decrement would prevail except in the immediate neighbourhood of exciting stars where the radiative decrement might hold.

Chamberlain made detailed applications to the Network nebula. Although it now appears that this particular nebula is more probably excited by radiation than by electron collisions, this analysis may be applied to other objects where the temperature of the electron gas may be high. The relative importance of collisional and radiative excitation

depends on the electron density and temperature, on the density of neutral hydrogen atoms, and on the dilution of the radiation. For any given situation it is necessary, therefore, to know the electron temperature, the dilution of the radiation, and the density. When these factors are given, the relative importance of the two contributions to the line excitation may be worked out. We can make some rough estimates for a representative planetary. As an example, consider a nebula similar to IC 418 for which we tentatively adopt the following values: $T_1=30,000^\circ\text{K.}$, $R=3R_1$, $N_e\sim 15\times 10^3$ electrons/cm.³, radius of shell $=1.6\times 10^{17}$ cm. If $T_e=20,000^\circ\text{K.}$, $\alpha_e=5.4\times 10^{-12}$, and from equation (125) we find $\mathcal{H}\sim 0.03$. With the aid of equation (122) and Tables IV : 1 and 9 we readily verify that the Balmer decrement will differ from that of the purely radiative model by an amount that is too small to detect. At lower temperatures the deviations will be even smaller. If T_e were as high as $30,000^\circ\text{K.}$ and $N_e\sim 3\times 10^4$, \mathcal{H} would be about 0.5, and deviations from the radiative decrement would begin to be important. In a thick nebular shell where W could become very small because of the influence of the $e^{-\tau}$ factor near the outer boundary, a zone in which collisional excitations become important might exist.

The cooling effect of the collisional excitation of the hydrogen lines might be estimated as a function of N_e and T_e . Even though only a small fraction of the actual intensities of the Balmer lines may represent collisional excitation, the dissipation of energy by this source is not negligible. Suppose that 2% of the atoms in the third level in hydrogen were excited by electron collision. Then 2% of the intensity of $H\alpha$ is to be attributed to collisions. On the other hand, the relative amount of energy liberated in $H\alpha$ and $Ly\beta$ will be in the proportion $A(H\alpha)\nu(H\alpha)/A(Ly\beta)\nu(Ly\beta)=0.14$. Therefore the actual amount of energy represented in collisional dissipation in the excitation of $H\alpha$ will be about 17% of the emission in $H\alpha$.

As we shall see in the next chapter, the electron temperatures of the planetaries fall between about 8000°K. and $20,000^\circ\text{K.}$ The dissipation of energy in the collisional excitation of the high hydrogen levels is probably not important in a typical planetary.

7. Transient Effects

So far we have treated the nebulae as in steady states, and this approximation probably holds for most planetaries and ordinary diffuse nebulae. For other objects such as the shells around novae and perhaps the radio sources, a steady state does not exist and recombination must be taken into account. No general solution of the problem can be given, and by way of illustration we shall treat as a very special example an ionized

filament of gas consisting of hydrogen with a trace of oxygen. We suppose that initially all the hydrogen was ionized and oxygen was ionized in the proportions N_1^0 , N_2^0 , and N_3^0 corresponding to O, O⁺, and O⁺⁺. The external source of excitation is suddenly cut off and the gas is allowed to recombine.

The electron density at any time will be controlled by the ionization of hydrogen. We can assume $N_e = N_i$, and shall suppose that T_e remains constant. Then

$$\frac{dN_e}{dt} = -\alpha_H N_e^2, \quad . \quad . \quad . \quad (126)$$

where the recombination coefficient α_H depends only on the electron temperature, T_e . Integrating this expression, we get

$$N_e = \frac{N_e^0}{1 + \alpha_H t N_e^0}, \quad . \quad . \quad . \quad (127)$$

where N_e^0 is the initial density of electrons (or hydrogen ions). The rate of depletion of O⁺⁺ ions by recombination will be

$$\frac{dN_3}{dt} = -\alpha_3 N_3 N_e, \quad . \quad . \quad . \quad (128)$$

where α_3 is the capture coefficient for electrons by O⁺⁺ ions.

$$N_3 = N_3^0 (1 + \alpha_H N_e^0 t)^{-(\alpha_3/\alpha_H)}. \quad . \quad . \quad (129)$$

The rate of change of the number of O⁺ ions will be given by

$$\frac{dN_2}{dt} = -\alpha_2 N_e N_2 + \alpha_3 N_e N_3. \quad . \quad . \quad (130)$$

This first order differential equation can be solved by conventional methods. We find

$$\begin{aligned} N_2 = & \left[N_2^0 - \frac{\alpha_3}{\alpha_2 - \alpha_3} N_3^0 \right] (1 + \alpha_H N_e^0 t)^{-(\alpha_2/\alpha_H)} \\ & + \frac{\alpha_3}{\alpha_2 - \alpha_3} N_3^0 [1 + \alpha_H N_e^0 t]^{-(\alpha_3/\alpha_H)}. \quad . \quad (131) \end{aligned}$$

Finally, the number of neutral oxygen atoms will increase at the rate

$$\frac{dN_1}{dt} = \alpha_2 N_e N_2. \quad . \quad . \quad (132)$$

Substitution from equations (127) and (131) yields

$$\begin{aligned} N_1 = & \left[\frac{\alpha_3}{\alpha_2 - \alpha_3} N_3^0 - N_2^0 \right] (1 + \alpha_H N_e^0 t)^{-(\alpha_1/\alpha_H)} \\ & - \frac{\alpha_2}{\alpha_2 - \alpha_3} N_3^0 (1 + \alpha_H N_e^0 t)^{-(\alpha_1/\alpha_H)} + N_1^0 + N_2^0 + N_3^0. \quad (133) \end{aligned}$$

The next step is the evaluation of the recombination coefficients. The rate of decrease of the number of ions, N_i , will be (cf. equation 67)

$$\frac{dN_i}{dt} = -N_i N_e \sum_j \int f(v) v \sigma_{\kappa j} dv, \quad (134)$$

where the recombination cross-section for level j is related to the absorption coefficient from the same level by equation (70). The absorption

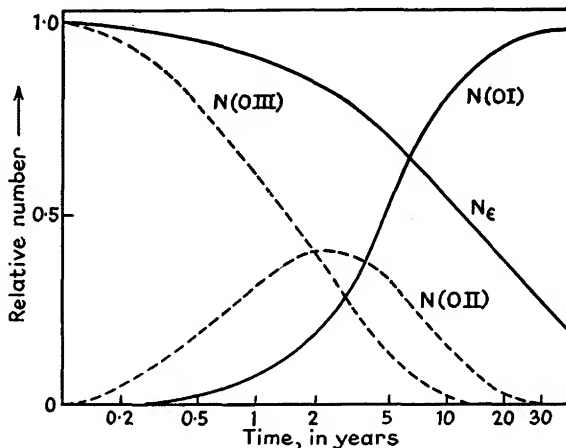


FIG. IV : 6. *Recombination of a Filament of Hot Gas.*

At $t=0$ it is assumed that all the hydrogen is ionized and oxygen is all doubly ionized as O^{++} . The numbers of ions or atoms are given in terms of the initial number of O^{++} ions and hydrogen ions. N_e^0 is taken as 10^4 electrons/cm.³, $T_e=20,000^\circ\text{K}$. and $N(O^{++}) \ll 10^4$.

coefficients for the ground-levels of O, O^+ , and O^{++} are given in Table IV:6. We may suppose that the higher levels are hydrogenic. For hydrogen itself we have simply

$$\alpha_H = \frac{KZ^4}{T_e^{3/2}} G_{T_e}. \quad (135)$$

If T is taken as $20,000^\circ\text{K}$., we find

$$\begin{aligned} \alpha_H &= 0.218 \times 10^{-7}, \\ \alpha_2 &= 0.955 \times 10^{-7}, \\ \alpha_3 &= 1.28 \times 10^{-7} \end{aligned}$$

if t is measured in days. As a numerical example, let us take a gaseous filament of density 10^4 atoms/cm.³ and suppose that initially $N_1^0 = N_2^0 = 0$. The change of concentrations of N_e , $N(O)$, $N(O^+)$, and $N(O^{++})$ with time (plotted on a logarithmic scale) is illustrated in Fig. 6. The expansion of the gas is neglected. If T_e increases, the rate of recombination will be cut down.

Grottrian gave a very interesting interpretation of the deep minimum in the light curve of DQ Herculis in terms of transient phenomena.⁽⁴⁴⁾

Exact quantitative treatments of non-equilibrium situations are extremely difficult, especially since the motions of gases in the diffuse nebulae (and possibly in the planetaries as well) may be complicated by magnetic fields.

REFERENCES

- (1) *Harvard Circular*, No. 335 (1928).
- (2) *M.N.R.A.S.*, **90**, 588 (1930).
- (3) *M.N.R.A.S.*, **92**, 820 (1932); **96**, 771 (1936).
- (4) *Ap. J.*, **86**, 70 (1937); **88**, 52 (1938).
- (5) *M.N.R.A.S.*, **96**, 77 (1935).
- (6) BOHM, DAVID, and ALLER, L. H., *Ap. J.*, **105**, 131 (1947).
- (7) See MENZEL, D. H., *Ap. J.*, **85**, 330 (1937). The value of K given in this paper I of the nebular series contains an error which is corrected in later papers of the series.
- (8) See, for example, *Astrophysics, The Atmospheres of the Sun and Stars*, by ALLER, L. H. (Ronald Press Co., New York, 1953), Chapter 5. Hereafter simply abbreviated as *Astrophysics I*.
- (9) See the discussion by JOHNSON, M. C., in *Observatory*, **73**, 91 (1953).
- (10) *Ap. J.*, **88**, 423 (1938).
- (11) *Pulkowa Obs. Circular*, **11**, 8 (1934).
- (12) *M.N.R.A.S.*, **96**, 980 (1936).
- (13) *Lick Obs. Bull.*, **18**, 57 (1937), No. 486.
- (14) *Ap. J.*, **113**, 25 (1951).
- (15) *Zeits. f. Ap.*, **1**, 98 (1930).
- (16) *M.N.R.A.S.*, **93**, 50 (1932); *Pulk. Bull.*, **13**, 3, 1933.
- (17) *Zeits. f. Ap.*, **9**, 266 (1935).
- (18) ALLER, L. H., BAKER, JAMES G., and MENZEL, D. H., *Ap. J.*, **90**, 601 (1939).
- (19) *Ap. J.*, **94**, 30 (1941).
- (20) *Ap. J.*, **108**, 243 (1948).
- (21) *Ap. J.*, **89**, 526 (1939).
- (22) *M.N.R.A.S.*, **106**, 423, 432 (1946).
- (23) *M.N.R.A.S.*, **109**, 698 (1950).
- (24) *Ap. J.*, **102**, 223 (1945).
- (25) *Ap. J.*, **108**, 354 (1948).
- (26) See GOLDBERG, L., *Ap. J.*, **90**, 414 (1939).
- (27) *Phys. Rev.*, **42**, 33 (1932).
- (28) *Phys. Rev.*, **57**, 36 (1930).
- (29) *Phys. Rev.*, **42**, 632 (1932).
- (30) *Ap. J.*, **96**, 78 (1942).
- (31) *Comptes Rendu*, **238**, 1099 (1954).
- (32) *Ap. J.*, **93**, 236 (1941).
- (33) *Ann. d'Phys.*, **9**, 273 (1931).
- (34) *Ap. J.*, **114**, 407 (1951).
- (35) *Ap. J.*, **91**, 215 (1940).
- (36) *Physik der Sternatmosphären* (Springer, Berlin 1938), p. 121.
- (37) *Astrophysics I*, p. 182.
- (38) *M.N.R.A.S.*, **106**, 159 (1946).
- (39) *Jap. Mem. Col. Sci.*, **21**, 173 (1938); *Contri. Inst. Ap. Kyoto*, Imperial Univ., No. 2.
- (40) *Ap. J.*, **108**, 142 (1948); **109**, 480 (1949).
- (41) *Ap. J.*, **117**, 387 (1953).
- (42) Thesis, London University (1949). See also BATES, FUNDAMINSKY, LEECH, and MASSEY, *Phil. Trans. Roy. Soc.*, A, **243**, 93 (1950), No. 860.
- (43) MOTT, N. F., and MASSEY, H. S. W., *Theory of Atomic Collisions* (Oxford University Press, London, 1950), p. 226.
- (44) *Zeits. f. Ap.*, **13**, 215 (1937).

CHAPTER V

The Forbidden Lines

1. Identification and Experimental Production of Forbidden Lines

In Chapter III we mentioned that in the gaseous nebulae the strongest lines were frequently the forbidden ones of light atoms in various stages of ionization. This chapter will be devoted to a more detailed discussion of this type of transition.⁽¹⁾

First let us consider the identifications of forbidden lines. Very few such lines can be observed in the laboratory. They are predicted from the energy differences between the metastable levels of the ground configuration. These levels are found from a detailed term analysis, often requiring a knowledge of intercombination lines which are weak and difficult to establish in light atoms.*

Among highly ionized atoms the term analyses are often incomplete and the metastable levels cannot be found directly.⁽²⁾ Under these circumstances an extrapolation procedure which is well illustrated by Edlén and Swings's identification of the $\lambda 3346$ and $\lambda 3426$ lines of the p^2 configuration of [NeV] is sometimes useful. These lines were identified independently by I. S. Bowen. First we write down the wave numbers of the nebular type transitions for the ions of the $2p^2$ electronic sequence, CI, NII, OIII, FIV (columns 2 and 3). The difference between columns 2 and 3 gives us the energy difference between 3P_2 and 3P_1 in wave number units (column 4).

Ion	$^3P_2-^1D_2$	$^3P_1-^1D_2$	$\Delta\tilde{\nu}$	$\sqrt{\Delta\tilde{\nu}}$	$^1D_2-^1S_0$	$^3P_1-^1S_0$
CI	10150 5034	10178	27.5	2.290 0.721	11455 5916	21632
NII	15184 4780	15267	82.2	3.011 0.718	17371 5542	32638
OIII	19964	20158	193.4	3.729 0.707	22913 5390	—
FIV	24624 4580	25011	387	4.436 0.702	28303 (5320)	—
NeV	(29204)	(29900)	(696)	(5.37)	(33623)	—

* Furthermore, the positions of the low-lying metastable levels are inferred from spectra lines in the far ultra-violet. An error in frequency units may be fairly large and the resultant $\delta\lambda$ may be of the order of several Angstroms. For example, if we use lines in the neighbourhood of 330 Å. to establish the position of a metastable term, an error of 0.01 Å. gives an error in the term value of $\Delta\tilde{\nu} = \delta\lambda/\lambda^2 = 0.01/(330)^2 = 9 \text{ cm.}^{-1}$. At $\lambda 4500$, the error would amount to two Angstrom units.

Experimental studies of isoelectronic sequences show that the fourth root of the term splitting varies nearly linearly with Z (column 5) at least for small Z . Hence we can predict the wave number separations $\Delta\tilde{\nu} \sim 696$ for the nebular lines of $[\text{NeV}]$ with some confidence, even though the positions of the lines, estimated at $\tilde{\nu} = 29204$ and 29900 are somewhat uncertain. Before the identification can be considered as satisfactory, the difference between the estimated and observed wavelength must be smaller than the limits allowable in the interpolation or extrapolation, and the separations of the lines in wave number units must agree with the predicted values. The intensity ratio must be the same in each object and approximately equal to that predicted by theory. Finally, if we are concerned with forbidden lines in planetary nebulae, the sizes of the images obtained on slitless spectrograms must be the same for both lines. The wavelengths predicted by this method are in satisfactory agreement with observed values. The measured separation between the lines in wave number units is in excellent agreement with theoretical predictions.

Transition	Pred. λ	Obsd. λ	$\tilde{\nu}$	$\Delta\tilde{\nu}$ obsd.
$^3P_2-^1D_2$	3424.2	3425.8	39190	697
$^3P_1-^1D_2$	3344.5	3345.9	29887	

In many nebulae the $[\text{NeV}]$ images are confused with certain ultra-violet $O\text{III}$ lines, so that intensity estimates cannot be made. If we exclude the objects with strong $O\text{III}$ lines we find the following intensity ratios from observations obtained at the Lick Observatory:

Nebula	$I(3426)/I(3346)$	
NGC 7027	2.1	Theoretical ratio = 2.6
NGC 2022	2.6	
Anon 21 ^h 31 ^m	3.2	
NGC 2440	2.4	

In view of the uncertainty of the observations, the agreement can be regarded as satisfactory.

For the production of the forbidden lines of $O\text{I}$ in the laboratory, McLennan, McLeod, and McQuarrie⁽³⁾ found that the best procedure was to use a heavy discharge either in pure oxygen at about 2 mm. pressure in a rather large tube—or in a trace of oxygen in an atmosphere of helium or argon. The latter technique yielded the larger intensity, presumably because $O\text{I}$ atoms in metastable levels cannot be de-excited by collisions with atoms of the noble gases. The energy levels of the noble gases are

all very high (10–20 e.v.), whereas the 1S level of OI has an excitation potential of 5.3 e.v. Atoms then tend to accumulate in the metastable levels from which they can escape only by radiative transitions to lower levels. Diffusion to the walls with consequent destruction of the metastable levels by collision is inhibited by the presence of the noble gas. In the pure oxygen discharge super-elastic collisions must be very effective in de-exciting the atoms so that the population of the 1S and 1D levels would be governed by the electron temperature in the tube. The total emission depends on the total number of radiating atoms in the available volume. That is, the emission per unit volume is

$$E = NAh\nu,$$

where N is the number of atoms in the upper level. If the density is low, the emission per unit volume is likewise small and the intensity will become too small to be observed. The rare gas mixture has the advantage of a low rate of de-excitation, but the pure oxygen has the advantage that the total number of OI atoms is very much larger.

Niewodniczanski⁽⁴⁾ used a high-frequency oscillator and external electrodes to excite forbidden lines of gases placed in a quartz tube. To obtain the spectrum of singly ionized atoms, e.g. $HgII$, a hollow cathode discharge tube (which gives a rapid voltage drop along the tube) yields better results.

Prokofjew,⁽⁵⁾ by means of an anomalous dispersion method, measured the relative f -values of the first member of the forbidden s^2S-d^2D and the first member of the permitted s^2S-p^2P doublets in the alkalis, Na, K, and Rb, and found the ratios to vary between 1×10^{-6} and 3×10^{-6} in good agreement with the predictions by A. F. Stevenson.⁽⁶⁾

Certain types of forbidden transitions, e.g. in helium, are produced under the influence of external electric fields. Such transitions, while of importance in stellar atmospheres, are not of significance in gaseous nebulae, and we shall not discuss them here.

Improvements in experimental techniques and excitation conditions may improve the laboratory studies of forbidden transitions. The study of forbidden lines in the highly ionized atoms of astrophysical interest, e.g. $NeIII$, $OIII$, etc., cannot be undertaken in the laboratory. It is impossible to produce sufficient numbers of ions in the requisite metastable levels to build up the intensities of the forbidden lines to observable values.

2. Dipole and Quadrupole Radiation

The spectral lines ordinarily met in physical experiments or solar and stellar observations are of the electric dipole type, i.e. their polarization properties, etc., resemble that of a dipole antenna. Forbidden lines on the other hand, correspond to *electric quadrupole* or *magnetic dipole*

radiation in classical radiation theory.⁽⁷⁾ We recall here very briefly those portions of the theory useful for our purposes.⁽⁸⁾

Maxwell's equations of the electromagnetic field express the fundamental relations between charges and currents on the one hand and electric and magnetic fields on the other. They include Coulomb's law, the law of electromagnetic induction, the continuity of magnetic lines of force, and Ampère's law generalized for the displacement current. A solution of these equations for the specified initial distribution of charges and their motions gives the values of \mathbf{E} and \mathbf{H} for the surrounding regions of space as well as in the immediate neighbourhood of the charges.

If a sphere is drawn, including all charges and currents, the integration of the *Poynting vector*,

$$\mathbf{N} = \frac{c}{4\pi} (\mathbf{E} \times \mathbf{H}), \quad . \quad . \quad . \quad (1)$$

over the entire surface of a sphere will give the total amount of energy radiated by the system of charges.

In many problems it is expedient to employ the so-called *vector* and *scalar potentials* \mathbf{A} and φ which are defined in terms of charge density ϱ and current density $\varrho\mathbf{v}/c$ as follows

$$\mathbf{A} = \int \frac{[\varrho\mathbf{v}]}{Rc} d\tau, \quad \varphi = \frac{1}{\epsilon} \int \frac{[\varrho]}{R} d\tau, \quad . \quad . \quad . \quad (2)$$

where R is the distance from the element of current or charge, $d\tau$ is the element of volume, ϵ is the dielectric constant, and the square brackets mean that the retarded potential is to be computed, i.e. \mathbf{A} and φ are to be calculated with ϱ and $\varrho\mathbf{v}$ values valid for the time $(t - R/c)$. We express charges in electrostatic units and currents in electromagnetic units. The electric and magnetic fields \mathbf{E} and \mathbf{H} are related to φ and \mathbf{A} by

$$\left. \begin{aligned} \mathbf{E} &= -\nabla\varphi - \frac{1}{c} \frac{\partial \mathbf{A}}{\partial t}, \\ \mathbf{H} &= \nabla \times \mathbf{A} = \text{curl } \mathbf{A}. \end{aligned} \right\} . \quad . \quad . \quad (3)$$

In electromagnetic units the magnetic moment of a closed circuit is $i\mathbf{a}$, where \mathbf{a} is the area of the circuit and i is the current. The current is given by $i = \varrho\mathbf{v}/c$, so that the magnetic moment becomes

$$\mathbf{M} = \frac{1}{2c} \int (\mathbf{r} \times \varrho\mathbf{v}) d\tau. \quad . \quad . \quad . \quad (4)$$

Now suppose that ϱ and $\varrho\mathbf{v}$ vary harmonically with the time, i.e.

$$\varrho = \varrho(x, y, z) \exp(2\pi i\nu t).$$

Then, with the aid of Maxwell's equations and the expression (3) for \mathbf{E} and \mathbf{H} we may calculate \mathbf{A} and φ . At large distances from the atom we find

$$\left. \begin{aligned} \varphi &= \frac{1}{r} \exp(2\pi i \nu t - ikr) [i \mathbf{k} \cdot \mathbf{D} - \frac{1}{2} k^2 \mathbf{i}_r \cdot \mathbf{Q} \cdot \mathbf{i}_r], \\ \mathbf{A} &= \frac{1}{r} \exp(2\pi i \nu t - ikr) [ik \mathbf{D} - i \mathbf{k} \mathbf{i}_r \times \mathbf{M} - \frac{k^2}{2} \mathbf{Q} \cdot \mathbf{i}_r] \end{aligned} \right\} \quad (5)$$

with $k = 2\pi\nu/c$, and

$$\mathbf{D} = \int \mathbf{e} r d\tau, \quad \mathbf{Q} = \int \mathbf{e} r r d\tau, \quad (6)$$

where \mathbf{i}_r is the unit vector in the direction of the radius r drawn from the origin, \mathbf{D} is the electric dipole moment (a vector), and \mathbf{Q} is the quadrupole moment (a dyad). We have neglected the terms $1/r^2$ as we are interested only in the electromagnetic waves at large distances from the atom, i.e. in the wave zone. The first term on the right-hand side of the expression for φ is the electric dipole term, and the second is the electric quadrupole term. The vector potential \mathbf{A} contains an electric dipole, a magnetic dipole, and an electric quadrupole term. From equations (3) and (1) we may calculate the Poynting vector for the three types of radiation. There results

$$\left. \begin{aligned} N_e &= \frac{1}{2} \frac{c}{4\pi} \frac{k^4}{r^2} [\mathbf{D} \cdot \mathbf{D} - (\mathbf{D} \cdot \mathbf{i}_r)^2] \mathbf{i}_r, \\ N_q &= \frac{ck^6}{32\pi r^2} [(\mathbf{Q} \cdot \mathbf{i}_r) \cdot (\mathbf{Q} \cdot \mathbf{i}_r) - (\mathbf{i}_r \cdot \mathbf{Q} \cdot \mathbf{i}_r)(\mathbf{i}_r \cdot \mathbf{Q} \cdot \mathbf{i}_r)] \mathbf{i}_r, \\ N_m &= \frac{c}{8\pi} \frac{k^4}{r^2} [\mathbf{M} \cdot \mathbf{M} - (\mathbf{M} \cdot \mathbf{i}_r)^2] \mathbf{i}_r, \end{aligned} \right\} \quad (7)$$

where N_e , N_q , and N_m refer respectively to the electric dipole, electric quadrupole, and magnetic dipole radiation fields.

That is, a system of moving electric charges emits not only electric dipole radiation but also magnetic dipole and electric quadrupole radiation. The terms corresponding to electric octopole and magnetic quadrupole radiation have been omitted as they are of no importance in optical spectroscopy. The report of Rubinowicz gives a good account of these radiations.

In applying these equations to the quantum theory we replace the classical definitions of \mathbf{D} , \mathbf{M} , and \mathbf{Q} given in equations (4) and (6) by the following

$$\begin{aligned} \mathbf{D} &= -e \sum_i \mathbf{r}_i, & \mathbf{Q} &= -e \sum_i \mathbf{r}_i \mathbf{r}_i, \\ \mathbf{M} &= \frac{-e}{2mc} \sum_i (\mathbf{L}_i + 2\mathbf{S}_i), \end{aligned} \quad (8)$$

where the summation is carried out over the electrons of the atom. The factor of (2) in the expression for M comes from the anomalous ratio of magnetic to mechanical moment for the electron spin. One may apply the correspondence principle to equations (7) to obtain the proper quantum mechanical expression (see Condon and Shortley, *Theory of Atomic Spectra*, p. 89 abbreviated as *TAS*). The rate of emission of energy over a sphere of large radius then will be

$$\begin{aligned} I_e &= \frac{64\pi^4\nu^4}{3c^3} \Sigma N(aJM)(aJM|\mathbf{D}|\alpha'J'M')^2 && \text{(electric dipole),} \\ I_m &= \frac{64\pi^4\nu^4}{3c^3} \Sigma N(aJM)(aJM|\mathbf{M}|\alpha'J'M')^2 && \text{(magnetic dipole),} \\ I_q &= \frac{32\pi^6\nu^6}{5c^5} \Sigma N(aJM)(aJM|\mathbf{Q}:\mathbf{Q}|\alpha'J'M')^2 && \text{(electric quadrupole).} \end{aligned} \quad (9)$$

Here $N(aJM)$ denotes the number of atoms in the upper state characterized by the quantum numbers $nLSJM$, which we abbreviate simply as aJM . The number of atoms in a given level, aJ , is $N(aJ) = (2J+1)N(aJM)$, assuming that $N(aJM)$ is independent of M . The matrix elements are defined by

$$\left. \begin{aligned} (aJM|\mathbf{D}|\alpha'J'M') &= e \int \psi(aJM)\mathbf{r}\psi(\alpha'J'M')d\tau, \\ (aJM|\mathbf{Q}|\alpha'J'M') &= e \int \psi(aJM)\mathbf{r}\mathbf{r}\psi(\alpha'J'M')d\tau, \\ (aJM|\mathbf{M}|\alpha'J'M') &= \frac{e}{2mc} \int \psi(aJM)(\mathbf{L}+2\mathbf{S})\psi(\alpha'J'M')d\tau, \end{aligned} \right\} \quad (10)$$

where the quantum number M denotes the M_J of the upper level of the transition, M' the M_J of the lower level. The summation is carried out over all Zeeman components comprising the transition $nLSJ-n'L'S'J'$. Following the terminology of Condon and Shortley, we define the sum of the squared matrix components occurring in equation (9) as the strength of the line,⁽⁹⁾ $S(aJ; \alpha'J')$. That is,

$$\left. \begin{aligned} S_e(aJ; \alpha'J') &= \sum_{M, M'} (aJM|\mathbf{D}|\alpha'J'M')^2, \\ S_m(aJ; \alpha'J') &= \sum_{M, M'} (aJM|\mathbf{M}|\alpha'J'M')^2, \\ S_q(aJ; \alpha'J') &= \sum_{M, M'} (aJM|\mathbf{Q}|\alpha'J'M')^2, \end{aligned} \right\} \quad (11)$$

where the summations are to be extended over all the $(2J+1)$ states of the upper level and the $(2J'+1)$ states of the lower level.

Since the intensity of a spectral line is given by

$$I(aJ; \alpha'J') = N(aJ)A(aJ; \alpha'J')h\nu, \quad (12)$$

the corresponding transition probabilities (*Einstein A coefficients*) are given by

$$A_e(aJ; a'J') = \frac{1}{2J+1} \frac{64\pi^4\nu^3}{3hc^3} S_e(aJ; a'J') \quad (13)$$

for electric dipole radiation,

$$A_m(aJ; a'J') = \frac{1}{2J+1} \frac{64\pi^4\nu^3}{3hc^3} S_m(aJ; a'J') \quad (14)$$

for magnetic dipole radiation, and

$$A_q(aJ; a'J') = \frac{1}{2J+1} \frac{32\pi^6\nu^5}{5hc^5} S_q(aJ; a'J') \quad (15)$$

for electric quadrupole radiation. The statistical weight of the upper level of the transition is $(2J+1)$.

If electric dipole radiation is permitted, the other types of transitions may be neglected. Only when the electric dipole component is missing do the other types of radiation become important.

Before calculating the transition probabilities by quantum mechanics we may find it worth while to discuss the order of magnitude of the transition probabilities to be expected and something about the selection rules. In making estimates of these quantities (and often other atomic quantities as well) it is expedient to make use of what are called *atomic units*⁽¹⁰⁾ instead of the usual anthropomorphic c.g.s. units. In this system the unit of length is the radius of the first Bohr orbit $a = 0.528 \times 10^{-8}$ cm., unit time τ is the interval required for an electron to go one radian in the first Bohr orbit, the unit of mass is the mass of the electron, and the unit of angular momentum is the quantum unit $\hbar = h/2\pi$.

First let us estimate the electric dipole transition probability for a line at $\lambda 5280$ whose wavelength is $10^4 a$ and whose wave number ν/c is consequently $10^{-4} a^{-1}$. The strength of the line will depend on whether the jump is between two nearby levels for which S is of the order of 1 or larger, or whether it is between a low and a high level. In the lower level the electron is close to the nucleus; in the higher level it moves in a remote orbit. In hydrogen, for example, the strengths of the individual transitions are

$$\begin{aligned} |(2p|\mathbf{D}|1s)|^2 &= 1.66, & |(3p|\mathbf{D}|1s)|^2 &= 0.267, \\ |(3p|\mathbf{D}|2s)|^2 &= 9.4, & |(4p|\mathbf{D}|1s)|^2 &= 0.093. \\ |(4p|\mathbf{D}|3s)|^2 &= 29.9, \end{aligned}$$

For our order of magnitude calculation let us take this dipole moment integral to be 1. Then A_e will be

$$\frac{64\pi^4\nu^3}{3hc^3} = \frac{32\pi^3}{3h/2\pi} \frac{1}{(10^4 a)^3} = \frac{32\pi^3}{3 \times 10^{12}} = 3.3 \times 10^{-10}$$

in atomic units. To get it in seconds we must multiply by $1/\tau$, where $\tau = 2.42 \times 10^{-17}$ sec. Thus

$$A_e \sim 1.4 \times 10^7 \text{ sec.},$$

which may be compared with the transition probabilities for the various components of $H\alpha$ which range from $0.1 \times 10^7 \text{ sec.}^{-1}$ to $1.6 \times 10^7 \text{ sec.}^{-1}$.

Now the ratio A_m/A_e depends on the size of $(aJM|M|a'J'M')^2$. Since

$$M = -\frac{e}{2mc} \Sigma(L_i + 2S_i),$$

and L and S are of the order of 1, A_m/A_e will be of the order of $1/c^2$, where $c=137$ in atomic units. Thus the magnetic dipole transition probability will be

$$\frac{1.4 \times 10^7}{(137)^2} \sim 1 \times 10^3 \text{ sec.}^{-1}.$$

We can estimate A_m in another way by noting that an electron moving in an orbit corresponds to a current ev/c which is $1/c$ in atomic units, since the electron velocity is unity as noted above. The size of the orbit is of the order of 1 atomic unit, so M (as defined via equation (4) and the corresponding quantum mechanical expression) will be $\sim 1/c$ atomic units.

Similarly we may calculate A_q/A_e . Taking the strengths again equal to 1, we find

$$\frac{A_q}{A_e} = \frac{32}{5} \frac{3}{64} \pi^2 \frac{\nu^2}{c^2} = 3 \times 10^{-8},$$

so that $A_q = 3 \times 10^{-8} A_e = 0.4 \text{ sec.}^{-1}$. In the X-ray region ν/c may be of the order of 1, and the quadrupole radiation could become much more important.

To summarize, we have the following estimates of relative and absolute transition probabilities for the single Zeeman components of lines.

	Electric Dipole	Magnetic Dipole	Electric Quadrupole
A/A_d	1	5×10^{-5}	3×10^{-8}
A	$1.4 \times 10^7 \text{ sec.}^{-1}$	10^3 sec.^{-1}	0.4 sec.^{-1}

In favourable circumstances where all the selection rules are obeyed, the transition probability will be higher than this because there will be several states to which jumps may take place. If the radial quantum integral is small, the lines will be weaker. Finally, due account must be taken of the ν^3 and ν^5 factors.

Thus the calculations of the A values reduces to the computation of the matrix elements given by equation (10).

3. Selection Rules

The symmetry properties (angular variations) of the wave functions are such that the matrix elements for electric dipole, magnetic dipole, and electric quadrupole radiation vanish unless rather restrictive conditions known as *selection rules* are satisfied. We summarize them in Table V : 1 to which we may append the following remarks.

The conditions imposed on the parity, which is odd if the sum of the l -values of the individual electrons is odd and even otherwise, are rigorous. Electric dipole transitions cannot occur between two levels of the same configuration, whereas electric quadrupole transitions may occur between two levels of the same configuration. In any instance where the configuration assignment is exact, the configurations between which the transitions take place cannot differ in the quantum numbers of more than one electron. The selection rules on J and M are rigorous except for perturbations produced by hyperfine structure.

TABLE V : 1
Selection Rules

Electric Dipole Radiation	Magnetic Dipole Radiation	Electric Quadrupole Radiation
Parity (determined by odd or even Σl)		
must change* (even - odd)	cannot change even - even odd - odd	cannot change even - even odd - odd
Configuration		
$\Delta n = \text{arbitrary}$ $\Delta l = \pm 1$	$\Delta n = 0^\dagger$ $\Delta l = 0$	$\Delta n = \text{arbitrary}$ $\Delta l = 0, \pm 2$
Inner Quantum Number J		
$\Delta J = \pm 1, 0^*$ $0 \rightarrow 0$ is not allowed	$\pm 1, 0$ $0 \rightarrow 0$ is not allowed	$0, \pm 1, \pm 2$ $(0 \rightarrow 0, \frac{1}{2} \leftarrow \frac{1}{2}, 1 \leftarrow 0$ are not allowed)
Magnetic Quantum number M		
$\Delta M = \pm 1, 0$	$\pm 1, 0$	$0, \pm 1, \pm 2$

* This rule is broken down under the influence of an electric field (i.e. in the Stark effect).

† This is equivalent to the statement that in magnetic dipole radiation, only transitions between terms of the same configuration occur.

In strict LS coupling, intersystem combinations are forbidden for all types of radiation (i.e. the spin quantum number, S , does not change). In electric dipole radiation $\Delta L=0, \pm 1$, and for electric quadrupole radiation $\Delta L=0, \pm 1, \pm 2$ except that the jump $0 \rightarrow 0$ does not occur. For pure LS coupling no magnetic dipole transitions are allowed except between two levels of the same term, e.g. ${}^3P_2-{}^3P_1$. Such transitions are of interest in connexion with the line spectrum of the corona. The green nebular lines $\lambda 4959$ and $\lambda 5007$ of $[OIII]$ represent magnetic dipole transitions between the 1D_2 and 3P terms. They occur only because of deviations from strict LS coupling, and we shall see in Section 4 that their strengths depend on a parameter χ which is essentially a measure of the departure from LS coupling.

4. An Illustrative Quantum Mechanical Calculation of the Strength of a Forbidden Line

The actual calculation of the line strengths given in equation (11) must be accomplished by quantum mechanics. For purposes of illustration, we may briefly review the calculation of the strengths of certain forbidden lines in $[OIII]$.

This section is intended accordingly for the reader who has some acquaintance with quantum mechanics and may be skipped without impairing the understanding of the remainder of this book.

The wave functions required for the calculation of the integrals (10) must be found from the solution of the wave equation for complex atoms:⁽¹¹⁾

$$H\psi = W\psi, \quad . \quad . \quad . \quad . \quad (16)$$

where

$$H = - \sum_i \left\{ \frac{\hbar^2}{8\pi^2m} \nabla^2 + \frac{Ze^2}{r_i} \right\} + \sum_{ij}' \frac{e^2}{r_{ij}} + \sum_i \xi(r) \mathbf{L} \cdot \mathbf{S}. \quad (17)$$

In this equation the term in $\{\}$ arises from the momentum of the electron and the Coulomb attraction of the nucleus of charge Z . The term in r_{ij} comes from the mutual electrostatic repulsion of the electrons while the LS term is magnetic in character; it arises from spin-orbit interaction. Here

$$\xi(r) = \frac{1}{2m^2c^2} \left(\frac{1}{r} \frac{\partial V}{\partial r} \right),$$

where V denotes the potential of the field in which the electron moves. The summation is carried out from $i=1$ to N . This wave equation is not separable and we cannot neglect the r_{ij} term even in the first approximation.

Slater⁽¹²⁾ suggested that for many purposes one could suppose that the cloud of electrons was more or less spherically distributed in a shell of some radius r_0 and acted to screen the nucleus. Hence when the electron was well outside the radius r_0 it moved in the field of a charge $Z-(N-1)$, while well inside r_0 it moved in the field of a charge Z . Slater supposed therefore that one could adopt as the first approximation a model in which each electron moved in a field of potential $U(r_i)$. The equation for the zero-order wave function becomes

$$-\sum_{i=1}^N \left[\frac{h^2}{8\pi^2m} \nabla^2 \psi_0 + U(r_i) \right] \psi_0 = W_0 \psi_0. \quad (18)$$

If we let $W_0 = \sum W_i$, we get N separate equations for N electrons, viz.

$$-\frac{h^2}{8\pi^2m} \frac{1}{\psi_i} \nabla^2 \psi_i + U(r_i) = W_i \quad i=1, \dots, N, \quad (19)$$

which may be solved to give zero-order wave functions which have hydrogen-like angular variables and non-hydrogenic radial functions. Hence

$$\psi_i = R(nl) \Theta_{lm_i} \Phi_{m_i} \Sigma_{m_s}, \quad (20)$$

where Σ_{m_s} represents the electron spin function $+1/2$ or $-1/2$. Here $n l m_l m_s$ are the usual zero-order quantum numbers. That is, n and l have their usual significance and m_l and m_s are the projections of the l and s vector on a magnetic field so strong as to break down the usual coupling to form M_L , M_s , or M_J . In the approximation to which we are working these zero-order wave functions all have the same energy which depends only upon the configuration nl , so that all the levels of the same configuration have the same energy.

The correct zero-order wave function of the atom is an antisymmetric sum of the products of the individual wave functions, i.e.

$$\psi_0 = \frac{1}{\sqrt{N!}} \begin{vmatrix} u_1(n^1 l^1 m_s^1 m_l^1) & u_2(n^1 l^1 m_s^1 m_l^1) & \dots \\ u_1(n^2 l^2 m_s^2 m_l^2) & \dots & \dots \\ \dots & \dots & \dots \\ u_1(n^N l^N m_s^N m_l^N) & \dots & \dots \end{vmatrix}, \quad (21)$$

where the u 's refer to wave functions and the $n^1 l^1 m_s^1 m_l^1$, etc., to the sets of quantum numbers. The subscripts of the u 's refer to the electrons. Such a determinantal form ensures consistency with the Pauli exclusion principle, since the interchange of two rows (or columns) changes the sign of the result.

Slater next calculated the perturbations due to the *electrostatic interaction* of the electrons, from integrals of the form

$$H_{gf} = \int \psi_g \frac{e^2}{r_{ij}} \psi_f d\tau,$$

and showed that this electrostatic interaction removed the degeneracy of the nl configuration, and resulted in the separation of the various terms. The splitting of the individual terms into the various J levels arises from spin-orbit interaction, i.e. the LS term in the Hamiltonian. If the electrostatic interactions are much more important than the *spin-orbit interaction*, the atom approaches LS coupling; if the opposite is true the atom approaches jj coupling.

Thus far we have spoken of the individual basic wave functions as expressed in the $nlm_s m_l$ representation (the individual wave functions are hydrogen-like except for the radial factor). When the $m_s m_l$ values of the individual electrons are given, we can calculate $M_L = \sum m_l$ and $M_S = \sum m_s$, and express the wave functions of the configuration in the $M_L M_S$ scheme. Finally, we can transform from a wave function with one set of $M_L M_S$ values to a wave function with another set of $M_L M_S$ values by means of the angular momentum operators.⁽¹³⁾

$$\begin{aligned} \mathcal{L} &= (L_x \pm iL_y) \psi_{FLM_L} = \sqrt{(L \mp M_L)(L \pm M_L + 1)} \psi_{FLM_L \pm 1}, \\ \mathcal{S} &= (S_x \pm iS_y) \psi_{FSM_S} = (\sqrt{S \mp M_S})(S \pm M_S + 1) \psi_{FSM_S \pm 1}, \quad (22) \\ \mathcal{J} &= (J_x \pm iJ_y) \psi_{FJM_J} = \sqrt{(J \mp M_J)(J \pm M_J + 1)} \psi_{FJM_J \pm 1}, \\ \mathcal{L}_Z &= M_L \psi_{FLM_L}, \quad \mathcal{S}_Z = M_S \psi_{FSM_S}, \quad \mathcal{J}_Z = M_J \psi_{FJM_J}. \end{aligned}$$

Our symbolism means that the operator $L_x + iL_y$ acting upon the wave function ψ_{FLM_L} will change it to the wave function ψ_{FLM_L+1} multiplied by the factor $\sqrt{(L - M_L)(L + M_L + 1)}$, and \mathcal{L}_Z acting upon this function will simply multiply it by M_L . It is clear that if we know ψ_{FSM_L} for any M_L we may find any other M_L by the application of these operators. To obtain the angular momenta in c.g.s. units multiply the right-hand side of eqn. (22) by \hbar .

We shall explain the use of these operators in the setting up of wave functions in the $nlSLM_L M_S$ scheme for the p^2 configuration. Our first task is to write down the possible combinations of m_s and m_l which the *Pauli Exclusion Principle* allows. Taking the $m_s m_l$ values in pairs with no two $m_s m_l$ values equal, we see that there are fifteen possibilities. Since the projection of the spin quantum number S on the magnetic field is either $+\frac{1}{2}$ or $-\frac{1}{2}$ we may denote it as $+$ or $-$.⁽¹⁴⁾ Thus $1+0^-$ means that for the first electron $m_l = +1$, $m_s = +\frac{1}{2}$, and for the second electron $m_l = 0$, $m_s = -\frac{1}{2}$. Each of these $(m_s m_l)$ pairs will correspond to a definite wave

function and we shall denote the functions in this scheme by letters of the Roman alphabet. Thus

		M_L	M_S	M_J	level	J	M_J	
$1+1-$	A	2	0	2	3P_2	2	2	α
$1+0+$	B	1	1	2	—	1		β
$1+0-$	C	1	0	1	—	0		γ
$1+-1+$	D	0	1	1	—	-1		δ
$1+-1-$	E	0	0	0	—	-2		ϵ
$1-0+$	F	1	0	1	3P_1	1	1	ζ
$1-0-$	G	1	-1	0	—	0		η
$1--1+$	H	0	0	0	—	-1		θ
$1--1-$	I	0	-1	-1	3P_0	0	0	ι
$0+0-$	J	0	0	0	1D_2	2	2	κ
$0+-1+$	K	-1	+1	0	—	1		λ
$0+-1-$	L	-1	0	-1	—	0		μ
$0--1+$	M	-1	0	-1	—	-1		ν
$0--1-$	N	-1	-1	-2	—	-2		ξ
$-1+-1-$	P	-2	0	-2	1S_0	0	0	π

Successive columns give the $m_l m_s$ values for the two electrons (n is not specified and $l=1$ is the same for all electrons), the Roman letter denoting the wave function, and the values of M_L , M_S , and M_J . There are fifteen Zeeman states characterized by L , S , J , and M_J , and these are entered in the table on the right-hand side of the page. Each level of a term has $2J+1$ states. The columns give J , M_J , and the Greek letter designation of the wave functions in the JM_J scheme.

We can also arrange the various zero-order wave functions according to their $M_L M_S$ values in a box as follows:

			M_L			
	2	1	0	-1	-2	
		B	D	K		+1
A		C, F	E, H, J	M, L	P	0
		G	I	N		-1

M_S

We see that the states in the $M_L M_S$ scheme correspond to

$M_L=2, 1, 0, -1, -2$
 $M_L=1, 0, -1$
 $M_L=0$

and

$M_S=0 (^1D_2)$
 $M_S=1, 0, -1 (^3P)$
 $M_S=0 (^1S).$

Hence a p^2 configuration, as a consequence of the Pauli Exclusion Principle, gives a 3P , a 1D , and a 1S term.

The $B=1^+0^+$ entry must certainly belong to the 3P_2 level with $M_J=2$. Similarly the $A=1^+1^-$ entry must belong to the 1D_2 term with $M_J=2$. Therefore it follows that the α and κ state wave functions in the M_J scheme must be equivalent to the B and A wave functions in the $M_L M_S$ scheme, i.e.

$$\begin{aligned}\alpha(J, M_J) &= B(M_L, M_S), \\ \kappa(J, M_J) &= A(M_L, M_S).\end{aligned}\quad . \quad . \quad (23)$$

The functions in the other boxes must likewise be related to one another. For example, we can say that $C+F$ is some combination of λ , ζ , and β . These combinations may be found with the aid of the angular momentum operators that express wave functions in the JM_J scheme in terms of those of the $M_L M_S$ scheme.⁽¹⁵⁾

Consider the operational equation

$$\mathcal{J} = \mathcal{L} + \mathcal{S} = \Sigma \mathcal{L}_i + \Sigma \mathcal{S}_i, \quad . \quad . \quad (24)$$

where the operator \mathcal{J} is to be used in the J, M_J scheme and the operators \mathcal{L} and \mathcal{S} in the $M_L M_S$ scheme, while $\Sigma \mathcal{L}_i$ and $\Sigma \mathcal{S}_i$ would be used in the $m_s m_l$ scheme. We find that

$$\begin{aligned}\mathcal{J}(\kappa) &= \mathcal{J}(2, 2) = \sqrt{4 \cdot 1}(2, 1) = 2\lambda, \\ \mathcal{L}(A) &= \mathcal{L}(1^+1^-) = \sqrt{2}(0^+1^-) + \sqrt{2}(1^+0^-) \\ &= -\sqrt{2}F + \sqrt{2}C, \\ \mathcal{S}(A) &= \mathcal{S}(1^+1^-) = (1^-1^-) = 0,\end{aligned}$$

hence

$$\lambda = \frac{1}{\sqrt{2}}C - \frac{1}{\sqrt{2}}F,$$

i.e.

$$(^1D^1_2) = \frac{1}{\sqrt{2}}(1^+0^-) - \frac{1}{\sqrt{2}}(1^-0^+), \quad . \quad . \quad (25)$$

where the superscript (1) on the upper right-hand corner of $(^1D_2)$ denotes the substate $M_J=1$. Thus we can express our wave functions in the $n l J M_J$ scheme in terms of the zero-order wave functions, A, B, C , etc. In so far as the angular portions are concerned, the latter may be written down at once from the hydrogenic wave functions.

The spin-orbit interaction represented by the term $\Sigma \xi_i(\mathbf{L} \cdot \mathbf{S})$ in the Hamiltonian produces the deviation from strict LS coupling that makes possible magnetic dipole transitions such as $^3P-^1D$, $^4S-^2D$, etc. It is this interaction that splits the 3P term into a 3P_0 , a 3P_1 , and a 3P_2 level whose mutual separations, although much smaller than the $^3P-^1D$ separation, are not negligible.

States of the same J and M_J perturb each other. For example, in the p^2 configuration under discussion the 1S_0 and 3P_0 levels perturb one another, and the 3P_2 level perturbs the 1D_2 level. Under these circumstances we may no longer regard L and S as "good" quantum numbers since the strict Russell-Saunders coupling is no longer obeyed. In spite of the fact that we may no longer speak rigorously of the terms as 1S , 1D , and 3P , since the 1S_0 term has some of the properties of 3P_0 and 1D_2 takes on some of the character of 3P_2 , in ions such as *OIII* or *NeV* the perturbed 1S_0 term will lie so very close to the unperturbed, strictly LS 1S_0 term that we may designate it by $^1S'_0$. Consequently the perturbed wave functions ought to be expressible in terms of the unperturbed wave functions, viz.

$$\left. \begin{aligned} (^3P'_2) &= a(^3P_2) + b(^1D_2) = \mathcal{A}, \\ (^1D'_2) &= e(^3P_2) + f(^1D_2) = \mathcal{B}, \\ (^3P'_1) &= (^3P_1), \\ (^3P'_0) &= c(^3P_0) + d(^1S_0), \\ (^1S'_0) &= g(^1S_0) + h(^3P_0), \end{aligned} \right\} \quad . \quad . \quad (26)$$

where the prime denotes the perturbed set. The perturbed as well as the pure LS wave functions form a normalized orthogonal set, i.e.

$$\int \mathcal{A}^2 d\tau = \int \mathcal{B}^2 d\tau = 1, \quad \int \mathcal{A} \mathcal{B} d\tau = 0.$$

Hence

$$\left. \begin{aligned} (^3P'_2) &= a(^3P_2) + b(^1D_2) = \mathcal{A}, \\ (^1D'_2) &= -b(^3P_2) + a(^1D_2) = \mathcal{B}, \\ (^3P'_0) &= c(^3P_0) + d(^1S_0), \\ (^1S'_0) &= c(^1S_0) - d(^3P_0). \end{aligned} \right\} \quad . \quad . \quad (27)$$

In strict LS coupling $a=c=1$ and $b=d=0$, while a and c decrease and b and d increase as jj coupling is approached. The splitting of the individual terms due to spin-orbit interaction as compared with the electrostatic separation of the terms provides a measure of the deviation from LS coupling. Let the total perturbation in the original Hamiltonian be denoted by

$$H' = H_1 + H_2, \quad . \quad . \quad . \quad (28)$$

where H_1 includes all perturbation terms of an electrostatic character while

$$H_2 = \xi(r_1)(L_1 \cdot S_1) + \xi(r_2)(L_2 \cdot S_2) \quad . \quad . \quad (29)$$

is the spin-orbit perturbation. Strict LS coupling corresponds to taking $H_2=0$, whereas in jj coupling H_2 is large compared with H_1 . Now $(^3P_2)$ and $(^1D_2)$ are wave functions which were calculated with the electrostatic

perturbation H_1 taken into account. In the language of quantum mechanics we say they are "diagonal" in H_1 because an integral like

$$({}^3P_2|H_1|{}^1D_2)$$

vanishes. Similarly when we take the complete perturbation into account, \mathcal{A} and \mathcal{B} must be "diagonal" in H' , i.e.

$$(\mathcal{A}|H_1+H_2|\mathcal{B})=\int[a({}^3P_2)+b({}^1D_2)]|H_1+H_2|[-b({}^3P_2)+a({}^1D_2)]d\tau=0. \quad (30)$$

For an atom near LS coupling $a^2 \sim 1$ and $b^2 \ll ab$, so we may neglect the terms in b^2 . We obtain

$$b=a \frac{({}^3P_2|H_2|{}^1D_2)}{({}^1D_2|H'|{}^1D_2)-({}^3P_2|H'|{}^3P_2)}. \quad (31)$$

The quantity in the denominator is simply the difference in energy between the 1D_2 and 3P_2 levels. The matrix element $({}^3P_2|H_2|{}^1D_2)$ arises from the spin-orbit interaction between 1D_2 and 3P_2 . From Condon and Shortley's table,⁽¹⁶⁾ we find that for a p^2 configuration

$$({}^3P_2|H_2|{}^1D_2)=\frac{\sqrt{2}}{2}\zeta(np). \quad (32)$$

The integral

$$\zeta(np)=\hbar^2 \int_0^\infty R^2(np)\xi(r)dr \quad (33)$$

may be evaluated from the splitting of the terms.⁽¹⁷⁾ For example, in a p^2 configuration the separation between the 3P_1 and 3P_0 levels is $\zeta({}^3P)=\frac{1}{2}\zeta(np)$. Thus the ratio b/a may be found directly from the observed term splittings and separations. Condon and Shortley have calculated the matrix elements of spin-orbit interaction for a number of configurations in terms of $\zeta(nl)$,⁽¹⁶⁾ the spin-orbit parameter that can be found from the level separation in a given spectral term.

Thus we see that for any level, b depends on the ratio of the spin-orbit splitting to the electrostatic splitting. For p^2 and p^3 configurations one may express b as a function of the parameter $\chi=\zeta/5F_2$, where $\zeta(nl)$ depends on the spin orbit interaction and F_2 , called the *electrostatic interaction parameter*, is a measure of the electrostatic splitting. F_2 is defined in terms of the radial quantum integral which involves the radial wave functions, $R(nl)$. G. H. Shortley and H. A. Robinson⁽¹⁸⁾ have worked out the values of the parameters ζ_p , F_2 , and χ for the p^2 , p^3 , and p^4 configurations of various ions by fitting the observed energy levels and energy separations to theoretical curves. The ratio of any pair of intervals, e.g. $({}^3P_2-{}^3P_0)/({}^1S_0-{}^1D_2)$ should be fixed uniquely by χ . Let 3P_c denote the centre of gravity of the triplet term (each level is assigned a weight $2J+1$).

Robinson and Shortley determined the χ values for the ions belonging to p^2 configurations by calculating it from the experimental value of the ratio $(^3P_2-^3P_0)/(^1D-^3P_0)$. For very small values of χ

$$\frac{(^3P_2-^3P_0)}{(^1D-^3P_0)} = \frac{5}{4}\chi + (\text{terms in } \chi^2, \chi^3, \text{ etc.})$$

is the asymptotic form of the theoretical relation between this particular interval ratio and χ (see *TAS*, p. 274).

For example, for *OIII* we have the following data: $^3P_2-^3P_0=306.8 \text{ cm.}^{-1}$, $^1D_2-^3P_0=20,271 \text{ cm.}^{-1}$, and $^3P_0=208 \text{ cm.}^{-1}$. Hence, $\chi=0.0122$ in good agreement with Robinson and Shortley's 0.0120.

Various other interval ratios may be plotted as a function of χ (once χ has been determined from one of them) and compared with the theoretical predictions. The agreement is good and along an isoelectronic sequence the residuals are regular. Robinson and Shortley were able to predict new levels in *KIV* and *CaVII*. They also found that F_2 , $\sqrt{\zeta}$, and $\sqrt{\chi}$ vary linearly with Z along an isoelectronic sequence, except for the first few members thereof.

Let us illustrate the calculation of the magnetic dipole moment by working it out for the Zeeman component $^3P_2-^1D_2$. We have that

$$\begin{aligned} (^1D_2)' &= a(1+1-) + b(1+0+), \\ (^3P_2)' &= -b(1+1-) + a(1+0+), \end{aligned}$$

and we want to calculate the matrix element

$$[(^3P_2)'\mathbf{L}+2\mathbf{S}|(^1D_2)'] = [(^3P_2)'\mathbf{J}+\mathbf{S}|(^1D_2)'], \quad (34)$$

since

$$\mathbf{L}+2\mathbf{S}=\mathbf{L}+\mathbf{S}+\mathbf{S}=\mathbf{J}+\mathbf{S}.$$

Now

$$\int (^3P_2)'\mathbf{J} (^1D_2)' d\tau = 0, \quad (35)$$

because \mathbf{J} operating on $(^1D_2)'$ will yield a function of the form $c_1(^1D_2)'+c_2(^1D_2)''$, which is still orthogonal to $(^3P_2)'$ since all the wave functions in the primed scheme are mutually orthogonal. Therefore, the dipole moment will depend upon the spin angular momentum $\mathbf{S}=\mathbf{S}_1+\mathbf{S}_2$. With the aid of the spin momentum operator we obtain

$$\begin{aligned} \mathbf{S} (^1D_2)' &= \mathbf{S}[a(1+1-) + b(1+0+)] \\ &= [\tfrac{1}{2}b(\mathbf{i}+\mathbf{j})][(1-0+)+(1+0-)] + b\mathbf{k}(1+0+), \end{aligned} \quad (36)$$

and finally

$$ab\mathbf{k} \int (1+0+)(1+0+) d\tau^2 = (ab)\mathbf{k}.$$

We have also to calculate

$$\int (^3P_2)'\mathbf{S} (^1D_2)' d\tau_1 d\tau_2 \quad (37)$$

to obtain the other Zeeman component arising from the $^1D_2^2$ state. By the method used in deriving equation (25) noting that $(^3P_2^2)=(1+0^+)$ and applying equation (24) we find that

$$(^3P_2^1) = \frac{1}{\sqrt{2}} D + \frac{1}{2} F + \frac{1}{2} C = \frac{1}{\sqrt{2}} (1^+-1^+) + \frac{1}{2} (1^+0^+) + \frac{1}{2} (1^+0^-). \quad (38)$$

From equations (27), (36), and (37) we get

$$\int (^3P_2^1)' S(^1D_2^2)' d\tau_1 d\tau_2 = [\mathbf{i} + \mathbf{j}] \frac{1}{2} ab, \quad (39)$$

and the total strength of the two Zeeman components arising from the $^1D_2^2$ state depends on $[\frac{1}{2}(\mathbf{i} + \mathbf{j}) + \mathbf{k}]ab$, the scalar amplitude of which is $\sqrt{3/2}$. The strength of the Zeeman component, $3/2a^2b^2$, must be multiplied by the statistical weight of the 1D_2 levels 5, to give the strength of the $^1D_2-^3P_2$ transition (see *TAS*, p. 72, equation (1)). We obtain accordingly,

$$S_m(^1D_2', ^3P_2') = \frac{15}{2} a^2 b^2.$$

Similarly

$$S_m(^1D_2', ^3P_1') = \frac{5}{2} b^2, \quad (40)$$

as follows from the calculation of

$$\int (^3P_1^1)' S(^1D_2^2)' d\tau.$$

Now a and b and hence S_m depend on the parameter χ . For small values of χ Shortley and his associates have given the expansions^(19, 26)

$$\left. \begin{aligned} a &= 1 - \frac{25}{144} \chi^2 - \frac{125}{864} \chi^3 + \dots, \\ b &= \frac{5}{12} \sqrt{2} \chi \left(1 + \frac{5}{12} \chi - \frac{25}{72} \chi^2 + \dots \right) \end{aligned} \right\} \quad (41)$$

The corresponding strengths, expressed in atomic units $e^2 h^2 / 16 \pi^2 m^2 c^2$, are:

$$\left. \begin{aligned} S_m(^1D_2', ^3P_2') &= \frac{15}{2} a^2 b^2 = \frac{375}{144} \chi^2 \left(1 + \frac{5}{6} \chi - \frac{125}{144} \chi^2 + \dots \right), \\ S_m(^1D_2', ^3P_1') &= \frac{5}{2} b^2 = \frac{125}{144} \chi^2 \left(1 + \frac{5}{6} \chi - \frac{25}{48} \chi^2 + \dots \right). \end{aligned} \right\} \quad (42)$$

For large values of χ the magnetic dipole strengths have been calculated from exact formulae. Estimates of χ may be made from the data in term tables or taken from the paper of Shortley and Robinson.

For example, for *OIII* we may adopt $b=0.0074$ and $\chi=0.0120$. Then S_m may be calculated from equation (42) and A computed from

equation (14). The $^1D_2-^3P_2$ transition corresponds to the $\lambda 5007 N_1$ line; the $^1D_2-^3P_1$ transition to the $\lambda 4959 N_2$ line. We find

$$\begin{aligned} A(^1D_2-^3P_2) &= 0.016 \text{ sec.}^{-1}, \\ A(^1D_2-^3P_1) &= 0.0054 \text{ sec.}^{-1}, \end{aligned}$$

in good agreement with the calculations of Pasternack,⁽²⁰⁾ A more accurate computation due to Garstang⁽²¹⁾ gives A values of 0.021 and 0.0071, respectively.

One important difference between the electric dipole and magnetic dipole radiation is that since the latter depends only on the spin component and not at all on the spatial coordinates of the electron, integration over space can give a result other than zero only if the initial and final level of the transition belongs to the same configuration. Thus is proven the selection rule stated in Table V:1.

The calculation of the strengths of the electric quadrupole lines depends upon the evaluation of integrals of the type

$$\int \psi^*(nlm_l m_s) \mathbf{r} \mathbf{r} \psi(n'l' m_l' m_s') d\tau, \quad (43)$$

which reduces to expressions of the form

$$S_q(LJ; L'J') = C_q(LJ; L'J') s_q^2(np, np), \quad (44)$$

where $C_q(LJ; L'J')$ arises from the angular factors in the wave functions and depends numerically on the value of χ . For example, we obtain for the auroral transitions in the p^2 configuration

$$\begin{aligned} C_q(^1S_0'; ^1D_2') &= \frac{5}{3} (bd + 2ac)^2 \\ &= \frac{20}{3} \left(1 - \frac{7}{24} \chi^2 + \dots \right). \end{aligned} \quad (45)$$

The s_q factor depends on the radial quantum wave function, viz.

$$s_q = s_q(np, np) = \frac{2}{5} \epsilon \int_0^\infty r^2 R^2(np) dr, \quad (46)$$

which must be evaluated independently for each ion. Since s_q^2 enters in the strength, it is evident that a very accurate knowledge of $R(np)$ is required for an accurate transition probability. In atomic units, s_q is of order of magnitude unity.

As an example, let us calculate the transition probability for the $\lambda 4363 ^1S_0-^1D_2$ transition of [OIII]. The factor χ is 0.0120, so we may calculate $C_q(^1S_0', ^1D_2')$ at once, but we can obtain S_q only if we know s_q . For our

illustrative calculation let us use the analytic representation of the Hartree radial wave function, viz.

$$R(r) = r^2(ae^{-br} + ce^{-dr}), \quad (47)$$

where $R(r)$ is subject to the normalization condition

$$\int R^2 dr = 1. \quad (48)$$

Hebb and Menzel⁽²²⁾ give the following values for the empirical coefficients:

$$a = 10.415, \quad b = 3.604, \quad c = 4.520, \quad d = 2.014,$$

when r is measured in atomic units. Hence

$$s_q = \frac{2}{5} \int_0^\infty r^2 R^2(np) dr = 0.525. \quad (49)$$

Thus

$$s_q({}^1S_0', {}^1D_2') \sim \frac{20}{3} s_q^2 = 1.85,$$

and the quadrupole transition probability is $A_q({}^1S_0 {}^1D_2) = 1.97 \text{ sec.}^{-1}$. The magnetic dipole moment for this transition is zero.

The result differs from that of Pasternack, who finds $A_q = 2.8$, and lies closer to that of Garstang, who finds $s_q = 0.479$ and $A_q = 1.6$. The source of the discrepancy is to be found in the radial quantum integral s_q , which Pasternack evaluated with the aid of hydrogen-like wave functions with screening constants, σ_n , evaluated from the F_2 integrals of Slater. In this way an s_q value of 0.636 is obtained. The screened wave function approximation is often rather poor for ions of low ionization.

To summarize, the electrostatic interaction between electrons separates the terms of a given configuration, whereas the spin-orbit interaction produces a splitting of the terms and deviations from the idealized situation of LS coupling. The ratio of spin-orbit to electrostatic splitting is expressed by a parameter χ , in terms of which the strengths of magnetic dipole lines may be computed. Finally, if the radial wave function is known, the quadrupole strengths can also be calculated.

The method assumes, among other things, that the perturbations of the levels arises from interactions between those of the same configuration. It does not take into account perturbations arising from interactions between terms of different configurations. That such an effect may be serious can be seen from a comparison of the observed and theoretical ratios $({}^1S-{}^1D)/({}^1D-{}^3P)$ for p^2 and p^4 . The theoretical value is 1.50 and the observed values are 1.13 for CI and 1.14 for OI, NII, and OIII. These departures may arise from the action of the $2p3p$ configuration, which probably affects the ${}^1D_2-{}^1S_0$ interval.

5. Formulae and Tables of Forbidden Line Strengths and Transition Probabilities; Comparison between Theory and Observation

The Einstein probability coefficient of spontaneous emission for magnetic dipole radiation, equation (14), may be written as

$$A_m(LJ; L'J') = 35,320 \left(\frac{\nu}{R} \right)^3 \frac{S_m(LJ; L'J')}{2J+1} \text{ sec.}^{-1}, \quad (50)$$

where ν denotes the frequency of the radiation, R that of the Lyman limit, and $S_m(LJ; L'J')$ is the magnetic dipole strength expressed in atomic units, $\epsilon^2 h^2 / 16\pi^2 m^2 c^2$, as in equation (42).

The corresponding coefficient for electric quadrupole radiation is

$$A_q(LJ; L'J') = 2648 \left(\frac{\nu}{R} \right)^5 \frac{S_q(LJ; L'J')}{2J+1} \text{ sec.}^{-1}, \quad (51)$$

provided the quadrupole strength S_q is expressed in atomic units $\epsilon^2 a_0^4$ (where a_0 denotes the radius of the first Bohr orbit).

Transition probabilities for certain forbidden lines appearing in the spectra of gaseous nebulae were estimated by A. Rubinowicz⁽²³⁾ and by A. F. Stevenson,⁽²⁴⁾ but the first reliable computations were those by E. U. Condon.⁽²⁵⁾ Some years later, when the number of known forbidden lines had been greatly increased by the work of Bowen and Wyse on the planetary nebulae, Simon Pasternack⁽²⁰⁾ calculated an extensive list of transition probabilities for many lines of astrophysical interest. At about the same time Shortley, Baker, Menzel, and the writer⁽²⁶⁾ published tables giving the line strengths for p^2 , p^3 , and p^4 configurations as a function of the parameter χ which measures the deviation from LS coupling. With the χ values taken from the compilation by Shortley and Robinson⁽¹⁸⁾ the A values computed from the tables of Shortley and his associates are in good agreement with those of Pasternack for magnetic dipole radiation, although for electric quadrupole radiation frequent differences are found because of the various estimates of the radial quantum integral. The advantage of the $S(\chi)$ formulation was that it could be applied to lines of additional ions, e.g. those appearing in the corona, whose importance could not have been anticipated in 1939.

The calculations of both Pasternack and of Shortley and his colleagues were based on the theory of *intermediate coupling* in which the perturbation was that due to the spin interaction of an electron with its own orbit. The predicted intensity ratios of various forbidden lines in the p^2 and p^4 configurations have been compared with the observations, and generally a good agreement has been found to within the uncertainties in the photometry. For example, the intensity ratio of the 5007/4949 or N/N_2 lines of [OIII] is 2.93, according to the calculations of Garstang. Photo-electric

measures (cf. Chapter II) by Liller and the writer give 3.03 with a mean error of 0.11.

A special problem was presented, however, by the $\lambda 3726.16$ and $\lambda 3728.91$ lines of [OII] corresponding to the $4S_{3/2}-2D_{3/2}$ and $4S_{3/2}-2D_{5/2}$ transitions. This radiation is prominent in low excitation planetaries such as NGC 40, but particularly in the diffuse nebulae in our own and other galaxies. For example, the emission nebulosities in the Triangulum spiral show it to be stronger than the green [OIII] lines which are the strongest emissions in most planetaries. The extensive distribution of this emission throughout the gaseous nebulae and the gaseous component of the interstellar medium hints that information on the A values for these lines might aid the understanding of the physical conditions in the gas where it originates. Now the doublet splitting of the $2D$ and $2P$ terms of the ground p^3 configuration of [OII], viz. -21.0 and -1.5 cm. $^{-1}$, indicate that the configuration is very close to pure LS coupling. The infra-red auroral $2D-2P$ transition is permitted even for pure LS coupling for electric quadrupole and magnetic dipole radiations. Jumps from $2P$ or $2D$ to $4S$ can occur as deviations from LS coupling. Pasternack and Shortley and his colleagues derived strengths for $\lambda 3729$ and $\lambda 3726$ by taking into account the second-order spin-orbit interaction. Thus they found the theoretical intensity ratio $I(3729)/I(3726)$ to be 1.9 and 1.64, respectively. Menzel and the writer pointed out that this ratio was in serious contradiction to the observed value, which is in the neighbourhood of 0.49. Ufford, Van Vleck, and the writer⁽²⁷⁾ showed that most of the discrepancy could be removed if one included not only the second-order effect of spin-orbit interaction but also the first-order effect of spin-spin interaction and spin-other-orbit interaction. The last-mentioned magnetic interaction actually has little influence on the intensity ratio, but does contribute to the splitting of the doublet D and P terms which should vanish in the first approximation for a p^3 configuration since the shell is half complete. Thus in addition to the parameter ζ which is involved in ordinary spin-orbit interaction of equation (33), there is also a parameter

$$\eta = \left(\frac{eh}{4\pi mc} \right)^2 \int_0^\infty \int_0^{r_1} r_2^{-3} R_{2p}^2(r_2) R_{2p}^2(r_1) dr_1 dr_2, \quad (52)$$

which is numerically much smaller than ζ , but becomes important in p^3 configurations. When the ζ and η factors are evaluated from the wave functions derived from the self-consistent fields of Hartree and Black, the $I(3729)/I(3726)$ ratio is found to be 0.58. A discrepancy of about 20% yet remains, but this may be due to polarization and configuration interaction.

Ufford and Gilmour carried out similar calculations for the p^3 configuration of [NI],⁽²⁸⁾ while Garstang treated [SII] in which he found that in

contrast to [OII] and [NI] the intensity ratio $I(2D_{5/2}-4S_{3/2})/I(2D_{3/2}-4S_{3/2})$ did not depend critically upon η . By using Hartree wave functions computed with electron exchange taken into account Garstang found a ratio of 0.47 for $I(3729)/I(3726)$ in OII.⁽²⁹⁾

Garstang has also computed the energies and A values for the p^2 and p^4 configurations, including the spin-spin interaction. He finds substantial differences between his results and those of Pasternack, due partly to improved estimates of s_q and ζ , the introduction of the η integral, and the use of experimental DP and SP term separations rather than theoretical calculations. Table V : 2 gives the A values for a number of ions of astrophysical interest. It is based on the calculations of Garstang, D. Osterbrock,⁽³⁰⁾ Ali Naqvi, and of Pasternack.

The transition probabilities for forbidden lines are in a relatively satisfactory form for many lines of astrophysical interest. Unfortunately, the intensities of forbidden lines in stars and nebulae depend not only on the transition probabilities but also on the target areas for collisional excitation. The theory for the latter cannot yet be regarded as completely satisfactory.

6. Collisional Excitation of the Forbidden Lines

Let N_A denote the number of atoms/cm.³ in a level A and N_e the corresponding number of electrons. If the velocity distribution of the electrons is $f(v)$, where $f(v)$ is given by equation (68) (Chapter IV), the total number of collisional excitations/cm.³/sec. to a level B will be

$$\mathcal{F}_{AB} = N_A N_e \int_{v_0}^{\infty} \sigma_{AB} v f(v) dv, \quad (53)$$

where the cross-section for collisional excitation σ_{AB} may be written in the form

$$\sigma_{AB} = \frac{1}{2J_A + 1} \frac{h^2}{4\pi m^2} \frac{\Omega(A, B)}{v^2} = \frac{4.17}{2J_A + 1} \frac{\Omega(A, B)}{v^2} \text{ cm.}^2. \quad (54)$$

The target area parameter $\Omega(A, B)$ is calculated by quantum mechanics. If equation (54) is put in equation (53) the total number of collisional excitations/cm.³/sec. will be

$$\begin{aligned} \mathcal{F}_{AB} &= N_A N_e \frac{\Omega(A, B)}{2J_A + 1} \frac{h^2}{2\pi m^2} \left(\frac{m}{2\pi k T_e} \right)^{1/2} e^{-\chi_{AB}/kT_e} \\ &= 8.54 \times 10^{-6} \frac{N_A N_e}{\sqrt{T_e}} \frac{\Omega(A, B)}{2J_A + 1} e^{-\chi_{AB}/kT_e}. \end{aligned} \quad (55)$$

where the energy difference between levels, χ_{AB} , is related to the velocity v_0 by

$$\frac{1}{2} m v_0^2 = \chi_{AB}. \quad (56)$$

TABLE V : 2
Transition Probabilities of Forbidden Lines Observed in the Spectra of Gaseous Nebulae
($2p^n$ and $3p^n$ Configurations)

$2p^2$ Configuration⁽¹⁾

Transition	Type	CI	NII	OIII	FIV	NeV
$^1D_2-^1S_0$	<i>e</i>	λ8727·4 0·50	5754·8 1·08	4363·21 1·6	3532·2 2·1	2972 2·6
$^3P_2-^1S_0$	<i>e</i>	λ4627·3 0·0 ⁴ 19	3070·0 0·0 ³ 16	0·0 ³ 71	0·0023	0·0068
$^3P_1-^1S_0$	<i>m</i>	λ4621·5 0·0026	3063·0 0·034	0·23	1·1	4·2
$^3P_2-^1D_2$	<i>m</i> <i>e</i>	λ9849·5 0·00023 0·0 ⁵ 12	6583·4 0·0030 0·0 ⁵ 94	5006·84 0·021 0·0 ⁴ 41	4060·2 0·098 0·0 ³ 13	3425·9 0·38 0·0 ³ 39
$^3P_1-^1D_2$	<i>m</i> <i>e</i>	λ9823·4 0·0 ⁴ 78 0·0 ⁶ 17	6548·1 0·00103 0·0 ⁵ 14	4958·91 0·0071 0·0 ⁵ 62	3997·4 0·034 0·0 ⁴ 21	3345·8 0·14 0·0 ⁴ 62
$^3P_0-^1D_2$	<i>e</i>	λ9808·9 0·0 ⁷ 55	6527·4 0·0 ⁶ 42	4931·0 0·0 ⁵ 19	0·0 ⁵ 64	0·0 ⁴ 19

$2p^4$ Configuration⁽¹⁾

Transition	Type	OI	FII	NeIII	NaIV
$^1D_2-^1S_0$	<i>e</i>	5577·350 1·28	4157·5 2·1	3342·9 2·8	3·1 (2)
$^3P_2-^1S_0$	<i>e</i>	0·0 ³ 37	0·0016	0·0051	
$^3P_1-^1S_0$	<i>m</i>	2972·3 0·078	0·49	2·2	
$^3P_2-^1D_2$	<i>m</i> <i>e</i>	6300·23 0·0069 0·0 ⁴ 24	4789·5 0·044 0·0 ⁴ 96	3868·74 0·20 0·0 ³ 30	3319·3 (2) 0·619
$^3P_1-^1D_2$	<i>m</i> <i>e</i>	6363·88 0·0022 0·0 ⁵ 32	4869·3 0·0138 0·0 ⁴ 13	3967·51 0·060 0·0 ⁴ 38	3445·9 (2) 0·185
$^3P_0-^1D_2$		0·0 ⁵ 11	0·0 ⁵ 41	0·0 ⁴ 12	

$3p^2$ Configuration⁽²⁾

Transition	Type	SiI	PII	SIII	CIV	AV	KVI
$^1D_2-^1S_0$	<i>e</i>	10991.52 2.1	7869.5 2.9	6312.1 3.6	5323.3 4.2	4625.5 4.8	4097 8.1 ⁽⁴⁾
$^3P_2-^1S_0$	<i>e</i>	6589.74 0.0030	4736.6 0.0099	3796.7 0.024	3203.2 0.055	0.10	0.30 ⁽⁴⁾
$^3P_1-^1S_0$	<i>m</i>	6526.85 0.0358	4669.5 0.223	3721.8 0.842	3118.3 2.56	6.76	
$^3P_2-^1D_2$	<i>m</i>	0.00273	11898.2 0.0169	9532.1 0.0642	8045.6 0.197	7005.7 0.519	6229.2 1.20
$^3P_1-^1D_2$	<i>m</i> <i>e</i>	0.000978	11483.2 0.00627	9069.4 0.0249	7530.5 0.0802	6435.10 0.224	5603.2 0.553

 $2p^3$ Configuration⁽²⁾

Transition	Type	NI	OII	FIII	NeIV	NaV
$^2P_{3/2}-^2D_{5/2}$	<i>m</i> <i>e</i>	10395.4 0.03558 0.081	7319.9 0.00500 0.14	5721.1 0.0281 0.15	4714.2 0.119 0.19	4011.2 0.406 0.24
$^2P_{3/2}-^2D_{3/2}$	<i>m</i> <i>e</i>	10404.1 0.03999 0.035	7330.7 0.00885 0.058	5733.0 0.0494 0.064	4724.2 0.211 0.082	4015.3 0.722 0.10
$^2P_{1/2}-^2D_{3/2}$	<i>m</i> <i>e</i>	10404.1 0.03620 0.070	7329.9 0.00553 0.12	0.0309 0.13	4725.6 0.132 0.16	4021.6 0.448 0.20
$^2P_{1/2}-^2D_{5/2}$	<i>e</i>	10395.4 0.047	7318.6 0.078	0.087	4715.6 0.11	4017.5 0.13
$^2D_{5/2}-^4S_{3/2}$	<i>m</i> <i>e</i>	5200.4 ⁽³⁾ 0.05104 0.0586	3728.91 ⁽³⁾ 0.05445 0.0441	0.04108 0.00012		
$^2D_{3/2}-^4S_{3/2}$	<i>m</i> <i>e</i>	5197.9 ⁽³⁾ 0.04245 0.0556	3726.16 ⁽³⁾ 0.03200 0.0427	0.00134 0.0477		
$^2P_{3/2}-^4S_{3/2}$	<i>m</i>	3466.4 0.00537				
$^2P_{1/2}-^4S_{3/2}$	<i>m</i>	0.00214				

$3p^4$ Configuration⁽²⁾

Transition	Type	SI	C/II	AIII	KIV	CaV	ScVI	TiVII
$^1D_2-^1S_0$	<i>e</i>	7724.7 2.6 (2); 4.1 (4)	6152.9 3.4 (2); 5.2 (4)	5191.4 3.9 (2); 6.2 (4)	4510.9 4.5 (2); 7.0 (4)	3996.3 5.1	3590.8 5.6	3263.1 6.2
$^3P_2-^1S_0$	<i>e</i>	4506.9 0.011 (2); 0.015 (4)	3583.0 0.028 (2); 0.044 (4)	3005.1 0.057 (2); 0.090 (4)	0.11 (2); 0.17 (4)			
$^3P_1-^1S_0$	<i>m</i>	4589.0 0.334 (2); 0.34 (4)	3675.0 1.28 1.3 (4)	3109.0 3.84 (2); 3.2 (4)	9.85			
$^3P_2-^1D_2$	<i>m</i>	10819.8 0.0276	8579.5 0.106	7135.8 0.321	6101.8 0.835	5309.2 1.94	4672.2 4.25	4144.8 8.42
$^3P_1-^1D_2$	<i>m</i>	11305.8 0.00806	9125.8 0.0294	7751.0 0.0838	6794.8 0.202	6086.9 0.432	5539.6 0.859	5104.5 1.52

 $3p^3$ Configuration⁽⁵⁾

Transition	Type	PI	SII	C/III	AIV	KV	CaVI
$^2P_{3/2}-^2D_{5/2}$	<i>m</i> <i>e</i>	0.017 0.30	0.057 0.38	8481.6 0.16 0.48	7237.3 0.42 0.57	6316.6 0.98 0.67	5587.2 2.1 0.78
$^2P_{3/2}-^2D_{3/2}$	<i>m</i> <i>e</i>	0.031 0.13	0.10 0.17	8433.7 0.29 0.21	7170.6 0.76 0.25	6223.4 1.8 0.29	5460.0 3.9 0.35
$^2P_{1/2}-^2D_{3/2}$	<i>m</i> <i>e</i>	0.019 0.25	0.062 0.33	8501.8 0.18 0.41	7262.8 0.46 0.48	6349.5 1.1 0.56	5631.0 2.3 0.64
$^2P_{1/2}-^2D_{5/2}$	<i>e</i>	0.17	0.22	8550.5 0.27	7332.0 0.31	6446.5 0.35	5766.4 0.39
$^2D_{5/2}-^4S_{3/2}$	<i>m</i> <i>e</i>	8787.6 0.0561 0.0358	6716.4 (3) 0.0428 0.0011	5517.7 0.0313 0.0021	4711.3 0.0354 0.0041	4122.6 0.0020 0.0055	0.0066 0.013
$^2D_{3/2}-^4S_{3/2}$	<i>m</i> <i>e</i>	8799.1 0.0328 0.0337	6730.8 (3) 0.0013 0.0367	5537.6 0.0058 0.0014	4740.2 0.024 0.0026	4163.3 0.088 0.0046	0.28 0.0081
$^2P_{3/2}-^4S_{3/2}$	<i>m</i> <i>e</i>	5332.4 0.099 0.0315	4068.6 0.32 0.0339	3342.7 0.90 0.0413	2.3 0.0439	5.4 0.0311	12 0.0329
$^2P_{1/2}-^4S_{3/2}$	<i>m</i> <i>e</i>	5339.7 0.040 0.0410	4076.4 0.13 0.0427	3353.4 0.37 0.0486	0.95	2.2	4.8

TABLE V : 2—REFERENCES

- (1) GARSTANG, R. H., *M.N.R.A.S.*, **111**, 115, 1951.
 (2) NAQVI, ALI M., *Thesis*, Harvard University (1951).
 (3) GARSTANG, R. H., *Ap. J.*, **115**, 506 (1952). Calculated A -values (taking into account electron exchange) with the following results:

	NI	OII	SII
$A(2D_{5/2}-4S_{3/2})$	6.95×10^{-6}	4.08×10^{-5}	6.31×10^{-4}
$A(2D_{3/2}-4S_{3/2})$	16.25×10^{-6}	13.15×10^{-5}	17.36×10^{-4}

- (4) OSTERBROCK, DONALD, *Ap. J.*, **114**, 469 (1951).
 (5) PASTERNAK, S., *Ap. J.*, **92**, 149 (1940).

The wavelengths of the forbidden lines are taken from Charlotte M. Sitterly's revised multiplet table *Princeton Observatory Contr.*, No. 20, 1945, and from I. S. Bowen, *Ap. J.*, **121**, 306 (1955).

Similarly the number of collisional de-excitations will be given by

$$\mathcal{F}_{BA} = 8.54 \times 10^{-6} \frac{N_B N_e}{\sqrt{T_e}} \frac{\Omega(A, B)}{2J_B + 1} \quad (57)$$

Notice that whereas only electrons with velocities greater than v_0 are capable of exciting the level B , this same level may be de-excited by electrons with any velocity whatever. Hebb and Menzel⁽²⁰⁾ calculated the target area parameters for the collisional excitation of [OIII]. Their results, as well as those obtained subsequently by Yamanouchi, Amemiya, and Inui for OI, by M. L. White and the writer for NII, and by the writer for OII were systematically too large.

The Ω 's obey a conservation theorem due to Mott, Bohr, Peierls, and Placzek⁽³¹⁾ which states that

$$\sum \frac{\Omega}{2J_A + 1} \leq (2l + 1), \quad (58)$$

where the summation is carried out over all levels of the ground configuration. $2J_A + 1$ is the statistical weight of the lower level from which collisional excitation takes place, and l is the azimuthal quantum number of the partial wave that contributes the largest share to the cross-section. This relation limits the "partial cross-sections", i.e. the contribution to the target area due to incident electrons of a particular quantum number, l . Thus the theorem is useful only when electrons of a special l value provide the major contribution to the cross-section. In exchange transitions only, one partial cross-section is appreciable and the theorem may be usefully applied. This type of transition is important for the excitation of the nebular lines since we are primarily concerned with excitation from a ground 3P or 4S term to a 1D or 1S or a 2D or 2P term.

More recently M. J. Seaton⁽³²⁾ has calculated target areas for the collisional excitation of the nebular lines by using explicitly anti-symmetric

wave functions of the Hartree-Fock type for continuous as well as for bound states. His target area parameters $\Omega(n, m)$ for various ions of astrophysical interest are given in Table V: 3. The ground (4S or 3P) term is denoted by "1", the middle metastable (2D or 1D) term by "2", and the highest metastable (2P or 1S) term is indicated by "3". Seaton estimates the absolute accuracy of the cross-sections to be of the order of $\pm 40\%$ for the entries for which detailed calculations were made. The relative accuracy of the cross-sections should be much better. The Ω 's vary less

TABLE V: 3

*Target Area Parameters for the Collisional Excitation
of Forbidden Lines**

2p ² Configuration				2p ³ Configuration			
Ion	$\Omega(1, 2)$	$\Omega(1, 3)$	$\Omega(2, 3)$	Ion	$\Omega(1, 2)$	$\Omega(1, 3)$	$\Omega(2, 3)$
NII	2.39	0.223	0.46	OII	1.44	0.218	1.92
OIII	1.73	0.195	0.61	FIII	1.00:	0.221:	3.11:
FIV	1.21:	0.172:	0.58:	NeIV	0.68:	0.234:	3.51:
NeV	0.84:	0.157:	0.53	NaV	0.43	0.255:	3.49:

2p ⁴ Configuration				3p ³ Configuration			
Ion	$\Omega(1, 2)$	$\Omega(1, 3)$	$\Omega(2, 3)$	Ion	$\Omega(1, 2)$	$\Omega(1, 3)$	$\Omega(2, 3)$
FII	0.95:	0.057:	0.17	SII	2.02	0.383	12.7
NeIII	0.76	0.077	0.27				
NaIV	0.61:	0.092:	0.30:				
MgV	0.54	0.112:	0.30:				

* SEATON, M. J., *Proc. Roy. Soc.*, **218**, 400 (1953). The less accurate values are denoted by the colon (:).

than about a per cent for the first few e.v.'s above the threshold. The $\Omega(2, 3)$'s are not small compared with $\Omega(1, 2)$ or $\Omega(1, 3)$. The Ω 's marked (:) were obtained by interpolation and are less accurate.

If the target areas are known, the relative intensities of the auroral and nebular transitions in ions like [OIII] or [NII] permit the estimations of electron temperatures. The rigorous formula for [OIII] was given by Menzel, Hebb, and the writer,⁽³³⁾ from a consideration of the statistical equilibrium of the 1S and 1D terms.

The 1D_2 level is populated by collisional excitations from the ground 3P term and by collisional and radiative de-excitations of the 1S term to the 1D term. Atoms escape from this level by the spontaneous emission of

the $^1D-^3P$ nebular transitions, by super-elastic collisions to the 3P term and by inelastic collisions to the 1S term. Thus, using the aforementioned notation of "1" for the 3P term, "2" for the 1D term, and "3" for the 1S term, the equation of statistical equilibrium is

$$\begin{aligned} N_1 C \frac{\Omega_{12}}{\varpi_1} e^{-x_{12}/kT_e} + N_3 C \frac{\Omega_{23}}{\varpi_3} + N_3 A_{23} \\ = N_2 C \frac{\Omega_{23}}{\varpi_2} e^{-x_{23}/kT_e} + N_2 C \frac{\Omega_{12}}{\varpi_2} + N_2 A_{21}. \end{aligned} \quad (59)$$

Similarly, the number of atoms entering the 1S level by collisions must equal the number leaving by collisions and radiative transitions

$$N_1 C \frac{\Omega_{13}}{\varpi_1} e^{-x_{13}/kT_e} + N_2 C \frac{\Omega_{23}}{\varpi_2} e^{-x_{23}/kT_e} = N_3 C \frac{\Omega_{23} + \Omega_{13}}{\varpi_3} + N_3 (A_{32} + A_{31}), \quad (60)$$

where

$$C = 8.54 \times 10^{-6} \frac{N_e}{\sqrt{T_e}}, \quad (61)$$

and $x_{23} = (x_3 - x_2)$ is the difference in excitation potential between the second and third level. From equations (59) and (60) we may calculate the relative populations of the 1S and 1D levels, viz.

$$\begin{aligned} \frac{N_3}{N_2} &= \frac{\varpi_3}{\varpi_2} e^{-x_{23}/kT_e} \frac{\left\{ 1 + \frac{\Omega_{23}}{\Omega_{12}} \frac{e^{-x_{23}/kT_e}}{(1 + \Omega_{23}/\Omega_{13})} + \frac{A_{21}\varpi_2}{C\Omega_{12}(1 + \Omega_{23}/\Omega_{13})} \right\}}{\left\{ 1 + \frac{(A_{32} + A_{31})\varpi_3}{\Omega_{13}C(1 + \Omega_{23}/\Omega_{13})} + \left[\Omega_{32} + \frac{A_{32}\varpi_3}{C} \right] \frac{e^{-x_{23}/kT_e}}{\Omega_{12}(1 + \Omega_{23}/\Omega_{13})} \right\}} \\ &= \frac{\varpi_3}{\varpi_2} e^{-x_{23}/kT_e} \left(\frac{b_3}{b_2} \right), \end{aligned} \quad (62)$$

where (b_3/b_2) measures the deviation from thermodynamic equilibrium at temperature T_e . As N_e increases, C increases and $b_3/b_2 \rightarrow 1$. Similarly we can write

$$\begin{aligned} \frac{N_2}{N_1} &= \frac{\varpi_2}{\varpi_1} e^{-x_{12}/kT_e} \frac{\left\{ \Omega_{12} + \Omega_{13} d e^{-x_{23}/kT_e} \right\}}{\left\{ \left(\Omega_{12} + A_{21} \frac{\varpi_2}{C} \right) + \Omega_{23} (1 - d) e^{-x_{23}/kT_e} \right\}} \\ &= \frac{\varpi_2}{\varpi_1} e^{-x_{12}/kT_e} \left(\frac{b_2}{b_1} \right), \end{aligned} \quad (63)$$

where

$$d = \frac{\Omega_{32} + \frac{A_{32}}{C} \varpi_3}{\Omega_{13} + \Omega_{23} + (A_{32} + A_{31}) \frac{\varpi_3}{C}}. \quad (64)$$

Finally,

$$\frac{b_3}{b_1} = \frac{\left\{ \Omega_{13} + \frac{\Omega_{12}}{p + e^{-x_{12}/kT_e}} \right\}}{\left\{ (\Omega_{23} + \Omega_{13}) + \frac{(A_{32} + A_{31})\varpi_3}{C} - \frac{\Omega_{23} + A_{32}\varpi_3/C}{1 + pe^{x_{12}/kT_e}} \right\}}, \quad (65)$$

where

$$p = \frac{\Omega_{12}}{\Omega_{23}} + \frac{A_{21}\varpi_2}{C\Omega_{23}}. \quad (66)$$

The equations (62)–(66) likewise hold for the p^3 configuration if “2” now refers to the $4S$ term, “2” to the $2D$ term, and “3” to the $2P$ term.

Let us consider first the ratio of the auroral and nebular line intensities.

$$\frac{I_a}{I_n} = \frac{N_3 A_{3,2} \nu_{3,2}}{N_2 A_{2,1} \nu_{2,1}} = \frac{\varpi_3 b_3 A_{3,2} \nu_{3,2}}{\varpi_2 b_2 A_{2,1} \nu_{2,1}} e^{-x_{12}/kT_e}. \quad (67)$$

Putting in the numerical data from Tables 2 and 3, and assuming T_e to lie in the neighbourhood of $10,000^\circ$ – $20,000^\circ$ K., we find the following approximate formula for [OIII] and [NII], viz.

$$[\text{OIII}]: \frac{I_{4363}}{I_{N_1+N_2}} = 13.1 \times 10^{-14,300/T_e} \left\{ \frac{1.012 + 2300 \sqrt{T_e}/N_e}{1.01 + 2.70 \times 10^5 \sqrt{T_e}/N_e} \right\} \quad (68)$$

$\sim 0.113 \times 10^{-14,300/T_e}$ for low densities,

$$[\text{NII}]: \frac{I_{5755}}{I_{6560}} = 61.5 \times 10^{-10,820/T_e} \left\{ \frac{1.01 + 320 \sqrt{T_e}/N_e}{1 + 1.94 \times 10^5 \sqrt{T_e}/N_e} \right\}. \quad (69)$$

The simultaneous solution of equations (68) and (69) permit a determination of T_e and N_e , provided the [NII] and [OIII] radiations both originate in the same parts of the nebula.

Some years ago M. L. White and the writer used this method to estimate N_e and T_e in typical planetaries.⁽³⁴⁾ The inaccuracies of the then available cross-sections did not permit accurate densities to be derived, although there was some suggestion of filamentary structure. More recently, Seaton⁽³⁵⁾ has employed similar considerations with his improved cross-sections, but conclusions concerning condensations drawn from forbidden line data must be regarded with caution until checked by independent evidence. Formulae similar to equations (68) and (69) may be derived for the [OII] and [SII] lines.

As an example, let us apply equations (68) and (69) to NGC 7027. We use intensity ratios adopted from the spectrophotometric studies of Minkowski and the writer, supplemented by the photo-electric measures.

The intensity ratios, corrected for the effects of space absorption as described in Section 7 are

$$\frac{I_{4363}}{I(N_1+N_2)} = 0.0155 \quad \text{and} \quad \frac{I_{5755}}{I_{6560}} = 0.056.$$

The simultaneous solution of these equations gives $T_e \sim 14,500^\circ\text{K.}$ and $N_e \sim 7.7 \times 10^4$ electrons/cm.³. On the other hand, if we employ only the [OIII] line data together with the surface brightness measured in $H\beta$ and corrected for the effect of space absorption and the assumed value of the parallax, N_e will be about 1.7×10^4 electrons/cm.³. A literal interpretation of this result would imply a considerable concentration of the material into filaments, a situation which is indeed possible in an object like NGC 7027.

The electron temperatures are usually derived from the ratio $I(4363)/I(N_1+N_2)$ which has been observed in many planetaries. The results for a number of typical bright planetaries have been given in column 8 of Table 7 of Chapter IV. Determinations of the electron temperature by independent methods is much to be desired.

7. The Determination of Ionic Concentrations from Line Intensities; Application to NGC 7027

If the relative emissions per unit volume are known for each of the observed nebular radiations, we may employ the considerations of this and the preceding chapter to determine the relative concentrations of the various ions. In most nebulae it is necessary to take into account the stratification. In NGC 7027 there appears to be no bona fide stratification, although the material may be concentrated in filaments. In a first approximation at least, we may set the relative emission per unit volume proportional to the tabulated intensity. We write

$$E_{JJ'} = N_J A_{JJ'} h\nu_{JJ'} = I_{JJ'} E_0, \quad (70)$$

where the upper and lower levels of the forbidden transition are denoted respectively as J and J' . Here E_0 is the constant of proportionality. Its numerical value will depend on the assumed parallax of the nebula, its surface brightness, and the extent to which the material is concentrated in individual filaments.

The number of ions N_1 in the ground term of any configuration that gives a forbidden line λ may be expressed as

$$\frac{N_1}{N_0} = \frac{I_\lambda}{I_0} \left(\frac{\lambda}{5000} \frac{5/9}{\varpi_l/\varpi_1} \frac{A_0}{A_\lambda} \right) 10^{(x_l - x_0)} \theta \frac{\eta_0}{\eta}, \quad (71)$$

where N_0 is the number of [OIII] atoms in the 3P term, $\theta = 5040/T_e$, I_0 is the intensity of the green nebular lines (mean wavelength ~ 5000 A.), $A_0 = 0.028$ is the Einstein A coefficient for the green nebular lines, $x_0 = 2.48$ e.v. is the excitation potential of the 1D_2 level, and $\eta_0 = b(^1D_2)/b(^3P)$

for [OIII]. Similarly, I_i is the intensity of the forbidden line of transition probability A_λ which arises from the level i , of statistical weight ϖ_i , for which $\eta = b_i/b_1$. The η 's are calculated from the data of Tables V: 2 and 3 with the aid of equations (63) and (65) once T_e and N_e are given.

We must now consider the recombination lines. Using equation (20), Chapter IV, with $n=4$, $n'=2$, and $g=0.822$, the emission in ergs/cm.³/sec. in $H\beta$ is

$$E_{H\beta} = 2.28 \times 10^{-19} \frac{N(H^+)N_e}{T_e^{3/2}} b_4(T_e) e^{x_1}. \quad (72)$$

Similarly, the emission in $\lambda 4686$ of $HeII$ is given by setting $Z=2$, $n=4$, and $n'=3$. Thus with $g=0.768$,

$$E_{4686} = 4.13 \times 10^{-18} \frac{N(He^{++})N_e}{T_e^{3/2}} b_4\left(\frac{T_e}{4}\right) e^{x_1}, \quad (73)$$

since the solution for the b_n 's for hydrogen at a temperature T_e is the solution for $HeII$ for the same value of

$$X_n = \frac{hRZ^2}{n^2kT_e} = \frac{hR}{n^2k(T_e/Z^2)}. \quad (74)$$

In other words, the solution for $HeII$ at 20,000° K. is equivalent to that for hydrogen at 5000° K.

The lines of the Pickering series may also be used by setting $n'=4$.

Let us now consider the lines of neutral helium. If we apply the combined Boltzmann and Saha equations, we find that the number of helium atoms in level j will be

$$N_j = b_j \frac{N(He^+)N_e}{T_e^{3/2}} \frac{h^3}{(2\pi mk)^{3/2}} \frac{\varpi_j}{4} e^{(I_0 - x_j)/kT_e}, \quad (75)$$

where ϖ_j and 2 are the statistical weight of the level j and of the He^+ ion, respectively, I_0 is the ionization potential of the helium atom, and x_j is the excitation potential of level j . Using equation (11), Chapter IV, for the population of the n th level in hydrogen, we find the ratio of the numbers of atoms in the upper levels j and n in helium and hydrogen, respectively, to be

$$\frac{N_j}{N_n} = \frac{b_j}{b_n} \frac{\varpi_j}{4n^2} \frac{N(He^+)}{N(H^+)} e^{(I_0/kT_e - x_n)}, \quad (76)$$

where $I_j = I_0 - x_j$. Let us suppose that we can compare the emission per unit volume E_{jj} in the helium transition ($j-j'$) with the emission per unit volume in $H\beta$, i.e. $E_{H\beta}$. Then

$$\frac{N_j}{N_4} = \frac{E(jj')}{E(H\beta)} \frac{A(H\beta)}{A(jj')} \frac{\lambda(jj')}{\lambda(H\beta)}, \quad (77)$$

whence the ratio of singly ionized helium to ionized hydrogen is

$$\frac{N(He^+)}{N(H^+)} = \frac{b_4}{b_j} \frac{4 \times 16 E(jj') A(H\beta) \lambda(jj')}{\varpi_j E(H\beta) A(jj') \lambda(H\beta)} \exp \left[X_n - \frac{I_j}{kT_e} \right]. \quad (78)$$

Goldberg has not only computed the A values for the principal lines of helium,⁽³⁶⁾ but has also investigated the b_j factors for helium atoms exposed to highly dilute temperature radiation.⁽³⁷⁾ He treated a somewhat simplified atom with the result that a single value of b_j is assigned to all the high triplet levels. Actually $b_j \rightarrow 1$ as $j \rightarrow \infty$.

For illustrative purposes let us apply these formulae to NGC 7027.⁽³⁸⁾ This object probably exhibits more lines than any other planetary nebula; on the other hand, it seems to be a somewhat atypical nebula. We shall base our discussion on line intensities measured photographically by Bowen, Minkowski, and the writer, supplemented by photo-electric measures of some of the brightest lines.

An examination of the hydrogen line intensities shows a very steep Balmer decrement suggestive of strong space absorption. On the assumption that the true Balmer decrement is given by Menzel and Baker's model B , and that the wavelength dependence of the absorption may be taken from the work of Whitford,⁽³⁹⁾ we can correct the measured line intensities for the interstellar extinction. It is found that the surface brightness in $H\beta$ (of Chapter IV) should be increased elevenfold so that with Berman's value of the parallax⁽⁴⁰⁾ N_e will be about 17,000 electrons/cm.³ if the nebula has an approximately constant density. From the relative intensities of the $\lambda 4363$ and $N_1 + N_2$ lines, we find T_e to be about 15,600° K.

If we assumed that the [NII] and [OIII] lines are formed in exactly the same strata, we saw that N_e would be about 7.7×10^4 and T_e would be depressed to about 14,500° K. A comparison of the intensities of the green nebular lines and $H\beta$ with the aid of equation (72) and the corresponding expression for $E(N_1 + N_2)$ then gives $N(\text{OIII}) = 14.3$. A comparison of the auroral ($\lambda \sim 7319$ Å.) and nebular transition ($\lambda 3727$) of [OII] suggests a somewhat lower density, whereas the [SII] transauroral and nebular line data indicates a much higher density. The conclusion to be drawn from these results is that either there is a pronounced concentration of the nebular material in individual knots or filaments with a low mean density in between, that the different ions are concentrated in different filaments, or that the target areas are subject to systematic errors. An overcorrection for space absorption would further complicate matters (p. 200). Most likely, NGC 7027 has a filamentary structure with possible differences in the proportions of the various ions. In other nebulae (cf. Chapters III and VII) different ions show very different concentrations. In IC 418, for example, the [NII] radiation occurs in an outer shell, whereas the [OIII] radiation tends to be concentrated closer to the nucleus—at least along the major axis. Estimates of the electron density may also be obtained from the doublet ratios of [OII] and [SII]. Some years ago Ufford, Van Vleck, and the writer noticed that the intensity ratio

$I(\lambda 3729)/I(3726)$ corresponding to $I(^2D_{5/2}-^4S)/I(^2D_{3/2}-^4S)$ in [OII] varied from one object to another in such a way as to suggest that the relative population of the $^2D_{5/2}$ and $^2D_{3/2}$ levels depended on the density. If the density is high, the populations must be in the ratio of the statistical weights, i.e. 6/4, but if it is low, radiative de-excitations are more important than collisional de-excitations so the ratio changes. Seaton has calculated the target area parameters for $\Omega(^2D_{5/2}-^2D_{3/2})$ in O^+ and S^+ and has derived formulae for estimating N_e from these forbidden line ratios.⁽⁴¹⁾

TABLE V : 4
Abundances of Ions in NGC 7027

Ion	Trans	$\bar{\lambda}$	A_n	χ	b_i/b_1	I_c	N_i
NII	N	6565	0.0040	1.88	0.40	124	0.900
	A	5755	1.08	4.03	0.0020	7.1	0.935
OII	N	3727	0.0*77	3.31	0.87	29	2.72
	A	7325	0.200	5.00	0.0065	22	0.97
OIII	N	5000	0.028	2.48	0.064	1850	14.3
FIV	N	4036	0.133	3.07	0.010	0.9	0.010
NeIII	N	3895	0.26	3.19	0.0032	124	6.7
NeIV	A	4724	0.534	7.38	0.00165	9.7	6.3
NeV	N	3400	0.52	3.70	0.00176	236	7.3
SII	N	6722	0.00107	1.84	0.400	4.7	0.063
SII	TA	4072	0.257	3.03	0.00132	12.0	0.53
SIII	A	6311	3.6	3.30	0.00056	6.8	0.58
CIII	N	5520	0.0042	3.69	0.1265	2.5	0.100
CHV	N	7840	0.277	1.60	0.0066	1.26	0.017
ClV	A	5322	4.2	3.92	0.00026	0.73	0.36
AlII	N	7360	0.404	1.68	0.00032	22	0.043
AlV	N	4720	0.0135	2.61	0.035	17	0.27
AlV	A	7250	1.75	4.31	0.00032	2.8	0.38
AV	N	6800	0.743	1.85	0.0017	6.5	0.134
KIV	N	6101	1.037	1.95	0.00090	1.2	0.007
KVI	N	6034	1.75	2.044	0.00048	<0.2	0.001
CaV	N	5000	2.37	2.22	0.00035	1.6	0.011

Since the electron density is found from the lines of a single ion, it will refer to the density in the filament or part of the nebula where the radiations of this particular ion predominate. From measures of the 3726/3729 [OII] ratio Osterbrock found N_e to vary from about 30,000 electrons/cm.³ in the brightest part of the Orion nebula to about 200 electrons/cm.³ in the fainter outer portions. The [SII] lines are useful at yet higher densities.

For the present let us estimate the ionic abundances assuming our space absorption correction is valid. Table V:4 gives the essential data. Successive columns give for each ion the character of the transition employed, nebular (N), auroral (A), or transauroral (TA), the mean wavelength of the forbidden line multiplet, the Einstein A coefficient, the excitation potential of the upper term of the multiplet, the factor (b_i/b_1),

the intensity of the whole forbidden multiplet (corrected for space absorption), and finally the relative number of ions, expressed approximately as numbers of ions/cm.³.

For the ions of chlorine, argon, potassium, and calcium it is necessary to estimate the cross-sections since no calculated values are available. Hence the concentrations estimated for these ions are to be regarded as rough estimates only. No emphasis can be placed on the discrepancies between the auroral and nebular line results for these ions. The discordances for [OII] and [SII] are probably to be attributed to differences in the densities of the filaments, and to the fact that different ions do not occur in different filaments in the same proportions.

The concentration of helium may be found by comparing the lines of *HeI* and *HeII* with *Hβ*. With the aid of equations (72) and (73) with $b_4 = 0.016$ for *HeII* at $T_e = 14,500$ together with the observed $I(4686)/I(H\beta)$ ratio, we find $H(He^{++})/N(H^+) = 0.066$. Similarly, if we apply equation (78) to the $\lambda 5876$, $\lambda 4471$, and $\lambda 4026$ *HeI* lines, and interpolate $b_j(HeI) = 0.50$ for all the high triplet levels, we find 0.029, 0.035, and 0.056 for the $N(He^+)/N(H^+)$ ratio. If a weighted mean value of 0.035 be adopted, the ratio of *He/H* by numbers of atoms is found to be 0.10, which is in good agreement with the value found some years ago by Menzel and the writer.

The determination of the actual abundances of the other elements whose ions are observed is a much more formidable task as allowance must be made for the distribution of ions among the various stages of ionization. The simplified ionization formula of Chapter IV cannot represent the observed distribution of the ions; hence, an empirical approach must be used.⁽⁴²⁾ One can compare the relative numbers of ions N_i/N_{i+1} as a function of ionization potential and draw a smooth empirical ionization curve. Such a curve is uncertain for two reasons. The ionic abundances themselves may be in error because of the limited accuracy of the observations and of the target areas. Furthermore, different ions may be concentrated in different proportions in different filaments or portions of the nebula. Finally, the assumption that the degree of ionization depends only on the ionization potential ignores the influence of strong bright lines in the far ultra-violet nebular spectrum. Thus the relative proportions of successive ions of a given element actually may be very different from what would be deduced from a smooth graph.

This step introduces greater uncertainties in the final result than does any other item! For some elements such as potassium and calcium the corrections for incompleteness in the observation of different stages of ionization are large; for others such as neon the corrections seem to be relatively small. The ratio of helium to hydrogen is extremely sensitive to the b factors and therefore to the electron temperature.

Table V : 5 compares the composition (numbers of atoms) of NGC 7027 with that of an average star. The stellar data are taken from the writer's recent compilation,⁽⁴³⁾ except that the helium abundance has been revised downward. The agreement for *H*, *He*, *N*, and *O* is good. Fluorine is uncertain in both the stars and nebulae. Neon comes out relatively less abundant, and sulphur more abundant than in the stars. Possibly differential concentrations in filaments may affect these elements, the target areas

TABLE V : 5

The composition of NGC 7027 compared with that of a normal star

Logarithm of Relative Numbers of Atoms		
Element	NGC 7027	Star
<i>H</i>	13.04	13.27
<i>He</i>	12.0	12.0
<i>N</i>	9.56	9.49
<i>O</i>	10.00	10.00
<i>F</i>	6.6:	7.7:
<i>Ne</i>	9.48	10.04
<i>S</i>	9.21	8.52
<i>Cl</i>	8.39	8.3
<i>A</i>	8.22	9.0:
<i>K</i>	6.2:	6.39
<i>Ca</i>	6.6:	7.72

may be in error, or most likely the distribution among various ionization stages may be very different from what has been assumed. The stellar values for chlorine and argon are uncertain. The nebular data for potassium and calcium are insecure; the abundance of calcium appears to have been under-estimated. One statement seems unassailable: composition differences between stars and nebulae will be difficult to establish.

Because of its great range in ionization and a possible extreme filamentary structure, perhaps NGC 7027 is not the best object for a detailed composition study. Other and probably more suitable objects include NGC 7662, NGC 6572, and NGC 1535. A realistic analysis of such nebulae requires that detailed attention be paid to their structural features. In Chapter VII we shall devote considerable attention to the structural features of the planetary nebulae.

REFERENCES

(1) For general reviews see:

BOWEN, I. S., *Rev. Mod. Phys.*, **8**, 55 (1936).

MROZOWSKI, S., *Rev. Mod. Phys.*, **16**, 153 (1944).

RUBINOWICZ, A., *Reports on Progress in Physics*, **12**, 233 (1949).

- (2) Identification of the coronal lines is discussed by EDLÉN, B., *Zeits. f. Ap.*, **22**, 30 (1942); see also *M.N.R.A.S.*, **105**, 323 (1945); *Ap. J.*, **98**, 116 (1943). EDLÉN, B., and SWINGS, P., *Comptes Rendu of Paris Academy*, **198**, 1748 (1934), and BOWEN, I. S., *P.A.S.P.*, **46**, 145 (1934), identified the [NeV] lines.
- (3) *Proc. Roy. Soc., A*, **114**, 1 (1927).
- (4) *Acta Physica Polonica*, **3**, 285 (1934).
- (5) *Zeits. f. Phys.*, **57**, 387 (1929).
- (6) *Proc. Roy. Soc., A*, **128**, 591 (1930).
- (7) For a very elementary account of these radiations, see, for example, the author's *Astrophysics—The Atmosphere of the Sun and Stars*, p. 115 (Ronald Press Company, New York, 1953). Hereafter simply referred to as *Astrophysics I*.
- (8) See CONDON, E. U., and SHORTLEY, G. H., *The Theory of Atomic Spectra* (Cambridge University Press, 1935), Chapter 4. Hereafter this work will be referred to as *TAS*. The radiation field of a dipole and the concepts of retarded potentials are discussed concisely in SLATER, J. C., and FRANK, N. H., *Introduction to Theoretical Physics* (McGraw-Hill Book Co., New York, 1933), pp. 286–305. See also MENZEL, D. H., *Mathematical Physics*, p. 329 (Prentice-Hall, New York, 1953) for a detailed development of the basic formulae for dipole and quadrupole radiation.
- (9) *TAS*, p. 98.
- (10) *TAS*, p. 428.
- (11) See, for example, *TAS*, p. 159, equation (2).
- (12) *Phys. Rev.*, **34**, 1293 (1929); *TAS*, Chapter 6.
- (13) *TAS*, p. 167.
- (14) This is the notation employed by Condon and Shortley, see *TAS*, p. 188–91.
- (15) This is the method of Gray and Wills, *Phys. Rev.*, **38**, 248 (1931).
- (16) *TAS*, p. 268.
- (17) *TAS*, p. 196.
- (18) *Phys. Rev.*, **52**, 713 (1937).
- (19) *Phys. Rev.*, **57**, 225 (1940).
- (20) *Ap. J.*, **92**, 129 (1940).
- (21) *M.N.R.A.S.*, **111**, 115 (1951).
- (22) *Ap. J.*, **92**, 408 (1940).
- (23) *Zeits. f. Phys.*, **65**, 662 (1930).
- (24) *Proc. Roy. Soc. A*, **137**, 298 (1932).
- (25) *Ap. J.*, **79**, 217 (1934).
- (26) *Ap. J.*, **93**, 178 (1941).
- (27) *Ap. J.*, **109**, 42 (1949).
- (28) *Ap. J.*, **111**, 580 (1950).
- (29) *Ap. J.*, **115**, 506 (1952).
- (30) *Ap. J.*, **114**, 469 (1951).
- (31) MOTT and MASSEY, *The Theory of Atomic Collisions* (2nd edition; Oxford, 1949).
- (32) *Proc. Roy. Soc., A*, **245**, 469 (1953); *Phil. Trans. Roy. Soc., A*, **218**, 400 (1953).
- (33) *Ap. J.*, **93**, 230 (1941).
- (34) *Astron. J.*, **54**, 181 (1949).
- (35) *M.N.R.A.S.*, **113**, 256 (1954).
- (36) *Ap. J.*, **90**, 414 (1939).
- (37) *Ap. J.*, **93**, 244 (1941).
- (38) Our procedure is very similar to that applied by Menzel and the writer in *Ap. J.*, **102**, 239 (1945).
- (39) *Ap. J.*, **107**, 102 (1948).
- (40) *Lick Obs. Bull.*, **18**, 57 (1937).
- (41) *Ann. d'Ap.*, **17**, 74 (1954).
- (42) See reference 38 especially Section V.
- (43) *Astrophysics I*, p. 327.

Note added in proof (Oct. 28, 1955).

The Paschen line intensities and the energy distribution in the continuum of NGC 7027 cannot be reconciled with the adopted space absorption. The true space absorption must be much less. The true Balmer decrement is therefore considerably steeper than Menzel and Baker's "case B". Collisional excitation must play an important role in the production of the hydrogen-line spectrum in the dense filaments of this object. (See R. Minkowski and L. H. Aller, *Ap. J.*, in press).

CHAPTER VI

The Stars that Illuminate the Gaseous Nebulae

1. Introduction

In preceding chapters we have seen that the nebulae derive all their energy from stars placed near or within them. In the diffuse reflection nebulae some of the light is simply scattered by small particles. The bright-line spectra, however, are produced by photo-ionization followed by recapture of electrons and by the dissipation of the energy of free electrons in the excitation of metastable levels. The ultimate controlling factor is the quantity and quality of the radiation emitted by the illuminating star. Many years ago Hubble noticed that diffuse nebulae illuminated by stars earlier in spectral class than about B2 showed spectra with emission lines, whereas nebulae illuminated by stars later than spectral class B2 yielded spectra that were simply reflections of the spectrum of the illuminating star.⁽¹⁾ At spectral class B2 the nebulae showed both emission and reflection types of spectra.

More recent work has demonstrated that this distinction is not entirely clear-cut. In Chapter III we mentioned the bright-line nebulosity surrounding the G dwarf star, T Tauri. The nebular variables provide a number of other exceptions.

The extended regions of low surface brightness and ionic density are presumably excited by the O stars in our galaxy, and fluorescence occurs whenever the necessary ultra-violet radiation can reach the atoms.

The outstanding difference between the O and B stars that excite the diffuse galactic nebulae and the central stars of the planetaries is primarily one of luminosity. The former have absolute visual magnitudes between -3 and -7 , whereas the absolute visual magnitudes of the planetary nuclei must be closer to 0 or -1 . The reason for the difference lies in the population types with which each is associated.

The Type I population which is characterized by the presence of dust and gas contains bright blue stars that fall in the upper left-hand corner of the Russell diagram. The main sequence extends from O and B through A down to the faint K and M dwarfs, and the upper part of the diagram contains a sprinkling of supergiants of all spectral classes. The Russell diagram for the Type II population is illustrated by the colour-magnitude

arrays for several globular clusters. The distribution of the stars is very different from that which obtains for the Type I population.⁽²⁾

The brightest stars in the globular cluster are red giants of absolute photo-visual magnitude about -3 . They form the upper end of a branch running to fainter, hotter stars as far as a colour index of 0.7 . Then the branch runs vertically on the colour-magnitude array to $M_v = +3$, turns again to higher surface temperatures and finally joins the main sequence. There is also a branch which separates from this main branch near $M_v = -1$ or 0 , and runs horizontally in the direction of higher surface temperatures. This branch is much more sparsely populated than the other, but it includes the cluster-type variables, better known as the RR Lyrae stars. Münch finds that the bluest stars of this branch often show peculiar spectral characteristics which differentiate them from Type I stars of the same colour or hydrogen line intensity.

Occasionally as in Messier-2, blue stars lie $1\frac{1}{2}$ – 2 magnitudes above the horizontal branch. In M15 a bona-fide planetary nebula appears. This object, in which the star appears to be brighter than the surrounding nebulosity, has been measured photo-electrically by Liller and the writer. Because of the crowding of the star field it will be necessary to combine these measures with photographic data to eliminate the effect of neighbouring stars. The upper limit to the brightness of the nebula is about $M_v = -2.1$.

2. The Magnitudes and Luminosities of the Central Stars of the Planetaries

Estimates of the absolute magnitudes of the planetary nuclei also can be made from their apparent magnitudes and distances as given, for example, by Berman.⁽³⁾ There are two difficulties—first in the measurement of the magnitudes of the central stars and second in the determination of the distances of the planetary.

The early estimates of the central star magnitudes by H. D. Curtis⁽⁴⁾ were not only affected by large accidental errors but gave the brighter stars as systematically too bright. Hubble,⁽⁵⁾ on the basis of pole-region comparisons of a number of planetary nuclei, reduced Curtis's measures to the usual magnitude scale. He found a systematic correction to be added to Curtis's apparent magnitude, m , viz. $\Delta = -0.173m + 3.37$. In his work on the planetaries A. van Maanen⁽⁶⁾ used the average relation between star count and magnitude for the galactic longitude and latitude of the field to estimate the magnitudes of the central stars. In fields where the number of stars is small, this method is likely to yield very misleading results, particularly for the brighter stars. Claude Anderson⁽⁷⁾ estimated the magnitudes of the nuclei of thirty-three planetaries by comparing the

images of the stars on his plates with a scale plate and finally reducing them to a standard exposure of Selected Area 61 for which the magnitudes were known. His magnitudes are only approximate, but may be good to the nearest half-magnitude except in instances where the nucleus is directly involved in the nebulosity. Berman⁽³⁾ has published a compilation of magnitudes of the planetary nuclei; some of the magnitudes are estimated

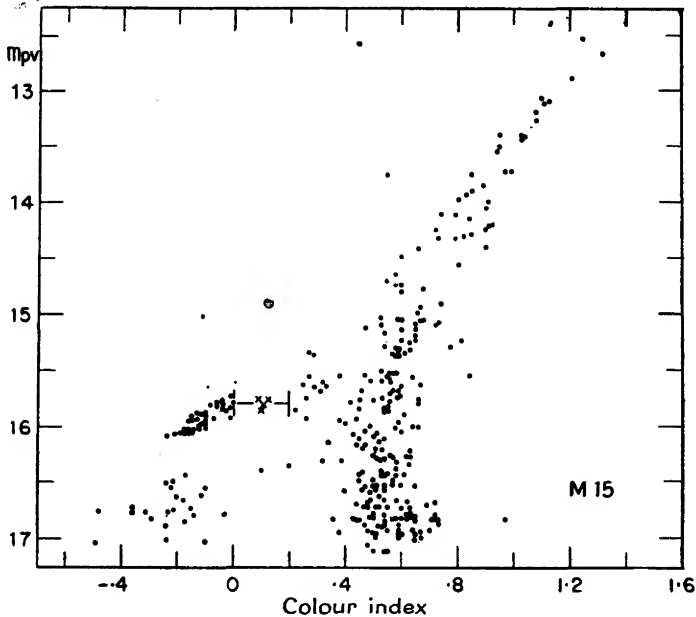


FIG. VI:1. *Colour Magnitude Diagram for the Globular Cluster Messier 15.*

Apparent photo-visual magnitude is plotted against colour index. The bars at $m_{pv}=15.8$, colour index=0 and $+0.2$ denote the limits of the region occupied by the RR Lyrae stars. The planetary nucleus falls at $m_{pv}=14.9$ and colour index= $+0.1$. Notice the strong clustering of blue stars at $m_{pv}=16$ and the number of fainter blue stars with colour indices between 0 and -0.4 . The branch of giant stars running from $m_{pv}=13$ and $CI=1.2$ to $m_{pv}=16$ and $CI=0.6$ is characteristic of the Type II population.

(Courtesy of H. C. Arp, Mt. Wilson and Palomar Observatories.)

by theoretical considerations. More recent work has shown that Berman's magnitude estimates are better than might have been expected. William Liller finds the differences shown in Table VI:1 between magnitudes measured photo-electrically (cf. Chapter II) and those determined by photographic and other techniques.⁽⁸⁾ These stars are rather blue intrinsically, and should be slightly brighter photographically than visually, perhaps by two- or three-tenths of a magnitude, except in so far as they are affected

by space absorption. Liller measured the brightness of the star plus nebular continuum at two points, one in the visual and the other in the photographic region. He then reduced the measured photo-electric magnitudes and colours to the photo-visual system. Thus there remains some uncertainty due to the nebular continuum. In fact, for several stars he finds that the published values of the intensity of the nebular continuum exceeds his measured intensity of star plus continuum! The difficulty with the nebular continuum can be overcome partly by going to larger telescopes

TABLE VI:1
Magnitudes of Planetary Nuclei

Nebula	Photovisual Magnitude	Photographic Magnitude
	Liller	Berman
NGC 40	11.2	11.3
NGC 2392	10.6	10.5
NGC 3242	12.0	11.9
IC 4593	11.2	10.2
NGC 6210	12.0	11.7
NGC 6543	—	11.2
NGC 6572	—	12.0
NGC 6720	14.2	14.4
BD + 30° 3639	10.1	10.3
NGC 6818	—	15.0
NGC 6826	10.6	10.7
NGC 7009	11.0	11.9

with the aid of which the contributions to the continuum by the nebula and by the star can be measured separately.

The measured magnitudes of many planetary nuclei are strongly affected by space absorption. The intrinsic colours of the planetary nuclei may be obtained from measures of objects in high galactic latitudes and in other regions known to be unaffected by obscuring particles. Such a study has been carried out at the Hamburg Observatory.⁽⁹⁾ Corrections for space absorption may also be made by comparing for any nebula the obscured Balmer decrement with the "standard" Balmer decrement exhibited by a number of planetaries which appear to be little affected by space absorption (see Chapter IV). Attempts have been made to correct for space absorption with the aid of the colour excesses of nearby B stars as measured by Stebbins and Huffer,⁽¹⁰⁾ but this procedure is poor because of the extremely spotty distribution of the interstellar material.

At the Mt. Wilson Observatory in 1954 Liller and the writer, using the photo-electric technique developed by the former, have measured the

brightnesses of a large number of planetary nebulae, and their central stars. These data when combined with now available spectrophotometric material on the nebular continuum and Balmer decrement should permit the determination of the apparent magnitudes and space absorption or colour excesses of a number of the central stars. Unfortunately, as we have seen, the distances of the planetaries are poorly known. Berman's determinations are probably statistically of the right order of magnitude, but the value for any individual parallax may be considerably in error. Perhaps our best information on the absolute magnitudes of the planetary nuclei will come from an analysis of those objects associated with the central bulge of the galaxy. Besides the planetary nucleus in M15 the only direct absolute magnitude determination is for the nucleus of NGC 246. This star is a double, whose companion is a dwarf late F star. Liller and the writer have measured the magnitude of this star and its companion, but an absolute magnitude is not yet available for the fainter component.

Since the planetary nuclei have a huge range in surface temperature (Section 6), their magnitudes alone do not tell too much of their true luminosities.

3. The Spectra of the Central Stars of the Planetary Nebulae

The nuclei of the planetary nebulae are all hot stars with temperatures ranging from 25,000°K. upwards.⁽¹¹⁾ Their spectra mimic those of certain stars of the Type I population, although their intrinsic luminosities are much lower.

The spectra may be described conveniently in four categories:

- (1) Wolf-Rayet type, e.g. the nuclei of NGC 40, NGC 6751, and HD 167362.
- (2) Combined emission and absorption features often of the Of type, e.g. the nuclei of NGC 6543 and IC 418.
- (3) O stars with absorption lines but no emission lines, e.g. the nucleus of IC 2149.
- (4) Continuous spectra with no trace of absorption or emission lines with the available dispersions, e.g. NGC 4361 and NGC 6720.

Before discussing these different kinds of objects in detail, a few remarks concerning the "classical" Wolf-Rayet stars of population Type I will be in order. These rare objects possess perhaps the most spectacular and least understood of stellar spectra. Upon a strong, high-temperature continuum are superposed broad, high-excitation, emission lines of the ions of light elements, particularly helium, carbon, nitrogen and oxygen. Often there are absorption lines associated with some of these strong emissions, but not all Wolf-Rayet stars show emission lines with absorption components.

Eðlén⁽¹²⁾ identified the emission lines on the basis of his term analyses of the spectra of light atoms. The interpretation of the spectra have been discussed by Beals,⁽¹³⁾ Menzel,⁽¹⁴⁾ Cecilia Payne-Gaposchkin,⁽¹⁵⁾ Swings,⁽¹⁶⁾ and others. Considerable attention has been paid to the eclipsing binary V 444 Cygni, "BD +38° 4010", which consists of a Wolf-Rayet component and an O star.⁽¹⁷⁾ The complexity of this system well illustrates the difficulties attending any attempt to explain the structures of the atmospheres of Wolf-Rayet stars. CQ Cephei, studied by Bappu, is another example.

There is a rich aggregate of early-type objects in Cygnus which includes a group of nine Wolf-Rayet stars. From the known absolute magnitudes of the B stars in the group plus measures of the magnitudes and colours of the others, Miss Roman finds these O, B, Wolf-Rayet, and P Cygni stars to be concentrated at a distance of 1600 parsecs.⁽¹⁸⁾ She finds the mean absolute magnitudes of the classical Wolf-Rayet stars to be -4.9 .

Some Wolf-Rayet stars appear to be much brighter than this. Thus, Henry J. Smith finds the following absolute magnitudes for the brighter stars observed in the southern hemisphere:

Star	Spec.	M	Notes	Star	Spec.	M	Notes
HD 33133	WN8	-8.0	(1)	HD 151932	WN7	-6.0	(3)
HD 38282	WN7	-8.9	(1)	HD 151804	O8f	-7.0	(3)
HD 32228	WC6pec.	-9.4	(1, 2)	HD 152408	O8f	-6.6	(3)

(1) In the large Magellanic Cloud for which $m-M$ is taken as 19.3. Several WC6 stars of $M = -6.2$ to -7.5 are also found there.

(2) Spectroscopically identical with θ Muscae.

(3) In NGC 6231.

The star, θ Muscae, which has a common proper motion companion of spectral class B8I on the Morgan-Keenan system has an absolute magnitude of -9.4 !

Wolf-Rayet stars are often components of binaries and the high luminosities found for some of these objects may simply represent the luminosity of the brighter O-type component. The Wolf-Rayet member of a system with a strong continuous spectrum may easily be two or three magnitudes fainter than its companion.

The classical Wolf-Rayet stars fall into two groups—a "carbon sequence" consisting of stars whose spectra show lines of helium, carbon, and oxygen in various stages of ionization, and a "nitrogen sequence" characterized by strong emission spectra of helium and nitrogen. Beals⁽¹⁹⁾ suggested the designations WC5, 6, 7, 8, 9 for the carbon stars and WN5, 6, 7, 8, 9 for the nitrogen stars. P. Swings⁽¹⁶⁾ and the writer⁽²⁰⁾

found independently that although the nitrogen stars contained a small trace of carbon, there was no evidence of any nitrogen in the stars of the carbon-oxygen sequence.

One star of intermediate type must be noted among the classical Wolf-Rayet stars. This object is HD 45166, spectral class W7n, which shows narrow emission lines of hydrogen, helium, carbon, nitrogen, oxygen, and silicon superposed on a continuum characterized by strong Balmer lines.⁽²¹⁾ In some respects this star resembles the Of stars almost as closely as it does the conventional Wolf-Rayet stars.

Henry Smith points out that HD 62910, a typical WN6 star also has strong lines of CIII, CIV, and OV, while the WN(4) star, HD 104994, has strong lines of OVI ($\lambda 3811$, $\lambda 3834$). HD 90657 W(N, C)(5) has $\lambda 4603$ –19 NV and $\lambda 4650$ CIII with about equal intensity.

The great breadth of the lines in the Wolf-Rayet stars has been attributed to expanding shells,^(13, 14) to the scattering by electrons of monochromatic radiations in a high-temperature atmosphere, and less plausibly to other causes. The high excitation character of the spectra of many of the stars shows that the temperatures of such objects must be high. Various authors,⁽²²⁾ including the present writer, have suggested that these radiations originate in a stratified atmosphere, whereas J. Weenan has tried to interpret the spectrum as coming from a source at a single temperature.⁽²³⁾ Photometric measures demonstrate that the stronger lines, such as $\lambda 4686$ of HeII, are affected by self-reversal.

No satisfactory atmospheric model for stars of the Wolf-Rayet type has been developed. The complexities exhibited by the Wolf-Rayet component of the binary V 444 Cygni have not been fully accounted for.

The planetary nuclei with spectra of the Wolf-Rayet type include the central stars of NGC 40, 6751, 6905, 7026, BD+30° 3639 and HD 167362. Perhaps the best known of these objects is BD+30° 3639, the interesting character of whose spectrum was first described by Mrs. Fleming.⁽²⁴⁾ Later, Campbell⁽²⁵⁾ found the star to be surrounded by a small nebula or envelope of hydrogen. Hence the object is often called "Campbell's hydrogen-envelope star", although the envelope is really a small planetary nebula. Swings and Struve found HD 167362 to be a very similar object and have published wavelengths and identifications for the lines in the spectra of this star and Campbell's object.⁽²⁶⁾

Photometric measures of the line intensities in BD+30° 3639 and the nucleus of NGC 40 have been published by the writer.⁽²⁰⁾ Campbell's star is remarkable in that although there are no nitrogen lines in its spectrum, the [NII] lines are very strong in the spectrum of the surrounding nebula. Helium, carbon, and oxygen in various stages of ionization contribute nearly all of the stellar lines. The relatively narrow emissions

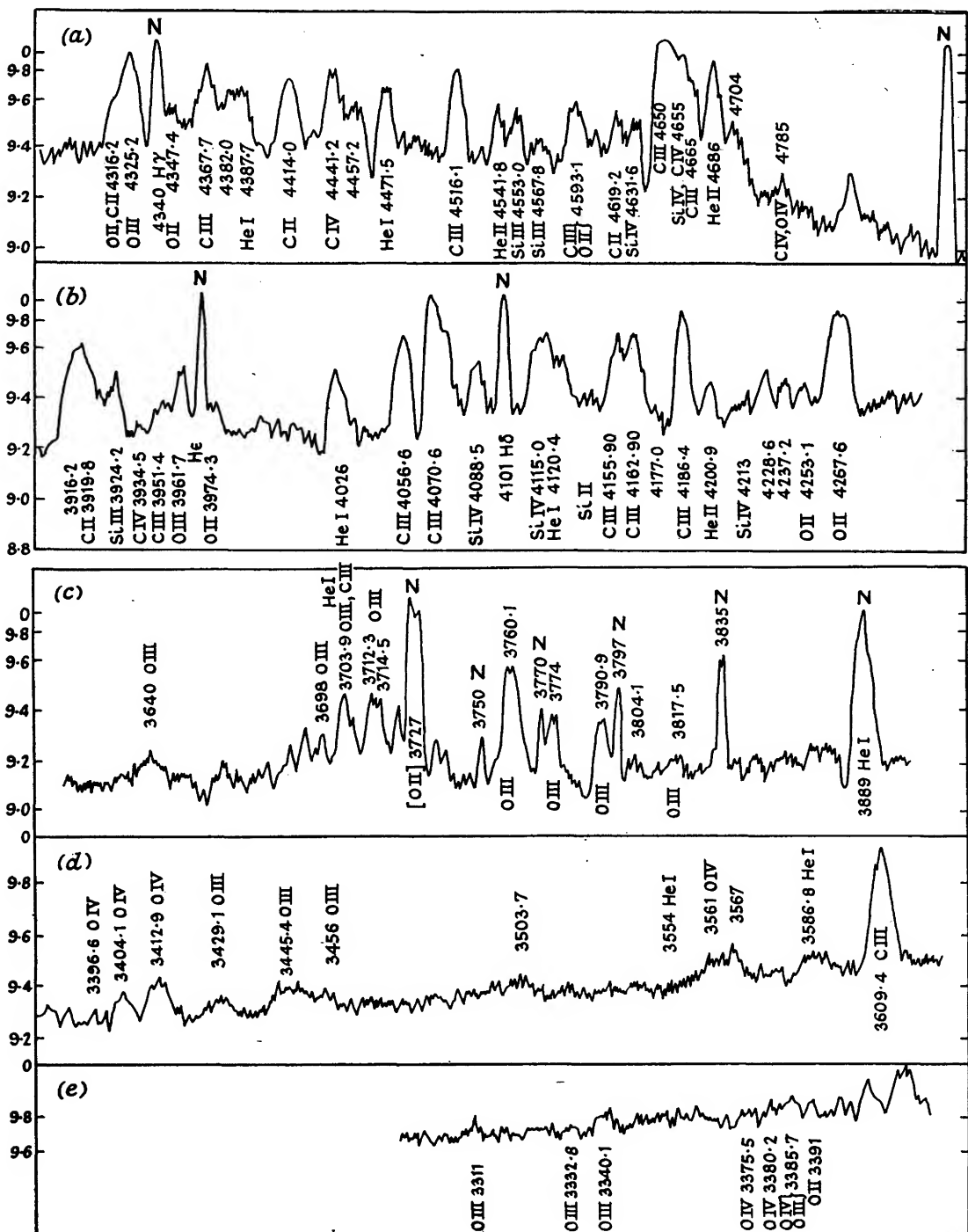


FIG. VI-2. *Tracing of the Spectrum of Campbell's Hydrogen Envelope Star BD + 30° 3639.* The scale on the side gives relative $\log I$. The wavelengths and indentifications are taken mainly from Struve and Swings (*Proc. Nat. Acad. Sci.*, **26**, 548 (1940).) The plate from which the tracing was made was obtained at the McDonald Observatory, September 1945. The lines of nebular origin are marked by *N*. Notice the numerous lines of carbon and oxygen and the difficulty of locating the continuum in this planetary nucleus of the Wolf-Rayet type.

of CII and CIII are particularly strong, the spectral class of the star is WC 8 (see Fig. 2).

The nucleus of NGC 40 displays a very similar WC 8 spectrum with a very strong CIII $\lambda 4650$ emission and bright lines that are somewhat broader than in BD+30° 3639. The surrounding nebula has a very low excitation with strong $\lambda 3727$ and weak $N_1 + N_2$.

Minkowski⁽²⁷⁾ has pointed out that the nuclei of several planetary nebulae, e.g. those of NGC 6751, NGC 6905, and IC 351, have line widths comparable with those found in the classical Wolf-Rayet stars, yet the nebular lines are as narrow as in planetaries whose nuclei have sharp emission lines. Thus if the ejection hypothesis for Wolf-Rayet atmospheres is invoked to explain the breadths of the stellar lines, the small velocity range of the gases in the surrounding nebula is difficult to comprehend.

The nucleus of NGC 7026 likewise shows broad emission lines near $\lambda 3800$ and $\lambda 4650$ with some suggestion of weaker diffuse lines in the ultra-violet. According to Swings and Swensson⁽²⁸⁾ the spectrum contains not only the lines of oxygen and carbon but also the 4641 MIII group. Photometric measures show that the $\lambda 3811$ – 3834 blend of OVI and the 4650, 4686, HeII, CIII, CIV blend contribute most of the light of the spectrum.⁽²⁹⁾ In this star the oxygen lines tend to be stronger than the carbon lines. On the other hand, in the nucleus of NGC 6751 most of the lines are weak compared with the $\lambda 4616$ – 4714 blend of carbon and ionized helium features. There is some possibility that this star may also contain nitrogen, which would place it in the Wolf-Rayet group of intermediate composition (see Fig. 3).

Turning to the Of stars which show strong continua, narrow emissions, and usually prominent absorption lines, let us first discuss the population Type I representatives and then the planetary nuclei.

The classical Of stars are very luminous objects. For the Of component of the binary 29 Canis Majoris, Kuiper finds a mass of forty-four suns and a bolometric magnitude of about -10 .⁽³⁰⁾ Miss Roman concludes that the Of stars in the Cygnus aggregate are definitely brighter than the pure absorption O stars and have an absolute visual magnitude of about -6.0 .⁽¹⁸⁾

Struve and Swings⁽³¹⁾ have discussed the spectroscopic characteristics of many of these stars, while Swings⁽¹⁶⁾ has grouped the Of stars into categories depending on the relative prominence of nitrogen and carbon. Some Of stars show bright lines of nitrogen with no trace of carbon, others such as 9 Sagittae show nitrogen and weaker carbon, yet others have CIII, $\lambda 5686$, and NIII, $\lambda 4641$, lines of comparable intensities, while in some $\lambda 5686$ is much stronger than $\lambda 4641$.

Perhaps the best known of the *Of* stars is 9 Sagittae. Fluorescence effects in the emission lines are marked. The $\lambda 4686$ line of the Paschen series of ionized helium appears as a weak emission, whereas the next line of the series, $\lambda 3203$, is a strong absorption line. The *NIII* radiations $\lambda 4634$, 4640 ($3p^2P-3d^2D$) show the P Cygni character, i.e. they consist of emission lines with absorption components on their shortward edges. Evidently these lines arise in a shell. On the other hand, $\lambda 4097-4103$ ($3s^2S-3p^2P$) are strong absorption lines. Furthermore, the high-level $\lambda 4379$ ($4f^2F-5g^2G$) line is in absorption. Hence the special fluorescent mechanism described in Chapter III for *NIII* in gaseous nebulae cannot apply. Also *CIII* $\lambda 5696$ ($3p^1P-3d^1D$) appears in emission. No high-level lines of *CIII* or of *NIII* appear in emission so that recombination in a shell cannot produce the bright lines. Selective fluorescence, however, gives a good explanation of the $\lambda 4686$ emission. P Cygni-type line profiles are found for selected lines of hydrogen, helium, carbon, nitrogen, and silicon in other *Of* stars. If the bright lines are attributed to an expanding shell, expansion velocities of the order of 200 km./sec. are indicated.

The most detailed quantitative study of the *Of* stars is that by J. B. Oke.⁽³²⁾ From an analysis of the intensities and profiles of the absorption lines he concludes that the gas pressure supports only a fraction of the weight of the atmosphere, the rest of the support being provided by radiation pressure and turbulence. He obtains indications of dimensions and luminosities in good accord with those found by Kuiper and by Miss Roman.

Oke concludes that the emission lines arise in the upper atmosphere of the star rather than in an extended envelope because: (a) the profiles of the emission and absorption lines are very similar in shape and width; (b) in HD 192281, which shows pronounced rotation, the emission lines yield the same rotational velocity as do the absorption lines; (c) the ratio of the intensities of 4640 to 4634 indicates considerable self-absorption. Recombination, which could be effective in an extended nebula, must be unimportant. He finds the radii of these stars to be about thirty times as great as that of the sun and the atmospheres themselves to have depths of the order of four million miles!

Oke measured the profiles and equivalent widths of the emission lines. These profiles must be corrected for the effect of the underlying stellar absorption. In *Of* stars, $\lambda 4686$ *HeII* appears in emission, whereas in the ordinary *O* stars the incipient 4686 emission does not fill in the stellar absorption.

The profiles of the *NIII* and $\lambda 4686$ lines show pronounced changes in periods of the order of several hours. The main part of the lines change considerably in shape and are accompanied by emission and absorption

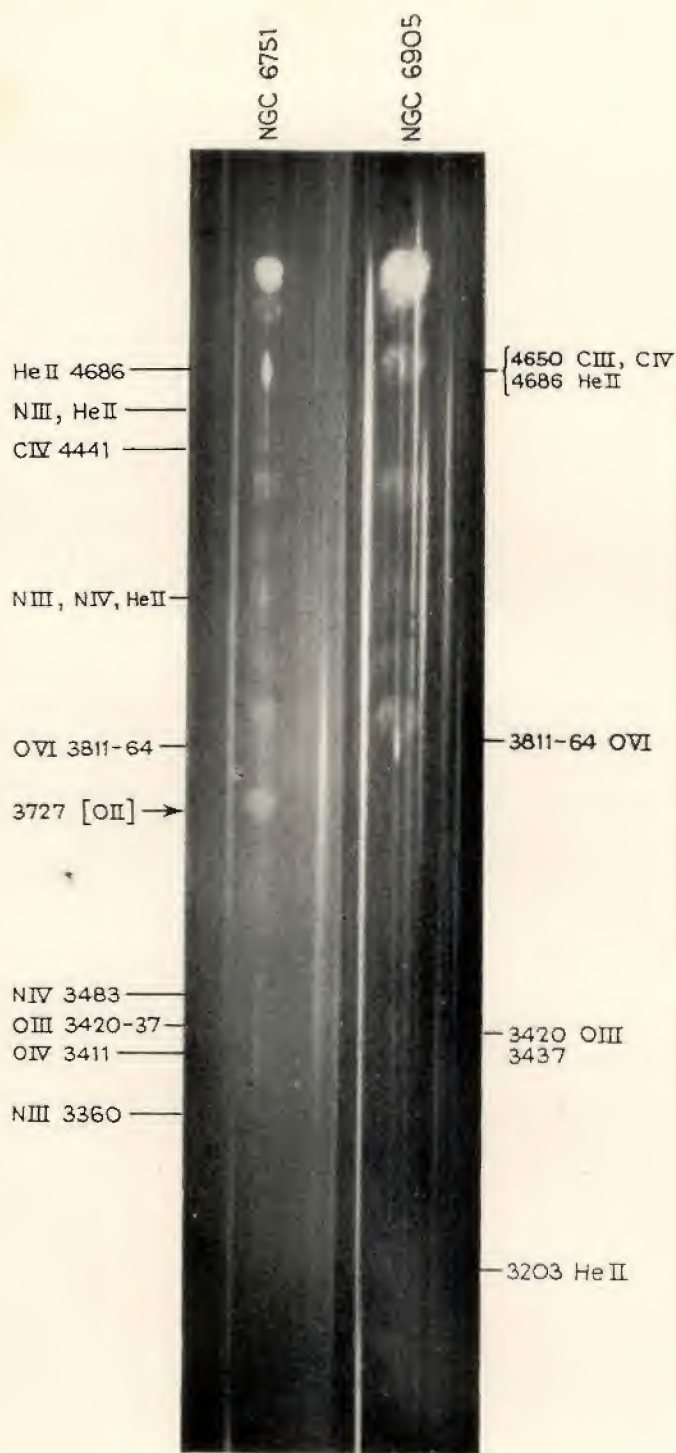


FIG. VI : 3. *The Spectra of the Planetary NGC 6751 and NGC 6905.*

The central star of NGC 6751 contains broad lines of carbon, nitrogen, oxygen and helium in various stages of ionization. The central star of NGC 6905 appears to belong to the carbon sequence. Notice the strong nebular images of 23727 [OII] in NGC 6751 and of 24686 of HeII in NGC 6905.

(Photographed with the quartz slitless spectrograph of the Crossley Reflector at the Lick Observatory in May 1945.)

satellites on the red and violet sides that come and go from plate to plate. These variations are probably sporadic rather than periodic, although more observation will be needed to settle this point. Presumably, the atmospheres of these stars contain great fields of prominences that change their configurations very rapidly.

TABLE VI : 2

The Spectrum of the Nucleus of NGC 6543
(photographic region)

λ	Ident.	Transition	W_λ
4685.8	HeII	3-4	13.8
4658.6	CIV	$5^2F^\circ-6^2G$	2.5
4646.5	CIV	5^2D-6^2F	1.6
4647.4	CIII _n	3^3S-3^3P	—
4619.4	NV	3^2S-3^2P	{ 0.40 0.20 A.
4603.2	NV	3^2S-3^2P	{ 0.74 0.34 A.
4541.6	HeII	—	0.85 A.
4088.9	SiIV	4^2S-4^2P	0.82
4057.8	NIV	3^1P-3^1D	{ 1.0 0.16 A.
3889.0	HI	2^2P-8^2D etc.	—
	HeI	2^3S-3^3P	1.3 A.
	HeII	4^2F-16^2G etc.	—
3835.2	HI	2^2P-9^2D etc.	0.6 A.
	HeII	4^2F-18^2G etc.	—
3797.3	HI	2^2P-10^2D etc.	0.7 A.
	HeII	4^2F-20^2G etc.	—
3563.4	OIV	$3p^2D-3d^2F$	0.64
3560.4	—	—	0.69
3484.9	NIV	$3s^3S-3p^3P$	0.42
3483.0	—	—	0.53
3478.7	—	—	0.53
3411.8	OIV	3^2P-3^2D	} 2.1
3409.8	—	$3s^4P-3p^4D$	
3403.6	—	3^2P-3^2D	
3396.8	OIV	$3s^4P-3p^4D$	0.23
3385.5	—	—	0.31
3381.3	—	—	0.29
3375.5	OIV	$3p^4S-3d^4P$	0.44

The planetary nuclei with Of type of spectra include the central stars of IC 418 and NGC 6210, while those of NGC 6826 and NGC 6543 probably lie between the Of and Wolf-Rayet groups. In some of these objects the emission lines are very prominent. The nucleus of NGC 2392 is also an Of star (see Section 4).

One of the most interesting of these objects is NGC 6543. Swings⁽³³⁾ has pointed out that the lines of CII, CIII, and NIII observed in the nebula are

all due to recombination, which seems to be unusually efficient in this object, whereas the strongest lines of the three ions CIV, NIV, and OIV appear with comparable intensities in the spectrum of the nucleus, which he classifies as W6.

Table VI:2, which is based upon observations secured by the writer at the McDonald Observatory in 1945, lists the nuclear lines observed in the photographic region of the spectrum. Successive columns give the line, its identification, the corresponding atomic transition, and finally the emission and absorption line intensities expressed in terms of equivalent widths

TABLE VI:3
*The Emission Line Spectra of the Nuclei of
IC 4997 and NGC 6826*

λ	Ident.	Transition	W_λ	
			IC 4997	NGC 6826
4685.8	HeII	3-4	—	1.8
4658.6	CIV	$5^2F^{\circ}-6^2G$	2.6	0.9
4650.2	CIII	3^3S-3^3P	0.67	0.7
4640.6	NIII	3^2P-3^2D	2.3	0.8
4634.2	NIII	3^2P-3^2D	1.9	0.4
4057.8	NIV	3^1P-3^1D	1.3	

referred to the underlying stellar continuum. Absorption lines are denoted by the letter *A*. Some of the higher members of the Balmer series are measurable, but the earlier members, $H\beta$, $H\gamma$, and $H\delta$ are masked by the strong nebular emission and are unobservable. The stellar CIV $\lambda 4646$ line is confused with the CIII $\lambda 4647$ line of nebular origin, but the 4658.6 CIV line is free of such blending. NIV and OIV are well represented, whereas SIV is represented only by $\lambda 4088.9$. The NV lines $\lambda\lambda 4603, 4619$ have profiles of the P Cygni type. Table VI:3, also based on observations secured at the McDonald Observatory in 1945, gives similar data for the nuclei of IC 4997 and NGC 6826. All three of these stars represent objects in which nitrogen and carbon lines appear with comparable intensities. The nucleus of IC 418 is also similar in this respect. IC 4997, whose nucleus is classified by Swings and Struve as a W7 star, has an abnormally strong $\lambda 4363$ [OIII] line, indicative of a high electron density.⁽³⁴⁾

4. The Nucleus of NGC 2392

This star, one of the brightest of planetary nuclei, has been studied in some detail. Its spectrum resembles that of certain classical Of stars, e.g. HD 14947 and HD 16691, although the HeII and NIII emission lines are very much narrower. The $\lambda\lambda 4634, 4640$ lines of NIII are present in

emission, whereas $\lambda\lambda 4097, 4103$ occur only in absorption. No carbon lines are observed.

Olin Wilson observed the spectrum of the nebula and its central star with the coude spectrograph at the 100-in. reflector.⁽³⁵⁾ He determined the radial velocity of the system from the single nebular [NeV] lines, from the mean of the components of the doubled nebular lines and from the stellar emission lines as +71 km./sec. The absorption lines in the spectrum of the central star did not give the same radial velocities. The absorption lines of highest excitation, those of NIV, gave essentially the velocity of the system. The NIII, HeII, and HeI lines gave +67, +63, and +57 km./sec. respectively, while the hydrogen lines gave a radial velocity of +45 km./sec. That is, lines of lower excitation show successively larger shortward displacements, which suggest a variation of outward velocity with depth in the central stars' atmospheres. The H lines are presumably formed highest in the atmosphere; the NIV lines deepest, in a region of much higher density and temperature.

A comparison of the profiles of the hydrogen lines in the nuclear spectrum with those observed in the normal O9 star 10 Lacertae show them to be generally weaker (as a consequence of the higher temperature in the atmosphere of the central star), although the profile shapes are generally similar. The other absorption lines are likewise all shallow although this star gives a richer absorption spectrum than do most other planetary nuclei.

Measures of the profiles of the emission lines in this and in other planetary nuclei suggest the possibility of time variations which may be similar to those found by Oke in the classical Of stars.

5. Spectrophotometry of Planetary Nuclei

Quantitative data on the profiles and total intensities of emission and absorption lines in the spectra of the planetary nuclei are necessary for an interpretation of these objects. Unfortunately all of these objects are faint. Many are involved in a bright nebula so that guiding at the telescope is difficult. Furthermore, the superposition of the bright nebular emission on the stellar absorption lines often fills in or badly distorts the profiles of the latter. The only way these difficulties can be even partially overcome is to employ high dispersions at a large telescope. Coude dispersions (~ 10 A./mm.) are adequate but the number of planetary nuclei that can be reached with such a spectrograph even with a 100-in. telescope is very small.

Some years ago the writer⁽³⁶⁾ observed the brighter central stars with the Cassegrain spectrograph at the McDonald Observatory with the highest attainable dispersions. These observations have been partially

superseded by coudé spectrograms secured by Olin Wilson. Measures of equivalent widths of absorption lines have been published for the central stars of IC 418, IC 2149, IC 4593, NGC 2392, NGC 6210, NGC 6543, NGC 6826, and NGC 6891. Profiles of emission and absorption lines in the nuclei of IC 418, 2149, 4593, and NGC 2392 have also been measured.⁽³⁷⁾ From these data estimates of the temperatures, electron densities, spectral classes, and chemical compositions can be made.

TABLE VI : 4
Spectral Classes of Planetary Nuclei

Object	Spectral Class	Excitation Temperature
IC 418	07	33,200
IC 2149	07.5	32,500
NGC 2392	06	34,500
IC 4593	07	33,400
NGC 6210	07	32,900
NGC 6543	07*	33,000
NGC 6826	06	34,600
NGC 6891	07	32,900

* Estimated from the intensities of lines not blended with nebular emissions.

The profiles of $H\gamma$ and $H\delta$ sometimes show an asymmetry in the sense that the wings are deeper on the shortward side—a consequence of the blending of a Balmer line with a Pickering line. Otherwise the lines show the type of profile anticipated for Stark broadening.

The equivalent widths of the hydrogen and helium lines may be employed to determine the spectral classes by the method of R. M. Petrie.⁽³⁸⁾ For most planetary nuclei it is possible to employ either the $HeI/HeII$ or $HeII/H$ ratios, viz.

$$\frac{HeI}{HeII} : \frac{I(\lambda 4471)}{\frac{1}{2}[I(\lambda 4200) + I(\lambda 4542)]},$$

$$\frac{HeII}{H} : \frac{\frac{1}{2}[I(\lambda 4200) + I(\lambda 4542)]}{\frac{1}{4}[I_c(H\gamma) + I_c(H\delta)]}$$

provided that the effects of blending with the nebular lines can be taken into account. Here $I_c(H\gamma)$ and $I_c(H\delta)$ are the intensities of $H\gamma$ and $H\delta$ corrected for blending with the ionized helium lines. In practice the blending of the stellar and nebular $\lambda 4471$ HeI lines is found to be quite troublesome so that the $HeII/H$ ratio is the more reliable. In Table VI : 4 we give the adopted spectral classes of the planetary nuclei whose absorption spectra have been observed with sufficient dispersion.

The corresponding temperatures are taken from Petrie's calibration of the excitation temperatures of normal O-type stars. They are not necessarily the same as the effective temperatures of these stars. At this point it is well to emphasize that Petrie's temperature calibration involves the assumption that the helium/hydrogen ratio is the same in all stars. If the helium/hydrogen ratio turns out to be larger in the planetary nuclei than in the Type I population O stars, the excitation temperatures will be lower than the values we have tabulated.

The equivalent widths of the *HI* and *HeII* lines may also be used to estimate electron densities and the number of hydrogen and ionized helium atoms in the second and fourth levels, respectively, "above the photosphere" of the star. The depth of the photosphere, or more precisely the quantity of matter per cm.² above an optical depth of say 0.5, is fixed by the opacity of the atmosphere. This opacity is produced by the continuous absorption of hydrogen atoms, of neutral helium atoms, of singly ionized helium atoms, and by electron scattering.⁽³⁹⁾ The relative importance of continuous absorption and of electron scattering will depend on the temperature and density.

If the higher members of the Balmer series are formed in an optically thin layer, the relation between the number of atoms above the photosphere in the second level, $N_{0,2}H$, and the equivalent width W_λ of the (2- n) transition will be

$$W_\lambda = \frac{\pi e^2}{mc^2} \lambda^2 f_{2n} N_{0,2} H, \quad . \quad . \quad . \quad (1)$$

where f_{2n} denotes the oscillation strength of the transition. In practice one calculates $\log N_{0,2}H$ from W_λ for each line of the Balmer series and plots $\log N_{0,2}H$ against n . For the earlier members of the series the computed value of $N_{0,2}H$ rises with increasing n , because the thin-layer approximation does not hold for strong lines. Gradually the $\log N_{0,2}H$ - n plot flattens off as the thin-layer approximation is more nearly fulfilled. Finally, however, the lines begin to coalesce, the W_λ 's are measured too small and $\log N_{0,2}H$ decreases. An extrapolation of the plot, as suggested by Unsöld,⁽⁴⁰⁾ gives a final estimate of $\log N_{0,2}H$. Unsöld has made extensive applications of this procedure to early-type stars,⁽⁴¹⁾ while the same principle was applied to the emission lines in the solar chromosphere many years ago by Menzel.⁽⁴²⁾

The application of this method to the four stars observed with the coude spectrograph yields values of $\log N_{0,2}H$ close to 15.4 as compared with 15.8 for 10 Lacertae,⁽⁴³⁾ and 15.8 and 15.7 for the supergiants λ Orionis (07.5) and 9 Cam (09).⁽⁴⁴⁾

The electron density in the atmosphere may be estimated from the

intensities of $H\gamma$ and $H\delta$ by a procedure employed by Unsöld⁽⁴⁰⁾ or from the number of resolvable lines of the Balmer series. If n_m is the principal quantum number of the last resolved Balmer line, the electron density is given by

$$\log N_e = 23.46 - 7.5 \log n_m, \quad (2)$$

a formula due to Inglis and Teller with the numerical value of the constant factor revised in accordance with the experimental work of W. Lochte-Holtgreven and W. Nissen at Kiel.⁽⁴⁵⁾ Further revisions in this formula appear to be required by recent studies of the hydrogen line profiles in the luminous shock tube at the University of Michigan.

In the nuclei of NGC 2392, IC 418, and IC 4593, $n_m=16$ so that $\log N_e=13.46$. In IC 2149 the Balmer series can be followed to $n_m=19$, corresponding to $\log N_e=12.86$. Estimates of $\log N_e$ found from $H\gamma$ and $H\delta$ are in good agreement with these values except for IC 2149. The electron densities are lower than in a main-sequence O star such as 10 Lacertae, and appear to be more nearly comparable with those found in supergiant atmospheres. A study of the higher members of the Balmer series indicates that these lines are formed in the higher levels of the atmosphere, i.e. near an optical depth of 0.2 or 0.3, as one would expect for an atom that became rapidly ionized with depth.

The observed data on the electron densities, temperatures, and mass of material above the photosphere may provide an estimate of the effective surface gravities of these stars provided the atmospheres are in hydrostatic equilibrium. At the base of the strata responsible for the stellar absorption lines, the gas pressure may be equated to the weight of the overlying layers, viz.

$$P_g = M_H g_{eff} \Sigma \mu NH, \quad (3)$$

where NH is the total number of atoms above the photosphere, μ is the molecular weight, and the effective surface gravity may be taken approximately as⁽⁴⁶⁾

$$g_{eff} = g - g'. \quad (4)$$

Here

$$g = g_0 \frac{M}{R^2} \quad (5)$$

is the ordinary surface gravity; M is the mass and R the radius of the star in terms of the corresponding solar quantities. Here

$$g' = k\sigma T_e^4/c \quad (6)$$

is the acceleration produced by radiation. T_e is the effective temperature, σ is the Stefan-Boltzmann constant, and k may be taken as the Chandrasekhar mean absorption coefficient. An estimate of g_{eff} can be

obtained in the following way: now $P_g = 2P_e$ for the highly ionized gas of the stellar atmosphere, and $\Sigma \mu NH$ can be computed from the observed intensities of the hydrogen lines and the combined Boltzmann and Saha equations for the assumed temperature of the star. Hence the right-hand side of equation (3) can be computed. Then the value of g itself can be guessed. If the radius of the star can be determined its mass can then be estimated.

If the star radiates as a black body at temperature T , its radius is related to its photographic absolute magnitude by

$$M_p = -0.83 - 5 \log R + \frac{36,600}{T} + 2.5 \log (1 - 10^{-14,600/T}). \quad (7)$$

If we adopt T as the excitation temperature corresponding to the spectral type, and M_p from the work of Berman, the radii of the planetary nuclei turn out to be comparable with that of the sun. The masses corresponding to $g_{\text{eff}} - g'$ are likewise comparable with that of the sun rather than with the values appropriate to their luminosities in accordance with the mass luminosity law.⁽⁴⁷⁾ To phrase the result a little more accurately we may say that the spectra of the planetary nuclei are consistent with the hypothesis that their masses are only slightly larger than that of the sun.

It is not possible to derive the actual stellar masses by the procedure we have described since we cannot be sure that the atmospheres are in hydrostatic equilibrium. The dependence of the radial velocity on the degree of ionization for the atoms in the atmosphere of the nucleus of NGC 2392 clearly show the difficulties to be encountered in the calculation of the structure of the actual atmosphere, a problem we shall mention in more detail in Section 8.

At this point some mention should be made of the central stars which show no lines of any kind. With available dispersions the central stars of nebulae, such as NGC 4361, NGC 3242, and NGC 6853, show continuous spectra with no trace of any stellar lines. The latter, if present at all, must be very weak and lost beneath the strong nebular emissions. At high temperatures the absorption line spectrum must eventually disappear, and this seems to occur for the hottest planetary nuclei. In high excitation objects such as NGC 7027 or NGC 2440 no central star spectrum appears at all!

The nuclei of NGC 1535 and IC 3568 seem to show strong $\lambda 4542$ HeII absorption lines, but other lines are masked by the nebular emission. Tentatively, we may assign them spectral classes near O7 or O8.

6. The Temperatures of the Central Stars of the Planetary Nebulae

In the preceding section we saw how the excitation temperatures of planetary nuclei with absorption line spectra may be estimated from their

spectral classes. The objects for which such methods could be applied turned out to have excitation temperatures between $32,000^\circ\text{K.}$ and $35,000^\circ\text{K.}$ Excitation temperatures might be derived for the Wolf-Rayet nuclei from their emission line spectra.

The temperatures of the planetary nuclei were first estimated, however, by entirely different methods based on theories of the excitation of the gaseous nebula. In Chapter III we saw that if the nebular shell was optically thick, all the radiation emitted by the central star beyond the Lyman limit would be absorbed. Zanstra⁽⁴⁸⁾ showed that under these circumstances each Lyman continuum quantum would be degraded into a Lyman α quantum plus a quantum of the Balmer series or continuum. The total number of quanta in the Balmer series plus continuum must equal the number of quanta emitted by the central star beyond the Lyman limit. Hence, from a comparison of the intensities of the nebular Balmer lines with the underlying stellar continua, the temperature of the central star could be determined provided the latter radiates as a black body. Similar arguments can be applied to high excitation nebulae in which the lines of *HeII* appear, except that here the Paschen and Brackett series of *HeII* rather than the Balmer series are observed. Hence, the relative intensities of the Brackett, Paschen, and Balmer series must be calculated (see Chapter IV). In this way *HeII* as well as *HI* temperatures can be determined. Ambarzumian⁽⁴⁹⁾ pointed out that one could also get an estimate of the temperature of the central star from the intensity ratio of $\lambda 4686$ to $H\beta$, provided the nebula was optically thick. The intensity of $\lambda 4686$ depends on the recombination rate of doubly ionized helium atoms, which in turn equals the rate of photo-ionizations of *HeII*. The latter depends on the energy available shortward of $\lambda 228$. The intensity of $H\beta$ involves the recombination rate of ionized hydrogen and therefore, since a steady state exists, on the stellar radiation field shortward of $\lambda 912$. If the central star radiates as a black body its temperature will be uniquely defined by the ratio

$$\int_{\nu_1}^{\infty} B_\nu(T) d\nu \bigg/ \int_{4\nu_1}^{\infty} B_\nu(T) d\nu,$$

where ν_1 denotes the frequency of the Lyman limit. The advantage of the Ambarzumian method is that one can compare the nebular lines $\lambda 4686$ and $H\beta$ without measuring the underlying stellar continuum. Thus the method is available for high excitation nebulae such as NGC 7027 where the stellar continuum cannot be observed at all.

The intensities of the forbidden nebular lines may also be employed to get the temperature of the central star. In the method due to Zanstra it is supposed that all the energy of the photo-electrically ejected electrons is

dissipated in the collisional excitation of the [OIII] lines. The energy required for the photo-ionization of each hydrogen atom is $h\nu_1$, so that the energy actually brought into the continuum is

$$\frac{1}{2}mv^2 = h(\nu - \nu_1). \quad (8)$$

Following Zanstra's notation we let

$$\frac{\partial L_s}{\partial \nu} = 4\pi R^2 \pi I_\nu \quad (9)$$

denote the energy emitted by the star per unit frequency interval at the frequency ν . If I_ν is given by the Planck function and we define $x = h\nu/kT$, the total amount of energy emitted per second by the star beyond the Lyman limit will be

$$E_u = \int_{\nu_1}^{\infty} \frac{\partial L_s}{\partial \nu} d\nu = \frac{8\pi^2 R^2 k^4}{c^2 h^3} T^4 \int_{x_1}^{\infty} \frac{x^3}{e^x - 1} dx. \quad (10)$$

If the nebula is optically thick all this energy will be absorbed. The corresponding number of quanta will be

$$N_u = \frac{8\pi^2 R^2 k^3}{c^2 h^3} T^3 \int_{x_1}^{\infty} \frac{x^2}{e^x - 1} dx. \quad (11)$$

Since the total energy of the free electrons,

$$E_f = E_u - N_u h\nu_1, \quad (12)$$

is assumed to be dissipated in the excitation of forbidden lines, we obtain from equations (10), (11), (12), and the definition of x , the total amount of energy, E , radiated in the forbidden lines, viz.

$$E = \frac{8\pi^2 R^2 k^4}{c^2 h^3} T^4 \left\{ \int_{x_1}^{\infty} \frac{x^3}{e^x - 1} dx - x_1 \int_{x_1}^{\infty} \frac{x^2}{e^x - 1} dx \right\}. \quad (13)$$

The total energy radiated in the [OIII] lines will be

$$E = \Sigma h\nu N_p, \quad (14)$$

where N_p is the number of forbidden line quanta. We may write

$$E = \frac{8\pi^2 R^2 k^4}{c^2 h^3} T^4 \sum \frac{x^4}{e^x - 1} A_\nu, \quad (15)$$

where we have used equation (9). The quantity

$$A_\nu = \frac{L_p}{\nu(\partial L_s / \partial \nu)} \quad (16)$$

is determined from the observations. Here L_p is the intensity of the nebular image, while $\partial L_s / \partial \nu$ is the energy per unit frequency interval in the

underlying stellar continuum measured at the same frequency. Thus A_ν is a dimensionless number. Equating equations (13) and (15), we obtain the transcendental equation

$$\int_{x_1}^{\infty} \frac{x^3}{e^x - 1} dx - x_1 \int_{x_1}^{\infty} \frac{x^2}{e^x - 1} dx = \sum \frac{x^4}{e^x - 1} A_\nu, \quad (17)$$

which has to be solved by trial and error for each observed value of A_ν .

Zanstra generalized this method to estimate central star temperatures from the magnitude difference between the star and the nebula. If it is supposed that the nebular magnitude is essentially that of the green nebular lines and that the stellar magnitude corresponds to the apparent brightness of the star at the effective photographic wavelength according to Brill, we can write

$$m_s - m_n = f(T), \quad (18)$$

where $f(T)$ is a known function apart from an additive constant, which is determined from one or more nebulae where a good temperature determination from equation (17) is available. Berman⁽⁵⁰⁾ estimated the ratio of the light of the nebula, l_n , to that of the star, l_s , to be given by

$$\frac{l_n}{l} = \frac{0.5 \int_{x_1}^{\infty} \frac{x^2}{e^x - 1} dx}{\int_{x_g}^{x_\nu} \frac{x^2}{e^x - 1} dx} + \frac{0.8 \int_{x_1}^{\infty} \frac{x^2(x - x_1)}{e^x - 1} dx}{\int_{x_g}^{x_\nu} \frac{x^2}{e^x - 1} dx}. \quad (19)$$

The first term on the right gives the ratio of the number of observed Balmer quanta (equal to the number of stellar quanta emitted beyond the Lyman limit) to the number of stellar photographic quanta between x_g (corresponding to $\lambda 5050$) and x_ν corresponding to $\lambda 3000$). The second term corresponds to the ratio of energy in the green nebular lines to that in the stellar spectrum between $\lambda 3000$ and $\lambda 5050$. The factor 0.5 allows for the omission of $H\alpha$ on photographs secured with ordinary emulsions, while the factor 0.8 allows for the lowered sensitivity of ordinary emulsions for the [OIII] radiation. Actually, the factors 0.5 and 0.8 have to be modified, depending on the emulsions and instruments used. Finally, the method fails for nebulae such as BD + 30° 3639, where the [OIII] lines are weak or absent. Berman has estimated the temperatures of the central stars for many nebulae in this way.

Zanstra has criticized Berman's modification of his method and remarks that, "from the point of view of photometry the use of stellar photographic quanta can mean only a very approximate estimate".

It must be emphasized that the nebular and stellar magnitudes, m_n and m_s , available to Berman, Zanstra, Vorontsov-Velyaminov, and others were rather inhomogeneous and poor. The replacement of such data by photo-electric values such as those obtained by Liller will go a long way towards resolving this difficulty.

Instead of comparing the nebular line intensities with the continuum of the illuminating star, Stoy⁽⁵¹⁾ compared the intensities of the nebular, Balmer and forbidden lines. The basic assumption is the same as that made by Zanstra in his "nebulium" method, namely the energy brought into the continuum by the electrons photo-electrically detached from hydrogen is all dissipated in inelastic collisions with ions of O^{++} , N^+ , etc.

If all ultra-violet quanta are absorbed in the nebula their total number will equal the number of Balmer quanta, i.e.

$$4\pi R^2\pi \int_{\nu_1}^{\infty} B_{\nu} \frac{d\nu}{h\nu} = \frac{8\pi^2 R^2}{c^2} \int_{\nu_1}^{\infty} \frac{\nu^2 d\nu}{e^{h\nu/kT} - 1} = \sum \frac{L_B}{h\nu_B}. \quad (20)$$

Here L_B denotes the energy radiated in the Balmer lines. The kinetic energy of an electron which has been ejected photo-electrically from an atom that has absorbed a quantum of frequency ν is given by equation (8). Not all of this is available for forbidden line excitation. Accordingly, we modify Stoy's treatment to take into account the fact that the final mean energy of the electrons is not zero but is given by

$$\frac{1}{2} m v_0^2 = \frac{3}{2} k T_e = h(\nu_e - \nu_1). \quad (21)$$

The energy contributed by each electron for the excitation of the nebular lines is

$$\frac{1}{2} m(v^2 - v_0^2) = h(\nu - \nu_e). \quad (22)$$

Since all of the stellar ultra-violet energy is assumed absorbed, the energy available for the collisional excitation of the forbidden nebular lines is the number of quanta times the energy per quantum

$$\frac{8\pi^2 R^2}{c^2} \int_{\nu_1}^{\infty} \frac{h\nu^3}{e^{h\nu/kT} - 1} \frac{1}{h\nu} h(\nu - \nu_e) d\nu = \Sigma L_N. \quad (23)$$

Then

$$\alpha(T) = \frac{\int_{\nu_1}^{\infty} \frac{\nu^3 - \nu_e \nu^2}{e^{h\nu/kT} - 1} d\nu}{\int_{\nu_1}^{\infty} \frac{\nu_{\beta} \nu^2}{e^{h\nu/kT} - 1} d\nu} = \frac{\Sigma L_N}{\Sigma L_B \frac{\nu_{\beta}}{\nu_B}}, \quad (24)$$

where ν_{β} is an arbitrary frequency which we take as the frequency of $H\beta$.

It is introduced in order to express both sides of the equation as a dimensionless ratio. The frequency of a Balmer line is denoted by ν_B .

In Table VI: 5 we compare the temperatures of planetary nuclei deduced in different ways. The second column gives the temperature estimated from the spectral class under the assumption that Petrie's temperature spectral class calibration is valid for these stars. The third column gives the

TABLE VI : 5
Temperatures of Planetary Nuclei
(in thousands of degrees)

Object	Spect. Class	Zanstra Method	Stoy Method	Remarks
Anon 0 ^h 25 ^m	—	40	55	(1)
IC 418	33.2	25	18	—
NGC 2392	34.5	35	56	(3)
IC 2149	32.5	40	26	—
II 3568	—	30	64	(2)
II 4593	33.4	25	31	—
6210	32	30	45	—
6543	—	35	33	(3)
6572	—	45	50	(4)
BD +30° 3639	—	25	18	(5)
6826	32	30	40	(3)
6891	32	30	42	—
IC 4997	—	30	39	(5)
7009	—	50	49	—
7027	—	80	65	(6)
7662	—	55	70	—

(1) Spectrum of star appears continuous with no trace of any absorption or emission lines.

(2) $\lambda 4541$ HeII present in absorption—probably late O.

(3) See text.

(4) Emission lines appear in spectrum of nucleus but no absorption lines are present.

(5) Wolf-Rayet type.

(6) Central star must be extremely hot and faint.

“Zanstra” temperatures obtained by Berman from the magnitude difference between star and nebula and from line intensity ratios. The fourth column gives the temperatures calculated by the Stoy method using the observed line intensities in the nebulae, under the assumption $T_e=0$. If the best estimates of the electron temperatures are made and the corresponding values of $\alpha(T)$ are computed, it is found that the nuclear temperatures are raised by several thousand degrees. The temperature of the IC 418 nucleus, for example, then comes closer to the other estimates. The Stoy method temperatures tend to show a greater range than do those found from spectral classes or the Zanstra methods. One must remark,

however, that the temperatures based on spectral types are limited to the small class of planetary nuclei that show absorption lines in their spectra.

What of the temperatures derived from $HeII$ and from a comparison of $\lambda 4686$ and $H\beta$? They turn out to be much higher than the Zanstra "hydrogen" or "magnitude-difference" temperatures. Wurm has discussed this question in some detail in his recent book on planetary nebulae.⁽⁵²⁾ He finds the temperature of the nucleus of NGC 7009 to lie between $85,000^\circ K.$ and $115,000^\circ K.$, whereas the nuclei of NGC 7027 and 7662 have temperatures between $110,000^\circ K.$ and $200,000^\circ K.$ Wurm and Singer⁽⁵³⁾ interpret the nebulae with very high ratios of $I(4686)/I(H\beta)$ as objects that are optically thick for radiation of wavelength shorter than $\lambda 228$, but thin for the radiation between $\lambda 912$ and $\lambda 228$. Hence the Zanstra condition of complete absorption of ultra-violet radiation holds for ionized helium but not for hydrogen. Some years ago Minkowski⁽⁵⁴⁾ established that many nebulae of low surface brightness must be optically thin in the Lyman continuum, but it seems doubtful that nebulae of high surface brightness are optically thin at the Lyman limit (see Chapter III).

Wurm has also derived temperatures of planetary nuclei from the ratio of the intensity in the nebular continuum at the Balmer limit to that of the continuous spectrum of the central star. This ratio depends on the temperature of the central star, the fraction of captures on the second level (which depends on the electron temperature), and upon the optical thickness of the nebula. On the basis of this method Page assigned lower limits of $50,000^\circ K.$, $120,000^\circ K.$, and $55,000^\circ K.$ to the nuclei of NGC 6543, NGC 6720, and NGC 7662.⁽⁵⁵⁾ One would expect these results to agree with those found from Zanstra's original hydrogen-line method, but the latter are much lower. In the absence of published details of his work a critical evaluation is not possible.

Zanstra's original method, his nebularium and star-nebula magnitude difference methods, as well as Wurm's Balmer continuum method all involve a comparison of the radiation of the central star in the accessible spectral region with its radiation in the far ultra-violet. On the other hand, the $I(4686)/I(H\beta)$ method and the Stoy method involve either the comparison of the stellar energy curve in one part of the far ultra-violet with that in another part of the far ultra-violet—or the comparison of the integrals of I_ν and I_ν/ν over the far ultra-violet. The assumption is made throughout that the central star radiates as a black body.

Actually, we have no direct means of testing the validity of this hypothesis. In Section 8 we shall show how a judicious guess of the ultra-violet energy distribution can be made by the method of model atmospheres. The predictions of such theories might be trusted for ordinary stars, but stars surrounded by extended envelopes are likely to have extremely complicated

ultra-violet energy distributions. Detailed calculations for envelope-free stars, particularly by W. Liller, suggest that the temperatures obtained by the original Zanstra method (or variants thereof that involve a comparison of the far ultra-violet energy with the energy in the observable region of the spectrum) give more reliable results than those that compare one part of the far ultra-violet with another, or that depend on a strict black body energy distribution in this region. We return to this question in Section 8.

7. The Chemical Compositions of the Planetary Nuclei

Present-day concepts of stellar evolution assign the nuclei of the planetaries to an ancient population. In the colour-magnitude arrays for the Type II population they lie near the horizontal branch of blue-white stars, although they appear to be intrinsically brighter than the ex-novae. Stars of a somewhat similar character have been found in high galactic latitudes. As an example one may mention BD +28° 4211, an extremely blue, diffuse-line object discussed by MacRae, Weston, and Fleischer.⁽⁵⁶⁾ Münch has found that stars of this type often show abnormal helium/hydrogen ratios.

As we have seen, the nuclei of the planetaries include Wolf-Rayet, *O*f type, and absorption-line objects. Differences in the nitrogen/carbon ratio seem to exist in the classical Wolf-Rayet and *O*f stars. Quantitative estimates of the composition differences in the Wolf-Rayet stars were first made by the writer some years ago, while Oke has recently determined the compositions of several *O*f stars.

The population Type II Wolf-Rayet stars that appear in planetary nebulae appear to mimic the composition differences that are found in the Type I high luminosity Wolf-Rayet stars. That is, helium appears to be more abundant than hydrogen and the ratios of carbon, nitrogen, and oxygen seem to fluctuate from one object to another. In Campbell's hydrogen envelope star or the nucleus of NGC 40, carbon appears to be eight or ten times as abundant as oxygen, while helium seems to be about ten times as abundant as carbon. On the other hand, in NGC 6543 the emission spectrum is consistent with equal abundances of oxygen and nitrogen with carbon about four times as abundant as either. No emphasis can be placed on these figures as emission-line spectra are strongly affected by special excitation mechanisms. Nevertheless, the spectral differences from one star to another strongly suggest that differences in chemical composition are real and striking.

Swings and Struve and, more recently, Swings and Swensson have emphasized that the Wolf-Rayet planetary nuclei often are of the "intermediate" type. That is, they resemble HD 45166, whose spectrum exhibits sharp lines of carbon, nitrogen, oxygen, hydrogen, and helium more closely than they do other "classical" Wolf-Rayet stars which fall in distinct

carbon-oxygen-helium or nitrogen-helium composition classes. Many of these nuclei have relatively sharp emission lines, and the writer often has called them *Of* rather than Wolf-Rayet stars. The demarcation line between *Of* and Wolf-Rayet stars is indistinct, particularly when planetary nuclei are classified according to this scheme which was developed for population Type I high-temperature stars.

Turning to the absorption line stars, we find that the determination of compositions is complicated by other factors. First, the lines of elements other than hydrogen and helium are usually very weak in the spectra. Second, the intensity ratio of the Pickering lines of ionized helium to the Balmer lines of neutral hydrogen depends critically upon the temperature and density. There is no evidence that the H/He ratios in the nuclei of IC 418, NGC 2392, IC 2149, and IC 4593 differ from those obtaining in "normal" Type I stars.

A planetary nucleus that appears definitely to be a helium star is the one associated with NGC 246. No hydrogen lines can be identified with certainty in its spectrum. The Pickering lines and $\lambda 4686$ are strong, but the CIII $\lambda 4650$ and CIV lines are yet stronger. There are no emission lines in the spectrum save those of OVI $\lambda 3811$ and $\lambda 3838$, nor is there any trace of any nitrogen. Berman assigns a temperature of $35,000^\circ\text{K}$. to this object, but this value seems to be too low.

We have already mentioned that the masses of the planetary nuclei are probably not much greater than that of the sun. Presumably they represent Type II stars that are near the end of their evolution. John Crawford⁽⁵⁷⁾ has suggested that the planetary nuclei derive their energy from Salpeter's helium-burning mechanism.⁽⁵⁸⁾ The presence of objects with varying proportions of carbon, oxygen, and nitrogen suggests that the element-building process may have gone beyond the carbon synthesis stage. These questions cannot be settled until the detailed evolutionary tracks of stars in the colour-magnitude diagram have been computed.⁽⁵⁹⁾ Further speculation at this time seems unwarranted.

8. The Energy Fluxes from O and B Stars

In striking contrast to the tiny blue stars that illuminate the planetary nebulae are the O and B stars that ionize the interstellar medium and excite the diffuse nebulae characteristic of the Type I stellar population. The sources of information on the radii, masses, and luminosities of these objects have been discussed in Chapter III. Here we shall concern ourselves with the characteristics of their radiation. The state of ionization of the interstellar medium and the level of excitation of gaseous nebulae depends upon the intensity and frequency distribution of the radiation beyond the Lyman limit in the spectra of the exciting stars.

Given the chemical composition of the superficial layers, their excitation temperature, and the surface gravity it should be possible to calculate the structure of the stellar atmosphere (i.e. the dependence of temperature and density on depth in the star), provided that it is in hydrostatic equilibrium. If the observable layers of the main sequence O and B stars of interest to us are composed primarily of hydrogen, we can assert that they are in radiative rather than in convective equilibrium.

We shall not attempt to give the detailed theory of the calculation of model atmospheres for high-temperature stars. Models have been calculated by Rudkjöbing,⁽⁶⁰⁾ by Anne Underhill,⁽⁶¹⁾ by Pecker,⁽⁶²⁾ by Jean McDonald,⁽⁶³⁾ by Neven and de Jager,⁽⁶⁴⁾ and by others.⁽⁶⁵⁾

The usual procedure has been to integrate the equation of hydrostatic equilibrium as a function of optical depth. If radiation pressure can be neglected,

$$\frac{dP_g}{dt} = -\frac{g}{k}, \quad (25)$$

where t is the optical depth in terms of the integrated radiation, and k is the mean absorption coefficient. If radiation pressure has to be taken into account, the equation of mechanical equilibrium is⁽⁶¹⁾

$$\frac{dP_g}{dt} = \frac{g}{k+\sigma} - \frac{\sigma_R}{c} T_e^4, \quad (26)$$

where σ is the coefficient of electron scattering and σ_R is the Stefan-Boltzmann constant. The calculation of the model atmosphere proceeds by successive approximations. Usually it has been assumed that in the first approximation the temperature distribution can be taken as that appropriate to a grey body, i.e.

$$T^4(i) = \sqrt{3} T_0^4 [i + q(i)], \quad (27)$$

where T_0 is the boundary temperature and $q(i)$ is a known function of i . The element of optical depth in the integrated radiation is given by

$$di = k q dx, \quad (28)$$

where k is the mean absorption coefficient. The calculation of a satisfactory k turns out to be extremely difficult. We would like to compute a mean absorption coefficient in such a way that if we define

$$i = \int k q dx, \quad (29)$$

the temperature will be the same function of t as T is of t for a grey atmosphere. For the late O and early B stars it does not seem possible to calculate a k that will satisfy this condition—at least in the initial stages of the calculations.

Some workers have started their calculations with the grey-body temperature distribution and the Rosseland mean absorption coefficient. The

convergence of the solution to a final model in which the flux is constant with optical depth and in which the condition of radiative equilibrium is fulfilled in each volume element is discouragingly slow. Indeed, Miss Underhill has pointed out that the Rosseland mean is not valid for the atmospheres of early-type stars. She has found that near spectral class O9 the Chandrasekhar type mean gives a much better, although still not entirely satisfactory, first approximation. Detailed calculations show that even at optical depths larger than those expected to contribute to the formation of the observable spectral lines the necessary conditions for the validity of the Rosseland mean are not yet fulfilled.

The most recent work suggests that it may be best to discard entirely the concept of a mean absorption coefficient and integrate the equation of hydrostatic equilibrium in terms of the optical depth τ_λ at some fixed wavelength, e.g. $\lambda 5000$. It is necessary to make a guess about the temperature distribution, but one can make a guess as good as the original grey-body approximation. The model atmosphere must be improved by iteration procedures until the conditions of radiative equilibrium and constancy of flux are fulfilled.

The grey-body approximation fails most severely as the boundary of the star is approached. The relation between the boundary temperature T_0 and the effective temperature T_e is

$$T_0 = \sqrt[4]{\frac{3^{1/2}}{4}} T_e \quad . \quad . \quad . \quad (30)$$

for a grey body. For a B star the boundary temperature is much lower than the value predicted by this formula. The radiation emergent beyond the Lyman limit is accordingly less than for a grey body of the same effective temperature, i.e. the same energy output.

The lowering of the temperature near the boundary is a consequence of the so-called *blanketing effect*—produced in this instance by the strong absorption beyond the Lyman limit. The qualitative effects may be predicted with the aid of a theory developed by Chandrasekhar in a study of the influence of the absorption lines upon the temperature distribution in the solar atmosphere.⁽⁶⁶⁾ Chandrasekhar assumed that the absorption lines were evenly distributed over the spectrum with a probability a_1 . Unsöld suggested that one could regard the Lyman absorption as equivalent in its action to that of absorption lines, and write

$$a_1/a_2 = \frac{\int_{\nu_1}^{\infty} F_\nu d\nu}{\int_0^{\nu_1} F_\nu d\nu}, \quad . \quad . \quad . \quad (31)$$

where F_v is the emergent flux from the star and ν_1 is the frequency of the Lyman limit.⁽⁶⁷⁾ Unsöld neglects the variation of this ratio with depth in the atmosphere and replaces the strongly wavelength-dependent stellar absorption coefficient k_v by constant values, i.e. k_1 and k_2 , for the spectral regions $0-\nu_1$ and $\nu_1-\infty$. He calculated these averaged values as Rosseland means taken over the appropriate spectral regions. The appropriate Rosseland mean absorption coefficient for the whole spectral region is then

$$\frac{1}{\bar{k}} = \frac{a_1}{k_1} + \frac{a_2}{k_2} \quad . \quad . \quad . \quad (32)$$

and if we put $x_1 = k_1/\bar{k}$ and $x_2 = k_2/\bar{k}$, we can then write the temperature distribution as a function of optical depth by

$$T^4 = 3/4 T_e^4 [\bar{i} + q(\bar{i})], \quad . \quad . \quad . \quad (33)$$

where $q(\bar{i})$ is given by Chandrasekhar's equation

$$q(\bar{i}) = \frac{2/3}{3+2\sqrt{3}A} \left[3 \left(\frac{a_1}{x_1^2} + \frac{a_2}{x_2^2} \right) + 2\sqrt{3}A - 3a_1a_2 \left(\frac{1}{x_1} - \frac{1}{x_2} \right) \left(\frac{x_2}{x_1} - \frac{x_1}{x_2} \right) A^2 e^{-\sqrt{3}x_1x_2A\bar{i}} \right], \quad (34)$$

where

$$A = \frac{1}{\sqrt{a_1x_1 + a_2x_2}}. \quad . \quad . \quad . \quad (35)$$

In the smallest optical depths the temperature falls below that of the corresponding grey body. Then the temperature rises for a time above the grey-body value, and finally converges to the grey-body approximation.

Neven and de Jager derived empirical model atmospheres in which they postulated that the hydrogen lines were formed in strict local thermodynamic equilibrium in accordance with an assumed formula for the hydrogen lines. The model atmospheres derived in this way for specific stars were not tested for constancy of flux nor for radiative equilibrium. The derived temperatures are perhaps too low and the temperature distributions appear to predict larger limb-darkening coefficients than are observed.

J. E. Milligan and the writer have adopted a somewhat different point of view.⁽⁶⁸⁾ Since hydrogen appears to be very much more abundant than helium, it suffices to consider a pure hydrogen atmosphere in the first approximation. The effect of the addition of a small amount of helium can be treated as a perturbation. To start the calculations it was assumed that the mean absorption coefficient approached the modified Chandrasekhar

mean⁽⁶⁹⁾ near the surface and the Rosseland mean at great depths. Except near the surface, where the temperature distribution was corrected for the blanketing effect in accordance with the Chandrasekhar-Hopf^(66, 70) theory, a grey-body temperature distribution was assumed. Three approximations to the temperature distribution were required before the flux became constant to within 2% over a range of optical depth 0 to 2.0. In the fourth approximation the flux was constant to within the errors of the calculation.

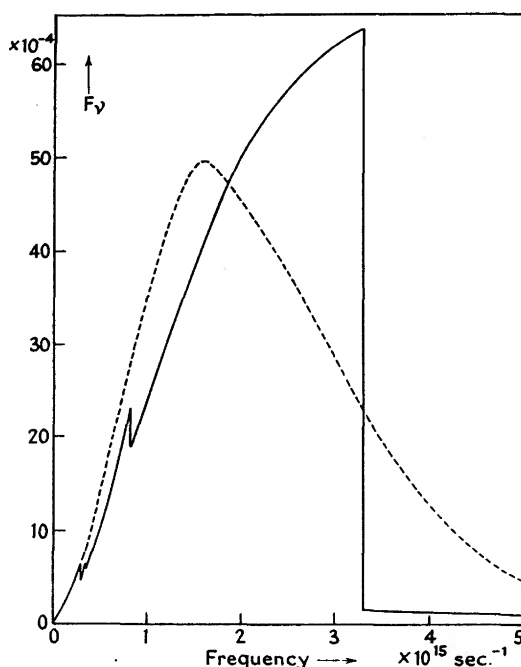


FIG. VI: 4. *The Emergent Energy Distribution in the Spectrum of a Hot Star.*

The star is assumed to be composed of pure hydrogen and to have an effective temperature of 29,500° K. Ordinates are $(\text{flux})/\pi = F_v$ in ergs/cm.²/sec.; the abscissa is the frequency, ν . The dotted curve gives the corresponding curve for a black body at this same temperature. (See reference 68.)

The boundary temperature was held constant at 18,000° K., and the surface gravity was taken as 1.6×10^4 degrees. The condition of radiative equilibrium was fulfilled to within the accuracy of the computation.

Fig. 4 shows the character of the emergent flux in comparison with that of a black body of the same effective temperature. Notice the copious flow of energy in the spectral region just redward of the Lyman limit and the depletion of the energy on the high-frequency side of this limit. Not only is the amount of energy cut, but its distribution is radically altered from that of a black body. If helium is present in quantity a strong absorption

will set in at $\lambda 504$, but in the interval $\lambda 912$ to $\lambda 504$ the energy distribution will still be "bluer" than for a black body of the same effective temperature.

The strong dependence of the energy distribution shortward of $\lambda 912$ on the hydrogen/helium ratio in the star is well illustrated by a comparison of these results with those found for a pure helium atmosphere of about the same effective temperature.⁽⁷¹⁾ Between $\lambda 1200$ and $\lambda 3400$ the grey energy distribution lies above that of the helium star, whereas from $\lambda 912$ to $\lambda 504$ the stellar radiation is considerably in excess of that of the grey body.

Thus the quantity and distribution of the energy emitted beyond the Lyman limit depends not only on the effective temperature of the star, but very much on its chemical make-up. Until the hydrogen/helium ratio is established for the star responsible for the excitation of a given nebula, little emphasis can be placed on "temperatures" derived from the quantity and quality of the energy in their far ultra-violet spectra.

Miss Underhill⁽⁶¹⁾ and, subsequently, Liller⁽⁷²⁾ have calculated the fluxes from stars with effective temperatures near $44,000^\circ\text{K}$. and $\log g = 4.20$ and 5.00 , respectively. The deviations of the energy distributions from that of a black body of the same effective temperature are striking, but, curiously, Liller finds that the correction to the temperature estimated by Zanstra's nebulium method is small. The correction is much larger for a star of effective temperature near $35,000^\circ\text{K}$.

To summarize: the excitation and ionization of gaseous nebulae or the interstellar medium are intimately controlled by the distribution of energy beyond the Lyman limit in the spectra of the illuminating stars. For a star in hydrostatic equilibrium this energy distribution will depend on: (1) the temperature distribution in the outermost layers (which is dependent on the blanketing effect); (2) the hydrogen/helium ratio.

The qualitative influence of these factors on the various types of "temperatures" derived from the energy in the far ultra-violet may be summarized briefly: methods which compare the total amount of far ultra-violet and visual region energies are going to be less affected than methods which depend on the energy distribution in the far ultra-violet at least for the hotter stars ($T > 45,000^\circ\text{K}$). For example, Zanstra's nebulium method should be less affected than Stoy's method.

A star composed mostly of helium might give too high a temperature by Zanstra's first method. In general, one might expect the *HI*, *HeI*, and *HeII* methods to give false temperatures. A pure hydrogen star whose energy distribution is strongly depleted just to the short wavelength side of $\lambda 912$ might radiate nearly as a black body near $\lambda 228$ so that the temperatures derived from the intensity ratio of $\lambda 4686$ to *H β* might be too high. Hence, Wurm's contention that the high $I(4686)/I(H\beta)$ ratio necessarily implies a thin optical shell for the radiation just shortward of the Lyman limit is not

rigorously justified. These matters cannot be investigated in a satisfactory fashion until appropriate model atmospheres for high-temperature stars have been calculated.

It is of considerable importance to the relation between the diffuse emission nebulae and their illuminating stars that the latter are often multiple. Frequently, in addition to the O star or stars that produce the excitation, there are also fainter B stars that are certainly physically associated with it. Such groupings have been discussed by W. W. Morgan, by V. A. Ambarzumian,⁽⁷³⁾ and particularly by Stewart Sharpless.⁽⁷⁴⁾ Multiple stars like the Trapezium in Orion are rather common, and even apparently single O stars may be very close multiples. Evidently such stars tend to originate in groups or associations. The gravitational interactions between the stars and their individual motions result in a loosening of the group. Some may escape and the remainder may form relatively stable configurations.

The best photographs of Messier 33 show that the illuminating "stars" of gaseous nebulae are here also often resolved into small, compact groups. For this reason the determination of the magnitudes and colours of the illuminating stars is extremely difficult.

The widespread prevalence of multiple stars as sources of the luminosities of diffuse nebulae must be taken into account in the theoretical work on specific objects.

REFERENCES

- (1) HUBBLE, E., *Ap. J.*, **56**, 162, 400 (1922).
- (2) See, for example, SANDAGE, A. R., *A.J.*, **58**, 61 (1953); ARP, H. C., BAUM, W. A., and SANDAGE, A. R., *A.J.*, **58**, 4 (1953); BAUM, W. A., *A.J.*, **58**, 222 (1953).
- (3) *Lick Obs. Bull.*, **18**, 57 (1937).
- (4) *Lick Obs. Publ.*, **13**, 57 (1918).
- (5) *Ap. J.*, **56**, 400 (1922).
- (6) *Mt. Wilson Contr. N.*, **463** (1933).
- (7) *Lick Obs. Bull.*, **17**, 21 (1933).
- (8) *Ap. J.*, **122**, 240, 1955.
- (9) Unpublished.
- (10) *Publ. Washburn Obs.*, **15**, 217 (1934).
- (11) An apparent exception is the nucleus of NGC 1514 which appears to be a dwarf AO star. It seems very likely that this star has an unresolved high-temperature companion that excites the nebula.
- (12) *Zeits. f. Ap.*, **7**, 378 (1933); *Vistas in Astronomy*, ed. by A. Beer (Pergamon Press, London, 1955).
- (13) *Pop. Astr.*, **37**, 577 (1929); *M.N.R.A.S.*, **90**, 202 (1929); *Publ. Dom. Ap. Obs.*, **4**, 272 (1930); *Journ. Roy. Astron. Soc. Canada*, **34**, 169 (1941).
- (14) *Publ. A.S.P.*, **41**, 344 (1929).
- (15) *Zeits. f. Ap.*, **7**, 1 (1933).
- (16) *Ap. J.*, **95**, 112 (1942).

- (17) See, for example, WILSON, O. C., *Ap. J.*, **91**, 379 (1940); **95**, 402 (1942); KRON, G. E., and GORDON, K., *Ap. J.*, **97**, 311 (1943); **111**, 454 (1950); and MUNCH, G., *Ap. J.*, **112**, 266 (1950).
- (18) *Ap. J.*, **114**, 492 (1951).
- (19) *Trans. I.A.U.*, **6**, 248 (1938).
- (20) *Publ. Amer. Astron. Soc.*, **10**, 157 (1942); *Ap. J.*, **97**, 135 (1943). Both this and Swings's paper (ref. 16) were presented at the Astronomical meetings and Spectroscopy Symposium held at the Yerkes Observatory, September 1941.
- (21) NEUBAUER, F. J., and ALLER, L. H., *Ap. J.*, **107**, 285 (1948). Miss Anger found the $\lambda 4640/\lambda 4686$ intensity ratio to vary with time, *Harv. Obs. Bull.*, 891 (1933).
- (22) See, for example, THOMAS, R. N., *Ap. J.*, **109**, 500 (1949); V. BAPPU, thesis, Harvard, 1952.
- (23) *B.A.N.*, **11**, 176 (1950).
- (24) *Astr. Nach.*, **125**, 155 (1890).
- (25) *Astr. and Ap.*, **13**, 461 (1894).
- (26) *Proc. Nat. Acad. Sci.*, **26**, 454, 548 (1940).
- (27) Quoted in *Ap. J.*, **97**, 162 (1943); footnote no. 41.
- (28) *Ann. d'Ap.*, **15**, 290 (1952).
- (29) See ALLER, L. H., *Ap. J.*, **113**, 139 (1951).
- (30) *Ap. J.*, **88**, 472 (1938).
- (31) *Ap. J.*, **91**, 546 (1940); **92**, 289 (1940); **92**, 295 (1940); **93**, 349, 356 (1941).
- (32) *Ap. J.*, **120**, 22 (1954).
- (33) *Ap. J.*, **92**, 289 (1940).
- (34) *Proc. Nat. Acad. Sci.*, **27**, 225 (1941).
- (35) *Ap. J.*, **108**, 201 (1948).
- (36) *Ap. J.*, **108**, 462 (1948).
- (37) WILSON, O. C., and ALLER, L. H., *Ap. J.*, **119**, 243 (1954).
- (38) *Publ. Dom. Ap. Obs.*, **7**, 321 (1947).
- (39) See, for example, the discussion in the author's *The Atmospheres of the Sun and Stars* (Ronald Press Co., New York, 1953), p. 182.
- (40) *Zeits. f. Ap.*, **21**, 38 (1941).
- (41) *Zeits. f. Ap.*, **23**, 100 (1944).
- (42) *Publ. Lick Obs.*, **17** (1931), "A Study of the Solar Chromosphere."
- (43) See ALLER, L. H., *Ap. J.*, **104**, 347 (1946).
- (44) *Ap. J.*, **90**, 439 (1939).
- (45) *Zeits. f. Phys.*, **133**, 124 (1952).
- (46) The assumption that g_{eff} is constant with optical depth in the star is really somewhat of an oversimplification. See Anne B. Underhill, *Publications Copenhagen Obs.*, **151** (1950).
- (47) See *Ap. J.*, **108**, 462 (1948)—Table 7. The $\log P_e$ for NGC 2392 is about ten times too high. If the value of the corresponding mass is corrected by the same factor, we find that $\log \bar{m} = 0.14$ for the objects listed.
- (48) *Ap. J.*, **65**, 50 (1927); *Dominion Astrophys. Obs. Publ.*, **4**, 209 (1931). *Zeits. f. Ap.*, **2**, 1 (1931).
- (49) *Poulkovo Obs. Circular No. 4*, **8** (1932).
- (50) *Lick Obs. Bull.*, **18**, 73 (1937).
- (51) *M.N.R.A.S.*, **93**, 588 (1933).
- (52) *Die Planetarischen Nebel*, Akademie-Verlag, Berlin (1951).
- (53) *Zeits. f. Ap.*, **30**, 153 (1952).
- (54) *Ap. J.*, **95**, 243 (1942).
- (55) *Astron. J.*, **55**, 77 (1950).
- (56) *Ap. J.*, **113**, 432 (1951).
- (57) *Publ. A.S.P.*, **65**, 210 (1953).
- (58) *Ap. J.*, **115**, 326 (1952); see also *Ann. Rev. of Nuclear Science*, **2**, 41 (1953).
- (59) SANDAGE, A., and SCHWARZSCHILD, M. have explained the lower part of the colour-magnitude array for globular clusters in terms of evolutionary processes. See *Ap. J.*, **116**, 463 (1952); HOYLE, F., and SCHWARZSCHILD, M. *Ap. J.*, Suppl. **2**, 1, 1955.
- (60) *Publ. Copenhagen Obs.*, **145** (1947).
- (61) *Publ. Copenhagen Obs.*, **151** (1950), and *Publ. Dom. Ap. Obs.*, **8**, 357, 385, (1951).
- (62) *Contributions of Astrophys. Inst.*, Paris Series B, No. 65 (1951).
- (63) *Publ. Dom. Ap. Obs.*, **9**, 269 (1953). This model is very similar to the one calculated by the writer for γ Pegasi. See *Ap. J.*, **109**, 244 (1949).
- (64) *B.A.N.*, **12**, 103, 1954.

- (65) Accounts of the calculation of model atmospheres will be found in WOOLLEY, R., and STIBBS, D., *The Outer Layers of a Star* (Oxford University Press, 1953), p. 282; CHANDRASEKHAR, S., *Radiative Transfer* (Oxford University Press, 1950), p. 312; KOURGANOFF, V., *Basic Methods in Transfer Problems* (Oxford University Press, 1953), Chapter 7; ALLER, L. H., *The Atmospheres of the Sun and Stars* (Ronald Press Co., New York, 1953), Chapter 7.
- (66) *M.N.*, **96**, 21 (1936).
- (67) *Zeits. f. Ap.*, **21**, 229 (1942).
- (68) *Astron. J.*, **58**, 44 (1953); *Proc. of the Indiana University Conference on Stellar Atmospheres*, ed. by M. Wrubel (1955).
- (69) See, for example, the author's *The Atmospheres of the Sun and Stars*, p. 230.
- (70) HOFF, E., *Mathematical Problems of Radiative Equilibrium*, Tract No. 31 (Cambridge University Press, 1934).
- (71) ALLER, L. H., HENIZE, K. G., MITCHELL, W., and WILKINSON, JOHN, *Publ. A.S.P.*, **64**, 262 (1952). The ordinate in the figure is not the flux, πF , but the quantity F .
- (72) Thesis, University of Michigan (1953).
- (73) *Abh. Deutsche Akad. Wiss. Kl. Naturw.*, No. 2 (1950).
- (74) *Ap. J.*, **119**, 334 (1954).

CHAPTER VII

Structure and Internal Motions of the Planetary Nebulae

1. Theory of the Ionization and Stratification of a Gaseous Nebula

In this chapter we are going to discuss in detail the structure and internal motions of the planetary nebulae. Our plan of attack is as follows. First we shall calculate the ionization of a nebula surrounding a hot star, following the suggestion by I. S. Bowen⁽¹⁾ and the theory by Bengt Strömgren.⁽²⁾ Then we shall examine the observed forms of the planetary nebulae to see how many of their features admit of a straightforward interpretation. It is necessary to consider not only the appearance of the nebulae upon direct photographs or slitless spectrograms but also the internal motions as revealed by the spectroscopic studies.

In an effort to interpret the clouds of ionized hydrogen observed by Struve and his co-workers⁽³⁾ in the neighbourhood of hot stars, Strömgren treated the ionization of a mass of hydrogen of uniform density exposed to dilute high-temperature radiation.⁽⁴⁾ These computations showed that in the immediate neighbourhood of the hot stars hydrogen is completely ionized, and remains so for a distance from the star that depends on the density of the gas and the available high-frequency radiation. Once neutral hydrogen atoms start to form from the free protons and electrons the process proceeds rapidly with the result that the transition from an ionized (*HII*) region to a neutral (*HI*) region takes place quickly. Thus the hydrogen ionization regions, which are defined by the faint glow of recombining protons and electrons, should have sharp boundaries as appears to be in harmony with the observations.

The original equations derived by Strömgren involved a number of approximations in the physical theory: (1) The frequency variation of the continuous absorption coefficient beyond the Lyman limit is neglected. (2) An approximate form of the ionization equation is employed wherein the recaptures on the higher levels are not taken into account. (3) The modification of the composition of the radiation field by radiative processes occurring within the nebula is neglected. Only the direct, diluted, radiation from the illuminating star is considered. Strömgren discussed the effects of some of these approximations and concluded that the main features of the ionization zones would not be greatly affected. We shall

try to allow for items (1) and (3) approximately, and take item (2) into account as well as the known atomic parameters permit.

The assumptions of uniform density and electron temperature were made for convenience. In the planetaries the nebular shell does not necessarily have a constant density or temperature throughout. Therefore we shall generalize Strömgren's method for an arbitrary variation of the density and electron temperature with distance from the exciting star.

Let us first consider the ionization in a nebula of hydrogen surrounding an illuminating star. Suppose that the number of hydrogen atoms plus ions, $N(s)$, and the electron temperature T_e depend only on the distance s from the central star. Furthermore, let us adopt the Wien approximation to the Planck law. The ionization equation for hydrogen, equation (65), Chapter IV, then assumes the form

$$\frac{N_i N_e}{N_1} = \frac{(2\pi m k T_e)^{3/2}}{h^3} \frac{\int_{y_1}^{\infty} W \frac{e^{-y}}{y} dy}{G_{T_e}}, \quad (1)$$

where $y = h\nu/kT_1$, T_1 is the colour temperature of the central star, and G_{T_e} depends on the electron temperature in accordance with equation (50), Chapter IV. The geometrical dilution factor is

$$W_s = \frac{R^2}{4s^2}, \quad (2)$$

and to this must be added the effect of the extinction of the starlight in the nebula. Strömgren uses for this factor the approximation

$$e^{-\tau_u},$$

where τ_u is the optical depth as measured from the inner boundary of the nebular shell at the Lyman limit. The corresponding element of optical depth is

$$d\tau_u = (1-x)N(s)\alpha_u \times 3.08 \times 10^{18} ds, \quad (3)$$

where the parsec (1 parsec = 3.08×10^{18} cm.) is chosen as the unit of distance for s , α_u is the absorption coefficient at the Lyman limit and x is the degree of ionization of hydrogen. That is,

$$N_i = N_e = xN \quad \text{and} \quad N_1 = (1-x)N_e. \quad (4)$$

Actually the ionization equation should be written in the form

$$\frac{N_i N_e}{N_1} = \frac{(2\pi m k T_e)^{3/2}}{h^3} \frac{R^2}{4s^2} \frac{1}{G_{T_e}} \int_{y_1}^{\infty} \frac{e^{-\tau_u - y}}{y} dy, \quad (5)$$

where the optical depth τ , at the frequency ν is related to that at the Lyman limit by

$$\tau_\nu = \tau_u \left(\frac{\nu_1}{\nu} \right)^3 (g/g_1), \quad (6)$$

since the absorption coefficient for hydrogen is given by

$$\alpha_\nu = \alpha_u \left(\frac{\nu_1}{\nu} \right)^3 (g/g_1). \quad (7)$$

Here ν_1 is the frequency of the Lyman limit and g is the Gaunt factor.

We shall attempt to allow for the influence of the variation of τ , with ν in the following approximate way. The integral on the right-hand side of equation (5) is replaced by the approximation

$$\int_{\nu_1}^{\infty} \frac{e^{-\tau_u \left(\frac{\nu_1}{\nu} \right)^3 \frac{g}{g_1} - \nu}}{\nu} d\nu \rightarrow e^{-\tau_u b} E_1(\nu_1), \quad (8)$$

where E_1 is the exponential integral function. The factor b is an empirical correction which will depend on the assumed optical depth of the nebula and on the temperature, T_1 . At high temperatures of the central star not only will b become small, but the Wien approximation to Planck's law will no longer be valid. The best we can do is to estimate an average value of b for the nebula under question. For example, with $T_1 = 30,000^\circ \text{K}$. and $\tau_u = 1.0$, $b = 0.70$.

The influence of the ultra-violet radiation produced by recapture of electrons on the ground-level is more troublesome to evaluate. Ambartsumian⁽⁵⁾ referred to this re-emitted Lyman continuum radiation as *diffuse radiation*, since the quanta escape from the atoms in random directions. On the other hand, the radiation from the central star is directed along the line from the central star to the point in question. A rigorous treatment of the problem would require the solution of the transfer equation for the continuum, but for present purposes we may be justified in following Zanstra and assuming that each Lyman continuum quanta is converted into a Lyman α quantum on the spot. The ionization equation is then written in the form

$$\frac{N_i N_e}{N_1} = \frac{(2\pi m k T_e)^{3/2}}{h^3} \frac{R^2}{4} \frac{E_1(\nu_1)}{G_{T_e}} \frac{e^{-\tau_u b}}{s^2}. \quad (9)$$

Making use of the equations (4), we find

$$\frac{x^2}{1-x} N = C_1(T_e) \frac{e^{-\tau_u b}}{s^2}, \quad (10)$$

where

$$C_1(T_e) = \frac{(2\pi m k)^{3/2}}{4h^3} \left(\frac{R}{R_0} \right)^2 \frac{R_0^2}{[3.08 \times 10^{18}]^2} \frac{E_1(\nu_1)}{G_{T_e}} T_e^{3/2}, \quad (11)$$

since s is measured in units of parsecs and R in units of the radius of the sun. Putting in numerical values there results

$$C_1(T_e) = 10^{-0.51} R^2 \frac{E_1(y_1)}{G_{T_e}} T_e^{3/2}. \quad (12)$$

The optical depth at the Lyman limit is chosen as the independent variable. Then

$$d\tau_u = 3.08 \times 10^{18} (1-x) N a_u ds. \quad (13)$$

Since T_e is presumed known as a function of s , $C_1(T_e)$ can be calculated as a function of s , viz. $C_1(s)$. Equation (10) can be written as

$$1-x = x^2 e^{\tau_{ub}} \frac{N(s)s^2}{C_1(s)} \quad (14)$$

and substituted into equation (13). We obtain

$$e^{-\tau_{ub}} b d\tau_u = e^{-t} dt = 3.08 \times 10^{18} a_u b x^2 \frac{N^2(s)}{C_1(s)} s^2 ds. \quad (15)$$

Let us introduce new variables, w and z , by

$$w = e^{-t}, \quad (16)$$

where $t = \tau_u b$, and

$$dz = 3.08 \times 10^{18} b a_u \frac{N^2(s)}{C_1(s)} s^2 ds. \quad (17)$$

Thus the relation between z and s becomes

$$z = 3.08 \times 10^{18} b a_u \int_0^s \frac{N^2(s)}{C_1(s)} s^2 ds, \quad (18)$$

where $z=0$ when $s=0$. The equations to be integrated numerically are then

$$\left. \begin{aligned} dw &= -x^2 dz, \\ \frac{1-x}{x^2} &= \frac{1}{w} \frac{s^2 N(s)}{C_1(s)} = \frac{\beta(z)}{w}, \end{aligned} \right\} \quad (19)$$

where $\beta(z)$ is known on the basis of the observed density and temperature distribution in the nebula.

To start the integrations we make use of the boundary conditions that $w=1$ when $z=0$, and that

$$w = 1-z \quad \text{for} \quad 1-x \ll 1. \quad (20)$$

In practice, one may plot $\beta(z)$ against z and obtain an approximation formula of the type

$$\beta(z) = Az^r, \quad . \quad . \quad . \quad (21)$$

where A and r are empirical constants. Thus

$$\frac{dw}{dz} = -x^2, \quad \frac{1-x}{x^2} = \frac{Az'}{w} \text{ for small } z. \quad . \quad . \quad (22)$$

Detailed application of the Strömgren theory to various model nebulae shows that despite the irregular density variations the hydrogen ionization zone has a very sharp boundary, so that the ionization decreases abruptly to zero over a short distance. The sharp boundaries of a number of planetary nebulae suggested to various writers that the luminous portions of such objects were merely the hydrogen ionization zones in a somewhat larger gas cloud.⁽⁶⁾ This condition cannot be true for all planetary nebulae.⁽⁷⁾ In some objects of low surface brightness we must be able to see the entire extent of the nebular gases. Nevertheless it appears to hold for certain nebulae of high surface brightness such as NGC 6826 whose luminous disk is surrounded by a very faint halo of extremely low surface brightness. Minkowski interprets this halo as marking the actual boundary of the nebula. It is faintly luminous because of radiation which leaks through from the inner region of the nebula, perhaps because of irregularities in the structure, e.g. filaments, etc. The Ring nebula, NGC 6720, also shows a faint outer halo; we recall that this object has a pronounced filamentary structure.

The Strömgren type of analysis can be applied to other gases as well. K. Wurm,⁽⁸⁾ for example, has discussed the problem of ionized helium—the formal theory of which is similar to that of hydrogen.

For HeI , one may employ equation (75), Chapter IV, where the ionization potential $\chi_1 = 24.46$ e.v., and the statistical weights are $\varpi_i = 2$, $\varpi_1 = 1.0$. The correction factor D may be calculated from the known absorption coefficients for the ground and certain excited levels, and with an assumed hydrogen-like absorption coefficient for higher levels (see Chapter IV, p. 142). For example, if $T_e = 10,000^\circ K.$, and $T_1 = 30,000^\circ K.$, we find

$$D = 0.88 W_g e^{-\tau b}, \quad . \quad . \quad . \quad (23)$$

where τ is the optical depth at the series limit. For most purposes it is sufficiently accurate to set $b = 1$ as $\alpha_1(\nu)$ does not vary too sharply with ν over the frequency range in question.

Since hydrogen is presumably much more abundant than helium we may have to take into account also the extinction produced by hydrogen at the helium series limit. That is,

$$d\tau = (1 - x_{He}) N_{He} 3.08 \times 10^{18} \alpha_1(v)_{He} ds + (1 - x_H) N_H 3.08 \times 10^{18} \alpha_1(v)_{H} ds. \quad (24)$$

At the helium series limit $\alpha_1(v)_{He} \sim 0.17 \alpha_1(v)_H$. In practice the influence of hydrogen will be important only if its atoms become neutral in appreciable quantities in regions where helium is yet ionized, a circumstance which seems unlikely. The transfer problem for helium may become more important than for hydrogen because of the large probability of recapture in the ground-level.

Oxygen offers an interesting application of the stratification theory. Lines of [OI], [OII], and [OIII] can all be observed in the gaseous nebulae, although the radiations usually observed are those of [OII] and [OIII]. Detailed illustrative applications are reserved for a later section, but we can mention here that in nebulae of fairly regular form and relatively low excitation the transition from [OIII] to [OII] takes place rather gradually.

2. The Forms of the Gaseous Nebulae

In this section we shall be concerned almost exclusively with the planetary nebulae. Despite their oft-times irregular and complicated appearance, most planetaries possess some suggestion of a symmetry that is entirely missing in the prominent diffuse nebulae. The latter often suggest random, unorganized masses of gas and small particles that have no more system of arrangement than do the clouds usually seen in the earth's atmosphere. The material which happens to be near sufficiently luminous hot stars is illuminated and caused to shine; that which is not so located may appear as dark lanes of obscuring matter (see Chapter VIII).

The shapes of the planetary nebulae, on the other hand, are often fairly symmetrical at least in the first approximation. Evidently they were formed by some ejection process involving the central star, although it seems likely that after the ejection ceased, the form of the nebula may have been appreciably modified by local radiation pressure and by other forces.

Regular forms such as IC 418, IC 4568, or IC 4406 appear to be relatively rare. Most nebulae have forms that cannot be interpreted in terms of simple elliptical, spherical, or cylindrical forms. Attempts have been made to classify them as ring, double-ring, amorphous, etc., forms, but Minkowski's photographs taken with the 200-in. telescope show the complexities to be such that more elaborate descriptions are necessary.

A detailed account of the observational data, illustrated by numerous photographs, will be found in Minkowski and Wilson's monograph on the planetary nebulae.⁽⁹⁾ In our present discussion we will refer to the isophotic contours of a number of the plates obtained at Palomar.

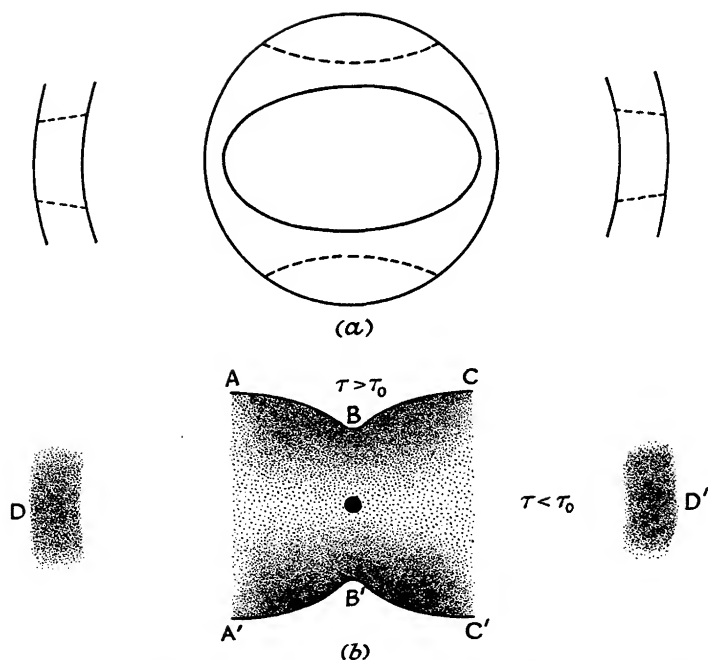
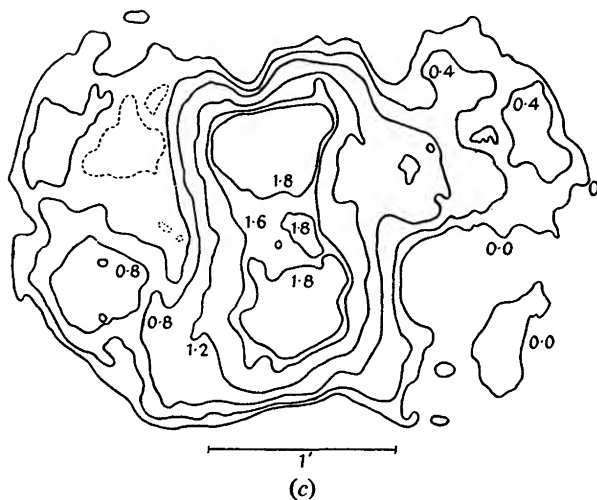


FIG. VII : 1. *The Structure of the Giant Planetary NGC 650-651 and Related Objects.*



(a) The idealized model for nebulae of this type consists of a roughly elliptical shell which is thinner in the equatorial plane than near the poles. There is also an outer envelope. The edge of the Strömgren ionization zone is denoted by the dotted line.

(b) Appearance of idealized model. The shaded area corresponds to the ionized region ($\tau < \tau_0$). The sharp boundary denotes the edge of the ionization zone ($\tau < \tau_0$). BB' denotes the axis of symmetry of the nebula. Along the lines ABC , $A'B'C'$ we see the edge of the ionization zone. At D and D' we see the edge of the ionized material itself.

(c) Isophotic contours of NGC 650-1 in the $[OIII]$ radiation. The contour lines correspond roughly to $\log I = 0.0, 0.4, 0.8, 1.2, 1.6$, and 1.8 . (Traced from plate PH 227M secured by R. Minkowski with the 200-in. telescope.)

Many planetaries show distinct effects of stratification. That is, the radiations of highly ionized atoms such as NeV , AlV are concentrated towards the central regions, $[OIII]$, $[NeIII]$, and H are found farther out, whereas $[OII]$ and $[SII]$ tend to have the largest images of all. We shall call attention to stratification effects in our discussions of the isophotic contours of slitless spectrograms of these objects (see Section 3).

Long exposures with the large reflectors show that some nebulae such as NGC 6543 and NGC 7662 have faint outer envelopes with a sharp limit. This faint limit may mark the extent of the actual nebular material or it may represent a shock front zone. The outer edges of luminous rings photographed with ordinary telescopes presumably mark the ends of the Strömgren ionization zones. If the structure of the nebula is filamentary some radiation may leak through tiny gaps in the material and produce a small amount of ionization in the surrounding shell of neutral gas.

A somewhat different situation appears to be presented by nebulae such as NGC 650-1, NGC 2346, and NGC 2371-2. Minkowski suggests that in portions of these objects we observe the edges of the Strömgren ionization regions, whereas in other portions we do not. The situation may be explained with the aid of Fig. 1 (*a*). Imagine that the nebular material was distributed in the form of an elliptical shell with a less dense outer envelope. We suppose that the elliptical shell was thicker and perhaps denser towards the poles than in the equatorial regions. Early in the expansion only the inner zones of the inner shell are ionized so that the nebula would appear as a ring-form structure. Later the equatorial zone would become so attenuated that radiation could penetrate it and excite the outer envelope. At the same time, the elliptical shell would still be so thick that the edge of the ionization zone indicated by the dotted line would lie well within its boundaries. A schematic representation of the appearance of a nebula such as NGC 650-1 is given in Fig. 1 (*b*). The shaded regions corresponding to $\tau < \tau_0$ (where τ_0 may be of the order of 5) are excited by the central star. The sharp boundary corresponds to the sudden depletion of the ionizing radiation. The isophotic contours of NGC 650-1 (Fig. 1 (*c*)) show the sharp falling-off of intensity on the edge of the ionization zone. NGC 650-1 shows condensations and spots that are enhanced on the $H\alpha$ and $[NII]$ photographs as compared with the $[OIII]$ photos.

The nebula NGC 650-1 cannot be symmetrical about the axis drawn through the central star and perpendicular to the longest diameter, nor is the latter axis an axis of symmetry. The surface brightness of the nebula is asymmetrically distributed so that it cannot be interpreted as an object with rotational symmetry.

A striking nebula that exhibits bilateral symmetry but defies any interpretation in terms of ejection hypotheses, rotation, etc., is the object

MHa 362 discovered by Minkowski in his *Ha* survey. In this general category one might also classify CD -29° 13998 which, on long exposures, resembles a bit of looped thread or a hysteresis loop. The isophotic contours (shown in Fig. 2) exhibit the symmetry characteristics in a semi-quantitative manner. Since the plates were not photometrically calibrated the intensities of the different contours are only approximate.

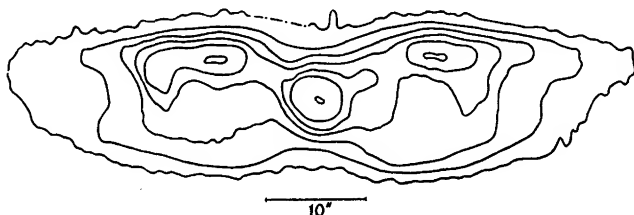
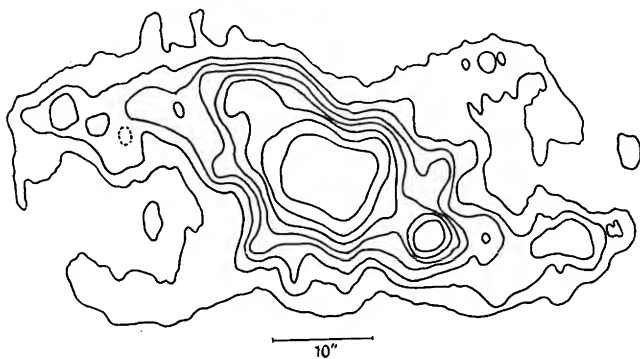


FIG. VII : 2.

(a) Isophotic contours of the planetary nebula, *MHa* 362, in the radiation of *Ha*+*[NII]*.

Notice the bright central condensation and the two wings which give the nebula the appearance of the type of emblem frequently seen at the top of a totem pole. Contours are traced at approximate $\log I$ values of 0.0, 0.4, 0.8, 1.0, 1.2, 1.4, and 1.6. The central star is at the centre of the nebula. (Traced from plate PH 182M secured by R. Minkowski.)



(b) Isophotic contours of CD -29° 13998 in the radiation of *Ha*+*[NII]*.

The brighter portions of this remarkable nebula show reverse S-shaped symmetry. The contours correspond roughly to steps of $\Delta \log I = 0.2$, i.e. a half-magnitude. (Traced from plate PH 187M secured by R. Minkowski.)

Neither of these objects are rotationally symmetrical.

The nebulosity associated with R Aquarii, NGC 6537, or Anon $19^{\text{h}}48^{\text{m}}12^{\text{s}} + 33^{\circ} 35.7'$ (1950), illustrate yet another kind of symmetry. Minkowski has suggested that the forms of these objects may be interpreted in terms

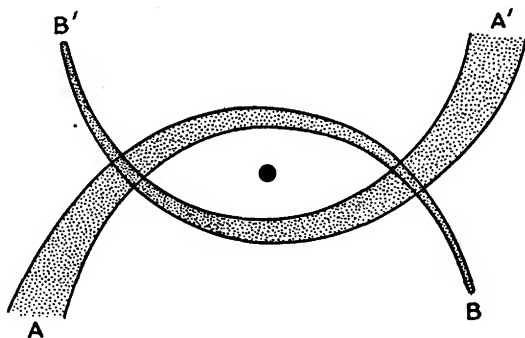
of a pair of looped filaments as indicated in Fig. 3 (b). Each filament AB or $A'B'$ is sharp at one end (B or B') and knotty at the other (A or A').

Many nebulae show extended filaments, spikes, or ansae. The classic example is NGC 7009, which shows two bright ansae at the ends of the major axis. The level of excitation is usually lower in the ansae than in the main body of the nebula. Thus for NGC 7009 the results given in Table VII:1 are found.⁽¹⁰⁾



FIG. VII:3.

(a) Isophotic contours of NGC 6537 in the radiation of $H\alpha$. Notice the four arms of the nebula and the rapid increase of brightness towards the centre. Contours are traced at approximate $\log I$ values of 9.8, 0.0, 0.3, 0.5, 0.7, 0.9, 1.1, 1.3, and 1.5. (Traced from plate PH 179M secured by R. Minkowski.)



(b) Possible schematic interpretation of nebulae such as NGC 6537 in terms of looped filaments.

TABLE VII : 1

Comparison of the Spectrum of the Main Body of NGC 7009 with that of Its Ansa

λ	Ion	Intensity		λ	Ion	Intensity	
		Main Body	Ansa			Main Body	Ansa
5007	[OIII]	96	106	4101	$H\delta$	2.5	2
5959	[OIII]	34	40	3967	[NeIII]	4.0	4
4861	$H\beta$	10	10	3889	$H\epsilon$	1.8	2
4686	HeII	1.4	0	3868	[NeIII]	8.0	11
4340	$H\gamma$	3.4	4	3727	[OII]	1.7	18

In each part of the nebula the intensities are referred to that of $H\beta$ as 10. Notice the great relative enhancement of [OII] λ 3727 and the disappearance of λ 4686 HeII in the ansae.

Features that we might refer to as ansae are often less symmetrically placed. For example, in NGC 7662 they appear as short spikes. The [OII] λ 3727 image in the Ring nebula, NGC 6720, shows pronounced tufts, whereas the [OIII] ring has merely a rough outer edge.

The filamentary structure characteristic of many planetary nebulae is probably better exhibited by photographs than by isophotic contours, although the latter give a better idea of the gradations in background intensity. The eye perceives sharp, small-scale intensity gradients, but tends to pass over slow intensity gradients.

Fig. 4 shows the isophotic contours of the low excitation planetary NGC 40 and of NGC 1501, which shows no stratification but exhibits on direct photographs an extremely filamentary appearance with twisted ring-like structures that range in size from less than one second of arc to about five seconds. Another example is the object numbered *MHa* 192; $\alpha=17^h18^m42^s$, $\delta=-38^\circ 26'$ (1950), in Minkowski's *Ha* survey. Short exposures show a splotch-ring structure with many delicate condensations. Longer exposures show a faint elliptical envelope covering the whole system.

NGC 6751 and 6905 are nebulae with Wolf-Rayet nuclei (see Fig. 3 of Chapter VI). The former shows an extremely mottled ring and considerably different appearance on the [OIII] and $H\alpha$ + [NII] photographs. The latter shows detailed structures similar to NGC 40, but the spectra of NGC 40 and of NGC 6905 are entirely dissimilar. Likewise, Merrill's planetary with the high-velocity Wolf-Rayet nuclear star shows an extremely irregular structure. At the other extreme is the Owl nebula, NGC 3587 (see Fig. 5). This object shows little evidence for stratification,

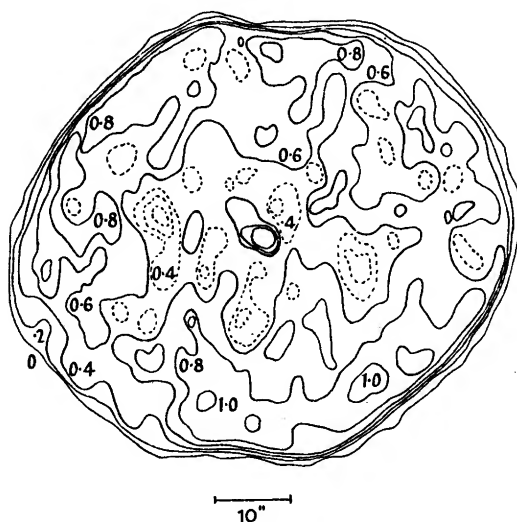


FIG. VII:4. *The Isophotic Contours of NGC 40 and NGC 1501.*

These planetaries exhibit a marked filamentary structure. Notice the large number of small knots and condensations. "Valleys" in the contour diagram are denoted by dotted lines. The position of the central star is indicated by a black dot. (Both plates, PH 21M and PH 121M, were secured by R. Minkowski.)

(a) NGC 40 in the radiation of $H\alpha$.

Notice the concentration of brightness at each end of the "minor axis". Contours are drawn at approximate $\log I$ values of 0.0, 0.3, 0.6, 0.75, 0.9, 1.0, 1.2, and 1.3.



(b) NGC 1501 in the $[OIII]$ radiation.

Notice the large number of deep "pits" in the contours and the abrupt decline in intensity at the edge of the nebula! Contours are drawn at $\log I$ values of 0.0, 0.2, 0.4, 0.6, 0.8, 1.0.

although the $H\alpha + [\text{NII}]$ ring may be a little larger and brighter. The striking feature of this nebula, however, is its perfectly smooth internal structure as photographed with the 200-in. telescope. Any fine structure in this nebula would require a scale of much less than $0.5''$.

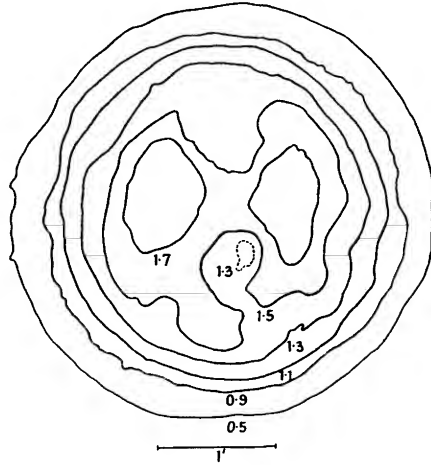


FIG. VII:5. *Isophotic Contours of the Owl Nebula, NGC 3587 in the $[\text{OIII}]$ Radiation.*

The surface brightness of this nebula declines smoothly towards the outer periphery. Each contour is labelled with its approximate $\log I$. Minkowski and the writer have discussed the structure of this nebula in *Ap. J.*, **120**, 261 (1954). (Traced from plate PH 49M secured by R. Minkowski.)

Minkowski emphasizes that the difficult phenomena to understand is not the filamentary structure of the large nebulae, but rather the smooth surface brightness of objects like the Owl nebula. At the dimensions, densities, and internal velocities of the planetaries, the Reynolds number is of the order of 10^7 to 10^8 , and all such objects should be turbulent structures.

The filamentary structure often differs from one type of ion to another. Sometimes the $[\text{NII}]$ radiations indicate much sharper features than do the $[\text{OIII}]$ images. The Dumbbell nebula in Vulpecula, NGC 6853, has an extremely mottled appearance. The outermost wisps are prominent and the nebula has somewhat of an hour-glass appearance in the $[\text{NII}] + H\alpha$ exposures, whereas the $[\text{OIII}]$ photographs show greatly enhanced narrow filaments. The largest planetary, NGC 7293, shows an extremely delicate structure of narrow thread-like filaments and small "hard" condensations.

Attention should be called to a number of ring planetaries of extremely low surface brightness. For example, Minkowski's planetary $\alpha = 16^{\text{h}}25^{\text{m}}39^{\text{s}}$,

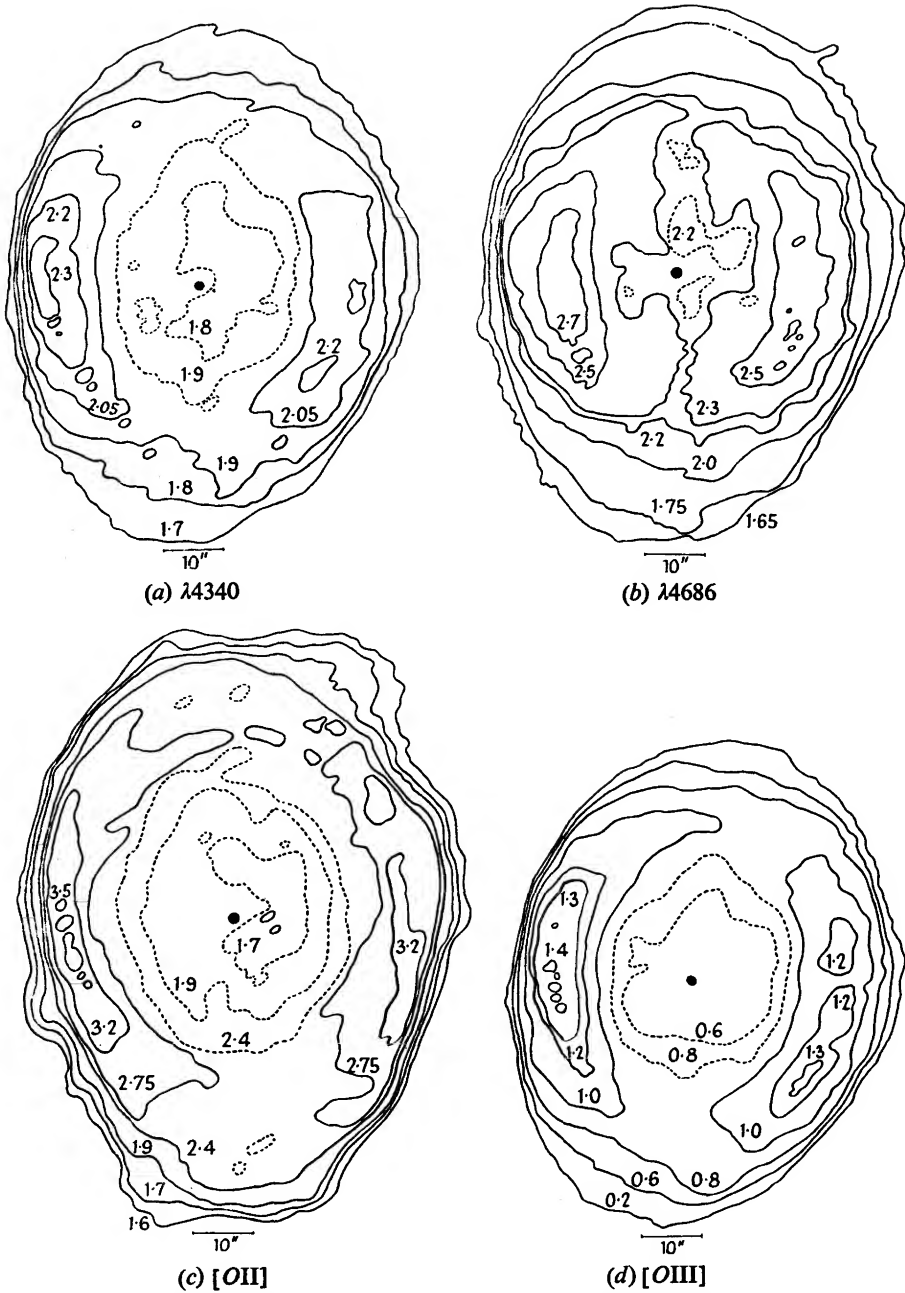


FIG. VII : 6. *Isophotic Contours of Various Images of the Ring Nebula, NGC 6720.*

For [OIII] we give the contours corresponding to approximate relative $\log I = 0.2, 0.6, 0.8, 1.0, 1.2, 1.3$, and 1.4 . For the other images it is possible to give only the plate densities corresponding to the various contours. The differences in size between the various images are well exhibited. The $\lambda 4686$ image is the smallest and the $\lambda 3727$ [OII] image very much the largest. Notice particularly the extremely low surface brightness at the centre of the 3727 image. (Traced from plates secured by R. Minkowski.)

$\delta = +28^\circ 5.4'$, has a sharp edge, but it cannot be a Strömgren sphere unless it is at an improbably high distance. The object $\alpha = 19^{\text{h}}4^{\text{m}}17^{\text{s}}$, $\delta = +6^\circ 19' 34''$ (1951), has a sharp outer boundary with a mottled ring inside, but a very low surface brightness.

The best-known planetary, NGC 6720, the Ring nebula in Lyra, shows an extremely interesting structure when photographed with the largest available scale and appropriate colour filters. The 3727 [OII] radiation gives the largest images. The [OIII] image is much smaller and the 4686 HeII image is the smallest of all. This nebula shows considerable complex structure in the rings with a maximum surface brightness at the ends of the minor axis. The distribution of intensity across the ring, however, is such that the [NeIII], [OII], and hydrogen emissions cannot be interpreted as even approximately uniform spherically symmetrical shells (see Fig. 6).

David S. Evans and A. D. Thackeray⁽¹¹⁾ carried out a photographic survey of the brighter southern planetaries with the Radcliffe reflector at Pretoria. Their observations are on a smaller plate scale, and do not include the filter-plate combinations necessary to isolate the various nebular lines. Nevertheless, a number of interesting objects have been described in their survey. They have classified their own objects and the ones photographed by H. D. Curtis⁽¹²⁾ on the basis of the nebular symmetry. They describe the various symmetrical forms as spherically symmetric such as the simple disk and ring, biaxially symmetric about two axes at right angles, centrally symmetric in which the structure is unchanged by reflection of each point of itself in the central star, and finally the helical form. To this they add what they call irregular nebulae which amounts to about 30% of the total. It is probable that when further photographic observations are made, the percentage of truly irregular objects will be greatly cut down.

One severe restriction placed upon the interpretation of the usual nebular photographs is that these often represent the composite effects of radiations of a number of different kinds of atoms in different stages of ionization. The picture obtained depends on the type of plate used, the reflectivity of the telescope mirror or the transmissivity of the objective, and the transparency of the atmosphere. The use of narrow band-pass filter combinations and special emulsions now available often permits nearly monochromatic photographs to be made. It is hoped that the southern planetaries can be rephotographed with plate-filter combinations similar to those used by Minkowski.

Among the southern nebulae must be mentioned the remarkable object IC 4406 which has been described by D. S. Evans,⁽¹³⁾ and whose shape and luminosity distribution has been interpreted by H. Zanstra and W. J. Brandenburg.⁽¹⁴⁾ The nebular image appears as a luminous band of nearly

constant width running approximately in the east-west direction, so it is rather sharply cut off on the north and south by two parallel, nearly straight lines. The east and west boundaries are rather vague. Zanstra and Brandenburg assumed that the luminous body of the nebula is restricted to a cylinder whose axis lies in the plane of the sky and whose radius is H (see Fig. 7). The positive axis of X points to the west, the Y -axis points to the south, and the Z -axis towards the observer. The central star is at O . It is supposed that within the small angle $d\Omega$, the nebula has a uniform emission/cm.³ for all values of r between $r=0$ and

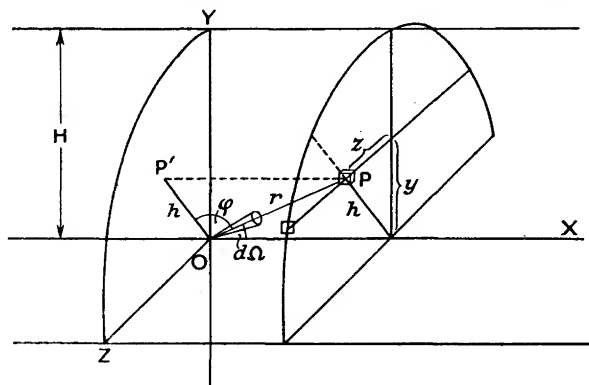


FIG. VII : 7. *Coordinate System chosen for the Interpretation of the Surface Brightness in IC 4406.*

It is assumed that the nebula is a cylinder whose axis lies in the plane of the sky. The X axis (axis of cylinder) and Y axis lie in the plane of the sky, while the Z axis points towards the observer. Here φ is the angle between the YZ plane and the radius vector.

(Courtesy H. Zanstra and W. J. Brandenburg, *Bull. Astr. Inst. Netherlands*, 11, 351, (1951).)

$r=R=H \sec \varphi$, where φ is the angle between the cone $d\Omega$ and the YZ plane, i.e. it is the angle between the radius vector drawn to the emitting point and the plane of symmetry of the nebula. The emission is proportional to $\cos^3 \varphi$. A comparison of the resulting isophotes with those obtained by Evans shows a fair amount of agreement, considering the simplicity of the model (see Fig. 8). The chief differences are that the theoretical isophotes are more closely spaced along the Y -axis (north-south directions) than are the observed isophotes, and that they show a more pronounced dent in the east and west direction. Possibly the amount of radiating material is greater in this direction. Conversely, it would be possible to invert the process by assuming cylindrical symmetry and deriving the emission per unit volume as a function of distance from the nebular axis.

One might suppose that IC 4406 could be taken as a model for ring nebula of the type described by Curtis in which the intensity inside the ring was too low as compared with the surface brightness in the ring.

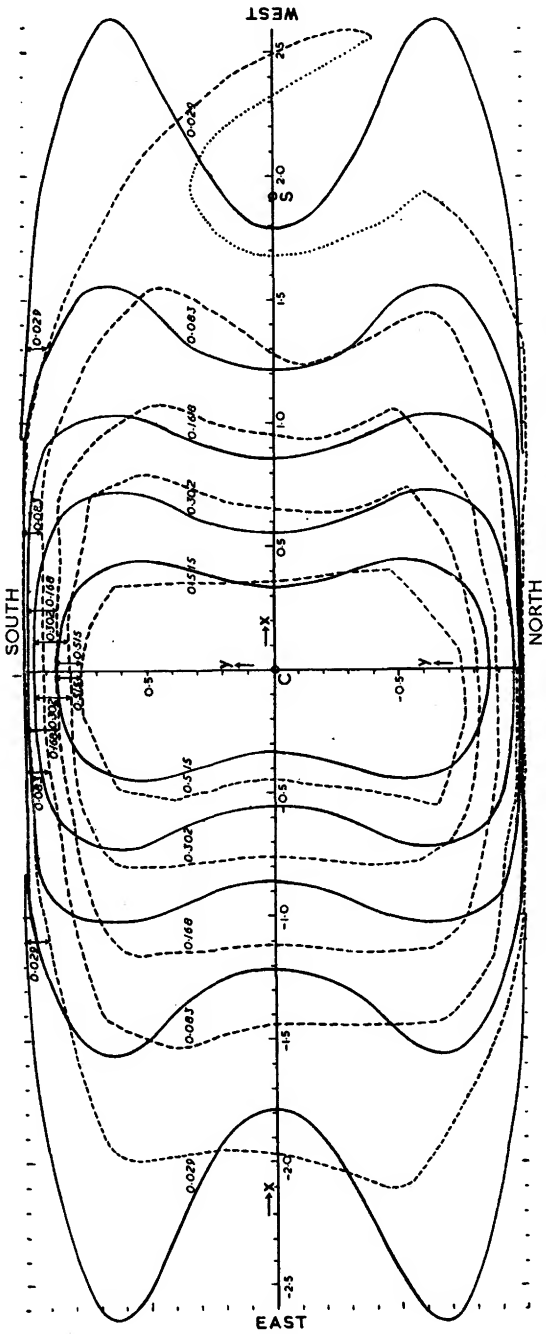


FIG. VII : 8. Comparison of the Isophotes for IC 4406 observed by Evans (dotted lines) with the Theoretical Isophotes of the Simple Model (solid lines). The intensities $I(X, Y)$ are expressed in terms of the central intensity as a unit. The unit of the scale is $17''.5$.

(Courtesy H. Zanstra and W. J. Brandenburgh, *Bull. Astr. Inst. Netherlands*.)

NGC 6720 is an example of such an object, and it has been suggested that a cylindrical form might account for the great brightness in the ring as compared with the centre in certain monochromatic images. The axis of the nebula would have to be pointed nearly in the direction of the observer. Zanstra and Brandenburg remind us that with a random distribution of axes in space we then should observe many nebulae similar to IC 4406, whereas only this one object is known. Adopting a distance of 1400 parsecs for the nebula, the radius of the cylinder is 24,000 astronomical units and its length is about 90,000 astronomical units.

3. Monochromatic Isophotic Contours of Planetary Nebulae

For a detailed understanding of the planetary nebulae it is necessary to have information on both the structure and the internal motions, i.e. the distribution of the radiating matter and its kinematics.

Qualitative descriptions based on direct photographs or slitless spectrograms are useful in a first reconnaissance of the problem but the construction of geometrical models for the nebulae requires quantitative data such as are provided by isophotic contours. The contours depicted in Figs. 1-6 were traced from certain of Minkowski's plates for which photometric standards were not available. Most of them involve emulsions and development conditions similar to those of his standardized plates, so we have been able to give the approximate intensities of the isophotic contours. In this section we shall describe some of the results obtained with photometrically calibrated Mt. Wilson and Palomar material and give interpretations in Sections 4 and 5. The pioneer work on isophotic contours for planetary nebulae was that by Louis Berman.⁽¹⁵⁾ He secured photometrically calibrated slitless spectrograms with the quartz slitless spectrograph on the Crossley reflector at the Lick Observatory. He then made successive tracings parallel to the dispersion across the monochromatic images. Each tracing gave a cross-section of each of the monochromatic images, and by combining successive tracings contour maps could be constructed. Berman measured plates of IC 4593, NGC 6543, 6572, 6826, 7009, 7027, and 7662, with particular emphasis upon NGC 6572. His isophotic contours show the relatively regular structure of NGC 6572, the complicated shells of NGC 7009, and the exceedingly intricate helical structure of NGC 6543 whose lack of symmetry makes a determination of its true structure difficult. He made no attempt to interpret the contours quantitatively in terms of the spatial distribution of the radiating matter, but he did determine the total relative intensities of the nebular images.

The determination of isophotic contours is beset with a number of difficulties. The finite size of the analysing beam of the microphotometer, the effects of bad seeing plus the inevitable guiding errors and the scattering

of light in the emulsion, all conspire to smear out the fine details in the nebular images. Finally, on slitless plates, the internal motions in the nebula tend to blur the nebular images by an amount depending on the velocity of the material along any given line of sight. Direct photographs secured with appropriate plate-filter combinations are very useful for the images of the strongest lines.

Some of these difficulties can be overcome by going to larger telescopes. Olin C. Wilson employed the coudé spectrograph of the 100-in. reflector in a slitless form. The equivalent focal length of the coudé arrangement is 250 ft., so that with a collimator of 290-cm. focus and a Schmidt camera of 81-cm. focus, a plate scale of $9.64''/\text{mm.}$ is obtained. This scale is about four times that of the spectrograph employed by Berman.

Many of Wilson's plates have been traced in the balanced-beam isophotometer. Objects of fairly symmetrical structure present no difficulty, but those characterized by numerous irregularities—such as NGC 2392, to mention an extreme example—require great care in tracing so that none of the “islands” and “valleys” are missed.

Typical isophotic contours based on calibrated direct photographs and slitless spectrograms are reproduced in Figs. 9, 10, 11, and 12. Among the simplest appearing nebulae is NGC 6572. Wilson's slitless spectrograms⁽¹⁶⁾ show the outer portions of this nebula to possess an amorphous structure. The nebula is not strictly elliptically symmetrical as earlier observations with smaller telescopes suggested. Nevertheless, the isophotes show a high degree of smoothness and regularity. $\text{MgI } \lambda 4571$ and $[\text{SII}]$ show a shell structure, whereas $\text{NIII } 4640$ and $[\text{AIV}] \lambda 4740$ apparently do not. The bright central star limits the study of the contours to the stronger lines since the weaker emissions are all blended with the spectrum of the nucleus. From tracings perpendicular to the dispersion direction Wilson and the writer have corrected the intensity distribution for the contribution from the central star and for the effects of seeing and guiding (see Section 4).

NGC 6210 also shows contours with the intensity decreasing monotonically outwards from the brightest part which, however, is not centrally located with respect to the central star or the system of contours (see Fig. 9). The extremely high excitation nebula NGC 6741 and the low excitation object IC 4593 show amorphous patterns similar to those of NGC 6210, but the bright central core appears double in the N_1 image of IC 4593 and in the $H\beta$, HeII , and $[\text{NeIII}]$ images of NGC 6741. Double cores appear in many nebulae. Fig. 10 illustrates the contours for NGC 2440. The outer portions of this nebula show an extremely complex structure.

Among the ring nebulae we may mention several examples. In Section 4

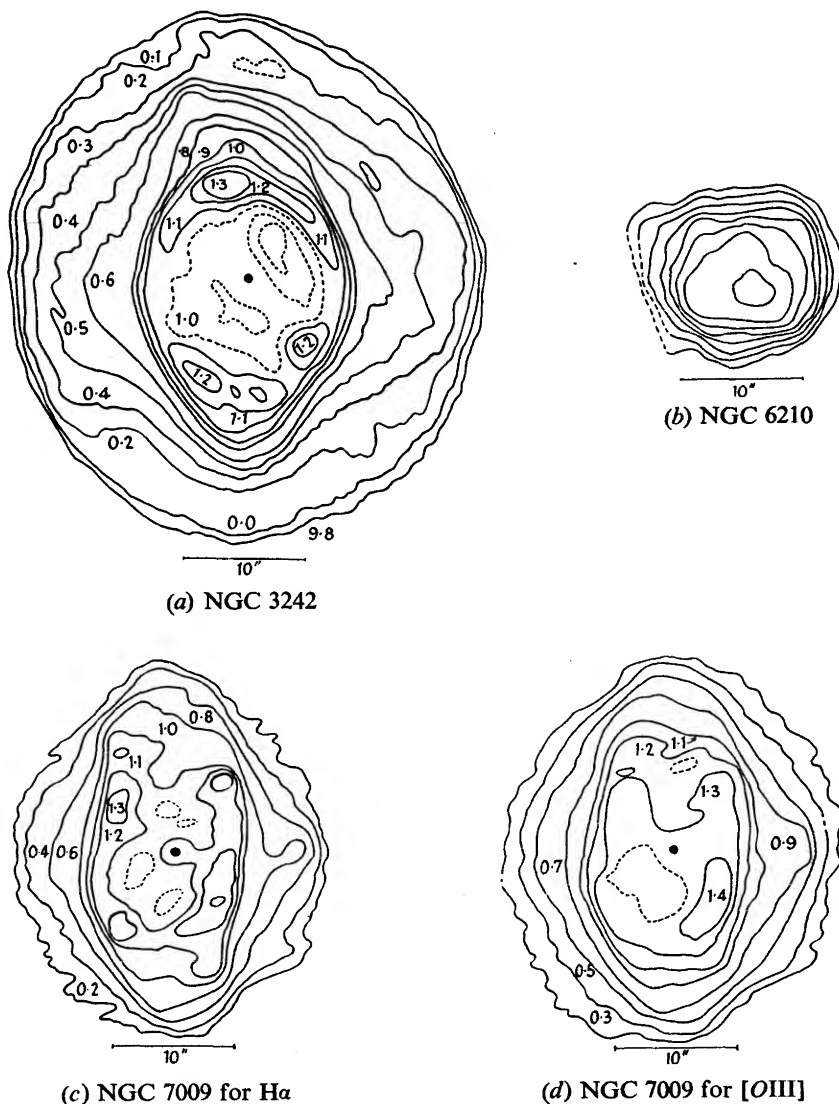


FIG. VII: 9. *Isophotic Contours of NGC 3242, NGC 6210, and NGC 7009.*

Minkowski obtained a photometric calibration for these images by using a fixed exposure time and different apertures.

(a) NGC 3242. Notice the sharp intensity decline at the edge of the inner ring and the low intensity of the central region. The contours are plotted at intervals of $\Delta \log I = 0.1$.

(b) NGC 6210 exhibits a monotonic decline in intensity outward from the centre. The values of $\log I$ are 9.9, 0.1, 0.3, 0.5, 0.7, 0.9, 1.1, 1.2, and 1.3. Contours of the [OIII] image are published in the author's *Astrophysics—Nuclear Transformations, Stellar Interiors, and Nebulae*, Ronald Press Co., New York, 1954, p. 199.

(c), (d) NGC 7009. Images for $H\alpha$ and [OIII] are depicted. The high ellipticity of the inner ring structure is well exhibited.

we shall describe the relatively regular structures IC 418 and IC 3568. Fig. 9 shows the isophotes of the $H\alpha$ images of the double-ring planetaries NGC 3242 and NGC 7009. Both of these objects display a relatively broken inner ring and a much fainter outer one. Contours of monochromatic images of NGC 7009 are reproduced in Chapter II, Fig. 10.

NGC 2440

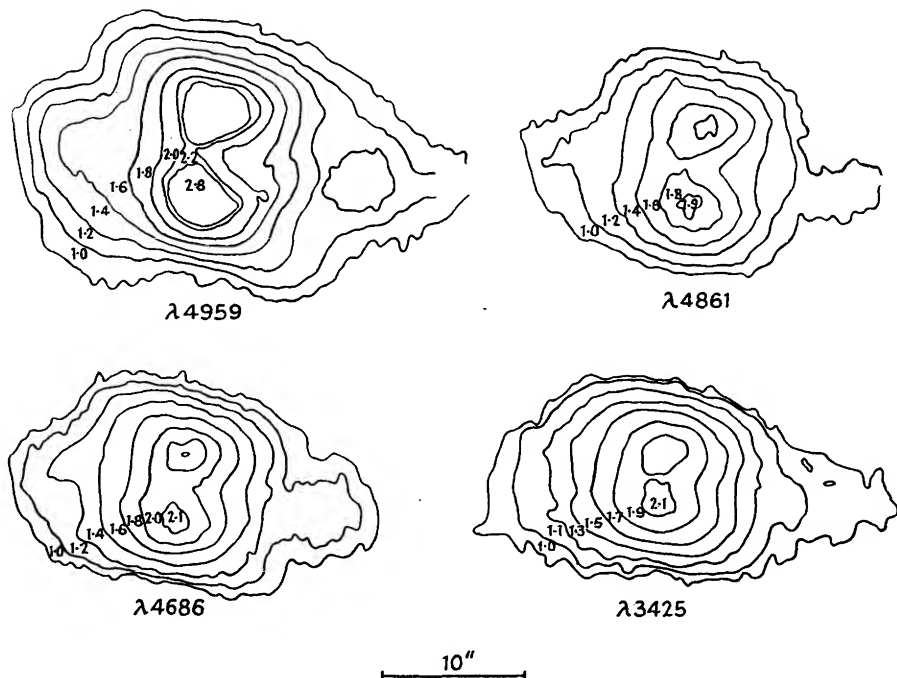


FIG. VII : 10. *Isophotic Contours of Monochromatic Images of NGC 2440.*

This planetary which resembles NGC 7027 in many respects has a double core or "condensation" and faint outer appendages. We depict the images for $\lambda 4959$ [OIII], $\lambda 4861$ $H\beta$, $\lambda 4686$ $HeII$, and $\lambda 3425$ [NeV]. The numbers on the contours give $\log I$.

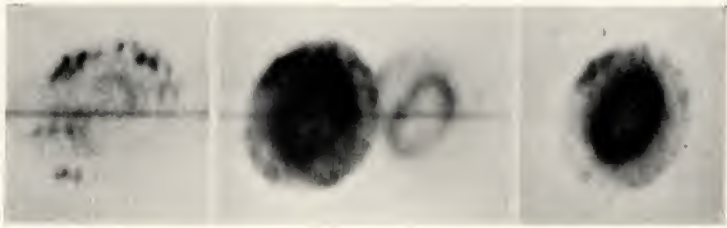
Compare also with NGC 650 which has a very much lower surface brightness.

(Traced from a slitless spectrogram secured by Olin C. Wilson with the coude spectrograph at the Mt. Wilson Observatory.)

Notice that the inner, brighter ring in NGC 7009 is elongated with the intensity minima along the major axis. The $HeII$ radiation is confined to the inner ring; the low excitation radiations extend to the ansae (cf. p. 244).

Detailed studies have been made of the Ring nebula in Andromeda NGC 7662. It consists of a bright, broken inner ring surrounded by a fainter, mottled outer ring. The contours for the radiations of [OIII], [NeIII], H , $HeII$, and $\lambda 3425$, [NeV] and $\lambda 3444$ [OIII] are illustrated in Fig. 11. Notice the striking similarity between the [OIII] and [NeIII] images. The irregular knots and condensations tend to be repeated from

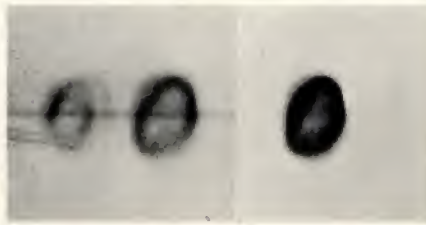
NGC 7662 (100").



$\lambda\lambda 3762, 29$ [OII]

$\lambda 3869$ [NeIII]

$H\beta$



$\lambda 3426$ [NeV], $\lambda 3444$ OIII

$\lambda 4686$ HeII

FIG. VII: 11 *Slitless Spectra and Isophotic Contours of NGC 7662.*

(a) The images for [OII], [NeIII], $H\beta$, $\lambda 3426$ [NeV], $\lambda 3444$ OIII, and $\lambda 4686$ HeII are reproduced from a slitless spectrogram secured by O. C. Wilson with the coudé spectrograph and 100-in. reflector.

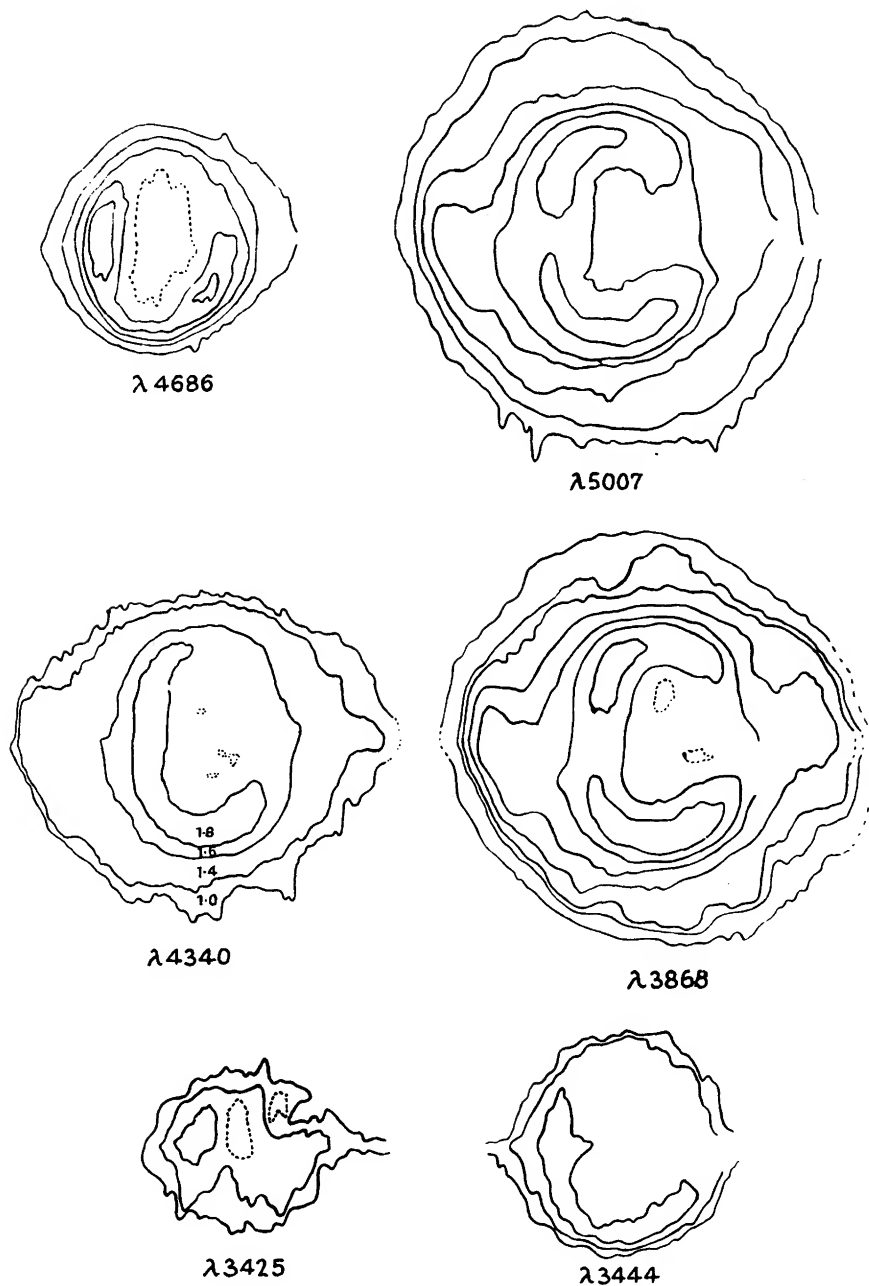


FIG. VII:11 (b)

The values of $\log I$ for the successive contours are as follows:

$\lambda 4686$ HeII 9.8, 0.2, 0.4, 0.5, 0.6.

$\lambda 5007$ [OIII] 0.1, 0.6, 0.9, 1.2, 1.3, 1.35.

$\lambda 4340$ H γ 1.0, 1.4, 1.6, 1.8.

$\lambda 3868$ [NeIII] 9.7, 0.1, 0.5, 0.7, 0.9, 1.1, 1.2.

$\lambda 3425$ [NeV] and 3444 OIII 0.0, 0.2, 0.4.

(Traced from a slitless spectrogram secured by O. C. Wilson with the 100-in. reflector.)

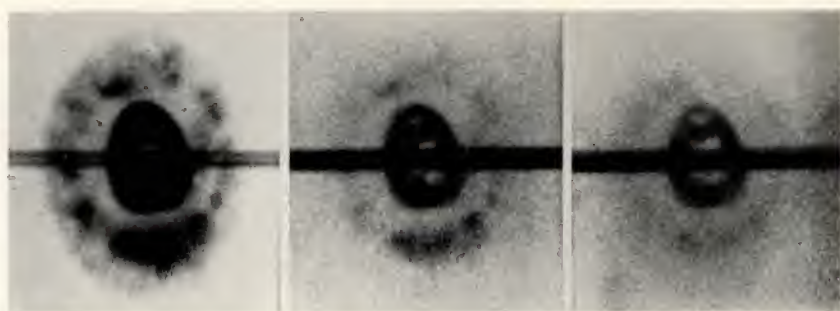
one image to the next; most of the irregularities in the outer contours of this nebula are real. The effects of plate grain, etc., are negligible in comparison. The zero point of the intensity in each image is arbitrary so the contours cannot be compared in detail. The inner ring in [OIII] and [NeIII] tends to have the appearance of a broken *C* with a saddle point on the minor axis. The hydrogen images do not show this saddle point, and the *HeII* and [NeV] images actually have a maximum of intensity here! The *HeII* radiation is missing completely from the outer ring. Olin Wilson observed not a trace of it in a three-night exposure with the coude spectrograph at the 100-in. The slitless data have been supplemented for this object by a direct photograph taken in the light of [OIII] by R. Minkowski with the Hale telescope. A comparison of the results shows that the distortion of the isophotic contours by the internal motions in the nebula is not great.

The most complex nebula for which isophotic contours have been measured is NGC 2392. This object has been classed as a double-ring structure, but a cursory examination shows that no simple shell can account for its complex features. The outer ring is very much fainter than the inner disk, as is well shown by the isophotes which crowd closely together at the edge of the inner disk (see Fig. 12). Notice the diminished surface brightness near the centre of the nebula. (Dotted lines are used to indicate "valley" contours.) The central star is very bright and distorts the contours along a line across the nebula. Notice that, in contrast to NGC 7662 where the *HeII* radiation was confined to the inner ring, the $\lambda 4686$ *HeII* radiation appears throughout the entire nebular structure. The pronounced filamentary structure of this nebula together with its complex internal motions place it among the most difficult objects for interpretation.

The isophotic contours have the advantage that they display the essential information of slitless spectrograms or direct photographs on a quantitative scale. They show, for example, that features that attract the eye are often no more than small perturbations on a flat background or steep intensity rise. On the other hand, they suffer from the limitations in seeing and guiding inherent in all direct photographs. In a few of the more symmetrical nebulae it is possible to trace the plates perpendicular to the dispersion and correct the intensity cross-sections for seeing and guiding errors. We shall illustrate these procedures for IC 418 and IC 3568.

4. Spatial Distribution of the Radiating Gases in Symmetrical Planetary

In Chapters IV and V we saw that formulae developed from theories of nebular line radiation almost invariably referred to the emission per unit volume at a certain point in the nebular shell. The observational data, on

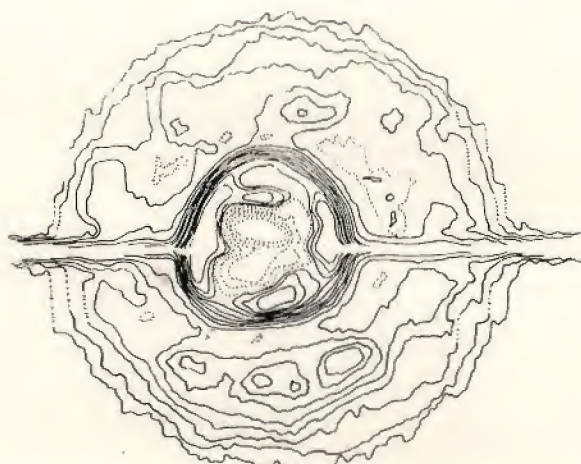


$\lambda 5007$ [OIII]

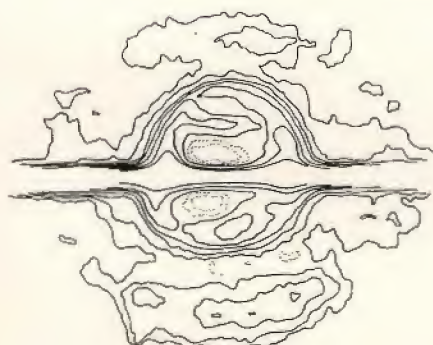
$H\beta$

$\lambda 4686$ HeII

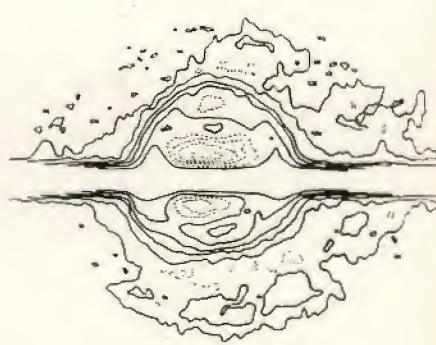
NGC 2392



$\lambda 5007$



$\lambda 4861$



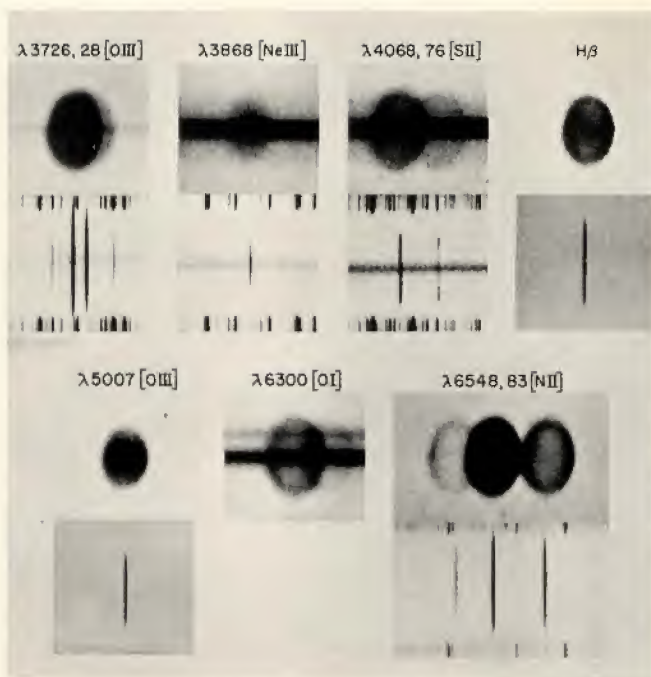
$\lambda 4686$

10"

FIG. VII: 12. *Slitless Spectrograms and Isophotic Contours of NGC 2392.*

(Top) The slitless spectrograms were secured by Olin C. Wilson with the coude spectrograph and 100-in. reflector. We reproduce the images for $\lambda 5007$ [OIII], $H\beta$, and $\lambda 4686$ HeII.

(Bottom) The contours for $\lambda 5007$ [OIII], $\lambda 4861$ $H\beta$, and $\lambda 4686$ HeII are traced in steps of $\Delta \log I = 0.1$.



IC 418

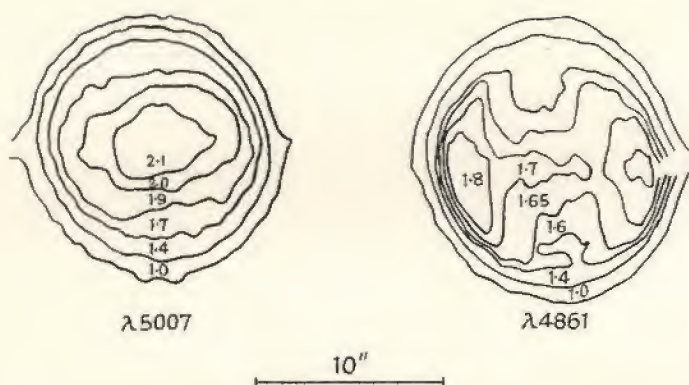


FIG. VII : 13. (Top) Slitless and Slit Spectra of various Images in IC 418.

These spectra were obtained by Olin C. Wilson with the coude spectrograph at the Mt. Wilson Observatory.

(Bottom) Isophotic Contours of the Image of [OIII] and $H\beta$.

Notice the concentration of intensity at the ends of the minor axis of the $\lambda 4861$ $H\beta$ image as though the density is greater in the polar regions and smaller in the equatorial plane. The surface brightness of the [OIII] radiation falls off monotonically away from the central star. The contours in these and in the images of certain other planetaries (e.g. NGC 2392) are distorted along a horizontal line passing through the centre by the effect of the continuous spectrum of the central star.

the other hand, consist at the best of isophotal contours of selected lines, the relative intensities (surface brightnesses) in the various radiations, and the average surface brightness of the [OIII] lines in nebulae where these radiations are strong. In nebulae of reasonably symmetrical structure it should be possible to estimate the emission per unit volume from the observed intensity distribution across the image. That is, on the assumption that the structure of the nebula, in the first approximation, can be represented as at least circularly symmetrical in a plane containing a line drawn across the nebula and the line drawn to the observer, the radial emission distribution may be derived.

Before describing the recent work on this problem some reference should be made to earlier attempts to obtain quantitative information on the nebular structures. Long ago, H. D. Curtis made qualitative comparisons between the nebular forms as observed by him on direct photographs secured with the Crossley reflector and various geometrical models of ellipsoidal shells, etc.⁽¹²⁾ He pointed out that uniform shell structures could not account for objects such as the Ring nebula in Lyra NGC 6720. W. K. Green's study of the structures of NGC 7009 and NGC 6543 was one of the earliest attempts at a quantitative investigation.⁽¹⁷⁾ He supplemented direct photographs taken with the Crossley reflector by radial velocity studies made with the 36-in. refractor and Mills's spectrograph. Green derived the variation of intensity across the nebular images in different position angles and compared them with theoretical intensity curves of ellipsoidal shells of gas. He tried to represent his radial velocity and photometric observations with a model nebula made of several shells of rotating gases.

In 1919, Reynolds⁽¹⁸⁾ photographed the Dumbbell nebula in Vulpecula on orthochromatic and ordinary plates and measured the intensity variations across the nebula in several position angles. Vorontsov-Velyaminov and Mrs. Cramer⁽¹⁹⁾ later concluded that this object was so complicated that it could not be interpreted by means of any unique theoretical model. Subsequent observations with large telescopes have tended to substantiate these conclusions.

Vorontsov-Velyaminov tried to study the structure of NGC 6720 on direct photographs taken at Simeis.⁽²⁰⁾ In view of the marked structural differences between the *HeII*, *H*, [OIII], and [OII] images in this nebula (cf. Fig. 6) little significance can be assigned to his quantitative results. He found that although the nebula does have a certain equatorial symmetry, the density must depend on the three spatial coordinates. For a study of NGC 6572⁽²¹⁾ he used Berman's isophotes of the monochromatic images and estimated the density variation of the radiating material by a method similar to that given by von Zeipel⁽²²⁾ and by Plummer⁽²³⁾ for the

evaluation of the spatial density of the stars in a spherical star cluster.⁽²⁴⁾

O. C. Wilson and the writer⁽²⁵⁾ have carried out a detailed analysis for the small, low excitation, planetary IC 418. Fig. 13 shows the isophotic contours of two of the principal nebular lines, NI and $H\beta$. The bright central star produces complications in the interpretation of the contours so that the actual analyses have to be carried out from microphotometer tracings made across the nebular images. The $[NII]$ and $[OII]$ images give the appearance of hollow shells. The $[OIII]$ image shows a concentration towards the central star as does (to a lesser degree) the hydrogen image. The outer ring in H , $[OII]$, and $[NII]$ has a minimum intensity along the major axis and a maximum intensity at the minor axis. The distribution of $[SII]$ is similar to that of $[OII]$, whereas that of $[NeIII]$ is similar to that of $[OIII]$. In order to secure data for both weak and strong images Wilson obtained a graded series of exposures made with the 100-in. coude spectrograph in the slitless form. The plates were traced in the microphotometer perpendicular to the dispersion; runs were made across the nebular images and also across the star spectrum close to the nebular image in order that the contribution of the starlight could be subtracted from the reduced tracing of the nebula.

Furthermore, the effects of seeing, guiding errors, and turbidity in the photographic emulsion blur the nuclear star spectrum into a fuzzy line of finite width, and likewise soften the features of the nebular image. Let us denote the relative intensity distribution along a line drawn perpendicular to the spectrographic dispersion in the broadened nuclear star spectrum by $K(S)$, where S is the distance from the centre of the image. Then, if the observed intensity distribution across a monochromatic nebular image after subtraction of the light of the central star be denoted by $I_0(x)$, while $I(x)$ denotes the true intensity distribution, we have

$$I_0(x) = \int_{-\infty}^{+\infty} K(y-x)I(y)dy. \quad (25)$$

The "diffusing function" K appears as the kernel of the integral equation. It must be normalized such that

$$\int_{-\infty}^{+\infty} I_0(x)dx = \int_{-\infty}^{+\infty} I(y)dy. \quad (26)$$

The problem of correcting the observed intensity distribution for the effects of guiding, seeing, and photographic turbidity is similar to that of correcting an observed frequency function for observational error, or an absorption line profile for the finite resolution of the spectrograph. In each instance the kernel K must be a known function, $I_0(x)$ is observed and the problem is to find $I(x)$.

Equation (25) must be solved by successive approximations.⁽²⁶⁾ If the kernel is narrow compared with the intensity variations across the nebula, the first approximation to the solution will often suffice. If the K function is broad, the solution may not converge at all and the fine details of the nebular structure certainly will be lost.

To obtain a first approximation to the solution of equation (25) we substitute I_0 for I under the integral, and solve the equation for a fictitious I_0 which we call I_0' . Then we form the difference $I_0(x) - I_0'(x)$ and add it to $I_0(x)$. This first approximation to $I(x)$ then may be checked by substituting it under the integral sign in equation (25) and comparing the predicted and observed $I_0(x)$. If the (seeing+guiding) kernel $K(s)$ is narrow the process will give reasonably satisfactory results (see Fig. 2 of Reference 25).

The most serious approximation is made in the next step of the analysis. This is the assumption that in the plane containing the observer and the direction of the tracing the emission in the nebula depends only on r , the distance from the central star. Actually this degree of symmetry does not really exist since $I(x) \neq I(-x)$, $x=0$ being the position of the central star. The two sides are sufficiently alike, however, to allow a mean curve to be drawn to represent the average radial intensity distribution. Subsequent measures along the minor (y) axis in $H\alpha$ and $[NII]$ slitless spectrogram images show a symmetrical structure, but although $I(y) \sim I(-y)$, $I(y) \neq I(x)$ in any approximation. Let us first consider the analysis of the major axis data.

Once suitable mean values of $I(x)$ have been chosen, the hypothesis of symmetry is invoked to obtain the relative emission/cm.³, $E(r)$. If the nebula is spherically symmetrical, the contribution to $I(x)$ by a volume of unit cross-section and length dz along the line of sight will be

$$E(r)dz = \frac{E(r)rdr}{\sqrt{r^2 - x^2}}. \quad (27)$$

The sum of all these contributions to the intensity $I(x)$ at x is thus found to be

$$I(x) = 2 \int_x^\infty \frac{E(r)rdr}{\sqrt{r^2 - x^2}}. \quad (28)$$

This integral equation was first formally solved by Abel. The solution

$$E(r) = -\frac{1}{\pi} \frac{\partial}{\partial r} \int_r^\infty \frac{I(w)dw}{\sqrt{w-r}}, \quad (29)$$

involves a differentiation of the observed $I(x)$. Now $I(x)$ involves the averaging of the intensity distribution from both sides of the nebula. Furthermore, it is affected by the inherent observational errors. Differentiation of this necessarily inexact observational function leads to yet larger

errors in the derived function; hence the computed $E(r)$ has much less accuracy than even the initial $I(x)$. Hence, a fairly large "range of solution" must exist in any $E(r)$ derived from equation (29).

In their treatment of a mathematically similar problem, the distribution of the true rotational velocities of the stars, Chandrasekhar and Münch⁽²⁷⁾ suggested that one assumes for $E(r)$ a plausible analytic function with adjustable parameters. The parameters are then found from the moments of the initial function $I(x)$. For shell nebulae, one might assume a function of the form

$$E(r) = Ar^a e^{-br}, \quad . \quad . \quad . \quad (30)$$

and evaluate the constants A , a , and b from the moments. In practice the representation of the IC 418 data by a formula of the type (30) was unsatisfactory. The sharp cut-off at the outer edge of the shell would have required additional terms. It appeared to be better to follow the method suggested by A. Wallenquist for the determination of the radial distribution of stars in a spherical cluster from star counts made in concentric rings around the centre.⁽²⁸⁾ We imagine that the nebula is composed of n concentric shells, each of constant luminosity $E(r)/\text{cm}^3$ or density of emission $d_1, d_2 \dots d_n$ and suitably chosen outer radii $r_1, r_2, r_3, \dots r_n$. The observed intensities, $I(x_1), I(x_2) \dots$, etc., measured at preassigned points in the nebula, $x_1, x_2, x_3 \dots$ may be expressed in terms of $d_1, d_2, d_3 \dots d_n$ by equations of the form

$$\left. \begin{aligned} I(x_1) &= a_{11}d_1 + a_{12}d_2 + \dots + a_{1n}d_n, \\ I(x_2) &= a_{22}d_2 + a_{23}d_3 + \dots + a_{2n}d_n, \end{aligned} \right\} \quad . \quad (31)$$

where the a 's are determined by purely geometrical considerations. The equations (31) are solved readily for the d 's in terms of the I 's, viz.

$$\left. \begin{aligned} d_1 &= b_{11}I(x_1) + b_{12}I(x_2) + \dots + b_{1n}I(x_n), \\ d_2 &= b_{22}I(x_2) + \dots + b_{2n}I(x_n), \text{ etc.}, \end{aligned} \right\} \quad . \quad (32)$$

where the numerical coefficients $b_{11} \dots b_{nn}$ which are derived from the a 's have been tabulated by Wallenquist. Some of the b 's are positive, some are negative, so that for a given d_j some of the $I(x)$'s enter in a positive and some enter in a negative way. Thus, in the calculation of $E(r)$ by the Wallenquist method, a histogram for $E(r)$ is obtained from an adopted $I(x)$ curve. As in other methods, the uncertainties in $I(x)$ are enhanced in the computed $E(r)$ values. A necessary, but not sufficient, condition that must be fulfilled is that the derived $E(r)$ functions when substituted in equation (28) reproduce the observed $I(x)$ to within the uncertainties of the observations. The $E(r)$ values are usually expressed on a relative scale.

Wilson and the writer adopted Berman's distance estimate of IC 418,⁽²⁹⁾ and took the relative intensities of the nebular lines from previous

published investigations.⁽³⁰⁾ The electron density could be fixed from the surface brightness in the Balmer continuum and the assumed size of the nebula. Unfortunately, the then available measurements of the surface brightness were poor. The radius of the central star was taken as three times that of the sun, and its temperature was adopted as 30,000° K. Finally, rough estimates of the target areas for collisional excitation permitted the $E(r)$ values to be converted to densities of individual ions.

Subsequently, direct photographs taken by Minkowski with the 200-in. and coudé spectrograms of the $H\alpha$ and [NII] images with a camera of longer focal length have permitted an improved determination of the intensity distribution across the images and more reliable $E(r)$ functions. Fig. 14 (*a-d*) summarizes the results for $H\alpha$ and [NII]. The $E(r)$ values for the major and minor axis naturally do not agree at the centre, because of the asymmetry of the nebular ring which is brighter along the minor axis than it is along the major axis (cf. Fig. 13). The photometric measures, corrected as far as possible for the influence of the central star and for the blurring effects of poor guiding and scintillation, confirm the hollow shell appearance of the [NII] lines and [OII], but they do suggest that the emission per unit volume of the radiations of [OIII], [NeIII], and also H have a small increase towards the centre of the nebulae.

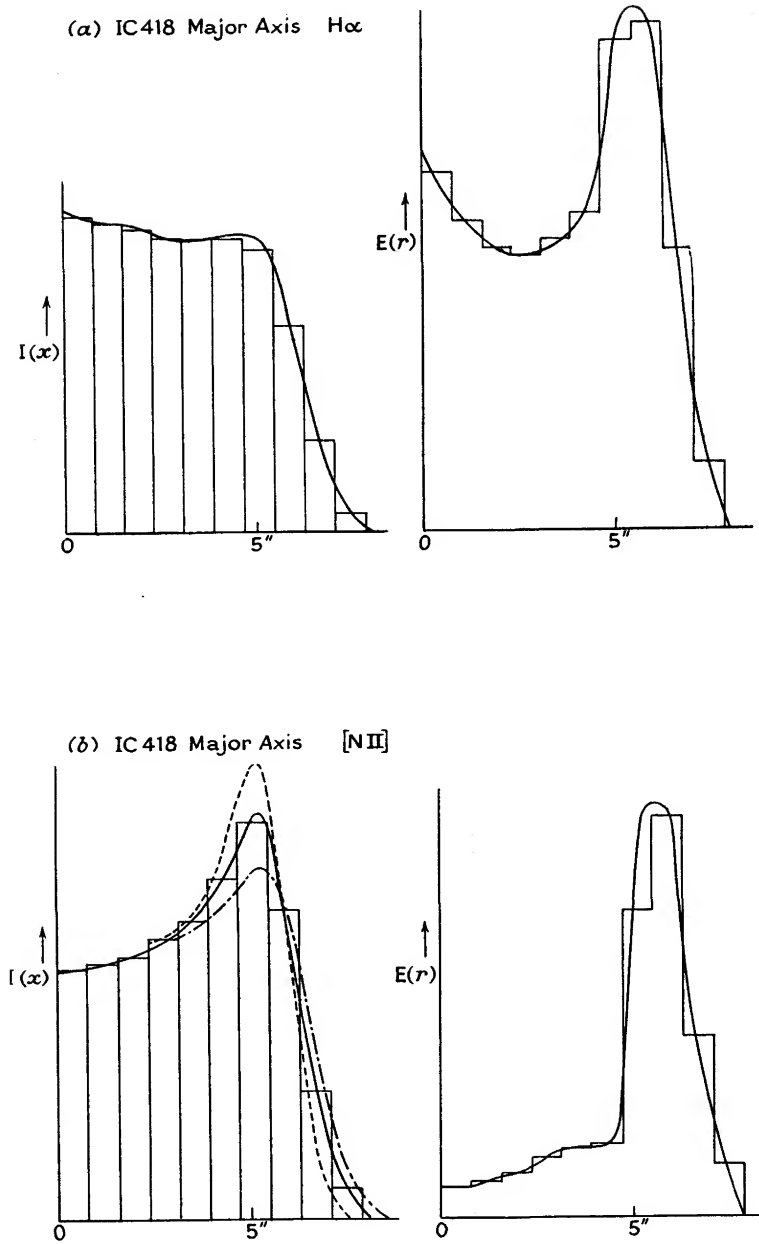
Although the Strömgren theory permits the radius of the shell to be accounted for with plausible values of N_e , T_e , and radius and temperature of the central star, we must emphasize that the determination of N_e is independent of any assumption concerning the completeness of the absorption of quanta in the Lyman continuum. The edge of the nebula does not appear to be as sharp as the Strömgren theory would demand, although inhomogeneities in the shell might "soften" the edge. The luminous body of IC 418 may be a Strömgren sphere, but we have no proof that it is!

Nevertheless, it is of interest to apply the ionization theory to other elements, e.g. oxygen and nitrogen. The ionized nitrogen is concentrated in the outer shell, and we suppose that it is ionized to NIII in the inner regions. Let us adopt the distribution of hydrogen from the $E(r)$ function for $H\alpha$ with $T_e=20,000^\circ\text{K.}$, assume the ratio of H/N to be 6000 and suppose this ratio to be constant throughout the nebula. The relevant equations for the Strömgren theory are then

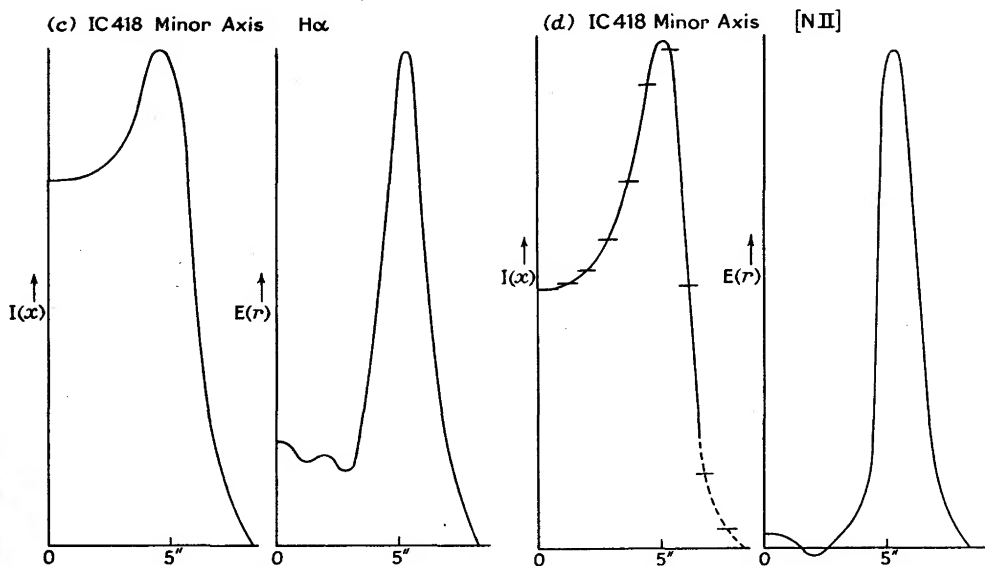
$$dz = \frac{N^2(s)}{6000} \frac{a_n}{C_1} s^{23.08} \times 10^{18} ds,$$

$$\frac{1-x}{x} = \frac{Ns^2}{C_1} \frac{1}{y}, \quad \frac{dy}{dz} = -x, \quad y = e^{-\tau}, \quad (33)$$

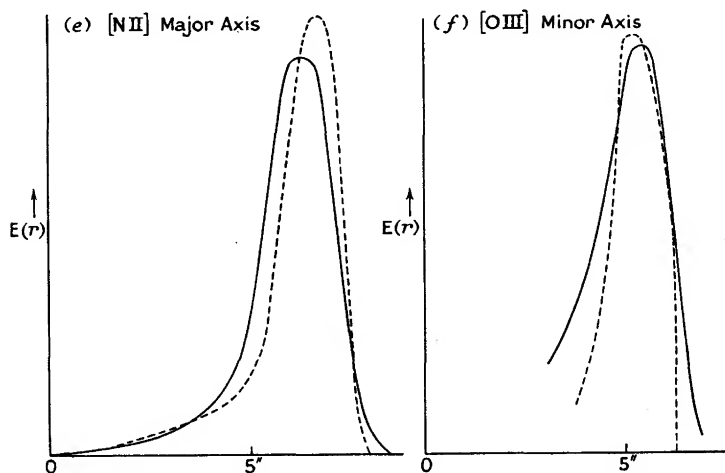
C_1 is defined for ionized nitrogen by an equation analagous to (11) while at $s=0$, $x=1=-dy/dz$. With the previously adopted N_e , the integrations



(a), (b) The intensity distribution $I(x)$ and the emission per unit volume $E(r)$ along the major axis in $H\alpha$ and $[NII]$. Smooth curves are drawn through the histograms. In the $I(x)$ curve for $[NII]$ the dashed and dot-dash curves show the results for opposite sides of the nebula. In the absence of spherical symmetry the results can be taken as of only qualitative significance.



(c), (d) $I(x)$ and $E(r)$ along the minor axis. Notice that although the $[NII]$ radiation exhibits a hollow shell, there is some indication of a slight rise of $E(r)$ towards the centre of the nebula in $H\alpha$.



(e) The emission function $E(r)$ for $[NII]$ (solid curve) is compared with the predicted concentration of N^+ ions along the major axis (dotted curve). It is assumed that the N/H ratio is constant throughout the nebula.

(f) The emission function $E(r)$ for $[OIII]$ (solid curve) is compared with the predicted concentration of O^{++} ions along the minor axis (dotted curves). The data of (f) are derived from a direct photograph by Minkowski; no information is available for the inner parts of the shell.

are carried out in the usual way. Here $a_n = 6.5 \times 10^{-18}$ and $I = 29.49$ e.v. The results of the calculation confirm our expectations that nitrogen is doubly ionized in the inner shell, and the predicted shape of the N^+ distribution agrees with the $[NII]$ emission function to within the error of observations (see Fig. 14 (e)).

In the radiation of $[OIII]$ the outer ring is visible at the extremities of the minor axis, but along the major axis the intensity simply declines monotonically (see Fig. 13). Similar calculations suggest that along the major axis the concentration of O^{++} may decline until in the region of the outer ring most of the oxygen exists as O^+ . Along the minor axis O^{++} prevails through the outer shell (see Fig. 14 (f)).

Application of these considerations to *SII* shows that sulphur is doubly ionized throughout most of the nebula. A small amount of *SII* appears in the region of the outer ring.

These calculations must be regarded as of an essentially qualitative nature because the influence of the energy distribution in the ultra-violet spectrum of the central star, the transfer problem in the radiation, and the mutual influences of the various continua are all neglected. Nevertheless, they do suggest that the elements are well mixed and that an understanding of the nebular images in terms of ionization stratification is possible for at least some of the most symmetrical nebulae.

Perhaps the most symmetrical planetary known is II 3568. This nebula cannot be observed with the 100-in. coudé, and our data consist of tracings of direct photographs taken by Minkowski with filters to isolate the $[OIII]$ and the $H\alpha$ radiations. Fig. 15 shows the intensity distribution across the nebula in the $H\alpha$ and $[OIII]$ images and the corresponding emission per unit volume. The emission near the central star cannot be determined very well because the stellar image is over-exposed. Hence the intensity distribution in only the outer part of the nebula can be measured reliably. II 3568 appears to consist of two concentric shells: an inner shell of relatively high density and an outer thin shell. Oxygen is almost completely doubly ionized in this nebula, the $[OII]$ image is very weak, even in the outer shell! For the same reason the nitrogen does not exist in observable quantities as N^+ ; M. L. White did not find the $[NII]$ lines in this object.⁽³¹⁾

Attempts to analyse nebular structure in terms of spherically symmetric models often run into severe difficulties. If such an assumption is made for many ring-shaped nebulae, regions of negative emission (absorption) are required to obtain a formal solution. Since this situation is physically impossible, the hypothesis of spherical symmetry must be abandoned.

Fortunately, assistance comes from another type of observation. If the spectrum is photographed with Wilson's multi-slit, a record of the radial

velocities in a series of parallel strips across the nebular image may be obtained (see Chapter II). In objects such as NGC 7662 the spectral lines are split in the inner region of the image and the approaching and receding

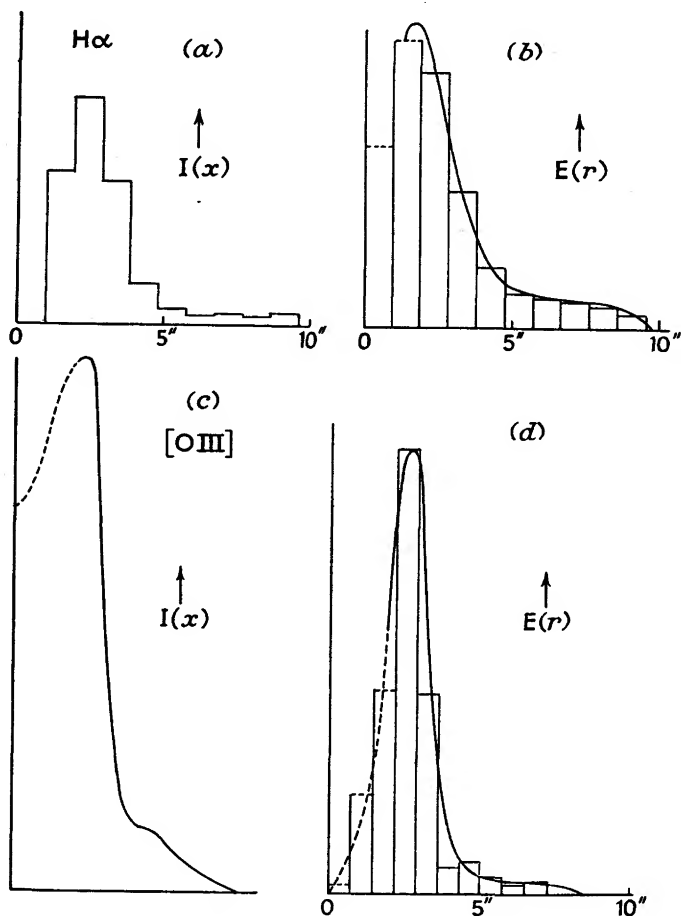


FIG. VII:15. Distribution of the H α and [OIII] Radiations in IC 3568.

- (a) $I(x)$ for H α . (b) $E(r)$ for H α .
 (c) $I(x)$ for [OIII]. (d) $E(r)$ for [OIII].

The scale of the ordinates of the figures can be established when the surface brightness and distance of this planetary are known. The nebula possesses a bright inner shell and a much fainter outer one. (Traced from a plate secured by R. Minowski with the 200-in. reflector.)

components are often clearly separated. Since the nebular shell is expanding, the red component is to be attributed to the far side of the shell, the violet component to the near side of the shell. Measurement of the separation of the components gives the rate of expansion of the shell, measurement

of the relative intensities of the components gives the relative emissions in the two sides of the shells. From a judicious combination of the isophotic contours and the radial velocity data, three-dimensional models of some planetaries may be constructed.

The results for NGC 7662 show that the bright inner ring (as well as the fainter outer one) has a variable thickness in the line of sight as well as perpendicular thereto. The smooth-shell approximation is extremely poor.

As a consequence of internal motion, the slitless images of some nebulae are to some degree blurred and distorted. A detailed comparison of the isophotic contours for the [OIII] images of NGC 7662 derived from both direct photographs and slitless spectrograms show that for this nebula, in which internal velocities of moderate magnitudes are observed, the effect is not pronounced. As previously mentioned, the effects might be large in NGC 2392, which has the largest internal motions of any planetary.

5. The Internal Motions in the Planetary Nebulae

At best, analyses of isophotic contours of monochromatic images of planetary nebulae can give us a rough idea of the distribution of the radiating gases. They tell us nothing about the kinematics of the nebular material. Is the nebula expanding, contracting, or rotating; are the gases in equilibrium or are they moving in turbulent currents?

The first thorough observational study of the internal motions of planetary nebulae was that undertaken by Campbell and Moore, who observed all the large and bright planetaries accessible to northern workers.⁽³²⁾ From a study of forty-three planetaries with the highest dispersions available to them, they found twenty-three objects which showed evidence of relative velocities, seventeen of which showed no such evidence and three for which evidence was suspected. Of the twenty-three showing internal motions, twenty-one were elliptical or elongated and only two were smaller than 5" in diameter. In nineteen of the twenty-three planetaries showing evidence of relative motion of one part of the nebula with respect to another, the observed motions could be interpreted as due to a rotation of the nebula about an axis coinciding with the shorter axis of figure. In four nebulae, particularly NGC 2392, Campbell and Moore remarked that the forms and inclinations of the lines do not admit a simple rotational interpretation.

Apparently Campbell and Moore did not consider the expansion hypothesis very seriously at this time, although they were well aware of certain of the difficulties of the rotational hypothesis.

The observations of Campbell and Moore showed that in many nebulae the lines were not monochromatic but were broadened, split, distorted, or twisted in appearance. The shapes of the lines are well illustrated in

Moore's drawings made to show the appearance of the lines on the Lick spectrograms. In view of the widespread occurrence of broadened and doubled lines in many nebulae, it is difficult to see how a rotational hypothesis could be entertained. A rotating shell of gas would present tilted lines on a spectrogram, and there would be no preferential broadening and splitting near the centre of the image. In NGC 7662 the $HeII\ 24686$ line was later observed to be a mirror image of the $[OIII]$ lines. On the rotational hypothesis this result would imply opposite rotations for the $[OIII]$ and $HeII$ shells!

Subsequently, Perrine⁽³³⁾ suggested that the doubling and distortion of the spectral lines was to be attributed to an expansion of the nebular shell, but the most convincing arguments in favour of the expansion hypothesis were those given by Zanstra.⁽³⁴⁾ He pointed out that the dark central portions of the nebular lines could not possibly arise from self-reversal as these are forbidden lines for which the transition probabilities are very low. On the other hand, the Balmer lines cannot show self-reversal because the population of the second level is very low.

The observed doublings and line shapes observed by Campbell and Moore are easily explained by an expansion hypothesis. Irregularities in the line forms are to be expected if different amounts of material were initially ejected in different directions. Furthermore, the expansion of a non-uniform shell can give the illusion of a rotational type of motion. The plausibility of the expansion hypothesis is further strengthened by a comparison of the expansion velocities with the velocity of escape. Using the expansion velocities estimated from the data of Campbell and Moore, and estimates of distance based on his own studies, Zanstra found the velocity of expansion to be much greater than the velocity of escape, even if we suppose the planetary nuclei to have masses as great as 100 times that of the sun.

The observations of Campbell and Moore thus indicated that the nebular shells were not in equilibrium but were slowly expanding. The interpretation of doubled, broadened, and distorted spectral lines in terms of an expanding shell leads to a consistent picture, whereas the rotational hypothesis encounters a number of severe difficulties. The expansion of the nebular shell is non-uniform, the irregularities, distortion, and mottling of the spectral lines all indicating large-scale motions which we usually associate with the term turbulence. These velocity irregularities appeared to be correlated with the appearance of the nebulae in the sense that those objects that appeared simple on direct photographs tended to have narrow, relatively unbroadened lines, whereas those that had a complex structure (e.g. NGC 2392) showed marked effects of turbulence.

The detection of internal motions in planetaries from a comparison of

direct photographs separated by many years eventually might be possible for a few planetaries, particularly NGC 2392. Such studies have been carried out for the Crab nebula, which is not a planetary but an ex-supernova.⁽³⁵⁾ Koslov tried to measure the internal motions in NGC 6543 from plates taken at the Moscow Observatory in 1904 and 1931, but his results appear to be inconclusive.⁽³⁶⁾ It is probable that many years will elapse before an actual expansion will be found in any of these objects.

The studies of Campbell and Moore were limited to the green nebular lines and $H\beta$. Comparison of expansion velocities of different lines can be undertaken best with a reflector. Olin C. Wilson used the coudé spectrograph at the 100-in. reflector, and made a systematic study of the brighter nebulae accessible with this telescope.⁽³⁷⁾ His first observations were made before the image rotator was available. More recently, by the introduction of the image rotator and the multi-slit, he has been able to preserve not only the fine structural details but is also able to observe several sections of the nebula simultaneously.

A concise summary of many of Wilson's results are given in Table VII: 2, which is reproduced from his paper. The first column gives the NGC or Index Catalogue designation. The nebulae are grouped according to the degree of excitation: H (high), M (medium), and L (low). The third column gives a rough description of the nebula as observed with slitless spectrograms. R denotes a ring nebula, DR a double ring, Irreg. an irregular structure. The fourth column gives the intensity ratio of the violet to the red component of the doubled lines. Notice that the number of nebulae with V/R greater than 1 is the same as the number with this ratio less than 1. The actual value of the ratio depends on the non-uniform distribution of the material. The fifth to the seventeenth columns summarize the separations ΔV of the line components of the different atoms and ions which are listed in order of the ionization potential of the next lower stage of ionization. For example, [OII] is listed with 13.6 e.v., which is the ionization potential of OI. Opposite each ΔV entry is given in parenthesis the total number of measures used in forming the value.

Notice that in many nebulae the ΔV values show large variations from one ion to another. A unique ΔV therefore cannot be assigned to each nebula. It is to be noted that the ΔV 's for H, [OIII], and [NeIII] are usually in good agreement so Wilson enters the mean ΔV for these atoms in the eighteenth column. The last column gives the mean deviation for all lines measured on more than one plate as a rough indication of the accuracy attained.

The most surprising result of Wilson's investigation is the variations in the ΔV 's for the different ions. In a simple expanding shell all ions should yield the same ΔV , but the observations show that [NeV] invariably yields

TABLE VII : II
Mean Separations of Double Lines in Planetary Nebulae
(km./sec.)

Nebula NGC	Ex- cita- tion	Form	V/R	[OI]	[SII]	H	[OI]	[NII]	HeI	NIII	[OIII]	OIII	[NIII]	HeII	[NeV]	Mean ΔV H _I (NIII) [OIII]	Mean M.D.
II 2165*	H	R	>1	—	—	—	106.0 (2)	—	—	—	40.0 (1)	—	39.9 (2)	—	0: (1)	40.0	1.7
2392*	—	DR	<1	—	—	—	65.6 (1)	61.5 (1)	—	—	105.2 (2)	—	113.9 (1)	—	0: (2)	107.3	11.4
2440	—	Irreg.	† 1	—	—	—	40.8 (22)	—	—	—	39.6 (2)	—	44.8 (1)	—	0: (1)	44.6	2.0
3242*	—	DR	† 1	—	—	—	44.2 (2)	42.1 (6)	—	—	35.6 (2)	—	39.0 (13)	33.6 (8)	—	39.8	1.6
6741*	—	R?	<1	—	—	—	55.5 (5)	—	—	—	41.6 (6)	—	41.0 (3)	—	0: (1)	41.4	3.3
6818*	—	R	<1	—	—	—	34.4 (1)	—	—	—	36.2 (12)	—	58.0 (5)	42.4 (4)	0: (2)	56.5	1.8
6886*	—	A	>1	—	—	—	45.3 (2)	—	—	—	32.8 (1)	—	40.6 (2)	—	0: (2)	37.1	1.4
7009*	—	R	>1	—	—	—	42.1 (20)	—	44.1 (4)	—	41.1 (11)	32.9 (3)	38.7 (7)	35.8 (4)	—	41.2	1.5
7027	—	Irreg.	<1	45.5 (1)	42.7 (2)	—	42.4 (4)	41.6 (2)	—	—	40.9 (5)	41.4 (1)	44.7 (7)	39.6 (2)	—	42.7	2.8
7662*	—	DR	<1	—	—	—	58.0 (2)	—	—	47.7 (1)	52.7 (15)	50.6 (11)	51.8 (12)	46.1 (5)	38.2 (1)	52.2	1.5
1351	M	—	>1	—	—	—	—	—	—	—	29.0 (2)	—	—	—	—	29.0	0.2
1335	—	DR	>1	—	—	—	—	—	—	—	40.0 (2)	—	39.0 (2)	—	—	39.5	0.3
1320	—	—	>1	—	—	—	40.3 (2)	—	—	—	—	—	34.6 (1)	—	—	34.6	—
II 2409*	—	A	>1	—	—	—	50.4 (2)	45.0 (1)	—	—	—	—	—	—	—	—	2.7
J 1500	—	A	<1	—	—	—	—	—	—	—	35.8 (1)	—	35.2 (4)	—	—	35.4	0.8
II 4593*	—	A	<1	—	—	—	71.1 (5)	71.1 (3)	38.3 (1)	—	—	—	—	—	—	—	—
6210*	—	A	† 1	—	—	—	42.1 (13)	—	—	—	42.8 (9)	—	41.6 (8)	—	—	42.2	1.6
II 4634	—	A	<1	—	—	—	35.6 (4)	71.5 (2)	—	—	29.8 (4)	—	28.6 (1)	—	—	29.6	1.0
6567	—	A	† 1	—	—	—	—	29.5 (1)	—	—	36.9 (6)	—	29.8 (1)	—	—	35.8	2.6
6720	—	A	<1	32.0 (1)	31.0 (1)	—	33.7 (3)	—	—	—	—	—	—	—	—	—	2.5
6803	—	A	† 1	—	—	—	—	—	—	—	—	—	60:	—	—	60:	0.6
6884	—	R	† 1	—	—	—	45.6 (1)	40.1 (4)	—	—	29.0 (3)	—	26.6 (2)	—	—	28.0	1.7
7026	—	Irreg.	† 1	—	—	—	81.7 (1)	—	—	—	45.5 (4)	—	42.0 (1)	—	—	44.9	—
I 418*	L	R	>1	49.9 (2)	34.7 (7)	0:	0:	* 0:	0:	—	—	—	—	—	—	81.7	—
HD 184738 = BD + 30° 3639*	—	R	†	—	43.2 (7)	52.8 (32)	59.6 (17)	51.9 (13)	—	—	—	—	—	—	—	0:	1.2
																52.8	4.3

* Further information will be found in Wilson's paper.

† Red components stronger at one end of line; violet components stronger at other end.
(Courtesy O. C. Wilson, *Ap. J.*, 111, 279 (1950).)

low values of ΔV , whereas high values are found from the low excitation radiations of [OII], [NII], or [SII].

The general rule is given by Wilson as follows:⁽³⁷⁾

"Where differences in component separation exist in the spectrum of a planetary nebula, the high-excitation particles show smaller separations, and the low-excitation particles higher separations, than [OIII] and [NeIII]. To this rule there is one universal exception, Hydrogen, which requires less excitation than either [OII] or [NII], always agrees closely in separation with the much more highly excited ions [OIII] and [NeIII]."

In some nebulae with $\overline{\Delta V}$ values ranging from 37 to 107 km./sec., the [NeV] lines are narrow, indicating a ΔV of less than 10 km./sec. The [NeV] image is always smaller than the *H*, [NeIII], or [OIII] image. No quantitative relation between differences in ΔV and differences in image size for the various ions appears. In fact, for NGC 2392 very large differences in ΔV correspond to very small differences in the sizes of the monochromatic images. The opposite appears to be true for NGC 7662, where the *HeII* and [NeV] radiations are strictly confined to the inner ring.

The low excitation nebula IC 418 is of special interest. Wilson observed it with higher dispersions at Mt. Wilson and Palomar and found the following correlation between ionization potential and component separation.⁽³⁸⁾

Ion	OI	MgI	SII	OII	NII	H	OIII	NeIII
Excitation (e.v.)	0	0	10.3	13.6	14.5	13.5	35.0	40.9
ΔV (km./sec.)	47	39	34	21	23	0:	0:	0:

On the high dispersion spectrograms the [OIII] lines remain sharp, but the *H* lines have a diffuse appearance. Probably they would appear double, were it not for the widening of the components. Wilson concludes that the [OI], [OII], and [OIII] radiations are rather completely separated, with very little overlapping. The analysis of the slitless data, discussed in Section 4, do not indicate a sharp demarcation between the [OIII] and [OII] radiations, and the Strömgren theory leads to results that are in at least qualitative agreement with the slitless data. Nevertheless the bulk of the [OII] and the [OIII] radiation comes from quite different quarters of the nebula.

Wilson calls attention to the close conformity of IC 418 to the spatio-kinematical structure principle exhibited by high excitation ring nebulae. In the high excitation objects the slitless images and expansion velocities of *H*, [OIII], and [NeIII] are closely similar, whereas in IC 418 the [OIII] and [NeIII] radiations occur in the innermost part of the nebula, and the

principal H emission is in the outer shell. Thus in IC 418, [OIII], and [NeIII] play the same role as [NeV] does in the high excitation object. At corresponding points in the nebular structure the level of ionization is much lower in IC 418 than in other objects.

The Ring nebula in Lyra, NGC 6720, shows the same type of internal motions as are found in other ring objects—the concept of a cylinder does not appear appropriate.

An ingenious comparison of slitless spectrograms of NGC 2392 secured with the 100-in. coudé and direct photographs of the same object obtained with the 200-in. was made by Wilson and Minkowski. The relative positions of knots and filaments on the slitless spectrogram are affected by their radial velocities; whereas no Doppler shifts occur on the direct photograph. These measures show that the knots and condensations in the outer ring are moving towards the observer on one side of the nebula—away from him on the other!

The observations of Olin Wilson that the ions of highest excitation in a nebula, such as NeV in NGC 7662, show a smaller expansion velocity than do ions of low excitation, e.g. $NeIII$ or $OIII$ in the same nebula, require one of two possible explanations. Either the different ions (although in roughly the same regions in the nebula) are drifting with respect to one another—or the velocity of a given ion gives the mass motion of the material in the region where the radiations of a given ionization stage predominate. That is, the [NeV] velocity is simply the velocity of material in the zone where [NeV] rather than [$NeIII$] radiations are produced.

Let us examine these alternatives in turn. In the first picture an actual differential drift of the different ions is imagined to occur—as a consequence of forces acting in one type of ion and differently or not at all upon another.

This situation is similar to the problem studied by McCrea for the solar prominences.⁽³⁹⁾ It is a well-known fact that gases of all different types remain thoroughly mixed in a solar prominence, even in spite of the fact that radiation forces, etc., must act selectively upon them. Evidently all gases tend to be dragged along together.

In the present context let us imagine a gas of two components, e.g. hydrogen and argon—the latter being several times ionized. We suppose that the hydrogen atoms are picking up momentum from the net outward flux of quanta. They tend to be accelerated away from the argon ions so that a net separation of elements would tend to occur. Collisions, however, tend to transfer momentum from the hydrogen to the argon atoms, and ultimately a steady state is set up in which the hydrogen and argon atoms drift apart at a steady rate. Clearly the rate of separation is going

to depend on the rate at which momentum is picked up by the hydrogen atoms and the rate at which it is transferred to the argon atoms.

Let the force acting upon a hydrogen atom be

$$f_1 = m_1 a_1, \quad . \quad . \quad . \quad . \quad (34)$$

where a_1 is the acceleration produced by the radiation pressure. For simplicity we assume that the argon ions are not absorbing radiation from the outgoing flux of the central star. McCrea's analysis shows that if the velocity of separation, U , is smaller than the thermal velocity, it will be given by

$$U = \frac{a_1}{2\rho\sigma^2\sqrt{\frac{2\pi kT}{m_1 m_2(m_1 + m_2)}}}, \quad . \quad . \quad . \quad . \quad (35)$$

where ρ is the density of the gas, σ is the collision radius, and m_1 and m_2 are the masses of the two interacting particles. In our present illustration we suppose that hydrogen is much more abundant than argon so that $\rho = N_e m_H$. For σ one should use the coulombic encounter cross-section. We can get an upper limit to the value of U by adopting $\sigma = 2 \times 10^{-8}$ as the encounter radius. Also $m_1 = m_H$ and $m_2 = 40m_H$. Making the necessary substitutions, we find

$$U = \frac{a_1}{2N_e m_H \sigma^2 \sqrt{\frac{2\pi kT}{m_H^2 \times 40 \times (41m_H)}}} = \frac{a_1}{4.5 \times 10^{-12} N_e} \quad (36)$$

for $T_e = 10,000^\circ \text{K}$. The acceleration due to radiation pressure is given by

$$m a_1 = \frac{\pi}{c} \int_{\nu_1}^{\infty} \alpha_\nu F_\nu d\nu, \quad . \quad . \quad . \quad . \quad (37)$$

where α_ν is the absorption coefficient and πF_ν is the flux from the central star. Putting in numerical values,

$$\alpha_\nu = \alpha_0 \left(\frac{\nu_0}{\nu} \right)^3,$$

where $\alpha_0 = 6.3 \times 10^{-18}$, $\pi F_\nu = \frac{2\pi h \nu^3}{c^2} \left(\frac{r}{R} \right)^2 e^{-h\nu/kT}$, $\nu_1 = 3.29 \times 10^{15}$ (frequency

of Lyman limit), T , the temperature of the star in the ultra-violet, is $30,000^\circ \text{K}$, $R = 3R_\odot$, and $r \sim 1.5 \times 10^{17} \text{ cm.}$, we find $a_1 \sim 10^{-3} \text{ cm./sec.}$ The gravitational acceleration produced by a central star of mass $M_0 (M_\odot = 1)$ is $0.6 \times 10^{-8} M_0$. Thus the gravitational attraction can be neglected entirely. If N_e is 5×10^3 , we find $U \sim 0.5 \text{ km./sec.}$ This velocity of separation applies only in the region where H is predominantly neutral and the collision radius is as low as the value given by the gas kinetic theory. Actually σ

is much larger and U is correspondingly smaller as the coulombic collision radius is greater than 10^{-7} cm. Hence no separation can occur unless the argon ions can acquire considerable momentum in the opposite direction to that in which hydrogen is moving. Ions such as $[NeV]$, $[AlV]$, etc., characteristic of the high excitation shell, have no resonance lines capable of absorbing Lyman line radiation. Hence no selective radiation pressure of hydrogen can act on them. The velocities of these ions are determined by the local velocity of the material at the zone in which they radiate.

Among the possible models considered by Olin Wilson was a thick shell in which the innermost observable zone was that of $[NeV]$. Within the $[NeV]$ zone he supposed that zones of more highly excited ions such as MgV , $NeVI$, etc., might exist. These ions do not produce observable forbidden lines, and Wilson supposed that the electron temperature was so high in this region that the recombination lines of hydrogen and helium did not occur. The material in the $[NeV]$ zone moves slowly outwards; its velocity is of the order of 5 km./sec. or less, and since very few H , HeI , or $HeII$ atoms are in the ground-level, few photo-ionizations can occur and the material acquires very little outward momentum. Towards the outer end of the $[NeV]$ zone the gas presumably is cooler and $HeII$ lines are produced as recombination sets in. Thus the bright ring of $HeII$ is produced; once $HeII$ is formed it can block all the outgoing radiation below $\lambda 228$ and pick up the corresponding momentum. The depletion of high frequency radiation permits the formation of $OIII$ and $NeIII$ ions, the temperature falls yet further, and recombination of hydrogen sets in. If the nebular shell is optically thick, hydrogen becomes neutral before the boundary is reached, and the momentum of the entire ultra-violet radiation is transferred to the nebular gases.

Wilson concluded that the actual amount of momentum absorbed in the nebular shell was comparable with that carried by the radiation emitted by the central star. The total number of quanta emitted per second by the central star of radius R and temperature T in the frequency interval ν to $\nu + d\nu$ is

$$\frac{8\pi^2 R^2 k^3}{c^2 h^3} T^3 \frac{x^2}{e^x - 1} dx, \quad . \quad . \quad . \quad (38)$$

where $x = h\nu/kT$. Since each quantum carries a momentum $h\nu/c$ the total amount of momentum carried by the stellar radiation beyond the Lyman limit is

$$F = \frac{8\pi^2 R^2 k^4}{c^3 h^3} T^4 \int_{x_1}^{\infty} \frac{x^3}{e^x - 1} dx. \quad . \quad . \quad (39)$$

If the radius of the central star is equal to that of the sun while its temperature is $100,000^\circ K.$, the momentum beyond the $HeII$ Lyman limit $\lambda 228$ will

be $F(\text{HeII}) = 1.4 \times 10^{26}$ gm. cm./sec.², whereas for frequencies between $\lambda 228$ and $\lambda 912$ the momentum will be $F(H) = 9.0 \times 10^{26}$ gm. cm./sec.². In this model it is supposed that within the shell, the total number of particles flowing across any spherical surface concentric with the illuminating star will be a constant. If r_1 is the radius of one surface at which the outward gas velocity is V_1 , the total number of particles crossing the surface per second will be $4\pi r_1^2 N_1 V_1 = 4\pi r_2^2 N_2 V_2$ where r_2 , N_2 , and V_2 , pertain to a second surface. Since each particle carries a momentum mV_1 at the inner surface and mV_2 at the outer surface, the momentum increment acquired by the gas will be

$$\Delta F = 4\pi m(n_2 r_2^2 V_2^2 - n_1 r_1^2 V_1^2) \sim 4\pi r^2 n_2 m V_2 (V_2 - V_1), \quad (40)$$

since r_1 is nearly the same as r_2 so that $n_1 V_1 = n_2 V_2$. If V_2 and $V_2 - V_1$ are of the order of 10 km./sec., $r = 10^{17}$ cm., $N_2 = 10^3/\text{cm.}^3$, and $m = m_H = 1.7 \times 10^{-24}$ gm., we obtain $\Delta F = 2 \times 10^{26}$ gm. cm./sec.², which is in fair agreement with the other calculation and indicates that the proposed model is a plausible one. Detailed examination shows that this model encounters a number of difficulties. The electron temperature is too low to account for a suppression of the emission of H and HeII in the inner zones. If the electron temperature were so very much higher in the inner zones than in the outer, a pronounced difference in the continuous spectra would be observed.

Another possibility is that the planetaries may be regarded as hollow shells. The slowly expanding shell increases gradually in size; the material on the inner surface is pushed backwards towards the star; that on the outer edge is pushed yet more rapidly outwards.

To understand how such a situation might come about we must briefly examine the effects of radiation pressure within the nebular shell. We recall that the essential feature of the Zanstra-Menzel picture of the passage of starlight through a gaseous nebula was the degradation of all quanta of the Lyman continuum into quanta of Lyman α and the Balmer lines plus other subordinate quanta. That is, if p is the probability that an electron will be captured on the ground-level, $1-p$ is the probability that it will be captured on some other level and subsequently cascade to the ground-level. In so doing, the atom is bound to emit two or more quanta which eventually (if they are not already fully broken down) will give rise to a Balmer quantum and a Lyman α quantum. This process of degradation of the " $(1-p)$ " quanta may not take place in the same volume element of the nebula, but may require several absorptions and re-emissions. In a first approach to this problem Ambarzumian made the simplifying assumption that a quantum of the Lyman continuum upon absorption by an atom has the probability p of being reradiated

as an ultra-violet quantum and a probability $(1-p)$ of being immediately degraded into a quantum of Lyman α in the same volume element.⁽⁴⁰⁾ He found that in a nebula of optical thickness 2 at the Lyman series limit, the mean density of the Lyman α radiation would be about 10^9 times larger than the density of the direct $Ly\alpha$ radiation. In the outer part of a static nebula the radiation pressure would build up to very high values—enormously in excess of the gravity of the central star.

Under these circumstances the nebular shell would be simply torn asunder. Actually, as was pointed out by Zanstra,⁽⁴¹⁾ the very process of expansion would reduce this radiation pressure and protect the nebula from catastrophic destruction. Zanstra's original treatment was schematic and the problem was handled more rigorously by Chandrasekhar,⁽⁴²⁾ who found that if the velocity difference between the inner and outer boundary of the nebular shell was about 3.5 times the velocity width of the undisplaced lines the pressure of the Lyman line radiation would be reduced by a factor of 10^4 and would cease to be important through most of the shell. Under certain conditions it might become comparable with that of L_c except near the inner and outer boundaries.

More recently Zanstra⁽⁴³⁾ has considered again the problem of the radiation pressure of $Ly\alpha$ in a stationary nebula, but one in which scattering occurs with a redistribution of frequency over the line profile, such that the scattering atoms set up a continuous interchange of energy between each element of frequency $\Delta\nu$ covered by the line. The line profile is that given by the Doppler theory. He showed that the radiation pressure in a stationary nebula with scattering redistribution of energy is hundreds of times smaller than in a nebula with strictly coherent scattering. The expansion of the nebula would further lessen the radiation pressure, but an exact evaluation of the amount would require an extension of Zanstra's treatment to an expanding shell.

We may illustrate how thermal Doppler effect acts to produce non-coherent scattering with the aid of Fig. 16 due to Zanstra. Suppose that atoms at O_1 emit $Ly\alpha$ quanta of frequency ν_1 in the X -direction. This radiation is assumed to be scattered by hydrogen atoms at point o , all of which have the same x -velocity v_{x_1} such that

$$v_{x_1} = \frac{\nu_1 - \nu_0}{\nu_0} c, \quad . \quad . \quad . \quad (41)$$

where ν_0 denotes the frequency at the centre of the line. These atoms, however, have a Maxwellian distribution of velocity in the Y -direction so that quanta emitted in this direction are distributed in frequency over the Doppler profile. Likewise, if the radiation is scattered at an angle ψ with

respect to the X -direction, the component of the thermal velocity in this direction will be

$$v = v_x \cos \psi + v_y \sin \psi. \quad (42)$$

If $\psi = 60^\circ$, for example, $v = 0.5v_{x_1} + 0.886v_y$, so that the quanta will be distributed in frequency according to a Doppler profile with a half-width $0.886v_D$, but with the line centre displaced by an amount $0.5(v_1 - v_0)$ from the undisplaced frequency v_0 . Thus it is clear that in a large majority of scattering processes a considerable redistribution of the frequency takes place. Zanstra adopts as an approximation that each scattering is accompanied by complete redistribution given by the thermal Doppler profile.

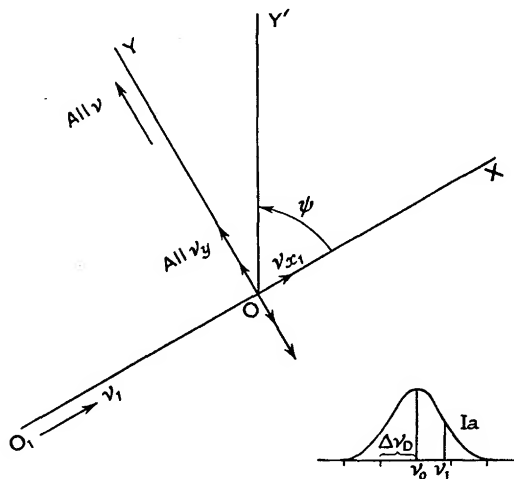


FIG. VII : 16. *Scattering with Thermal Doppler Effect.*
The insert 1a depicts the thermal profile of the line.
(Courtesy H. Zanstra, *Bull. Astron. Inst. Netherlands*, 11, 4 (1949).)

Zanstra's formulation of the problem leads to an integral equation connecting the rate at which the radiation in the Lyman continuum is converted into Lyman α with the total emission per unit volume. The equation turns out to be difficult to solve, and Zanstra obtained an approximate answer by essentially a trial-and-error process. The results show that by taking the redistribution of energy with frequency into account, the radiation pressure in the static nebula is reduced by a factor of 300 as compared with the result obtained from the theory of strict coherent scattering! The physical reason for this result may be explained as follows. A nebula whose optical thickness at the Lyman limit is unity and whose electron temperature is about 9000°K . has an optical thickness of about 10^4 at the centre of the $L\gamma\alpha$ profile. Well inside the nebula a $L\gamma\alpha$ quantum emitted at the centre of the line would have a chance of $\exp(-10,000)$ of escaping, which means it would never get out were the scattering strictly

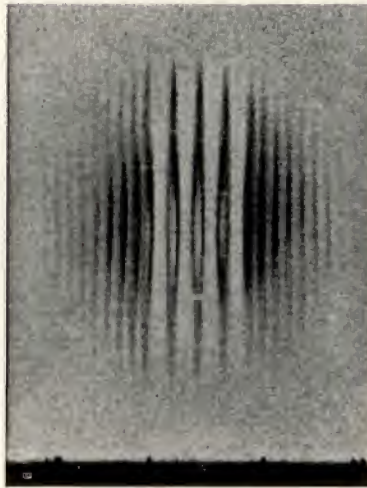
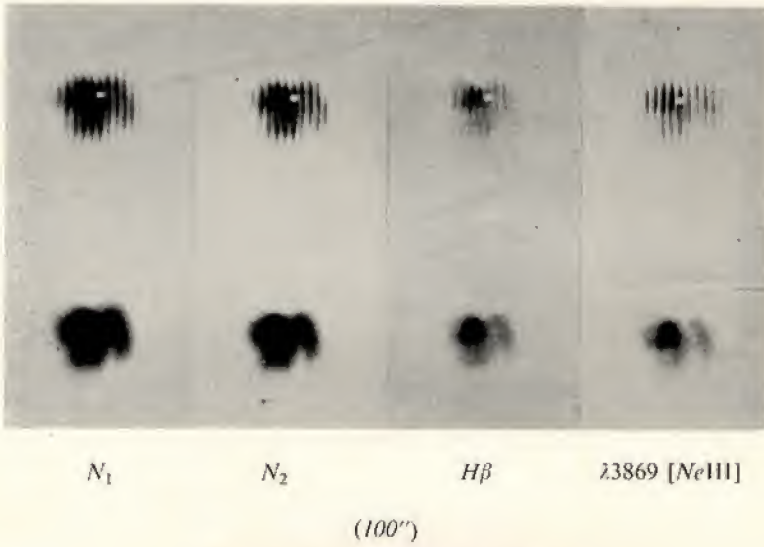


FIG. VII : 17. *Internal Motion in the Planetary Nebulae NGC 7027 and NGC 7662.*

(Top) Multi-slit images of NGC 7027. The small white square is a fiducial mark to enable the observer to relate all positions in the nebula to the same coordinate system. Notice the doubling and complex character of the lines. The lower row shows the ordinary slitless images secured with the coudé. In this planetary all images have about the same internal intensity distribution.

(Bottom) The $\lambda 3869$ [NeIII] image in NGC 7662 (compare Fig. 11) as observed at Palomar. The separation between slits is chosen to be larger near the centre of the image where the line splitting is greater. Compare with Fig. II : 13. (Observations by Olin C. Wilson, Mt. Wilson and Palomar Observatories.)

coherent. Since the scattering is non-coherent, as it is governed by the Doppler profile, there is a chance of about 2×10^{-5} it might be re-emitted in the wing of the profile where the optical depth is 1 or less, so that it might escape. Because a given quantum is repeatedly scattered it finally escapes in the wing.

Further discussions of the intensity and radiation pressure in Lyman α in planetary nebulae have been given by Shotaro Miyamoto,⁽⁴⁴⁾ T. Saigusa,⁽⁴⁵⁾ and by Wasaburo Unno.⁽⁴⁶⁾ Unno deduced the exact form of the equation of transfer, taking into account the frequency redistribution in the line profile. He found that the radiation pressure in Lyman α was reduced via the Zanstra effect to about 3×10^{-3} that of the older theory except at the extreme outer boundary. This result is in good agreement with Zanstra's estimate except at the outer edge of the nebula, where the radiation can escape even at the line centre.

All these calculations are idealized in that they refer to static nebulae and sometimes also include idealized profile shapes. Nevertheless, certain implications for expanding shells may be foreseen. In particular it seems likely that Chandrasekhar's conclusion that the inner edge of the nebula is pushed back towards the star while the outer edge is accelerated outwards must hold. Thus in certain of the ring-shaped nebulae the low [NeV] velocities may simply represent the velocities in the inner shell edge that is being pushed back towards the star. Olin Wilson favoured this mechanism for IC 418, which he believed to be a hollow shell in so far as the H , [OII], and [NII] radiations are concerned. As we saw, however, more recent work suggests that the H shells are not strictly hollow. In IC 418, [NeIII] and [OIII] play the same roles as does [NeV] in objects of higher excitation, i.e. they show the lowest velocities of expansion.

Because of the hopelessly complicated geometry of the nebulae, exact calculations of the $L\gamma\alpha$ radiation pressure are impossible in any practical model. Differential velocities between one part of the shell and another alone would suffice to enormously complicate the problem. The idealized and schematic computations do indicate the general trends of the behaviour of radiation pressure, and suggest mechanisms that may account for some of the observed phenomena.

REFERENCES

- (1) *Ap. J.*, **81**, 1 (1935).
- (2) *Ap. J.*, **89**, 526 (1939).
- (3) *Ap. J.*, **88**, 364 (1938); **89**, 119 (1939).
- (4) An analogous procedure is applied by DE JONG, J. H., *B.A.N.*, **11**, 345 (1951).
- (5) *M.N.R.A.S.*, **93**, 50 (1932).

- (6) See, for example, ALLER, L. H., and MENZEL, D. H., *Ap. J.*, **102**, 258-9 (1945). PAGE, THORNTON, and GREENSTEIN, JESSE, *Ap. J.*, **114**, 98 (1951), postulated that the observed disks of planetaries were to be interpreted as *HII* regions and used this assumption to adjust the published magnitudes of the central stars and nebular surface brightnesses.
- (7) See MINKOWSKI, R., *Ap. J.*, **95**, 243 (1942). Wurm has argued that most planetary nebulae are optically thin at the Lyman limit. (Reference 8.)
- (8) *Die Planetarischen Nebeln*, Akademie-Verlag, Berlin (1951), p. 85.
- (9) In preparation.
- (10) ALLER, L. H., *Ap. J.*, **93**, 236 (1941); Tables 2 and 4.
- (11) *M.N.R.A.S.*, **110**, 429 (1950).
- (12) *Lick Obs. Publ.*, **13**, 57 (1918).
- (13) *M.N.R.A.S.*, **110**, 37 (1950).
- (14) *B.A.N.*, **11**, 350 (1951).
- (15) *Lick Obs. Bull.*, **15**, 86 (1930).
- (16) *A.J.*, **55**, 70 (1950).
- (17) *Lick Obs. Bull.*, **9**, 92 (1917).
- (18) *M.N.R.A.S.*, **90**, 200 (1919).
- (19) *Russ. A.J.*, **14**, 301 (1937).
- (20) *Russ. A.J.*, **14**, 194 (1937).
- (21) *Zeits. f. Ap.*, **12**, 247 (1936).
- (22) *Annales de l'Observatoire de Paris Memoirs*, **25**, F29 (1908).
- (23) *M.N.R.A.S.*, **71**, 460 (1911).
- (24) An account of these methods as applied to the specific example of a globular star cluster is given, for example, in SMART, W. M., *Stellar Dynamics* (Cambridge University Press, 1938), p. 297.
- (25) *Ap. J.*, **114**, 421 (1951).
- (26) Methods of solving the integral equation (25) are given, for example, by VAN DE HULST, H. C., *Bull. Astron. Inst. Netherlands*, **10**, 75 (1946); TRUMPLER, R. J., and WEAVER, H. F., *Statistical Astronomy* (Univ. of California Press, Berkeley, 1952), Chapter 1.4.
- (27) *Ap. J.*, **111**, 142 (1950).
- (28) *Upsala Medd.*, No. 65 (1936).
- (29) *Lick Obs. Bull.*, **18**, 57 (1937).
- (30) WYSE, A. B., *Ap. J.*, **95**, 356 (1942); ALLER, L. H., *Ap. J.*, **93**, 195 (1941).
- (31) *Ap. J.*, **115**, 71 (1952).
- (32) *Lick Obs. Publ.*, **13**, 77 (1918).
- (33) *Ast. Nach.*, **237**, 89 (1929).
- (34) *Zeits f. Ap.*, **2**, 329 (1931).
- (35) See the discussions by BAADE, WALTER, *Ap. J.*, **96**, 188 (1942); and by MINKOWSKI, R., *Ap. J.*, **96**, 199 (1942).
- (36) *Ast. Nach.*, **254**, 137 (1935).
- (37) *Ap. J.*, **111**, 279 (1950).
- (38) *Ap. J.*, **117**, 264 (1953).
- (39) *M.N.R.A.S.*, **95**, 509 (1935).
- (40) *Pulkova Obs. Bull.*, **13**, 3 (1933).
- (41) *M.N.R.A.S.*, **95**, 84 (1934).
- (42) *Reviews of Modern Physics*, **17**, 138 (1945); *Ap. J.*, **102**, 402 (1945).
- (43) *B.A.N.*, **11**, 1 (1949); **11**, 359 (1951).
- (44) *Publ. Astron. Soc. Japan*, **2**, 23 (1950).
- (45) *Publ. Astron. Soc. Japan*, **4**, 16 (1952).
- (46) *Publ. Astron. Soc. Japan*, **3**, 158 (1951).

CHAPTER VIII

The Diffuse Gaseous Nebulae

1. Introduction

In this final chapter we shall discuss some of the characteristics of diffuse galactic nebulae in more detail. As we have emphasized previously, the diffuse nebulae represent really only denser regions of the interstellar medium. Hence much of the theory of the diffuse nebulae is essentially part of the theory of the interstellar medium, an excellent account of which is being prepared by Lyman Spitzer, Jr. Accordingly, although we shall pay particular attention to the gaseous diffuse objects, we shall mention some of the work on the Orion nebula, which contains great quantities of solid particles as well as of gas.

Extensive studies of the diffuse galactic nebulae of low surface brightness have been carried out by Shajn and Hase at Simeis, by G. Courtes in Haute Provence (the programme was initiated by B. Strömgren and C. Fehrenbach in 1950), by Hugh Johnson, B. Strömgren, and W. W. Morgan at the McDonald Observatory in Texas, by R. Minkowski, S. Sharpless and others at Palomar, by K. Henize and by the Harvard Observatory in South Africa, and by C. S. Gum at Canberra, Australia.⁽¹⁾

The chief interest in the interstellar medium in general, and the diffuse nebulae in particular, lies in their association with the processes of star formation, a subject we have mentioned in Chapter III. The invariable association of stars of high luminosity in our own and other galaxies with the grains and gas of the spiral arms, the requirement of astrophysical theories of energy generation that the very luminous stars be younger than the age of the galaxy, and the direct evidence found by Blaauw and Morgan⁽²⁾ for the common origins of groups of B stars all point to the desirability of investigations that will show how stars are actually formed from the interstellar medium. Stars of a great range of mass and luminosity appear to be formed continually from the grains and gas. The very luminous ones are easy to identify; certain fainter objects perhaps appear in the course of their formation as T Tauri stars. Others would seem less easy to identify.

An account of theories of star formation lies outside the scope of our discussions. Spitzer⁽³⁾ has proposed a plausible mechanism for star formation from an inhomogeneous medium. On the other hand, Hoyle and Lyttleton⁽⁴⁾ and more recently McCrea⁽⁵⁾ have favoured the building-up of normal stars by a process of accretion until their masses are such as to permit them to shine as B or O stars. These theories are of a rather schematic nature.

The work of W. W. Morgan and his associates at the Yerkes Observatory and of Ambarzumian, Shajn and Hase, and their associates in the Soviet Union strongly favour the hypothesis that groups of massive stars (O associations) and of stars more nearly similar to the sun (T associations) are formed directly from the interstellar medium. The colour-magnitude array for the galactic cluster NGC 2264 suggests that the process of star formation may actually be taking place before our eyes. Merle Walker finds that the luminous stars are already on the main sequence, whereas the cooler, fainter stars fall to the right of the main sequence. These stars may be in a state of Kelvin contraction, not yet shining by nuclear sources. A similar process of star formation may be going on in Orion, where massive as well as faint stars are being formed, and in Taurus, where only dwarf stars appear to be in the process of formation.

Over periods of time equal to the age of the galaxy, the depletion of the interstellar medium by the process of star formation might be expected to be rather marked. On the other hand, novae, supernovae, planetary nebulae, P Cygni stars, Wolf-Rayet stars, rapidly revolving close binary systems, and even the corpuscular radiation from solar-type stars are constantly adding material to the interstellar medium. Estimates by Vorontsov-Velyaminov, L. Biermann, and Otto Struve suggest that between one and ten solar masses may be added to the interstellar medium each year. Since the added material presumably is enriched in heavier elements as a consequence of nuclear processes occurring within stars we might expect the mean composition of the interstellar medium to change gradually with the time. Probably, also, the interstellar medium is not "holding its own", but is gradually being depleted in the process of star formation.

The evolution of a dark cloud or a diffuse nebula into a star or cluster of stars will depend on the chance configuration of the stars in its neighbourhood, on the mass, density, temperature, and internal motions in the cloud, as well as on the ratio of solid grains to gas. Not only are the mean values of such parameters as temperature and density of importance, but the mean fluctuations of these quantities are also urgently wanted.

The greater part of this reflection nebula is bluer than its central star, although some features are distinctly redder. Notice the different appearance of the nebula-sity to the north-west of the centre of the nebula. Also, compare the south-east and north-east regions with those to the east and west. On reproductions of equal contrast, the nebula has a softer texture in blue or ultra-violet light than in red or infra-red. (The star images are enlarged in the red photograph due to the variation in focus during the long exposure.) The illuminating star, HD 200775, of spectral class B5V, possesses a variable hydrogen shell and exhibits weak, variable $[FeII]$ emission lines in its spectrum. Most of the faint red stars within 4' of the centre of the nebula are variable and show $H\alpha$ emission in their spectra.

(Courtesy E. B. Weston, University of Michigan Observatory.)



Red

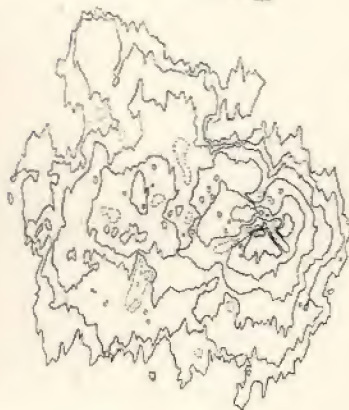
Blue

FIG. VIII: 1. NGC 7023 photographed in Red and Blue Light.

(*Top, left to right*) Photographs in the radiation of $[OIII]$, $H\alpha + [NII]$, and $[OII]$ secured with the Curtis Schmidt telescope.

(*Bottom*) The corresponding isophotic contours in steps of a factor of 2 in surface brightness. The smaller size of the nebula in the $H\alpha$ radiations than in the $[OIII]$ radiations is unusual. The surface brightness in the continuum is very much lower than in $H\alpha$ and the corresponding isophotes resemble those of $[OII]$ more closely than they do those of $H\alpha$.

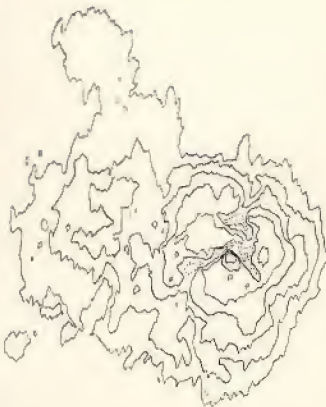
(Courtesy, Albert Boggess.)



M20: $[OIII] \lambda\lambda 4959, 5007$.
Log I : 0.0, 0.3, 0.6, 0.9, 1.2, 1.5, 1.8.



M20: $H\alpha \lambda 6563 + [NII]$.
Log I : 0.0, 0.3, 0.6, 0.9, 1.2, 1.5.



M20: $[OII] \lambda 3727$.
Log I : 0.0, 0.3, 0.6, 0.9, 1.2, 1.5, 1.8.

2. The Observable Parameters for the Diffuse Nebulae

Let us recapitulate briefly some of the observations that can be made for diffuse nebulae.

Usually the exciting stars can be easily identified and their spectral classes, temperatures, and absolute magnitudes established. If their colour excesses can be measured, the effect of galactic absorption can be evaluated and the distance of the nebula can be found. Angular distances in the nebula can be converted to distances in parsecs and the area and volume of the radiating material estimated. If the nebula is of the reflection type its colour, surface brightness, and polarization can be measured as a function of position angle and distance from the illuminating star. From an analysis of these data estimates of the albedos and sizes of the reflecting grains can be made.

The difference between nebulae that owe their surface brightness primarily to the scattering and reflection of light by small particles and those that shine by fluorescence are well exhibited by direct photographs obtained with appropriate filters and emulsions. In Figs. 1 and 2 we compare photographs of NGC 7023, obtained by E. B. Weston, and of M20 (the Trifid nebula), obtained by A. Boggess. NGC 7023 shows a spectrum that is a faithful replica of its illuminating star with little, if any, indication of emission lines. The Trifid nebula has an emission spectrum and a weak continuum. A comparison of NGC 7023 photographed in the region of $H\alpha$ and in the nearby continuum shows no differences. On the other hand, photographs obtained with a blue-sensitive emulsion show considerable differences. The nebula is definitely blue.

The Trifid nebula is very much brighter in $H\alpha$ than in the nearby continuum. Curiously, the continuous and $[OIII]$ radiations extend over a much larger volume of space than does the $H\alpha + [NII]$ radiation. This behaviour is well illustrated in the corresponding isophotic contours.

If the surface brightness in $\text{ergs/cm}^2/\text{sec}$. in each of these monochromatic radiations can be determined by comparison with an appropriate source of known intensity distribution, further progress can be made. If the dimensions of the radiating volumes can be estimated from their angular sizes and the distance of the nebula, and if the electron temperature can be found, the emission per unit volume can be evaluated. If the emission in the hydrogen lines comes from the recombination of protons and electrons, Menzel and Baker's "case B"⁽⁶⁾ will hold, and the density of ions and electrons may be computed at once.

Furthermore, from the fluctuations in surface brightness it is possible to supplement estimates of the mean density $\bar{\rho}$ by estimates of $(\bar{\rho} - \bar{\rho})^2$. The

internal motions in extended nebulosities may also be measured. The expansion of the Network nebula across the line of sight is easily seen in the blink comparator on plates taken at the Mt. Wilson Observatory. In most gaseous nebulae the knots and filaments move with smaller speeds and are less well defined, so that radial velocities give us the most reliable picture of the internal motions. The radial velocities can be measured by a slit spectrograph or by the Fabry-Perot etalon technique.

Finally, slit spectroscopic observations are desirable to separate the contributions of [NII] and $H\alpha$, for example, and to get the general level of excitation in the nebula. It is well to reiterate at this point that slit spectrographic work on extended diffuse nebulae can be done much better with fast spectrographs on small telescopes than on larger telescopes. For faint extended nebulae, speed rather than a large scale is essential. Spectroscopic observations give data on the kinematics as well as on the density fluctuations in the gas.

The geometrical and physical relationship of the exciting star to the diffuse nebula is also an important parameter. Bright nebulae tend to include not just single early-type stars but whole associations. Sometimes there are vast clouds of dust and gas, but no early-type stars (as in Aquila); in other instances (as in Perseus) the centre of concentration of the hot stars does not coincide with that of the nebulosity. Shajn and Hase observed many instances of faint nebulae not associated with hot stars, and also that among the bright nebulae one in eight (e.g. NGC 7822) is not associated with a star of class W, O, B0, or B1. They found only a feeble tendency of the association between stars and nebulae to increase with stars of higher temperature. In particular, the stars that one might expect to be shedding material most rapidly into the interstellar medium, Be stars and Wolf-Rayet stars, do not appear to be associated with nebulosities more closely than do ordinary O and B stars.

3. Physical Processes in Diffuse Nebula

A diffuse nebula, such as the Orion nebula, differs from the gaseous nebulae we have discussed previously in two important respects: (a) in addition to the gas, small solid particles are usually also present; (b) the nebula is often optically very thick.

The presence of the grains may exert a profound effect on the relation between the electron temperature and the energy distribution in the radiation field to which the atoms are subjected. Atoms and electrons may strike the cold grains and give up kinetic energy to the excitation of internal modes of vibration of the grain. The result is that in regions where grains are present in appreciable numbers the electron temperature

will be markedly lowered. Spitzer and Savedoff⁽⁷⁾ have discussed this question in detail.

The large optical thickness of the Orion nebula is manifested by the appearance of absorption lines of helium produced by the nebula and by the character of the energy distribution in the Balmer continuum.

Some years ago, O. C. Wilson⁽⁸⁾ noticed that the narrow, sharp absorption line $\lambda 3889$ corresponding to the 2^3S-2^3P transition appeared in the spectra of the stars of the Trapezium in the Orion nebula. In θ^1C Orionis he measured an equivalent width of 0.20 Å. On the other hand, the $\lambda 5016$ and $\lambda 3965$ lines corresponding to the 2^1S-3^1P and 2^1S-4^1P transitions did not appear. Both the 2^3S and 2^1S levels are metastable. From the known f values of these lines he estimated the population of the 2^3S level to be at least twenty-five times larger than that of the 2^1S level. The theory of the excitation of the levels of HeI by dilute temperature radiation was given by O. Struve and K. Wurm⁽⁹⁾ and has recently been improved by P. Wellmann.⁽¹⁰⁾ This theory predicts that for very small dilution factors the ratio $N(2^3S)/N(2^1S)$ varies from 147 for an electron temperature of $10,000^\circ K.$ to 84 for an electron temperature as high as $25,000^\circ K.$ ⁽¹¹⁾ Hence the non-appearance of the lines arising from the metastable 2^1S levels is not surprising.

An even more striking effect of the large optical thickness of the Orion nebula is shown by the energy distribution in the Orion nebula beyond the Balmer limit. Ten years ago Barbier⁽¹²⁾ found the colour temperature of this continuum to be in the neighbourhood of $11,000^\circ K.$ Greenstein,⁽¹³⁾ using higher dispersion, subsequently measured the energy distribution in the continuum with respect to that of θ^1C Orionis, whose colour temperature had been determined both photographically and photo-electrically. He found a colour temperature of $12,000^\circ K.$ on both sides of the Balmer limit. If the energy distribution in the Balmer continuum is considered to arise from a pure recombination process, an electron temperature of $65,000^\circ K.$ is implied as one can readily verify from the equations in Chapter IV. From the relative intensities of the $[OIII] \lambda 4363$ and N_1+N_2 lines, and the Hebb-Menzel target areas, the writer had suggested an electron temperature of about $10,500^\circ K.$ ⁽¹⁴⁾ The use of Seaton's target area data will not change this estimate very much. Greenstein showed that the colouring action of the grains would tend only to increase the discordances.

The clue to the answer lies in the metastability of the 2^2S level of hydrogen mentioned in Chapter IV. Greenstein suggests that a sufficient number of hydrogen atoms accumulate in this level for absorptions from it to occur. If the nebula is considered to be a homogeneous, plane-parallel slab of thickness x_0 and at a constant electron temperature T_e , the

intensity I_ν of the emergent radiation in unit frequency interval would be

$$I_\nu = \int_0^{x_0} F_\nu e^{-\tau_\nu} dx, \quad . \quad . \quad . \quad (1)$$

where

$$F_\nu = A_1 N_1 N_e T_e^{-3/2} e^{-h\nu/kT_e} \quad . \quad . \quad (2)$$

is the emission per unit volume and solid angle

$$\tau_\nu = \int_0^x N_2 \alpha_{2\nu} dx, \quad . \quad . \quad . \quad (3)$$

where N_2 is the number of atoms in the second level, and

$$\alpha_\nu = A_2 \nu^{-3} \quad . \quad . \quad . \quad (4)$$

is the continuous absorption coefficient. Then

$$I_\nu = \frac{A_1 N_1 N_e}{A_2 N_2} \frac{\nu^3 e^{-h\nu/kT_e}}{T_e^{3/2}} [1 - e^{-\tau_\nu^0}] \quad . \quad . \quad (5)$$

is the intensity of the emergent beam. If the optical thickness in the Balmer continuum

$$\tau_\nu^0 = N_2 A_2 \nu^{-3} x_0$$

is small

$$I_\nu \rightarrow C_1 e^{-h\nu/kT_e}, \quad . \quad . \quad . \quad (6)$$

and we have the same functional dependence of I_ν on ν as for the Balmer continuum in the planetaries. On the other hand, if τ_ν^0 is large,

$$I_\nu \rightarrow C_2 \nu^3 e^{-h\nu/kT_e}, \quad . \quad . \quad . \quad (7)$$

which is the Wien approximation to the Planck law. That is, if the nebula is optically thick at a frequency ν the dependence of I_ν on ν will resemble that of a black body at T_e . Although strong self-absorption occurs in the Balmer continuum, there is no metastable Paschen level. Hence the continuous absorption coefficients should show a strong discontinuity at the Balmer limit, which Greenstein finds to amount to 1.6 magnitudes in the Orion nebula. The amount of this discontinuity is lower than might be expected, probably as a consequence of the superposition of starlight scattered by small particles.

If the 2^2S level is so well populated as to render the nebula optically thick in the Balmer continuum, an electron temperature of $12,000^\circ\text{K.}$ can be reconciled with a colour temperature of $12,000^\circ\text{K.}$ If this hypothesis is correct, the filamentary structure of the inner part of the nebula should be much less pronounced in the ultra-violet than in the blue. On the assumption that the Strömgren theory⁽¹⁵⁾ could be applied to the luminous

zone of the Orion nebula, Greenstein estimated the total number of neutral and ionized hydrogen atoms to be about $300/\text{cm}^3$. On the assumption that the distance of the nebula was 1300 light-years he estimated the luminous portion to have a radius of about 1.5 light-years. The actual extent of the dark portion of the nebula must be very much greater, although its density probably falls off at large distances from the Trapezium.

The entire Orion region is one of great complexity. In it are found several rich aggregates or associations of early-type stars. One is connected with the belt stars; several are found in the region of the sword.

TABLE VIII : 1

Gaseous Nebulae in the Large Magellanic Cloud

Nr.	Shape	ergs/sec./cm. ²	N_e	Theor. Sp. Class	Obs. Sp. Class
186 e	faint ring	0.70×10^{-4}	1.6	B2	(B2)
198	faint ring	1.24	2.1	B0	0a
9	crescent	1.06	4.1	B3	0e5
30 c	crescent	1.7	5.7	B1	P Cyg (B1)
200	crescent	0.49	1.7	B0	0a
44 e	bright knot	12.3	25.5	B0	0
191 a	bright knot	21.0	30.4	B2	(B2;)
180	irregular (knots)	~ 11.0	~ 18.0	$r < s_0$	
206	irregular (background) (knots)	3.0 ~ 3.0	3.0 ~ 9.0	$r < s_0$	
		Max. meas. value	65	45	
		Max. value (est.)	~ 600	~ 200	

The best known of these associations is the one connected with θ Orionis. The faint outer loop discovered by Barnard has an overall radius of curvature of about 50 parsecs and is not symmetrical with respect to the Orion nebula. The 21-cm. data (cf. p. 311) obtained at Harvard indicates a total mass of neutral hydrogen gas in the Orion region of the order of 60,000 solar masses.

The chaotic structures and great quantities of solid particles present in the diffuse nebulae make them even less tractable for theoretical work than the planetaries which at least appear to be purely gaseous throughout.

The Strömgren theory has often been applied to the interpretation of diffuse nebulae in our galaxy, although the irregularities are frequently so great that a detailed quantitative treatment is not possible.

A number of the diffuse nebulae in the Large Magellanic Cloud suggest Strömgren ionization zones in an extended cloud of neutral hydrogen. Table VIII : 1, prepared by Henize, Doherty, and the writer⁽¹⁶⁾ gives some of the salient data. The first column gives the number from Henize's catalogue, the second a brief description of the appearance of the nebula,

and the third gives the surface brightness in $H\alpha$ expressed in $\text{ergs/cm}^2/\text{sec}$. The electron density in numbers/ cm^3 as calculated from the surface brightness, and linear dimensions of the radiating filament, is given in the fourth column. From the radius of the ionized region (assuming it to be a Strömgren sphere) and the given electron density, one can estimate the spectral class required by the ionization theory. The spectral classes estimated in this way are entered under the column "*Theor. Sp. Class*". The observed spectral class is given in the last column. Notice that in a number of nebulosities the observed spectral class is earlier than the predicted one. In such instances the nebula may be smaller than the region capable of complete ionization. The radio observations by Kerr and Hindman⁽¹⁷⁾ in Australia (see Section 7) show that both Magellanic Clouds contain large quantities of neutral gas. They substantiate the interpretation of certain emission nebulae as ionization zones in an extended medium as well as the order of magnitude of the densities obtained from the optical region studies.

TABLE VIII : 2
*Data for Bright Diffuse Galactic Nebulae**

	Distance kilo- parsecs	Total Luminosity				A	\bar{N}_e	M
		$H\alpha$	$\lambda 5850$	OII	OIII			
NGC 6514	1.4	4.8	0.0061	3.8	1.8	4	87	120
6523	1.3	50.0	0.012	22.0	17.0	2	90	550
6611	2.3	16.0	0.0062	3.6	3.6	7	60	800
6618	2.0	26.0	0.012	—	18.0	13	180	1000

The luminosity is given in units of 10^{35} erg/sec. A gives the suggested reduction of intensity at $H\alpha$ due to space absorption, i.e. $A = S_{\text{true}}/S_{\text{obs}}$. The distances in kiloparsecs for the first three nebulae are from Morgan, Whitford, and Code, *Ap. J.*, **118**, 318 (1953); that of the fourth from Cederblad, *Lund Medd.*, 2, No. 119 (1946).

* Albert Boggess III, Thesis, Univ., of Michigan (1954).

Recently, Albert Boggess has made a detailed photometric study of the four bright galactic nebulae, NGC 6523 (M8), the Lagoon nebulae, NGC 6514 (M20), the Trifid nebula, NGC 6611 (M16), and NGC 6618 (M17). Table VIII:2 summarizes his results. The second column gives the distance in kiloparsecs. The third, sixth, fifth, and fourth columns give the total luminosity in the monochromatic radiations of $H\alpha$, the forbidden oxygen lines, and the continuum at $\lambda 5850$ as obtained from an integration over the isophotic contours. The space absorption correction factor A is determined by a comparison of radio-frequency and optical observations (see Section 7). The mean electron density is \bar{N}_e , while M is the estimated mass of the luminous region of each nebula in solar masses. These are much larger than the values estimated for the Orion nebula.

The Trifid nebula is a smooth, symmetrical body with a density that falls off steeply from the centre, although it does not fall to zero at the edge. M20 appears to be a "classical" Strömgren sphere illuminated by a central star of luminosity, 2.9×10^{36} ergs/sec. The M8 nebula appears to comprise several density condensations grouped about a central one of high surface brightness. This is the largest object of the four and possesses very faint extensions that may represent radiation leakage from the main body of the nebula. NGC 6618 is probably heavily obscured so that its actual mass and luminosity may be even larger than Boggess estimated. NGC 6611 is also an amorphous body of low surface brightness that also may have a larger total mass than has been computed.

On the other hand, Shajn and Hase have obtained electron densities for NGC 6523, 2237, and 6618 of 54, 28, and 110/cm.³, and masses of 3200, 5800, and 260 solar masses from measures of the surface brightness of *H α* . The discrepancy for NGC 6523 is striking, whereas that for NGC 6618 may be at least partially understood in terms of space absorption. Yet larger masses have been derived by Shajn and Hase for emission nebulosities in the external galaxies M31, M33, M101, and NGC 6822. They find an electron density, $N_e=100/\text{cm}^3$, for NGC 604 in M33 (compare Table 1, Chapter I) and a total mass of about 200,000 solar masses! The scale of their plates is much too small to permit any account to be taken of the filamentary structure of these objects. The determination of accurate densities and total masses will require observations secured with large telescopes. In order to excite a gaseous nebula with a radius of 20 or 30 parsecs and a density of 50 ions or electrons per cm.³, a whole association of O and B stars is needed. Hence it is not surprising that nebulosities such as NGC 595 and NGC 604 or the nebulae in NGC 2070 contain dozens of B and O stars. The observations of Shajn and Hase and those of G. Haro show that the largest gaseous nebulae tend to be found in *Sc* spirals rather than in *Sb* systems.

Shajn and Hase concluded that in certain nebulae such as NGC 6523 or NGC 6618 there is a tendency for the material to be concentrated in the periphery or at least at some distance from the centre. They base their deduction on the observed vestiges of rings, arcs, and layers that are disposed in a more or less symmetrical fashion with respect to the central region, the thickening near the edges, and the presence of luminous rings. They believe that masses of outward-moving material may overtake one another or encounter the braking action of the surrounding interstellar medium (see p. 300).

Fortunately, many of these questions may eventually be settled by observations such as those secured by G. Courtes. Whereas Boggess was restricted to objects of rather high surface brightness, the use of the

narrow band-pass Savart-Lyot filter permits the St. Michel observers to measure the intensities of very dim nebulosities. Furthermore, the Fabry-Perot etalon enables the measurement not only of the internal radial velocities but also the contributions of weak lines such as the [NII] pair near $H\alpha$.

The internal motions in the diffuse nebulae, i.e. the kinematics of the gaseous knots and filaments have come in for increasing attention. In general, we deal here with a compressible fluid which may move in free space at supersonic velocities in the presence of a magnetic field. Before discussing this interesting hydrodynamical problem let us briefly mention the evidence for the interstellar magnetic field.

4. The Galactic Magnetic Field

One of the outstanding classical problems of galactic structure has been the explanation of the spiral arms in external galaxies such as the Triangulum and Andromeda spirals. Early attempts were made to identify these arms as arms of stars, but the work of Baade⁽¹⁸⁾ has conclusively shown that they are arms of gas and solid grains. The question naturally arises: What keeps the gas in the spiral arms? Why does it not diffuse throughout the entire plane of the galaxy? The answer seems to lie in the existence of a general galactic magnetic field.

Some years ago Hiltner⁽¹⁹⁾ and Hall⁽²⁰⁾ discovered that the light of distant stars in the galactic plane is often polarized as though by scattering produced by systematically oriented elongated grains. The only plausible mechanisms capable of maintaining such particles oriented parallel to one another over large regions of space require an interstellar magnetic field.⁽²¹⁾ These aligned, elongated particles scatter different amounts of light respectively parallel to and perpendicular to the magnetic field.

Plots of the orientation of the polarization vector against galactic longitude and latitude suggest that the interstellar magnetic field runs along the local spiral arm, even though large local irregularities exist. Hence the direction of the field cannot be constant; the direction of the lines of force must be warped and distorted. Hiltner's data indicate that the mean deviation, α , of the direction of the field from that of the spiral arm must be about 0.2 radian.⁽²²⁾

Chandrasekhar and Fermi⁽²³⁾ pointed out that there must be a relationship between α and H . As the ionized gas of the interstellar medium is pushed about by radiation pressure, gravitational forces, etc., so that density fluctuations are produced, the lines of magnetic force are twisted and turned. If the magnetic field were strong, the turbulent motions would be powerfully inhibited as the lines of force would tend to keep themselves straight. Hence the angle α would be small. On the other hand, α would be

large if the field is weak, because the random motions of the interstellar clouds would be little affected by the magnetic lines of force. They would be twisted and turned as the clouds moved about.⁽²⁴⁾

Chandrasekhar and Fermi established a relation between α and H by the following argument.⁽²⁵⁾ The motion of a disturbance in a magnetized, tenuous gas is governed by the combined action of hydrodynamic and electromagnetic principles. If ϱ is the density of the interstellar material (which has a high conductivity) and H is the strength of the interstellar magnetic field,

$$V = \frac{H}{\sqrt{4\pi\varrho}} \quad . \quad . \quad . \quad . \quad . \quad (8)$$

is the velocity of the transverse oscillations of a given line of force.⁽²⁶⁾ This magneto-hydrodynamic wave can be represented by the expression

$$y = A \sin \frac{2\pi}{\lambda} (x - Vt), \quad . \quad . \quad . \quad . \quad . \quad (9)$$

where y is the displacement of the line of force in a direction perpendicular to that of the propagation of the wave, x . Here λ is the wavelength of the disturbance. Now

$$\frac{\partial y}{\partial x} = \frac{2\pi A}{\lambda} \cos \frac{2\pi}{\lambda} (x - Vt), \quad . \quad . \quad . \quad . \quad . \quad (10)$$

$$\frac{\partial y}{\partial t} = \frac{2\pi A}{\lambda} V \cos \frac{2\pi}{\lambda} (x - Vt), \quad . \quad . \quad . \quad . \quad . \quad (11)$$

so that

$$V^2 \left(\frac{\partial y}{\partial x} \right)^2 = \left(\frac{\partial y}{\partial t} \right)^2. \quad . \quad . \quad . \quad . \quad . \quad (12)$$

Now $\partial y / \partial x$ represents the tilt of a line of force with respect to the plane of the spiral arm. Hence

$$\left(\frac{\partial y}{\partial x} \right)^2 = \alpha^2. \quad . \quad . \quad . \quad . \quad . \quad (13)$$

Furthermore, if the turbulent velocities, v , of the gas clouds are isotropic,

$$\overline{v^2} = \overline{v_x^2} + \overline{v_y^2} + \overline{v_z^2}, \quad . \quad . \quad . \quad . \quad . \quad (14)$$

and in particular since the lines of force are anchored in the material,

$$\left(\frac{\partial y}{\partial t} \right)^2 = \frac{1}{3} \overline{v^2}. \quad . \quad . \quad . \quad . \quad . \quad (15)$$

From equations (8), (12), (13), and (15) we now find:

$$H^2 = \frac{4}{3} \pi \varrho \frac{\overline{v^2}}{\alpha^2}. \quad . \quad . \quad . \quad . \quad . \quad (16)$$

Chandrasekhar and Fermi adopted the following numerical values as appropriate to the local spiral arm:

$$\begin{aligned}\rho_u &= 2 \times 10^{-24} \text{ gm./cm.}^3, \quad (27) \\ v &= 5 \times 10^5 \text{ cm./sec.}, \quad (28) \\ \alpha &= 0.2 \text{ radian.}\end{aligned} \quad (17)$$

Hence

$$H = 7.2 \times 10^{-6} \text{ gauss.} \quad (18)$$

A second estimate of the value of H was obtained from the condition that the gas and dust in the spiral arm be in equilibrium with respect to sideways expansion or contraction. They equated the pressure due to the gravitational attraction of the spiral arm upon itself to the sum of the material and magnetic field pressures.

The gravitational force arises from the action of all matter (stars plus gas and grains), but we are interested only in the gravitational pressure on the interstellar matter. Suppose that the spiral arm is a cylinder of constant density and total radius R . At a point whose distance from the centre of the cylinder is r , the gradient of the gravitational pressure will be

$$\frac{dP}{dr} = -\frac{2GM(r)}{r} \rho = -2G\pi r \rho_i \rho, \quad (19)$$

since $M(r) = \pi r^2 \rho_i$ is the mass per unit length within the radius r . Here ρ_i is the average density of all matter in the spiral arm. Integrating equation (19), we obtain

$$P_{gr} = \pi G(R^2 - r^2) \rho_i \rho. \quad (20)$$

Near the centre of the arm

$$P_{gr} \sim \pi G \rho_i R^2. \quad (21)$$

For equilibrium we must have

$$P_{gr} = p_{kin} + p_{mag}, \quad (22)$$

where

$$p_{kin} = \frac{1}{3} \rho v^2 \quad (23)$$

is the kinetic pressure produced by the turbulent gas. The magnetic pressure is

$$p_{mag} = \frac{H^2}{8\pi}. \quad (24)$$

If the radius of the spiral arm is taken as $250 \text{ parsecs} = 7.7 \times 10^{20} \text{ cm.}$ and $\rho_i = 6 \times 10^{-24} \text{ gm./cm.}^3$, $P_{gr} = 1.5 \times 10^{-12} \text{ dynes/cm.}^2$, $p_{kin} = 0.2 \times 10^{-12} \text{ dynes/cm.}^2$, hence $p_{mag} = 1.3 \times 10^{-12} \text{ dynes/cm.}^2$, and H turns out to be $6 \times 10^{-6} \text{ gauss.}$

In a second paper⁽²⁹⁾ Chandrasekhar and Fermi give yet another method

for estimating the strength of the galactic magnetic field. They consider the conditions necessary for the stability of an infinite cylinder of incompressible fluid with a magnetic field along its axis when it is subjected to periodic transverse deformations. If the wavelength of these deformations exceeds a certain critical value which depends on the field strength, the cylinder will break up. The magnetic field tends to prevent the instability from being set up. If these considerations be applied to the spiral arms of our own galaxy (approximated as cylinders of density $\rho = 2 \times 10^{-24}$ gm./cm.³ and radius $R = 250$ parsecs), they find that a field of 7×10^{-6} gauss will effectively prevent the arms from disintegrating. If the field is 6.25×10^{-6} gauss, disintegration of the spiral arms will set in after about 2.5×10^9 years.

These estimates by Chandrasekhar and Fermi seemingly give a reliable estimate of the mean strength of the magnetic field, but there are good reasons for believing that the field is not uniform within the spiral arms themselves. The observations by Hiltner and by Hall indicate that the direction of the interstellar magnetic field is strongly affected by local turbulence which acts to change the density of the gas and, therefore, the strength of the local field that is dragged along with the material.

The density of the interstellar medium fluctuates over a range exceeding a hundredfold as a consequence of the perturbing effects of radiation pressure, gravitational attraction of nearby stars and clusters, and the tidal action of the central bulge of the galaxy. Hence a fiftyfold variation in the intensity of the field from one point to another is not unlikely, and tenfold variations seem distinctly probable.

Although most loops and arches observed in gaseous diffuse nebulae are probably to be interpreted as fragments of Strömgren spheres, the character of the loops in some objects such as 30 Doradus in the Large Magellanic Clouds suggest the presence of large-scale non-uniform magnetic fields. Some gaseous nebulae contain long, thin filaments, strongly oriented as though by a magnetic field. One of the best examples of this phenomenon is exhibited by the Network nebula in Cygnus, which we shall discuss in Section 6.

5. Turbulence in Galactic Nebulae and the Interstellar Medium

In astronomical objects in general and in the interstellar medium in particular, smooth laminar flow is rarely encountered. The *Reynolds number* is

$$R = \frac{\rho v l}{\eta}, \quad . \quad . \quad . \quad . \quad (25)$$

where l is the linear size of the objects, while v is identified with the relative motions of the fluid. Here ρ is the density and η is the viscosity;

the ratio $\nu = \eta/\rho$ is called the *kinematical viscosity*, which is usually very large. If the diameter of a large diffuse cloud is taken as about 10^{19} cm., the speed of the cloud as 10^6 cm./sec. and the kinematical viscosity⁽³⁰⁾ as 10^{19} cm.² sec.⁻¹ (as compared with values of 0.15 cm.² sec.⁻¹ and 0.01 cm.² sec.⁻¹ for air and water respectively) we find R to be of the order of 10^6 . Since laminar flow breaks down into turbulent flow for Reynolds's numbers in excess of 1000, we can expect motions within the diffuse galactic nebulae to be turbulent in character.

The mathematical discussion of the theory of turbulence lies outside the scope of this book, and we shall restrict ourselves to a few general comments.⁽³¹⁾ In a fluid in turbulent motion, suppose that we could measure the velocity as a function of position at a given instant, t . We might make an harmonic analysis of this velocity field $\mathbf{v}(\mathbf{r}, t)$ of the form

$$\mathbf{v}(\mathbf{r}, t) = \sum_k \mathbf{v}_k(t) \exp(i\mathbf{k} \cdot \mathbf{r}), \quad (26)$$

which amounts to interpreting the instantaneous velocity field as the superposition of harmonic variations of all possible wavelengths, λ , which are related to the wave number k by $k = 2\pi/\lambda$. The lower limit of k is fixed by the dimensions of the container in which the turbulence occurs. The upper limit is controlled by the fact that the very smallest eddies are continually being wiped out by viscosity. Since a Fourier analysis of this type will require the simultaneous presence of eddies of many different sizes, there will exist what is called a *hierarchy of eddies*. The amount of mechanical energy residing at any instant in a unit mass in eddies of wave numbers between k and $k+dk$ will be $F(k)dk$, where the function $F(k)$ specifies the *spectrum of turbulence*. For small values of k (large eddies), the character of this function will depend on the exact means by which mechanical energy is supplied to the fluid. The transfer of energy from these large to smaller eddies is accompanied by an increasing degree of disorder. The forces or temperature gradients that supply energy to the large eddies usually do so in a non-isotropic fashion, but the passage of the energy to the smaller eddies is accompanied by an increasing approach to isotropy in the motion. The reason why the small-scale turbulence tends to be isotropic is to be sought in the fact that pressure differences play a large role in the degradation of the motions. A compressed region tends to expand in all directions so that any directionally dependent properties of turbulence tend to be wiped out in the small eddies.

Furthermore, each eddy of a given k dissipates as heat some of the energy it receives from the larger eddies. The rest is passed on to smaller eddies as kinetic energy of motion. In eddies of some size, say $\sim k_s$, the dissipation of energy by viscosity will become important, and the motion within the tiny whirl will be laminar. The frequency of eddies of yet

smaller size will fall off very rapidly. If the Reynolds number, defined by equation (25) is sufficiently large, there will exist a large region of the turbulence spectrum, i.e. for eddies of intermediate sizes, $k_0 \ll k \ll k_s$, for which thermal dissipation will be negligible. In this domain the distribution function $F(k)$ will depend on ε , the rate at which energy is supplied to the largest eddies, as well as on the viscosity.

Now $F(k)$ has the dimensions $(\text{velocity})^2 \times \text{length}$, while k has the dimension $(\text{length})^{-1}$. Now for $k \gg k_0$, $F(k)$ will depend on $e = \varepsilon/\rho$ and the kinematical viscosity $\nu = \eta/\rho$ (ratio of ordinary viscosity to density). As $\nu \rightarrow 0$, the spectrum depends more and more closely on e .

In order to obtain some notion of the character of the turbulence spectrum in this region, Kolmogoroff employed a dimensional analysis. The dimensions of ε are $(MV^2/T)L^{-3} = ML^{-1}T^{-3}$, ρ has dimensions ML^{-3} . Hence e has dimensions V^2T^{-1} , while those of ν are L^2T^{-1} .

Combinations of ν and e , having the dimensions required for $F(k)$ and k , are:

$$\begin{aligned} F(k): [L/T]^2 \times [L] &= [(\nu^2 e)^{1/4}] \\ k: [L]^{-1} &= \left[\left(\frac{\nu^3}{e} \right)^{1/4} \right]^{-1}, \end{aligned} \quad (27)$$

and hence $F(k)$ must have the form

$$F(k) = (\nu^5 e)^{1/4} f(k \nu^{3/4} e^{-1/4}). \quad (28)$$

Since k has the dimensions L^{-1} , the quantity in $()$ in $f()$ is dimensionless.

If the Reynolds number is very large (which corresponds to $\nu \rightarrow 0$), $F(k)$ should be independent of the viscosity. Thus we require that

$$F(k) \rightarrow A(\nu^5 e)^{1/4} \left(\frac{\nu^3}{e} \right)^{-5/12} k^{-5/3} = A e^{2/3} k^{-5/3} \quad (29)$$

for $F(k)$ to be independent of ν ; A is constant. That is, the larger the Reynolds number, the more closely will the turbulence spectrum approach the *Kolmogoroff approximation*,

$$F(k) \sim k^{-5/3}. \quad (30)$$

Let us define v_k as the mean velocity of all eddies with wavelength less than λ_k in accordance with the expression

$$v_k = \left[\int_k^\infty F(k) dk \right]^{1/2}. \quad (31)$$

If the Kolmogoroff approximation can be applied, we see

$$v_k = \frac{c_1}{k^{1/3}} = \frac{c_1}{\sqrt[3]{2\pi}} \lambda^{1/3}, \quad (32)$$

where c_1 is a constant. Kolmogoroff's method of developing the asymptotic form of the equilibrium spectrum gives no information concerning the

domain in which energy is dissipated by turbulence. A more comprehensive, although less reliable, theory which enables the spectrum in the dissipation range to be determined has been given by Heisenberg. For stationary, fully developed turbulence in which ε_k is a constant, independent of k , Chandrasekhar has shown that

$$F(k) = \text{const.} \left(\frac{k_0}{k} \right)^{5/3} \frac{1}{[1 + (k/k_s)^4]^{4/3}} \quad k > k_0, \quad \dots \quad (33)$$

$$F(k) = 0 \quad k < k_0,$$

where k_s is a parameter that depends on the Reynolds number and the wave number k_0 of the largest eddy.

The equilibrium theories, i.e. those concerned with the small-scale motions, postulate that the small-scale motions are isotropic and statistically steady (i.e. have times of change small compared with their characteristic periods), whatever the nature of the large-scale motion. Modifications of the elementary theory are required in the domain of the larger eddies that contain the kinetic energy as soon as the compressibility of the fluid and the presence of magnetic fields are taken into account.

A gaseous nebula can be treated as a compressible fluid from the standpoint of turbulence theory only so long as the mass motion of one part of the object with respect to another part of the object is less than the velocity of sound. This condition is not always fulfilled and Mach numbers, M , exceeding one may occur.⁽³²⁾ A rigorous generalization of the equilibrium theories to compressible fluids would be difficult although some kind of a perturbation treatment may be possible. Some general qualitative remarks may be made. Even at subsonic speeds the finite compressibility of the gas will cause compressional (longitudinal) waves to be set up in addition to the shear (transverse) waves. Lighthill has discussed the mechanism for the generation of compressional waves. Pressure fluctuations in the medium can be regarded as the source of the acoustical waves which carry away a small amount of energy if the Mach number is small. Under these circumstances the turbulence will not be much affected. The dissipation of energy in noise rises rapidly, however, as M increases. At large values of M it is not possible to give a quantitative discussion of the problem. The acoustical waves evolve into a random distribution of shock waves which interact with one another and with the transverse waves. The amount of energy dissipated by the shock waves is comparable with that degraded by the transverse waves. As $M = u/c$, where u is the velocity of the material and c is the velocity of sound, becomes very large, say ~ 14 or 15 , the shock waves become intense and we can no longer speak of a hydrodynamical connexion between different parts of the fluid. Thus the proper picture of motion in certain gaseous nebulae may well become that

of a number of separate non-interacting elements which have no hydrodynamical connexion with one another.

It is to be expected that the energy will be introduced into the largest eddies in a non-isotropic fashion. For example, radiation pressure from stars and clusters of stars will almost certainly be directionally dependent. Nevertheless, because of the role of pressure in the transfer of energy from one eddy size to another the turbulence tends to become isotropic. The lifetime of these larger eddies will be simply the time required for one of them to make a revolution and decay. In this time interval,

$$T = l(\bar{u}^2)^{-1/2}, \quad (34)$$

energy will be transferred from the large-scale to the small-scale eddies. For a gaseous nebula of diameter $l = 19 \times 10^{17}$ cm. ≈ 2 light-years, and $(\bar{u}^2)^{1/2} = 10^6$ cm./sec. the time-scale of decay of the energy in the largest eddy will be of the order of 1.9×10^{12} sec. $\approx 60,000$ years. Chandrasekhar has discussed the change of the shape of the turbulence spectrum when the driving force is cut off and the turbulence is allowed to decay. In gaseous nebulae, however, we cannot be sure that decaying turbulence is observed. It seems more likely that the energy going into the larger eddies fluctuates with the time. As the energy is passed down through the hierarchy of eddies the effect of these fluctuations tends to be smoothed out. In the smaller eddies the turbulence may be relatively stationary for long periods of time. In objects like the Orion nebula, however, the largest eddies may fluctuate in size and motion as the driving force of the turbulence changes. Over large regions of the spiral arm one might expect radiation and gravitational forces to keep the material rather well churned up.

In view of the probable existence of a magnetic field pervading the interstellar medium and diffuse nebulae the interaction between turbulence and this field assumes considerable importance. Turbulence is a random and diffusive phenomenon. Hence the separation between any two points in the fluid will tend to increase with the time. Since the lines of magnetic force are frozen into the medium, the lines of force will tend to follow the motion and be stretched out. There will be a sharing of the energy between the magnetic field and the kinetic energy of motion. Bierman, Schluter, Alfvén, Fermi, and others have suggested that because of the strong coupling between magnetic and kinetic energies,

$$\frac{H^2}{8\pi} \sim \frac{1}{2} \rho v^2.$$

On the other hand, G. K. Batchelor has suggested that not all of the turbulent energy is available for transfer to the magnetic field. Equipartition of magnetic energy will occur with the small eddies in which a maximum dissipation of energy occurs.

Batchelor finds that if a small magnetic field is initially present in the interstellar medium it will be built up to value for equilibrium with turbulence in the course of a few thousand years. The rate of decay of an interstellar magnetic field through the mechanism of setting up electric currents that dissipate their energy through ohmic heating is so very slow that these fields must be regarded as essentially permanent. The presence of this field must be taken into account in all hydrodynamical studies of diffuse nebulae.

The most detailed application of turbulence theory concepts to the interpretation of the internal radial velocities in a gaseous nebula was carried out by S. von Hoerner for the Orion nebula.⁽³³⁾ He assumed that this object could be treated as an incompressible fluid in a steady state and applied the Kolmogoroff spectrum law in the form

$$[(V_1 - V_2)^2] = C^2 |\mathbf{r}_1 - \mathbf{r}_2|^{2/3}, \quad (35)$$

where $V_1 - V_2$ is the difference in radial velocity between two points of a pair located by the vectors \mathbf{r}_1 and \mathbf{r}_2 . The constant C depends on the nebular density.

The observed radial velocity V at any point in the nebula will comprise contributions from radiating volumes all along the line of sight. S. von Hoerner considered two limiting models: I, a fully transparent nebula; and II, a nebula that is almost opaque. The emission is assumed to decline exponentially with distance into the nebula. He considered also the effects of (a) measuring errors, (b) the finite surface area covered by the spectrograph slit, and (c) the statistical departures of the observed values of $|V_1 - V_2|^2$ from the expected values.

The basic observational data are those of Campbell and Moore,⁽³⁴⁾ who measured the radial velocity at eighty-five points in the Orion nebula. The greatest number of observations were secured in the inner, brighter portions of the object. Hence von Hoerner treated the inner portion separately. In order to find a satisfactory statistical interpretation of the observations he found it necessary to suppose that the depth to which we can see in the nebula is less than 0.10 parsec at the centre and 0.40 parsec elsewhere in the nebula. The corresponding extinction coefficient must be greater than 0.11 magnitude per parsec at the centre of the nebula! The densities, computed on the assumption that the sizes of the particles are roughly the same as elsewhere in the interstellar medium, exceed 8×10^{-23} gm./cm.³ at the centre of the nebula and 2×10^{-23} gm./cm.³ elsewhere. The mass of the whole nebula was estimated to be about six solar masses—as compared with ten solar masses found by Greenstein by entirely different methods! The total mass of gaseous material in the Orion region is very much greater, however (cf. p. 311).

On the basis of the agreement between the theoretical curves and the velocity-pair statistics for the observed points, von Hoerner concluded that the Orion nebula exhibited a turbulence spectrum. The exponent in the law (cf. equation (32))

$$v_k = \text{const. } \lambda^n \quad (36)$$

fell between $1/4$ and $1/2$. He was not able to find the dimensions of the smallest turbulent elements, and was only able to conclude they were larger than 0.02 parsec—a distance very much larger than the mean free path of a gas ion.

When the velocity distributions derived from the point-pair statistics as analysed by the turbulence theory are compared with the velocity distributions deduced from the widths of the spectral lines as measured by Baade and Minkowski, a serious discrepancy is found. The line width velocities are about three times as great as those found from the von Hoerner analysis. That is, if two radiating elements lie at a distance h behind one another, the average difference of their radial velocities is about three times as great as if they lie side by side!

S. von Hoerner also compared the values of the constant C for the inner portion and whole of the Orion nebula with estimates carried out for the interstellar sodium and calcium lines and for emission nebulae in the Milky Way and Magellanic clouds. The results suggested that the turbulent energy density is much higher in Orion. Accordingly, von Hoerner suggested that energy is not only dissipated in the nebula but is transported from the inner regions near the Trapezium to the outer portion. An anisotropy of the turbulence in the smaller elements might result. A satisfactory interpretation of this discrepancy within the framework of the usual turbulence theory is not obvious. One thinks of the energy being supplied to anisotropic large eddies and passed down to smaller and smaller eddies which become increasingly isotropic. If the smaller eddies are not isotropic, the whole application of the concepts of homogeneous turbulence to the Orion nebula is open to question. Further observational data on the Orion and other galactic nebulae should be very useful in establishing the character of the turbulence existing in such objects. New observations being secured at Mt. Wilson should enable a much more satisfactory study of the kinematics of the Orion nebula to be made.

The scarcity of radial-velocity data for other galactic nebulae, particularly for those of low surface brightness, now precludes further analyses similar to those made by von Hoerner. The need for some other line of attack is indicated. Traditional turbulence theories have been concerned mostly with the correlations between the velocity differences and the distances between selected points in the fluid. Since the density, pressure, and velocity of a given volume element in turbulent motion are all

connected, the results of the theory can be generalized to discuss the effects of turbulence upon the densities and pressures. Hence, if the radial velocity variations from one point to another in a gaseous nebula are not known, we can use the fluctuations in its surface brightness, provided that these fluctuations are produced by random variations in the density of the radiating gases. We assume that T is constant in the HII region.

The shapes of bright-line clouds such as Messier 8 or the Trifid nebula depend not only on the spatial distribution of the material but also on the arrangement of the exciting stars. The two effects must be taken into account. In certain regions of the Milky Way, however, it does appear to be possible to select areas where the bright nebosity is distributed at random and is excited by stars that are some distance away. Care must also be exercised to make sure that there is no obscuration produced by dark clouds in the line of sight.

Such a region appears to be located in Cygnus between $\alpha=20^h1^m$, $\delta=+38.0^\circ$ and $\alpha=20^h13^m$, $\delta=+34.5^\circ$. Some years ago the writer made a detailed study of this region on plates taken with the Palomar 48-in. Schmidt and plate-filter combination to isolate the $H\alpha$ radiation.⁽³⁵⁾ If the surface brightness, $I(x)$, can be measured as a function of the distance along a line drawn in the plane of the sky,

$$I(x) = \int_{-\infty}^{+\infty} E(z, x) dz, \quad . \quad . \quad . \quad (37)$$

where z is the distance along the line of sight, and E is the emission in $H\alpha$ per unit volume. Now $E \sim N_i N_e \sim N_e^2 \sim \rho^2$, where ρ is the density. Actually, since the turbulence produces density variations in a gas of some mean density ρ_0 , we are concerned with fluctuations in the intensity $I(x)$ about a mean value I_0 . If the turbulence is homogeneous, the turbulence spectrum of $I'(x) = I(x) - I_0$ is the same as the turbulence spectrum of $E(z, x) - E_0$, which is related to $\rho^2 - \rho_0^2$. In practice the measured quantities were the galvanometer deflections registered by the microphotometer. These are roughly proportional to the intensity since the latter varies over only a small range. The correlation function $g(r)$,

$$g(r) = \frac{\Sigma I'(x) I'(x+r)}{\Sigma I'(x)^2} \quad . \quad . \quad (38)$$

is related to the turbulence spectrum by

$$F(k) = \sqrt{\frac{2}{\pi}} \int_0^\infty g(r) \cos kr dr. \quad . \quad . \quad (39)$$

Detailed numerical analysis shows that $F(k)$ has a sharp maximum corresponding to an eddy size of $34'$. Thereafter $F(k)$ falls off roughly as $k^{-1.8}$. If the results are interpreted in terms of the turbulence spectrum,

this means that the largest whirls have a sufficient store of energy to maintain a flow of energy down the hierarchy of eddies. If the diffuse clouds lie at a distance of 1000 parsecs, as their association with nearby supergiant stars would suggest, the largest eddy is about 10 parsecs in diameter.

We speak of the "turbulence spectrum" of these gas clouds. Yet it may be that although the Fourier analysis of the brightness variations yields a function that resembles a turbulence spectrum, it is really not a turbulence spectrum at all in the accepted meaning of the term! The Mach numbers are often large, and turbulence under these conditions is poorly understood. Large amounts of energy are probably dissipated quickly in acoustical and shock waves rather than by slow leakage in the course of passage through the hierarchy of eddies.

The sharpness of the interstellar *H* and *K* lines shows that the internal motions in large clouds of attenuated gas are frequently very small. D. ter Haar suggests that these clouds shed material until the motions inside are laminar.⁽³⁶⁾ The stabilization process takes about one year. The sizes of the cloud are determined by the requirement that they are the largest units within which no turbulence will occur. The clouds are continually being destroyed by the tidal action of the galactic centre, by encounters with stars, and particularly by collisions with other clouds, which limit their lifetimes to about ten million years.

The lifetimes of the denser galactic nebulae like Orion must be measured in millions of years. Eventually they disappear as the material of which they are composed is dissipated in space or collected into stars.

Further work along the lines indicated by McVittie, Burgers, van de Hulst, and von Hoerner is needed to clarify the many hydrodynamical problems of the interstellar medium.

6. The Network Nebula in Cygnus

One of the most fascinating of gaseous nebulae is the Network nebula in Cygnus. Direct photographs reveal an intricate lace-like structure that covers a considerable area. The filaments show the characteristic bright lines of a hot gas—there is no evidence of any solid particles. This object presents a host of perplexing problems.

For example, photographs taken at Mt. Wilson forty years apart show a motion of the filaments across the line of sight, but no perceptible change in their delicate, wispy structures. The work of Burgers⁽³⁷⁾ indicates that such a filament in a vacuum should expand at a rate so as to double its initial radius in less than a century. Evidently some forces must act to maintain the shapes of these filaments, and one is tempted to suppose that local magnetic fields may play a role.

The source of excitation of the nebular spectrum presents an even more challenging problem. Searches by Hubble⁽³⁸⁾ and more recently by Wachmann at the Hamburg Observatory revealed no hot star enclosed within the region defined by the nebula that might serve as a source of thermal excitation. It has been suggested that such a star might lie behind an obscuring cloud. Star count studies do not indicate an adequate amount of absorption within the loop of the Network nebula.⁽³⁹⁾ On the other hand, there exists the possibility that the Network nebula may lie at the same distance from the sun as the cluster of early-type stars described by Miss Roman,⁽⁴⁰⁾ and draw its excitation from them. J. W. Chamberlain estimates that if there is no extinction of the radiation between the cluster and the loop, about 10% of the hydrogen could be ionized if T_e is as low as 10,000° K.⁽⁴¹⁾

The loop appearance of the nebula and the fact that the two brightest portions are slowly moving apart have suggested to various workers that the object may be the relic of an ancient nova outburst. Humason's radial velocity measures of various filaments show that the internal motions are somewhat irregular and cannot be interpreted as a simple expansion. Adopting the nova-shell hypothesis, Oort⁽⁴²⁾ suggested that the source of excitation of the nebular radiation might lie in the dissipation of the kinetic energy of the gases as they moved through a resisting medium. Under these circumstances the Balmer lines would be excited primarily by collisional processes. The Balmer decrement might be substantially different than that for purely radiative excitation.

The Oort hypothesis is amenable to a quantitative check. The amount of energy radiated by the filaments may be observed directly. Since the speeds of these filaments are known and lower limits to their masses may be found, the rate of dissipation of energy may be compared with the total store of kinetic energy. J. W. Chamberlain used the 24-in. Curtis Schmidt telescope at the Portage Lake Station of the University of Michigan to make a study of the Network nebula by photographic photometry. He employed appropriate combinations of plates and filters to isolate the $H\alpha + [NII]$, the $[OII]$, and the $[OIII]$ emissions. Following a suggestion by F. D. Miller he established the surface brightness of the nebula in these various radiations by photographing the companion to the Andromeda spiral, M32, with the same plate-filter combinations and exposure times. The spectral energy distribution, total magnitude and surface brightness of M32 along its major and minor axes have been measured by Stebbins and Whitford⁽⁴³⁾ and by R. O. Redman.⁽⁴⁴⁾ The spectral energy distribution in Messier 32 is very similar to that of the sun. When the transmissions of the filters and optical equipment, the spectral sensitivity of the emulsion, and the atmospheric transparency effects were allowed for, it

was possible to determine the surface brightnesses of various selected filaments in the light of $\lambda 3727$, $H\alpha + [\text{NII}]$, and the green nebular lines.

Chamberlain's photographs show pronounced excitation differences from one part of the nebula to another. For example, in NGC 6960 certain filaments that are prominent in the forbidden oxygen lines are weak or missing in $H\alpha + [\text{NII}]$.

On the assumption that the filaments are cylinders of uniform density, Chamberlain derived the mean emission in $\text{ergs/cm}^2/\text{sec}$. in the various monochromatic radiations in seven different regions of the nebula. For an average filament and an assumed distance of the nebula of 500 parsecs he finds $E(H\alpha) = 1.37 \times 10^{-19} \text{ ergs/cm}^2/\text{sec}$. The emission in $\lambda 3727$ $[\text{OII}]$ and $N_1 + N_2$ $[\text{OIII}]$ averages 5.6 and 2.8 that of $H\alpha$. In order to interpret these numbers in terms of densities the physical mechanisms of excitation and the electron temperature must be known. The ratio of 4363 to $N_1 + N_2$ indicates a very high temperature of the order of $100,000^\circ\text{K}$. on the basis of Seaton's cross-sections. Chamberlain found that his observations could be interpreted with a variety of temperatures between $20,000^\circ\text{K}$. and $40,000^\circ\text{K}$., and either collisional excitation or radiative excitation by a distant high-temperature source.

Slit spectrograms of the loop nebula have been secured by Humason, van de Hulst, and most recently by Minkowski.⁽⁴⁵⁾ These observations showed that generally $[\text{OII}]$ 3727 was strongest, $N_1 + N_2$ $[\text{OIII}]$ next, while $H\gamma$, 4363 $[\text{OIII}]$, and $[\text{NeIII}]$ were weaker; the relative intensities showed pronounced fluctuations from filament to filament. Minkowski finds that the red $[\text{NII}]$ lines are not of negligible intensity. The ratio $H\alpha/[\text{NII}]$ varies from about 3.2 to 4.1. The $H\alpha/H\beta$ ratio becomes about 1.2 to 1.4, whereas the theoretical ratio for radiative excitation is between 2 and 3 for electron temperatures between 40,000 and $160,000^\circ\text{K}$. Nor can the extremely small $H\alpha/H\beta$ ratio be attributed to collisional excitation. Chamberlain finds that the Balmer decrement remains steep ($H\alpha/H\beta \sim 3$) even for temperatures as high as $160,000^\circ\text{K}$. The decrement is steepened if the nebula is optically thick. The measurement of the $H\alpha/H\beta$ intensity ratio needs verification.

A high electron temperature does not necessarily imply the dissipation of mechanical energy. The energy could be supplied to the filaments by radiative processes to maintain a high electron temperature. The hydrogen energy levels could be excited by collisions with electrons.

Chamberlain's data permit a quantitative test of Oort's hypothesis that the excitation of the Network nebula arises from the dissipation of the kinetic energy of an expanding nova shell colliding with an interstellar gas cloud. From the emission in $H\alpha$ it is possible to estimate the total rate at which energy is radiated away by the filaments. The velocities of the

filaments are known from the data of Humason, and their masses can be guessed from the rate at which they emit energy. In this way Chamberlain finds that the rate of energy dissipation is such that the entire kinetic energy of the moving filament could be used up in about thirty years. Since the filaments have not changed in appearance by detectable amounts in nearly fifty years some other source of excitation must be sought. The Cygnus cluster of O and B stars possibly supplies enough radiant energy, but here again the rate of energy supply may not be enough unless these stars have very rich sources of ultra-violet energy.

Burgers^(37, 46) and others⁽⁴⁷⁾ have attempted to apply aerodynamical methods to the problem of the collision between a gaseous nebula and the interstellar medium. A solution appears practicable if the loss of energy by radiation and thermal conduction can be neglected, but Chamberlain's work shows that such approximations are not permissible for the Network nebula. When the radiation losses are important, the equations become intractable and a solution has not been obtained. Burgers has also suggested that bright emission regions may arise when shock waves pass through an extended gaseous nebula. Effects of this type may appear in the various diffuse galactic nebulae. Kantrowitz has suggested the possibility that the Network nebula may represent a luminous shock front, analogous to the phenomena observed in shock tubes. The measured radial velocities would not then be connected with the motion of the luminous body of the nebula.

Shajn and Hase have discovered additional objects in which the orientation and delicacy of the filaments strongly suggest the presence of a galactic magnetic field. The wisps tend to lie parallel to the galactic plane as they do in the Network nebula.* Furthermore, these filamentary nebulosities also appear to have no early-type stars to which their excitation can be ascribed.

The Network nebula has not yet been observed as a radio source, although it is possible that with the development of powerful new equipment it can be found by these techniques. A somewhat similar nebula, IC 443, has been detected as a radio source (see p. 305).

7. Gaseous Nebulae as Radio Sources

Since Jansky's discovery of "cosmic static" twenty years ago, the new field of radio astronomy has been rapidly developed. Progress has been particularly rapid since 1945 as new techniques devised under the stimulation of the war effort could be applied to astronomy.⁽⁴⁸⁾

* It is of interest that long filamentary dust clouds described by W. W. Morgan likewise tend to be oriented parallel to the galactic plane—or more precisely to the Gould belt of bright stars.

We shall not attempt a detailed discussion of galactic radio astronomy nor of the observational techniques employed, but shall concentrate our attention on sources of radio-frequency radiation identified with gaseous nebulae.

The earlier surveys with low-resolution equipment by Grote Reber and others showed that the galactic radio noise was strongest in the direction of the Milky Way with strong concentrations near the galactic centre and in Cygnus.

The sun was discovered to be a strongly variable radio noise source, but it was at once evident that the sources of galactic radio noise must be very much more powerful. Thousands of millions of stars, each radiating as strongly as the disturbed sun, would be required to match the observed energy output.

The development of high-resolution techniques revealed the presence of a number of discrete sources, which for a time were called "radio stars", although none of them could be identified with actual stars. The strongest of these sources have been identified with optically observable objects—all of which have turned out to be remarkable. Most of the weaker discrete sources have not been identified. In fact, of the 200 strong discrete sources that have been listed by various observers, only a handful have been identified with optical objects.⁽⁴⁹⁾ These include the Cassiopeia and Puppis sources, Cygnus A, the Crab nebula, NGC 5128 (Centaurus), and NGC 4486 (Virgo). Unlike the bright stars, the strongest sources are concentrated to the plane of the galaxy. The weaker sources, which are believed to be randomly distributed, are probably to be identified with external galaxies. B. Y. Mills refers to these two kinds of objects as Class I and Class II sources, respectively. In fact, the radio-frequency radiation from eight or nine "normal" galaxies (i.e. systems like our own galactic system) has been detected as well as emission from unusual galaxies that emit an abnormal amount of radio noise. The "normal" galaxies include the Andromeda spiral and several objects in the Virgo cluster. Curiously, the Triangulum spiral Messier 33 has not been detected. In fact, no Sc spiral has so far been found, and it may be that these predominately Type I populations are not strong radio sources.

The character of the galactic discrete sources so far identified with optical objects is such that the weaker sources must lie beyond the limits of the most powerful of existing telescopes, even if they are not partially obstructed by the interstellar absorption. Interferometric techniques show that these sources have finite diameters. For example, the diameter of the Cassiopeia source, assuming it to be a uniform disk, was found to be about 5.6' in good agreement with the optical observations.⁽⁵⁰⁾

The strong sources so far identified include the Cassiopeia source ($\alpha=23^{\text{h}}21^{\text{m}}11.38^{\text{s}}$, $\delta=+58^{\circ}31'52.9''$ (1950)), Cygnus *A* ($\alpha=19^{\text{h}}57^{\text{m}}44.5^{\text{s}}$, $\delta=+40^{\circ}35'46.3''$ (1950)), Puppis ($\alpha=8^{\text{h}}20^{\text{m}}$, $\delta=-42^{\circ}15'$), Tycho's supernova of 1572, and the Crab nebula. The last-mentioned was the first source identified; the energy distribution in its radio-frequency spectrum is different from that of other radio sources. Kepler's supernova of 1604 has not yet been found, but no radio-telescope of adequate power has yet been used on this object.

Direct photographs of the Cassiopeia source secured with the 48-in. Schmidt show a number of sharp, unusual filaments, unlike any gaseous nebulae heretofore known.⁽⁵¹⁾ The spectra and velocities of the first three filaments observed by Minkowski illustrate some of the complexities involved.⁽⁵²⁾ Filament No. 1 shows strong radiations of [NII], [OIII], and [OI], although *H α* and *H β* are absent.

Each line profile extends over a velocity range of 3000 km./sec. with maximum intensities corresponding to velocities of -1000 km./sec. and greater than $+2200$ km./sec.! Filament No. 2 shows lines of [NII], [OI] with a weak *H α* . The third filament shows strong [NII]. The line is tilted and narrow, corresponding to a 400–500 km./sec. difference in speed between the extreme ends of the filament. The sharpness of the lines indicates that any expansion of the filaments must be very small compared to the mass motions of the filaments themselves.

Minkowski and the writer⁽⁵³⁾ suggested that the absence of hydrogen emission in the spectrum of filament No. 1 was to be attributed not to the absence of hydrogen in the nebula, but to the conditions of excitation. If the electron temperature is about $15,000^{\circ}\text{K.}$, *H α* will not be collisionally excited enough to produce an observable line, although [OII], [NII], and [OIII] will appear with some strength. The filaments' spectrum indicated that it was not in ionization equilibrium.

Minkowski subsequently secured additional observations of the filaments in the Cassiopeia source. He finds two kinds of nebulous objects: (1) Diffuse filaments and condensations visible on both blue and red exposures. (2) Sharp, short filaments and semi-stellar condensations visible only on red-sensitive plates.

The two groups differ not only in their spectra but also in their radial velocities. The diffuse (1) objects have large radial velocities and velocity spreads, and observable transverse motions after two years. The sharp (2) objects have small radial velocities and moderate velocity spreads, but show no transverse motions in two years. Minkowski gives the following description of the spectra of the two kinds of objects. He estimated the line intensities by comparison with the spectrum of NGC 7027.

TABLE VIII : 3

Spectra of Filaments in the Cassiopeia Radio Source

λ	Diffuse Objects			Sharp Objects
3727 [OII]	4	6	6	—
3869 [NeIII]	—	—	(2)	—
4069 [SII]	2	2	2	—
4076 [SII]	1	1	1	—
4959 [OIII]	15	20	15	—
5007 [OIII]	45	60	50	—
6300 [OI]	20	20	20	—
6364 [OI]	10	10	10	—
6548 [NII]			} 23	150
<i>Hα</i> <i>H</i>				100
6584 [NII]				450
6716 [SII]	30	70	15	
6730 [SII]	50	110	24	

From the fact that the sharp filaments do not appear in the blue, one can estimate that $H\beta/H\alpha \ll 1/3$, Minkowski concludes that the line intensities for the diffuse filaments interpreted with the aid of Seaton's cross-sections require that the filaments cannot be in ionization equilibrium. If the electron temperature is as low as $15,000^\circ\text{K}$. so that $H\alpha$ will not be strongly excited by collisions, the observed intensities in the diffuse filaments would require proportions of $N[\text{OIII}]:N[\text{OII}]:N[\text{OI}]=10:1:2$. Since changes are observed in the structures of the diffuse details in a period of two years, and since the relaxation times for the ionization equilibrium may be expected to be much longer than this, it is safe to assume that the ionization equation cannot be applied and abnormal-looking ratios are to be expected. In the two brightest diffuse filaments Minkowski has succeeded in observing $\lambda 4363$. Temperatures of $15,000^\circ\text{K}$. and $40,000^\circ\text{K}$., respectively, are indicated by the $4363/(N_1+N_2)$ ratio. The absence of $H\alpha$ in the hotter filament is puzzling, unless the filament is so very dense that the collisional de-excitations of the 1D_2 level of OIII become important.

The radio observers also find an extended source in Cygnus—sometimes referred to as “Cygnus X”. Measures with the interferometer show that it cannot be a source of uniform surface brightness. Minkowski finds filaments similar to these characteristic of the Cassiopeia source in this area also. Most of the area is so filled with obscuring nebulosity that many of the structures are probably hidden. The Puppis source has a diameter of about a degree, and shows a filamentary structure similar to that of the Cassiopeia source.

A nebula, IC 443, somewhat similar to the Network nebula in Cygnus has recently been identified as a radio source. This object is much more

remote than the Network nebula; the small proper motion of the filaments is barely visible on the blink microscope in fourteen years. The spectrum shows strong radiations of $H\alpha$ and $[NII]$. We might expect the Network nebula to be a detectable radio source, but it lies so close to Cygnus X and the strong Cygnus A source that the resolution presents a serious problem.

The first radio source to be identified, Taurus A , was shown to coincide in position with the Crab nebula. This object is the remnant of an extremely luminous supernova that was observed in 1054.⁽⁵⁴⁾ Direct photographs show it to consist of an amorphous mass upon which is superposed a network of intricate filaments. J. C. Duncan's measurements of these filaments showed the nebula to be expanding.⁽⁵⁵⁾ N. U. Mayall observed the spectrum of this filamentary structure and found a radial expansion of 1100 km./sec.⁽⁵⁶⁾ When the radial velocity measurements are combined with the lateral expansion rates in seconds of arc per annum, the distance of the nebula is found to be 1100 parsecs.⁽⁵⁷⁾

Detailed studies of the spectra of the filaments (by Minkowski)⁽⁵⁸⁾ show them to resemble ordinary planetary nebulae of high density. The $[OI]$ and $[SII]$ lines are particularly strong. On the other hand, the hydrogen lines are very weak compared with those of both neutral and ionized helium. Thus hydrogen must really be very much less abundant than helium.

It has been suggested that supernovae originate from very dense stars in whose interiors hydrogen has been converted into helium and heavier elements have been built up by reactions involving α -particles. For example, Borst⁽⁵⁹⁾ has suggested that Be^7 may be formed by a collision of two α -particles in which 19 M.e.v. of energy is absorbed. Subsequently Be^7 decays by capture to Li^7 . Another possible process is the building of C^{12} from three α -particles as suggested by Salpeter.⁽⁶⁰⁾ Actually, except for the small ratio of hydrogen to helium no unusual proportions of any elements have been established. In particular, there is no evidence for excess quantities of lithium or carbon.

The amorphous mass of the Crab nebula shows a strong, continuous spectrum with no trace of any lines. Minkowski attributed this strong continuum to free-free emissions in a highly ionized gas. It is possible that the electron temperature may be considerably higher than Minkowski originally assumed. If a discontinuity can be observed at the Balmer limit, the electron temperature must be less than 400,000° K. If this jump cannot be observed and if the mass of the nebula is as great as thirty-six times that of the sun, the electron temperature can be as high as 2,000,000°. The electron densities must be comparable with those existing in typical high excitation planetaries, but the volume of the radiating gas is very much larger. If the electron temperature is as high as 1,000,000° the

thermal energy content of the nebula is enormous, and the rate of emission of energy in free-free transitions is low. Minkowski and Greenstein⁽⁶¹⁾ have pointed out that if the emission of energy in possible far ultra-violet forbidden lines is neglected the dissipation of 1% of the kinetic energy of the expanding nebula would supply its energy for a thousand years. Since the expansion of the nebular gases occurs at supersonic velocities, the kinetic energy could be dissipated by shock waves. Excitation and ionization by electron impact probably dominates except for the ions of highest ionization potential where radiative ionization may occur. A central star may help maintain the ionization level in the nebula, but it does not appear to be absolutely necessary to supply the observed excitation.

The most unusual feature of the Crab nebula as a radio source is the character of the energy distribution in its spectrum. "Normal" radio sources such as Cassiopeia or Puppis have a spectrum in which the radio-frequency flux appears proportional to wavelength from about 2 to 15 m. The flux of the Taurus source appears to be constant from 20 cm. to 10 m., but it appears to fall off between 20 cm. and 9.4 cm.

An optically thin source in which free-free emissions provide the radio-frequency radiation will emit a spectrum in which the energy distribution is also nearly independent of wavelength. We may show this rather easily by the following argument.

The thermal emission from a column of gas of length h containing N_i ions/cm.³ N_e electrons/cm.³ will be

$$I_\nu = \int_0^{\tau_{\nu 0}} \frac{j_\nu}{4\pi k_\nu} e^{-\tau_\nu} d\tau_\nu, \quad . \quad . \quad . \quad (40)$$

where j_ν is the total emission/cm.³ in all directions, k_ν is the absorption coefficient and $d\tau$, the element of optical depth. If the gas has a temperature of the order of 1,000,000° K., the bound-free emissions can be neglected and only the free-free emissions will be of importance. The corresponding absorption coefficient per cm.³ of the gas will be

$$k_\nu' \sim N_i N_e Z^2 \nu^{-2} g_{\text{III}}, \quad . \quad . \quad . \quad (41)$$

where Z is the ionic charge and g_{III} is the Gaunt factor. The effect of negative absorptions is included in k_ν' . Since Kirchhoff's law holds,

$$j_\nu = 4\pi k_\nu B_\nu(T). \quad . \quad . \quad . \quad (42)$$

In the far infra-red the Planck function $B_\nu(T)$ reduces to

$$B_\nu(T) \sim \frac{2kTv^2}{c^2}. \quad . \quad . \quad . \quad (43)$$

Then by integration of equation (40)

$$I_\nu = B_\nu [1 - e^{-\tau_{\nu 0}}] \sim B_\nu \tau_{\nu 0} = B_\nu k_\nu' h \quad . \quad . \quad . \quad (44)$$

for an optically thin source. Thus the ν^2 factor disappears and I_ν is

independent of ν except for the dependence of g_{III} on ν . Hence, if the radio-frequency radiation of the Crab nebula is the low-frequency end of an optical spectrum which is primarily due to free-free emission, the fluxes in the optical and radio continua cannot differ by more than an order of magnitude.

The most careful examination of this hypothesis was made by Greenstein and Minkowski. At a frequency of 100 megacycles/sec. the total emission in the Crab nebula is 2.8×10^{24} ergs/sec./unit frequency, according to the measurements of Stanley and Slee.⁽⁶²⁾ At $\lambda 4250$, R. Minkowski finds the total flux to be 3.4×10^{21} ergs/sec./unit frequency, i.e. 800 times smaller! Since the g_{III} factor is about 1.0 in the optical region and 9 in the radio-frequency region, the hypothesis of thermal emission fails by a factor of 80.

Therefore it is necessary to attribute the radio-frequency radiation from the Crab nebula to some non-thermal source. A significant clue is provided by a recent photo-electric observation by J. Oort and T. Walraven, who found a polarization exceeding 30% in certain directions in the nebula. The polarization directions are parallel near the centre but oriented at random in the outer parts of the nebula where the resultant polarization finally drops to zero. This polarized radiation cannot be explained by free-free transitions. Oort and Walraven attribute it to the "synchrotron" emission of high-speed electrons in a strong magnetic field. The polarised radiation is confined almost entirely to the direction of the electrons motion. Radiation emitted according to this mechanism has a characteristic energy spectrum that falls off at very high frequencies but also extends to very low frequencies. Hence, the radio-frequency emission as well as the continuous optical emission and short-period changes in the nebula can be explained. A field of the order of 0.001 Gauss is required. The particles must be supplied continuously to the nebula and cannot have originated in the supernova explosion. An enormous total magnetic flux plus a huge supply of energy is required.

Other strong galactic radio sources like the Cassiopeia and Puppis sources also involve non-thermal radio-frequency radiation. Possibly synchrotron radiation occurs there also but the weakness of the optical continuum suggests a different spectral energy distribution.

Minkowski has pointed out that a very pronounced correlation exists between the velocity dispersion in the nebulous filaments and the radio-frequency emission per unit volume. The Cassiopeia source whose individual filaments show velocity differences of the order of 1000 km./sec. shows a much stronger emission than does IC 443, in which the irregular motions are of the order of 100 km./sec. The non-thermal emission invariably seems to be associated with high velocities of the moving gases.

Extragalactic radio sources of high-power output are also known. The most powerful of these sources, Cygnus A ($\alpha=19^h57^m45^s$, $+40^\circ 35' 46''$), appears to be two colliding galaxies. As Spitzer and Baade showed,⁽⁶³⁾ when two galaxies collide the stars pass side by side without any collisions. On the other hand, the gas becomes very hot, and we should observe a continuum of stars plus high excitation emission lines. Spectrograms obtained by Minkowski show a radial velocity of 16,830 km./sec. The cluster to which this nebula belongs lies at a distance of 33,000,000 parsecs. The strongest lines are [NeV], but there are also lines of [OI], [OII], [OIII], [NII], $H\alpha$, $H\beta$, and [NeIII]. The spectrum thus resembles that of a planetary nebula.

These two colliding galaxies appear to be the brightest objects in this particular cluster. They are comparable, therefore, with our own galaxy. Baum found the line emission to be comparable with the radio-frequency emission and greater than that of the stars. A similar object is found in Perseus. The huge ellipsoidal galaxy NGC 5128 and Messier 87, one of the brightest spheroidal galaxies in the Virgo cluster, are also abnormally intense radio sources. Direct photographs of M87 show a jet of very unusual appearance which may be associated with the radio emission. The Andromeda nebula and the Magellanic clouds, on the other hand, are examples of "normal" galaxies similar to our own in so far as the ratio of radio-frequency radiation to optical radiation is concerned.

Although the Crab nebula and Tycho's supernova of 1572 have been identified as radio sources, it does not seem likely that all galactic radio sources are remnants of ex-supernovae. Since the very strongest sources like Cassiopeia are near the limit of existing optical telescopes we must expect that the bulk of the galactic sources detected by the larger radio telescope will lie beyond the reach of existing optical equipment. Many of the extra-galactic sources may be objects like M87.

Although thermal free-free emission cannot account for the radiation from the prominent discrete sources, we might expect to detect some thermal radiation from large clouds of ionized hydrogen in the spiral arms. Furthermore, calculation shows that most observed emission nebulosities can also produce absorption of radio-frequency radiation. Thus discrete sources like Cygnus X, which presumably lies behind clouds of ionized gases, might have their spectral energy distributions flattened as a consequence of this absorption. At frequencies greater than 500 megacycles/sec. the flat thermal spectrum of free-free emission should be observed from extended HII emission regions.

Since these HII regions are strongly concentrated towards the galactic plane, a line of sight along a spiral arm should penetrate several of them. P. A. G. Scheuer and M. Ryle⁽⁶⁴⁾ reported a strip of radio emission

confined to a belt 4° wide centred on the galactic equator. They concluded that this emission was to be attributed to ionized hydrogen of a density similar to that found by optical methods. The required electron temperature was about $20,000^\circ\text{K}$.

Can emission from individual galactic nebulae be detected? The planetary nebulae are all too small, but we might expect that bright objects such as the Orion nebula would lie above the threshold of detectability. At the Cavendish laboratory J. E. Baldwin⁽⁶⁵⁾ was unable to find it at a frequency of 210 megacycles/sec. At a frequency of 3200 megacycles/sec. (9.4 cm.), Haddock, Mayer, and Sloanaker,⁽⁶⁶⁾ working at the Naval Research Laboratory, were able to detect not only the Orion but also several other diffuse nebulae. Their measurements indicated that if the source were spherical in shape the average electron density within $7.5'$ of the centre would be about $400/\text{cm}^3$, a value consistent with Baldwin's failure to detect it at $\lambda 140\text{ cm}$. It is of interest that M17 is substantially brighter in radio frequencies than the Orion nebula, even though it is very much fainter in the optical region of the spectrum. The Naval Research Laboratory investigators have detected also the Trifid and Messier 8 nebulosities. Boggess has combined his optical observations of NGC 6514, 6523, 6611, and 6618 with these radio-frequency observations to secure estimates of the space absorption.⁽⁶⁷⁾ The surface brightness in $H\alpha$ will depend on N_e and T_e , according to the formulae we have developed. The radio-frequency emission per unit volume at frequency ν will be

$$E_{rf}d\nu = N_i N_e \frac{kK}{2RT_e^{1/2}} \bar{Z}^2 g_{III} e^{-h\nu/kT_e} d\nu, \quad (45)$$

where

$$g_{III} = \frac{\sqrt{3}}{\pi} \ln \frac{(2kT_e)^{3/2}}{4 \cdot 22\pi \sqrt{m} Z e^2 \nu}, \quad (46)$$

if the condition

$$9.1 \times 10^{-7} \frac{\nu}{T_e^{1/2} N_i^{1/3}} > 1 \quad (47)$$

is fulfilled. This will be true if $N_i \leq 3000$ and $T_e \leq 40,000^\circ$ at $\nu = 3200$ megacycles/sec. Here Z^2 is the mean square charge and $K = 3.26 \times 10^{-6}$. The ratio of emission per unit volume in $H\alpha$ to that in radio-frequency radiation is found to be

$$\frac{E_{H\alpha}}{E_{rf}} = 7.24 \times 10^{18} \frac{b_3 e^{17500/T_e}}{g_{III} \bar{Z}^2 T_e}. \quad (48)$$

Since the $H\alpha$ and radio-frequency radiations originate in the same volume element, we may equate this ratio to $S_{H\alpha}/S_{rf}$, i.e. the ratio of the surface brightnesses, and solve for the electron temperature provided there is no

space absorption. Space absorption diminishes the optical brightness, but not the radio brightness of a radio source. If the electron temperature can be found from the forbidden lines, one may find the space absorption. Since no independent data on the forbidden line intensities were available, Boggess adopted a value of $10,000^{\circ}\text{K}$. (appropriate to the Orion nebula) and solved for the amount of space absorption. In this way the values of the quantity A in Table VIII:2 were obtained. The desirability of further observations of the forbidden line intensities and of the Balmer decrement for the purposes of establishing the electron temperature and the space absorption from purely optical data is evident.⁽⁶⁸⁾

The 21-cm. radiation corresponds to the energy difference between two hyperfine states in the ground-level of hydrogen. This line is emitted only in regions where neutral hydrogen is present. Measures of its profile and displacement give information on the motions, densities, and temperatures of clouds of neutral hydrogen in the line of sight. These studies have proven to be a very powerful tool for probing the spiral arms of the galaxy and evaluating the physical conditions in the *HI* regions.⁽⁶⁹⁾

In this connexion we must mention the work of Bok and his associates at Harvard who have measured accurate profiles of the 21-cm. line with a velocity resolution of 3 km./sec. They find that the neutral hydrogen gas does not seem to be concentrated in regions where the particle density is high. The complex distribution of gas in the spiral arms is emphasized in Matthews's investigations of the Perseus-Orion region. That the neutral hydrogen gas tends to be found in the same clouds as the atoms producing the interstellar lines or ionized calcium seems to be indicated by R. Lawrence's study of high latitude fields where G. Münch had found stars with strong interstellar lines.

T. K. Menon's observations of the great Orion complex are of particular interest. The 21-cm. profiles may be interpreted in terms of an expanding shell of neutral gas, whose centre of expansion corresponds to the supposed origin point of μ Columbae and AE Aurigae. The total areas under the profiles remain the same from one point in the region to another, although the profiles tend to be sharper in the neighbourhood of the dust clouds of the Horsehead nebula.

The line is usually observed in emission, although J. P. Hagen and E. F. McClain⁽⁷⁰⁾ have observed it in absorption in front of sources of high radio-frequency brightness. The Australian observers, F. J. Kerr, J. F. Hindman, and B. J. Robinson,⁽⁷¹⁾ have studied the 21-cm. radiation from the two Magellanic clouds. They find that the neutral hydrogen extends well beyond the easily visible regions of each cloud and is much less concentrated towards the nucleus than are the bright stars. Although the amount of dust and bright-line nebulosity is very different for the two

clouds, the neutral hydrogen content is more nearly equal. It amounts to 6×10^8 and 5×10^8 solar masses for the Large and Small Clouds, respectively, provided they are optically thin in the 21-cm. radiation. The average density, about 0.2 atom/cm^3 , is the same order of magnitude as that found from the ionic density in the ionized regions of the Large Cloud averaged over the volume of the cloud.

At other radio frequencies B. Y. Mills finds evidence that the non-thermal emission from the Large Magellanic Cloud is probably more important than the thermal emission. The radio emission is distributed rather like the neutral hydrogen and bright stars rather than the unresolved nebulosity. Thermal radiation does appear to exist in the neighbourhood of the Loop nebula, 30 Doradus, the brightest emission in the Large Cloud.

Radio astronomy will yield many important new results in the study of the diffuse nebulae and the interstellar medium. The sensitivity of existing equipment in certain frequency ranges is often low. Furthermore, this low resolution of these instruments means that only the gross features of the interstellar medium can be studied. Eventually small objects like planetary nebulae may be observable with some of the larger radio-telescopes that are projected. On the other hand, certain of the intense radio sources prove to have very interesting optical spectra which indicate that they are far from ionization equilibrium. The hydrodynamical and other properties of the objects will certainly lead to many engaging problems.⁽⁷²⁾

REFERENCES

- DUFAY, JEAN, *Nébuleuses Galactiques et Matière Interstellaire*, Albin Michel, Paris (1954).
- (1) See, for example, *Sky and Telescope*, **13**, 150 (1954); **14**, 11, 93 (1954); Gum, C. S. *Observatory* **72**, 151 (1953). The work of Shajn and Hase is summarized in *Trans. Internat. Astron. Union*, **8**, 693 (1954).
 - (2) BLAAUW, A., and MORGAN, W. W., *Ap. J.*, **117**, 256 (1953). See also BLAAUW, A., *B.A.N.*, **11**, 459 (1952).
 - (3) Centennial Symposia, Harvard College Observatory Monographs No. 7 (Cambridge 1948), p. 87.
 - (4) HOYLE, F., and LYTTLETON, R. A., *Proc. Camb. Phil. Soc.*, **35**, 405 (1939).
 - (5) MCCREA, W. H., *M.N.R.A.S.*, **113**, 162 (1953).
 - (6) *Ap. J.*, **88**, 52 (1938).
 - (7) *Ap. J.*, **111**, 593 (1950).
 - (8) *Ap. J.*, **91**, 360 (1940).
 - (9) *Ap. J.*, **88**, 84 (1938).
 - (10) *Zeits. f. Ap.*, **30**, 71 (1952).
 - (11) See WELLMANN, P., *Ap. J.*, **116**, 452 (1952).
 - (12) *Ann. d'Ap.*, **7**, 80 (1944).
 - (13) *Ap. J.*, **104**, 414 (1946).
 - (14) *Publ. A.S.P.*, **58**, 165 (1946).
 - (15) *Ap. J.*, **89**, 526 (1939).

- (16) *Ast. Journ.*, **58**, 215 (1953).
- (17) *Ast. Journ.*, **58**, 218 (1953).
- (18) *Publ. Obs. Univ. of Mich.*, **10**, 7 (1951).
- (19) *Ap. J.*, **109**, 471 (1949).
- (20) *Science*, **109**, 166 (1949).
- (21) See DAVIS, L., and GREENSTEIN, J. L., *Ap. J.*, **114**, 206 (1951); also SPITZER, L., and TUKEY, J. W., *Ap. J.*, **114**, 187 (1951). Present evidence favours the Davis-Greenstein theory.
- (22) *Ap. J.*, **114**, 241 (1951).
- (23) *Ap. J.*, **118**, 113 (1953).
- (24) In a medium which is a sufficiently good conductor the lines of force may act as though they were frozen in the medium. The situation may be summarized by the following argument due to G. K. Batchelor. The equation for \mathbf{H} is

$$\frac{\partial \mathbf{H}}{\partial t} - \nabla \times (\mathbf{v} \times \mathbf{H}) = \lambda \nabla^2 \mathbf{H},$$

where

$$\lambda = \frac{1}{4\pi\mu\sigma}.$$

Here σ is the specific conductivity. The condition for the lines of \mathbf{H} to be frozen in the medium is that the term on the right-hand side of the equation should be negligible compared with the other terms. When all terms are made non-dimensional by using a representative length l and velocity V_0 , the condition becomes $\lambda/IV_0 \ll 1$. A medium which is a good conductor for large-scale motions may actually be a "poor" conductor for small-scale motions. Another statement of the criterion is that the time of decay due to Ohmic losses ($\sim l^2/\lambda$) must be large compared with the time-scale of the hydrodynamic motion ($\sim l/V_0$) and this again leads to $IV_0/\lambda \gg 1$. We may regard IV_0/λ as equivalent to a "magnetic" Reynolds number.

- (25) *Ap. J.*, **118**, 113 (1953). A somewhat similar argument was given by DAVIS, LEVERETT, JR., *Phys. Rev.*, **81**, 890 (1951).
- (26) See ALFVEN, H., *Cosmical Electrodynamics*. New York, Oxford University Press (1950).
- (27) This value is based on the 21-cm. line radiations as discussed by OORT, J., *Ap. J.*, **116**, 223 (1952).
- (28) BLAAUW, A., *B.A.N.*, **11**, 405 (1952).
- (29) *Ap. J.*, **118**, 116 (1953).
- (30) For an ordinary gas the kinematical viscosity is $\nu = 0.49\nu_L$, where L is the mean free path, and ν the mean velocity of the atoms. When the mean free path is long as in the interstellar medium, ν becomes very large. Exact formulae for the viscosity and thermal conductivity of a completely ionized gas have been given by CHAPMAN, S., *Ap. J.*, **120**, 151 (1954).
- (31) Excellent discussions of the theory of turbulence will be found in:
CHANDRASEKHAR, S., *Ap. J.*, **110**, 329 (1949); BATCHELOR, G. K., *Reports on Progress in Physics*, **15**, 101 (London, 1952); *The Theory of Homogeneous Turbulence* (Cambridge University Press, 1953).
- (32) The turbulent Mach number is the ratio of the mean turbulent-motion velocity to the mean velocity of sound in the medium.
- (33) *Zeits. f. Ap.*, **30**, 17 (1951).
- (34) *Publ. Lick Obs.*, **13**, 96 (1918).
- (35) *Ap. J.*, **113**, 120 (1951).
- (36) *Zeits. f. Ap.*, **32**, 251 (1953).
- (37) *Proc. Kon. Ned. Akad. Wetensch.*, **49**, 589 (1946).
- (38) *Mt. Wilson Contr.*, Nos. 241 and 250; *Ap. J.*, **56**, 196, 420 (1922).
- (39) See, for example, MILLER, F. D., *Harvard Ann.*, **105**, 297 (1937); BALONOWSKY and HASE, *Pulkova Bull.*, **14**, 2 (1935).
- (40) *Ap. J.*, **114**, 492 (1951).
- (41) *Ap. J.*, **117**, 399 (1953).
- (42) *M.N.R.A.S.*, **106**, 159 (1946).
- (43) *Ap. J.*, **108**, 413 (1938).
- (44) *M.N.R.A.S.*, **96**, 588 (1936).
- (45) *Proc. Roy. Soc., A*, **218**, 400 (1953).

- (46) *Proc. Kon. Ned. Akad. Wetensch.*, **49**, 600 (1946); **50**, 262, 332, and 442 (1947).
- (47) *Problems of Cosmical Aerodynamics*, Dayton (Central Air Documents Office, 1951).
- (48) See, for example, VAN DE HULST, H. C., *A Course in Radio Astronomy*, Leiden (1951); LOVELL, A. C. B., and CLEGG, J. A., *Radio Astronomy*, Chapman and Hall, London (1952).
- (49) See, for example, BROWN, R., HANBURY, M. N., and HAZARD, C., *M.N.R.A.S.*, **113**, 109, 123 (1953).
- (50) The diameters were measured and published simultaneously by observers at Sydney, Australia, Jodrell Bank, and Cambridge, England. See *Nature*, **170**, 1061 (1952).
- (51) BAADE, W., and MINKOWSKI, R., *Ap. J.*, **119**, 206 (1954).
- (52) MINKOWSKI, R., *Ap. J.*, **119**, 215 (1954).
- (53) BAADE, W., MINKOWSKI, R., and ALLER, L. H., *Ap. J.*, **119**, 232 (1954).
- (54) MAYALL, N. U., and OORT, J., *P.A.S.P.*, **54**, 95 (1942).
- (55) *Proc. Nat. Acad. Sci.*, **7**, 179 (1921); *Ap. J.*, **89**, 482 (1939).
- (56) *Publ. A.S.P.*, **49**, 10 (1937).
- (57) BAADE, W., *Ap. J.*, **96**, 188 (1942).
- (58) *Ap. J.*, **96**, 199 (1942); *Ann. d'Ap.*, **9**, 97 (1946).
- (59) *Phys. Rev.*, **78**, 807 (1950).
- (60) *Ap. J.*, **115**, 326 (1952).
- (61) *Ap. J.*, **118**, 1 (1953).
- (62) *Australian J. Sci. Res.*, **A**, **3**, 234 (1950).
- (63) *Ap. J.*, **113**, 413 (1951).
- (64) *M.N.R.A.S.*, **113**, 3 (1953).
- (65) *Observatory*, **73**, 155 (1953).
- (66) *Ap. J.*, **119**, 456 (1954).
- (67) BOGGESE, A., Thesis, University of Michigan (1954).
- (68) See the discussion of the Kramers-Gaunt factor by Elwert: *Zeits. f. Naturforsch.*, **3a**, 477 (1948); *Zeits. f. Ap.*, **25**, 310 (1948).
- (69) See H. C. van de Hulst's Halley Lecture for 1953.
- (70) *Ap. J.*, **120**, 368 (1954).
- (71) *Australian Journ. of Physics*, **7**, 297 (1954).
- (72) See *Gas Dynamics of Cosmic Clouds*, ed. by VAN DE HULST, H. C., and BURGERS, J. M., North Holland Publishing Co. (Amsterdam, 1955).

Name Index

AIRY, GEORGE, 50
 Alfvén, H., 295
 Ambarzumian, V. A., 26, 33, 41, 42, 75, 76,
 97, 105, 132, 218, 231, 274, 236, 280
 Amemiya, A., 190
 Anderson, Claude, 49, 50, 54, 202
 Andriolat, H., 69, 146, 154
 Auwers, G. F., 49

BAADE, W., 3, 4, 12, 16, 89, 97, 98, 138, 288,
 297, 309
 Babcock, H. D., 21
 Babcock, H. W., 41
 Baker, J. G., 12, 113, 118, 121, 122, 123, 127,
 130, 136, 148, 157, 158, 184, 196, 281
 Baldwin, J. E., 310
 Barbier, D., 39, 40, 68, 70, 91, 146, 154, 283
 Barnard, E. E., 3, 84, 90
 Batchelor, G. K., 295, 296
 Bates, D. R., 141, 145
 Baum, William, 309
 Beals, C. S., 206
 Berman, L., 25, 26, 28, 49, 51, 52, 53, 54, 67,
 68, 128, 129, 147, 196, 203, 204, 205, 217,
 220, 221, 222, 251, 252, 257, 260
 Bester, M. V., 85, 86
 Bethe, H., 146
 Biermann, L., 280, 295
 Blaauw, A., 279
 Boggess, Albert III, 28, 90, 96, 281, 287, 310,
 311
 Boggess, Nancy W., 28
 Bohr, N., 190
 Bok, B. J., 85, 86
 Bond, G. P., 11
 Borst, L. B., 306
 Bourget, H., 15, 16
 Bowen, I. S., 18, 19, 20, 43, 58, 59, 65, 70,
 78, 80, 81, 82, 184, 234
 Boyce, J., 78
 Brahe, Tycho, 5, 304
 Brandenburg, W. J., 248, 249, 250, 251
 Bredichin, T., 49
 Brill, A., 220
 Bruhns, K. C., 49
 Buisson, H., 15, 16
 Burgers, J. M., 299, 302
 Burnham, S. W., 102

CAMM, G. L., 53
 Campbell, W. W., 17, 43, 51, 57, 72, 90, 91,
 101, 155, 207, 224, 266, 267, 268, 296
 Cannon, A. J., 65, 96
 Carroll, J. A., 112
 Cassini, J. D., 93
 Cederblad, S., 1, 85, 86, 90, 95
 Chalonge, D., 39, 68, 70
 Chamberlain, J. W., 127, 155, 156, 157, 158,
 159, 300, 301, 302
 Chandrasekhar, S., 132, 142, 216, 227, 228,
 229, 260, 275, 277, 288, 289, 290, 291, 294

Cillie, C. G., 71, 112, 127, 130
 Code, A., 31, 43, 70, 89, 90
 Condon, E. U., 169, 175, 179, 184
 Copeland, R., 91
 Cramer, Mrs. O., 257
 Crawford, John, 225
 Curtis, H. D., 24, 35, 49, 50, 56, 86, 90, 148,
 202, 248, 249, 257

D'ARREST, H. L., 102
 de Jager, C., 226, 228
 Dennison, Edwin, 28
 Doherty, Lowell, 9, 97, 285
 Draper, Henry, 11
 Draper catalogue, 65
 Dreyer, J. L. E., 1
 Dufay, J., 91
 Duncan, J. C., 48, 90, 306
 Dunham, T., 84

EDLÉN, B., 58, 78, 164, 206
 Elvey, C. T., 36, 92, 93
 Evans, David S., 50, 57, 248

FABRY, CHARLES, 15, 16
 Fath, E. A., 101
 Fehrenbach, C., 14, 279
 Fermi, E., 288, 289, 290, 291, 295
 Fleischer, R., 224
 Fleming, W. P., 207
 Fundaminsky, A., 156

GARSTANG, ROY, 184, 185, 186
 Gilmour, R. M., 185
 Goldberg, L., 76, 77, 145, 146, 196
 Goos, F., 16, 138
 Green, W. K., 257
 Greenstein, J. L., 85, 91, 103, 104, 105, 151,
 152, 153, 154, 283, 284, 285, 296, 307, 308
 Grotrian, W., 163
 Gum, C. S., 279

HADDOCK, F., 310
 Hagen, J. P., 311
 Hall, John, 31, 288
 Haro, Guillermo, 8, 9, 97, 103
 Harris, Daniel III, 88
 Hase (Gaze), B. F., 2, 85, 93, 98, 279, 280, 282
 Hatanaka, T., 84
 Hebb, M. H., 150, 183, 190, 283
 Hendrix, D. O., 21
 Henize, K. G., 2, 9, 27, 48, 97, 285
 Henyey, L., 85, 91
 Herbig, George H., 102, 103, 104, 105
 Herschel, Sir John, 1, 2, 49, 56, 84, 90, 96
 Herschel, Sir William, 1, 2, 56, 84, 90
 Hiltner, W. A., 9, 28, 32, 36, 288
 Hind, J. R., 102
 Hindman, J. F., 286, 311
 Hoag, Arthur, 31
 Hoffleit, D., 86

- Holden, E. S., 5, 56
 Holetschek, J., 25, 24
 Holmberg, E., 23
 Hopf, E., 229
 Hoyle, F., 280
 Huang, Su shu, 143, 146
 Hubble, E. P., 24, 25, 86, 90, 94, 95, 98, 100, 101, 103, 201, 202, 300
 Huffer, C. M., 88, 204
 Huggins, W., 2, 17, 57, 90, 91
 Humason, M. L., 101, 300, 302

 INGLIS, D., 216
 Inui, T., 190

 JANSKY, P., 302
 Johnson, Harold, 33, 88
 Johnson, Hugh M., 92, 93, 279
 Johnson, M. C., 130
 Jose, P., 59

 KANTROWITZ, A., 302
 Keeler, J. E., 11, 50, 56, 90
 Keenan, P. C., 96
 Kerr, F. J., 286, 311
 Kholopov, P., 105
 Kienle, H., 39, 70
 Koch, P. P., 16, 138
 Kolmogoroff, A. N., 293, 296
 Koslov, V., 268
 Kron, G. E., 6
 Kuiper, G. P., 25, 209, 210

 LACAILLE, N. L., 84, 93
 Lalande, J., 49
 Lassell, W., 56, 102
 Lawrence, R., 311
 Lighthill, M. J., 294
 Liller, W., 26, 31, 32, 33, 34, 35, 41, 55, 72, 185, 202, 203, 204, 205, 224, 230
 Lochte-Holtgreven, W., 216
 Lockyer, Norman, 17, 57
 Lundmark, K., 49
 Lyttleton, R. A., 280

 MCCLAIN, E. F., 311
 McCrea, W. H., 271, 280
 McDonald, J., 226
 McLennan, J. C., 165
 McLeod, J. H., 165
 McQuarrie, W. C., 165
 MacRae, Donald, 31, 41, 42, 224
 McVittie, G., 299
 Matthews, T. A., 311
 Mayall, N. U., 20, 67, 98, 100, 101, 306
 Mayer, C. H., 310
 Mayer, Maria Goeppert, 151
 Menon, T. K., 311
 Menzel, D. H., 25, 35, 71, 74, 78, 82, 84, 113, 114, 118, 120, 121, 123, 127, 130, 136, 141, 147, 148, 150, 157, 158, 183, 184, 185, 190, 191, 196, 198, 206, 215, 274, 281, 283
 Merrill, P. W., 4, 46, 244
 Messier, C., 90
 Miller, F. D., 300
 Milligan, James E., 228
 Mills, B. Y., 303, 312
 Milne, E. A., 132

 Minkowski, R., 2, 6, 12, 16, 39, 43, 46, 48, 54, 55, 57, 59, 66, 69, 70, 71, 86, 93, 106, 138, 146, 154, 193, 196, 209, 223, 238, 239, 241, 242, 244, 246, 248, 251, 256, 261, 264, 271, 279, 297, 301, 304, 305, 306, 307, 308, 309
 Miyamoto, S., 155, 277
 Mohler, O. C., 28
 Moore, J. H., 43, 51, 72, 90, 101, 266, 267, 268, 296
 Morgan, W. W., 1, 14, 85, 87, 88, 89, 90, 104, 231, 279, 280
 Moseley, H. G. J., 78
 Mott, N. F., 190
 Münch, G., 224, 260, 311

 NAVOI, ALI, 186, 190
 Neven, L., 226, 228
 Newkirk, B. L., 49
 Newkirk, G., 98
 Niewodniczanski, H., 166
 Nissen, W., 216

 OKE, J. B., 210, 213, 224
 Oort, J., 53, 154, 300, 308
 Osterbrock, D., 1, 85, 88, 93, 186
 Oxmantown, Lord, 91

 PAGE, T. L., 28, 39, 40, 65, 68, 69, 71, 72, 92, 146, 147, 150, 223
 Paraskevopoulos, J., 90
 Parenago, P., 25, 53, 55
 Pasternack, S., 183, 184, 185, 186, 190
 Payne-Gaposchkin, C., 65, 78, 206
 Pease, F. G., 98
 Pecker, J. C., 226
 Peierls, R., 190
 Pekeris, C. L., 114, 118, 120, 123, 141, 147
 Perrine, C. D., 50, 267
 Petrie, R. M., 214, 215, 222
 Pettit, E., 35
 Placzek, G., 190
 Plaskett, H. H., 59, 67, 70, 112
 Plummer, H. C., 257
 Prokofjew, W., 166

 REBER, GROTE, 303
 Redman, R. O., 300
 Reynolds, J. H., 257
 Ritchey, G. W., 5
 Robinson, B. F., 311
 Robinson, H. A., 179, 180, 181
 Roman, N., 206, 209, 210, 300
 Rosino, L., 96
 Rosse, Lord of (Parsons), 2, 11, 56
 Rubinowicz, A., 168, 184
 Rudkjobing, M., 226
 Ryle, M., 309

 SAIGUSA, T., 277
 Salpeter, E., 225, 306
 Sandage, A., 98
 Savedoff, M., 283
 Schaeberle, J. M., 56
 Scheiner, J., 37
 Scheuer, P. A. G., 309
 Schlüter, A., 295
 Schon, M., 40

- Seaton, M. J., 141, 154, 190, 191, 193, 197, 283, 301, 305
 Seyfert, Carl K., 97, 101, 102
 Shajn, G. A., 2, 85, 93, 98, 128, 279, 280, 282
 Shapley, Harlow, 97
 Sharpless, S., 1, 7, 85, 86, 88, 89, 90, 93, 104, 231
 Shortley, G. H., 84, 169, 175, 179, 180, 181, 184, 185
 Singer, O., 223
 Slater, J. C., 144, 145, 174, 175, 183
 Slee, O. B., 308
 Slipher, V. M., 98, 101
 Sloanaker, R. M., 310
 Smith, Henry J., 206
 Spitzer, L., 151, 152, 153, 154, 279, 283, 309
 Stanley, G. J., 308
 Stebbins, J., 33, 85, 88, 204, 300
 Stevenson, A. F., 166, 184
 Stock, J., 31, 41, 42
 Story, H., 96
 Stoy, R., 57, 58, 69, 221, 222, 223, 230
 Strömgren, B., 1, 9, 14, 32, 36, 85, 140, 141, 234, 235, 238, 241, 248, 261, 270, 279, 285, 287
 Struve, O., 6, 9, 22, 36, 85, 92, 93, 96, 103, 207, 209, 212, 224, 234, 283, 280
 Struve, O. (the elder), 102
 Struve, W., 49
 Swensson, J. W., 209, 224
 Swings, P., 59, 78, 164, 206, 207, 209, 211, 212, 224

 TCHENG, MAO-LIN, 91
 Teller, E., 76, 151, 216
 Ter Haar, D., 299
 Thackeray, A. D., 50, 57, 248
 Trumpler, R. J., 90

 UFFORD, C. W., 185, 196
 Underhill, Anne, 226, 227, 230
 Unno, Wasaburo, 277
 Unsöld, A., 153, 215, 216, 227, 228

 VAN DE HULST, H. C., 299
 Van de Kamp, P., 49
 Van Maanen, A., 49, 50, 54, 202
 Van Vleck, J. H., 185, 196
 Vinti, J. P., 146
 Von Gothard, E., 57
 Von Hahn, 93
 Von Hirsch, R., 40
 Von Hoerner, S., 296, 297, 299
 Von Zeipel, H., 257
 Vorontsov-Velyaminov, B., 25, 51, 57, 221, 257, 280
 Vyssotsky, A., 49

 WACHMANN, A. A., 300
 Wade, Campbell M., 85, 86
 Walker, Merle, 280
 Wallenquist, Ake, 90, 260
 Weenen, J., 207
 Weston, E. G., 96, 105, 224, 281
 White, M. L., 190, 193, 264
 Whitford, A. E., 33, 70, 85, 88, 89, 90, 196, 300
 Williams, R. C., 28, 39, 70
 Willis, Howard, 50
 Wilsing, G., 37, 49
 Wilson, A., 48
 Wilson, Harvia H., 79
 Wilson, O. C., 22, 28, 43, 44, 72, 91, 213, 214, 239, 252, 256, 258, 260, 264, 268, 269, 270, 271, 273, 277, 283
 Wilson, R. E., 51, 87, 96
 Wirtz, C., 24, 25, 49
 Wolf, Max, 57, 84
 Wright, W. H., 57
 Wurm, K., 223, 230, 238, 283
 Wyatt, S. P., 28
 Wyse, A. B., 19, 20, 58, 59, 69, 70, 78, 91, 184
 YAMANOUCHI, T., 190
 Yü, C. S., 26

 ZANSTRA, H., 51, 66, 74, 75, 95, 218, 219, 220, 221, 222, 223, 224, 230, 236, 248, 249, 250, 251, 267, 274, 275, 276, 277

Subject Index

- ABEL'S INTEGRAL EQUATION, 259
- Absorption coefficients, *see* continuous absorption coefficients
- Aggregates (or associations) of B stars, 89, 231
- Ampère's law, generalized for displacement current, 167
- Andromeda spiral nebula (M31), 5, 8, 28, 89
- emission nebulae in, 8, 97, 100
- as a radio source, 303
- Angular diameters of planetaries, as an index of distance, 54
- Angular momentum operators, 175, 177
- Anomalous dispersion, 166
- Ansa of planetary nebulae, 57, 243, 244, 254
- Associations, 89, 231
- Atmospheric extinction, dependence on wavelength, 37, 38
- Atomic units, 143, 170
- Auroral transitions defined, 79
- BALMER CONTINUUM. Measurement of intensity in planetary nebulae, 71
- origin of, 74, 146–50
- Balmer decrement, 112, 148
- and space absorption, 54, 66, 127, 128, 200, 209
- calculation of, 122–5
- experimental studies of, 130
- influence of collisions on, 155–9
- in Network nebula, 301
- observations of, 127, 128, 129
- Tables of, 126, 127, 158
- Balmer discontinuity, dependence on temperature and density, 153, 154
- Blanketing effect in stellar atmospheres, 227
- Boltzmann equation for hydrogen, 118
- Born approximation, 156
- Bowen fluorescent mechanism, 81, 82, 83, 84
- Brackett series of hydrogen, 75
- CALIFORNIA NEBULA (NGC 1499), 6, 146
- Campbell's hydrogen envelope star, 207, 208, 224
- Cassiopeia radio source, 304, 305
- Catalogues, of nebulae and clusters, *see* NGC
- of diffuse nebulae, 84
- of emission nebulae in external galaxies, 97, 98
- Central stars of planetary nebulae
- compositions of, 224, 225
- luminosities of, 204, 205
- magnitudes of, 202–4
- position in Russell diagram, 202
- spectra of, 205–13
- spectrophotometry of, 213
- temperatures of, 217–24
- Chandrasekhar mean absorption coefficient, 216, 227, 228, 229
- Chemical composition of planetary nebulae, 58, 198, 199
- Classification of spectra of planetaries, 66, 73
- Coal sack, 7
- Collisional excitation of Balmer lines, 154–60, 200, 300
- cooling effects of, 160
- Collisional excitation of forbidden lines, 186–94
- target areas for, 191
- Collisional cross-sections for hydrogen lines, 156
- Conservation of energy, for pure radiative equilibrium, 115
- Conservation Theorem for target areas, 190
- Continuous absorption coefficient for hydrogen, 120
- for complex atoms, 141, 142
- for helium, 146
- for oxygen, 145
- Continuous spectra, of planetary nebulae; measurements of, 71
- of diffuse nebulae, 91, 94
- of Orion nebula, 91
- theory of, 146–54
- Contours, isophotic measurement of, 27–31
- Coma corrector, 14
- Combination variables, *see* variable stars, combination
- Correspondence principle, 169
- Coulomb's law, 167
- Crab nebula (NGC 1952), 4, 5, 268
- as a radio source, 306, 307, 314
- Crossley reflector, 11, 21, 50, 51, 56, 68, 98, 128, 251, 257
- Curtis Schmidt telescope, 7, 8, 41, 98, 300
- DARK NEBULAE, 84
- Diffuse nebulae, 84–102
- catalogues of, 84, 92
- dimensions of, 86
- distances and galactic concentration, 87
- illumination of, 93–6
- in external galaxies, 96–100, 284, 285
- photography of, Chapter II
- photometry of, 35, 36, 286
- physical processes in, 282, 283, 284
- polarization of, 96
- spectra of, 91, 92, 93
- Diffuse radiation in gaseous nebulae, defined, 236
- Dipole radiation, 166 *et seq.*
- selection rules for, 172
- Dumbbell nebula in Vulpecula (NGC 6853), 217, 246, 257
- EDDINGTON APPROXIMATION, 132
- Einstein coefficient of spontaneous emission, 81, 119, 170, 184
- for 2-photon emissions, 152
- Einstein probability coefficient, expressed in terms of line strengths, 170, 184
- Electric dipole moment, 168

- Electric dipole radiation, 166, 170. *See also* dipole radiation
- Electric quadrupole radiation, 166, 170, 184.
See quadrupole radiation
- Electron densities from Balmer continuum, 147, 148
— from forbidden lines, 193
- Electron scattering, 146, 215
- Electron temperature
— from continuous spectrum, 150, 153, 154
— from forbidden lines, 193–4
— Theory of for a nebula with “impurities”, 135, 136
— Theory of, for a pure hydrogen nebula, 130–8
— observed values, 149
— of Orion nebula, 284
- Electrostatic interaction between electrons in complex atoms, 175, 179, 182
- Electrostatic interaction parameter, 179
- Emission line intensities in gaseous nebulae, measurement of, 67–70
- Emission measure, 86, 92
— defined, 36
- Exchange effects in collisional excitation, 77
- Expansion of gaseous nebulae, 266–77
- FABRY-PEROT INTERFEROMETER, 12, 14, 15, 16, 17, 43, 282
- Filamentary structure of gaseous nebulae, 196, 246, 256, 299, 301
— of strong radio sources, 304
- Filters for photography of gaseous nebulae, 12, 85
- Filters, interference type, 13, 14, 23, 32, 33, 85
- Fluorescence by solid particles, 94
- Fluorescence in gaseous nebulae, 81. *See also* Bowen fluorescent mechanism
- Fluorescence in stars, 210
- Forbidden lines
— collisional excitation of, 186–95
— experimental production of, 164–6
— identification of, 164
— in planetary nebulae, 58, 73, 75, 78–81
— transition probabilities of, 170–86, 187–9
— types of, defined, 79
- Free-free transitions as a source of continuous spectrum, 147, 150, 152
- GALACTIC NEBULAE, TYPES OF, 2
— diffuse, 7, 84 *et seq.*
— planetary, 2
- Galactic rotation and planetary nebulae, 52
— formula for, 87
- Gaunt correction factor, 118, 120, 121, 123
— asymptotic formula for, 147
— for radio-frequency radiation, 310
- Globular cluster M15 (NGC 7078) and associated planetary nebula, 55
- Globules, 7
- HAIDINGER FRINGES, 15
- Hamburg Observatory, 204, 300
- Hartree wave functions, 144, 145, 183
- Harvard College Observatory, 11
- Harvard standard regions, 25
- Helium, spectrum of in gaseous nebulae, 75, 76, 77, 195
— forbidden lines of, 166
— ionization of, 238
- Henney-Greenstein camera, 12, 85
- Hierarchy of eddies, 292
- High excitation nebulae in external galaxies, 101
— as radio sources, 102
- Hind's variable nebula (NGC 1555), *see* T Tauri
- Hubble's variable nebula (NGC 2261), 103
- Hydrogen, ionization of, 138, 234 *et seq.*
— nebula, Chapter IV
- IMAGE-ROTATOR, 22, 268
- Image slicer, 18, 19, 20, 58
- Index catalogue of clusters and nebulae, 1
- Intermediate coupling, 173–84
- Internal motions in gaseous nebulae, 266–77
- Interstellar absorption and Balmer decrement, 54, 127
- Interstellar lines, as an index of distance, 87
- Ionization equation for gaseous nebulae and the interstellar medium, 138–42, 234–9
— including effects of collisional ionization, 159
- Isoelectronic sequences, 165
- Isophotic contours of gaseous nebulae, 27, 32, 240, 241, 242, 243, 244, 245, 246, 247, 248, 251–6
- Isophotometer, cathode-ray tube, 28
— balanced beam, 28, 29, 31, 252
- jj* COUPLING, 175, 178
- KINEMATICAL VISCOSITY, 292
- Kolmogoroff approximation to turbulence spectrum, 293
- Kramer's formula, 118
- LADENBURG f. *See* oscillator strength
- Lamont-Hissey Observatory, 48
- Lick Observatory, 11, 20, 21, 49, 50, 59, 65, 67, 68, 69, 98, 102, 128, 165, 251
- Loop nebula (30 Doradus), 8, 31
- LS or Russell Saunders coupling, 173, 175, 178, 185
- Lucite, use as a diffuser in spectrophotometry, 39, 68
- Lyman radiation in gaseous nebulae, 74
— theory of, 111 *et seq.*
- MCDONALD OBSERVATORY, 14, 21, 22, 68, 91, 102, 212, 213
- McMath-Hulbert Observatory, 32, 33
- Mach number, 294
- Magellanic Cloud, Large, 8, 9, 27, 51, 96, 97, 100, 285, 286, 291, 312
- Magellanic Cloud, Small, 8, 9, 51, 97, 312
- Magnetic dipole radiation, 78, 168, 169, 170, 171, 172, 184
— selection rules for, 172
- Magnetic field, in galaxy, 288–99
- Maxwellian distribution of velocities
— deviations from, 114
— expression for, 139
- Maxwell's equations, 168

- Messier 8 nebula (NGC 6523) Lagoon, 7, 8, 28, 84, 86, 89, 90, 93, 96, 286
- Messier 31 (*see* Andromeda Spiral)
- Messier 33 (*see* Triangulum Spiral)
- Messier's catalogue, 1
- Metastable levels of helium, 75, 76
 - of ground configurations, 80, 164 *et seq.*
 - of hydrogen, 150–4, 283
- Model atmospheres, for early-type stars, 225–31
- Morgan-Keenan systems of spectral classification, 88
- Motions within gaseous nebulae
 - by radio methods, 44
 - interpretation of, 271, 277, 295–7
 - measurement of, 43, 44, 266–8, 282
- Mt. Wilson Observatory, 2, 5, 8, 31, 35, 41, 43, 49, 50, 59, 70, 71, 204, 251, 270, 282, 297, 299
- Multi-slit, 44, 264, 268
- Multiple stars and excitation of gaseous nebulae, 231
- NAVAL OBSERVATORY (U.S.A.), 32
- Naval Research Laboratory, 310
- Nebula, definition of, 1. *See also* galactic nebulae
 - extra-galactic, 11
 - spiral, 1
 - “white” 2
- Nebular transitions, defined, 79
- Nebulium, 78
- Negative absorptions, 118
- Network or Veil Nebula (NGC 6960, 6992, 6995), 5, 154, 159, 282, 299–302
- New General Catalogue of Clusters and Nebulae* (NGC), 1
- Non-coherent scattering, 275, 276
- North America nebulae (NGC 7000), 154
- Nova Aquilae, 1918, 3
- Nova (DQ) Herculis, 1934, 3, 163
- Nova Persei (1901), 3
- Novalae, relation to gaseous nebulae, 3
- OORT CONSTANT, 87
- Oort relation, 87
- Operational equation in quantum mechanics, 177
- Orion nebula (NGC 1976, M42), 1, 2, 7, 8, 9, 11, 17, 24, 36, 40, 43, 59, 84, 88, 91, 93, 96, 97, 98, 103, 105, 154, 155, 283, 284, 285, 296, 297, 310, 311
 - spectrum of, 91
 - variables in, 105
- Oscillator strength, 81, 118
 - for hydrogen, 117
 - for continuum, 142
- Owl nebula (NGC 3587), 11, 244, 246
- PALOMAR SCHMIDT SKY SURVEY, 6, 14, 85, 298
- Palomar 200-in. Hale telescope, 8, 41, 57, 59, 251, 256
 - coude spectrograph, of, 19, 59, 270
- Paschen series of hydrogen, 75
 - of ionized helium, 218
- Pauli exclusion principle, 174, 175, 177
- P Cygni characteristics in stellar spectra, 210, 212
- Pfund series, 75
- Photography of gaseous nebulae, 12, 13
- Photometric calibration, methods of, 39, 40, 41
- Photometry of gaseous nebulae, 23
 - by photo-electric methods, 23, 31–6, 204
 - by photographic methods, 24–7
 - by visual methods, 24
- Planetary nebulae, 2
 - central stars of, 202–24
 - chemical compositions of, 199
 - dimensions and forms of, 51, 54, 55, 56, 57
 - distances of, 49–55
 - interpretation of spectra of, 72–84
 - membership in population type II, 2, 51, 55
 - space distribution of, 46, 48
 - spectra of, 57–72
- Pleiades nebulosity, 91, 93, 146
- Polarization of light in diffuse nebulae, 96
- Poynting Vector, 168
 - defined, 167
- Primary mechanism for excitation of hydrogen lines and helium lines, 74, 75, 77. *See also* recombination spectra
- Proper motions of planetary nebulae, 50
- QUADRUPOLE RADIATION, 166–71, 184
 - selection rules for, 172
- Quadrupole moment, 168
- Quantum mechanics, equations for radiation, 169
 - calculation of line strengths by, 173 *et seq.*
- RADCLIFFE REFLECTOR, 248
- Radial quantum integral for dipole transitions to continuum, 142, 144
 - for forbidden lines, 183, 184
- Radiation pressure
 - and mechanical equilibrium of stellar atmospheres, 226
 - in expanding planetaries, 275–7
 - in static planetaries, 275
 - separation of ions by, 271, 272
- Radiative equilibrium, for helium, 77
 - for OIII, 82
 - of a gaseous nebula, 111
- Radio-frequency observations of gaseous nebulae (21 cm.), 89, 311, 312
- Radio-frequency thermal radiation from diffuse nebulae, 90, 310, 312
- Radio-frequency sources, 302–12
- Rayleigh scattering in earth's atmosphere, 38
- Recombination spectra in afterglows, 130
- Recombination spectra in gaseous nebulae
 - continuous, 146, 147, 148
 - of carbon, 77
 - of hydrogen, 74, 75
 - of oxygen, 78, 80
 - theory of, 111 *et seq.*
- Reynolds's number
 - and relation to turbulence spectrum, 292–4
 - defined, 291
 - for planetary nebulae, 246

- Ring nebula (NGC 6720), 2, 56
 - early observations of, 11
 - internal motions of, 271
 - isophotic contours of, 247
 - outer halo of, 238
 - photo-electric observations of, 32
 - structure of, 244, 248, 257
- Rosette nebula (NGC 2237, 2238, 2246), 6, 86, 88, 93
- Rosseland mean absorption coefficient, 226, 227, 228, 229
- Rydberg formula, 114
- ST. MICHEL OBSERVATORY IN HAUTE PROVENCE, 14, 279
- Scalar potential, defined, 167
- Schmidt cameras
 - Baker super-Schmidt, 12
 - use for photography of nebulae, 6, 8, 12
- Schuster-Schwarzschild approximation, 132
- Scorpio Centaurus cluster, 88, 89
- Selection rules for radiation, 172, 173
- Simeis Observatory, 2, 257, 279
- Slater's rules for calculation of wave functions, 144, 145
- Slitless spectrograph, 21, 27, 31
- Solar spectral energy distribution used as standard for nebular spectrophotometry, 35
- Space distribution of planetary nebulae, 46, 48
- Spatial structure of planetary nebulae, 256–66
 - relation to internal motions, 270
- Spectra of gaseous nebulae, *see* diffuse nebulae, planetary nebulae, spectra of, etc.
- Spectrographs for nebular work, 17–23
- Spectrophotometry of gaseous nebulae by photographic methods, 37–41, 67, 72
 - by photo-electric methods, 69
 - errors in, 69
 - of Orion nebula, 91
- Spin-orbit interaction, 173, 175, 177, 183, 185
 - second-order effect in, 185
- Spin-orbit perturbation, 178
- Spin-other-orbit interaction, 185
- Spin-spin interaction, 185
- Spiral arms, defined by emission regions, 88, 89
- Spot sensitizer, 39
- Stark broadening of lines in stellar spectra, 214, 216
- Statistical equilibrium
 - in excited levels, 82
 - in ground configurations of complexes, 192
 - in hydrogen, 113, 115, 118, 123
- Stellar energy distributions, 39
 - theory of, 225–30
- Stellar population types, 2, 4, 5, 98, 100, 201, 202
- Stimulated emissions, 118
- Stratification of a gaseous nebula, theory of, 234–9
 - observations of, 88, 89, 241, 246, 248–56
- Strength of a spectral line, defined, 169
 - formulae and tables of, 184, 185, 186–90
- Supernovae, 4
 - as radio sources, 304
- Surface brightness of nebulae
 - by method of relative exposures, 24
 - measurement of, 23–36
 - photometric standards of, 36
- T ASSOCIATIONS, DEFINED, 105
- Target area for collisional excitation of forbidden lines, 186–93
 - tables of, 191
- Temperature of gaseous nebulae, kinetic, 17. *See also* electron temperature
- Temperatures of illuminating stars, 217–23, 228
- Thermodynamic equilibrium, deviations from, 118 *et seq.*
- Tonantzintla Schmidt telescope, 8, 9, 97
- Transauroral transitions, defined, 79
- Transient effects of ionization and excitation in gaseous nebulae, 161, 162
- Transition probabilities, for forbidden lines, 170–85
 - calculation of, 173–83
 - tables of, 187–90
- Triangulum spiral (M 33), 8, 9, 87, 98, 99, 100, 185, 231, 303
- Trifid nebula (NGC 6514), 7, 84, 90, 93, 96, 281, 287, 310
- Trigonometric parallaxes of planetary nebulae, 49
- T Tauri variables, 94, 102–6
- Turbulence, in gaseous nebulae, 16, 17, 268, 291–9
 - in relation to galactic magnetic field, 288, 295, 296
 - spectrum of, 293, 294
 - theory of, 293–5
- Two-photon emission in hydrogen, 151–4
 - in helium, 75
- Types of stellar population. *See* stellar population types
- ULTRA-VIOLET RADIATION as source of excitation of Balmer lines, 74, 75
- VARIABLE NEBULAE, 102, 103
- Variable stars, combination (or symbiotic), 4
 - associated with diffuse nebulae, 102–106
- Vector potential, defined, 167
- Veil nebula. *See* Network Nebula
- WARNER AND SWASEY OBSERVATORY, 41
- Wave functions, 143, 144
 - for complex atoms, 173, 174, 177, 178
 - zero-order, 174, 176, 177
- Wolf-Rayet stars, 81, 205, 206
 - as central stars of planetaries, 207, 224
- Yerkes Observatory, 1, 22, 92
- ZEEMAN COMPONENTS
 - states, 176, 177
 - transition probabilities for, 169, 171, 180, 181

★ Gaseous Nebulae ★
L. H. ALLER ★

C & H